



**US Army Corps
of Engineers**
Waterways Experiment
Station

Technical Report GL-96-17
October 1996

Installation Restoration Research Program

Assessment of Geophysical Methods for Subsurface Geologic Mapping, Cluster 13, Edgewood Area, Aberdeen Proving Ground, Maryland

by *Dwain K. Butler, Michael K. Sharp, Keith J. Sjostrom,
Janet E. Simms, Jose L. Llopis, WES
David V. Fitterman, U.S. Geological Survey*

DTIC QUALITY INSPECTED 2

Approved For Public Release; Distribution Is Unlimited

19961216 054

Prepared for Directorate of Safety, Health, and Environment

The contents of this report are not to be used for advertising, publication, or promotional purposes. Citation of trade names does not constitute an official endorsement or approval of the use of such commercial products.



PRINTED ON RECYCLED PAPER

Assessment of Geophysical Methods for Subsurface Geologic Mapping, Cluster 13, Edgewood Area, Aberdeen Proving Ground, Maryland

by Dwain K. Butler, Michael K. Sharp, Keith J. Sjostrom,
Janet E. Simms, Jose L. Llopis

U.S. Army Corps of Engineers
Waterways Experiment Station
3909 Halls Ferry Road
Vicksburg, MS 39180-6199

David V. Fitterman

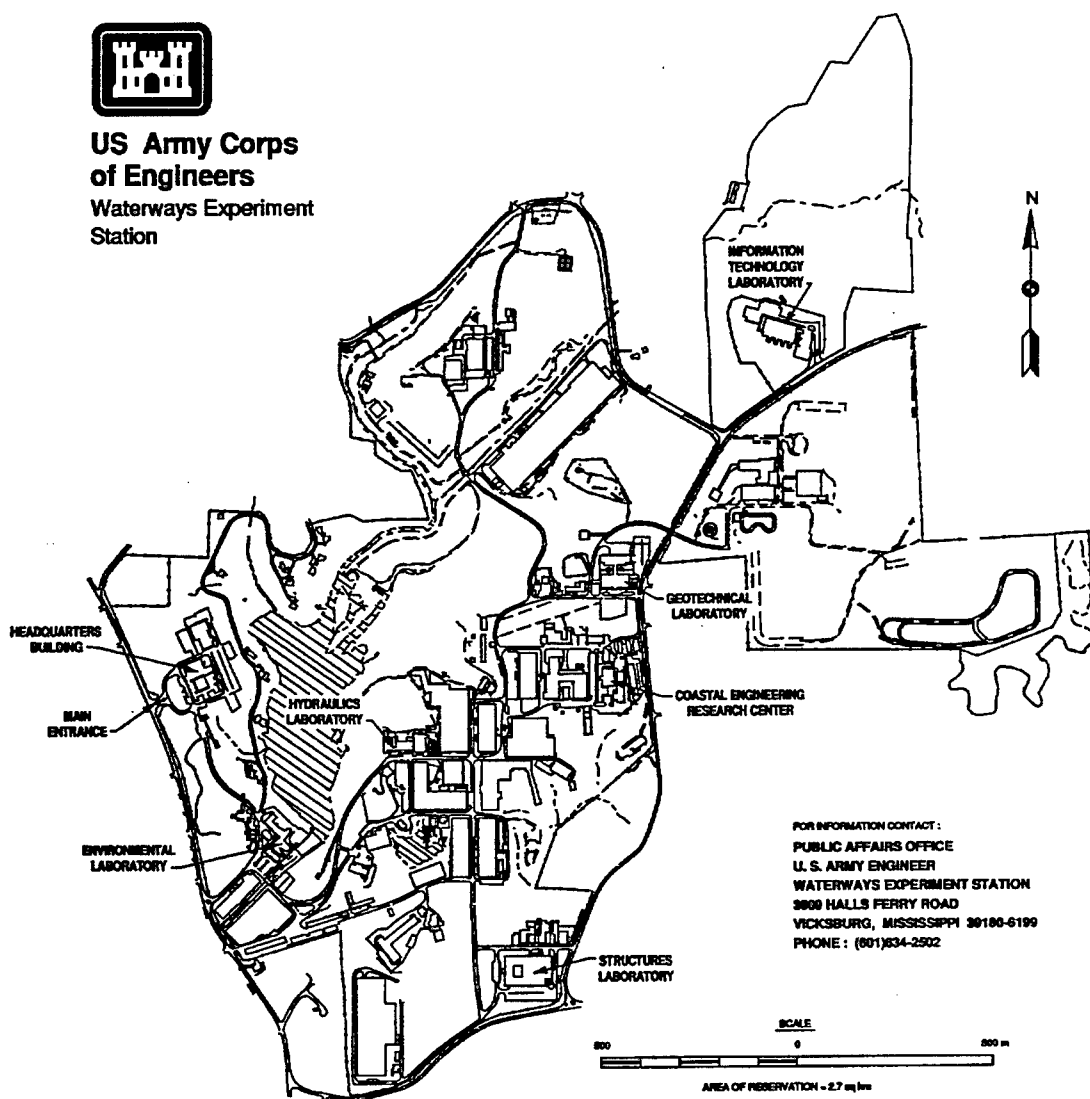
U.S. Geological Survey
Box 25046, MS 964
Denver Federal Center
Denver, CO 80225

Final report

Approved for public release; distribution is unlimited



**US Army Corps
of Engineers**
Waterways Experiment
Station



Waterways Experiment Station Cataloging-in-Publication Data

Assessment of geophysical methods for subsurface geologic mapping, Cluster 13, Edgewood Area, Aberdeen Proving Ground, Maryland / by Dwain K. Butler ... [et al.] ; prepared for Installation Restoration Program, Directorate of Safety, Health, and Environment. 288 p. : ill. ; 28 cm. — (Technical report ; GL-96-17)
Includes bibliographic references.

1. Geophysical well logging — Maryland — Aberdeen Proving Ground. 2. Geological mapping — Maryland — Aberdeen Proving Ground. 3. Geological mapping — Evaluation. 4. Prospecting — Geophysical methods — Evaluation. I. Butler, Dwain K. II. United States. Army. Corps of Engineers. III. U.S. Army Engineer Waterways Experiment Station. IV. Geotechnical Laboratory (U.S. Army Engineer Waterways Experiment Station) V. Installation Restoration Program. VI. Aberdeen Proving Ground (Md.). Directorate of Safety, Health, and Environment. VII. Series: Technical report (U.S. Army Engineer Waterways Experiment Station) ; GL-96-17.
TA7 W34 no.GL-96-17

Contents

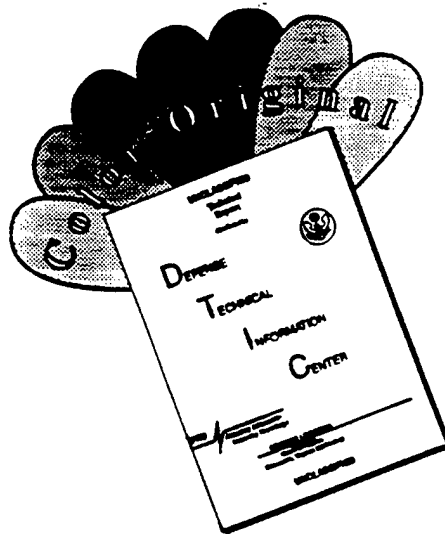
Preface	vii
Executive Summary	viii
Conversion Factors, Non-SI to SI Units of Measurement	x
1—Introduction	1
Background	1
Purpose	7
Scope of Report	7
2—Physiography and Geology of the Edgewood Area and Cluster 13 ..	8
Regional Physiographic and Geologic Setting	8
Geology of the Edgewood Area and Cluster 13	11
3—Plan of Investigation	23
Site Survey Grid	23
Geophysical Investigation Strategy	23
Basic Physical Concepts and Survey Procedures	28
Seismic refraction (SR) method	28
Electrical resistivity (ER) method	29
Transient electromagnetic (TEM) method	30
Borehole geophysical logging methods	31
4—Results of the Investigation	33
Seismic Refraction Analysis	33
Data: Procedures and time-distance plots	33
Interpretation: Procedures and cross-sections	35
Interpretation: Seismic velocity cross sections and assessment ...	38
Electrical Resistivity Analysis	41
Data: Procedures and apparent resistivity plots	41
Interpretation: Procedures and best-fit models	42
Interpretation: Electrical resistivity cross-section and assessment .	42
Transient Electromagnetic Analysis	49
Data: TEM procedures and sounding curves	49
Interpretation: Procedures and best-fit models	50
Interpretation: 3-D portrayal of results	50
Interpretation: Assessment of TEM results	53

Borehole Geophysical Logs	79
Summary of Integrated Geological Assessment	80
5—Summary and Conclusions	86
References	88
Appendix A: Seismic Refraction Time-Distance Data Plots	A1
Appendix B: Electrical Resistivity Sounding Data	B1
Appendix C: Transient Electromagnetic Sounding Data	C1
Appendix D: Borehole Geophysical Logs	D1
SF 298	

List of Figures

Figure 1.	Lauderick Creek area cluster locations	3
Figure 2.	Location of Cluster 13, Edgewood Arsenal Area, and Sites 1-4	5
Figure 3.	Physiographic provinces in Maryland	9
Figure 4.	Generalized cross-section of the Coastal Plain sediments . .	10
Figure 5.	Shallow stratigraphy in the Cluster 13 area	13
Figure 6.	Potentiometric surface map for Cluster 13 area (from shallow monitoring wells)	17
Figure 7.	Deep stratigraphic borings in the vicinity of Cluster 13 . . .	19
Figure 8.	Cross-section between stratigraphic borings LC-1 and TH-2 (approximately NE-SW)	21
Figure 9.	Survey grid for Site 4, Cluster 13, and locations of four survey profile lines	25
Figure 10.	Typical seismic refraction time-distance plot, for refraction spread centered at (2.5, 1.5) or 405 ft (123.4 m) from beginning of line, showing assignments of layer number to each arrival	34
Figure 11.	Typical seismic refraction time-distance plot (left), for refraction spread centered at (2.5, 1.5) or 405 ft (123.4 m) from beginning of line, showing straight lines through arrivals from each layer and a model (right) from a traditional intercept time interpretation	36
Figure 12.	Velocity-stratigraphic cross section for long line seismic refraction survey (2.5, 1.5); dashed lines are the planar interface model.	37

DISCLAIMER NOTICE



THIS DOCUMENT IS BEST QUALITY AVAILABLE. THE COPY FURNISHED TO DTIC CONTAINED A SIGNIFICANT NUMBER OF COLOR PAGES WHICH DO NOT REPRODUCE LEGIBLY ON BLACK AND WHITE MICROFICHE.

Figure 13.	Long line seismic velocity stratigraphic cross section, showing three mappable velocity units	39
Figure 14.	Cross line 1 seismic velocity stratigraphic cross section, showing three mappable velocity units	40
Figure 15.	Typical electrical resistivity sounding data and best fitting model for location (2.5, 1.5)	43
Figure 16.	Parameters of best-fit model (Figure 15) and comparison of measured data with best-fit model values (Synthetic) for resistivity sounding at location (2.5, 1.5)	44
Figure 17.	Electrical resistivity cross section along long line, showing resistivity ranges in ohm-m	46
Figure 18.	Color-coded version of the electrical resistivity cross section shown in Figure 17, emphasizing the interpreted resistivity "facies"	47
Figure 19.	TEM data, best-fit model, and best-fit model parameters list for sounding at location (2.5, 1.5)	51
Figure 20.	Cluster 13 survey grid and TEM sounding number grid cell assignments	52
Figure 21.	Cross sections from the TEM volume model along the long line and cross lines 1-3; resistivity ranges for the layers are given in the text	55
Figure 22.	TEM layer 1 resistivity map	57
Figure 23.	TEM layer 2 resistivity map	58
Figure 24.	TEM layer 3 resistivity map	59
Figure 25.	TEM layer 4 resistivity map	60
Figure 26.	Surface elevation map	61
Figure 27.	Depth to layer 1 - layer 2 interface in TEM volume model	62
Figure 28.	Depth to layer 2 - layer 3 interface in TEM volume model	63
Figure 29.	Depth to layer 3 - layer 4 interface in TEM volume model	64
Figure 30.	Layer 1 thickness in TEM volume model	65
Figure 31.	Layer 2 thickness in TEM volume model	66
Figure 32.	Layer 3 thickness in TEM volume model	67
Figure 33.	View of complete 4-layer TEM volume model, looking northeast	69

Figure 34.	View of complete 4-layer TEM volume model, looking southwest	71
Figure 35.	View of 4-layer TEM volume model with vertical- horizontal bench cut, looking southwest	73
Figure 36.	View of top of layer 2 with color-coded elevation contours, looking southwest	75
Figure 37.	View of top of layer 3 with color-coded elevation contours, looking southwest	77
Figure 38.	Borehole geophysical logs for WLC-37	81
Figure 39.	Borehole geophysical logs for WLC-39	82
Figure 40.	Long line seismic velocity cross-section, with hydrogeologic interpretations and borehole logs projected onto section	83
Figure 41.	Long line TEM cross-section, with geologic interpretations	84

Preface

A field investigation was performed at Cluster 13, the Edgewood Area of Aberdeen Proving Ground (APG), Maryland, during the period 7-14 November 1994. This work was performed under the Installation Restoration Program for the Directorate of Safety, Health and Environment, APG, Maryland. APG Technical Monitor for the work was Mr. Jerry Burgess. Mr. Donald Green was the APG Area Manager. The work was performed by personnel of the U.S. Army Engineer Waterways Experiment Station (WES).

This investigation was performed by Messrs. Michael K. Sharp, Keith J. Sjostrom, and Jose L. Llopis, and Drs. Janet E. Simms and Dwain K. Butler, Earthquake Engineering and Geosciences Division (EEGD), Geotechnical Laboratory (GL), WES, and Dr. David V. Fitterman, Branch of Geophysics, U.S. Geological Survey. Dr. Fitterman assisted with the field work and the data interpretation. This report was prepared by Dr. Butler. The work was performed under the general supervision of Dr. Arley G. Franklin, Chief, EEGD, and Dr. William F. Marcuson III, Director, GL.

At the time of publication of this report, Director of WES was Dr. Robert W. Whalin. Commander was COL Bruce K. Howard, EN.

The contents of this report are not to be used for advertising, publication, or promotional purposes. Citation of trade names does not constitute an official endorsement or approval of the use of such commercial products.

Executive Summary

Detailed subsurface geological information is not available for many areas at Aberdeen Proving Ground (APG), Maryland. Remedial investigations (RI) at APG require detailed subsurface geological information for planning monitoring well placement, depth, and installation details, and for modeling ground water flow and possible contaminant transport. The detailed geological information is also needed for subsequent feasibility studies (FS). Among the information needed are surficial soil thickness and variation, depths to the water table, depths to the Pleistocene-Cretaceous boundary, vertical and lateral heterogeneity within units or formations, and depths to the Precambrian basement (crystalline rocks). A geophysical investigation performed at Cluster 13, Edgewood Area, APG, demonstrates the capability of geophysical methods for contributing to a detailed subsurface geological mapping program.

Seismic refraction, electrical resistivity, and transient electromagnetic surface surveys and borehole geophysical logging were conducted at a portion of Cluster 13, Edgewood Area of Aberdeen Proving Ground, Maryland. Seismic refraction cross sections map the "topsoil" layer and the water table (saturated zone). The water table elevations from the seismic surveys correlate closely with water table elevations in nearby monitoring wells. Electrical resistivity cross sections reveal a very complicated distribution of sandy and clayey facies in the upper 10 - 15 in of the subsurface. A continuous surficial (topsoil) layer correlates with the surficial layer of the seismic section and nearby boring logs. Below the surficial layer, the complicated facies distribution has resistivities ranging from 25 ohm-m (likely clay) to several thousand ohm-m (dry sands and/or gravels). The complexity and details of the electrical resistivity cross section correlate well with boring and geophysical logs from nearby wells.

The transient electromagnetic surveys map the Pleistocene-Cretaceous boundary, the saprolite, and the top of the Precambrian crystalline rocks. Conducting the transient electromagnetic surveys on a grid pattern allows the construction of a 3-D representation of subsurface geology (as represented by variations of electrical resistivity). Depths to the Pleistocene-Cretaceous boundary are consistent with the interpreted depths from borings at Cluster 13 and other areas of the Edgewood Area. Thickness and depth of the saprolitic layer and depth to top of the Precambrian rocks are consistent with generalized geologic cross sections for the Edgewood Area and depths projected from

reported depths at the Aberdeen Proving Ground NW boundary using regional dips. The average depth to top of the Precambrian rocks beneath Cluster 13 is 100 m.

Conversion Factors, Non-SI to SI Units of Measurement

Non-SI units of measurement used in this report can be converted to SI units as follows:

Multiply	By	To Obtain
acres	4,046.873	square meters
feet	0.3048	meters(m)
mho	1.0	Siemen (S)
mho/ft	3.2808	Siemen/m (S/m)
ohm-ft	0.3048	ohm-m

1 Introduction

Background

The Edgewood Area of Aberdeen Proving Ground (APG), Maryland, was placed on the National Priorities List in February 1990. The Installation Restoration Program at APG seeks to characterize the nature and extent of risks posed by uncontrolled hazardous waste sites, evaluate potential remedial options, and carry out remediation when required. A fundamental part of the site characterization is developing an understanding of the geology and hydrogeology. Overall, the geology of APG is poorly understood and documented. The present work is part of an ongoing effort to investigate the geology of APG and of the clusters and sites at the Edgewood Area specifically.

Cluster 13 is one of more than 50 clusters of potentially contaminated sites under study at the Edgewood Area. Each cluster may contain multiple sites for purposes of characterization and remediation. Cluster 13 is located in the Lauderick Creek Area of the Edgewood Area (Figure 1). For purposes of the remedial investigation and feasibility study (RI/FS) for Cluster 13, four sites have been defined, as shown in Figure 2. This report will present results of work performed at Site 4 and will ultimately become part of the RI for Cluster 13. Geophysical investigations at Sites 1-3 were performed separately and documented in Sharp and Lee (1995).

The U.S. Army Chemical School occupied portions of the Edgewood Area from 1920 to 1951. One of the primary field training areas used by the Chemical School was the Lauderick Creek Area. Portions of the Area used for field training are designated as School Fields #1-10 (Figure 1). From Figures 1 and 2, School Field Training Area #2 is seen to coincide with Site 4, Cluster 13. The School Fields in general were used for a wide variety of chemical warfare related activities. Training activities included: storage, use and firing of chemical ordnance; identification of chemical agents; decontamination; clothing impregnation and laundering; disposal of chemical agents, chemical agent contaminated materials; and chemical ordnance. School Field #2 also had several small dump sites. At the dump sites, empty drums were present on the surface and at one site partially buried drums were visible. The dump sites also contained empty or expended munitions, miscellaneous junk, and the remains of an old aircraft (AEHA 1990). This description of the dump sites was valid during the geophysical surveys discussed in this

392250E 4365000N

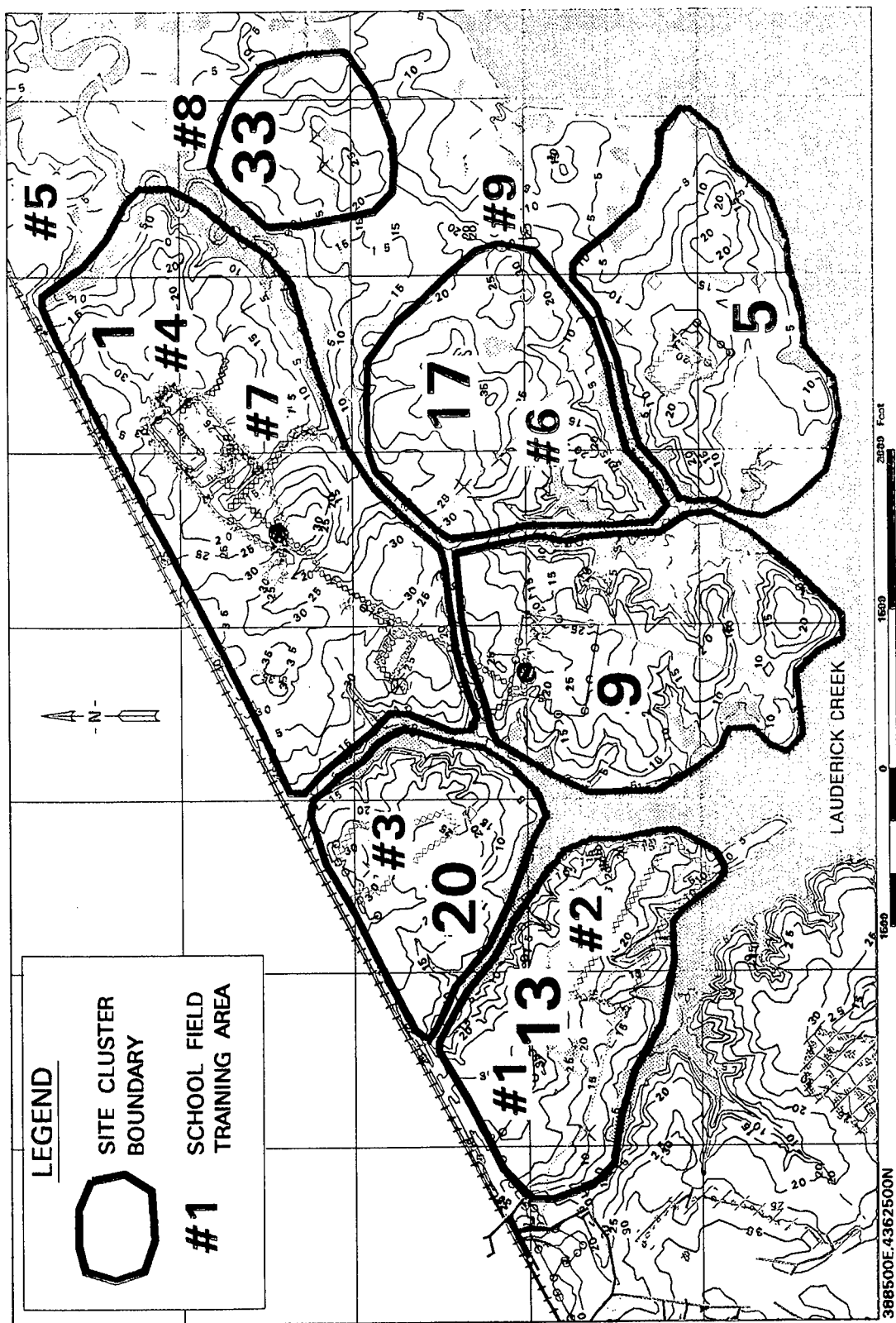


Figure 1. Lauderick Creek area cluster locations

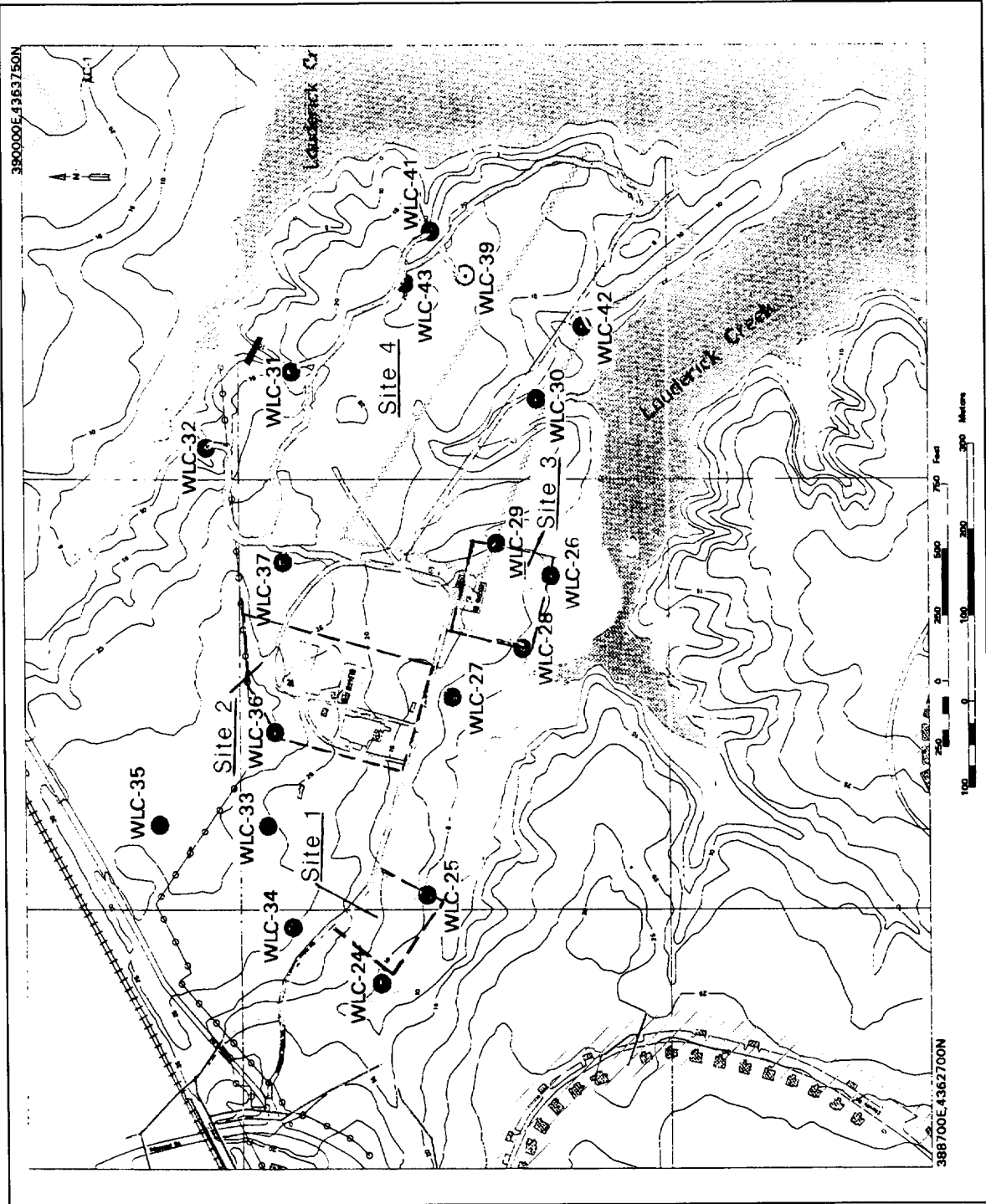


Figure 2. Location of Cluster 13, Edgewood Arsenal Area, and Sites 1-4

report; however, the dump sites were cleaned up in a removal action by the Corps of Engineers in 1995 (R&R International 1995).

Purpose

The purpose of the present work at Site 4 of Cluster 13 is to assess the capability of geophysical methods to map details of subsurface geology (stratigraphy) in the APG geologic setting. Specific mapping objectives are (1) the location and continuity of sand and clay facies in the shallow subsurface (< 15-20 m), (2) depth to the water table, (3) the depth to the Pleistocene-Cretaceous boundary (estimated to be approximately 50 ft or 15 m deep beneath Cluster 13), and (4) the depth to the Precambrian crystalline rock (basement). Existing boreholes in Cluster 13 for monitoring wells are quite shallow, < 14 m, and widely scattered. Boreholes to depths of approximately 76 m exist in other areas of The Edgewood Area; but, due to the complexity of the sedimentary section, projections of the stratigraphy to such depths beneath Cluster 13 are tenuous at best. The geophysical investigations were planned to allow detailed stratigraphic mapping to depths of approximately 15 m and general stratigraphic indications to greater depths (possibly to the depth of the Precambrian basement).

Scope of Report

The general physiography and geology of APG and the Edgewood Area and specifically of Cluster 13 are briefly presented in Chapter 2. Chapter 3 summarizes the plan of the investigations at Cluster 13; Site 4, and surveys the basic concepts of the geophysical methods. Results of the investigations are detailed in Chapter 4, and finally conclusions and suggestions for approaches to mapping the subsurface geology at other clusters at Edgewood Area are presented in Chapter 5.

2 Physiography and Geology of the Edgewood Area and Cluster 13

Regional Physiographic and Geologic Setting

APG is located on the Chesapeake Bay, approximately 25 km northeast of Baltimore, Maryland, in Harford County. APG is located in the Coastal Plain Physiographic Province. Maryland extends across five physiographic provinces, which parallel the Atlantic coastline in belts of varying width from New England almost to the Gulf of Mexico (Fenneman 1938; Vokes 1957; Whitten et al. 1992). Figure 3 shows the physiographic provinces of Maryland and the location of APG. APG is elongated in a northeast-southwest direction, occupying approximately 79,000 acres. The Edgewood Area occupies the southwestern portion of APG, bounded to the northeast by the Bush River.

The Coastal Plain Province in Maryland is bounded to the north and west by the Fall Line, actually a transition zone varying in width from approximately 5 to 15 km between the Cretaceous and younger Coastal Plain sediments (south and east of the Fall Line) and the Precambrian Piedmont Crystalline Complex (igneous and metamorphic rocks, west and north of the Fall Line). Coastal Plain sediments form a seaward-thickening wedge deposited on the seaward (eastward) continuation of the Piedmont Crystalline Complex, which forms the Precambrian basement under the Coastal Plain. The wedge consists of both marine and non-marine sedimentary formations that increase in thickness and decrease in dip for successively younger formations. The formations decrease in dip from an average of approximately 15 m/km near Precambrian basement to an average of 2 m/km for the uppermost formations. There are significant variations both vertically and laterally in lithology and texture. In the APG area, the Fall Line approximately parallels U.S. Highway 40, 3 to 6 km from the northwest boundary of APG.

A generalized cross-section of Coastal Plain sediments is shown in Figure 4. The stratigraphic framework and lithologic description of the sediments in Harford County are given in Table 1. A generalized hydrogeological assessment of the formations is also presented on the right side of Figure 4

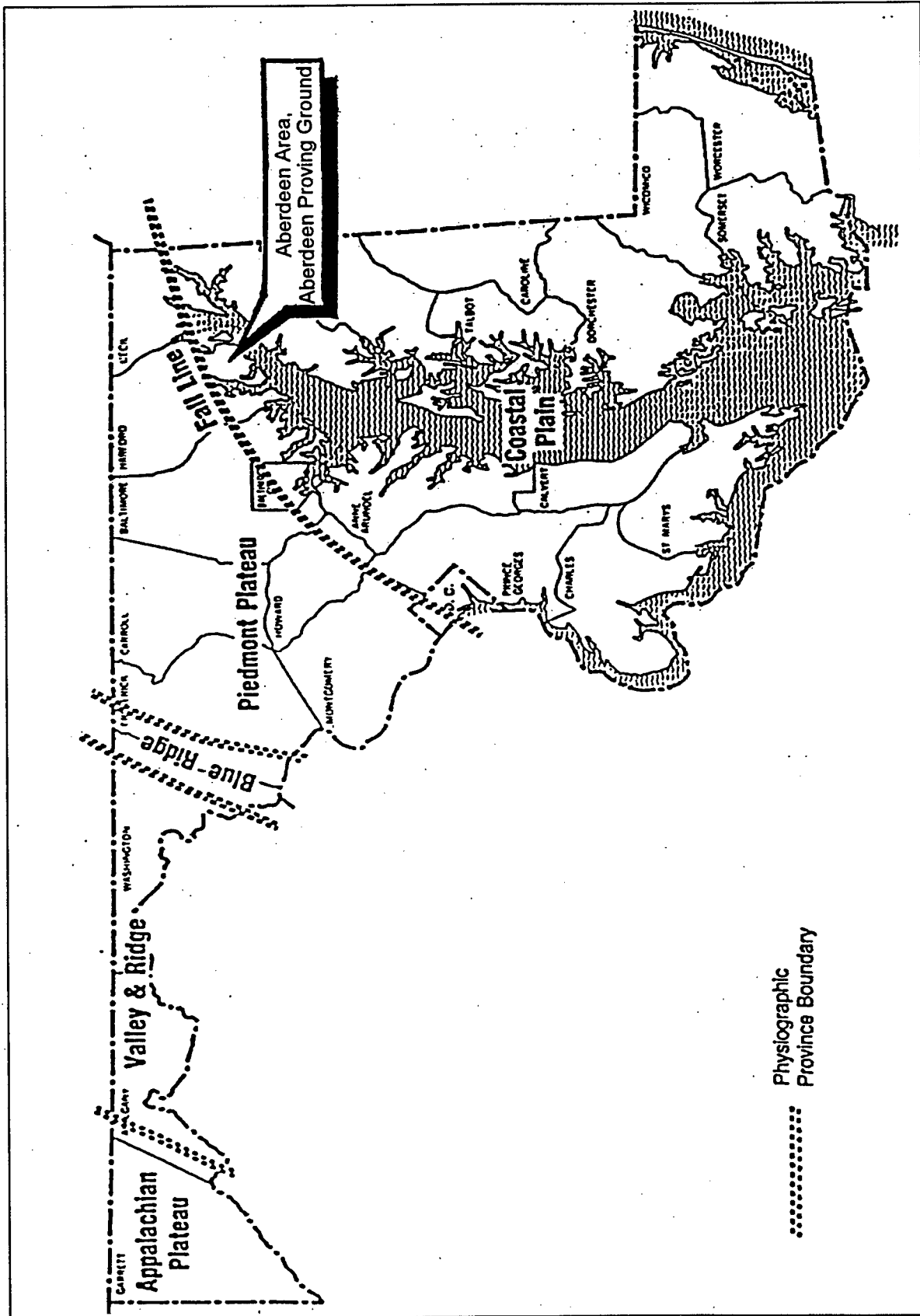


Figure 3. Physiographic provinces in Maryland.

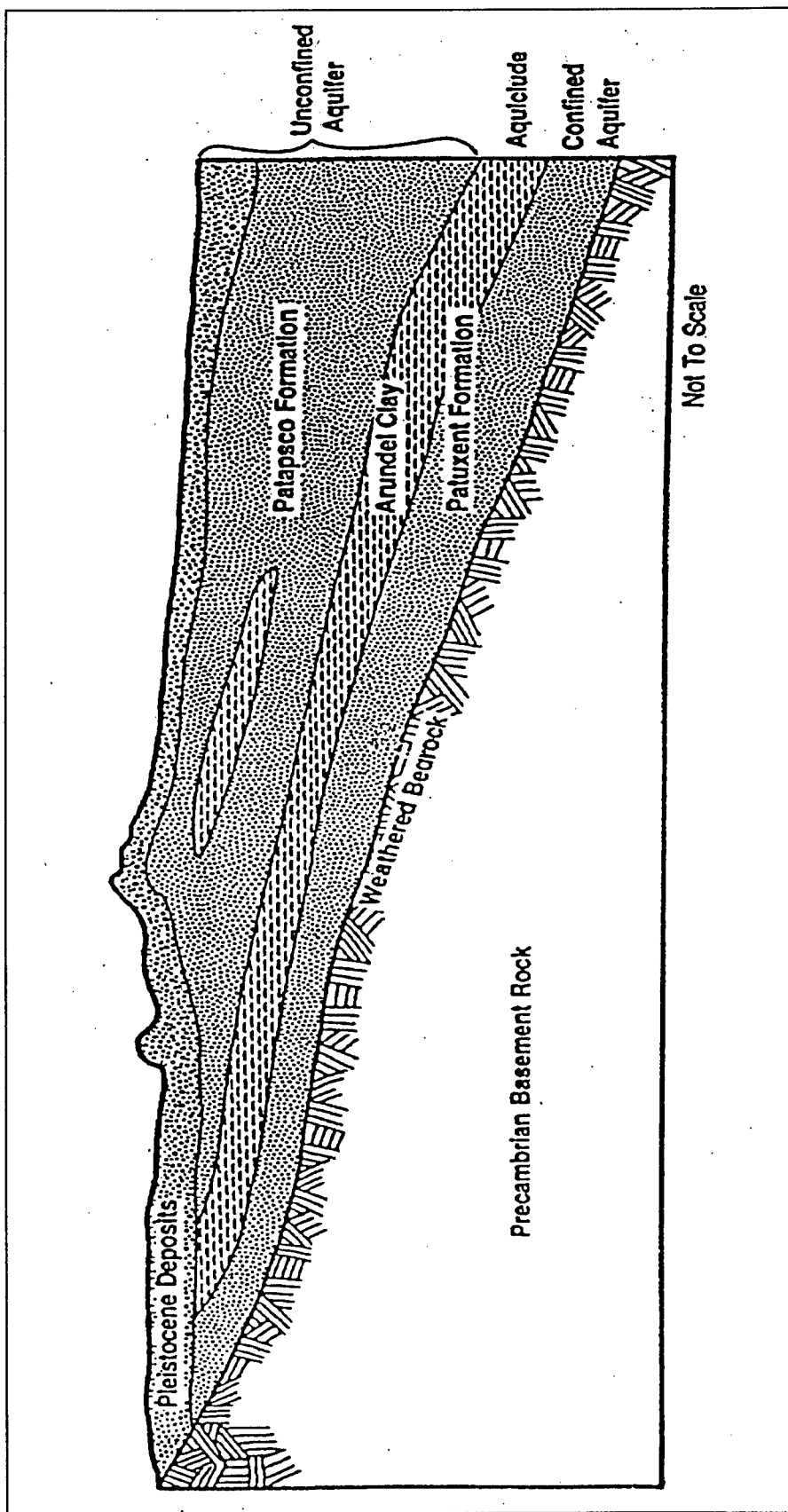


Figure 4. Generalized cross-section of the Coastal Plain sediments

and Table 1. Note that the top of the Precambrian basement rock is a saprolite (rock weathered in place but retaining most of the original rock structure). The thickness of the saprolitic zone is unknown. A more detailed discussion of the individual formations can be found in Whitten et al. (1992) and other references given there.

Geology of the Edgewood Area and Cluster 13

Cluster 13 is situated on a peninsula bordered by two tributaries of Lauderick Creek, as shown in Figures 1 and 2. The cluster is bordered to the northwest by the installation boundary. Elevations vary from 0 at the water edge to approximately 9 m in the northwest portion of the cluster (7.6 m maximum elevation within Site 4). Areas close to the water edge are marshy (shown in green in Figure 2), while the higher elevations of the peninsula are covered by trees (hardwoods) and brush. The ground surface of Site 4 has a thick layer of leaves and roots. The surficial soil is a dark brown loam, likely the surface layer of the Sassafras Soil Series (Corps of Engineers 1994).

The boreholes indicated in Figure 2 as WLC-26 to WLC-43 are shallow (< 15 m) groundwater monitoring wells. Fence diagrams for these wells are shown in Figure 5, where the general stratigraphy, water table, screened interval, and projections between well locations are indicated. A ground water elevation map is shown in Figure 6, although the contours are not well defined by wells in the central part of Site 4.

In addition to the shallow wells at Cluster 13, there are deeper stratigraphic borings in the Lauderick Creek Area (Figure 7). A geologic cross-section between stratigraphic borings LC-1 and TH2 is shown in Figure 8; the stratigraphic information from three of the shallow wells is also shown in the cross-section. The simple color coding in Figure 8 is gold for sands and gravels and maroon for clays. In addition to the lithologic logs for LC-1 and TH2 shown in Figure 8, borehole geophysical logs (natural gamma, self potential, and single point resistivity) exist (Corps of Engineers 1994). The greatest depth of any of the stratigraphic borings is to elevation -76.8 m (-252 ft), which is not deep enough to encounter the basement rocks. The basement crystalline rocks are estimated to lie at depths of approximately 100 m (approximately 328 ft) beneath the northwestern boundary of the Edgewood Area.

Table 1
Generalized Lithology of the Coastal Plain Sediments

System	Series	Group	Formation	Thickness Range (ft)	Lithology (Generalized)	Water-Bearing Properties
Quaternary	Holocene			0 - 30	Clay, silty sand, and gravel	May yield large quantities of water where recharge can be induced from nearby streams
	Pleistocene		Talbot	20 - 30	Fine to medium silty sand with mixtures of fine gravel and lenses of silt and clay	Water table aquifer where composed of coarse grained water-bearing materials as in Aberdeen and Havre de Grace. Yields up to 500 gpm
Cretaceous	Lower Cretaceous	Potomac	Patapsco	60 - 90	Fine to medium sand, silt, and clay	Thin and of limited areal extent. Yields some water to domestic wells in Harford County
			Arundel	40 - 90	Silty clay to clayey silt with lenses of organic silty clay and lignite and ironstone nodules	Not a water-bearing formation except where penetrated by a few wells in outcrop area
			Patuxent	80 - 100	Silty fine to medium sand with minor clay lenses	Source of water for numerous domestic and small commercial ground water supplies along U.S. Highway 40. Thickens rapidly toward southeast and becomes an excellent aquifer yielding up to 1,000 gpm
Precambrian	Glenarm		Wissahickon (undivided)		Saprolite—hard silty clay to clayey silt with some sand lenses	Not a water-bearing formation

Fence Diagram for Shallow Monitoring Wells at Cluster 13

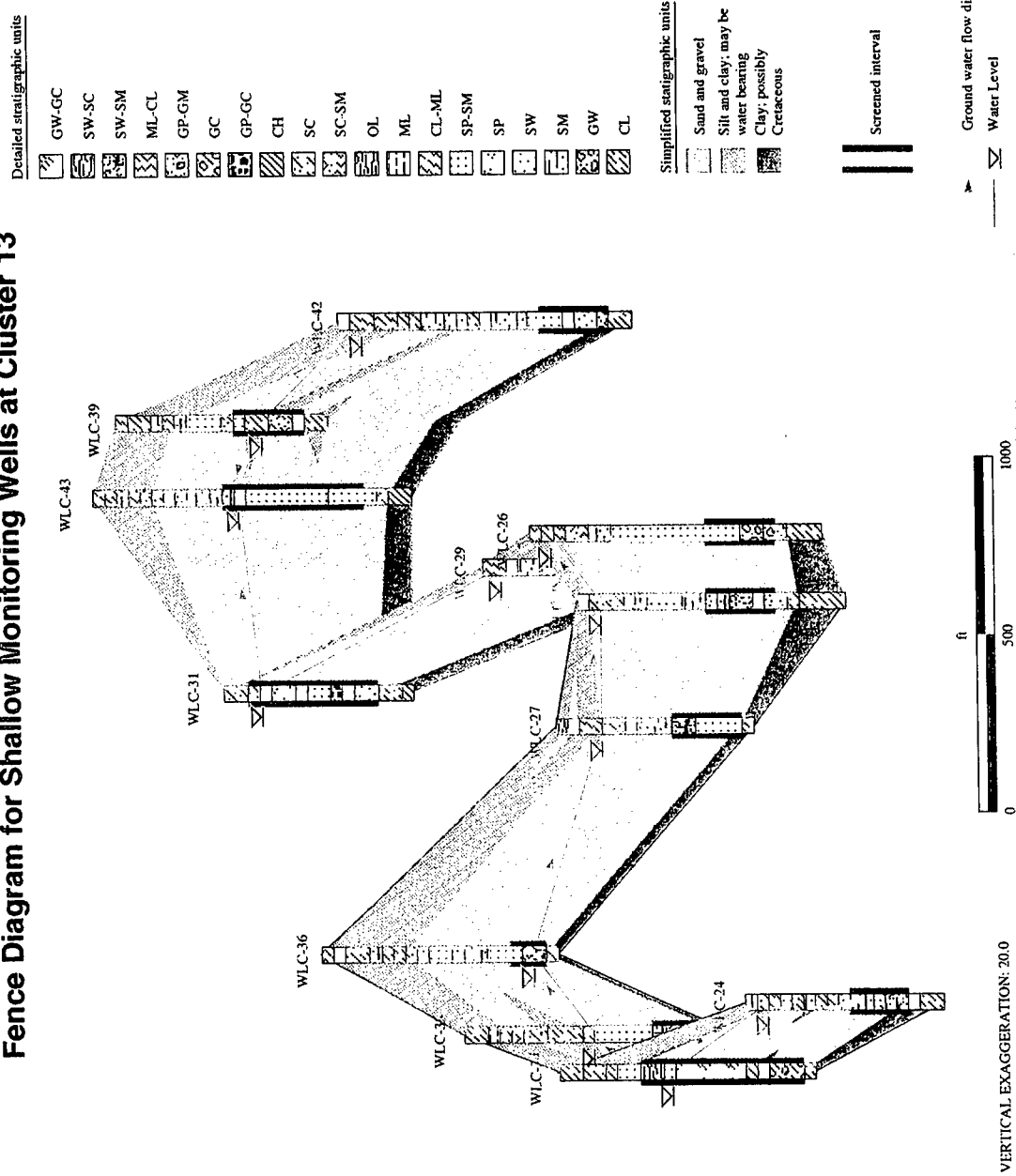


Figure 5. Shallow stratigraphy in the Cluster 13 area (Continued)

Fence Diagram from Shallow Monitoring Wells at Cluster 13

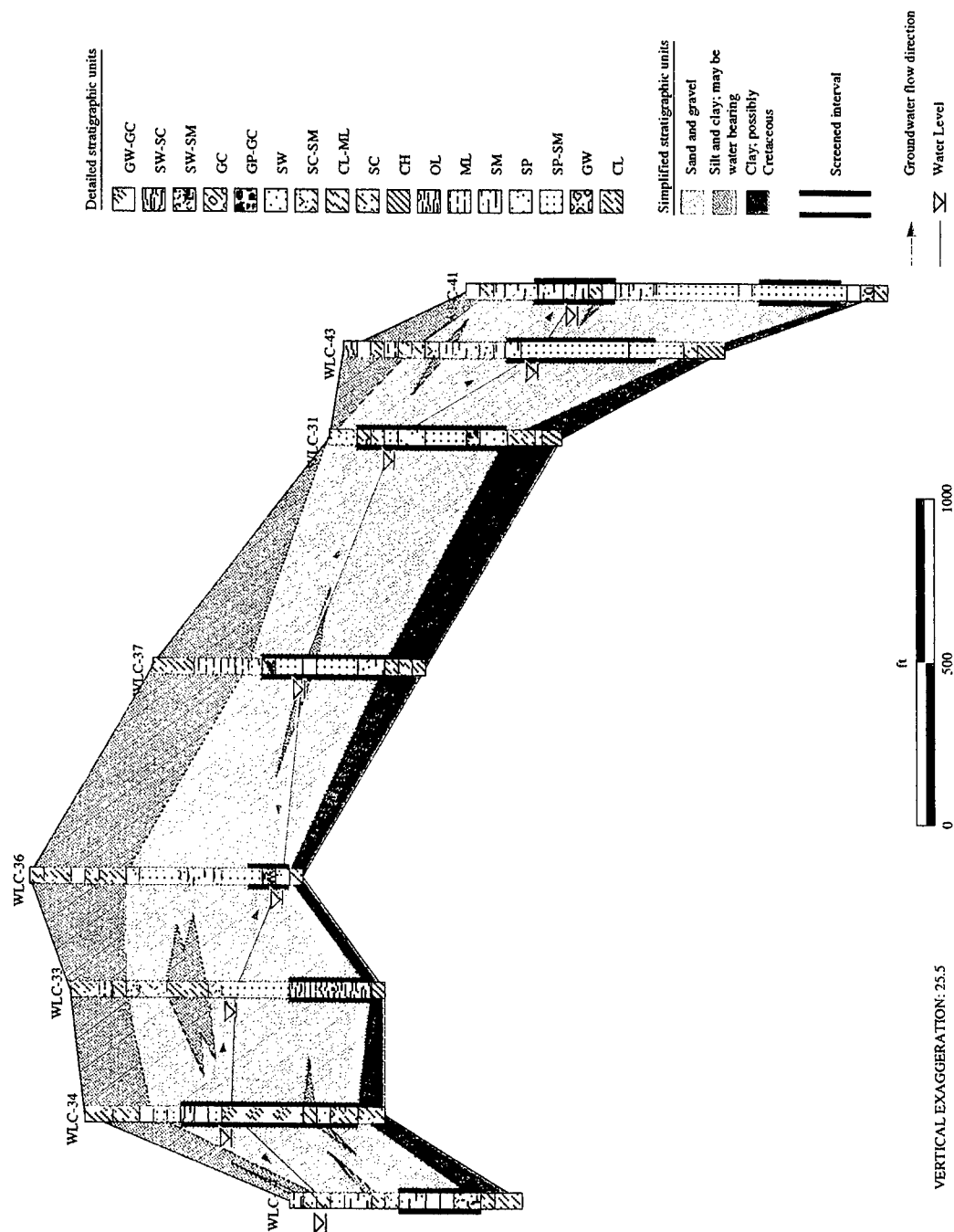


Figure 5. (Concluded)

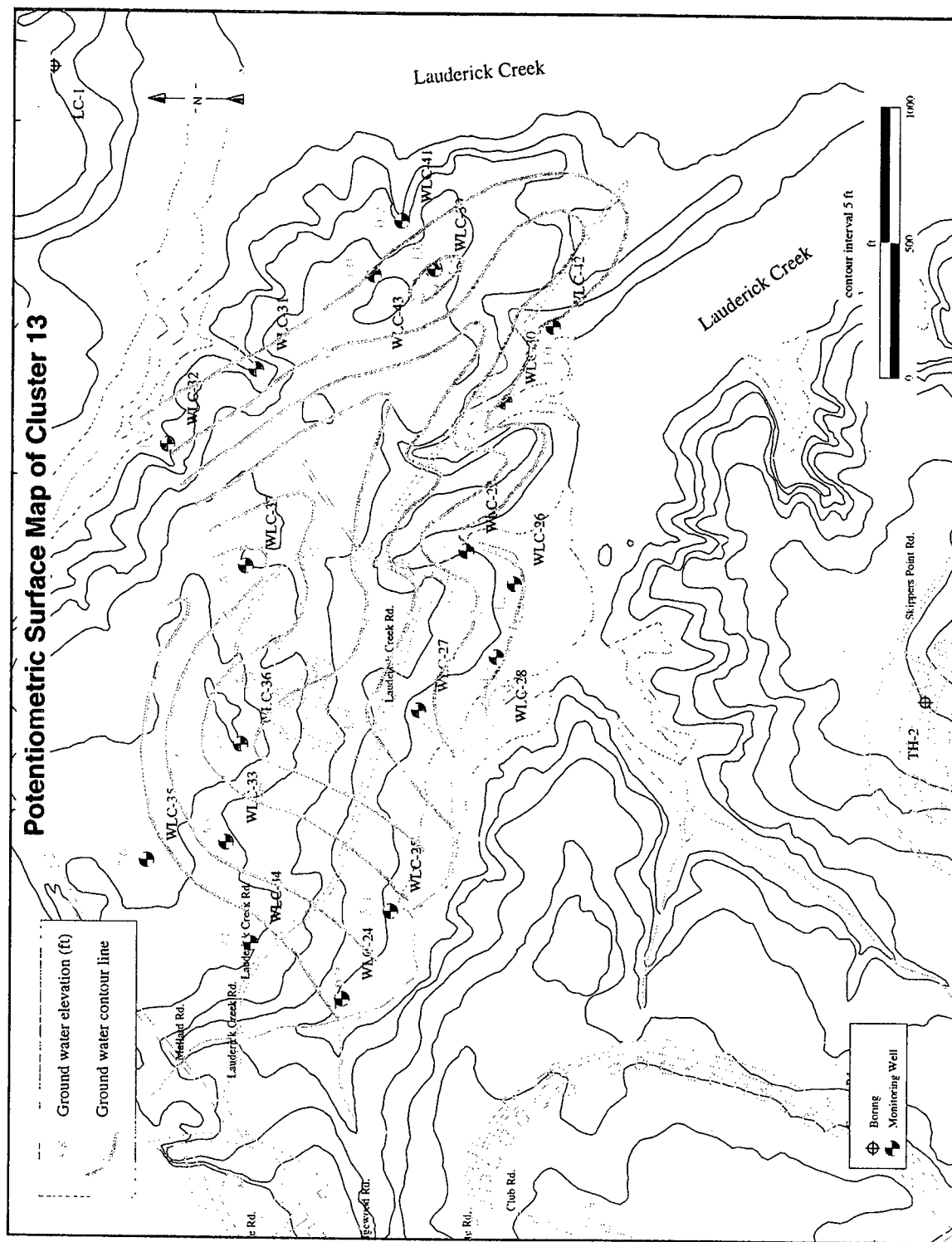


Figure 6. Potentiometric surface map for Cluster 13 area (from shallow monitoring wells)

Figure 8

Geologic Cross Section of the Cluster 13 Area

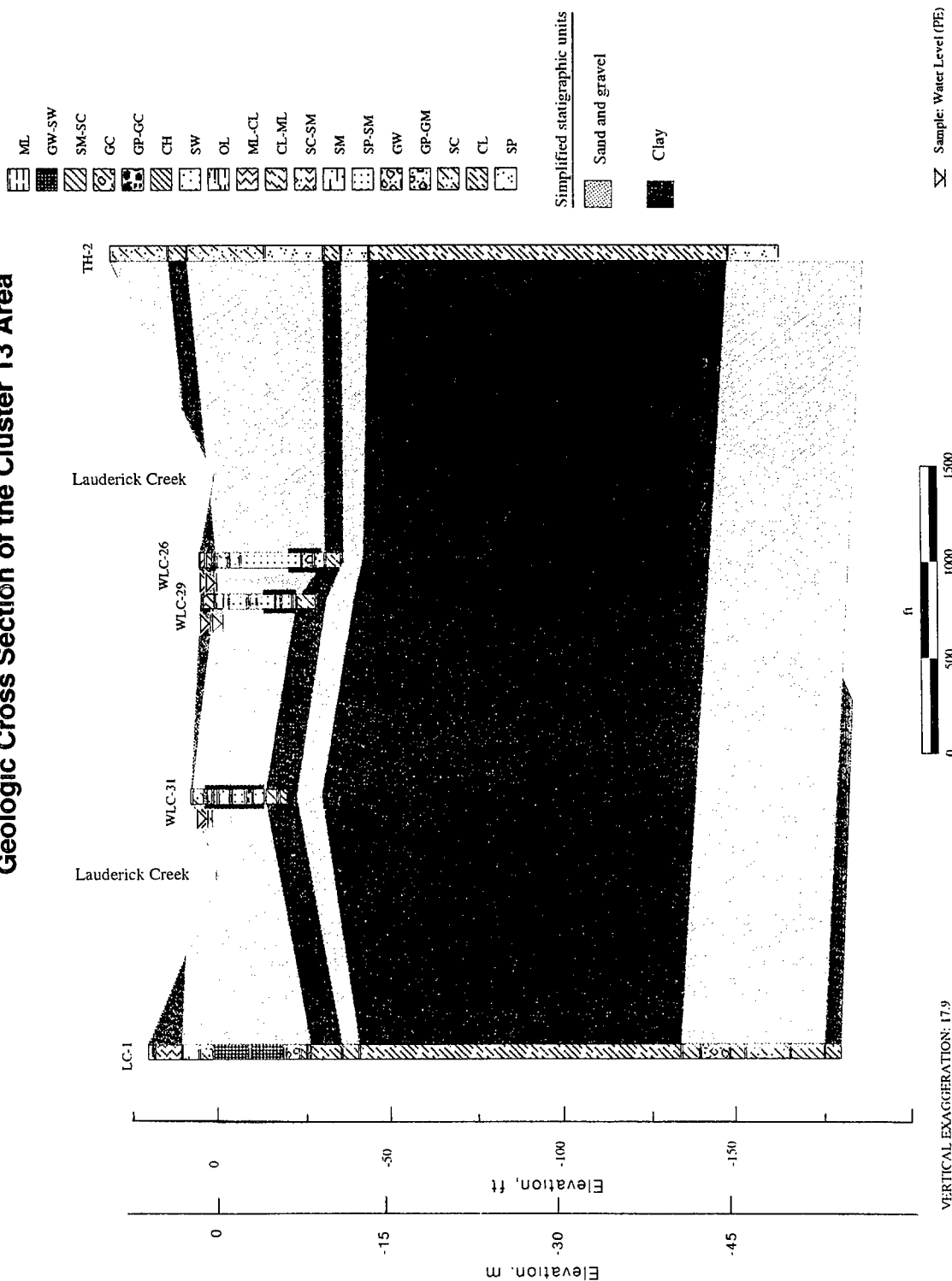


Figure 8. Cross-section between stratigraphic borings LC-1 and TH-2 (approximately NE-SW)

3 Plan of Investigation

Site Survey Grid

A 100×100 ft (approximately 30.5×30.5 m) grid was established at Site 4, as shown in Figure 9. The grid was established with an electronic total station surveying system, using the indicated bench mark (BM 13-2) as a starting reference. Grid points consisted of wooden hubs labeled with the coordinates. This grid served as a reference system for all geophysical field work and for all geophysical results in this report. For example, reference to a grid coordinate such as (1.5, -3.5) indicates a physical location 150 ft East and 350 ft South relative to the (0,0) origin shown in Figure 9. Also indicated in Figure 9 are four reference lines (dashed), along which geophysical cross-sections are constructed. The zero distance reference for the Long Line is from the northwest end, and for Cross Lines 1-3 the zero distance reference is from the southwest ends; selected grid coordinates are included on cross-sections for complete referencing. Coordinates of the intersections of the Long Line with Cross Lines 1-3 are (2.5, 1.5), (6.5, -2.5), and (10.5, -6.5), respectively.

Geophysical Investigation Strategy

The geophysical investigation was planned around three guiding principles: (1) acquisition of complementary geophysical survey data; (2) acquisition of both profile and areal coverage information; (3) integrated interpretation of geophysical and existing geological data. Complementary geophysical methods are those from which different physical properties of subsurface materials can be interpreted or inferred, e.g., density and seismic velocity, seismic velocity and electrical resistivity, and other combinations. Comparison of geophysical properties allows qualitative lithological and hydrogeological characterization. The tabulation below gives a possible, qualitative, hydrogeological interpretation of seismic velocity and electrical resistivity values for geologic materials based on a classification of values into high, intermediate, and low ranges (Butler et al. 1990):

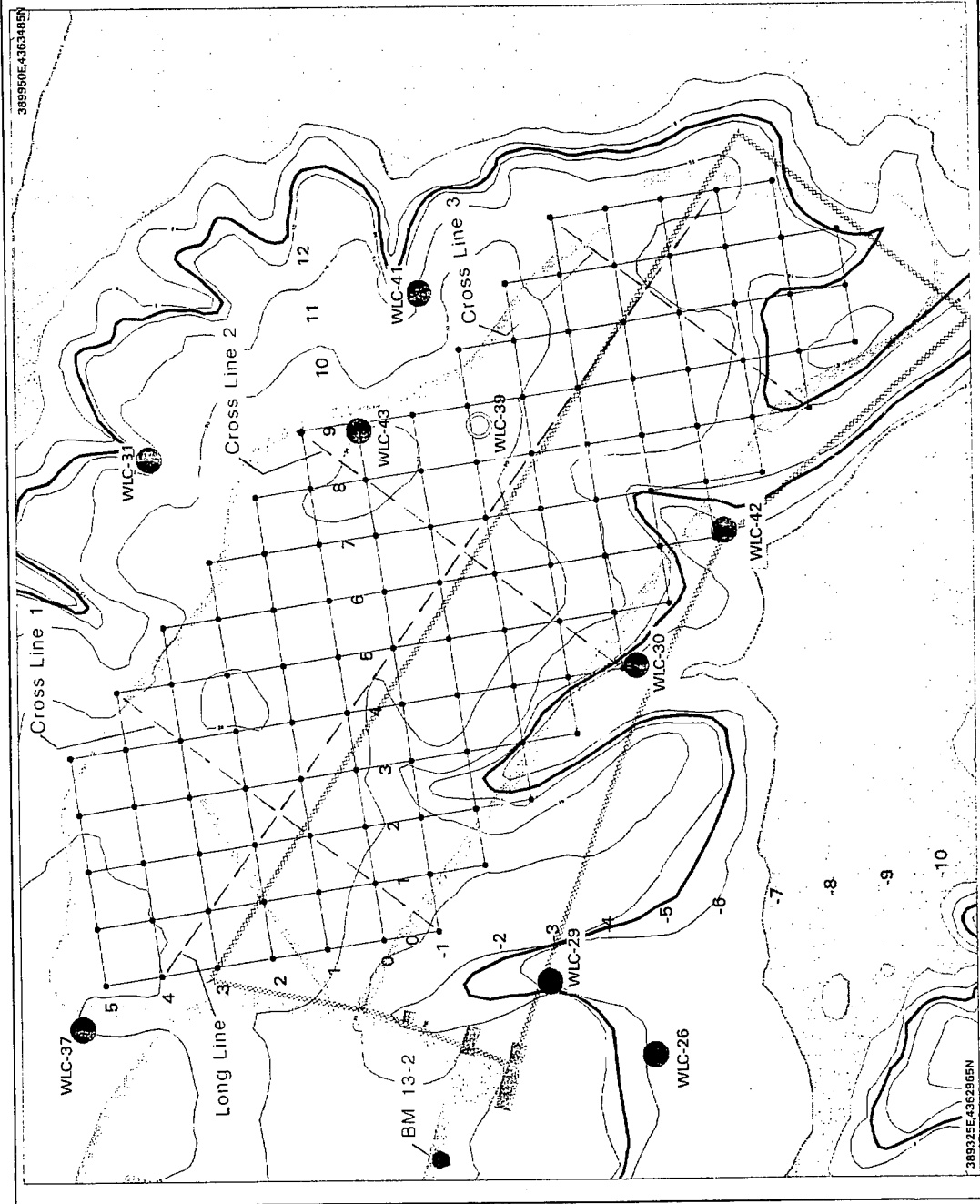


Figure 9. Survey grid for Site 4, Cluster 13, and locations of four survey profile lines

Seismic Velocity (m/s)	Electrical Resistivity (Ohm-m)	Qualitative Hydrogeological Interpretation
High	High	Impermeable rock
High	Intermediate	Rock. Possible aquifer
High	Low	Rock. Possible aquifer; probably brackish
Intermediate	High	Dry unconsolidated sediments at depth; weathered or fractured rock
Intermediate	Intermediate	Possible aquifer in unconsolidated sediments; weathered rock
Intermediate	Low	Clay or brackish water saturated sediments
Low	High	Dry unconsolidated sediments; no clay
Low	Intermediate	Unconsolidated, wet sediments
Low	Low	Wet, clayey sediments
Seismic Velocity -- High (>3,000 m/s); Low (<1,000 m/s)		
Electrical Resistivity -- High (>1000 Ohm-m); Low (<30 Ohm-m)		

An integrated interpretation just refers to the fact that a geophysical investigation should never be conducted independently of other data sources; all available geologic information should be utilized for both planning and interpreting geophysical surveys. The concepts of complementary methods and integrated interpretation are discussed and illustrated in detail by Butler and Llopis (1984), Butler (1986), Butler and Fitterman (1986), and Butler (1994).

Three surface geophysical survey methods were employed: seismic refraction (SR); electrical resistivity (ER); transient electromagnetic method (TEM). The SR and ER methods were employed in a complementary manner along the four cross section lines shown in Figure 9, with surveys conducted at the centers of the 100 × 100 ft grid cells along the lines (the survey procedures and physical concepts are described in the next section). This procedure resulted in surveys every 140 ft along the lines. The SR and ER surveys were planned to provide detailed subsurface mapping information to depths of approximately 50 ft (~ 15 m) along the cross-section lines. At the intersection points of the lines, both SR and ER surveys were conducted for each line (i.e., at right angles to each other), which will give an indication of the effects and significance of lateral heterogeneity.

TEM surveys were conducted at each grid cell (the survey procedure and physical concepts are described in the next section). Thus the entire area of Site 4 was covered by TEM surveys with a spacing of 100 ft, and in the process TEM data was acquired along the cross section lines for comparison and integration with the SR and ER data. The TEM surveys were planned to provide moderately detailed subsurface mapping information to depths of 200-300 ft (~ 60-90 m) or greater.

Borehole geophysical surveys were conducted in 26 of the monitoring wells at Cluster 13. The methods included electrical conductivity and natural

gamma surveying (logging) as a function of depth. All wells were logged to the maximum accessible depths in the wells, ranging from a minimum of 13 ft (4 m) to a maximum of 45 ft (13.7 m). The geophysical logs from all the wells will add to and complement the background database for Cluster 13. Also, wells WLC-30, WLC-37, WLC-39, WLC-42, and WLC-43 are very close to or within the Site 4 survey grid and are relevant for integrating with and comparing to the surface geophysical survey results.

Basic Physical Concepts and Survey Procedures

Seismic refraction (SR) method

For the seismic methods, energy is input to the earth by an impulsive or explosive source. The energy travels in the form of compressive, shear and surface waves that are detected at the surface by sensors called geophones. Geophones are arranged in linear arrays (or *spreads*) in line with the energy source. Typically 12 or 24 geophones are connected to the recording seismograph. The energy travels directly to the geophones through the near surface material and is also reflected and refracted from interfaces between subsurface geologic materials with contrasting physical properties. The SR method makes use of the direct and refracted waves to determine the seismic velocities of geologic "layers" and depths to interfaces. The compressive waves typically utilized in seismic refraction surveying are always the first arriving energy. Plotting the arrival times of the waves versus the distance of the geophones from the energy source (time-distance plot) results in data points that can be connected by a series of intersecting best-fitting straight lines. The slopes of the straight lines yield the velocities of successively deeper layers of soil and rock, and an analysis of the arrival times at the individual geophones relative to the best-fitting lines yields depths to interfaces between different materials beneath the geophones.

The seismic velocities can be considered a fundamental physical property of geologic materials, depending on depth, degree of induration, mineralogy, porosity, etc., and ultimately on bulk density, compressibility and rigidity. In unconsolidated sedimentary materials, the compression wave (P-wave) seismic velocity will increase dramatically at the water table (100 percent saturation), and the seismic velocity will generally be higher in clays than in unsaturated sands and gravels. An example of a time-distance plot and the interpreted seismic cross sections are given in the next chapter, while further details of the SR method, seismic velocities, and interpretation procedures can be found in standard and specialized references, e.g., Redpath (1973), Scott (1973), Butler et al. (1982), Butler and Llopis (1984), and Telford et al. (1990).

The SR surveys were conducted along the four cross section lines shown in Figure 9. Spreads of 24 geophones, spaced 10 ft (3.05 m) apart, were oriented along the diagonals of each grid cell along the cross section lines. The energy source for the surveys was a sledge hammer impact on a surface

metal plate. Source locations were offset 10-ft from each end and at the center (or between geophones 12 and 13) of the geophone spreads. The centers of the 24-geophone spreads and also the central source location were at the centers of each grid cell. Total distance from the offset shot points and the farthest geophone was 240 ft (~ 73 m). Since the distance between grid cell centers was only 140 ft (approximately), there was considerable overlap in the surface coverage of adjacent geophone spreads. A rule-of-thumb is that the spread length should be 4-5 times the desired depth of investigation; thus the desired depth of investigation of 50 ft should be achieved with the SR surveys.

Electrical resistivity (ER) method

The surface ER methods involve the use of four metal electrodes that are driven into the ground to make electrical contact. Current (I) is injected through two of the electrodes, and a potential difference (ΔV) is measured with the remaining two electrodes. The current penetrates the earth to depths dependent on the current electrode spacing and the geoelectric structure of the subsurface. A quantity known as the *apparent resistivity* is then calculated according to the following relation:

$$\rho_a = K (\Delta V / I) \quad (1)$$

where K is a geometric factor defined by the arrangement and spacings of the four electrodes. Electrical resistivity is a fundamental physical property of geologic materials that depends on porosity, pore fluid and saturation, mineralogy, degree of induration and other factors. The electrical resistivity of clays will generally be considerably less than for sands, gravels, and carbonates. Also, the electrical resistivity of saturated and even partially-saturated materials in the subsurface will be less than the same materials in an unsaturated state.

For a very thick surface layer relative to the electrode spacings, the apparent resistivity equals the true resistivity of the material; and for a very thin surface layer relative to the electrode spacings overlying a thick layer, the apparent resistivity will approximately equal the true resistivity of the underlying layer. However, for the general case of layers of arbitrary thickness relative to the electrode spacings, the apparent resistivity will be a complex volume weighted average of the true resistivities of the subsurface layers. By systematically varying the electrode spacings from small to large values, electrical resistivity data can be collected that enables the determination (interpretation) of true electrical resistivity as a function of depth. A plot of apparent resistivity versus current electrode spacing is known as the sounding curve. From the sounding curve, an estimate or initial model of the subsurface can be obtained. The minimum number of layers required to explain the sounding curve is determined by inspection of characteristic features (e.g., minima, maxima and points of inflection) of the sounding curve. Estimates of layer thicknesses and resistivities are determined by examination of the asymptotic

behavior of the sounding curve. True layer resistivities and layer thicknesses are determined from the VES data and the initial model by a process known as inversion, where the data are inverted to find a layered model of the subsurface that best reproduces or explains the data, i.e., the sounding curve (Butler et al. 1982; Simms and Butler 1992; Interpex 1988). The layered model is assumed to apply beneath the center point of the electrode array. An example of a ER sounding curve and its interpretation is given in the next section.

The ER surveys were conducted along the four cross section lines shown in Figure 9. A collinear electrode arrangement or array known as the Schlumberger array was used for all the surveys. The array is expanded symmetrically about the center point of each grid cell along the cross sections lines to obtain vertical electrical sounding (VES) data. A multiconductor sounding cable, switching box, and resistivity meter were used to acquire the data (Simms and Butler 1992). The depth of investigation of the ER VES survey is a function of the maximum spacing between the current electrodes. Maximum current electrode spacings for the surveys ranged from 200 to 300 ft (61 to 91.4 m). A rule-of-thumb is that the maximum spacing between the current electrodes should be 4-5 times the desired depth of investigation; thus the desired depth of 50 ft should be achieved for the ER surveys. The ER VES data are fitted to four, five or six-layer models.

Transient electromagnetic (TEM) method

The TEM method determines the electrical resistivity of the subsurface as a function of depth by the process of electromagnetic induction. A transmitter loop, which is generally laid on the surface, although ground contact is not required, is energized by an electrical current that is turned off very rapidly. The changing magnetic field caused by the turn off of the current induces electrical currents in subsurface materials by electromagnetic induction. The subsurface currents generate secondary magnetic fields that are detected as an induced voltage by a surface receiver loop. Initially, the induced currents are concentrated beneath the transmitter loop; however, with time, the currents diffuse to greater depths and lateral distances from the transmitter loop. The magnitude of the induced current at any depth is directly related to the conductivity ($= 1/\text{resistivity}$) of the geologic material. The measured quantity at the receiver loop is voltage as a function of time after transmitter turn off. A quantity called the late-stage apparent resistivity can be computed from the receiver loop voltage at any time. A plot of the apparent resistivity versus time then constitutes a TEM sounding curve, where early times correspond to shallow depths and later times correspond to greater depths (Butler and Fitterman 1986). The TEM sounding data are inverted to give a subsurface model consisting of layer resistivities and thickness, similar to the results of ER interpretation. A typical TEM sounding data set and its interpretation is given in the next section, and greater detail regarding the physical concepts, field procedures, and interpretation procedures is given by Butler and Fitterman (1986).

TEM soundings were conducted at each cell of the survey grid. The transmitter loop was 100×100 ft (30.5×30.5 m) and was "laid out" using the survey stakes as a form. The receiver was always placed outside the transmitter loop, 80 ft (24.4 m) from the center or 30 ft from the nearest side of the transmitter loop. Interpreted subsurface models are assumed to apply beneath the centers of the grid cells. The shallowest, reliably detectable interface depth will likely be in the range 15-50 ft, depending primarily on the first layer resistivity and time of first measurement after transmitter shut off. Depth of investigation will likewise depend on the subsurface resistivities and the greatest measurement time for which the signal exceeds the noise level, but should be 200-300 ft or greater. The TEM sounding data are fitted to four or five layer models.

Borehole geophysical logging methods

The electrical conductivity logging method measures the conductivity of a volume of material surrounding the borehole as a function of depth. Similar to the TEM method, the conductivity is determined as a result of electromagnetic induction processes, with an electromagnetic transmitter and receiver separated by 1.3 ft (0.5 m) in the borehole. Unlike the TEM method, the borehole conductivity logging system operates at a constant frequency (39.2 kHz). The system is calibrated to read directly in conductivity units (mS/m); and, in the absence of lateral and vertical conductivity variations within the volume of influence of the system, the measurement will be the true conductivity of the surrounding material. For all cases involving lateral and vertical conductivity variations, the measured conductivity will be a volume averaged or apparent conductivity. The system averages the conductivity of material from a zone approximately 0.7 - 3.3 ft (0.2 - 1.0 m) from the borehole, and is most sensitive to material located approximately 1.0 ft (0.3 m) from the borehole. In the vertical direction, the effects of an interface between two different materials will be averaged or "smeared" over a vertical distance of approximately 3 ft (1 m), since the effects of the material on either side of the interface will be "sensed" prior to reaching the interface and after the interface is passed. The location of the interface can still be accurately located as the point of steepest slope of the response curve. Thin layers of material will be detected by the system, but the true conductivity of the thin layer will not be indicated due to effects of the surrounding material on the measurements within the thin layer. Taylor et al. (1989) review the above concepts and further details of the conductivity logging system.

Natural gamma logging involves measuring the natural rate of emission of gamma radiation by geologic materials surrounding the borehole. In shallow sedimentary materials, uncontaminated by artificial radioisotopes, the common gamma-emitting isotopes are potassium-40 and daughter products of the uranium and thorium decay series. Through various processes, these natural radioisotopes become concentrated in clays (hence shales) and clay-rich sediments; thus clays and other clay-rich sediments (i.e., fine-grained detrital sediments) tend to be more radioactive than quartz-rich sands and gravels and carbonates. Although there are exceptions and a knowledge of local geology

is invaluable, soils and rocks can generally be classified by their level of gamma activity. In the shallow sedimentary section, gamma logging provides a valuable tool for qualitative lithological characterization and stratigraphic correlation between boreholes.

Conductivity and natural gamma measurements were acquired approximately every 0.33 ft (0.1 m) in the boreholes and are plotted side-by-side as a function of depth for each borehole. The side-by-side plots facilitate qualitative lithological identification, since clays and clay-rich sediments will generally have both high electrical conductivity (low resistivity) and high gamma count rate, while quartz-rich sands and gravels will have lower conductivity and low gamma count rate.

4 Results of the Investigation

Seismic Refraction Analysis

Data: Procedures and time-distance plots

The seismic data were examined as acquired in the field for quality and preliminary, qualitative assessment of seismic velocities and interface depths and then stored on floppy disks for subsequent analysis. The first step in the data analysis consists of picking the first arrival times for all the seismic records. Then plots of first arrival times versus distance from the source points (time-distance plot) are examined and each data point is assigned a number. The data point number assignments refer to the interpretation of the data point as belonging to a direct arriving event (= 1) or to a refracted arrival event (= 2, 3, 4,). A direct arriving event (= 1) travels from the source directly to the geophones through layer 1. The first refracted event (= 2) travels down to, along, and up from the interface between layers 1 and 2. The second refracted event (= 3) similarly travels down to, along, and up from the interface between layers 2 and 3.

A typical time-distance plot is shown in Figure 10 for the Long Line refraction spread *centered* at (2.5, 1.5) or 405 ft from the beginning of the Long Line, which is also the location of the intersection of Cross Line 1 with the Long Line. The refraction spread extends from 280 ft to 530 ft, with source points indicated by A, B, and C at 280, 405, and 530 ft. Locations of the 24 geophones are indicated along the bottom axis. The arrival times at the geophones are obtained from the vertical axis in milliseconds (msec). The data are interpreted to represent a direct and two refraction events, i.e., three layers.

Time-distance plots of the data for all seismic refraction surveys conducted at Cluster 13 are contained in Appendix A, in the order Long Line, Cross Line 1, Cross Line 2, and Cross Line 3.

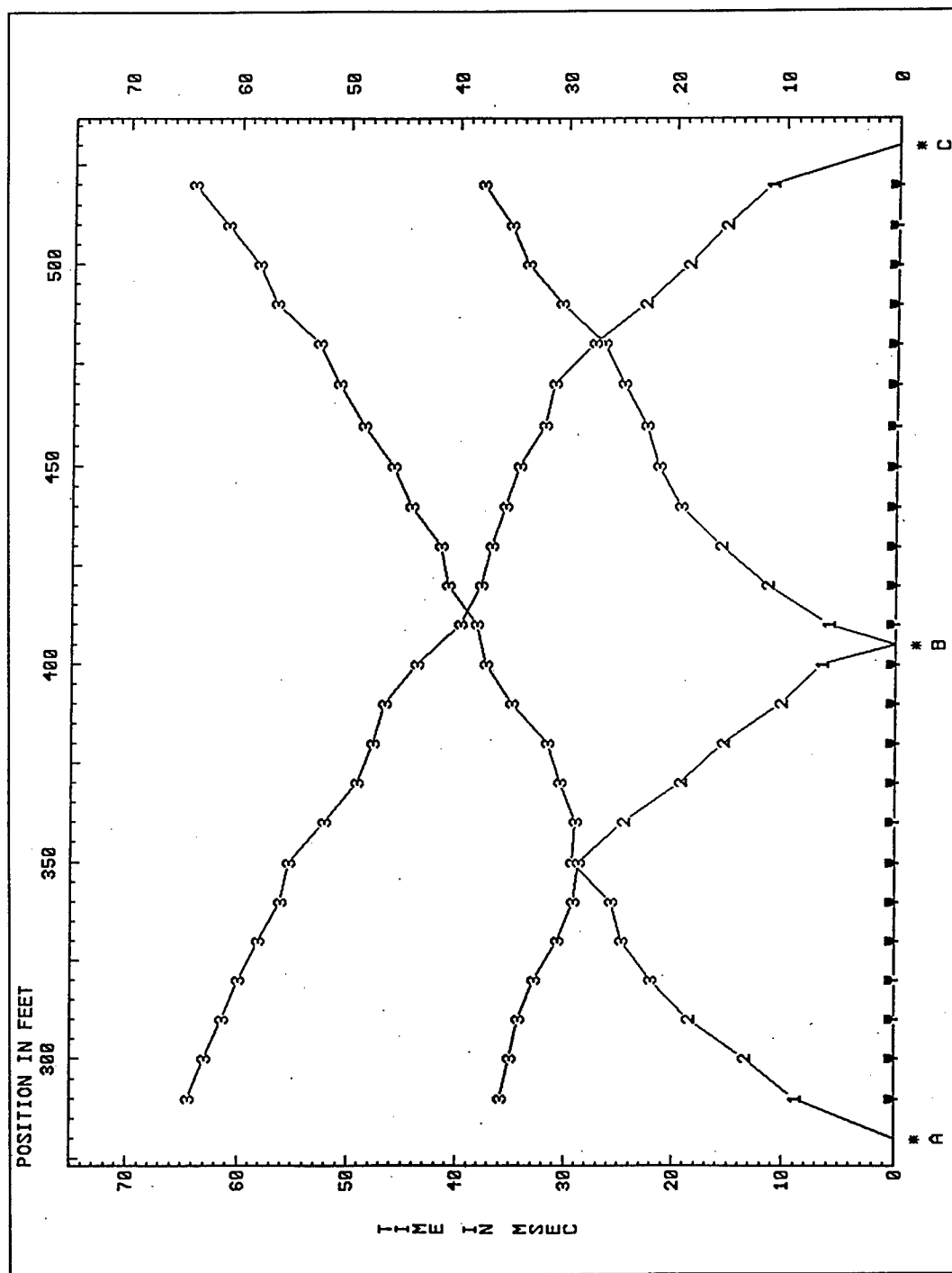


Figure 10. Typical seismic refraction time-distance plot, for refraction spread centered at (2.5, 1.5) or 405 ft (123.4 m) from beginning of line, showing assignments of layer number to each arrival

Interpretation: Procedures and cross-sections

The next step in the analysis of seismic refraction survey data is to develop a model of the subsurface from the time-distance data. The model consists of layers (velocity-stratigraphic units; Butler and Curro 1981) characterized by their seismic velocities and thicknesses. If the subsurface actually consists of discrete layers of geologic material separated by planar interfaces, the time distance plot will consist of data defining a straight line for each layer with slope equal to the inverse of the seismic velocity. For example, the data in Figure 10 are interpreted to represent three layers, where the third layer is thick relative to the length of the seismic geophone spread.

The data from Figure 10, Long Line survey (2.5, 1.5), are shown again in Figure 11, where straight lines have been fit to the time-distance data. The data deviate from the straight lines due to several factors: possible arrival time "picking" errors (typically ± 1 msec or less); ground surface elevation changes; seismic velocity heterogeneity; variations in interface elevations (i.e., interface topography). An approximation to the subsurface model can be obtained by using the traditional intercept time interpretation method to produce a planar interface model (Butler et al. 1982; Telford et al. 1990; Burger 1992), such as shown to the right of the time-distance plot in Figure 11, where the layer velocities are shown in feet/second and the interface depths are shown in feet at each end of the interfaces in the model. The intercept time interpretation procedure was used for a preliminary analysis of the data and for comparison with the electrical resistivity results.

A more detailed interpretation analysis is used for the final analysis of the seismic refraction data, where depths beneath each geophone are determined. The analysis procedure uses the delay time method of Pakiser and Black (1957) to obtain a first approximation depth model and then uses iterative ray tracing and model adjustment to minimize errors between the model-predicted arrival times and the actual data (Scott 1973). Computer program SIP (Rimrock Geophysics 1995) performs the analysis and produces a cross section model from the interpreted layer-arrival events (e.g., Figure 10). The interpreted cross section corresponding to the time-distance plot and event layer assignments in Figure 10 is shown in Figure 12. Velocities of the three layers are given in the Legend to the right of the cross section. The velocities are averages for the layers that include the results of the central source point (B) for the spread as well as the results of the adjacent spreads. The two interfaces are highly irregular. The dashed straight lines are the planar model interfaces from the intercept time interpretation model in Figure 11, shown for comparison with the irregular interface interpretation.

While the cross section in Figure 12 corresponds in physical location with the time-distance data in Figure 10, the interpretation procedures used by SIP considers all the data from the overlapping, adjacent geophone spreads. Thus the cross sections corresponding to any geophone spread will match with cross sections from adjacent spreads at all common or overlapped surface locations. SIP processes up to five spreads together to produce a continuous cross section. Cross sections from adjacent groups of five spreads along a survey line,

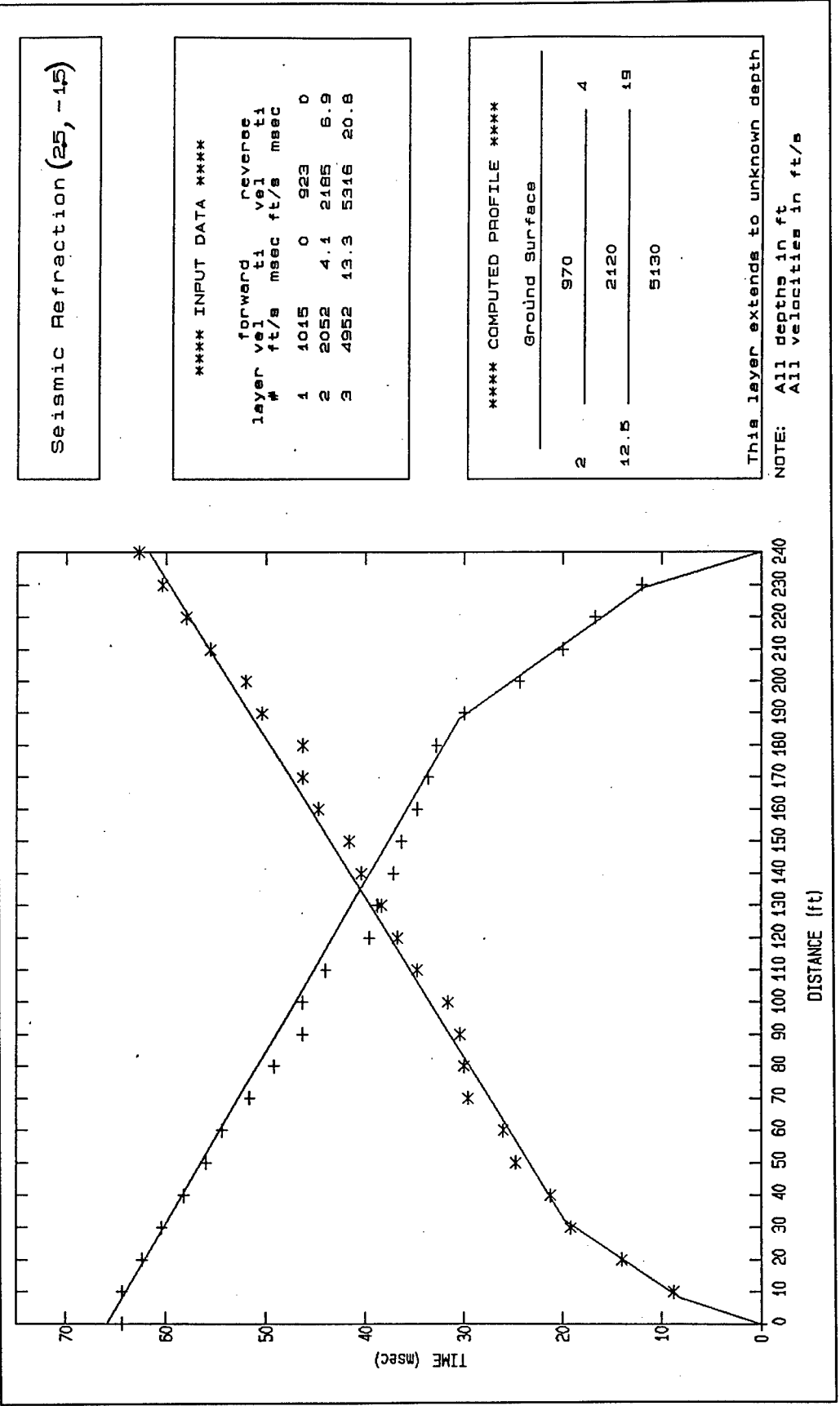


Figure 11. Typical seismic refraction time-distance plot (left), for refraction spread centered at (2.5, 1.5) or 405 ft (123.4 m) from beginning of line, showing straight lines through arrivals from each layer and a model (right) from a traditional intercept time interpretation

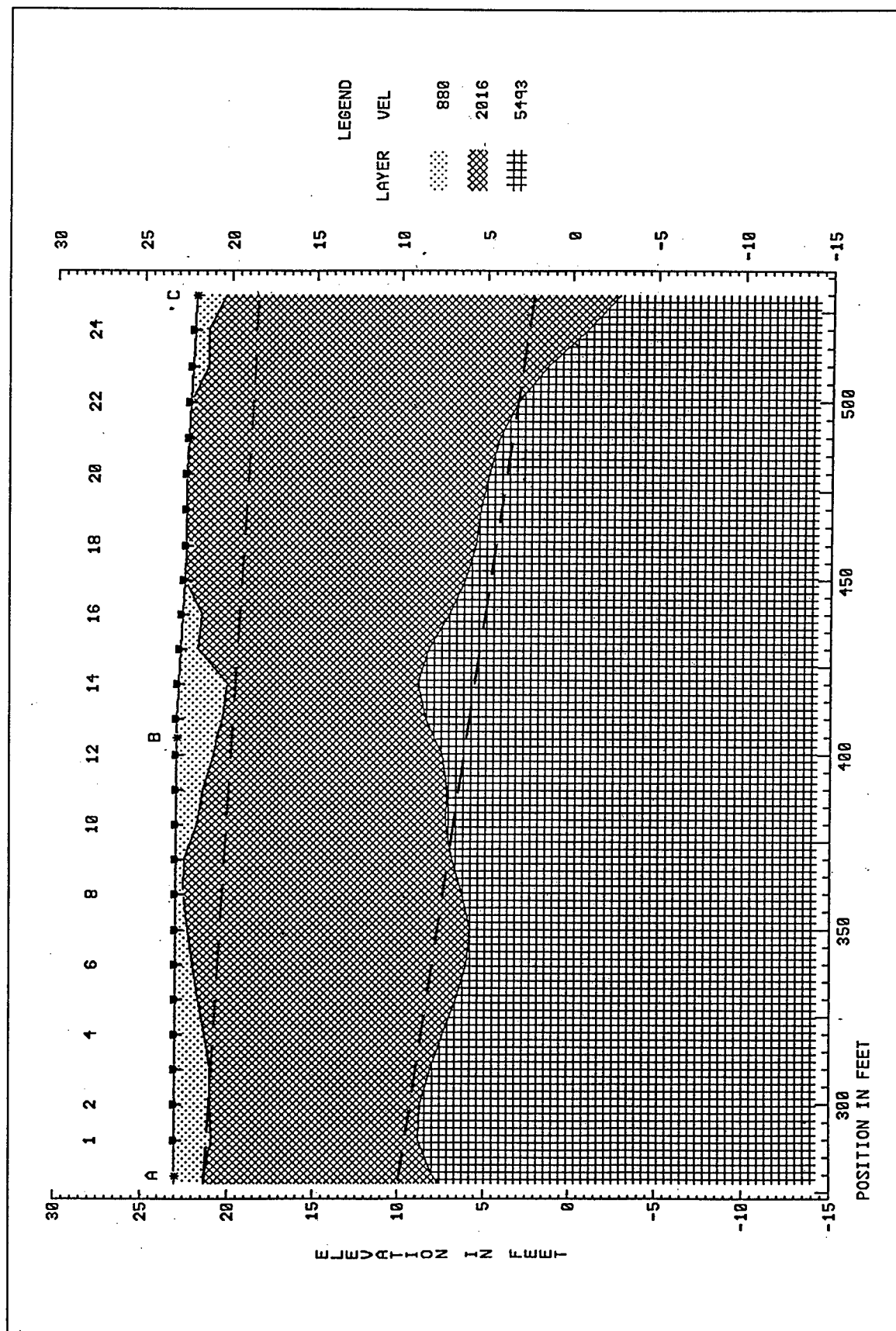


Figure 12. Velocity-stratigraphic cross section for long line seismic refraction survey (2.5, 1.5); dashed lines are the planar interface model

such as the Long Line, are not constrained to match. Individual cross section plots, such as Figure 12, for all the seismic refraction spreads are presented in Appendix A in groups of five (or less) immediately following the corresponding time-distance plots.

Interpretation: Seismic velocity cross sections and assessment

The individual cross section plots for the Long Line and Cross Line 1 are matched and joined in groups up to five to produce the composite cross sections shown in Figures 13 and 14, respectively. The cross sections are all three layer models of the subsurface (including Cross Lines 2 and 3), with a relatively small range of average, interpreted P-wave velocities for each layer:

Layer	P-Wave Velocity Range, ft/s (m/s)
1	775 - 880 (236 - 268)
2	1,670 - 2,015 (509 - 614)
3	5,240 - 5,815 (1,597 - 1,772)

Locations where the Cross Lines intersect the Long Line are indicated in Figure 13, while the intersection of the Long Line with Cross Line 1 is indicated in Figure 14. A good indication of the quality of the overall survey and the interpretation procedure is given by the differences in the subsurface model at survey line intersection points. The following tabulation summarizes the comparison of the cross sections at the intersection points:

	Intersection of Long Line with		
	Cross Line 1	Cross Line 2	Cross Line 3
Maximum Interface Depth Difference (ft)	<2	<5	<2
Velocity Difference, Layer 1 (percent)	6	4	1
Velocity Difference, Layer 2 (percent)	10	0	14
Velocity Difference, Layer 3 (percent)	5	2	2

A typically accepted rule of thumb accuracy for seismic refraction depth determinations is ± 10 percent of the depth; the maximum interface depth differences at the intersection points are within this accuracy. The average velocity difference is approximately 5 percent. The two larger velocity differences for Layer 2 may be caused by lateral heterogeneity; however, there is no consistent directional trend difference for any of the layer velocities, i.e., no definitive evidence for horizontal velocity anisotropy.

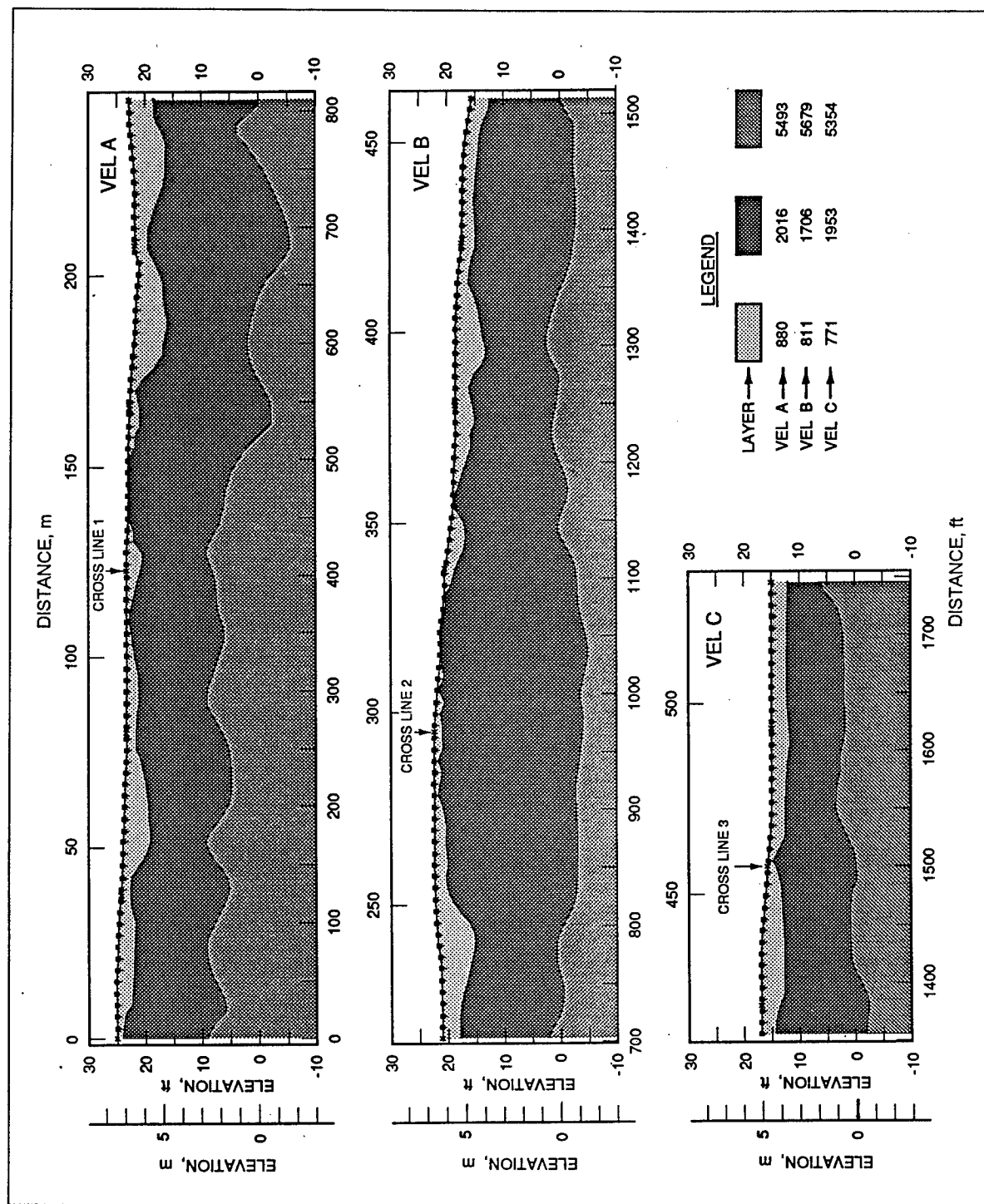


Figure 13. Long line seismic velocity stratigraphic cross section, showing three mappable velocity units

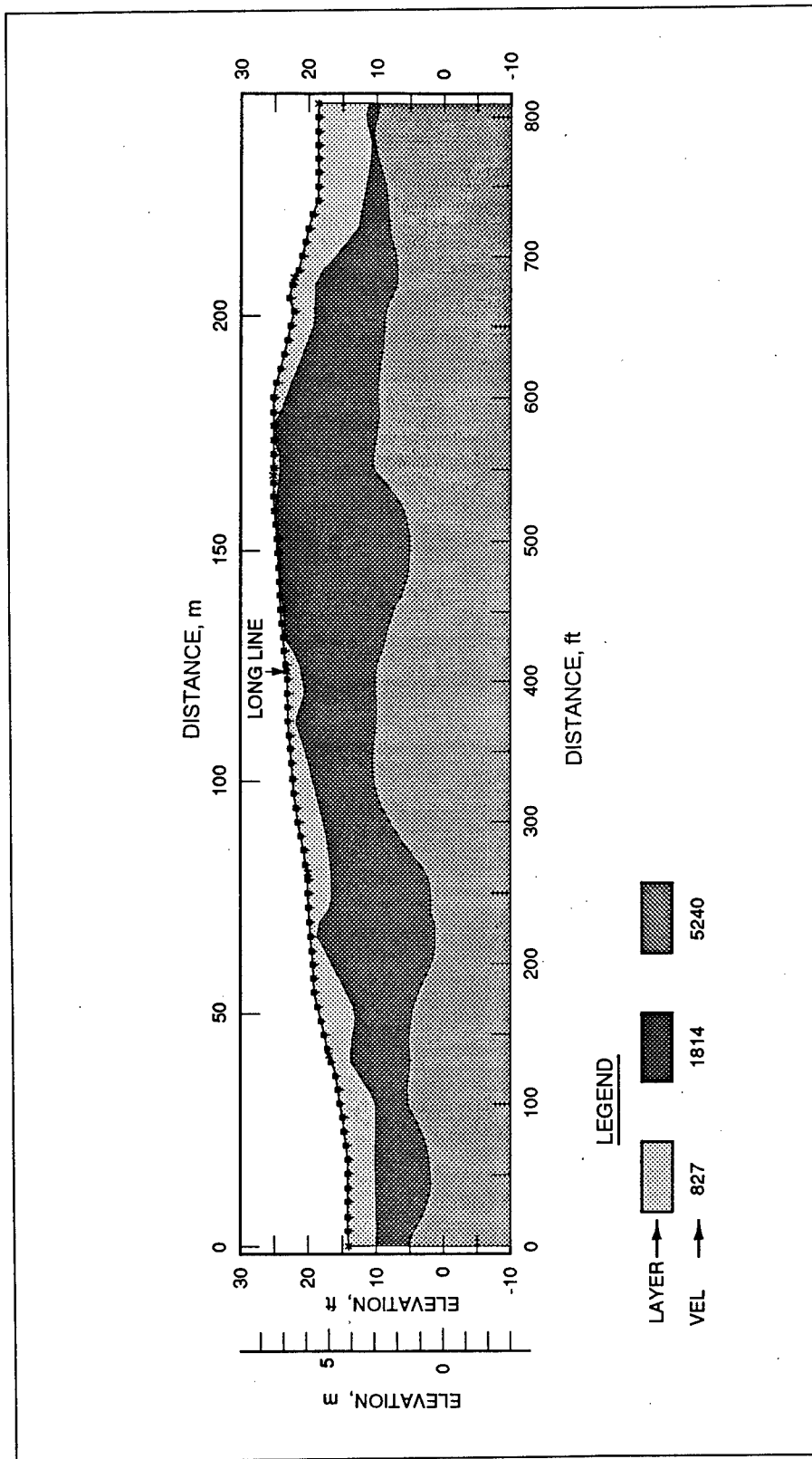


Figure 14. Cross line 1 seismic velocity stratigraphic cross section, showing three mappable velocity units

Certain qualitative assessments regarding the nature and/or state of the materials forming the three layers can be deduced from the seismic velocities and layer geometries, without consideration of the complementary geophysical, geologic, and hydrogeologic data for the site. The P-wave velocity of *Layer 1* is so low that the material must be *very loose with high porosity*; consistent with the observed thick layer of organic materials and the very loose nature observed when driving electrode rods during the ER surveys. The *Layer 2* P-wave velocity is consistent with a wide range of *unconsolidated, unsaturated* sediment types, from sands and gravels to sandy clays. A number of possibilities are suggested by the P-wave velocity of *Layer 3*, e.g., saturated materials (i.e., the interface is the water table), weathered rock or other low density, weak rock, or a massive clay. The velocity value, the contrast in velocity between *Layers 2* and *3*, and geometry considerations suggest that *Layer 3* materials are *saturated* and that the *Layer 2 - Layer 3* interface is the *water table*. Elevation of the interface varies from +7 ft to -5 ft, with a mean close to 0 ft or approximately mean sea level, as expected since the site is essentially a peninsula into the Chesapeake Bay.

From Figure 13, *Layer 1* along the Long Line cross section (along the long dimension of the peninsula) is seen to be typically 2-3 ft thick, varying from 1 ft or less to as much as 6 ft thick. Along the Cross Line 1 cross section (perpendicular to the long dimension of the peninsula), Figure 14, *Layer 1* varies in thickness from 1 ft or less in the central portion (425-575 ft) to 4-8 ft at each end of the cross section. *Layer 2*, along the Long Line cross section in Figure 13, varies in thickness from 10-15 ft near the ends of the line to 20-25 ft in the central portion (800-1,100 ft). Along the Cross Line 1 cross section, *Layer 2* is 20 ft thick in the central portion (425-575) and dramatically thins to 1-4 ft thick near the ends.

Electrical Resistivity Analysis

Data: Procedures and apparent resistivity plots

The electrical resistivity data were converted to apparent resistivity values ρ_a using the geometric factor K for the Schlumberger array

$$K = \pi s [(L/s)^2 - 1/4] \quad (2)$$

where s is the spacing between the two potential electrodes (commonly referred to as M and N ; $s = MN$, where MN is the distance between M and N) and L is the spacing between the sounding point (center point) and the current electrodes (commonly referred to as A and B ; $L = AB/2$). Field sounding plots were made of the apparent resistivity versus L for quality control. If a data point appeared to deviate from defining a smooth sounding curve, additional readings were acquired and the multiple values were averaged to produce a single value for each electrode spacing; this procedure was simplified

since the data were acquired using the multiconductor sounding cable and electrode switching box.

The Long Line VES data for location (2.5, 1.5) are shown in Figure 15 (squares). This location corresponds to that for the seismic refraction example shown in Figure 10 and is the location of the intersection of the Long Line with Cross Line 1. VES plots for all the electrical resistivity surveys conducted at Cluster 13 are contained in Appendix B, in the order Long Line, Cross Line 1, Cross Line 2, and Cross Line 3. Site physical constraints prevented acquiring sounding data at all the cross line locations, resulting in only three soundings for Cross Line 2 and two soundings for Cross Line 3. Instrumentation problems prevented completion of data acquisition for Cross Line 1; only one sounding was conducted.

Interpretation: Procedures and best-fit models

VES interpretation procedures were described in Chapter 3. The results of the interpretation of the VES dataset for Long Line location (2.5, 1.5) are shown in Figure 15, where the best-fit five-layer model is shown in the plot to the right of the sounding plot. The theoretical sounding curve corresponding to the best-fit model is shown as the solid line in the sounding plot. The best-fit theoretical sounding curve has the appearance of a best-fit line through the data points. True resistivity and thickness values for the best-fit model and a comparison of the theoretical apparent resistivities (labeled "Synthetic") versus measured values for the case in Figure 15 are given in Figure 16. The information in Figure 16 also shows that the average fitting error is 0.962 percent; this represents a very good fit of the theoretical sounding curve to the measured sounding data. Due to noise and lateral heterogeneity effects on the data, fitting errors for many of the VES data sets are in the range 2-5 percent. Some of the VES datasets which could not be modeled in detail (i.e., larger fitting errors), were evidently affected by lateral heterogeneities. Best-fit model information sheets for each of the VES datasets, such as Figure 16, are included in Appendix B.

Interpretation: Electrical resistivity cross-section and assessment

Unlike the seismic refraction interpretation procedure which produces a continuous cross-section, the VES interpretation procedure is a one-dimensional (1-D) process (beneath the center of the electrode array). The resistivity cross-section must be constructed by examining the individual 1-D interpretations (e.g., the model in Figures 15 and 16) placed side-by-side and drawing inferences about the two-dimensional (2-D, i.e., the cross-section) distribution of resistivities. Generally the interpreted cross-section is constructed by grouping similar resistivity values and utilizing "geological reasonableness" and any knowledge about the stratigraphy of the site. The 1-D interpretation cannot totally account for the effects of lateral heterogeneity

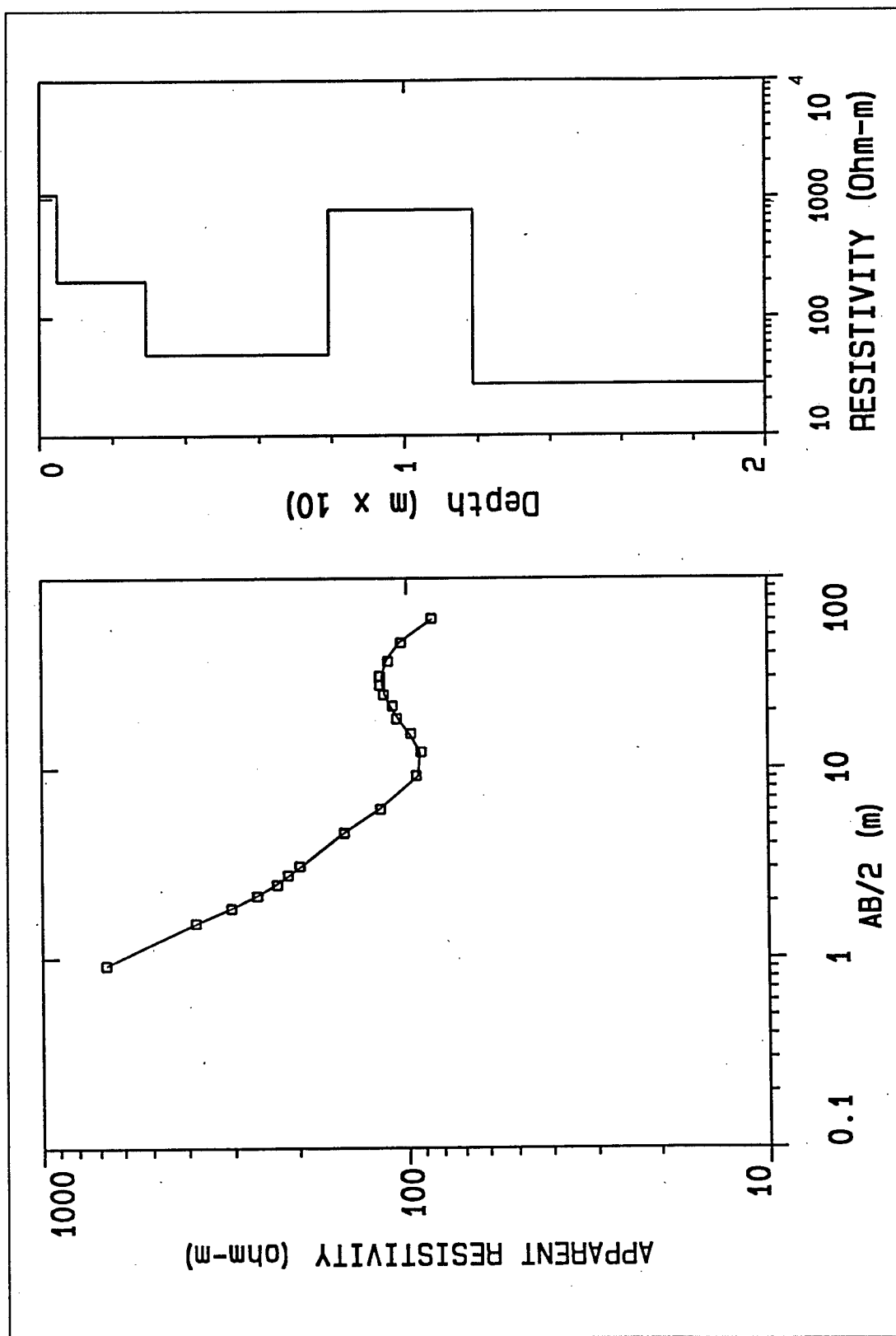


Figure 15. Typical electrical resistivity sounding data and best fitting model for location (2.5, 1.5)

CLIENT: Aberdeen Proving Ground
LOCATION: Cluster 13
COUNTY:
PROJECT:
ELEVATION: 6.95
SOUNDING COORDINATES: X: 2.5000 Y: 1.5000

DATE: Nov 1994
SOUNDING: 3
AZIMUTH:
EQUIPMENT:

Schlumberger Configuration

FITTING ERROR: 0.962 PERCENT

L #	RESISTIVITY (ohm-m)	THICKNESS (meters)	ELEVATION (meters)	LONG. COND. (Siemens)	TRANS. RES. (Ohm-m ²)
			6.95		
1	1082.5	0.485	6.46	4.482E-04	525.1
2	201.9	2.43	4.02	0.0120	492.1
3	48.40	4.99	-0.968	0.103	241.8
4	796.1	3.95	-4.92	0.00497	3147.7
5	27.16				

ALL PARAMETERS ARE FREE

No.	SPACING (m)	RHO-A (ohm-m)		DIFFERENCE (percent)
		DATA	SYNTHETIC	
1	0.914	670.5	671.5	-0.149
2	1.52	381.0	378.8	0.575
3	1.82	304.7	305.2	-0.153
4	2.13	259.0	259.9	-0.344
5	2.43	228.6	231.1	-1.09
6	2.74	213.3	211.4	0.886
7	3.04	198.1	196.7	0.672
8	4.57	149.3	149.7	-0.277
9	6.09	118.8	119.6	-0.633
10	9.14	94.48	93.32	1.23
11	12.19	91.44	92.10	-0.728
12	15.24	97.53	98.63	-1.12
13	18.28	106.6	105.7	0.828
14	21.33	109.7	111.4	-1.53
15	24.38	115.8	115.0	0.660
16	27.43	118.8	116.8	1.66
17	30.48	118.8	117.1	1.42
18	36.57	112.7	114.2	-1.34
19	45.72	103.6	104.7	-1.10
20	60.96	85.34	84.89	0.526

Figure 16. Parameters of best-fit model (Figure 15) and comparison of measured data with best-fit model values (Synthetic) for resistivity sounding at location (2.5, 1.5)

under or to either side of the electrode array, particularly heterogeneities smaller than the spacing between VES locations.

In the presence of lateral heterogeneities, the cross-section construction can be complicated. The resistivity cross-section along the Long Line is shown in Figure 17. Dashed and "wavy" lines indicate interpreted geoelectrical facies, i.e., a grouping of interpreted electrical resistivities into areas or zones of similar values. The cross-section displays considerable vertical and lateral variations; some of the "facies" groupings include a large range of resistivity values. Figure 18 is a color-coded version of Figure 17, where materials that are interpreted to be similar in nature based on resistivity ranges and geologic reasonableness are colored the same.

The shallow section at the site is known to consist of clays, silts, sands, gravels, and mixed sediments of varying percentages of these constituents; the percentage of clay in the mixed sediments is a major controlling factor on resistivity. In addition, the water content of the sediments varies from some residual value near the surface to 100 percent below the water table. The resistivity of ground water from the shallow monitoring wells at Cluster 13 range from 17 to 250 ohm-m with a mean of approximately 50 ohm-m. The bulk resistivity ρ_{bulk} of saturated clean (no clays) sands and gravels will be controlled by the pore water resistivity ρ_{pw} , and can be estimated by a simplified form of Archie's Law (Butler and Llopis 1984)

$$\rho_{bulk} \sim \rho_{pw} \phi^{-2} \quad (3)$$

A porosity range of 20 to 50 percent should encompass most clean sands and gravels. For this range of porosity and for the stated range and mean of pore water resistivity, the bulk resistivity of the in situ sands, gravels, and mixtures can be approximated as follows.

Pore Water Resistivity (ohm-m)		Bulk Resistivity (ohm-m) Porosity	
		20 percent	50 percent
Low	17	425	68
Mean	50	1,250	200
High	250	6,250	1,000

The presence of clays in the saturated mixtures of sediments will lower the bulk resistivities, since the clays are conductive.

The color coding in Figure 18 is qualitatively interpreted below in terms of likely material type, based solely on the resistivity ranges and general knowledge about site geology:

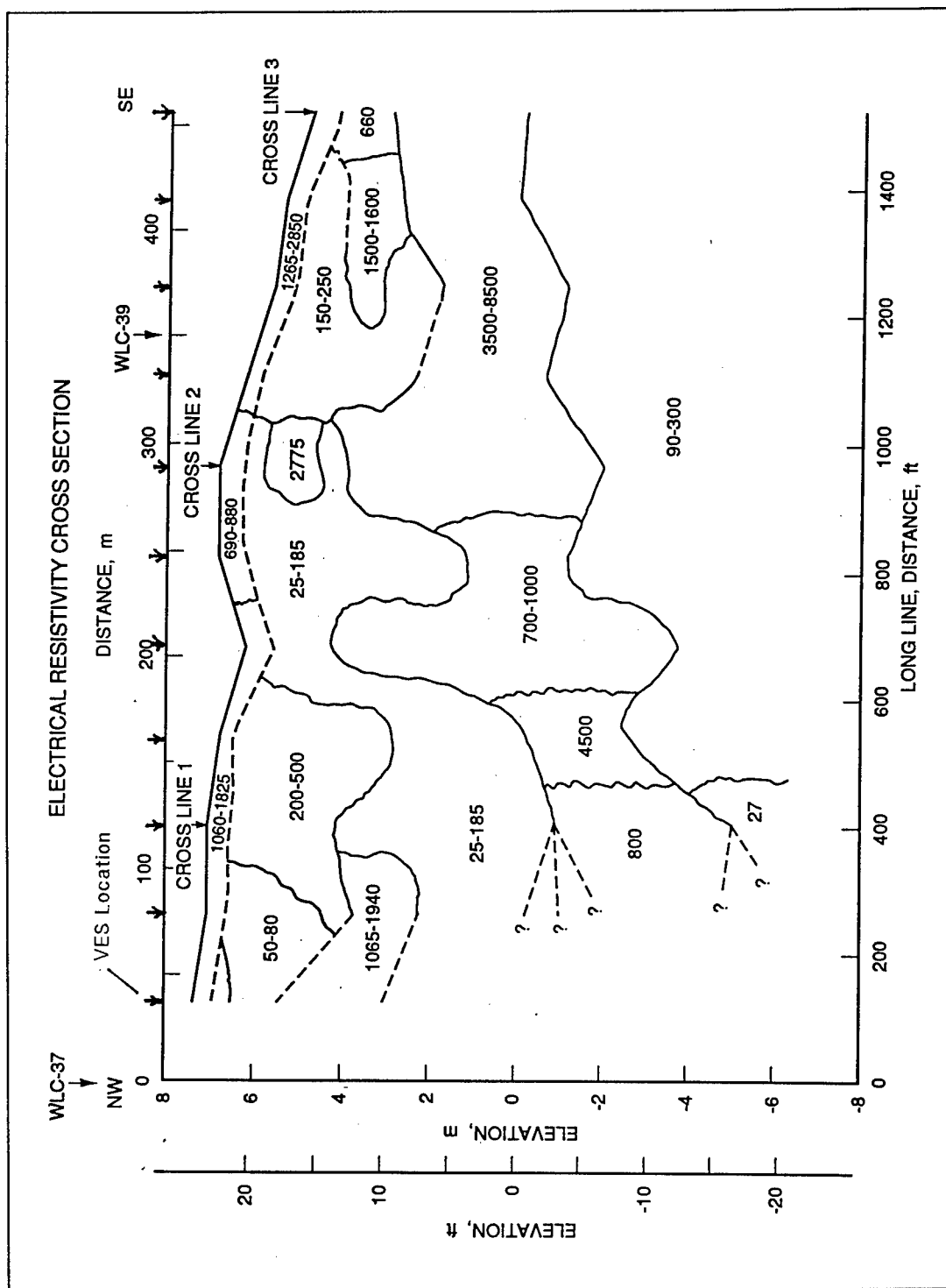


Figure 17. Electrical resistivity cross section along long line, showing resistivity ranges in ohm-m

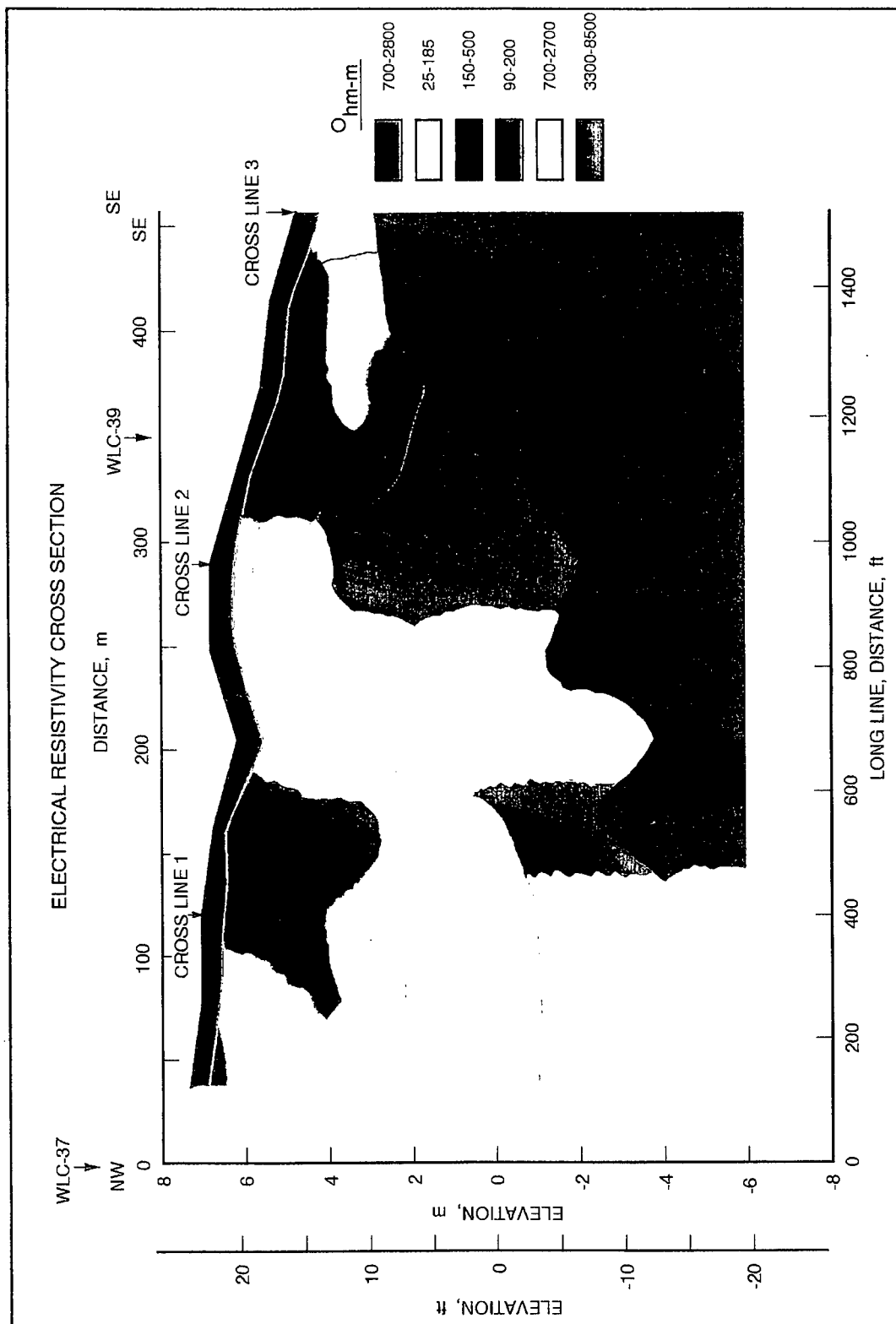


Figure 18. Color-coded version of the electrical resistivity cross section shown in Figure 17, emphasizing the interpreted resistivity "facies"

Green	—	organic surface layer, with sand and clay, very high air content, dry to moist
Brown	—	clayey, silty sand, dry to moist
Gray	—	clay; sandy, silty clay; moist to saturated
Yellow	—	sands; maybe some gravels and small percentage of silts and clays; moist
Orange	—	clean silty, sandy gravels, dry
Blue	—	clayey, silty, sands and gravels, saturated

Many of the boundaries in Figures 17 and 18 are subjective and poorly defined.

In spite of the lateral heterogeneity evident in the resistivity cross-section, some continuities across the section are notable:

- a. A high-resistivity layer, varying in thickness from approximately 0.4 to 0.6 m, extends across the section; this layer is interpreted to be the high porosity organic layer (mat of leaves, roots, and decaying trees) observed at the site.
- b. A zone or layer of high to very high resistivity material (yellow and orange in Figure 18), varying in thickness from 2 to 4 m or greater, extends across the section from less than 1 m depth (elevation approximately 4 m or 13 ft) at the SE end of the section to 8 m depth (elevation approximately -1 m or -3 ft) at the NW end of the section.
- c. A zone of low to intermediate resistivities (blue in Figure 18) extends approximately two-thirds of the distance across the section from the SE end to approximately the 500 ft (150 m) position. The top of the zone is at elevation 0 at the SE end.

The gray-colored areas in Figure 18 are interpreted to be clays or sandy, silty clays; the permeabilities of these areas are likely low enough to serve as barriers to groundwater flow.

Transient Electromagnetic Analysis

Data: TEM procedures and sounding curves

A total of 92 TEM soundings were conducted. The data were acquired in the form of receiver voltage in millivolts as a function of time, and a plot of voltage versus time forms the TEM sounding curve. Each sounding curve is

an average or stack of seven sounding datasets obtained at each location. However, before interpretation, the TEM voltages are converted to apparent resistivities using procedures described in detail in Butler and Fitterman (1986) and McNeill (1980). The TEM sounding plot becomes apparent resistivity versus time, where the time axis corresponds to the electrode spacing axis of an electrical resistivity sounding plot. The TEM sounding data are interpreted using a numerical inversion computer program (Interpex 1993) and procedure similar to the method used for inverting electrical resistivity data.

Interpretation: Procedures and best-fit models

The TEM apparent resistivity versus time data for sounding APG59 is shown in Figure 19. Sounding designation APG59 refers to the numerical order in which the soundings were acquired in the field; sounding numbers are indicated on a grid map in Figure 20. Thus APG59 refers to sounding number 59, which is located at (4.5, -1.5). The location is indicated in the lower part of Figure 19 as "Sounding Coordinates: E: 450.0 N: -150.0." Similarly to the case of resistivity interpretation, the squares in the sounding plot (left plot) are the TEM data. The best-fit 5-layer model is shown in the right plot, while the theoretical sounding curve for the model is shown in the sounding plot and appears as a best-fitting curve to the data. Also shown in the lower part of Figure 19 are the fitting error and the model layer resistivities and thicknesses. Note that the shallowest interface (elevation -7.7 m or -25 ft) in the TEM best-fit model is deeper than the deepest interface detected with the ER and SR surveys.

The complete set of TEM sounding data and best-fit models are contained in Appendix C, starting with APG91 in the NW corner, proceeding across each row of grid cells and ending with APG47 in the SE corner (see Figure 20). Each TEM sounding was fitted with 4- and/or 5-layer models; fitting errors ranged from 1.5 to 7.5 percent with an average of approximately 3 percent. While no constraints were placed on the parameters during the inversion process, the *initial* model for each sounding contained a high resistivity lowermost layer with a resistivity of 3,000 ohm-m. The best-fit models proved rather insensitive to the choice of the initial resistivity of the lower layer in the inversion as long as it was much larger than other resistivities in the initial model. Four of the TEM sounding datasets were not interpretable due to high noise levels: APG19, APG83, APG84, APG85. These four TEM sounding locations were near large numbers of 55-gal drums and other metallic objects on the surface, which produced the high noise levels.

Interpretation: 3-D portrayal of results

As discussed previously and shown in Figure 20, the TEM results form a 2-D, 100 ± 100 ft grid of resistivity versus depth models. The results can be modeled and graphically portrayed (visualized) as interfaces and volumes in

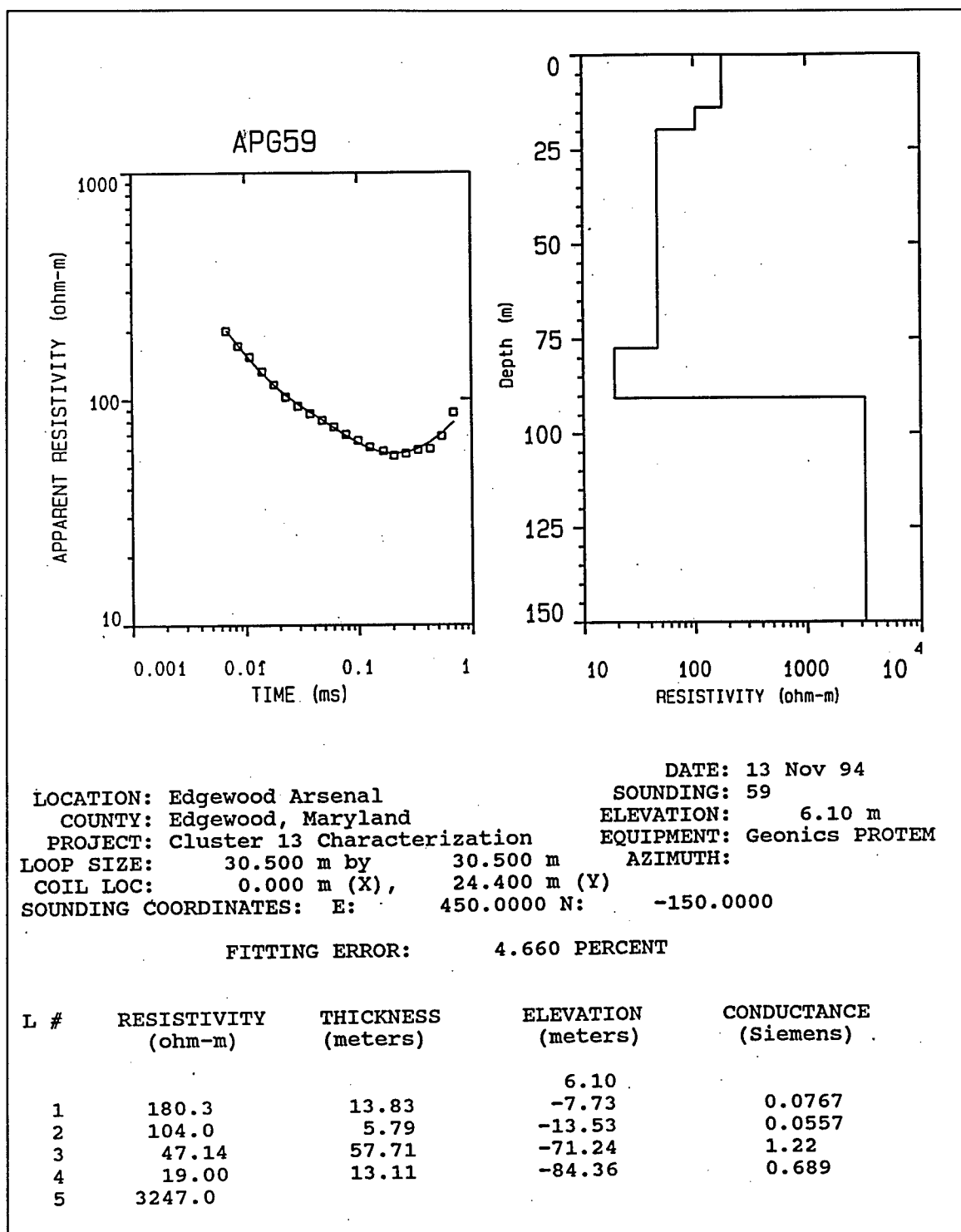


Figure 19. TEM data, best-fit model, and best-fit model parameters list for sounding at location (2.5, 1.5)

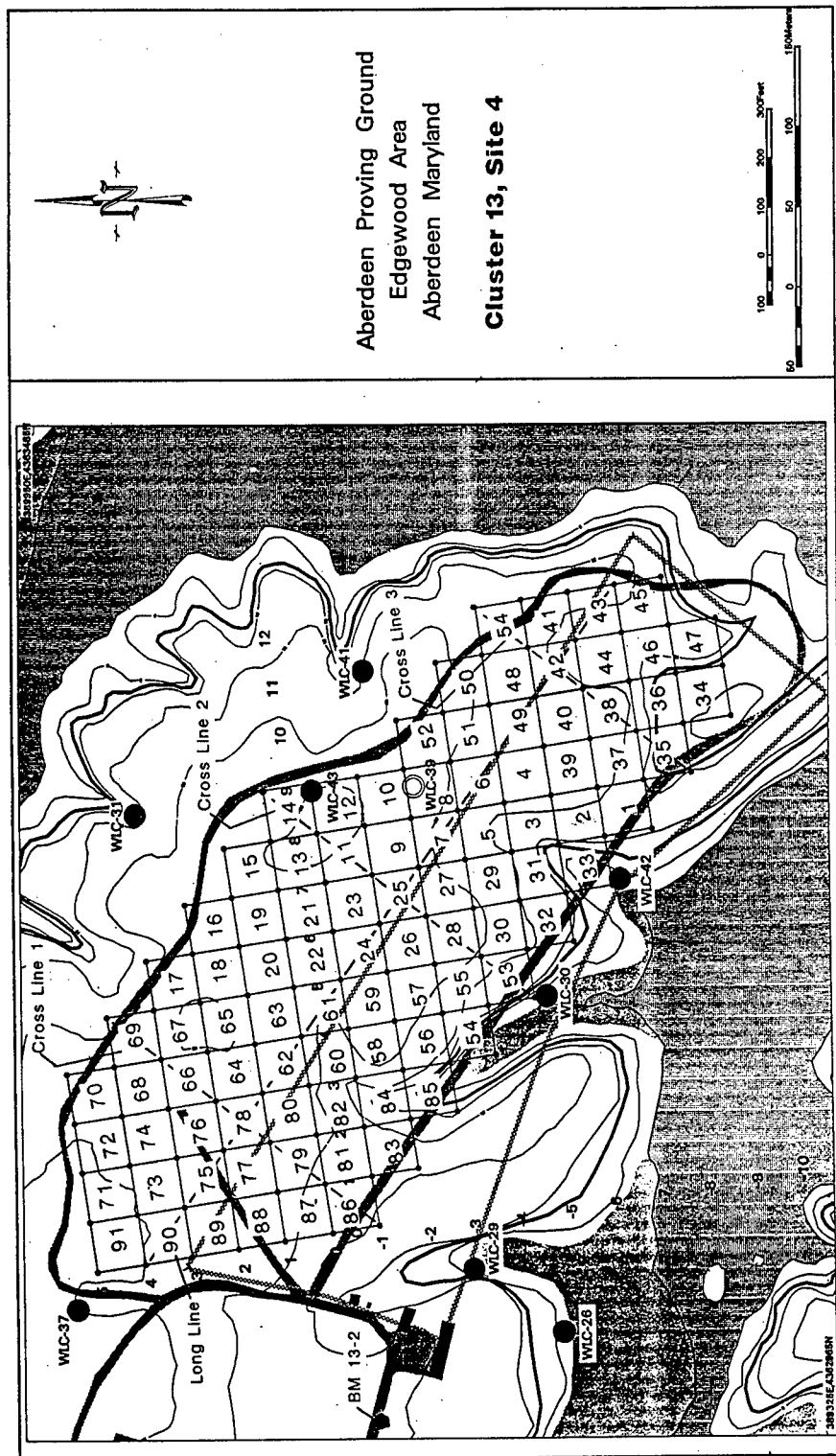


Figure 20. Cluster 13 survey grid and TEM sounding number grid cell assignments

three dimensions 0(3-D). Once the 3-D volume model is formulated, the data can be viewed on any cross-section or cut through the volume. For purposes of the volume model, only four layers are considered; for any case where five layers were fitted to the data such as APG59 (Figure 19), the upper two layers were combined and the "average" resistivity used for the volume model.

The easiest way to introduce the volume model of the TEM results is to view cross sections along the Long Line and Cross Lines as shown in Figure 21. The lower right corner of Figure 21 reproduces the grid map and shows the locations of the cross-section lines for reference. The cross-sections are color coded relative to the four layers but not to resistivity variations within the layers. Within a layer in the volume model, resistivity varies laterally but not vertically. The depth axis corresponds to elevation, i.e., 0 depth is 0 elevation.

Lateral resistivity variations for the four layers in the volume model are shown in Figures 22-25. From Figures 22-25, resistivity variations within each layer are approximately as follows:

Layer	Resistivity Range and Mean (ohm-m)	
1	50 - 500	200
2	40 - 66	50
3	12 - 38	20
4	2,600 - 5,500	3,000

Details of the volume model are completed in Figures 26-32, where the elevations of the surface and the three layer interfaces (Figures 26-29) in the model and the thicknesses of the upper three layers (Figures 30-32) are shown.

Finally Figures 33-37 show various perspective views of the four-layer TEM volume model. For these views of the model, the +x-axis is approximately East, the +y-axis is approximately North, and the +z-axis is up. Thus the views in Figures 33 and 34 are "looking" approximately Northeast and down and approximately Southwest and down, respectively. Figure 35 displays a vertical-horizontal bench-cut through the volume, that reveals the dip of the top of layer 4. Figures 36 and 37 are views of the top of layers 2 and 3, respectively, with color-coded elevation contours to enhance depth perception.

Interpretation: Assessment of TEM results

The interpreted volume model of the subsurface at Cluster 13, based on the TEM results, consists of four layers with variable thicknesses and electrical resistivities. Except for layer 1, the resistivity variations within the four layers are quite small. The thickness of layer 1 varies from 12 m to 36 m

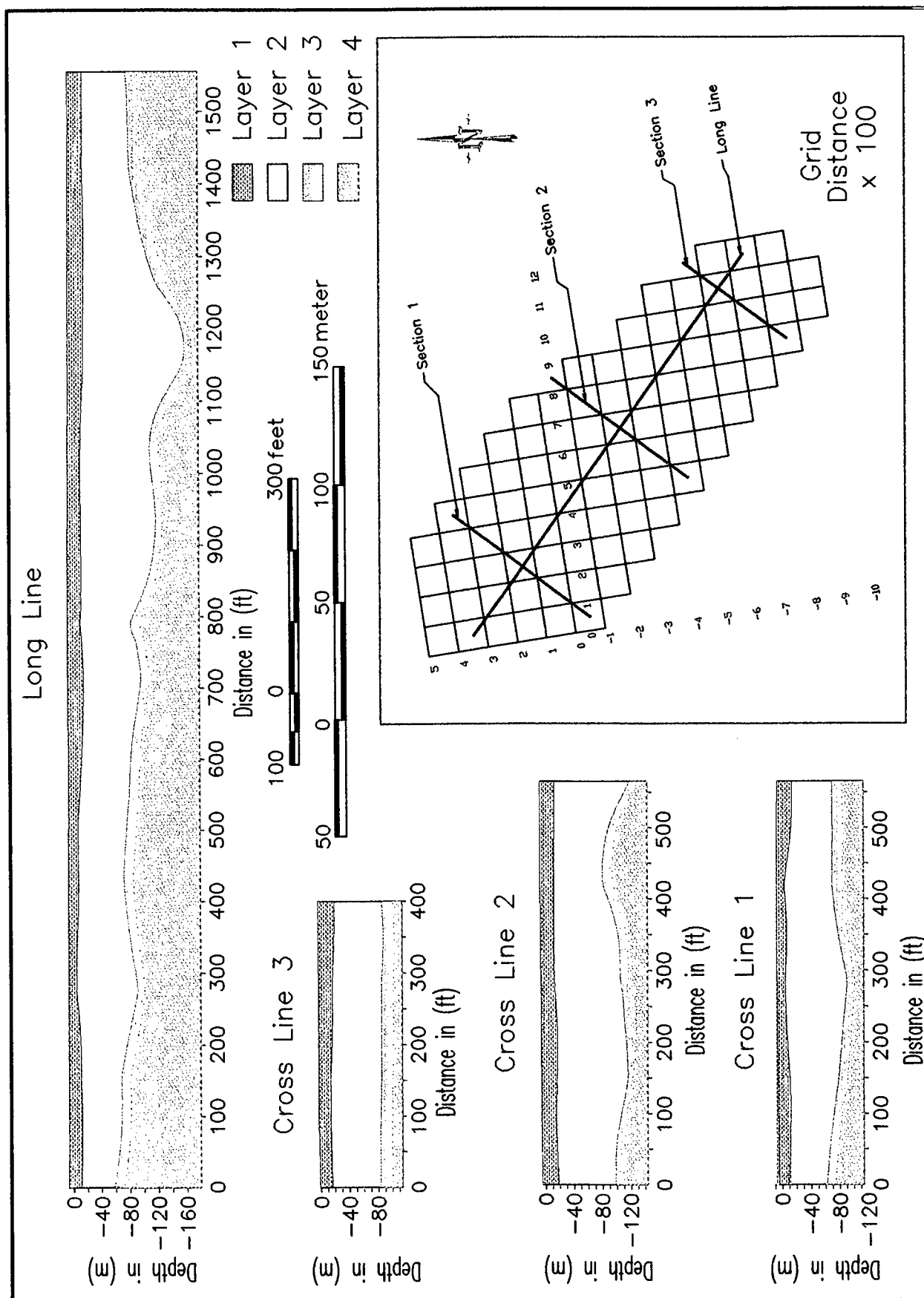


Figure 21. Cross sections from the TEM volume model along the long line and cross lines 1-3; resistivity ranges for the layers are given in the text

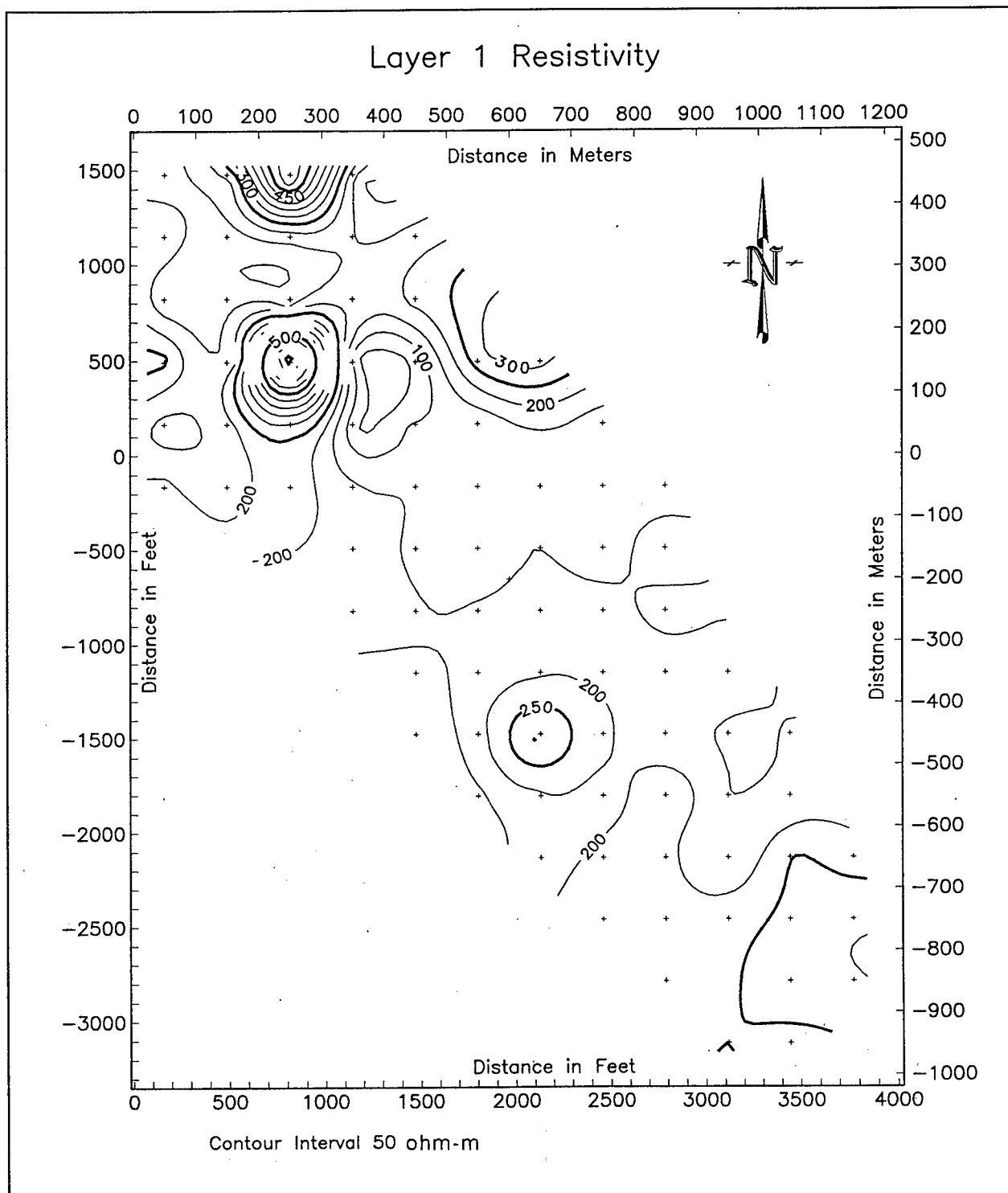


Figure 22. TEM layer 1 resistivity map

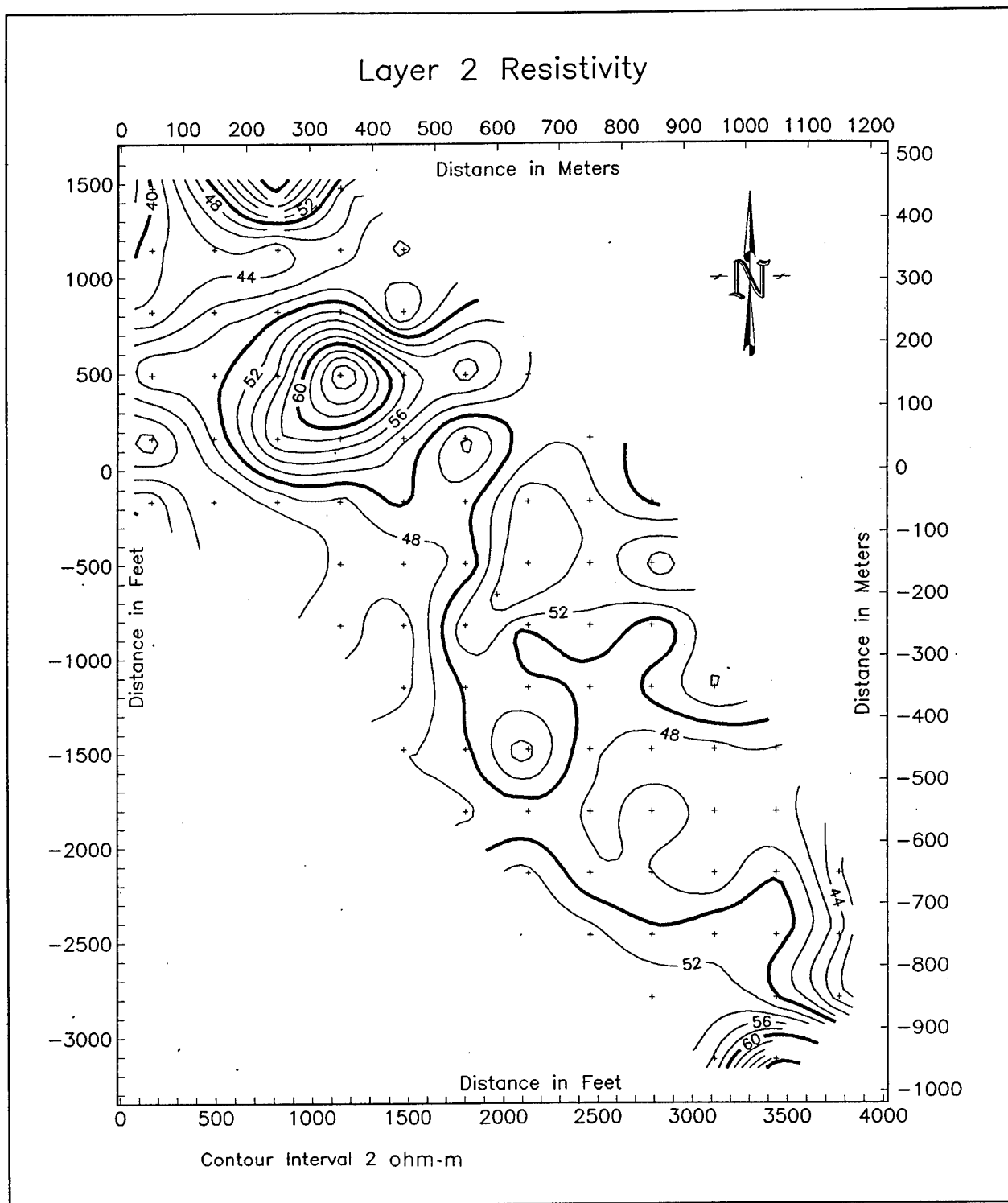


Figure 23. TEM layer 2 resistivity map

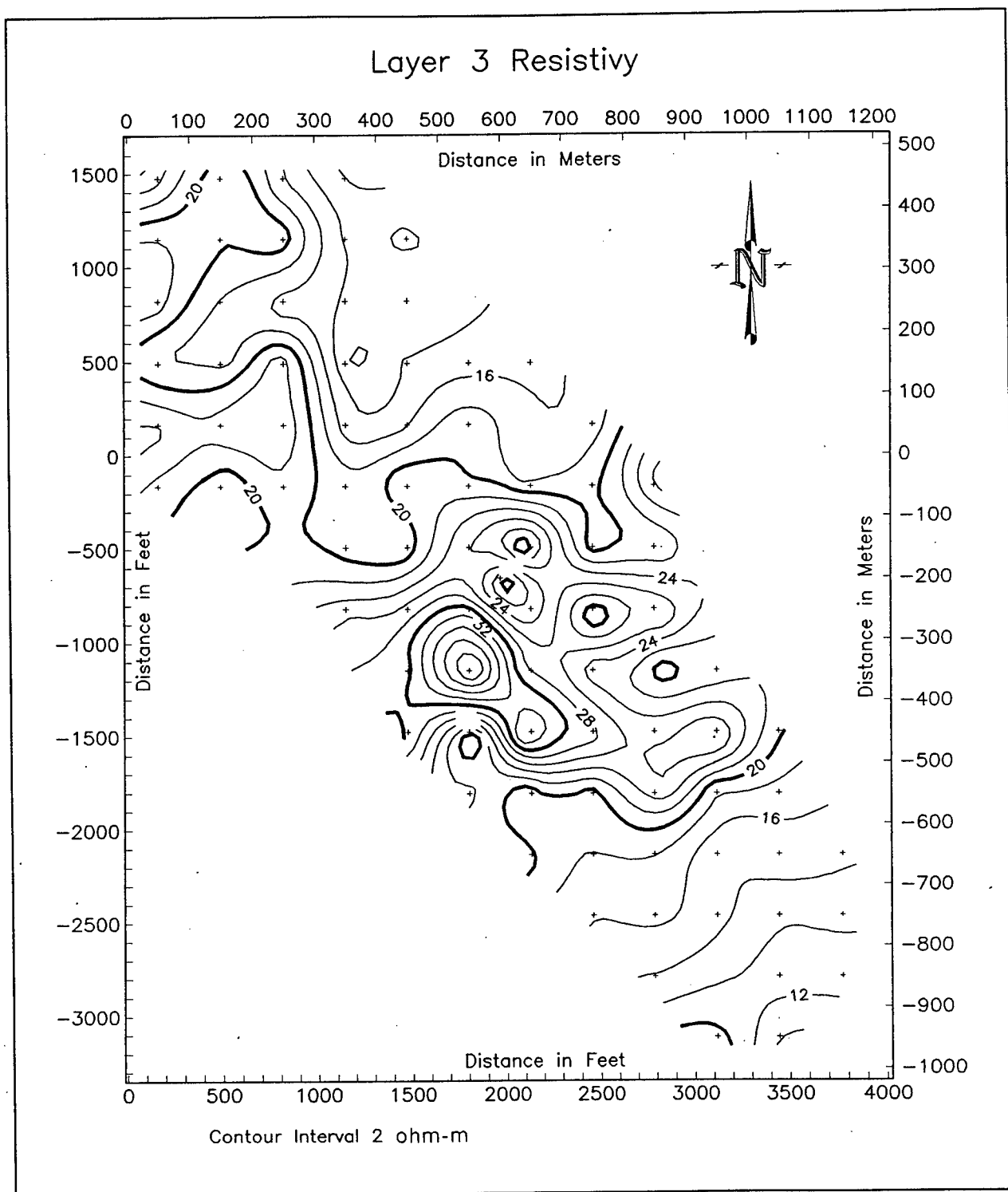


Figure 24. TEM layer 3 resistivity map

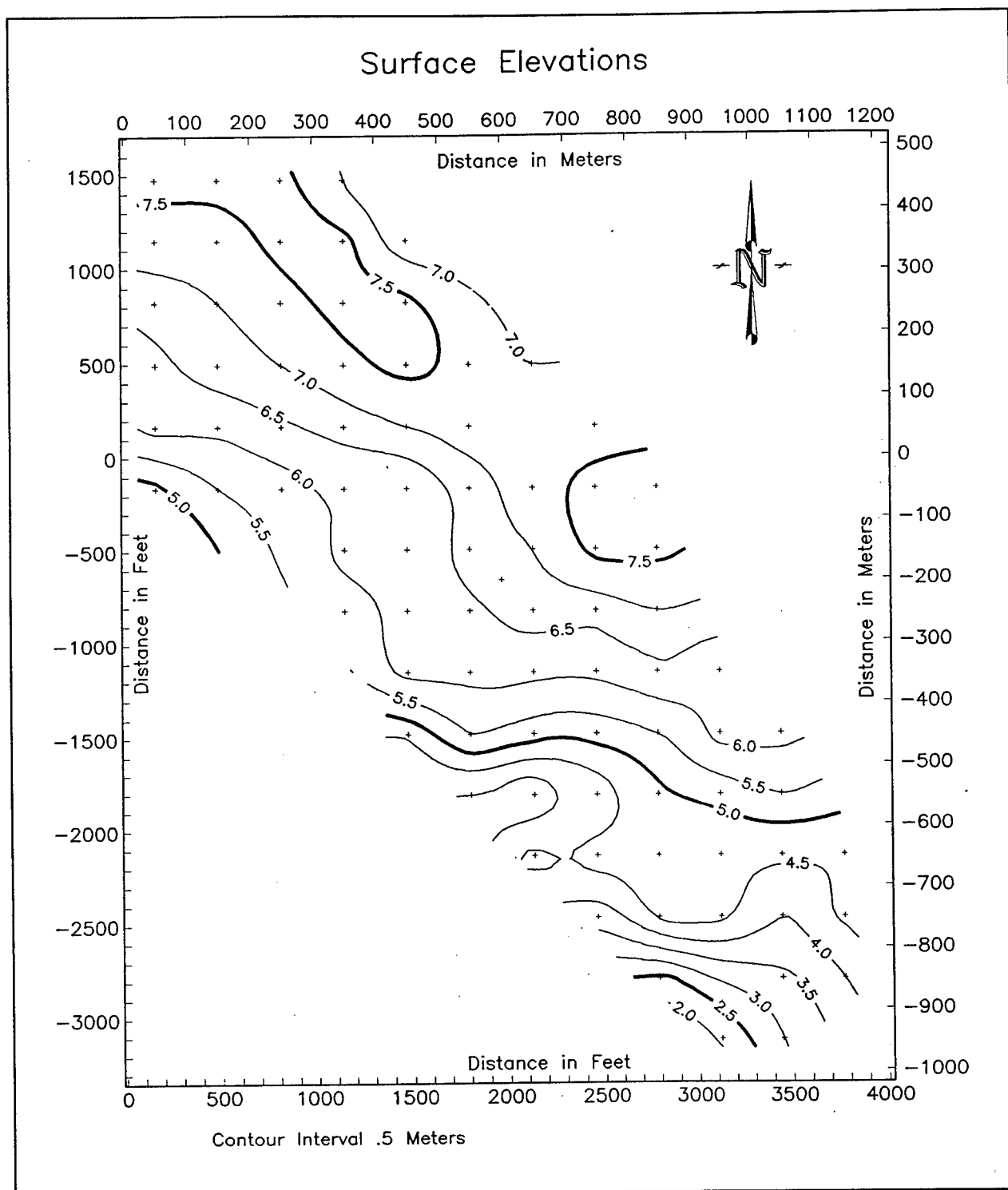


Figure 26. Surface elevation map

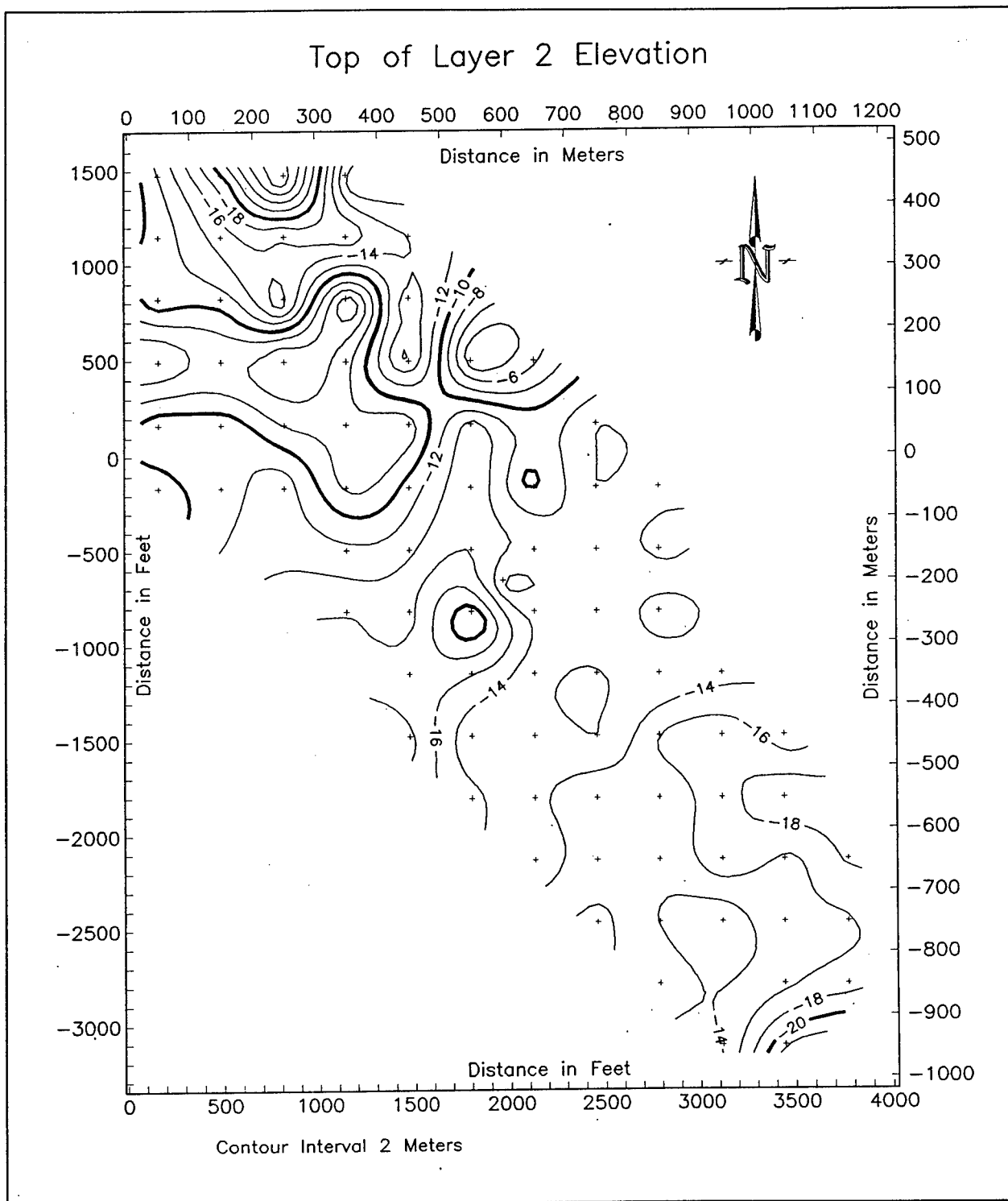


Figure 27. Depth to layer 1 - layer 2 interface in TEM volume model

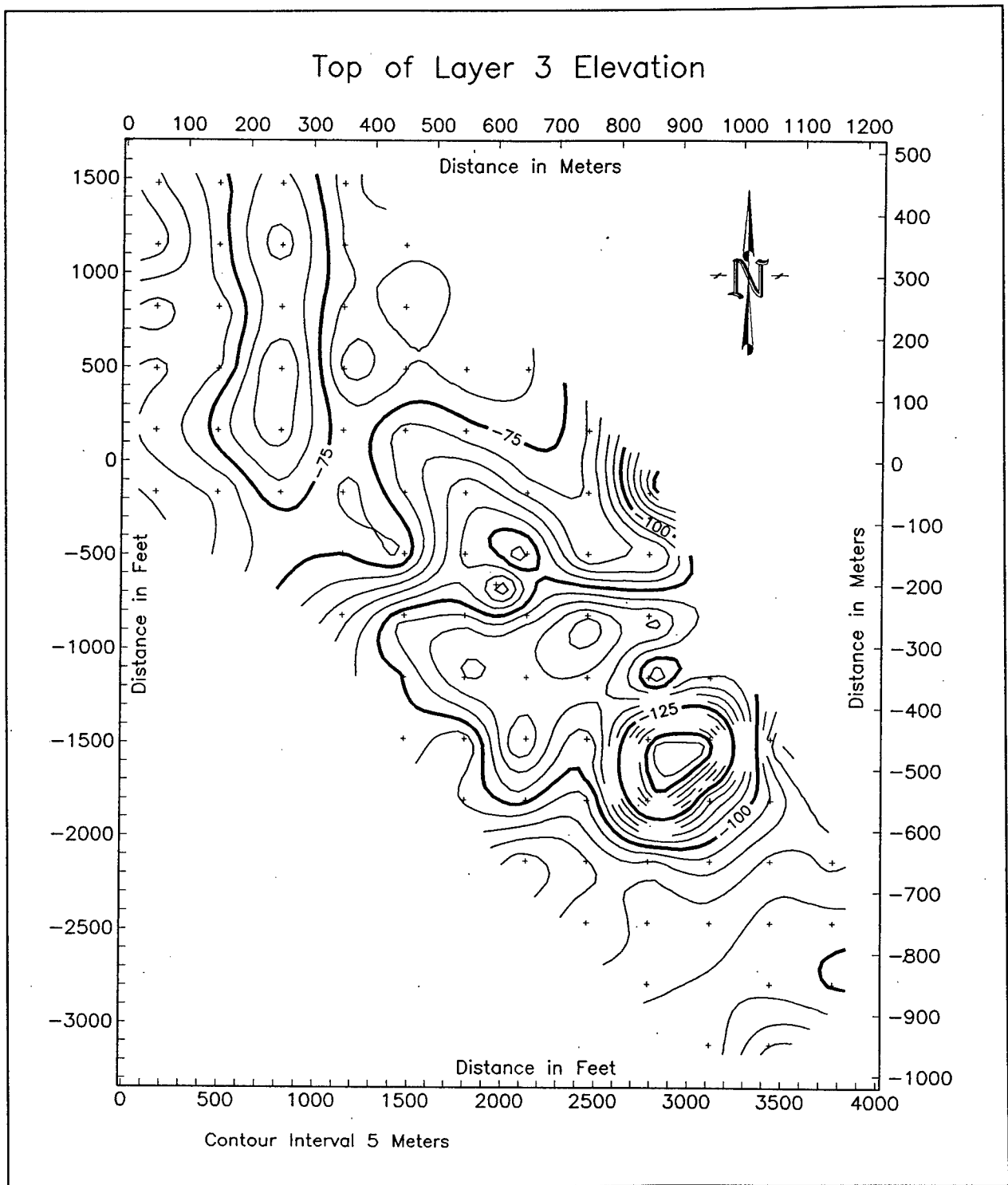


Figure 28. Depth to layer 2 - layer 3 interface in TEM volume model

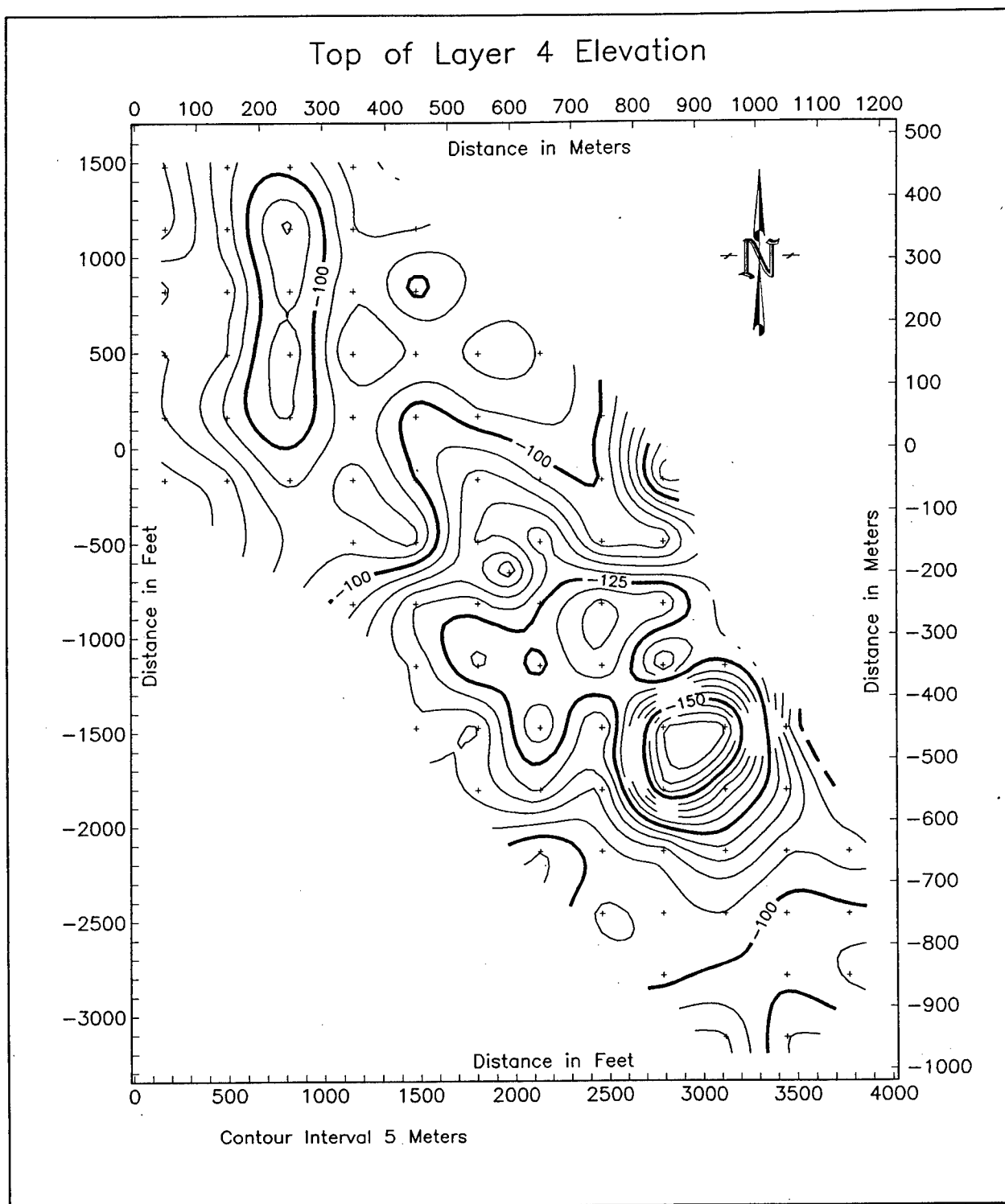


Figure 29. Depth to layer 3 - layer 4 interface in TEM volume model

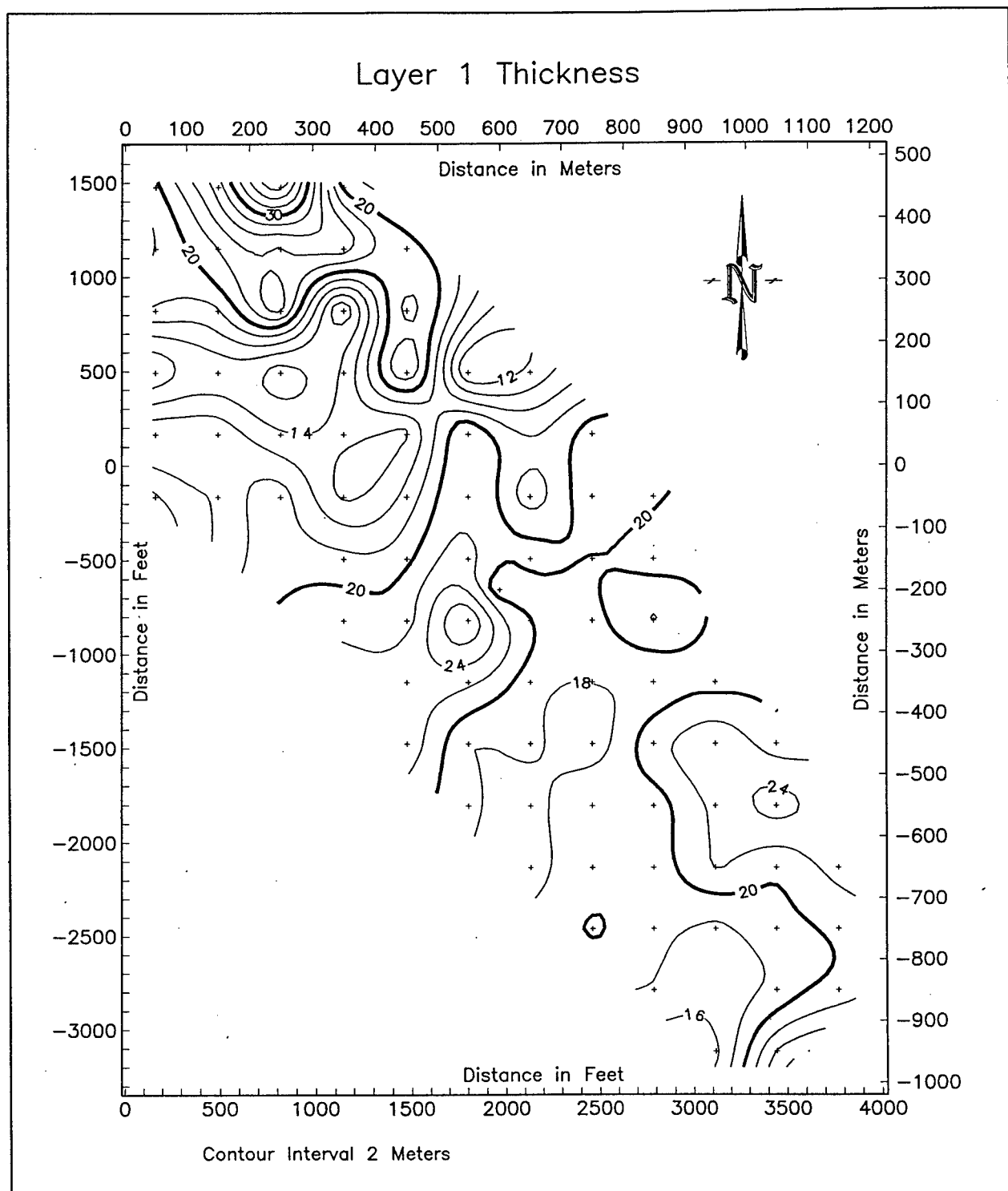


Figure 30. Layer 1 thickness in TEM volume model

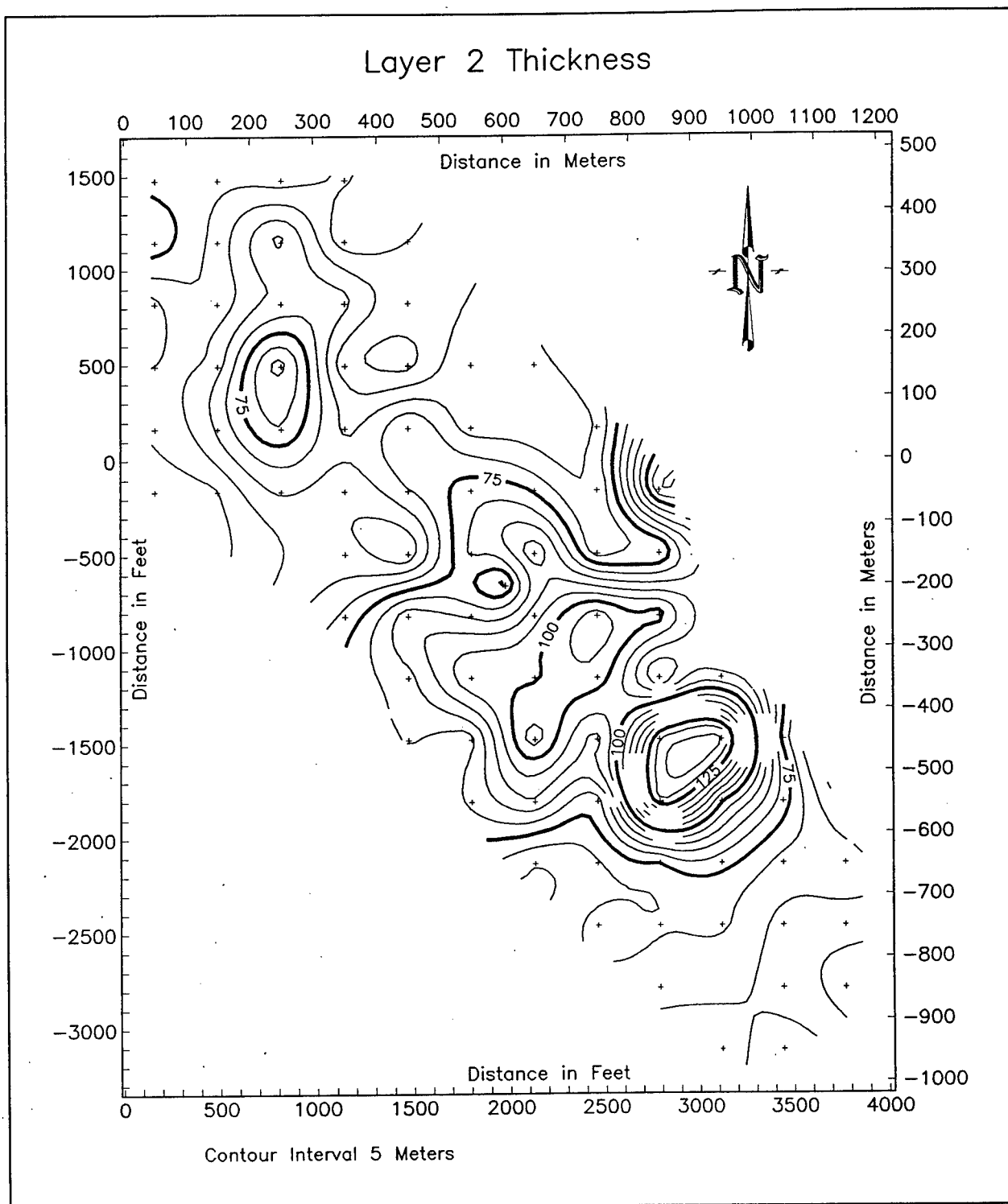


Figure 31. Layer 2 thickness in TEM volume model

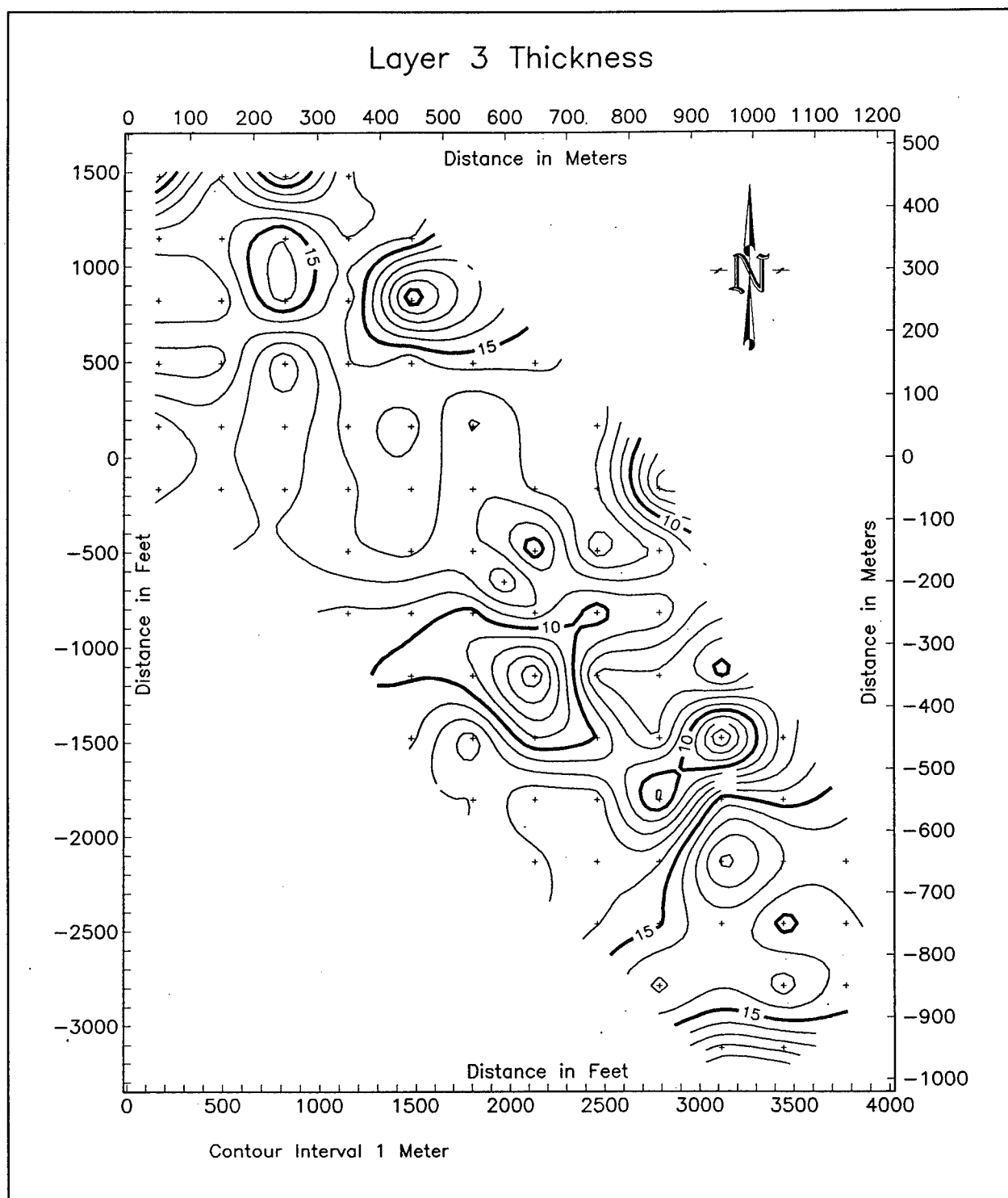


Figure 32. Layer 3 thickness in TEM volume model

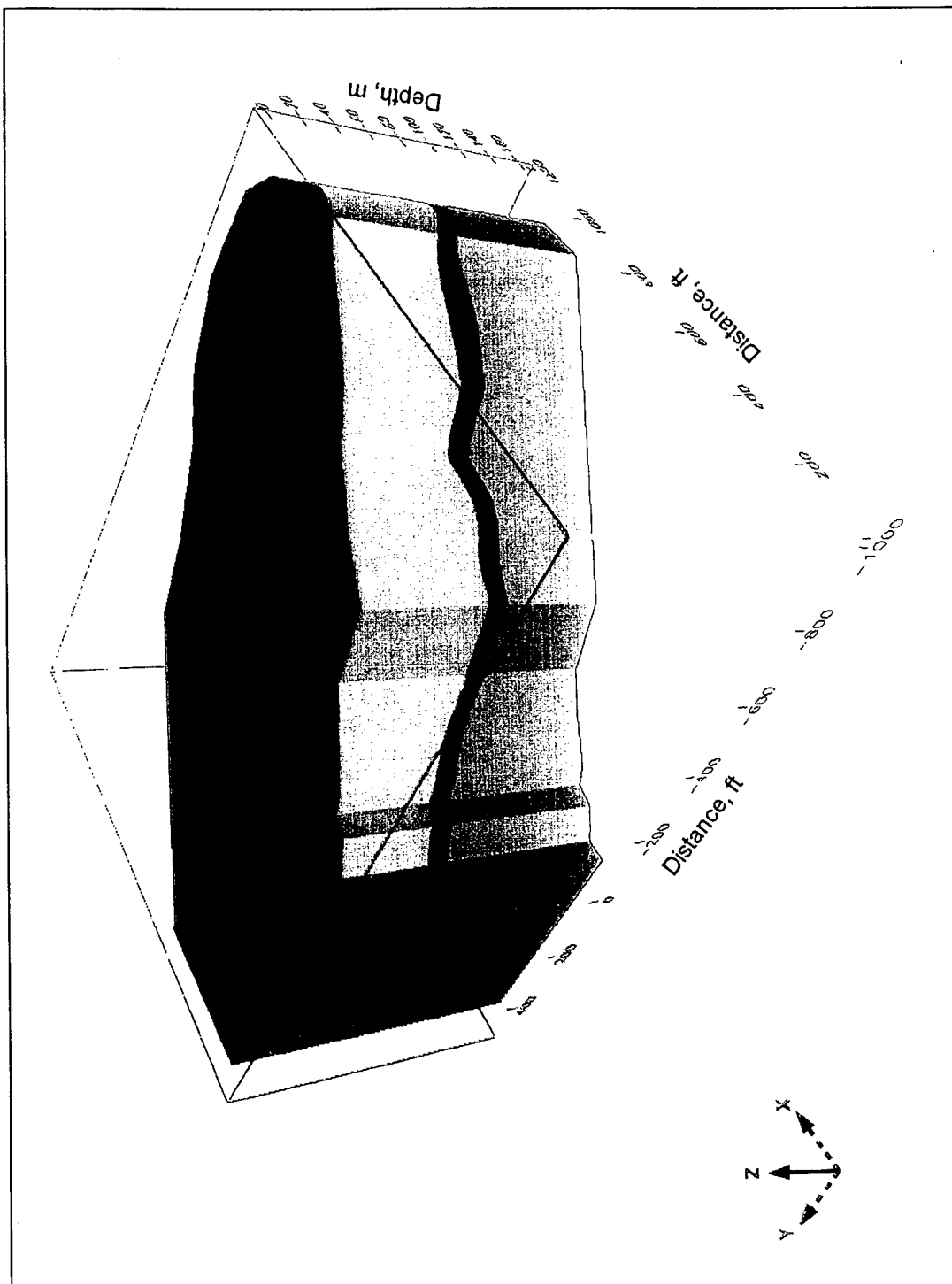


Figure 33. View of complete 4-layer TEM volume model, looking northeast

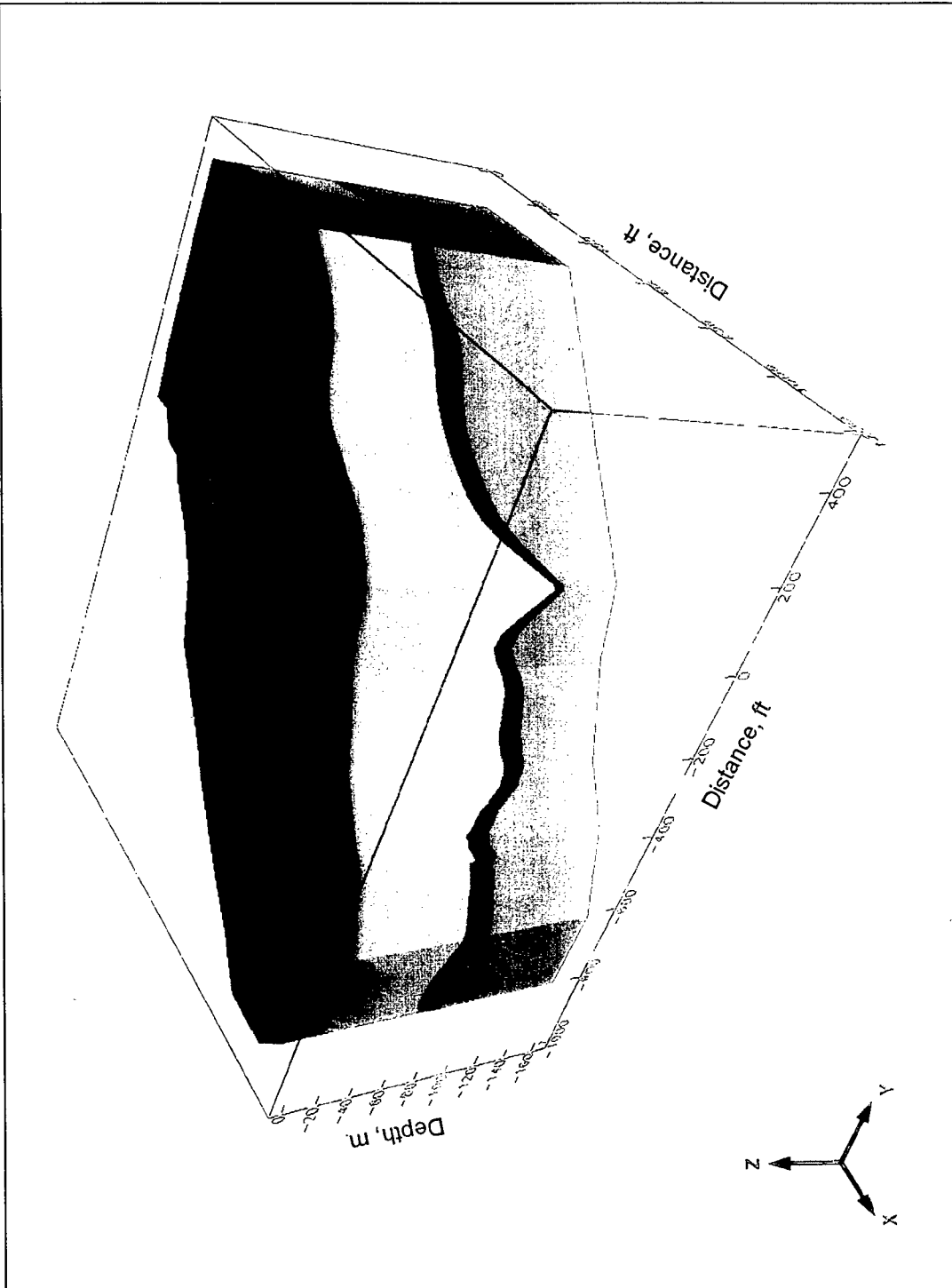


Figure 34. View of complete 4-layer TEM volume model, looking southwest

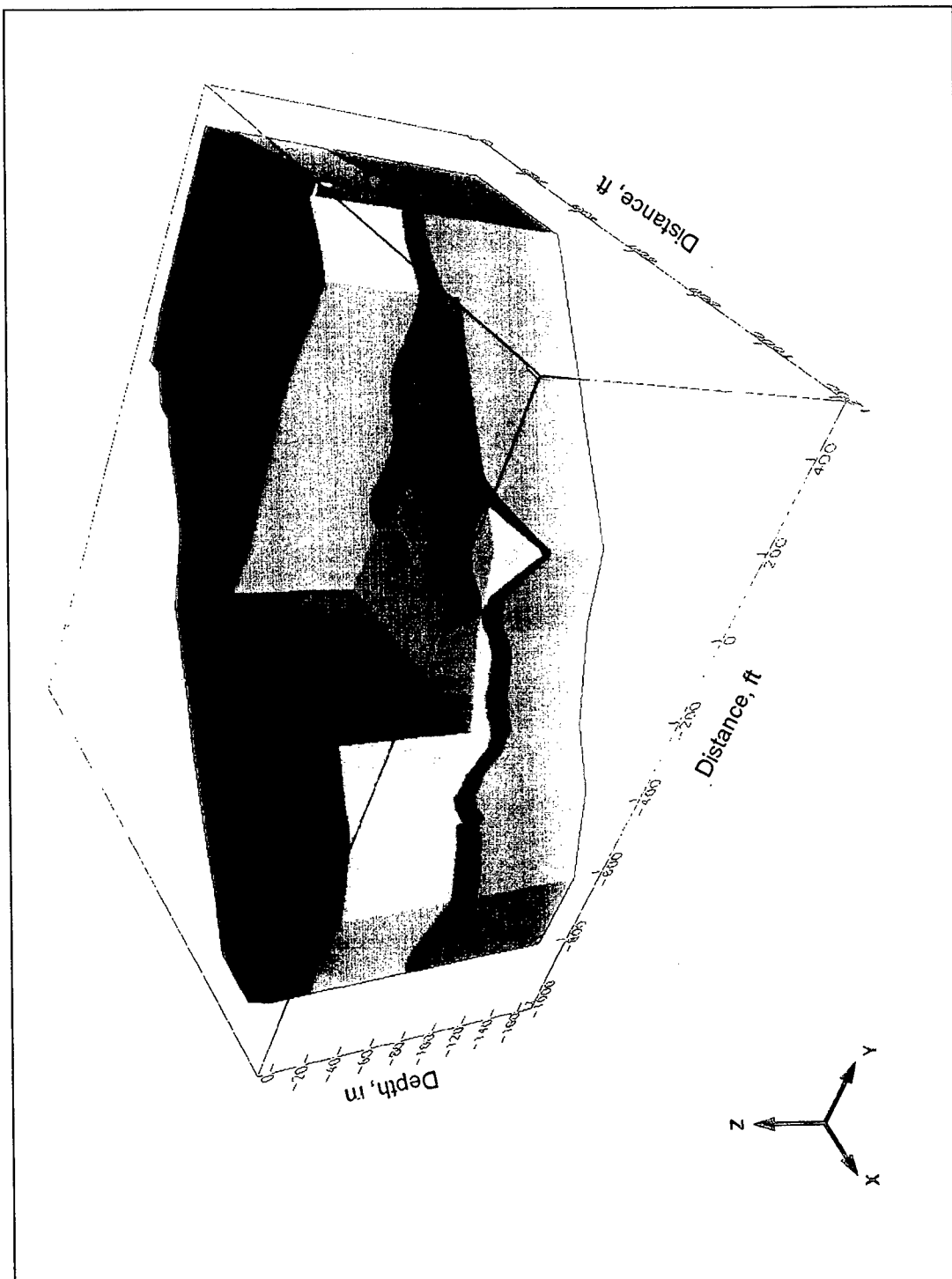


Figure 35. View of 4-layer TEM volume model with vertical-horizontal bench cut, looking southwest

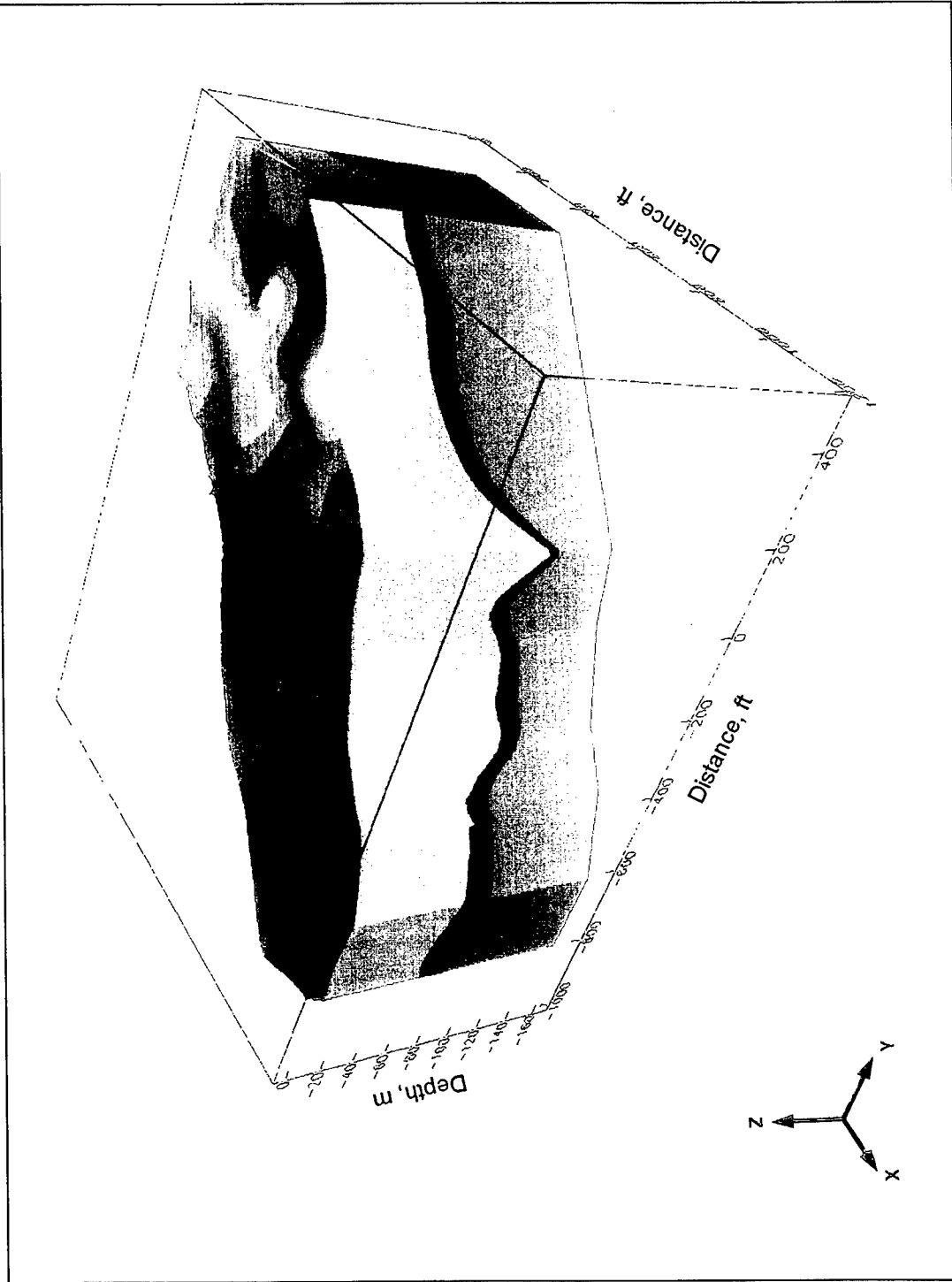


Figure 36. View of top of layer 2 with color-coded elevation contours, looking southwest

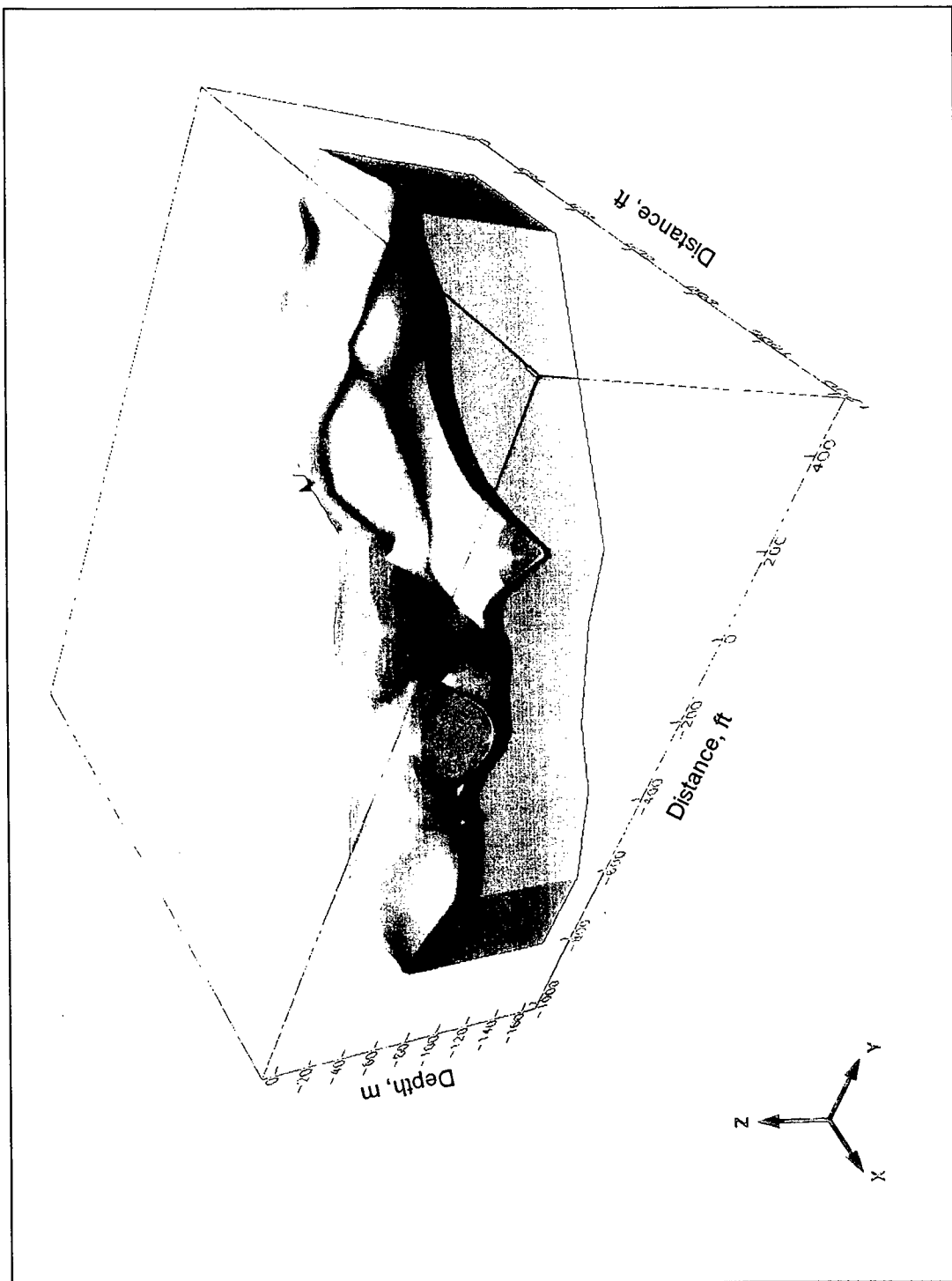


Figure 37. View of top of layer 3 with color-coded elevation contours, looking southwest

(Figure 30). As noted previously, layer 1 from the TEM results includes all the materials investigated by the ER and SR surveys. Thus the resistivity for TEM layer 1 is a volume average of the resistivities of materials in the upper 12-36 m, some of which are revealed in the ER results and cross sections (Figure 17 and 18 and Appendix B).

Layer 2 varies in thickness from 60 m to 135 m, but has a relatively small variation in resistivity (40-66 ohm-m). The mean resistivity, 50 ohm-m, indicates that Layer 2 likely has a large clay content and is saturated. There is strong indication, based on the depth to top and resistivity, that the top of layer 2 (layer 1/layer 2 interface) may represent the Pleistocene-Cretaceous boundary beneath Cluster 13.

Layer 3 is a relatively thin unit (7-20 m thick) with mean resistivity of 20 ohm-m. Based on the low resistivity value, layer 3 is likely composed predominantly of clays. Also, based on its thickness and pervasive presence over layer 4 (Figures 21 and 33-37), layer 3 is identified as the saprolite overlying the basement crystalline rock. The saprolite layer is typically shown as being from 6 to 12 m thick in geologic cross sections and is at an elevation consistent with TEM layer 3.

The resistivity of layer 4 is consistent with a dense, impervious rock. Based on the depth or elevation and the resistivity of layer 4, it is tentatively identified as the basement crystalline rock. Elevation of the top of layer 4 is approximately -80 m at the NW end of the survey area and -100 m beneath the SE end, but the topography on top of layer 4 is irregular (Figure 37) and includes an apparent erosional feature down to elevation -160 m between the positions of Cross Lines 2 and 3. The elevation of the top and apparent physical nature of layer 4 is consistent with the predicted depth and the known physical nature of the basement crystalline complex rocks.

Thus the tentative geological assessment of the four layers of the TEM results based on the model properties and general knowledge of the geology are as follows:

Layer	Mean Resistivity (ohm-m)	Geological Interpretation
1	200	Surficial silts, sands, gravels, and clays, including the surficial aquifer; Pleistocene
2	50	Silty, sandy clays, likely saturated; Cretaceous
3	20	Clays. Precambrian saprolite
4	3,000	Crystalline rock. Precambrian

Borehole Geophysical Logs

Borehole geophysical logs, consisting of conductivity and natural gamma logs, obtained in the shallow exploratory borings and monitoring wells of

Cluster 13 are contained in Appendix D. The geophysical logs for WLC-37 and WLC-39 are shown in Figures 38 and 39, respectively; these wells are closest to the Long Line and hence most relevant for comparison to the Long Line cross sections. The data are presented as acquired, since the measurements are plotted directly in conductivity units ($\text{mmho/m} = \text{mS/m}$) and natural gamma count rate (counts/s). The dashed lines in Figures 38 and 39 indicate interpreted interfaces between different material types.

Due to the details of the conductivity logging instrument response, the conductivity of the more conductive layers will be underestimated by the dashed lines, while the conductivity of the less conductive layers will be overestimated. The layers of high conductivity also have high natural gamma activity, consistent with the identification of such layers as having high clay content (labeled "C" for clay in Figures 38 and 39). Similarly, layers with low conductivity also have low natural gamma activity, consistent with the identification of such layers as predominantly sand and/or gravel (labeled "S" for sand in Figures 38 and 39). Most of the wells have a protective steel casing extending to approximately 1.5 - 2 m depth; thus the conductivity log is not meaningful shallower than 2 m depth due to the response of the steel. Also noted on Figures 38 and 39 are the water table depths as deduced from Figure 6 and the drilling logs. The position of the water table in relation to the overlying clay in Figures 38 and 39 suggests that groundwater may be locally confined vertically; such as WLC-37, Figure 38, where the water table is at the base of the clay unit or facies. In WLC-39, the slight rise in conductivity at 6 m depth (Figure 39) may be due to the occurrence of the water table; otherwise the water table has little effect on the geophysical logs. In other wells, the geophysical logs and drilling logs suggest perched ground water conditions.

Summary of Integrated Geological Assessment

In order to better compare the seismic, TEM, and resistivity cross sections, the continuous seismic and TEM cross sections (Figures 13 and 21) are replotted in Figures 40 and 41, respectively, as discontinuous interface cross sections (interface depth data every 140 ft along the section) for direct comparison with the resistivity cross section in Figures 18. The sections in Figures 40 and 41 have all of the tentative interface identifications and soil/rock type and condition assessments indicated. Also, Figure 40 has information from WLC-37, WLC-43 and WLC-39 projected to the cross section; these wells are 55, 30 and 80 m, respectively, laterally from the Long Line cross section, however the surface elevations for the wells are about the same as at the projected location on the cross section.

The close agreement of the three projected water table locations from the wells with the seismic interface identified as the water table in Figure 40 strengthens the assessment. The seismic interface (water table) is shown dashed between the 400 to 540 ft (122 - 165 m) position of the cross section,

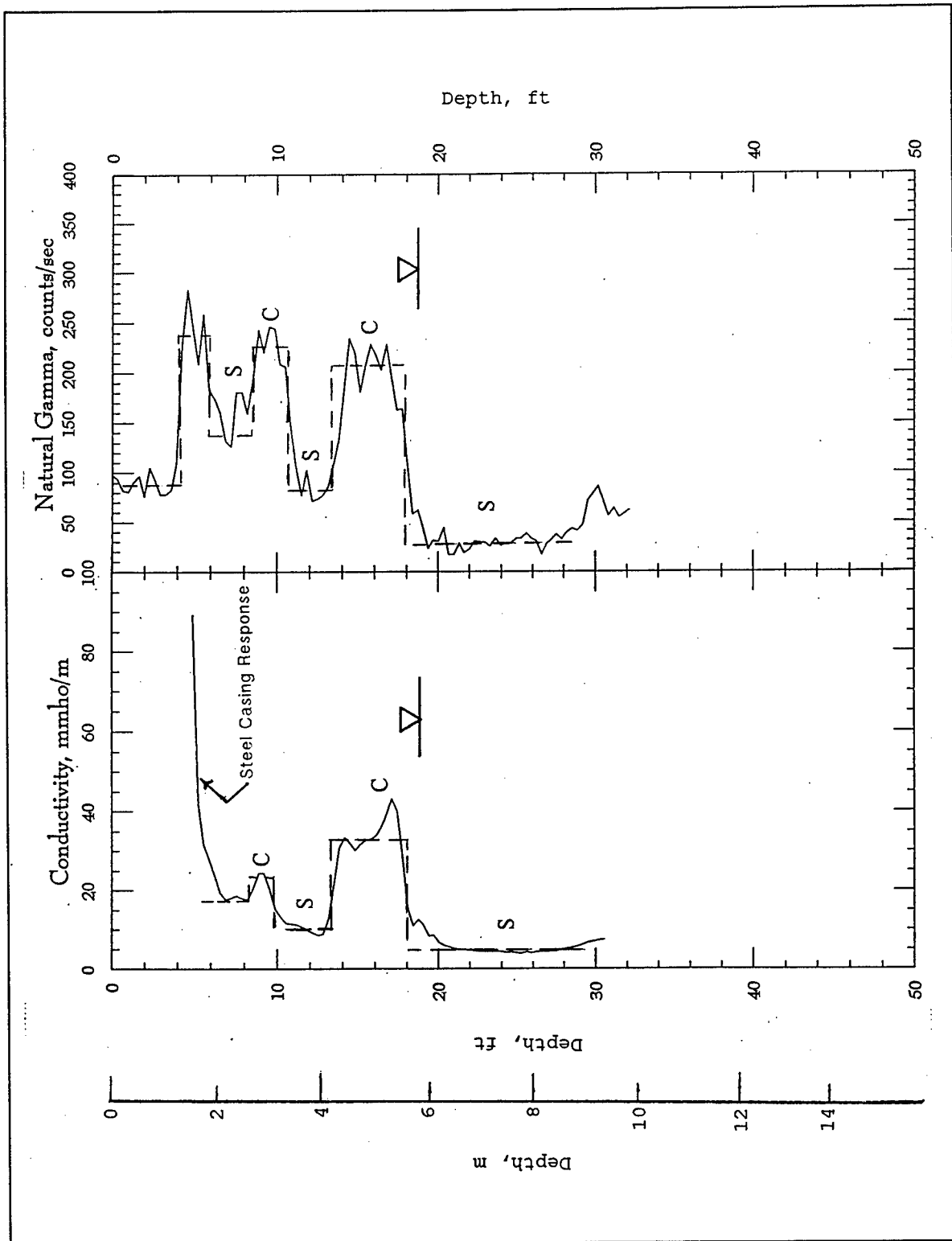


Figure 38. Borehole geophysical logs for WLC-37

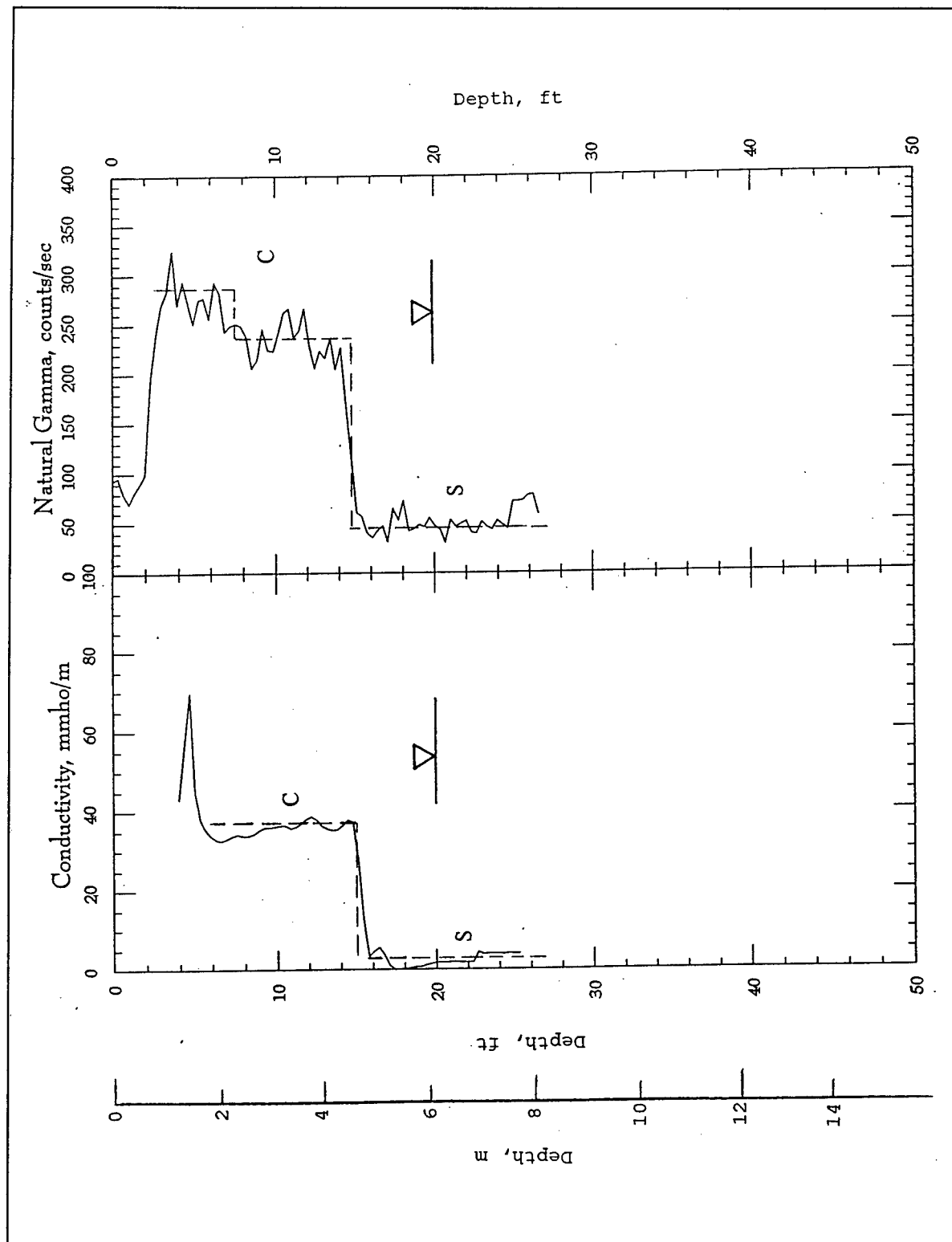


Figure 39. Borehole geophysical logs for WLC-39

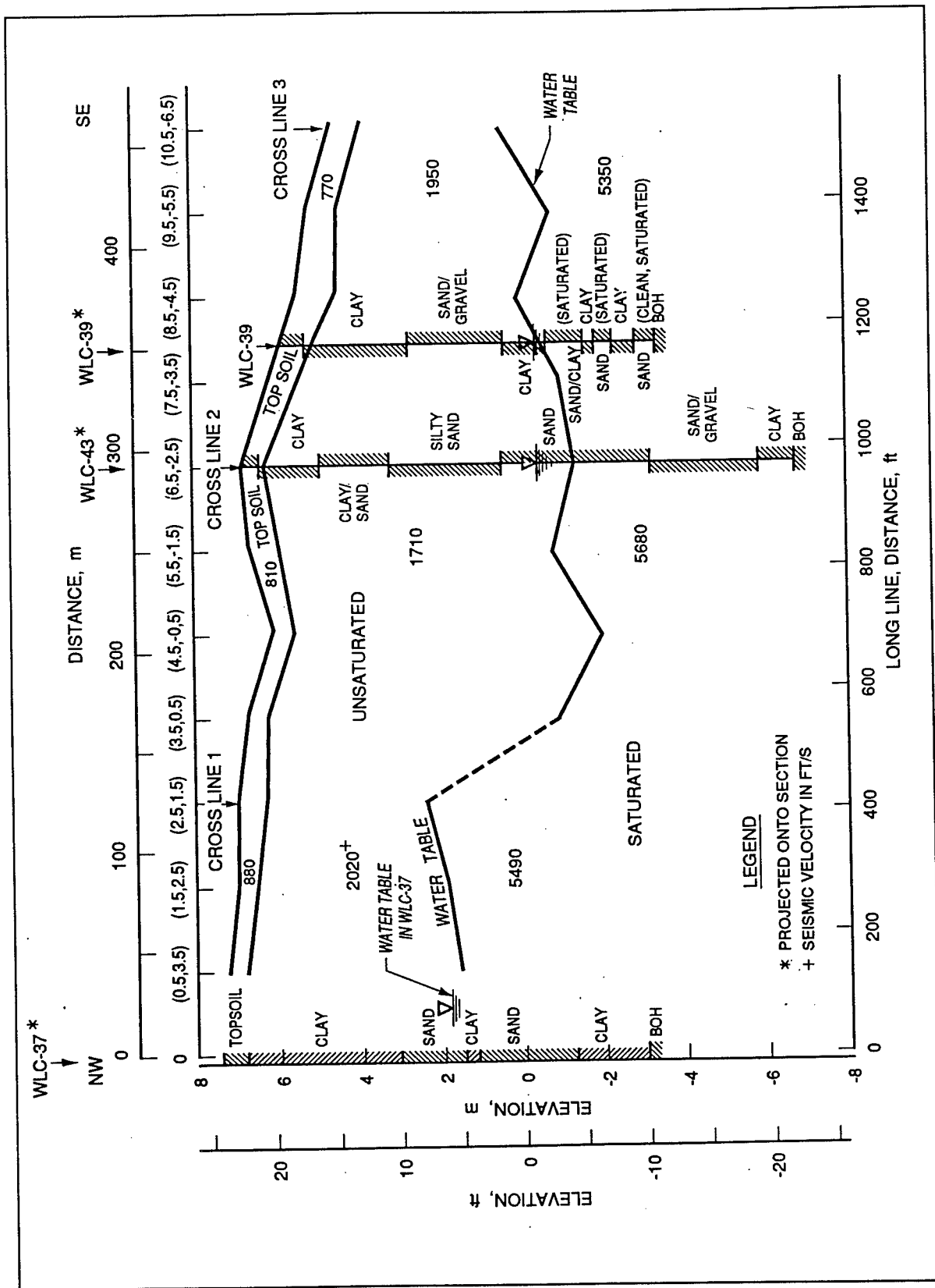


Figure 40. Long line seismic velocity cross-section, with hydrogeologic interpretations and borehole logs projected onto section

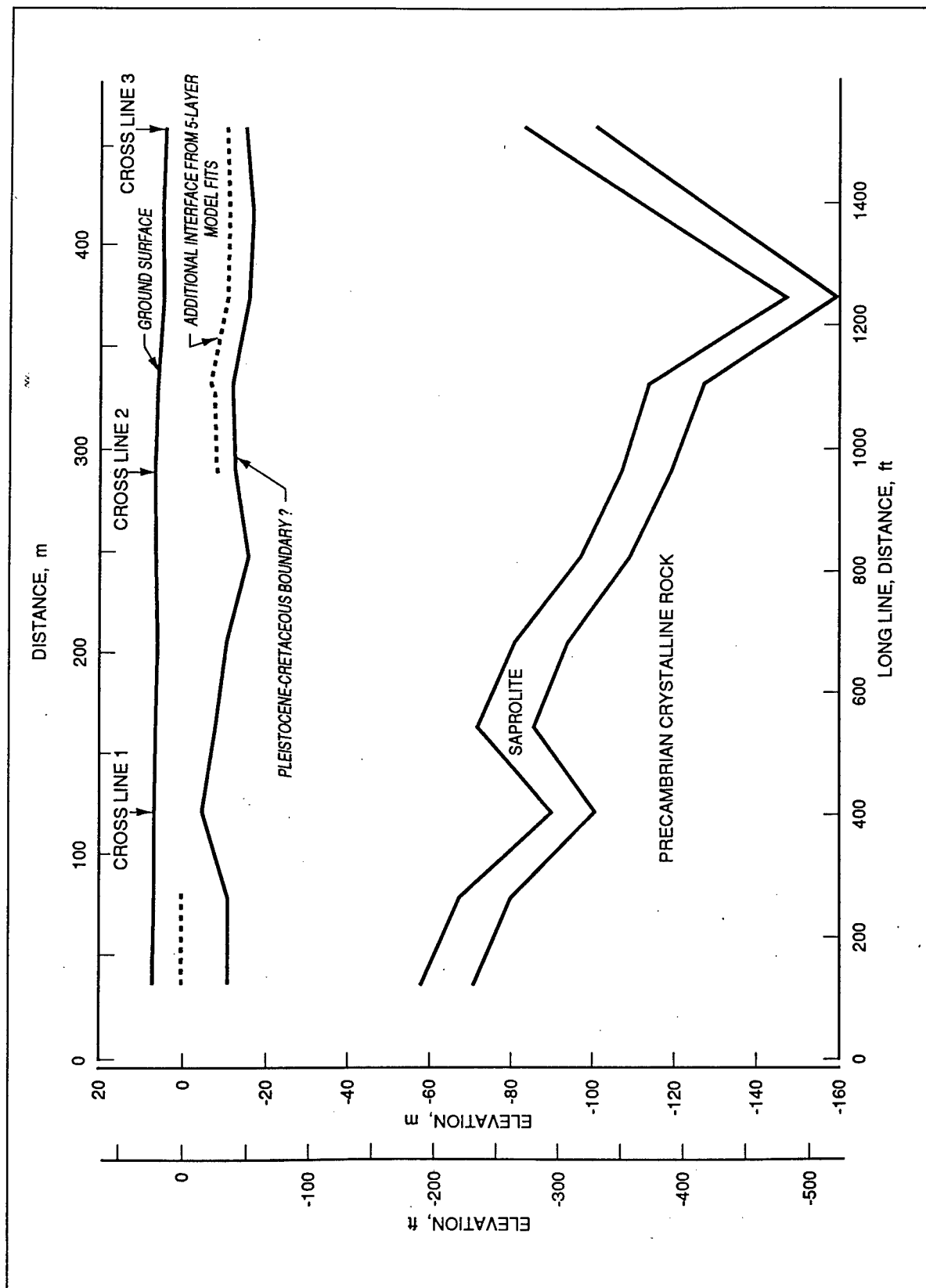


Figure 41. Long line TEM cross-section, with geologic interpretations

due to the dramatic change in the seismic interface between those positions. Comparison of Figures 40 and 18 indicates that the interface between the orange and blue regions of the resistivity cross section agrees closely with the seismic interface (water table) from the approximate position 800 ft (245 m) to the SE (right) end of the section. From the 800 ft position to the NW (left) end of the section, there is no indication of the water table in the resistivity cross section (Figure 18); this is the same region of the section where the seismic interface (water table) increases in elevation from approximately -2 m to +2 m. Considering the suggestions of clay at the NW (left) end of the section in Figure 18 (gray-colored regions) and the clay in the boring log for WLC-37, the water table at the NW end of the section may be perched. The clay with top at elevation -1.5 m in WLC-37 may serve as a perching layer and the facies may have a geometry laterally that blocks the lateral extension of the water table from SE to NW in the section.

Comparing Figures 41 and 18, confirms that the uppermost TEM interface, tentatively identified as the Pleistocene-Cretaceous boundary, is everywhere deeper than the deepest interface in the resistivity section except for one location. At the 400 ft (122 m) position in the TEM cross section, the Pleistocene-Cretaceous boundary rises to elevation -5 m; and at exactly this location in the resistivity section a low resistivity area is tentatively identified as clay, consistent with the expected nature of the upper part of the Cretaceous materials. The depths indicated in Figure 41 for the Pleistocene-Cretaceous boundary are consistent with depths shown on cross sections developed to support RCRA investigations at the Edgewood Area of APG. Additionally, comparing the complex stratigraphy revealed by the three boring logs in Figure 40 with the nature of vertical and lateral variations shown by the resistivity section (Figure 18) validates the complex resistivity section.

5 Summary and Conclusions

This report presents the results of geophysical surveys conducted over a portion of Cluster 13 at the Edgewood Area of Aberdeen Proving Grounds, Maryland. The primary objective of the investigation was to demonstrate the capability of geophysical methods for mapping subsurface geology and thus to supplement and extend the existing information on subsurface conditions. Of particular interest as specific mapping objectives were (1) the location and continuity of sand and clay facies in the shallow subsurface ($< 15\text{-}20\text{ m}$), (2) depth to the water table, (3) the depth to the Pleistocene-Cretaceous boundary, and (4) the depth to the Precambrian crystalline rock (basement). Three geophysical methods were applied at the site. Seismic refraction and electrical resistivity surveys were conducted along four intersecting profile or cross-section lines. Transient electromagnetic soundings were conducted on a grid pattern over the whole area of interest, which included the four profile lines. The results of the geophysical surveys are correlated with all known, existing geological information for the site.

The geologic mapping objectives of this investigation were achieved in varying detail. Seismic refraction and electrical resistivity surveys revealed details about the shallow geology. Seismic refraction cross-sections map the thickness and continuity of the "topsoil" layer and the water table (saturated zone); the water table is detected at depths of approximately 4 m to 8 m or at elevations from -2 m to 2 m. The water table elevations from the seismic surveys correlate closely with water table elevations measured in nearby monitoring wells. Electrical resistivity cross-sections reveal a very complicated distribution of sandy and clayey facies in the upper 10 - 15 m of the subsurface. A continuous surficial (topsoil) layer is mapped that correlates with the surficial layer of the seismic section and nearby boring logs. Below the surficial layer, the complicated facies distribution has resistivities ranging from 25 ohm-m, which is most likely clay, to several thousand ohm-m, which represents dry sands and/or gravels. The complexity and details of the electrical resistivity cross-section correlate well with boring and geophysical logs from nearby wells. The effective maximum mapping depth of the seismic refraction and electrical resistivity surveys *as conducted at the site* is 10 - 15 m. To achieve greater mapping depths would require longer surface geophone spreads and electrode arrays which would be difficult to accomplish at the site due to the limited size of the Cluster 13 peninsula and the topography. The

refraction and resistivity surveys *as conducted* did not detect or map the Pleistocene-Cretaceous boundary at the site.

The transient electromagnetic surveys *as conducted* did not resolve the details of the upper 10 - 15 m of the subsurface at the site. However, the Pleistocene-Cretaceous boundary, the saprolite, and the top of the Precambrian crystalline rocks were successfully mapped by the transient electromagnetic surveys. Conducting the transient electromagnetic surveys on a grid pattern allowed the construction of a 3-D representation of subsurface geology (as represented by variations of electrical resistivity). Planning the transient electromagnetic surveys to give detail in the upper 10 - 15 m would sacrifice the depth of investigation capability for the deeper interfaces. Depths to the Pleistocene-Cretaceous boundary are consistent with the interpreted depths from borings at Cluster 13 and other areas of the Edgewood Area area. Thickness and depth of the saprolitic layer and depth to top of the Precambrian rocks are consistent with generalized geologic cross-sections for The Edgewood Area and depths projected from reported depths at the Aberdeen Proving Grounds NW boundary using regional dips. The average dip of the top of the Precambrian rocks from the transient electromagnetic cross-section (~ 20 m/km) is larger than the reported average dip (~ 15 m/km) but this difference could just be a localized effect.

This report provides results that successfully demonstrate application of a complementary suite of geophysical surveys to map details of subsurface geology at the Edgewood Area area of APG. Seismic refraction and electrical resistivity surveys were used for shallow mapping (< 15 m depth) and transient electromagnetic surveys for deeper mapping (~ 15 m to ~ 170 m). The transient electromagnetic method has potential for shallow mapping (< 15 m) as well as mapping to greater depths (> 170 m), but would require separate surveys with smaller and larger transmitter loops respectively. Another geophysical method with potential for subsurface geologic mapping in the APG setting is high-resolution seismic reflection surveying (Miller et al. 1995), which has the potential for higher vertical and horizontal resolution than the transient electromagnetic method. Miller et al. (1995) successfully mapped subsurface reflectors in the depth range 20 to 230 m; over this depth range and also for shallower and greater mapping depths, several acquisition geometries (source-geophone spacings and offsets) will be required for optimum mapping success. Seismic reflection surveys alone, however, may not detect some interfaces between clayey sediments and sandy sediments that are easily detectable by transient electromagnetic and electrical resistivity methods. As with any subsurface geologic mapping investigation, a complementary suite of geophysical methods is required for the APG setting, with the methods chosen based on specific mapping objectives and site details and physiography. Scopes of work for geophysical investigations should contain detailed mapping objectives and desired vertical and horizontal resolution. The suite of geophysical methods to be used for a specific investigation at APG should be selected and *justified* (relative to the mapping objectives and resolution requirements) by knowledgeable geophysicists and not specified in scopes of work prepared by others.

References

- AEHA. (1990). "RCRA facility assessment, Edgewood Area, Aberdeen Proving Ground, MD," No. 39-26-0490-90, U.S. Army Environmental Hygiene Agency, Aberdeen Proving Ground, MD.
- Burger, H. Robert. (1992). *Exploration Geophysics of the Shallow Sub-surface*, Prentice Hall, Englewood Cliffs, New Jersey.
- Butler, Dwain K. (1986). "Military Hydrology, Report 10: Assessment and field examples of continuous wave electromagnetic surveying for ground water," Miscellaneous Paper EL-79-6, U.S. Army Engineer Waterways Experiment Station, Vicksburg, MS.
- Butler, Dwain K. (1994). "Environmental geophysics: The best kept secret of environmental cleanup," *Proceedings of the 1994 Geotechnical Lecture Series: Current Topics in Geotechnical/Geoenvironmental Engineering*, Geotechnical Division, Illinois Section, American Society of Civil Engineers.
- Butler, Dwain K., and Curro, Joseph R. (1981). "Crosshole seismic testing: Procedures and pitfalls," *Geophysics*, Vol 46, pp 23-29.
- Butler, Dwain K., Gangi, Anthony F., Wahl, Ronald E., Yule, Donald E., and Barnes, Donald E. (1982). "Analytical and data processing techniques for interpretation of geophysical survey data," Miscellaneous Paper GL-82-16, U.S. Army Engineer Waterways Experiment Station, Vicksburg, MS.
- Butler, Dwain K. and Llopis, Jose L. (1984). "Military Hydrology, Report 6: Assessment of two currently fieldable geophysical methods for military ground-water detection," Miscellaneous Paper EL-79-6, U.S. Army Engineer Waterways Experiment Station, Vicksburg, MS.
- Butler, Dwain K., and Fitterman, David V. (1986). "Transient electromagnetic methods for ground-water assessment," Miscellaneous Paper GL-86-27, U.S. Army Engineer Waterways Experiment Station, Vicksburg, MS.

- Butler, Dwain K., Llopis, Jose L., Yule, Donald E., Sharp, Michael K., and Dardeau, Elba A. (1990). "Water Detection Response Team Geophysics Element case histories," Technical Report GL-90-23, U.S. Army Engineer Waterways Experiment Station, Vicksburg, MS.
- Corps of Engineers. (1994). "Remedial investigation and feasibility study, Cluster 13, Edgewood Area, Aberdeen Proving Ground, Part 1: Remedial investigation," Draft Final (June 1994), U.S. Army Engineer Waterways Experiment Station and U.S. Army Engineer District, Baltimore.
- Fenneman, Nevin M. (1938). *Physiography of Eastern United States*, McGraw-Hill, New York.
- Interpex. (1993). "TEMIXGL v. 3.0--User's Manual," Interpex, Ltd., Golden, CO.
- Interpex. (1988). "RESIX Plus, User's Manual," Interpex, Ltd., Golden, CO.
- McNeill, J.D. (1980). "Applications of Transient Electromagnetic Techniques," Technical Note TN-7, Geonics, Ltd., Mississauga, Ontario, Canada.
- Miller, Richard D., Xia, Jianghai, Anderson, Joe M., Laflen, David R., and Marcus, Sara. (1995). "High resolution seismic reflection profiling at Aberdeen Proving Grounds, Maryland," Open-File Report No. 95-22, Kansas Geological Survey for U.S. Army Engineer Waterways Experiment Station, Lawrence, KS.
- R&R International, Inc. (1994). "Work plan for removal action of surface debris at the School Fields training areas, Edgewood Area, Aberdeen Proving Ground, Maryland," for Baltimore District, U.S. Army Corps of Engineers.
- Redpath, Bruce B. (1973). "Seismic refraction exploration for engineering site investigations," Technical Report E-73-4, U.S. Army Engineer Waterways Experiment Station, Vicksburg, MS.
- Scott, James H. (1973). "Seismic refraction modeling by computer," *Geophysics*, Vol. 38, pp 271-284.
- Sharp, Michael K., and Lee, Landris T. (1995). "Geophysical Investigation of Cluster 13, Edgewood Area, Aberdeen Proving Ground, Maryland," Miscellaneous Paper GL-95-9, U.S. Army Engineer Waterways Experiment Station, Vicksburg, MS.
- Simms, Janet E. and Butler, Dwain K. (1992). "Assessment and selection of an automated electrical resistivity interpretation procedure,"

Technical Report GL-92-12, U.S. Army Engineer Waterways Experiment Station, Vicksburg, MS.

Taylor, K. C., Hess, J. W., and Mazzela, A. (1989). "Field evaluation of a slim-hole borehole induction tool," *Ground Water Monitoring Review*, Vol. IX, No. 1, pp 100-104.

Telford, W. M., Geldart, L. P., and Sheriff, R. E. (1990). *Applied Geophysics*, Cambridge University Press, New York.

Vokes, H. E. (1957). "Geography and geology of Maryland," Bulletin 19, Maryland Geological Survey, Baltimore, MD.

Whitten, Charlie B., Miller, S. Paul, Derryberry, Nancy A. (1992). "Aberdeen Area Fire Training Area, Hydrologic Assessment, Aberdeen Proving Ground," Technical Report GL-92-20, U.S. Army Engineer Waterways Experiment Station, Vicksburg, MS.

Yule, Donald E., and Sharp, Michael K. (1990). "Seismic refraction data processing software: Seismo Version 2.7," Instruction Report GL-90-2, U.S. Army Engineer Waterways Experiment Station, Vicksburg, MS.

Appendix A

Seismic Refraction Time-Distance Data Plots

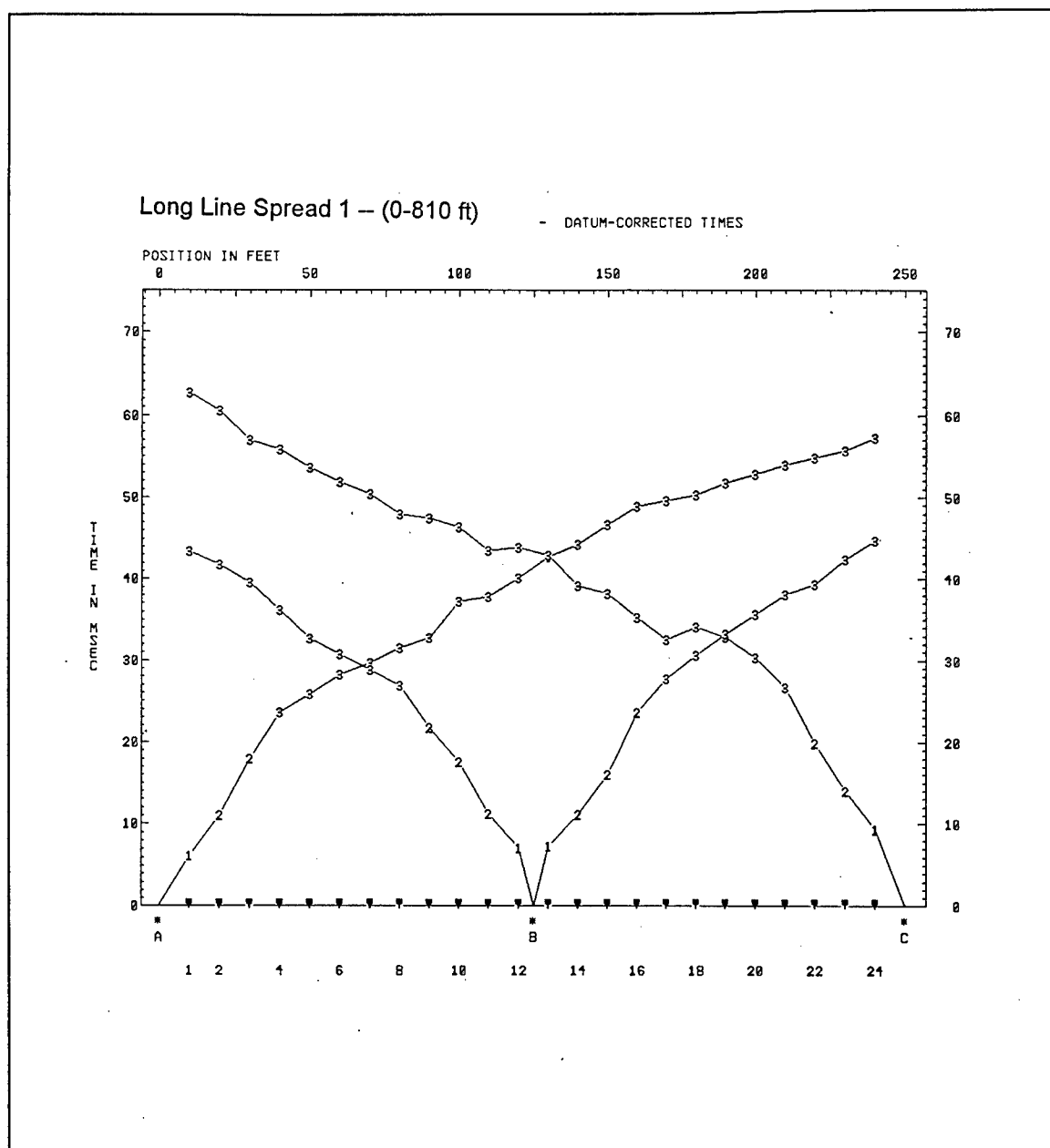


Figure A1. Long line spread 1—time-distance (Sheet 1 of 5)

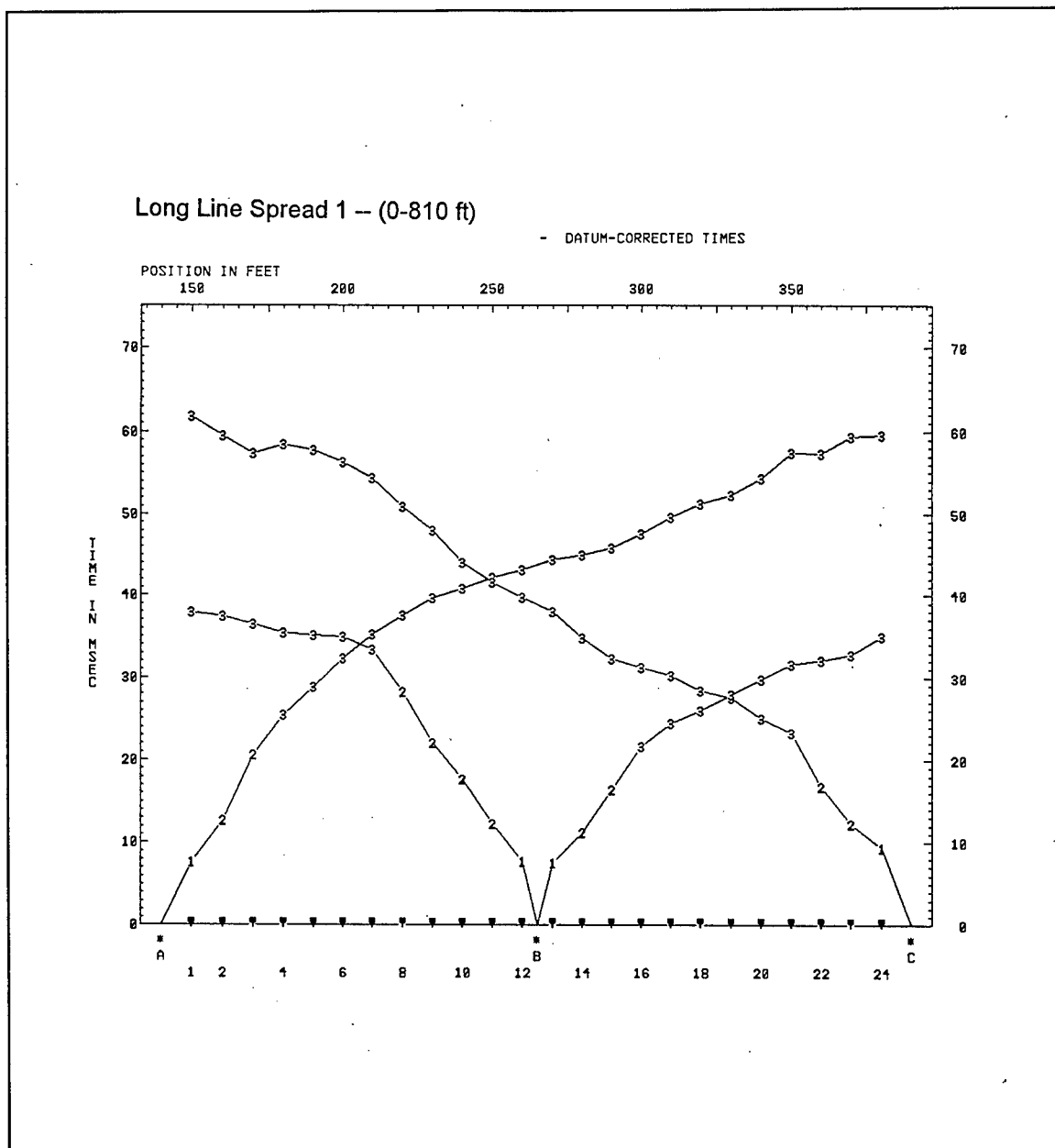


Figure A1. (Sheet 2 of 5)

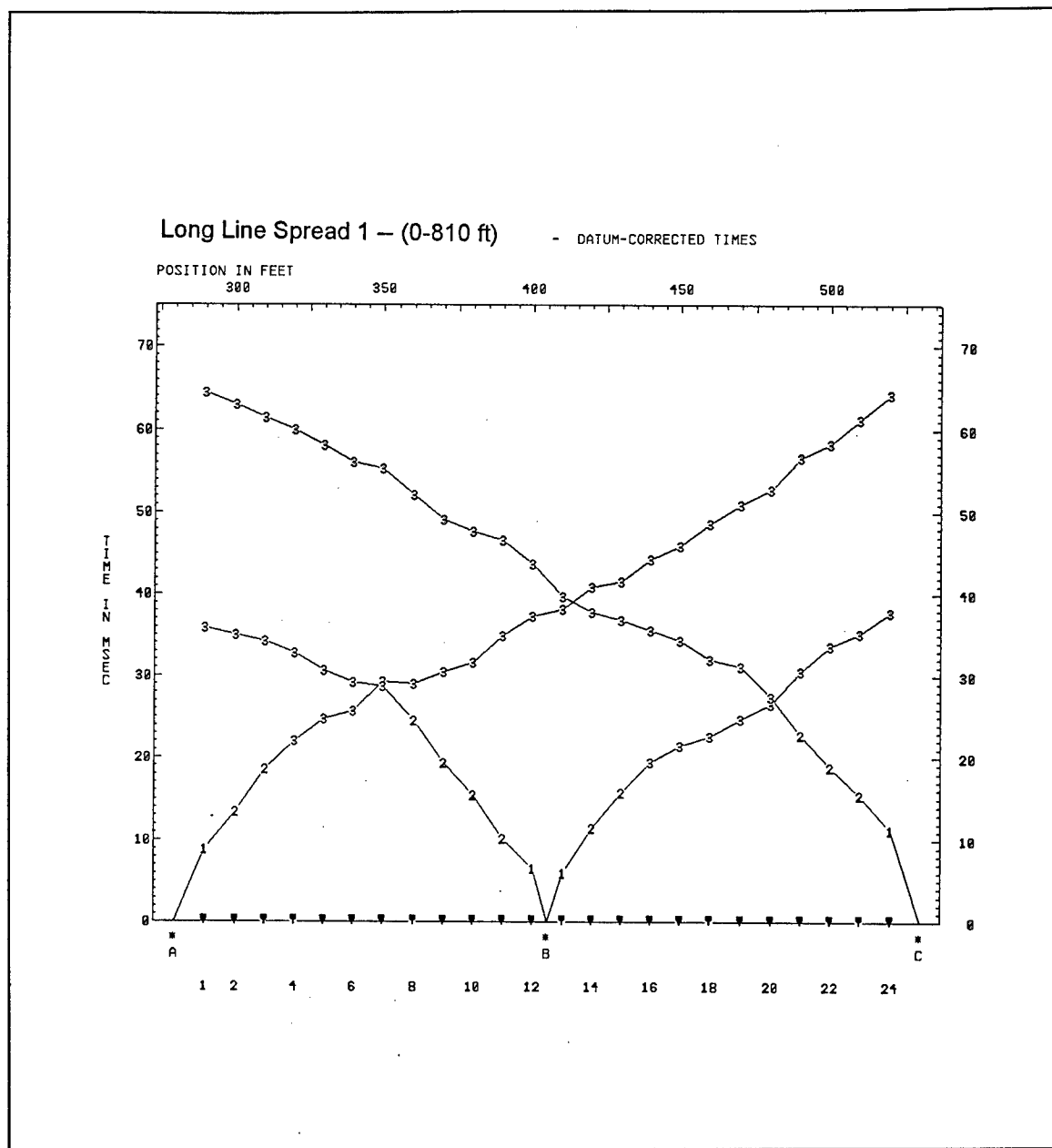


Figure A1. (Sheet 3 of 5)

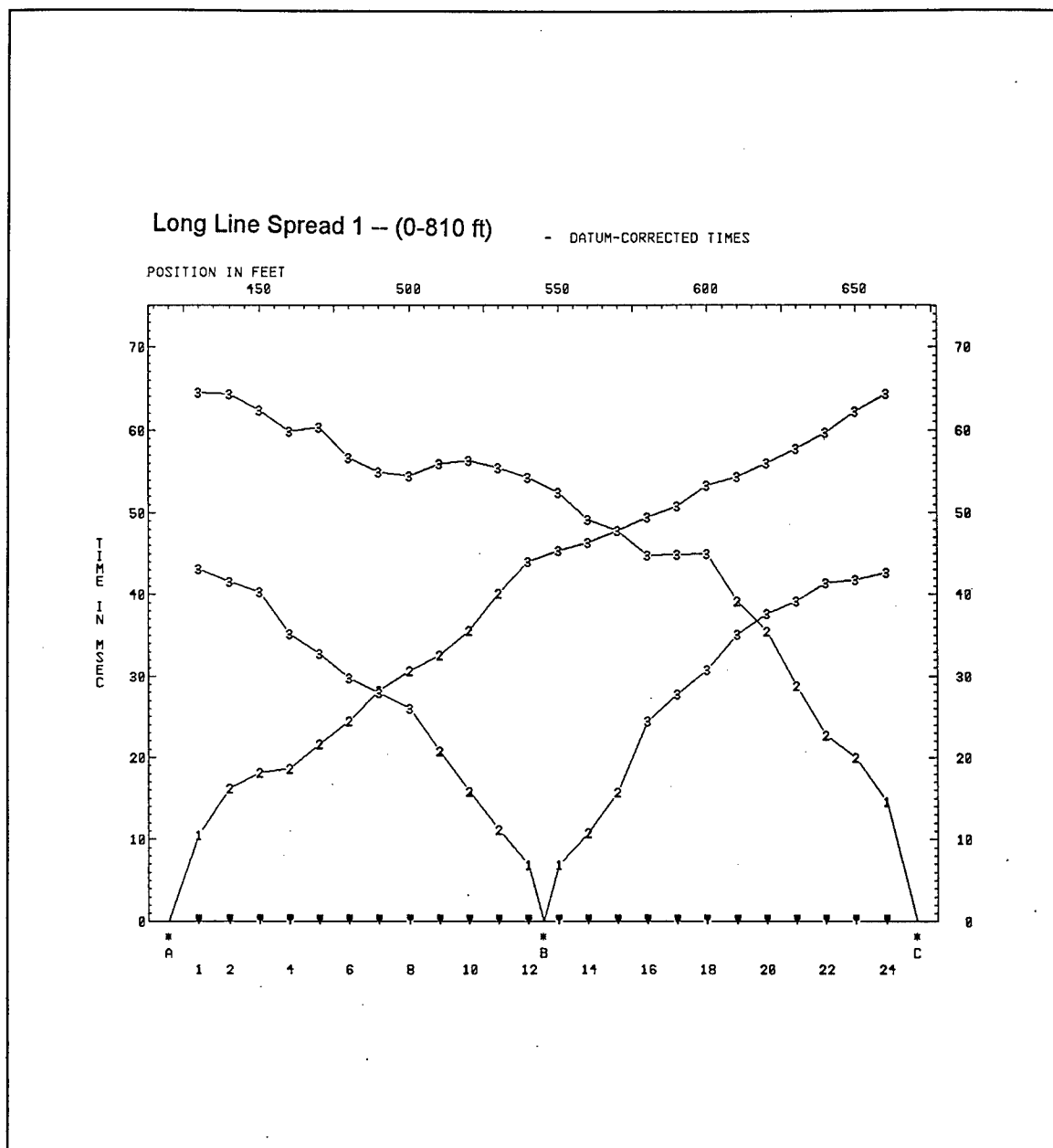


Figure A1. (Sheet 4 of 5)

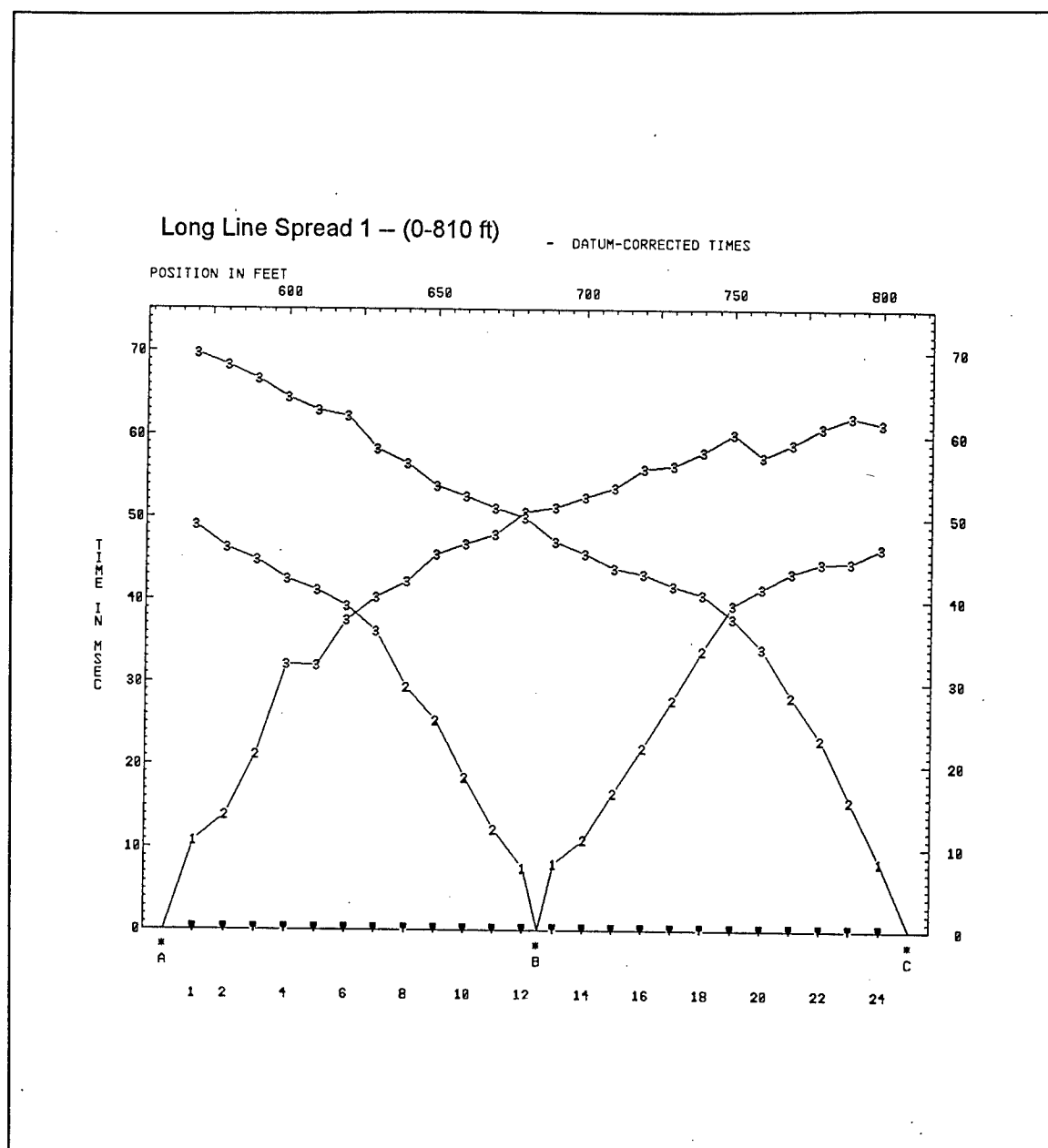


Figure A1. (Sheet 5 of 5)

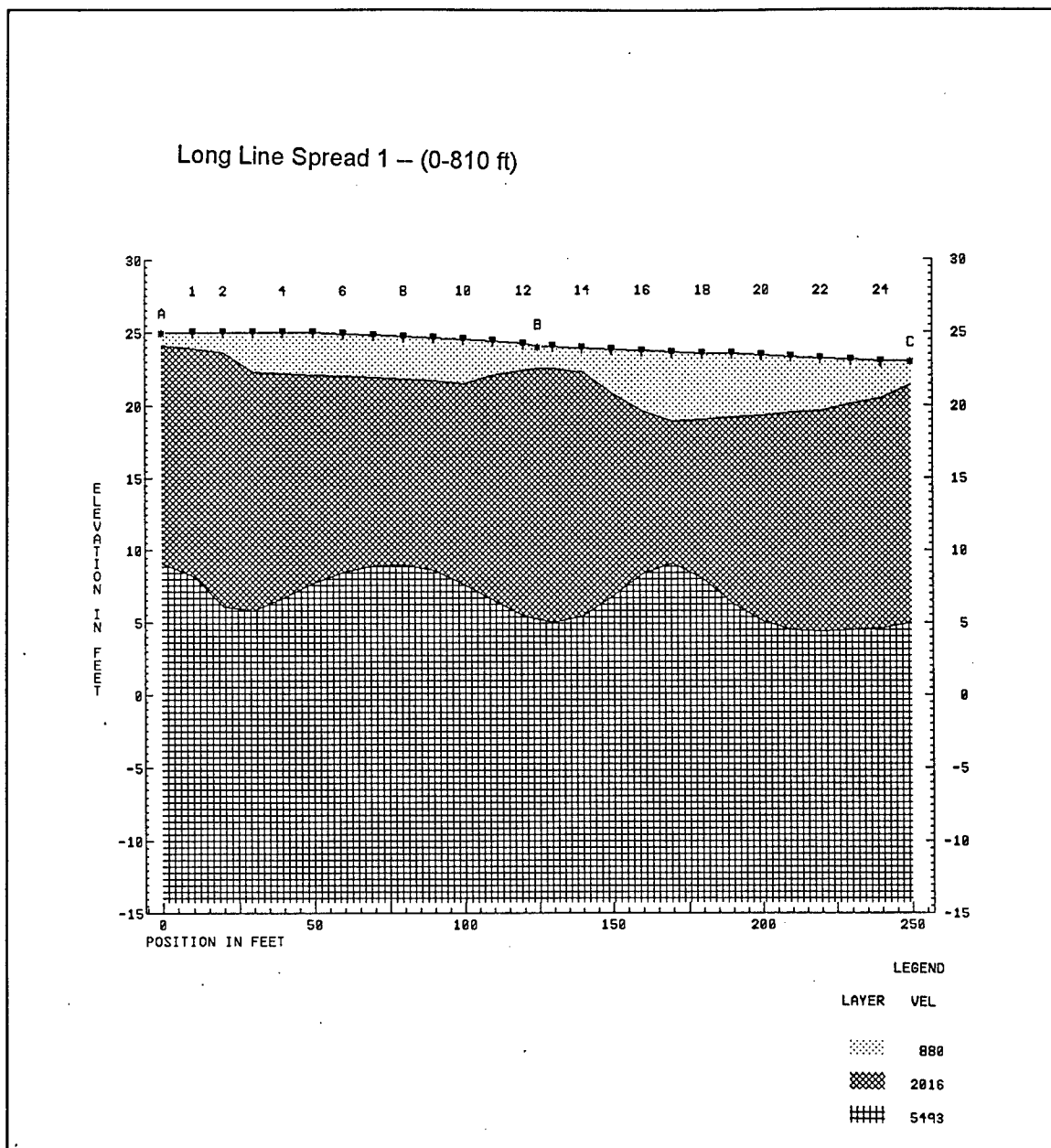


Figure A2. Long line spread 1—cross-section (Sheet 1 of 5)

Long Line Spread 1 -- (0-810 ft)

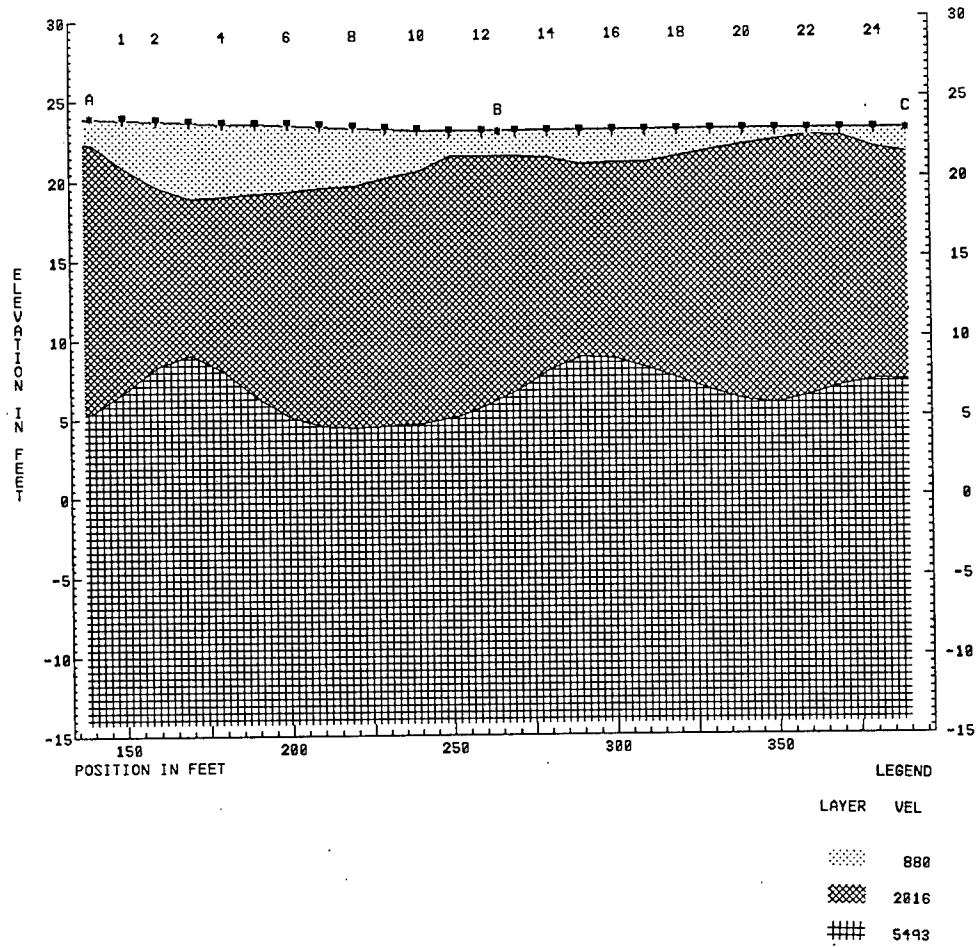


Figure A2. (Sheet 2 of 5)

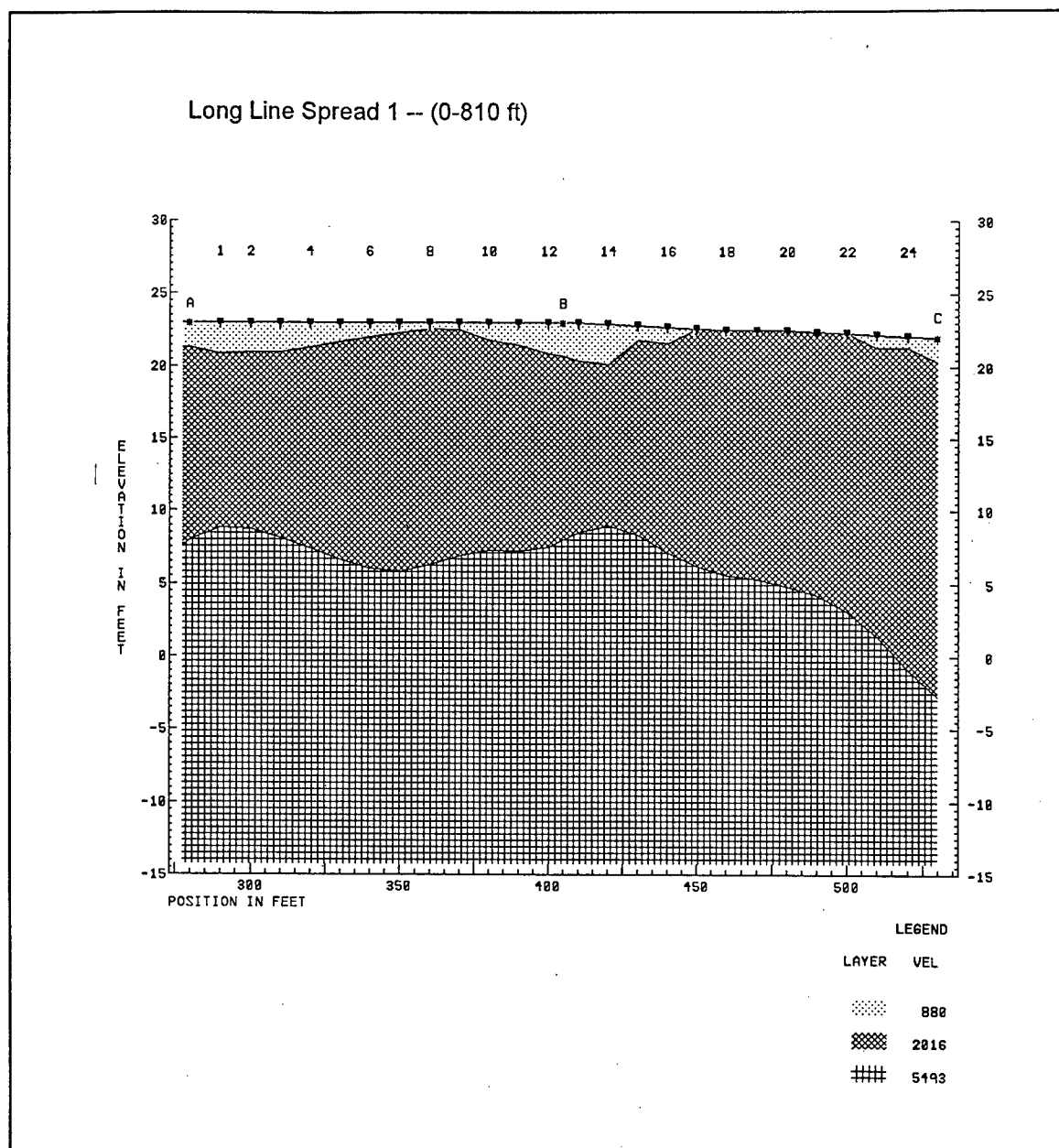


Figure A2. (Sheet 3 of 5)

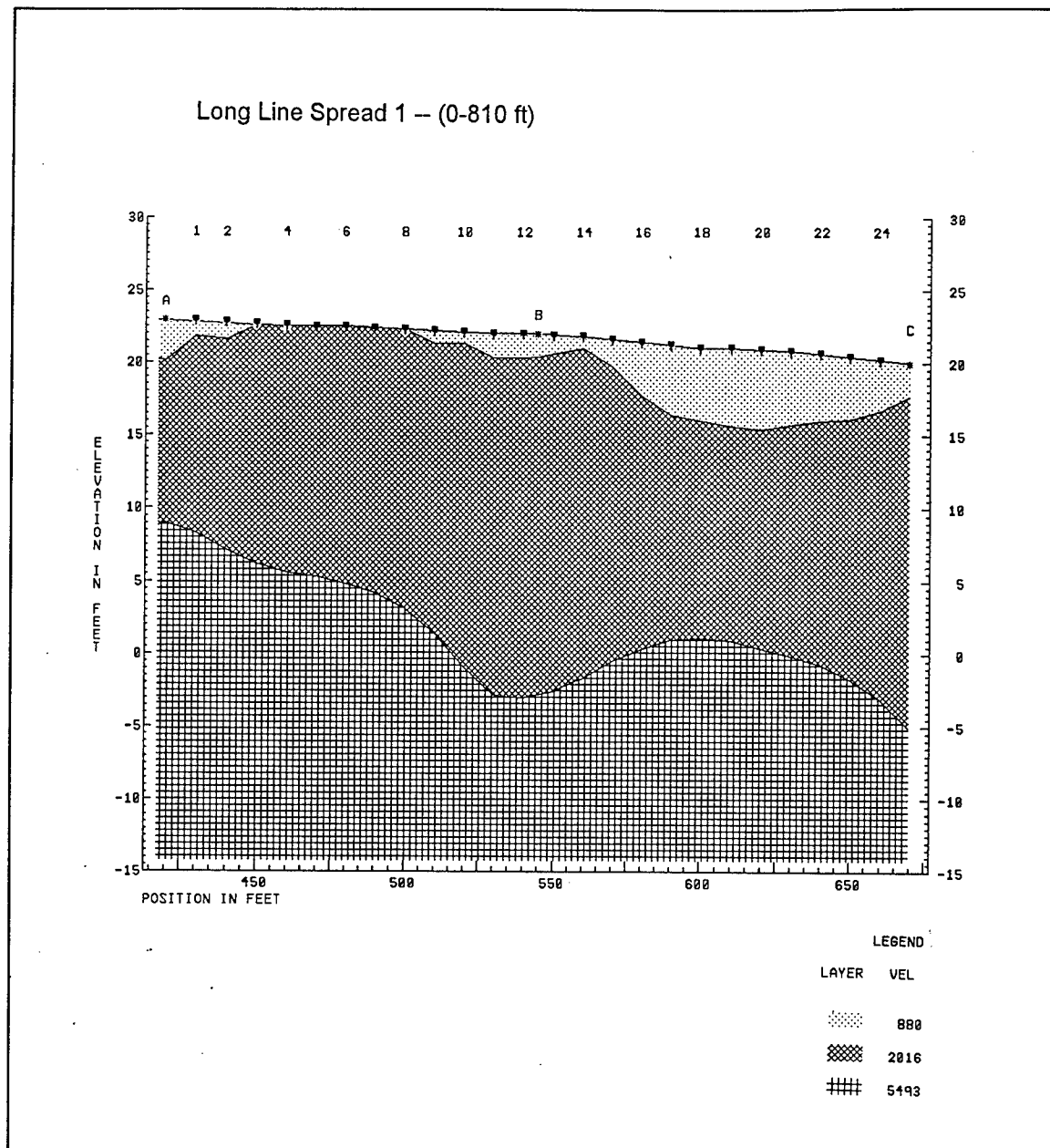


Figure A2. (Sheet 4 of 5)

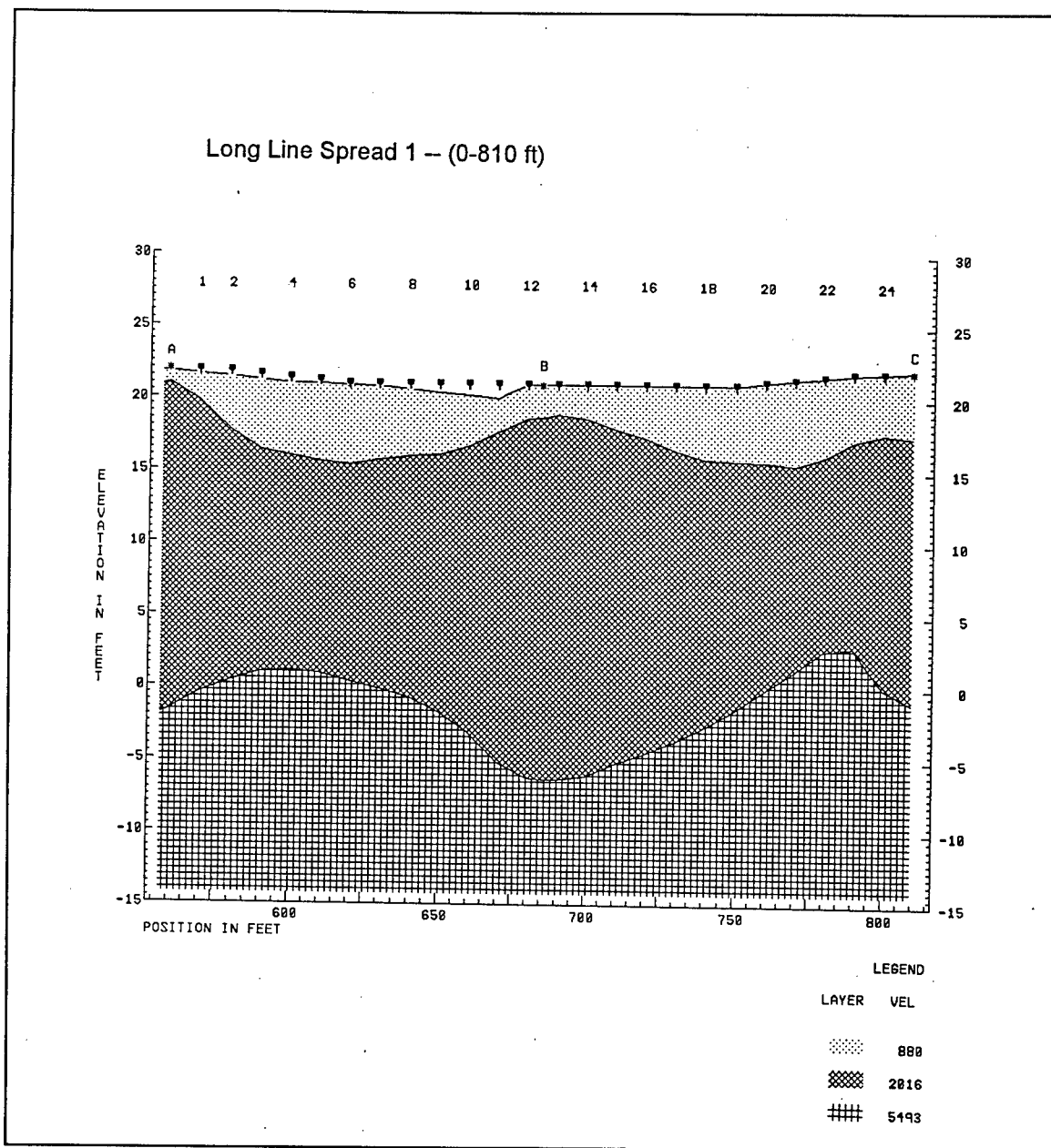


Figure A2. (Sheet 5 of 5)

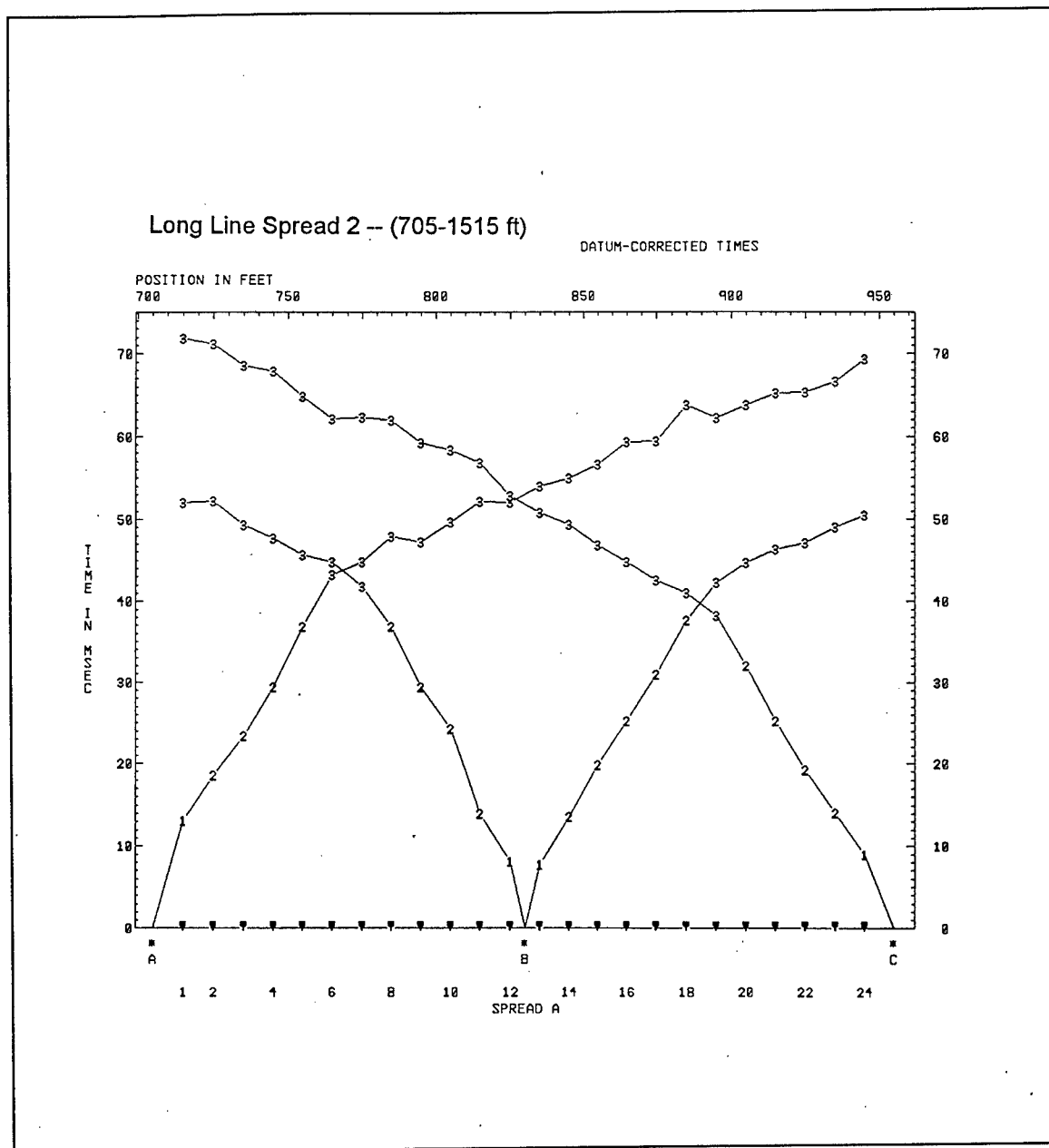


Figure A3. Long line spread 2—time-distance (Sheet 1 of 5)

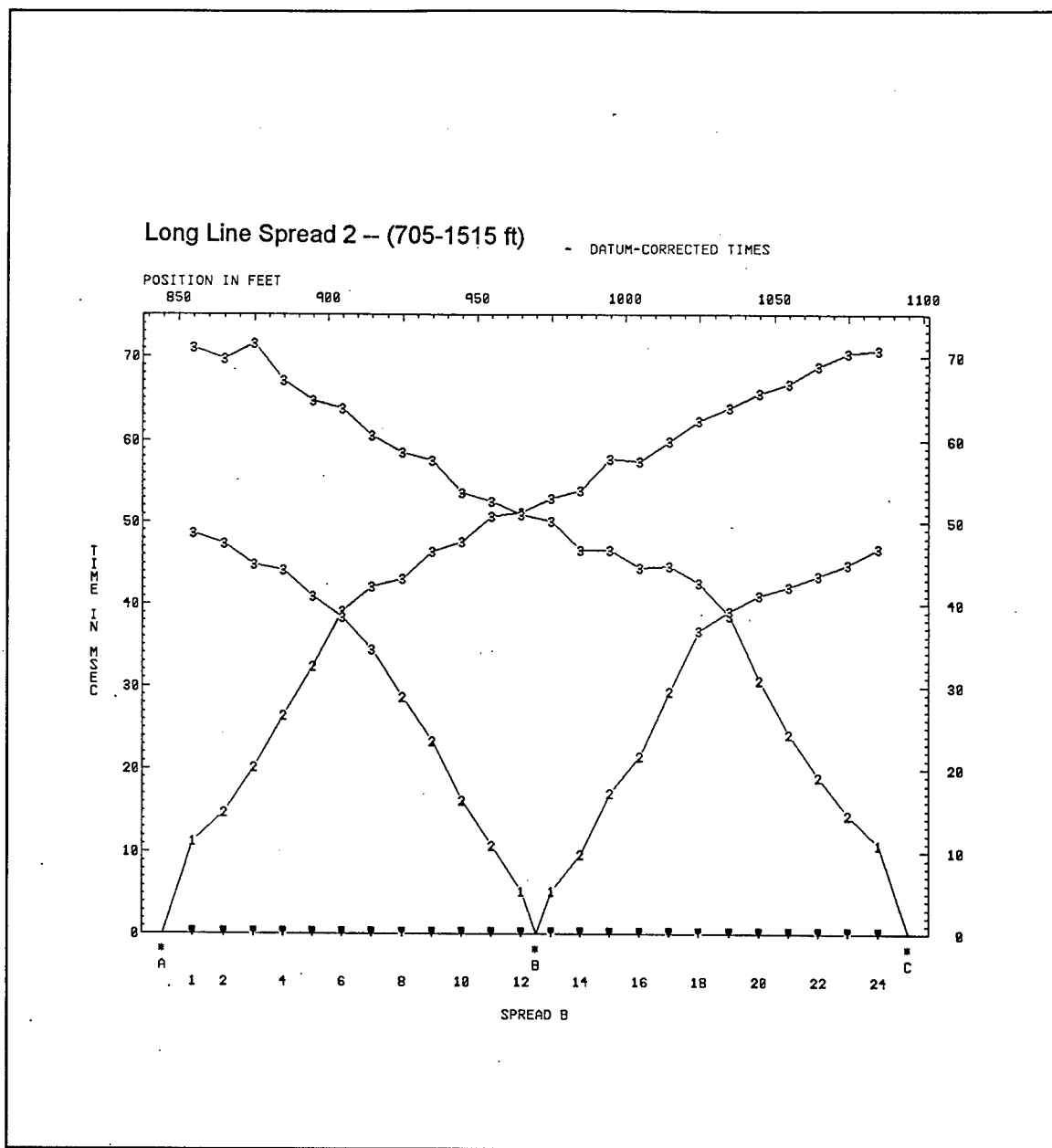


Figure A3. (Sheet 2 of 5)

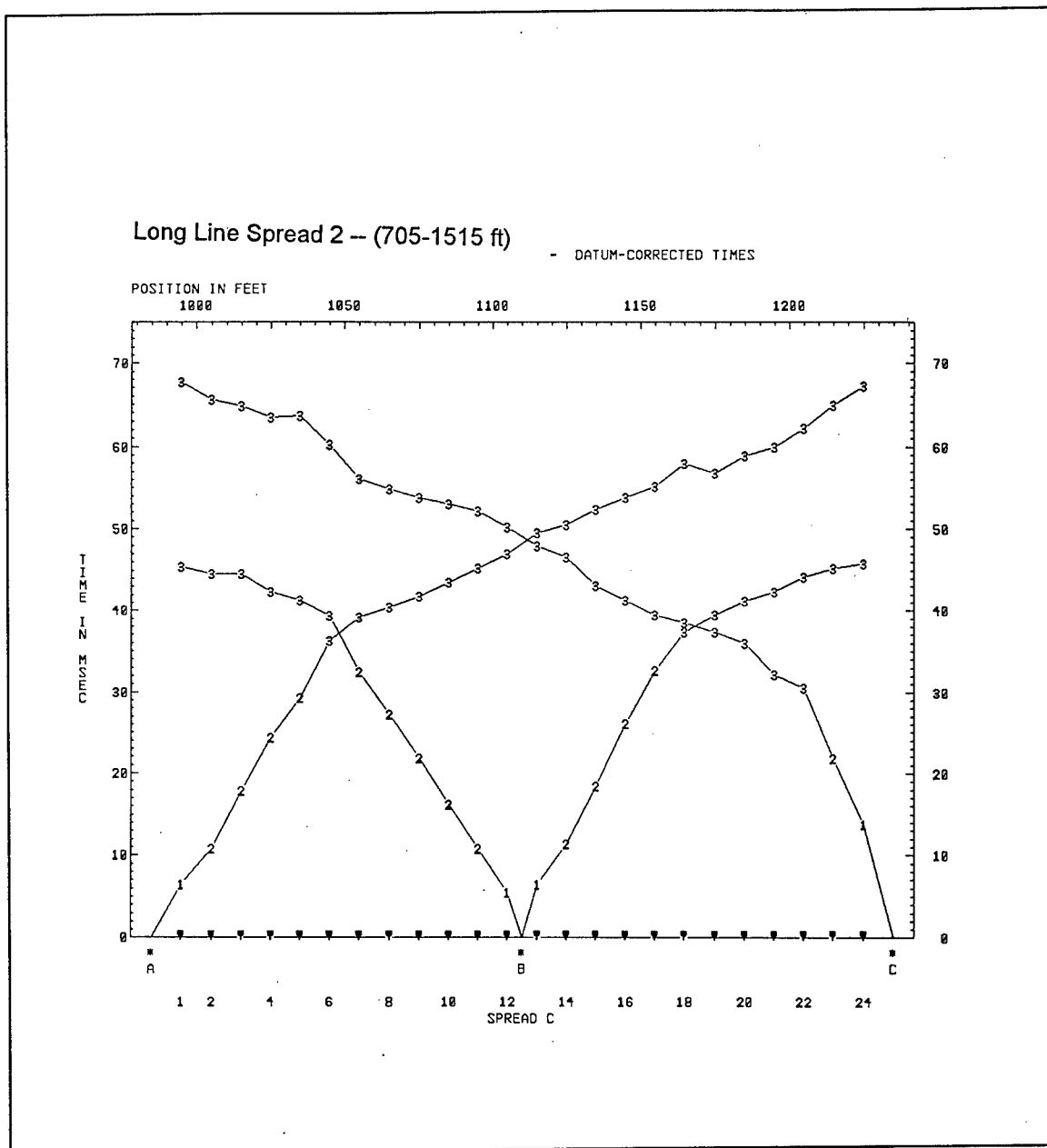


Figure A3. (Sheet 3 of 5)

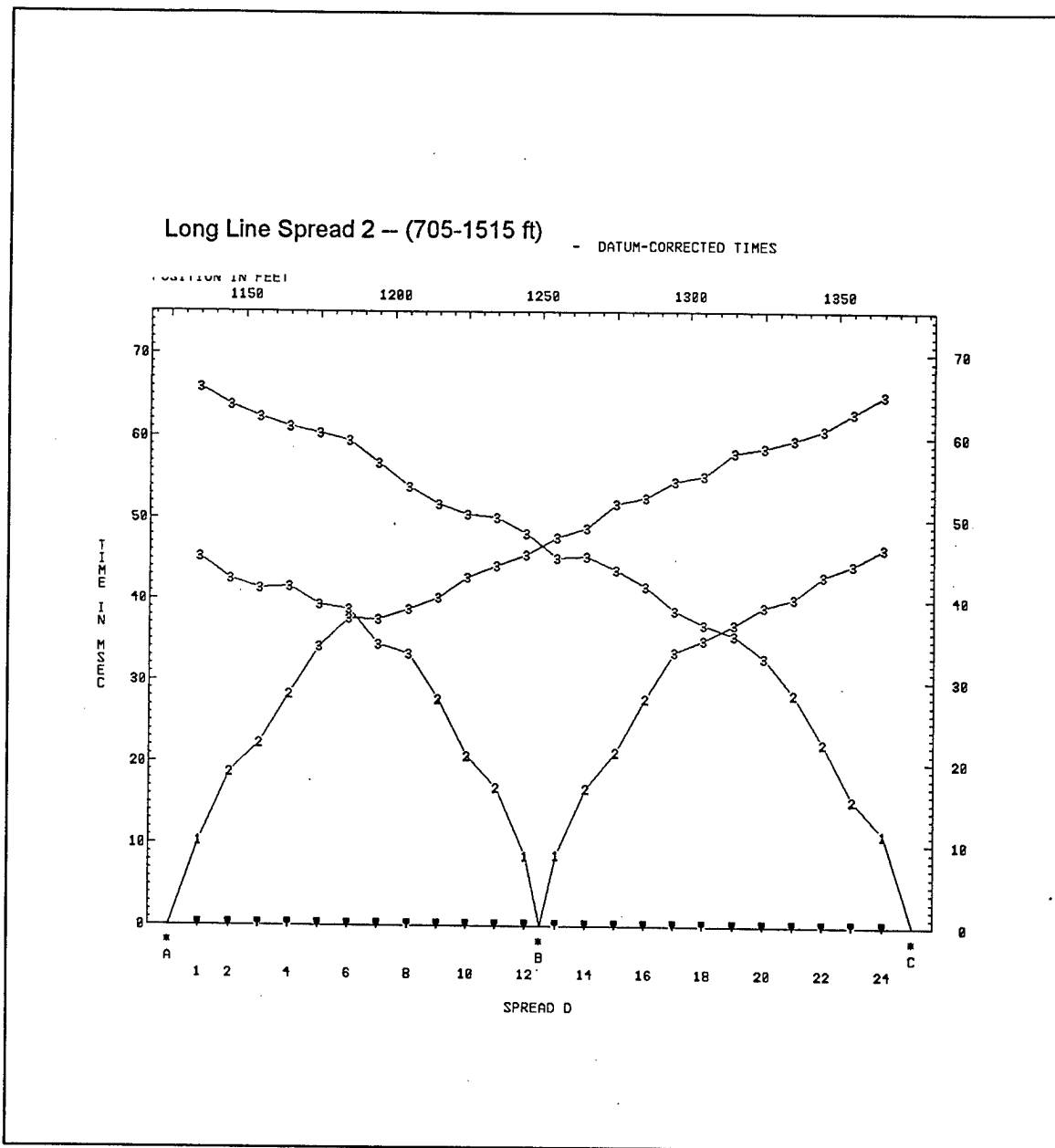


Figure A3. (Sheet 4 of 5)

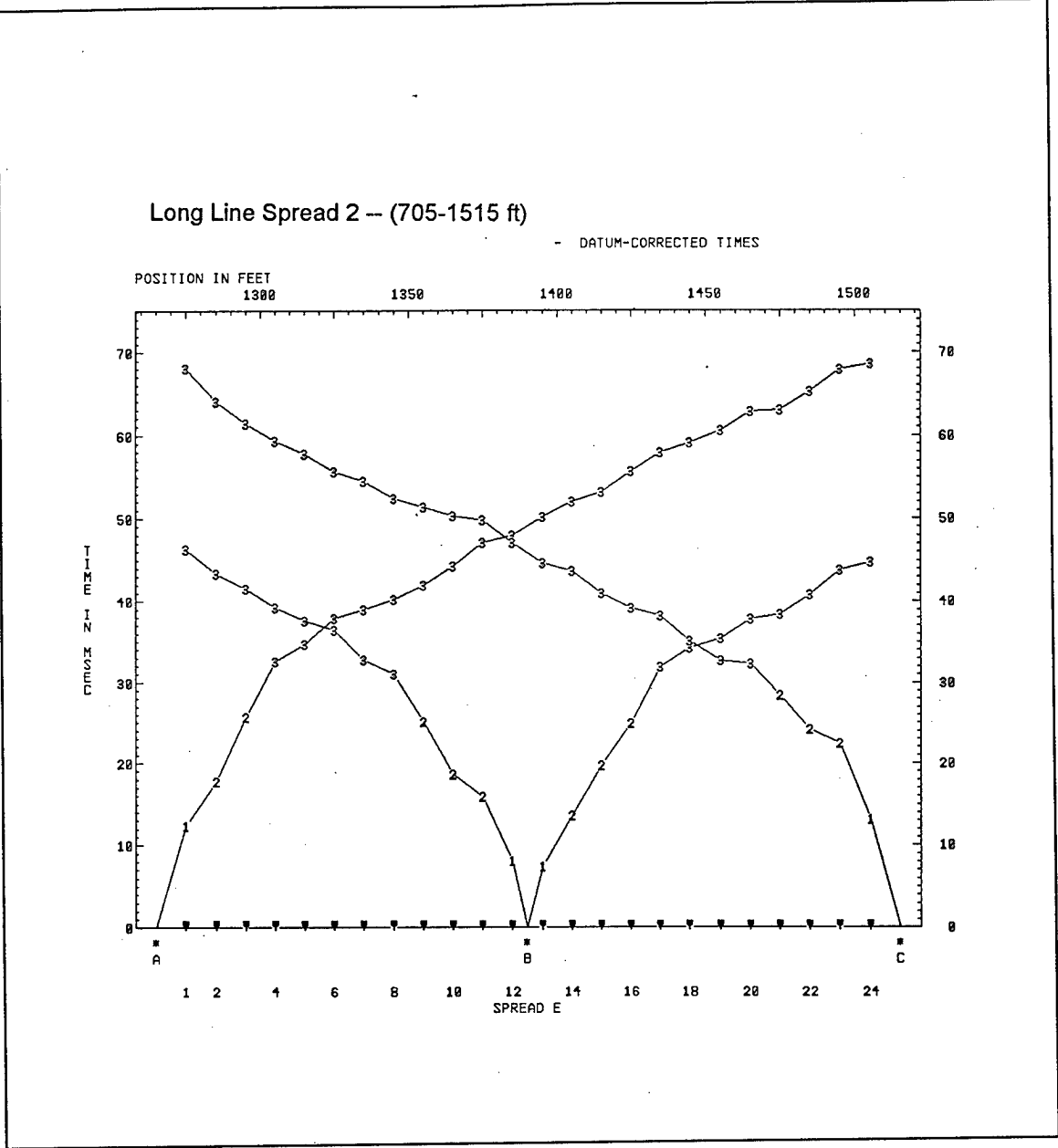


Figure A3. (Sheet 5 of 5)

Long Line Spread 2 -- (705-1515 ft)

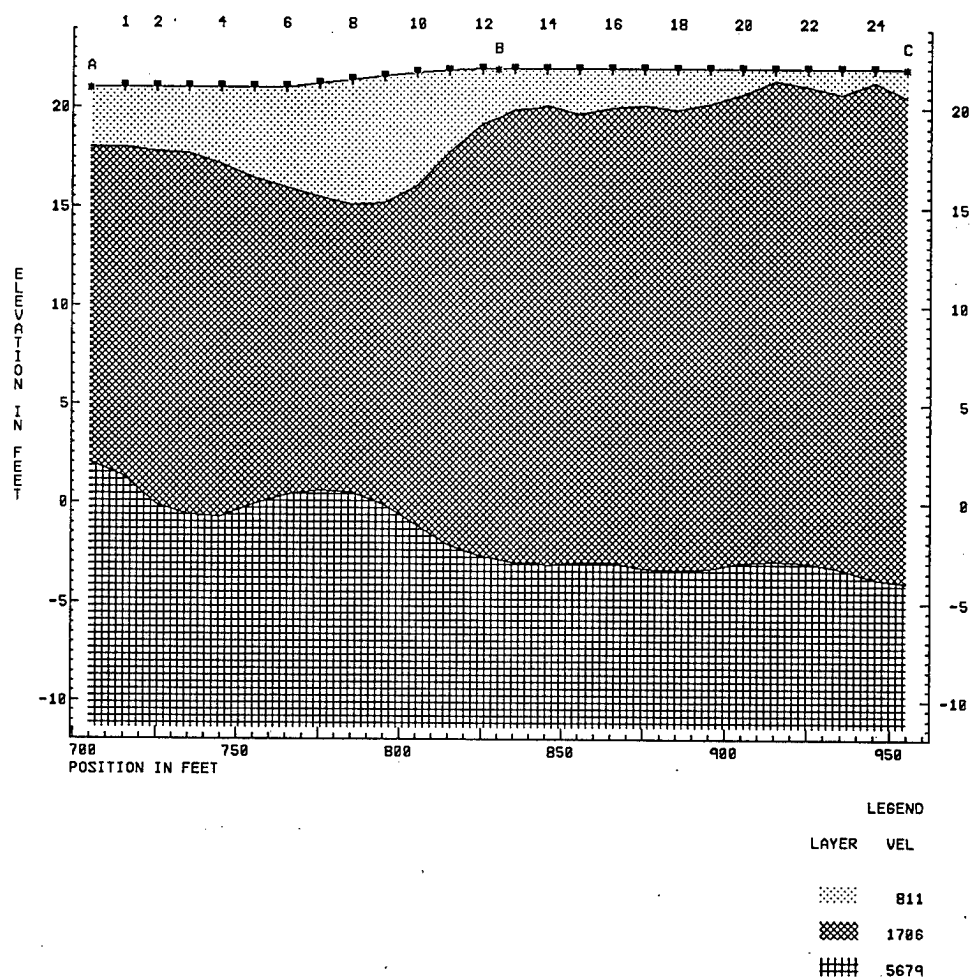


Figure A4. Long line spread 2—cross-section (Sheet 1 of 5)

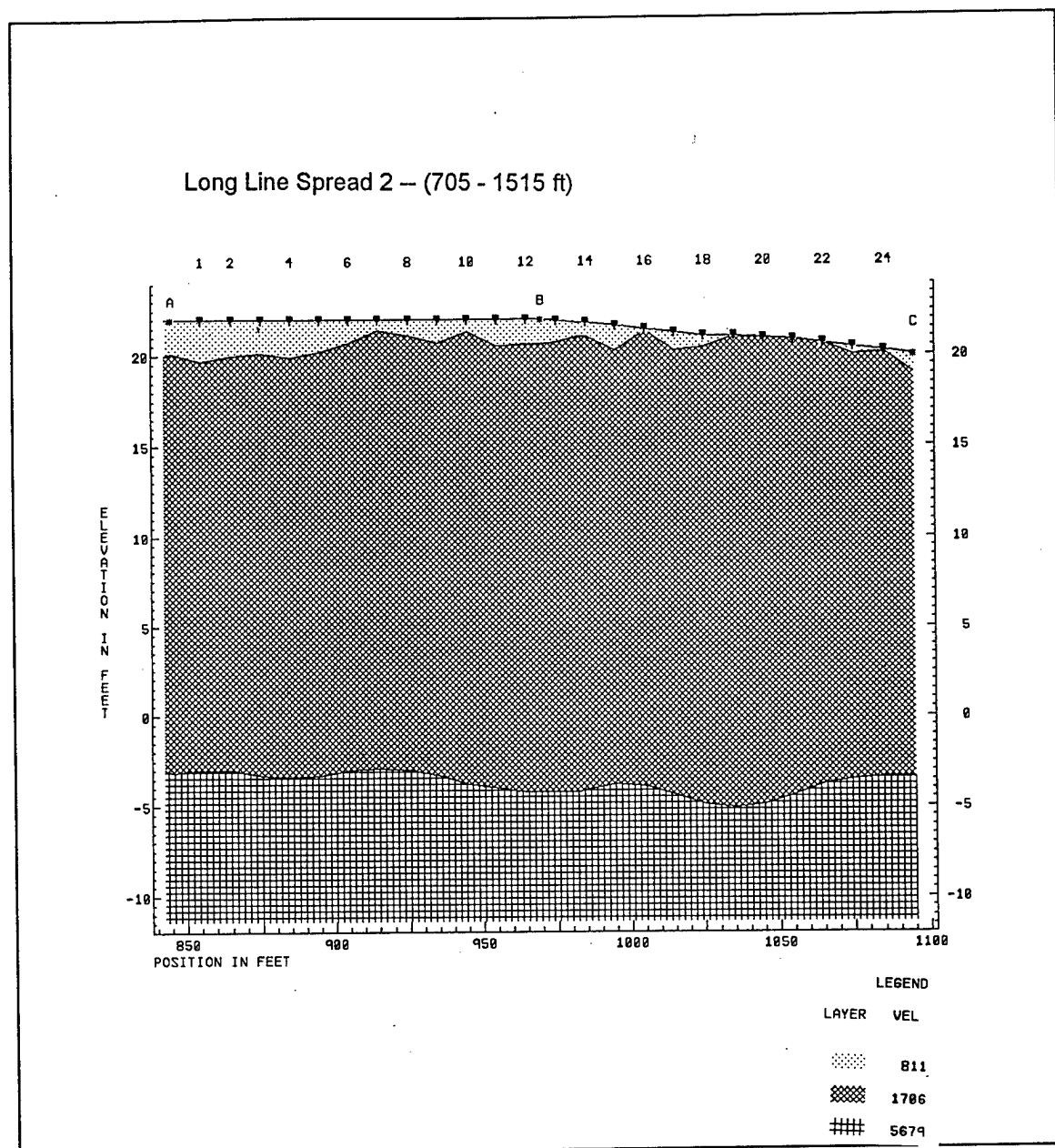


Figure A4. (Sheet 2 of 5)

Long Line Spread 2 -- (705 - 1515 ft)

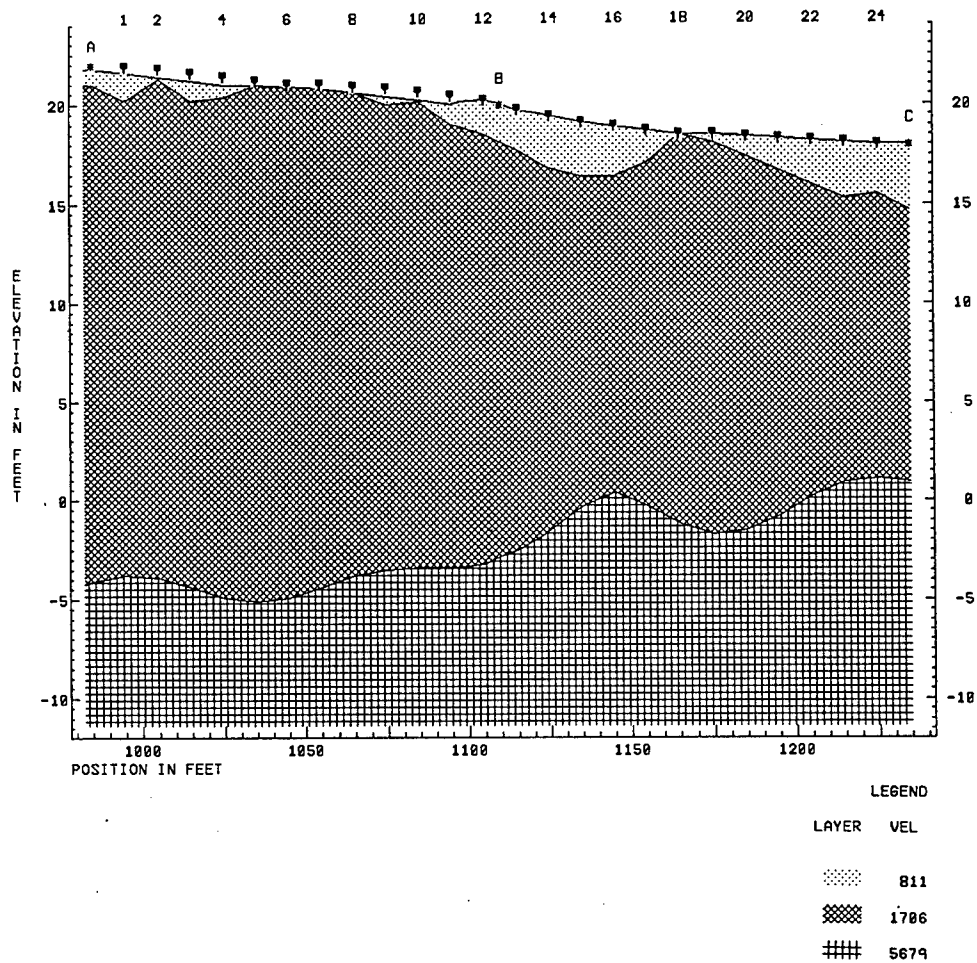


Figure A4. (Sheet 3 of 5)

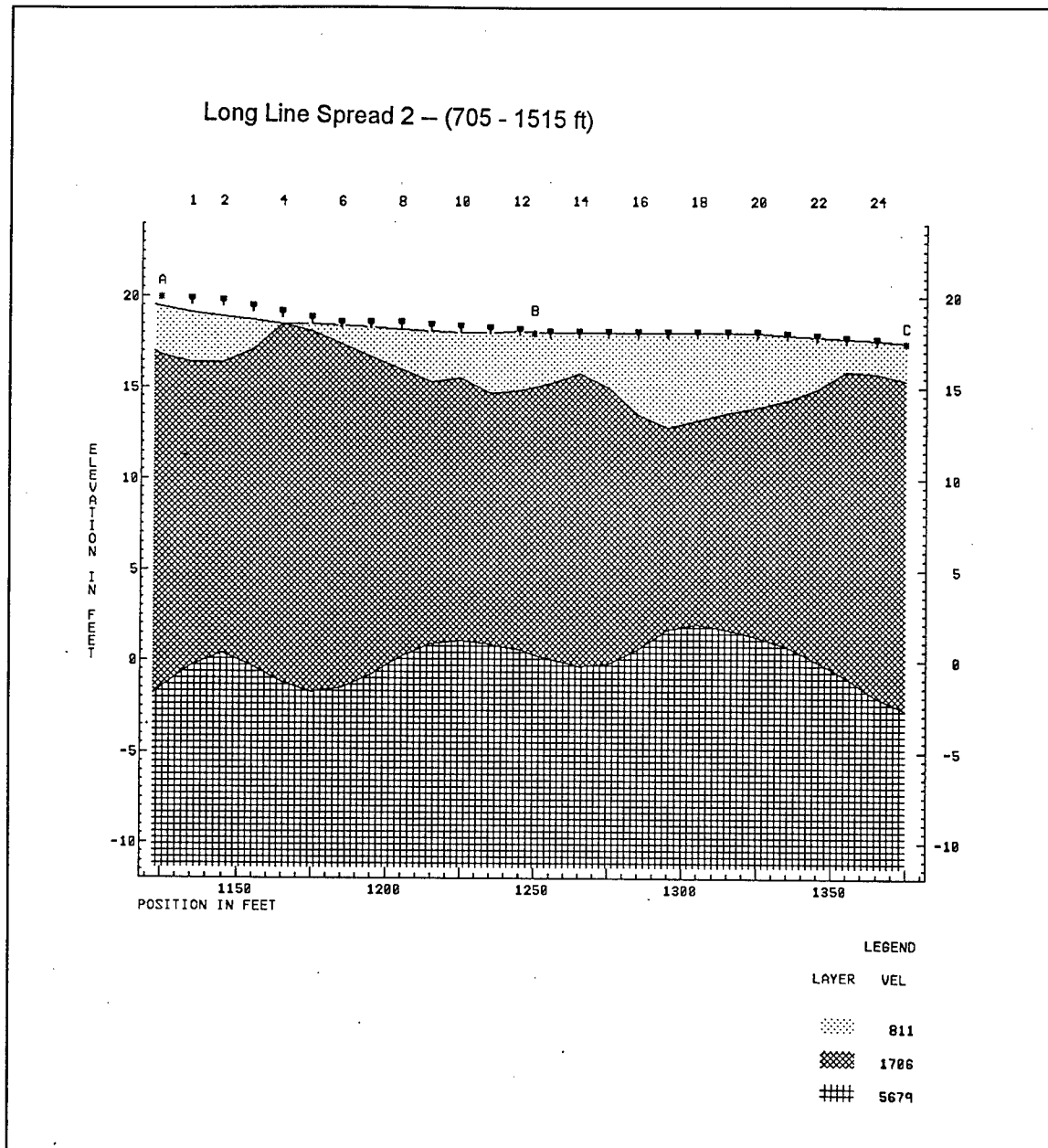


Figure A4. (Sheet 4 of 5)

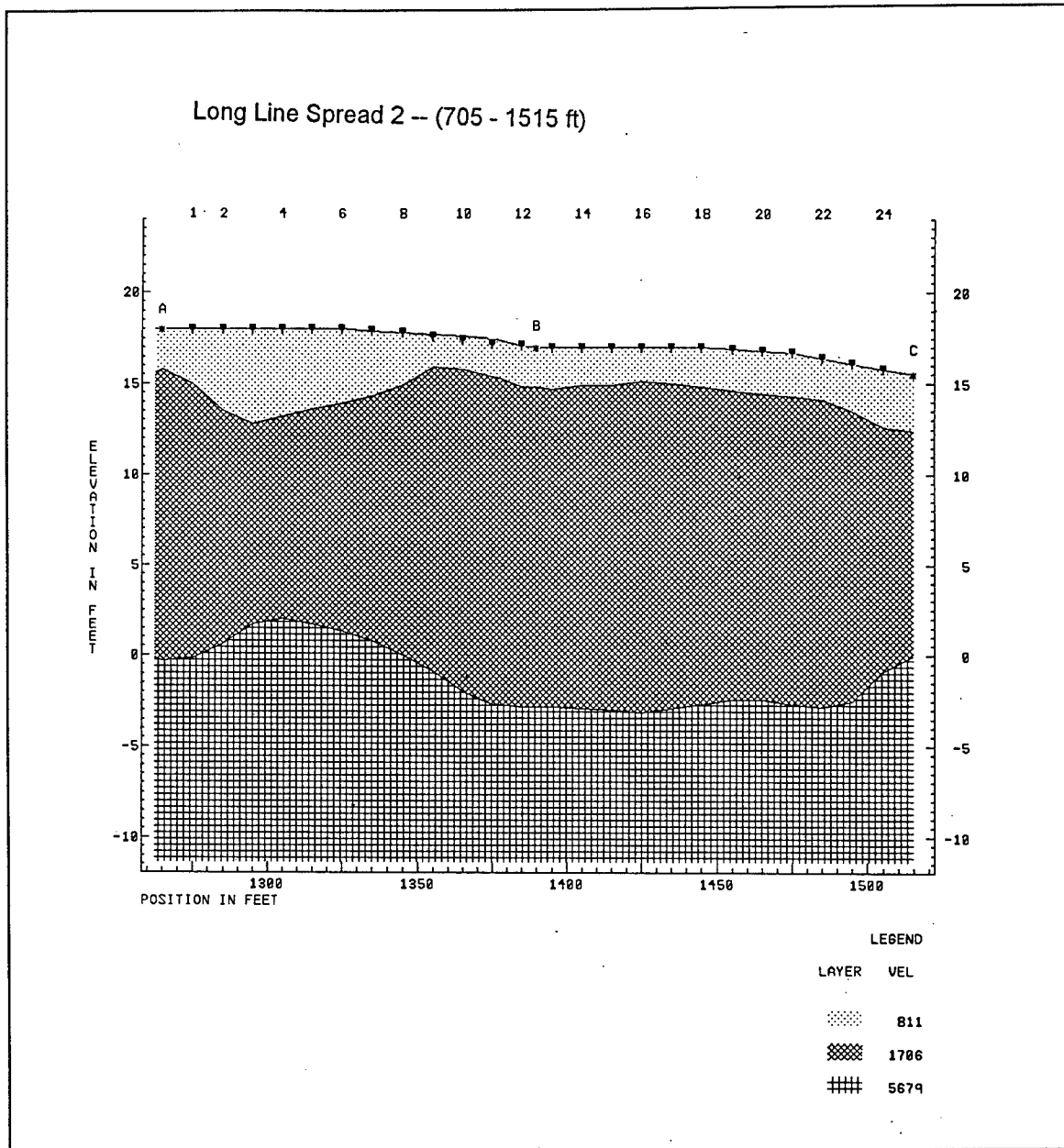


Figure A4. (Sheet 5 of 5)

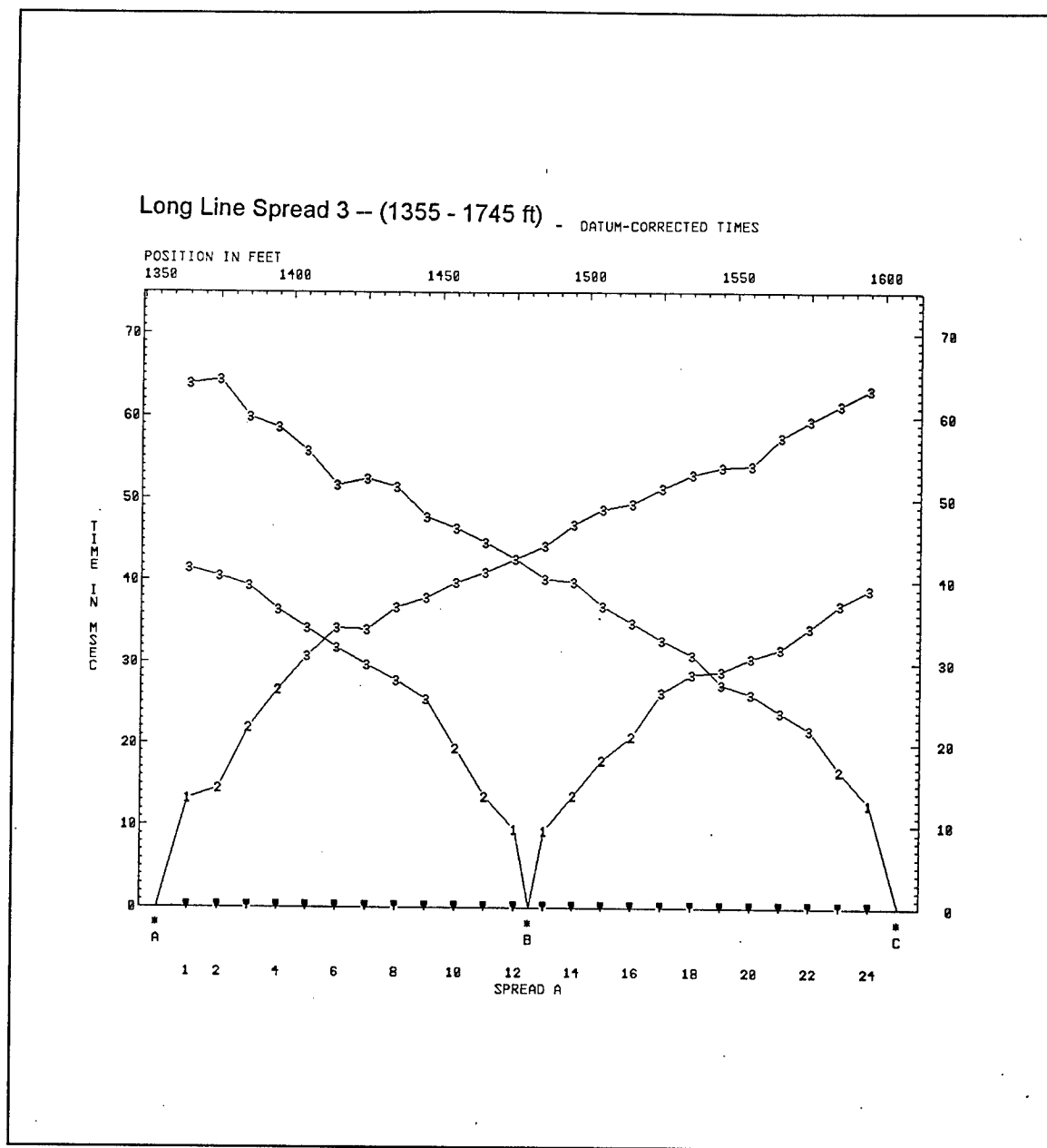


Figure A5. Long line spread 3—time-distance (Continued)

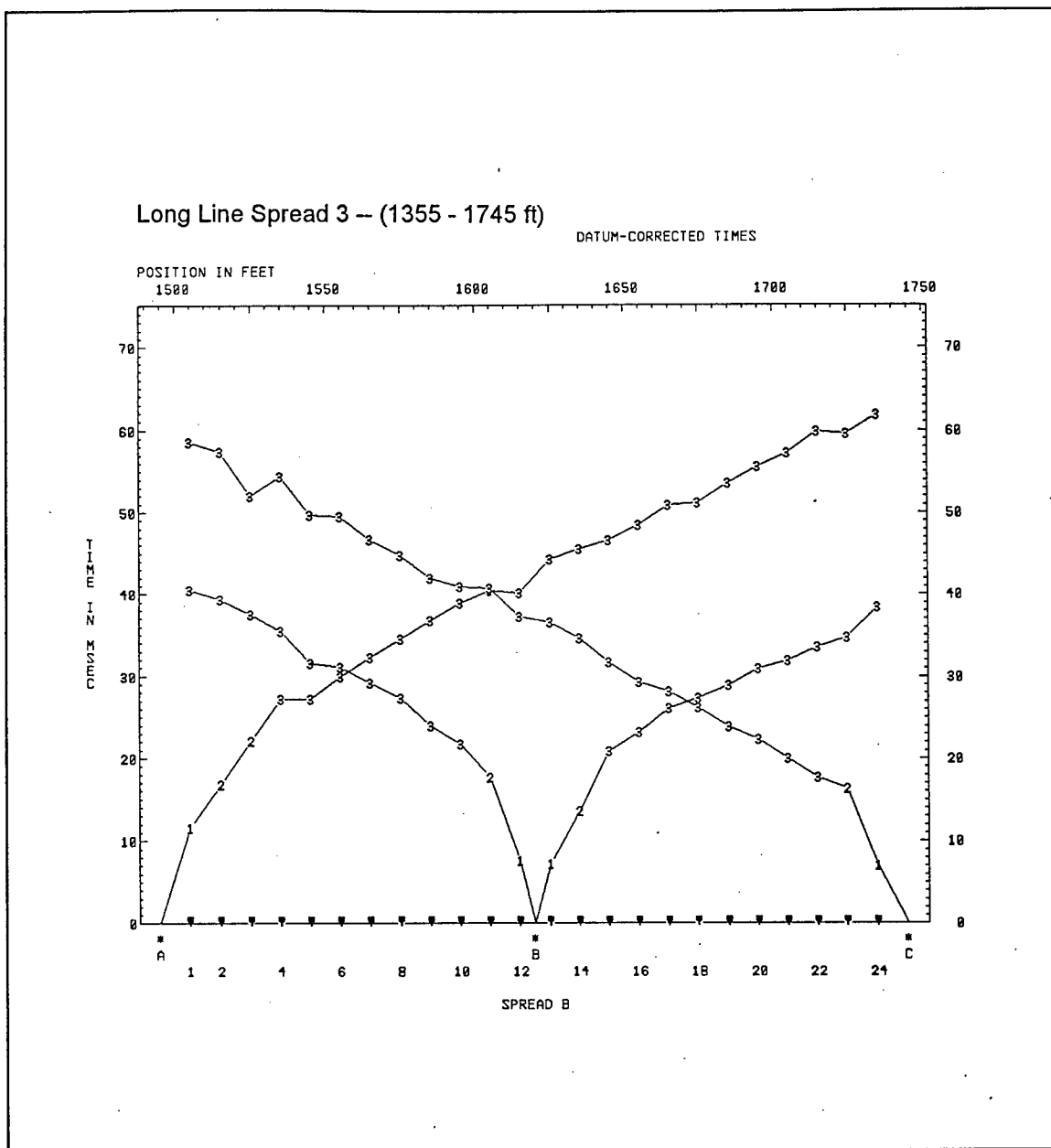


Figure A5. (Concluded)

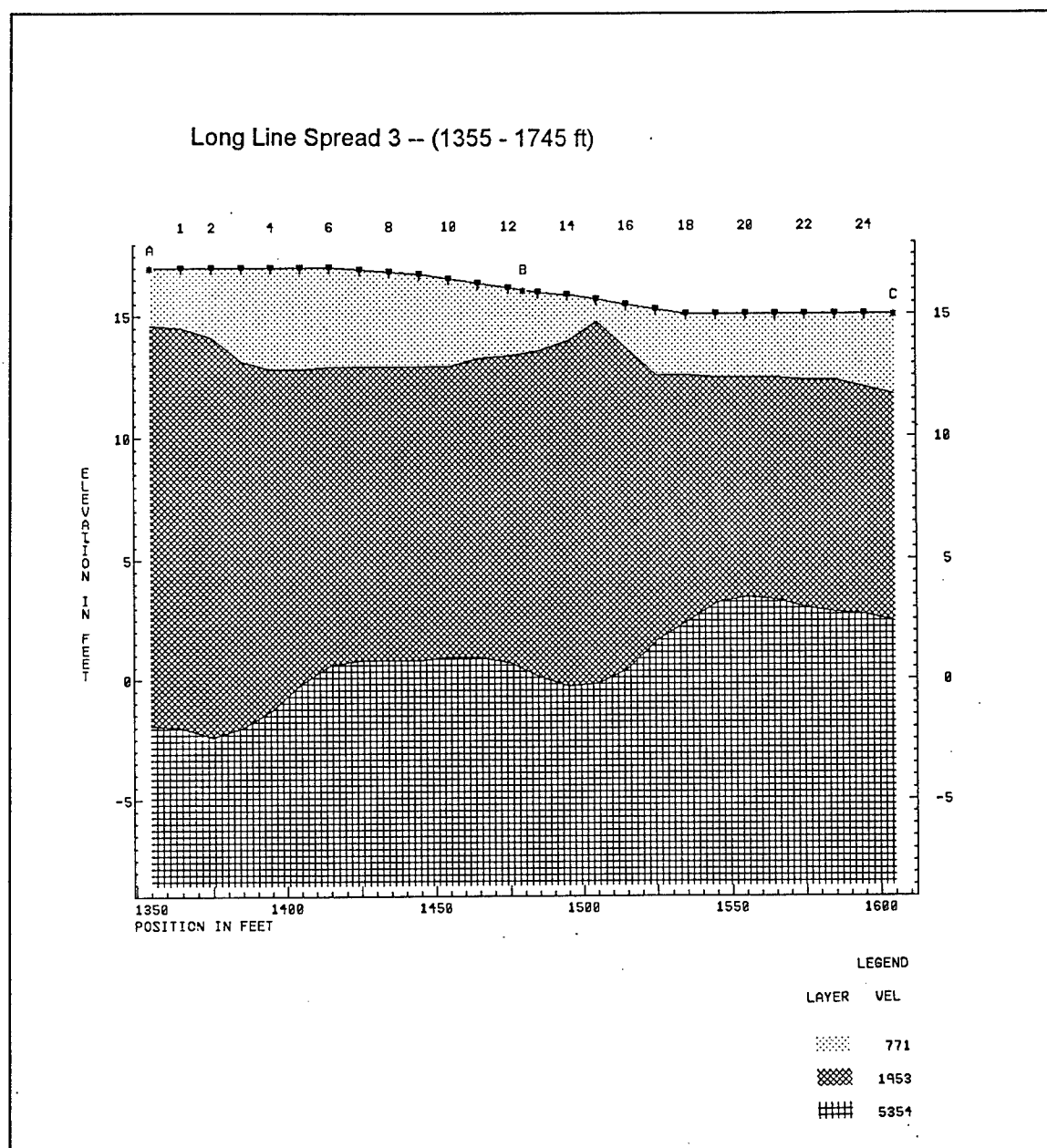


Figure A6. Long line spread 3—cross-section (Continued)

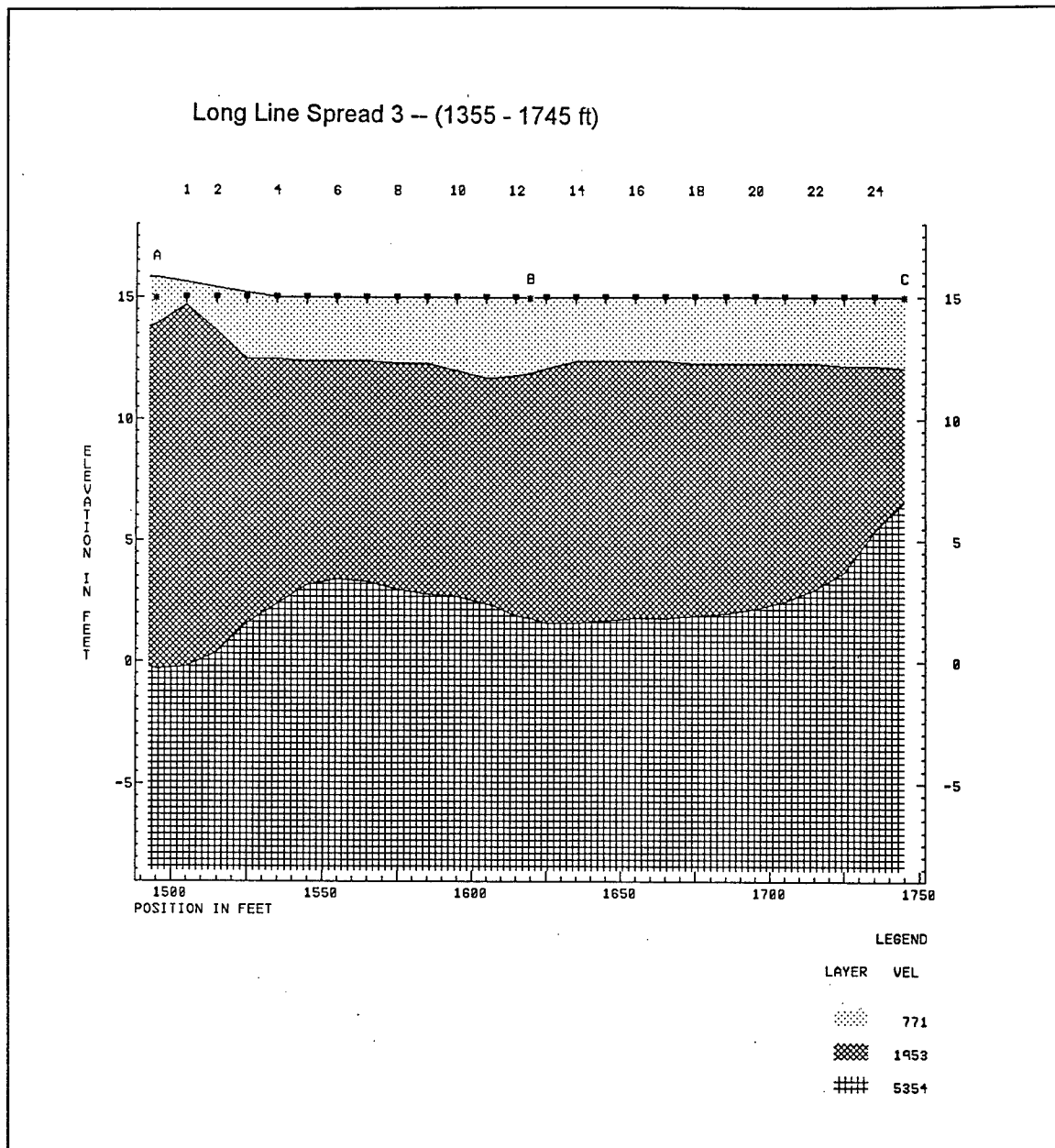


Figure A6. (Concluded)

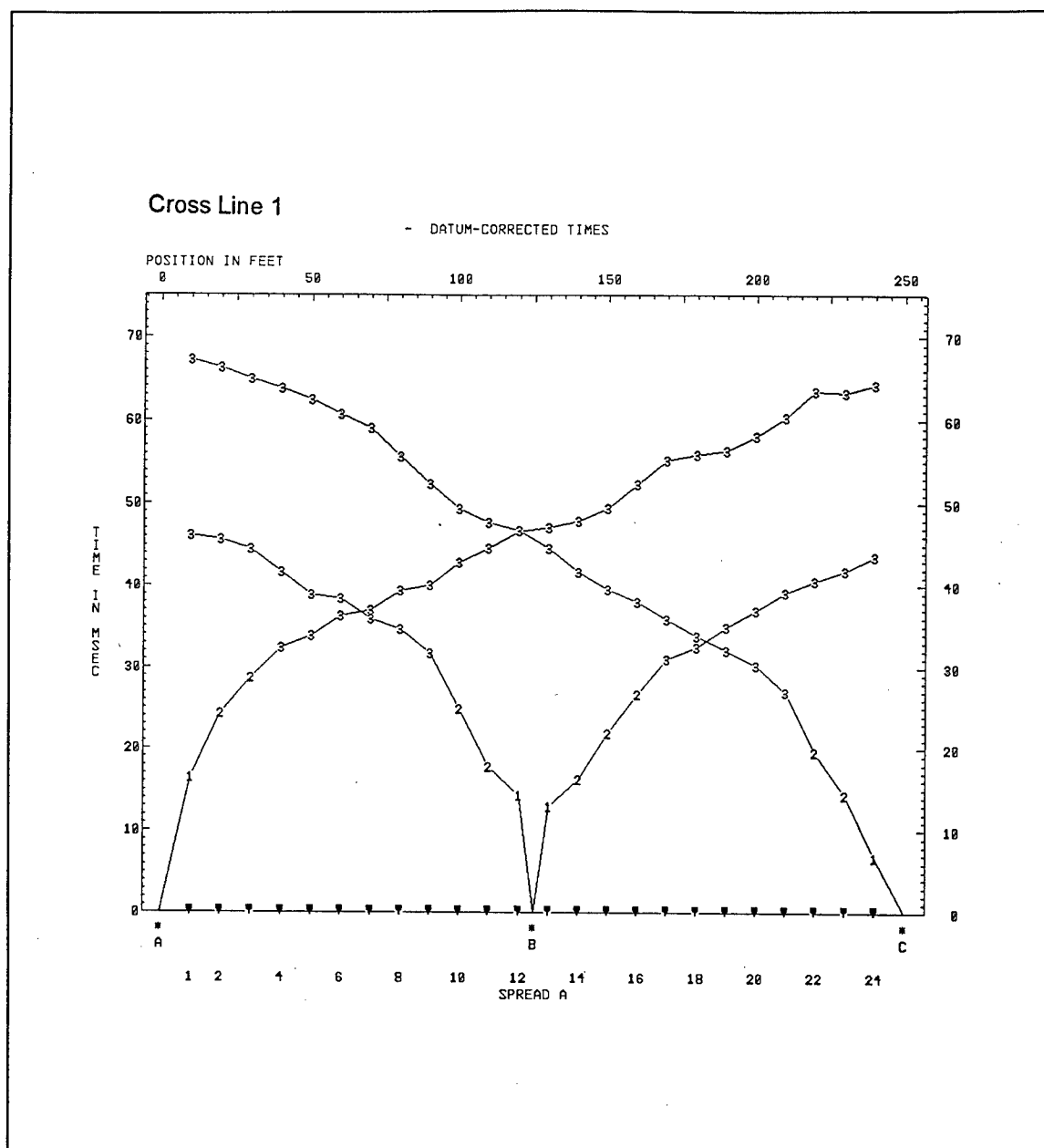


Figure A7. Cross line 1—time-distance (Sheet 1 of 5)

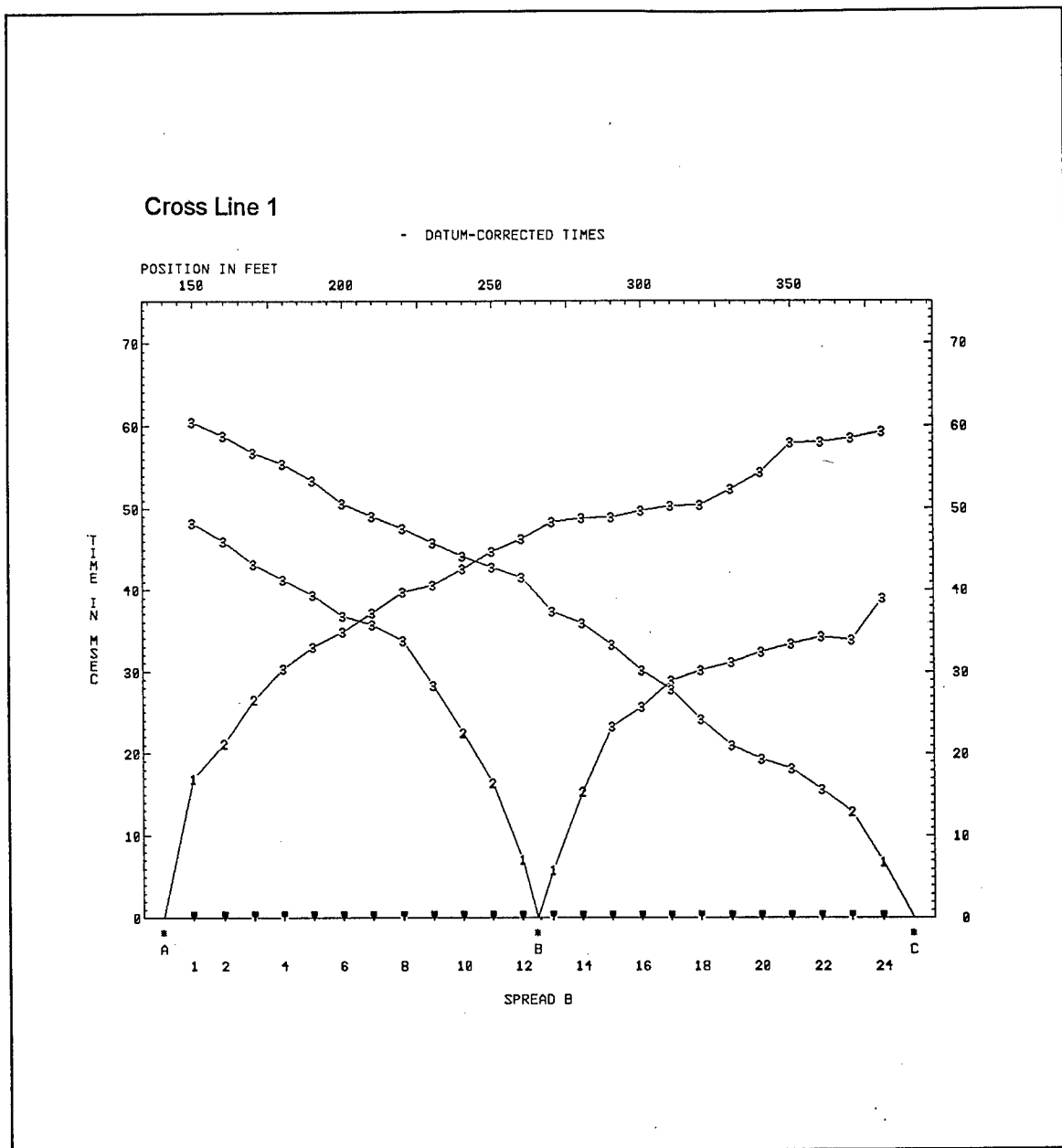


Figure A7. (Sheet 2 of 5)

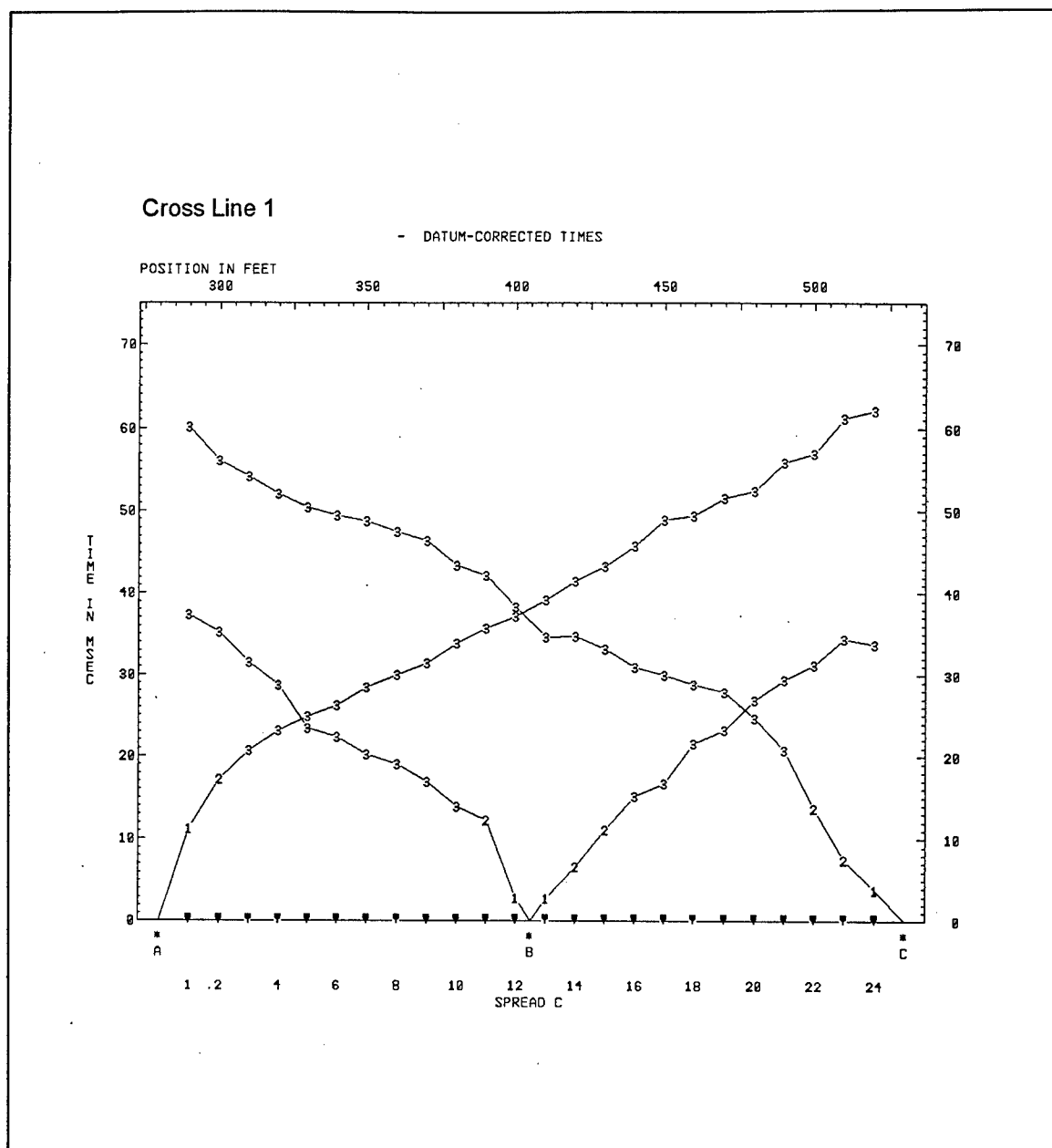


Figure A7. (Sheet 3 of 5)

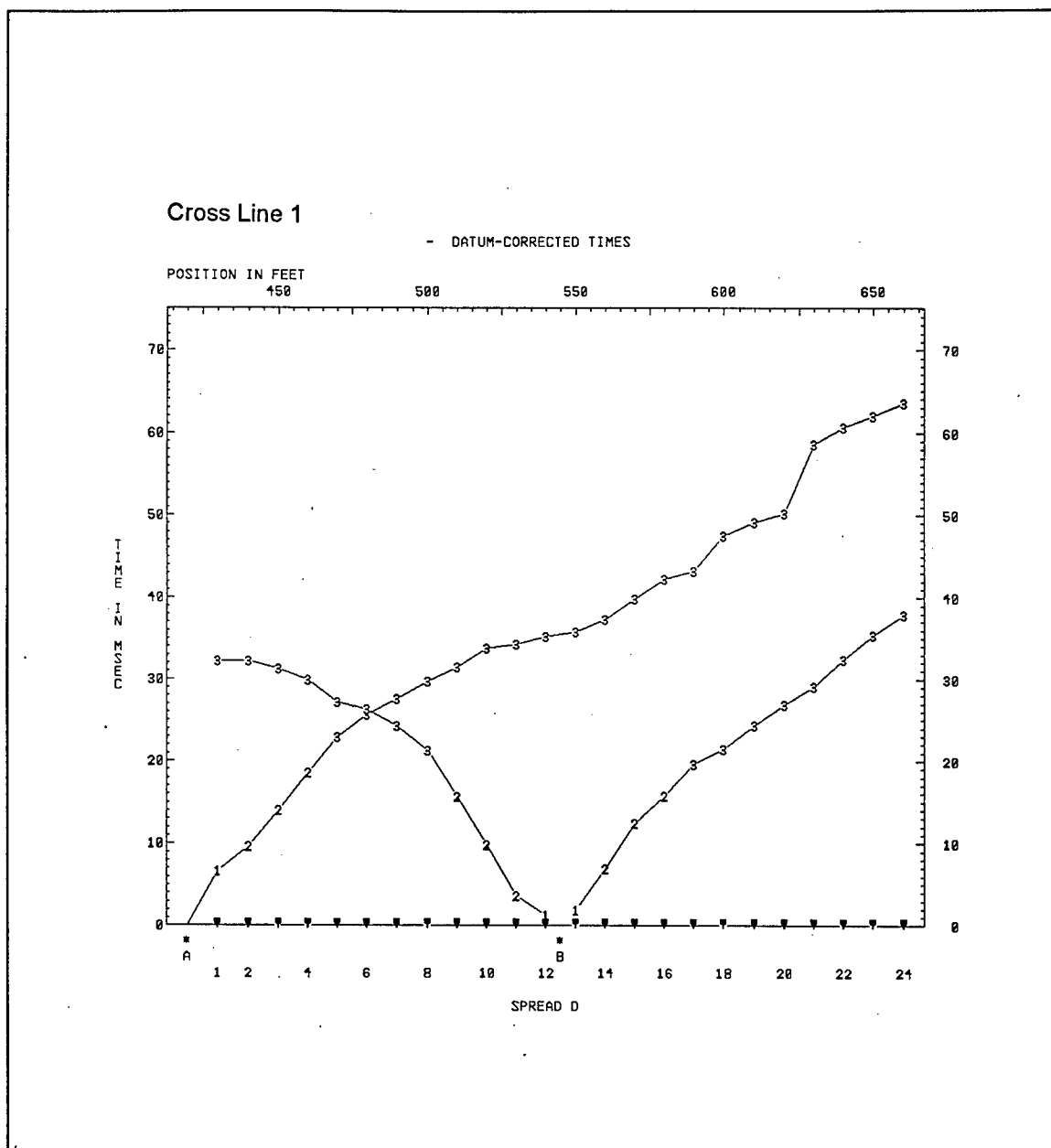


Figure A7. (Sheet 4 of 5)

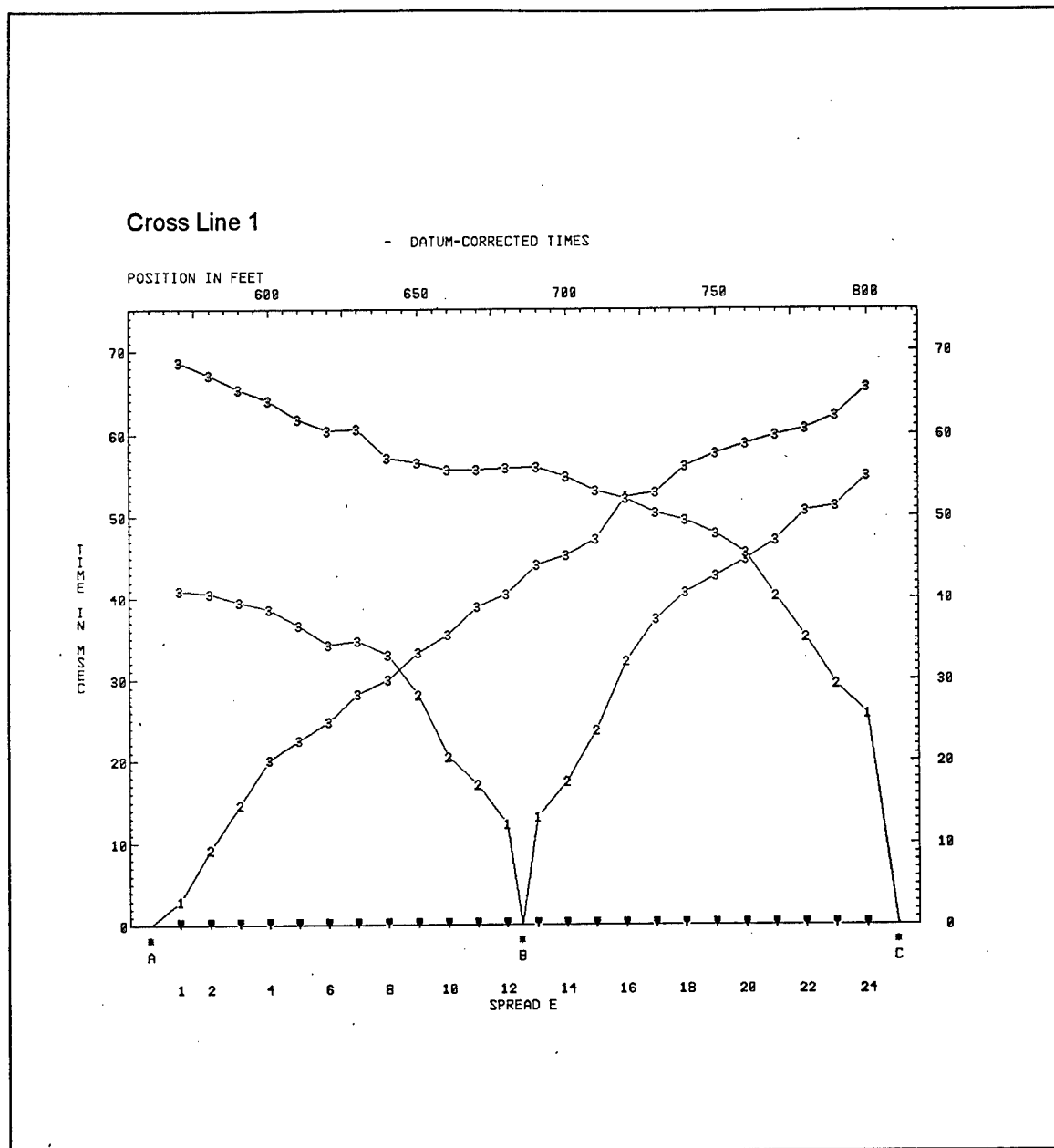


Figure A7. (Sheet 5 of 5)

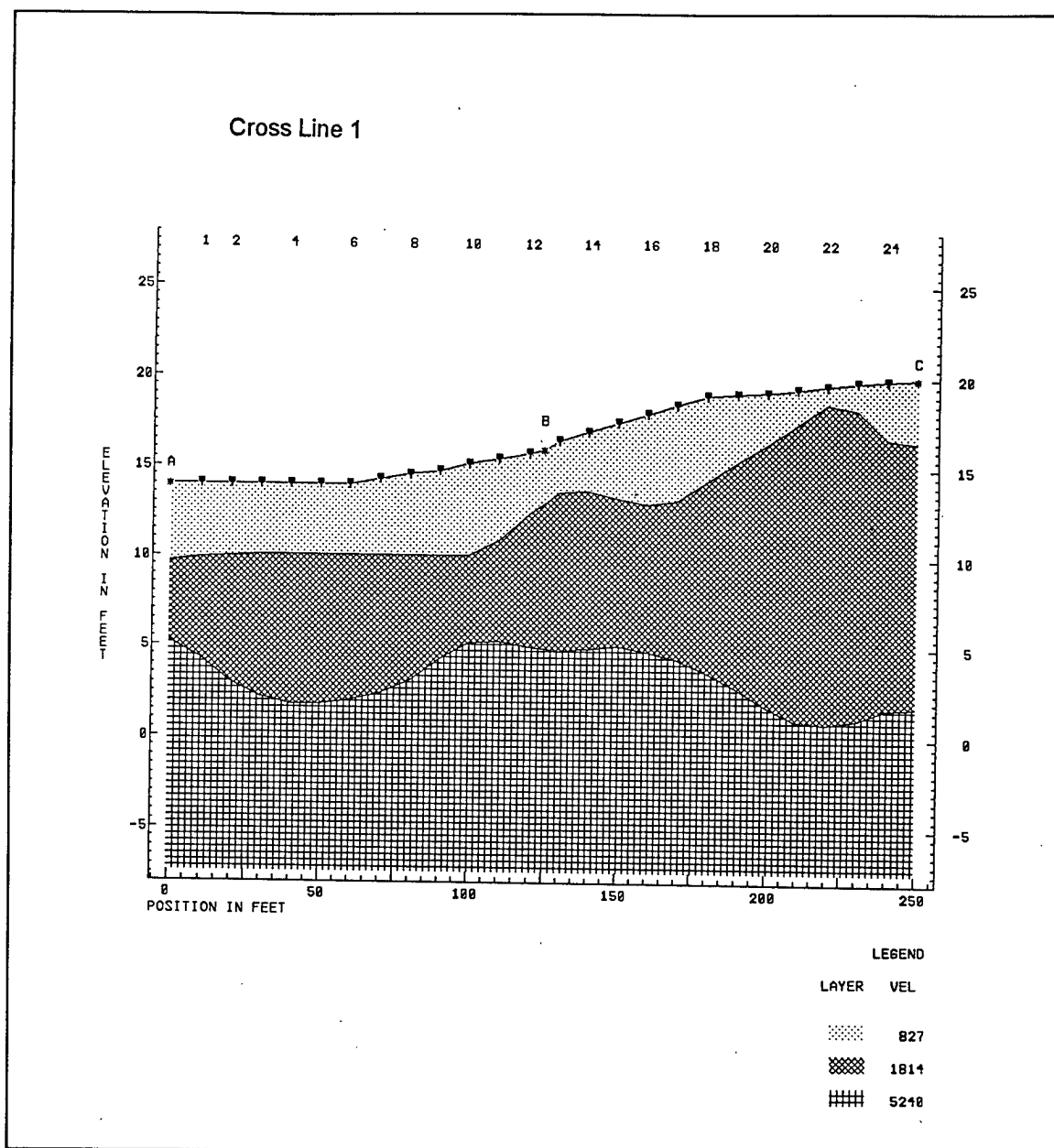


Figure A8. Cross line 1—cross-section (Sheet 1 of 5)

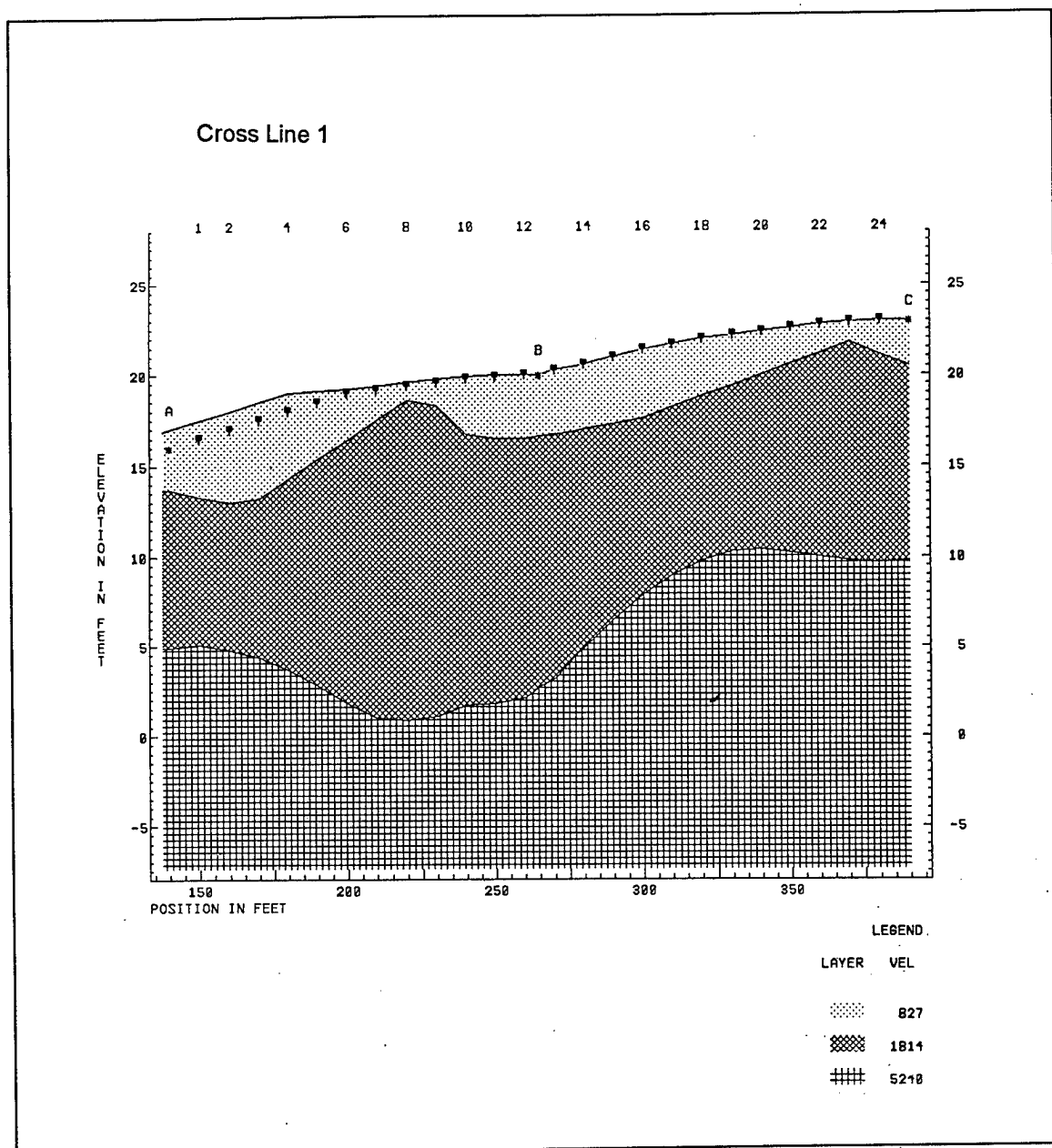


Figure A8. (Sheet 2 of 5)

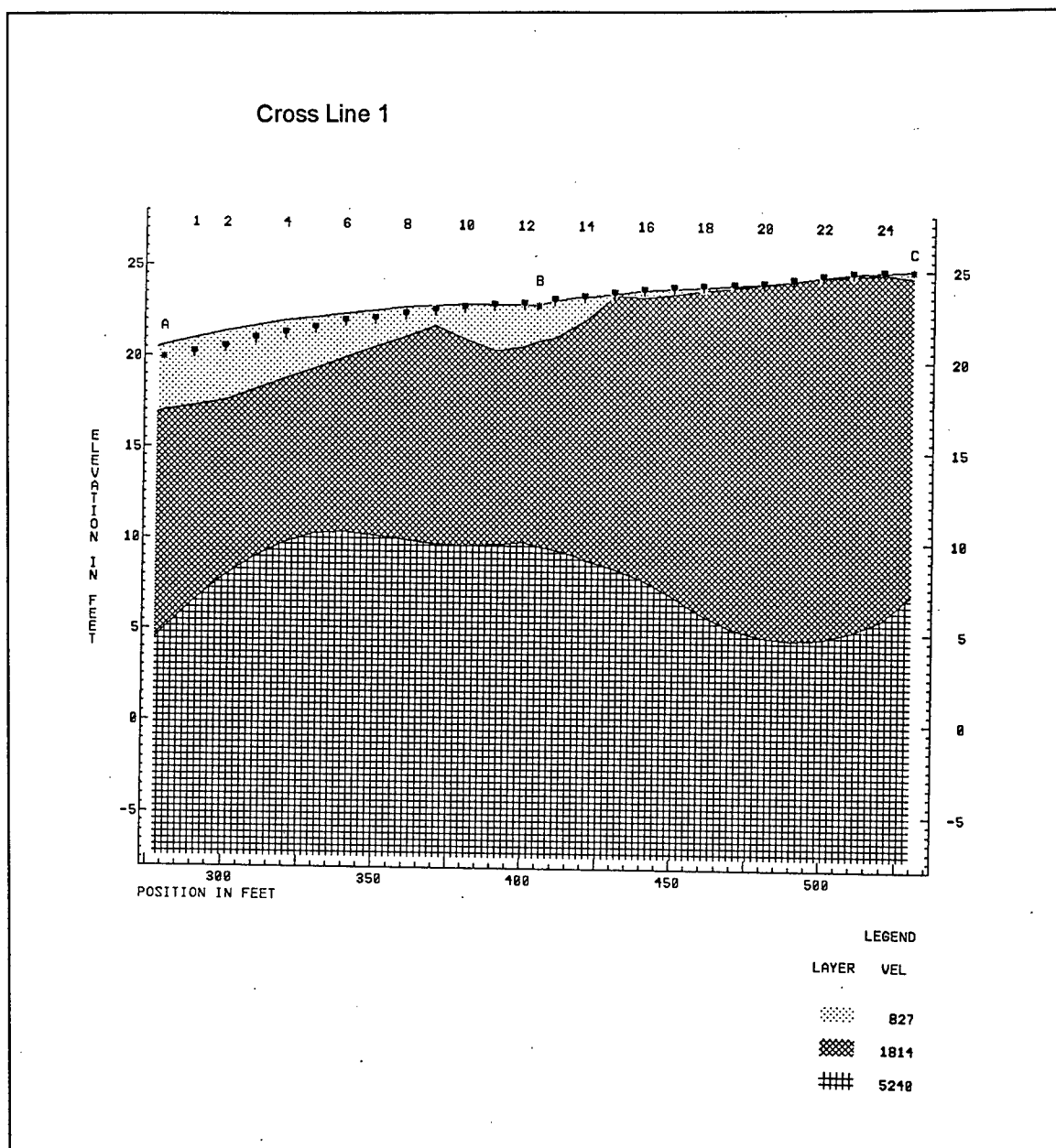


Figure A8. (Sheet 3 of 5)

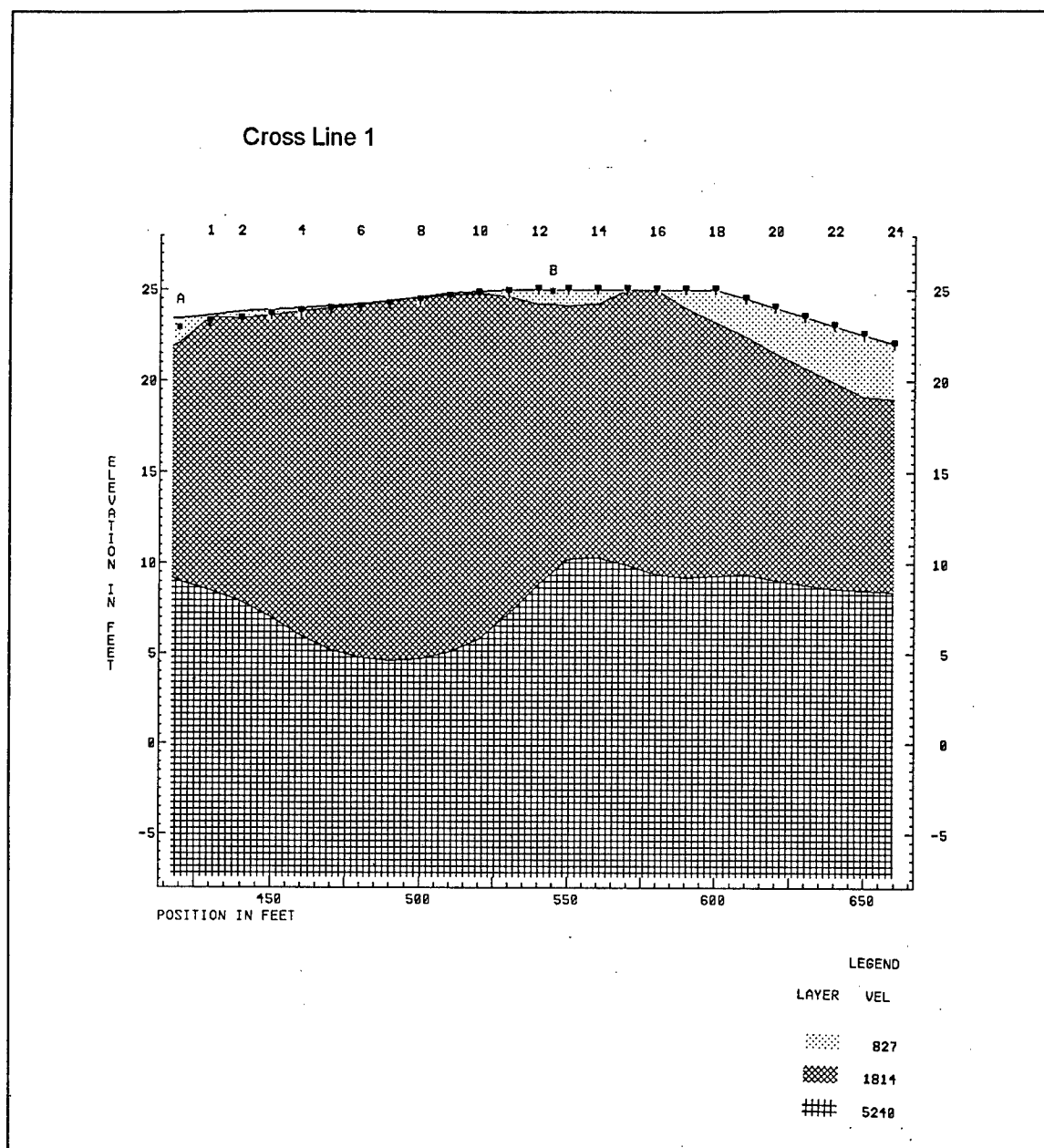


Figure A8. (Sheet 4 of 5)

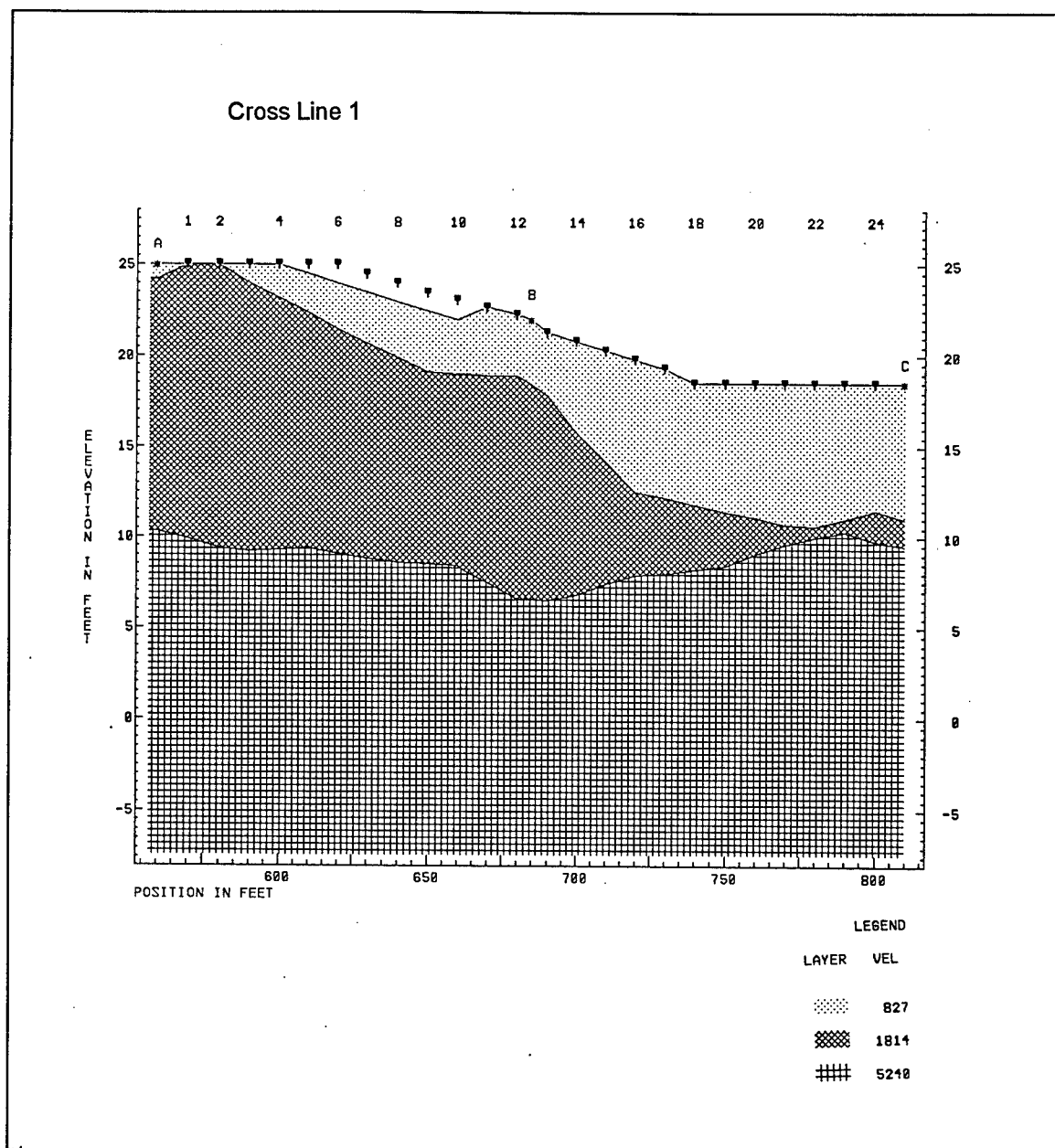


Figure A8. (Sheet 5 of 5)

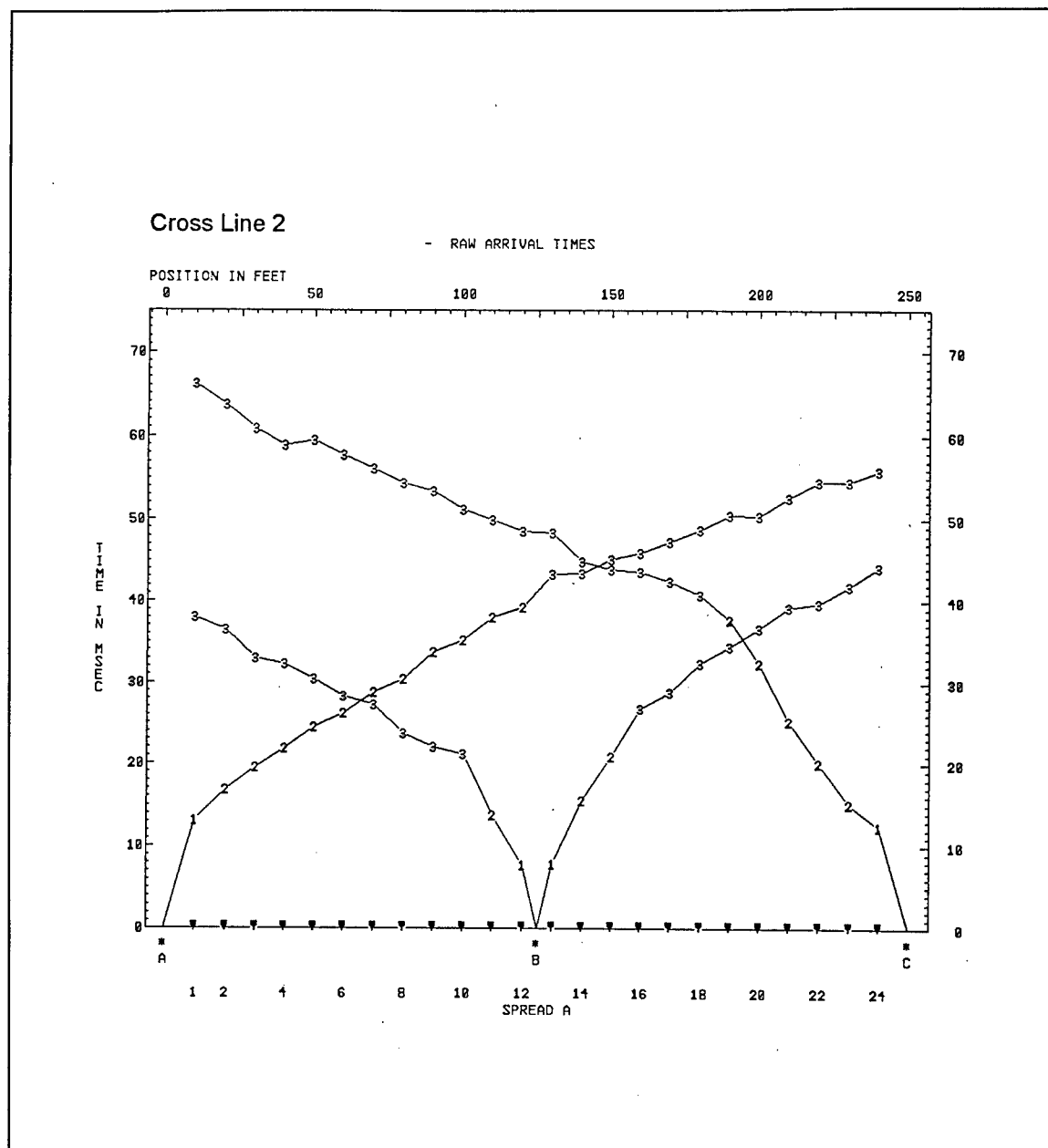


Figure A9. Cross line 2—time-distance (Sheet 1 of 5)

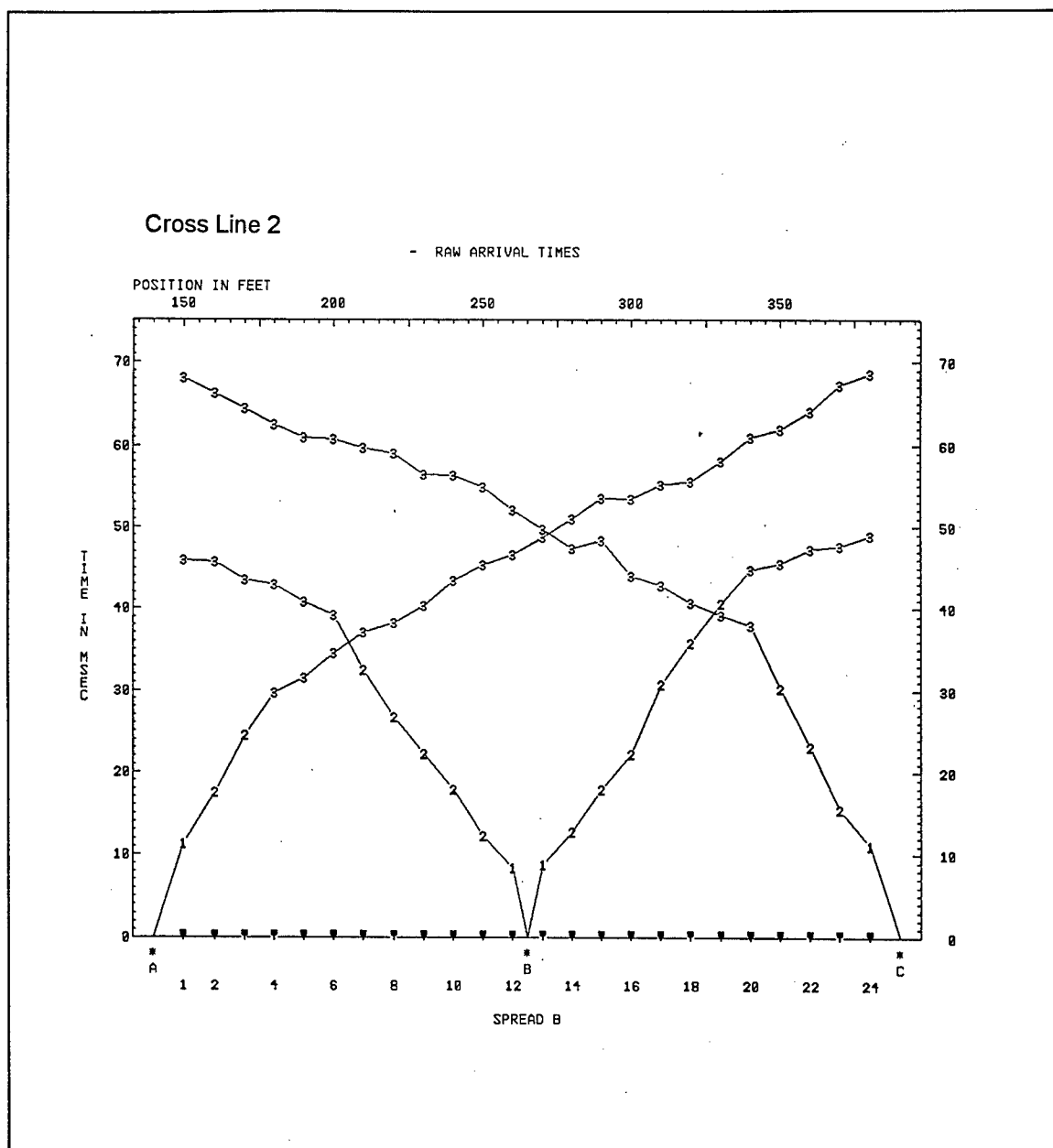


Figure A9. (Sheet 2 of 5)

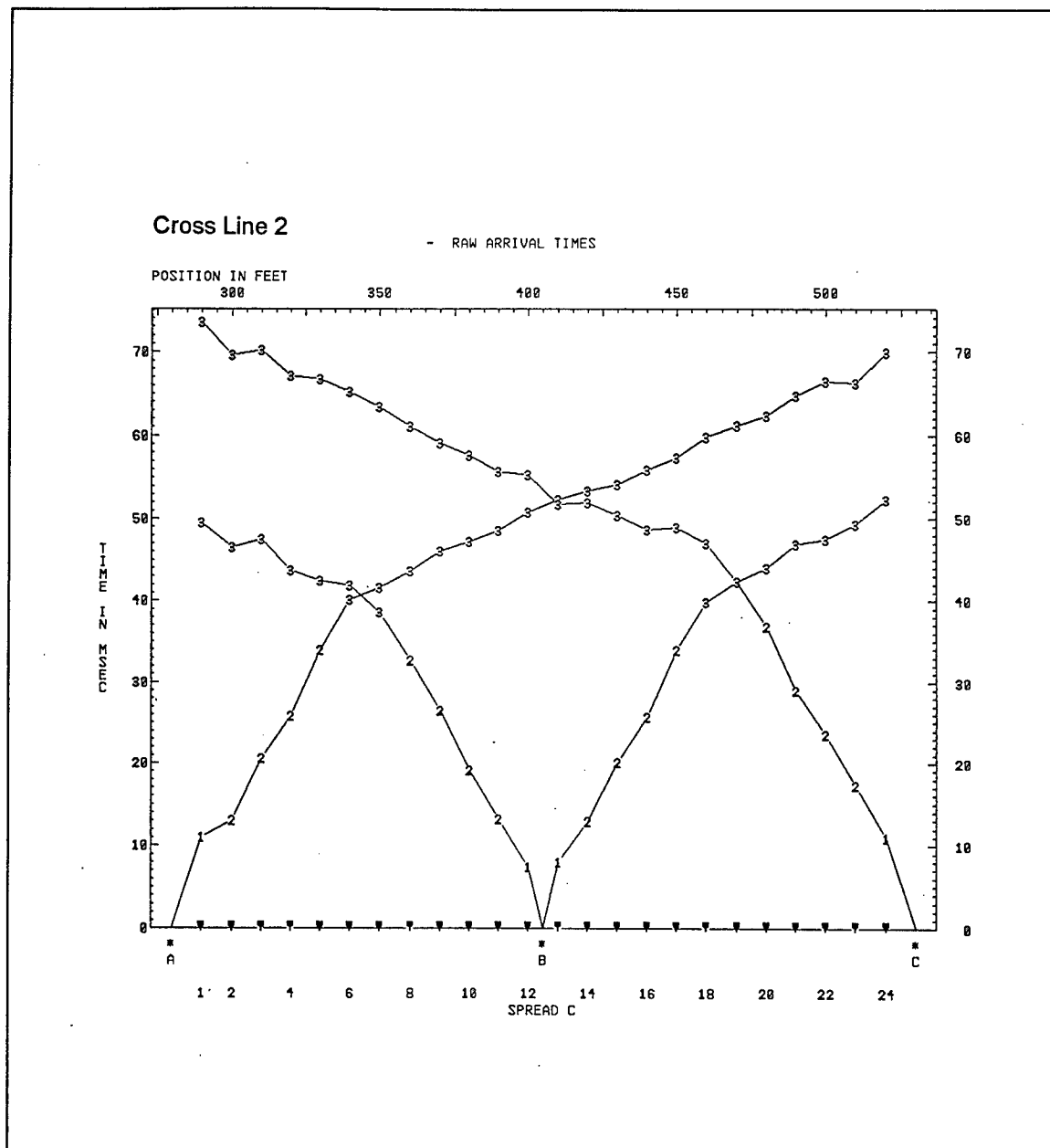


Figure A9. (Sheet 3 of 5)

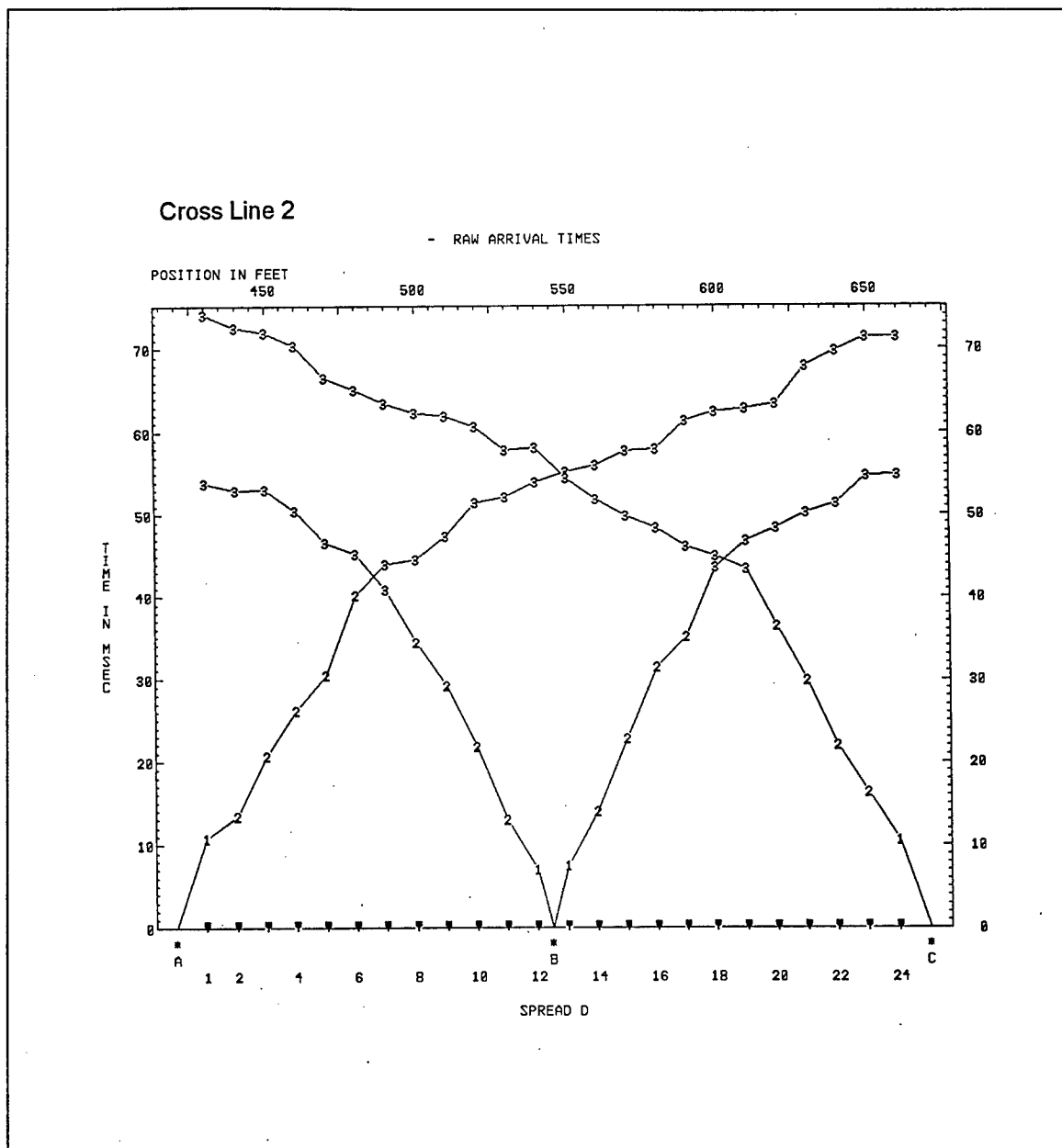


Figure A9. (Sheet 4 of 5)

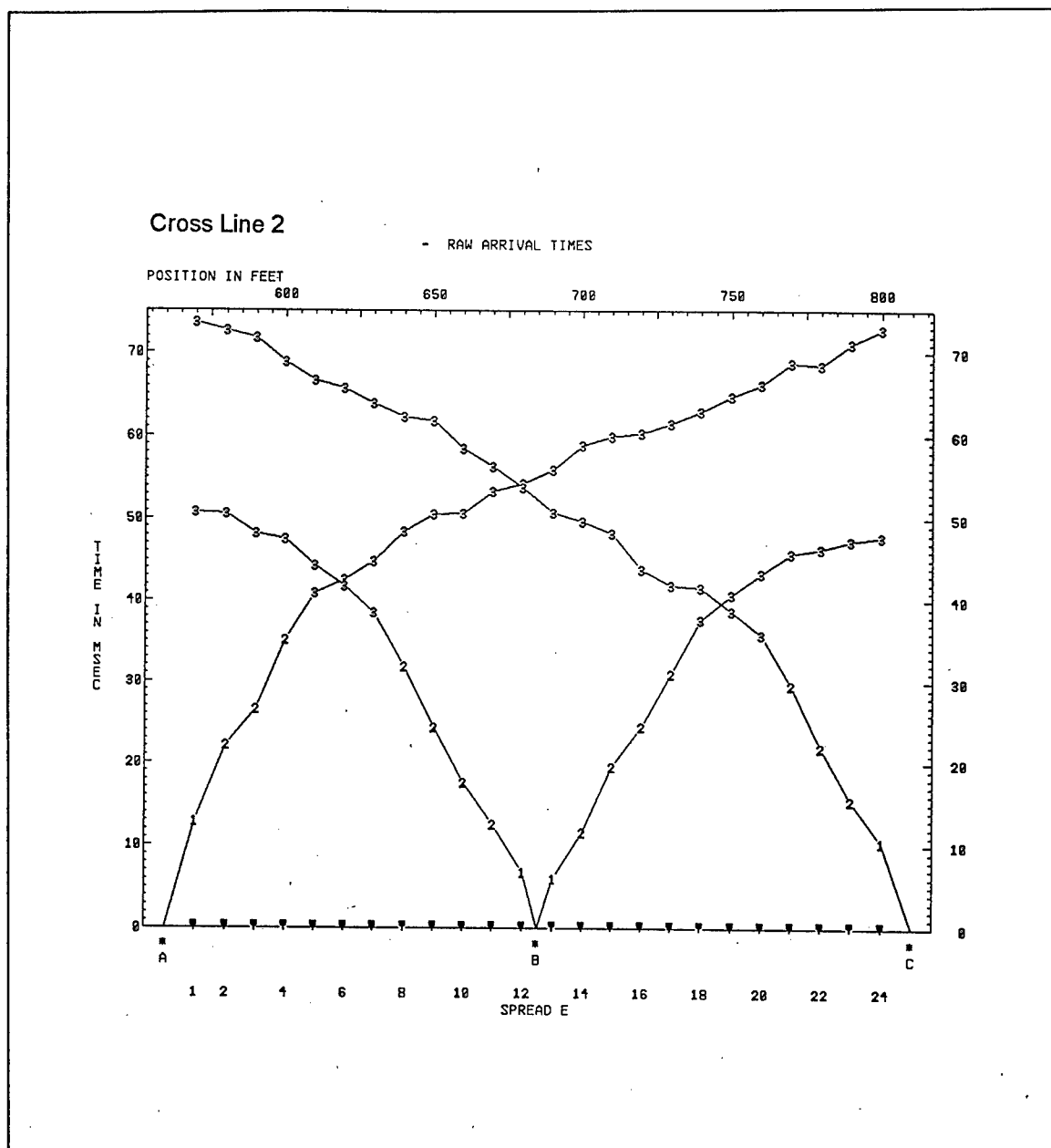


Figure A9. (Sheet 5 of 5)

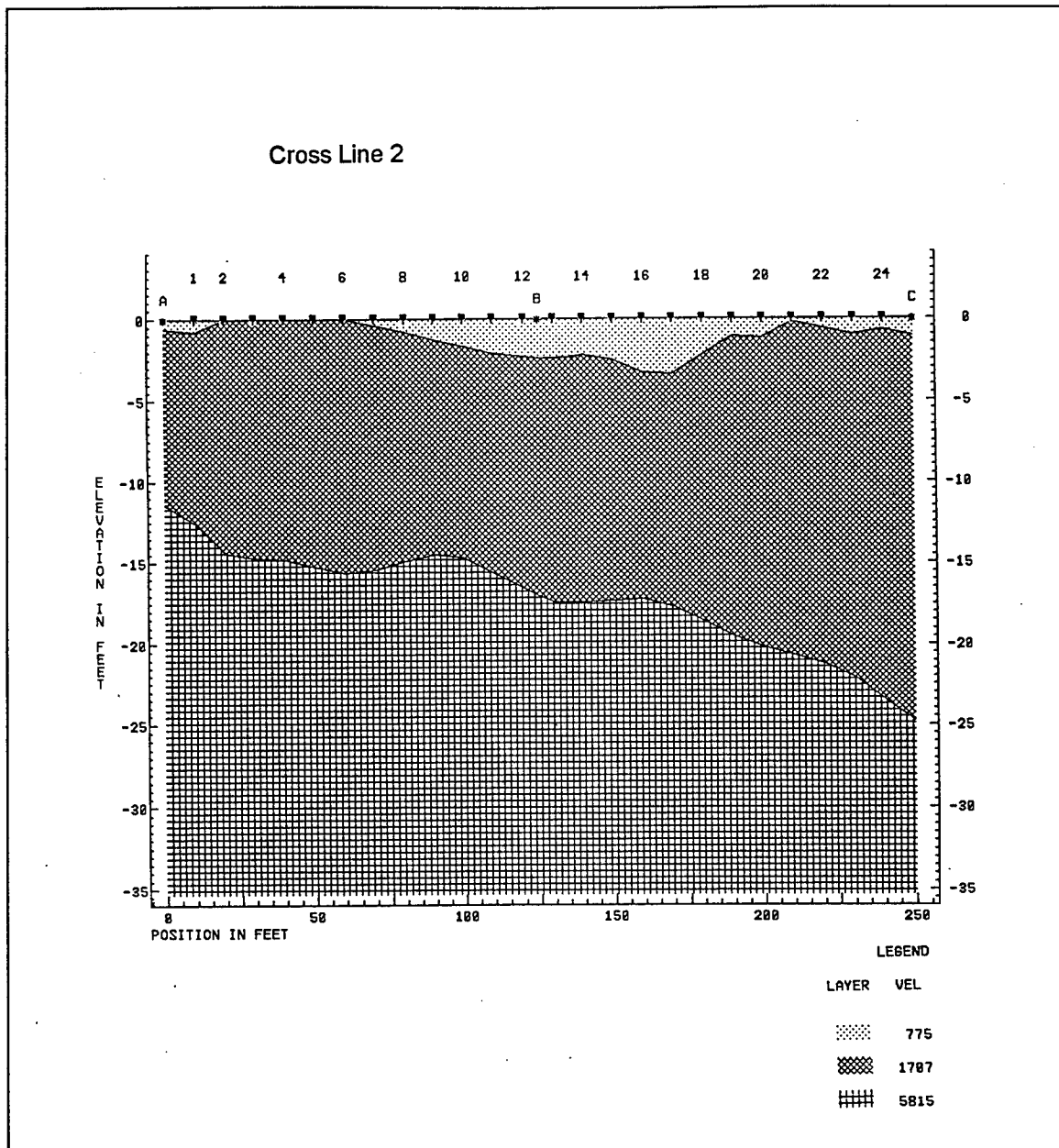


Figure A10. Cross line 2—cross-section (Sheet 1 of 5)

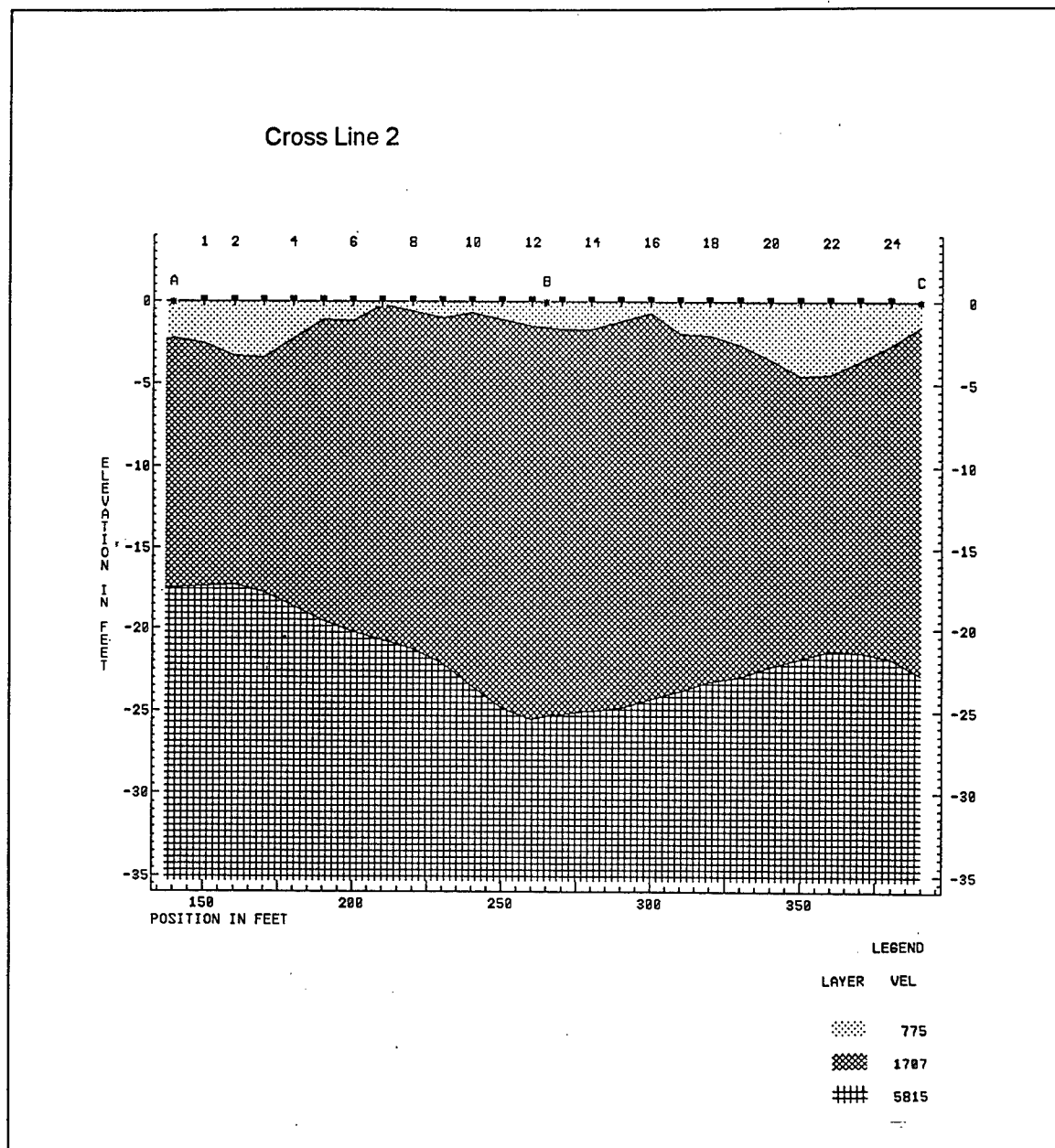


Figure A10. (Sheet 2 of 5)

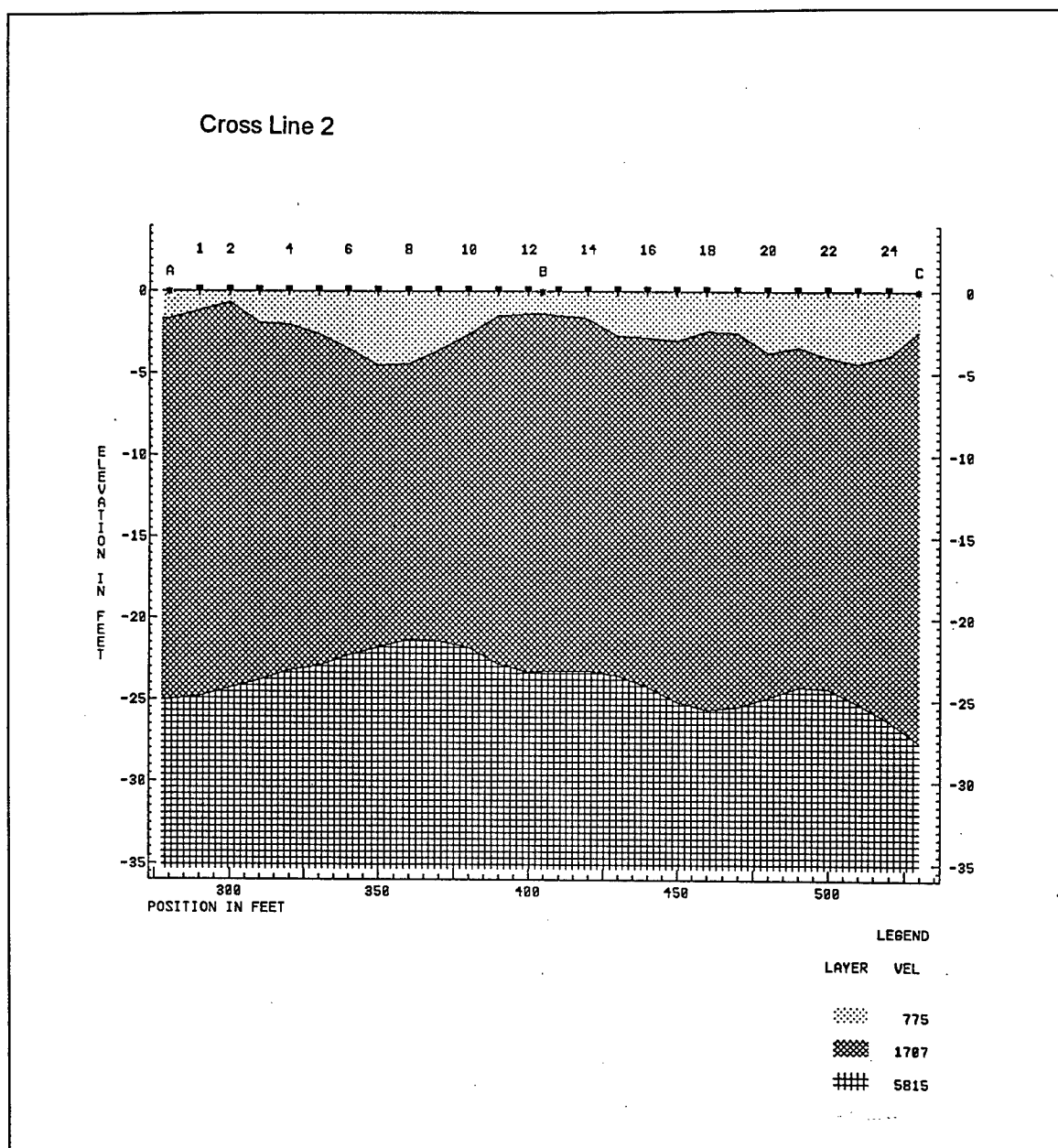


Figure A10. (Sheet 3 of 5)

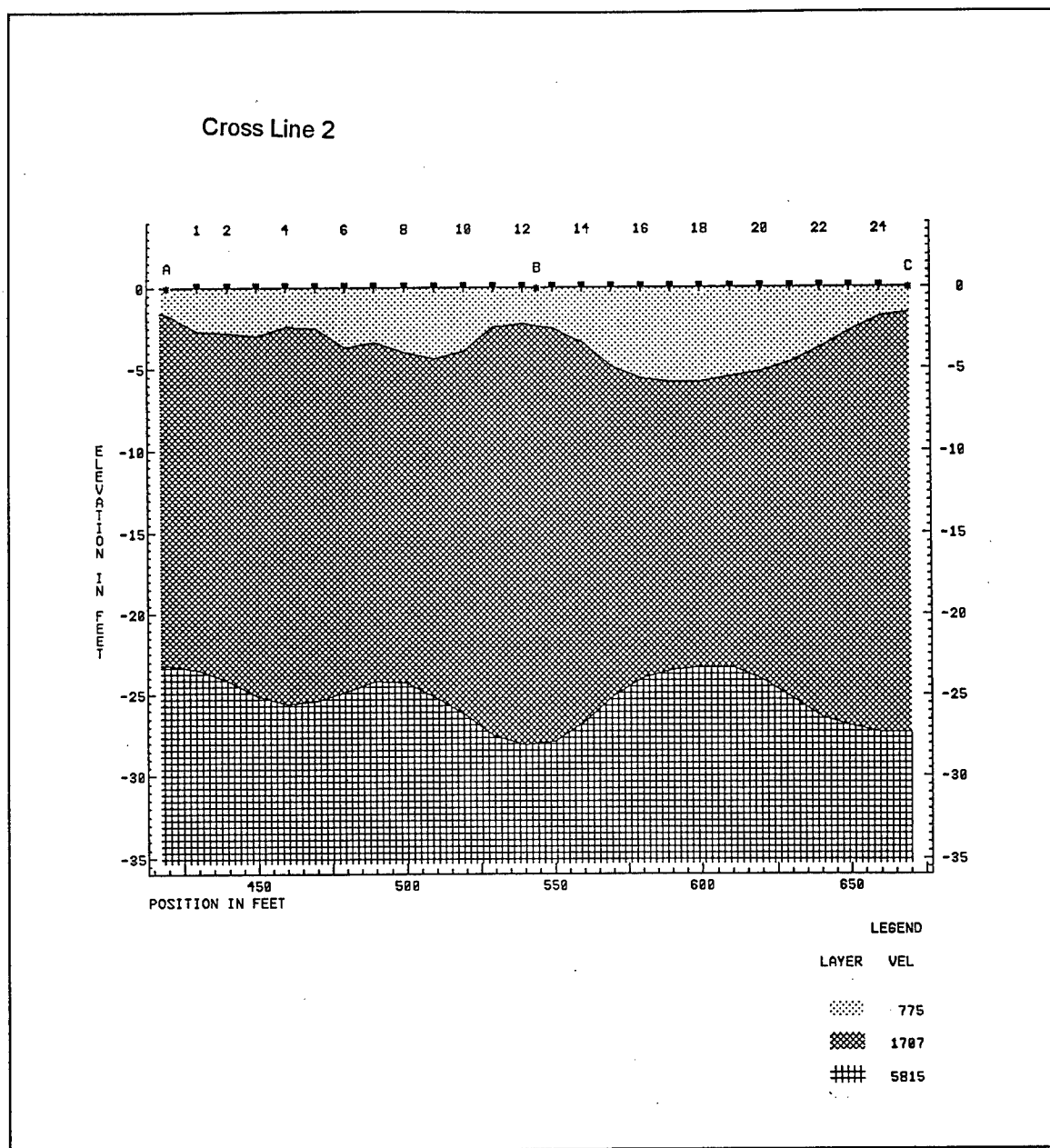


Figure A10. (Sheet 4 of 5)

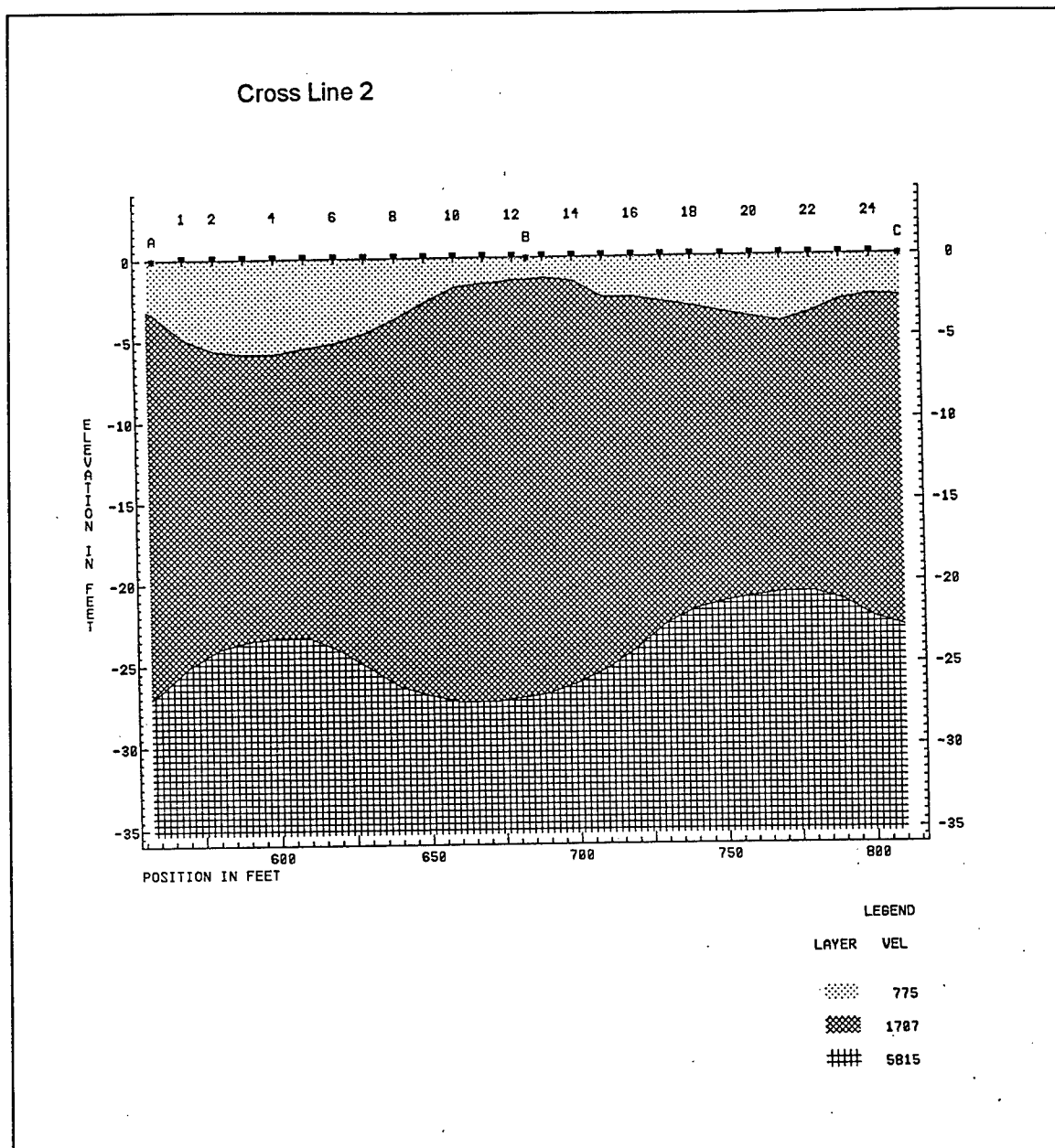


Figure A10. (Sheet 5 of 5)

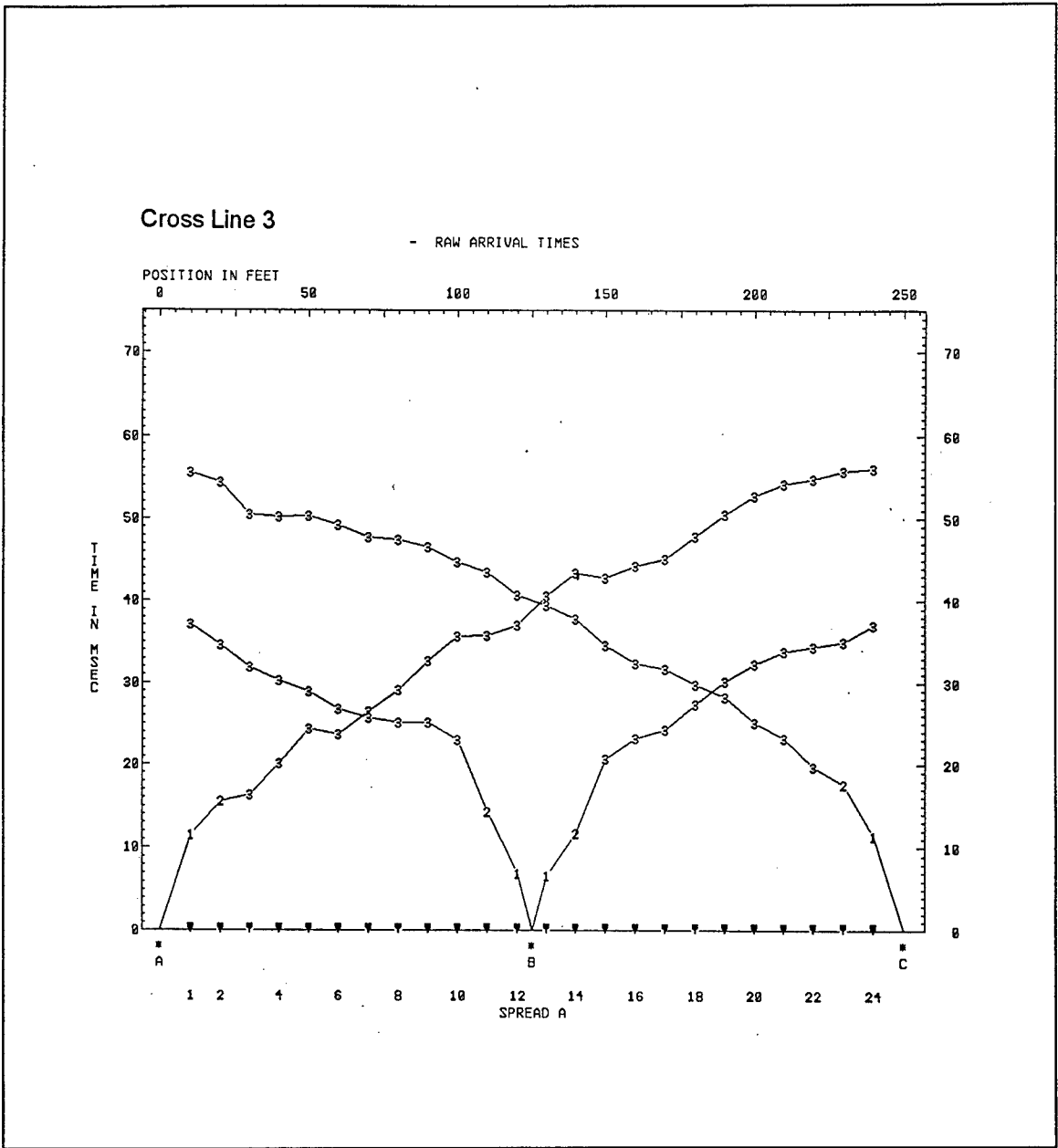


Figure A11. Cross line 3—time-distance (Sheet 1 of 4)

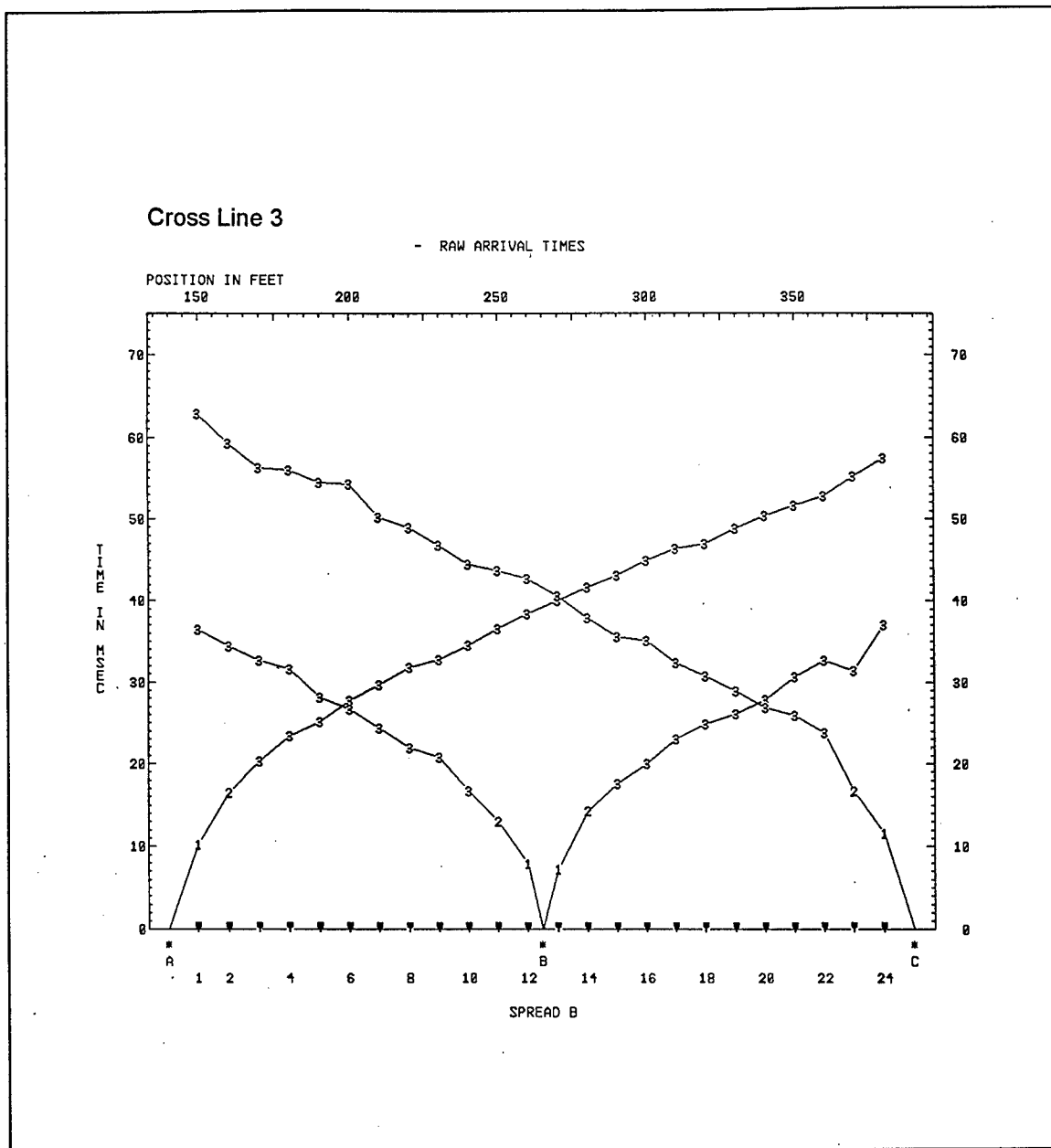


Figure A11. (Sheet 2 of 4)

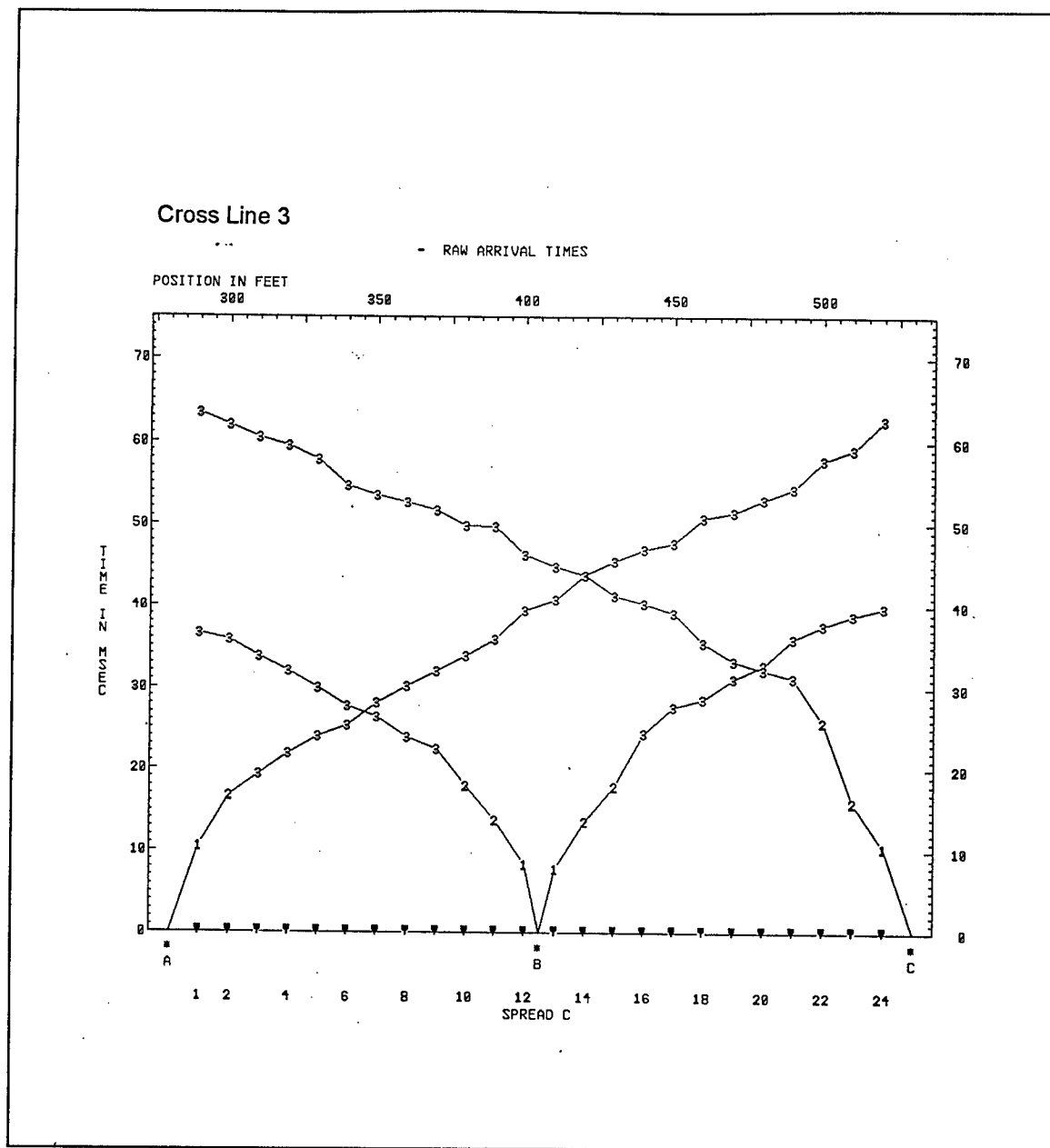


Figure A11. (Sheet 3 of 4)

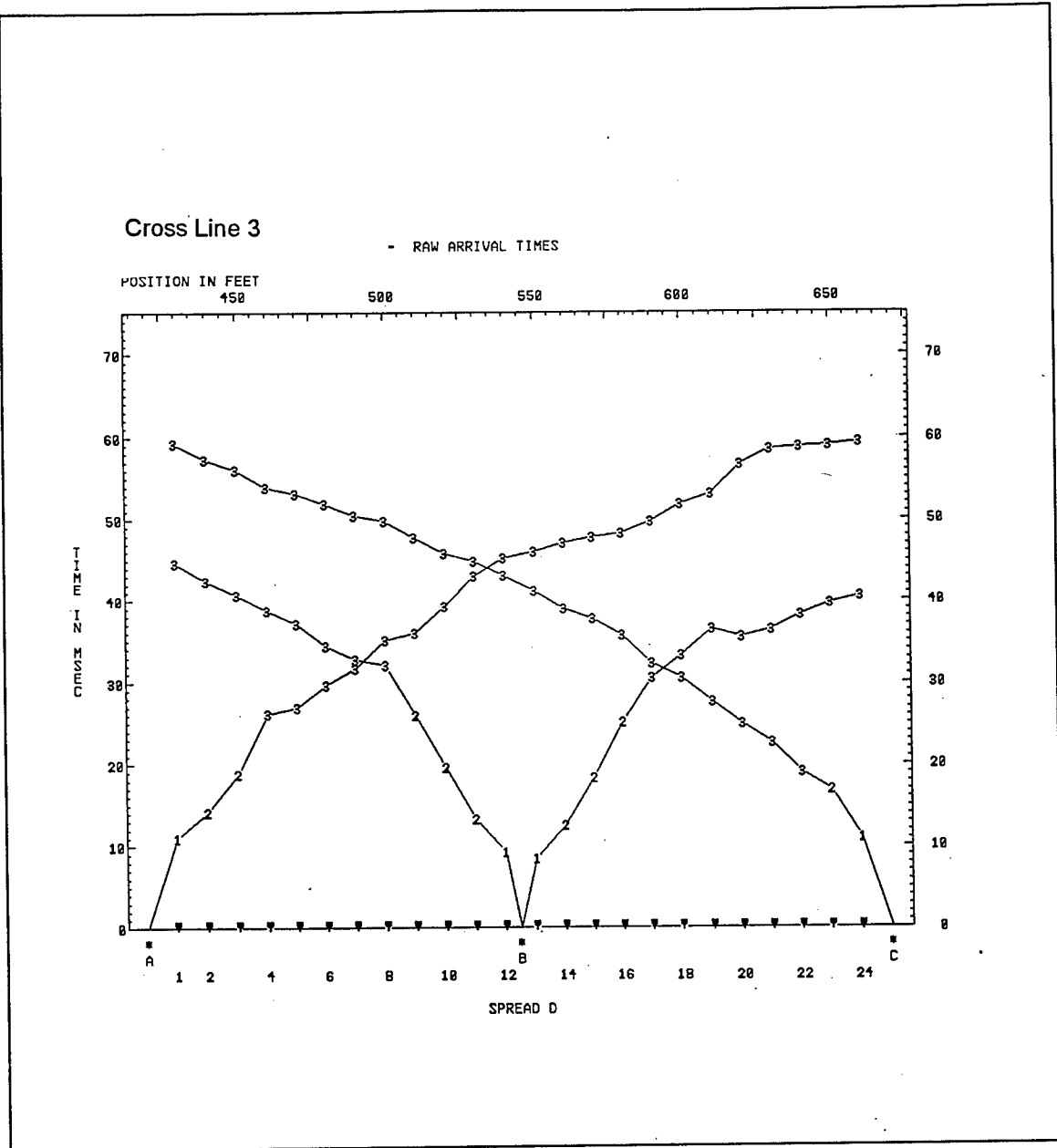


Figure A11. (Sheet 4 of 4)

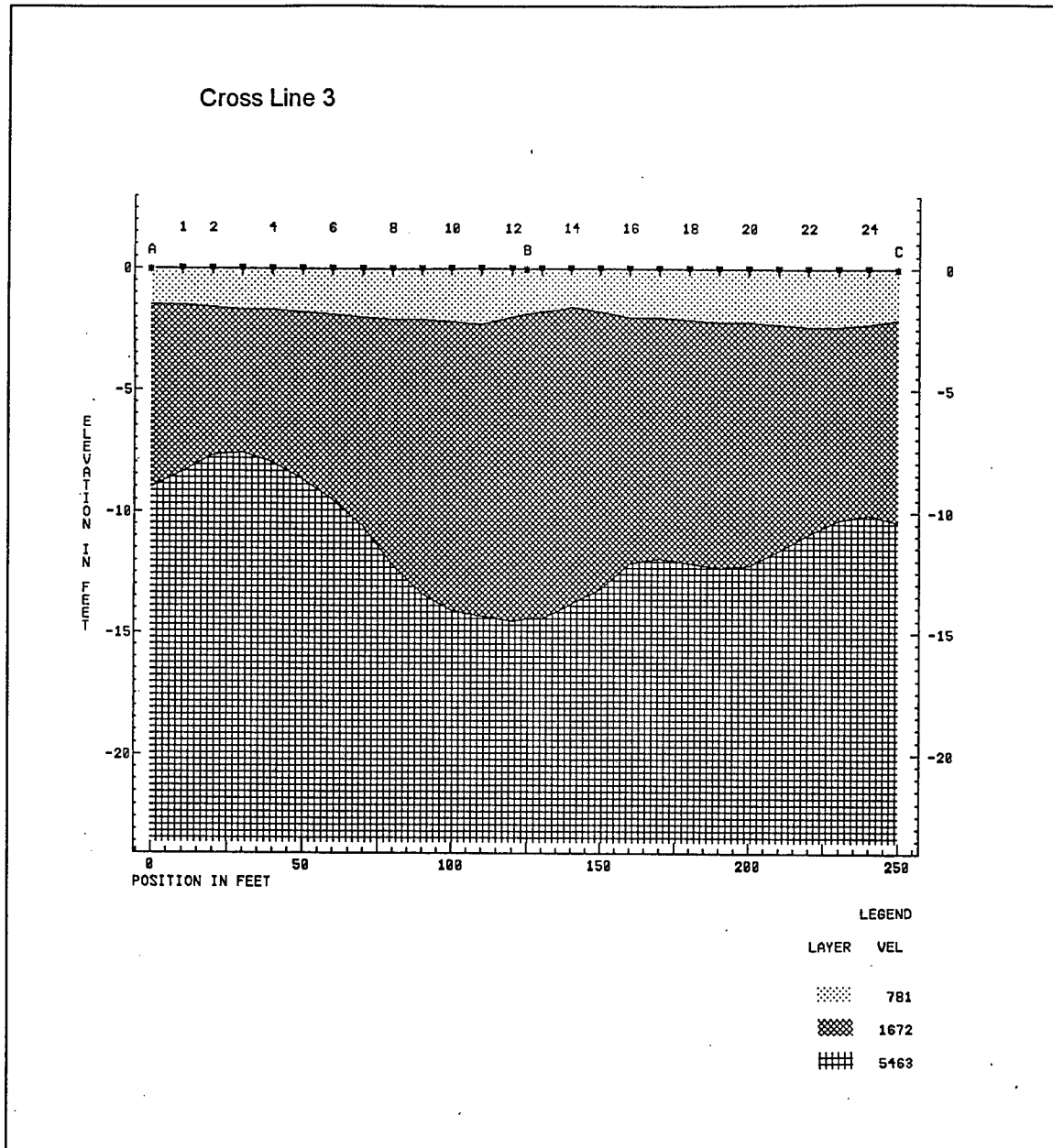


Figure A12. Cross line 3—cross-section (Sheet 1 of 4)

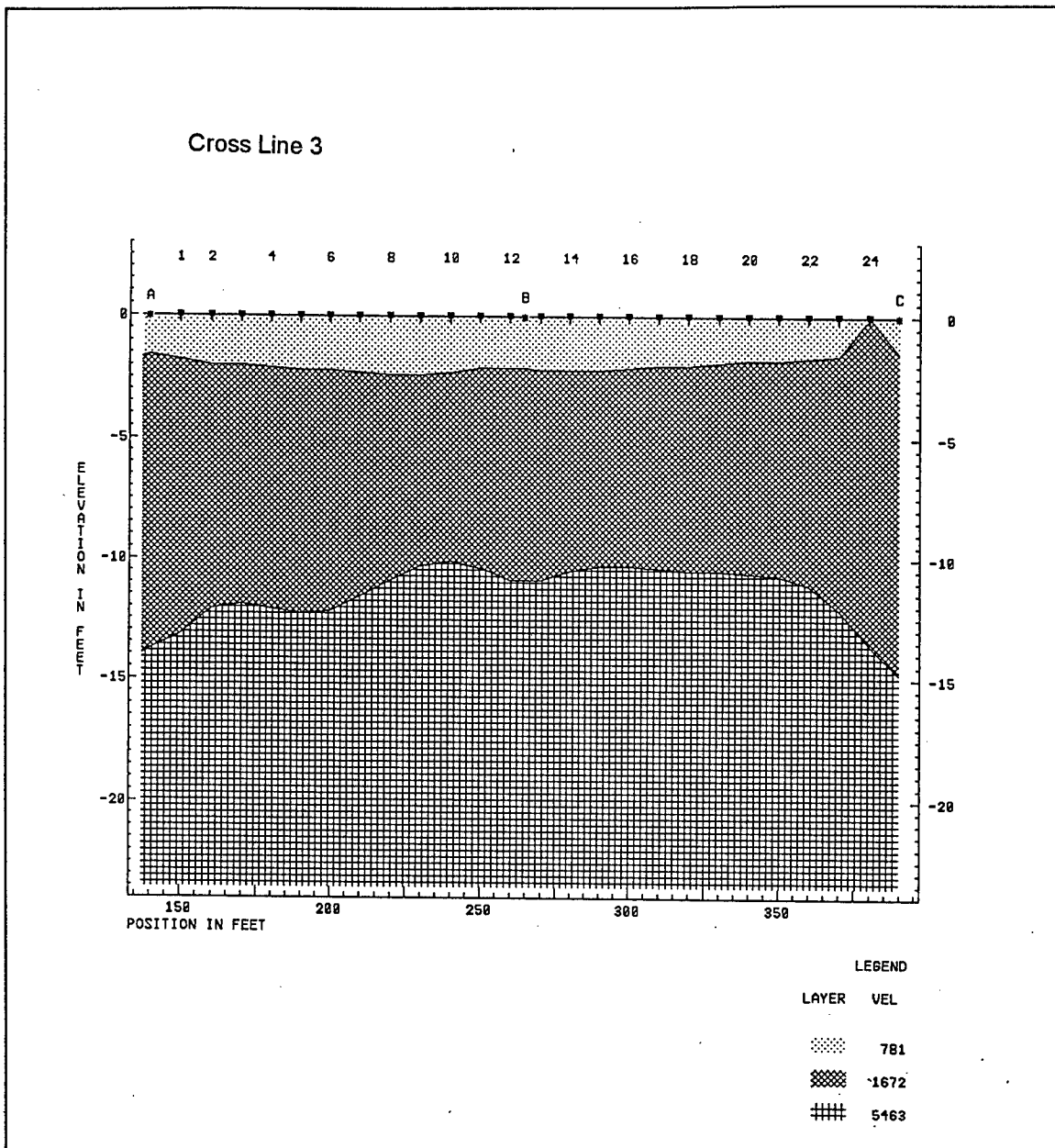


Figure A12. (Sheet 2 of 4)

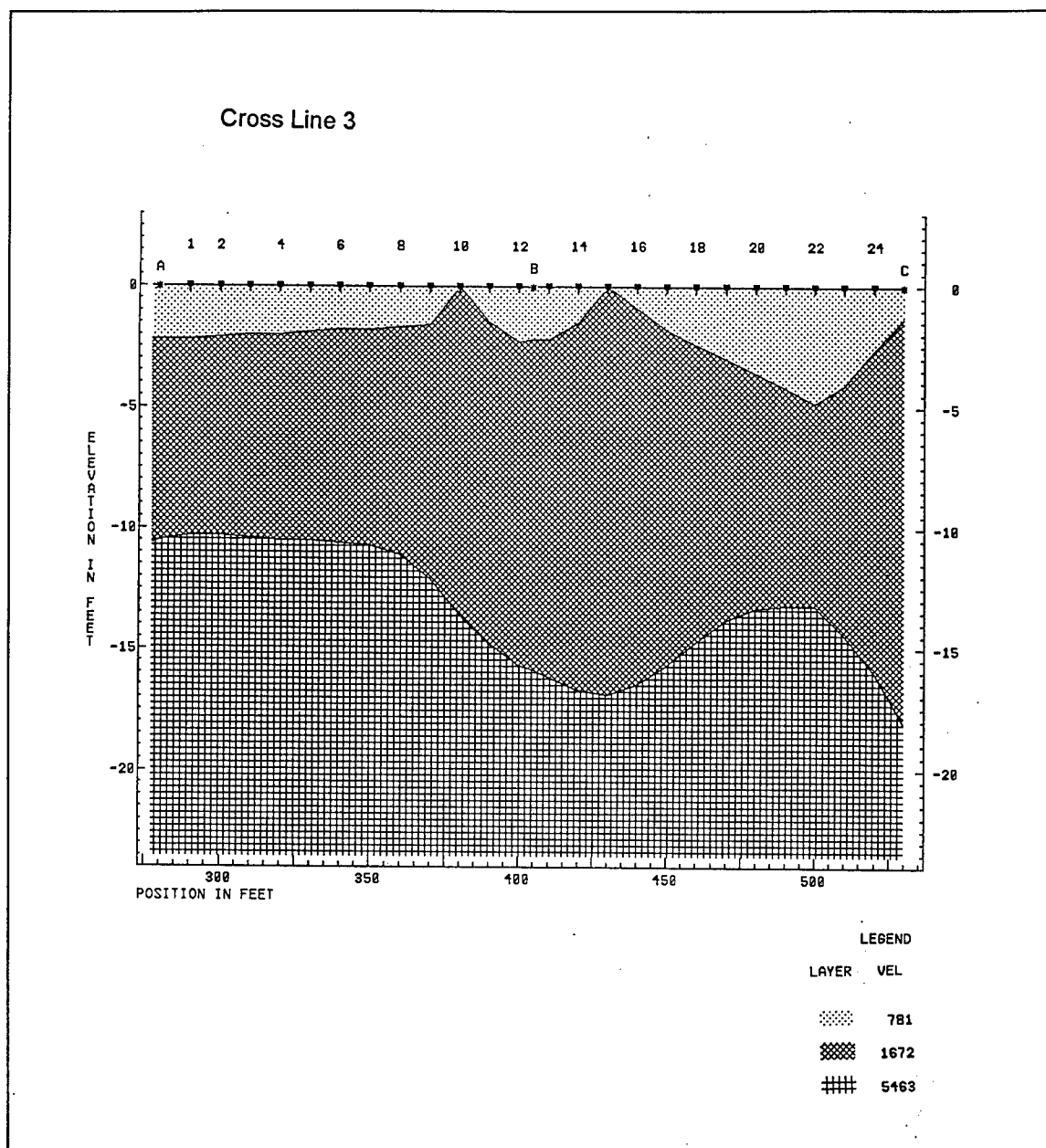


Figure A12. (Sheet 3 of 4)

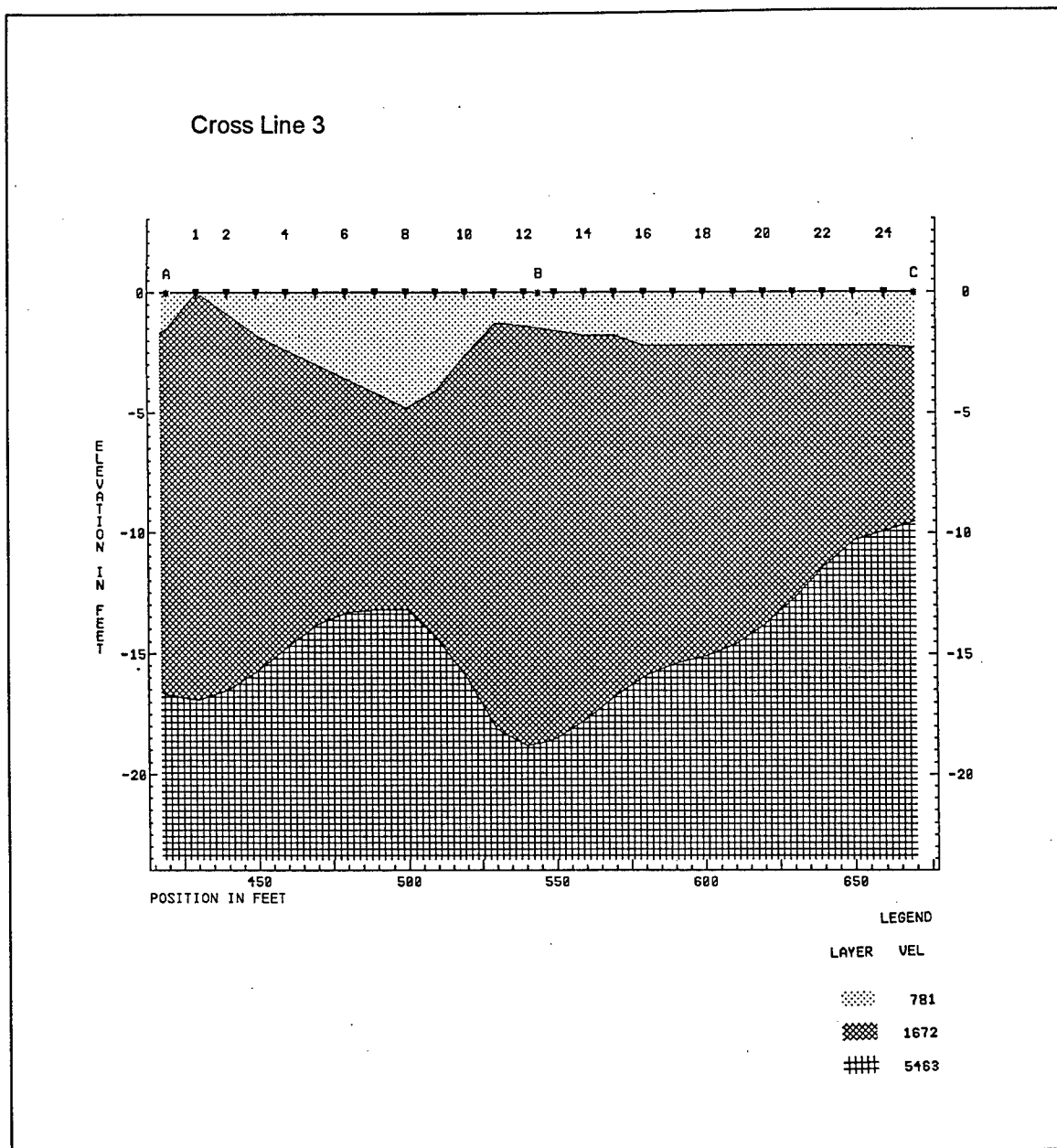


Figure A12. (Sheet 4 of 4)

Appendix B

Electrical Resistivity

Sounding Data

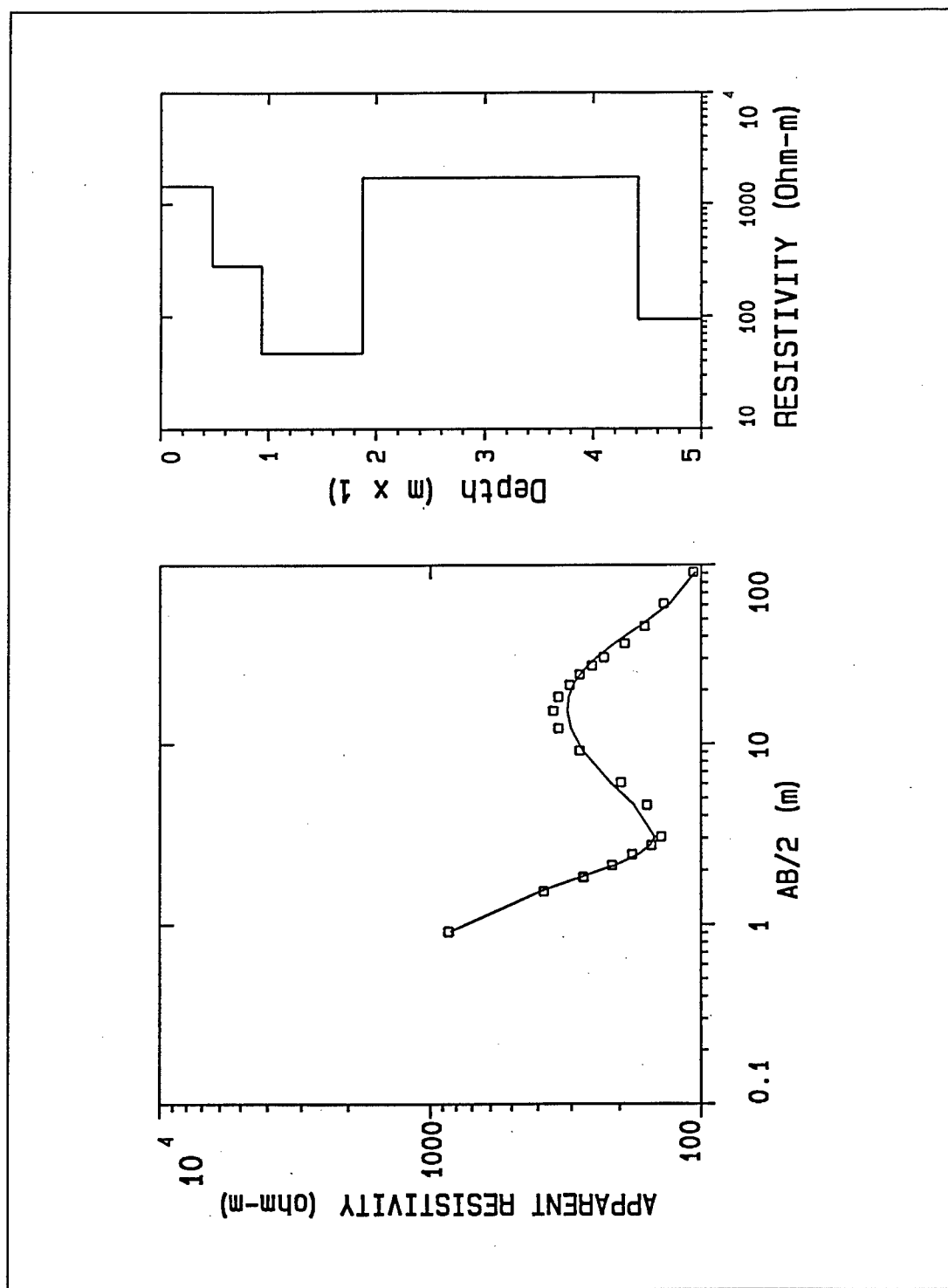


Figure B1. Long line electrical resistivity sounding (0.5, 3.5)

DATA SET: 1

CLIENT: Aberdeen Proving Ground DATE: Nov 1994
 LOCATION: Cluster 13 SOUNDING: 1
 COUNTY: AZIMUTH:
 PROJECT: EQUIPMENT:
 ELEVATION: 0.00
 SOUNDING COORDINATES: X: 0.5000 Y: 3.5000

Schlumberger Configuration

FITTING ERROR: 6.342 PERCENT

L #	RESISTIVITY (ohm-m)	THICKNESS (meters)	ELEVATION (meters)	LONG. COND. (Siemens)	TRANS. RES. (Ohm-m ²)
			0.0		
1	1464.1	0.464	-0.464	3.172E-04	679.9
2	317.1	0.436	-0.901	0.00138	138.5
3	52.69	1.06	-1.96	0.0202	56.16
4	1838.4	2.36	-4.33	0.00129	4356.9
5	94.53				

ALL PARAMETERS ARE FREE

No.	SPACING (m)	RHO-A (ohm-m)		DIFFERENCE (percent)
		DATA	SYNTHETIC	
1	0.914	853.4	843.9	1.11
2	1.52	381.0	391.4	-2.73
3	1.82	271.2	275.4	-1.55
4	2.13	213.3	207.8	2.59
5	2.43	179.8	171.3	4.73
6	2.74	152.3	154.1	-1.16
7	3.04	140.2	148.3	-5.82
8	4.57	158.4	176.8	-11.58
9	6.09	198.1	216.2	-9.13
10	9.14	280.4	272.2	2.91
11	12.19	335.2	301.1	10.18
12	15.24	350.5	310.5	11.39
13	18.28	335.2	307.0	8.42
14	21.33	304.7	295.4	3.06
15	24.38	280.4	279.3	0.366
16	27.43	252.9	261.3	-3.30
17	30.48	228.6	242.9	-6.26
18	36.57	192.0	208.6	-8.65
19	45.72	161.5	168.6	-4.38
20	60.96	137.1	130.1	5.12
21	91.44	106.6	104.9	1.61

Figure B2. Long line electrical resistivity sounding (0.5, 3.5) best-fit model information

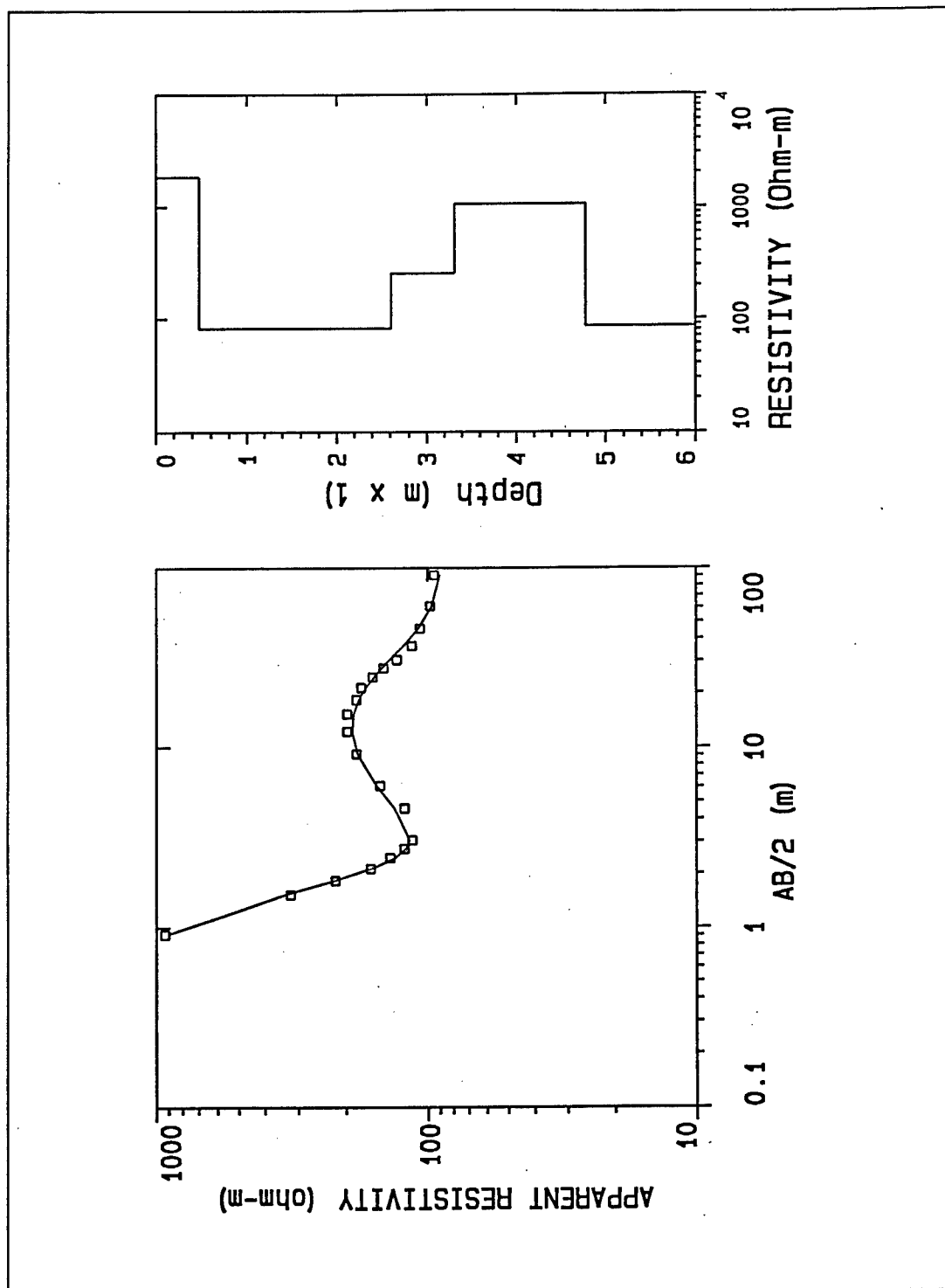


Figure B3. Long line electrical resistivity sounding (1.5, 2.5)

DATA SET: 2

CLIENT: Aberdeen Proving Ground DATE: Nov 1994
 LOCATION: Cluster 13 SOUNDING: 2
 COUNTY: AZIMUTH:
 PROJECT: EQUIPMENT:
 ELEVATION: 0.00
 SOUNDING COORDINATES: X: 1.5000 Y: 2.5000

Schlumberger Configuration

FITTING ERROR: 3.983 PERCENT

L #	RESISTIVITY (ohm-m)	THICKNESS (meters)	ELEVATION (meters)	LONG. COND. (Siemens)	TRANS. RES. (Ohm-m ²)
			0.0		
1	1825.6	0.471	-0.471	2.582E-04	860.6
2	82.20	2.13	-2.60	0.0259	175.5
3	256.5	0.705	-3.31	0.00275	181.0
4	1065.5	1.46	-4.78	0.00138	1565.0
5	86.02				

ALL PARAMETERS ARE FREE

No.	SPACING (m)	RHO-A (ohm-m)		DIFFERENCE (percent)
		DATA	SYNTHETIC	
1	0.914	929.6	905.9	2.55
2	1.52	320.0	336.6	-5.17
3	1.82	219.4	219.0	0.170
4	2.13	161.5	159.7	1.11
5	2.43	137.1	131.8	3.86
6	2.74	121.9	120.2	1.33
7	3.04	114.3	116.6	-2.08
8	4.57	121.9	132.3	-8.51
9	6.09	149.3	153.5	-2.82
10	9.14	182.8	180.7	1.14
11	12.19	198.1	189.5	4.34
12	15.24	198.1	187.0	5.58
13	18.28	182.8	178.8	2.20
14	21.33	175.2	168.2	4.00
15	24.38	158.4	157.2	0.804
16	27.43	144.7	146.8	-1.40
17	30.48	129.5	137.4	-6.12
18	36.57	114.3	122.4	-7.17
19	45.72	106.6	108.0	-1.25
20	60.96	97.53	96.51	1.04
21	91.44	94.48	89.75	5.00

Figure B4. Long line electrical resistivity sounding (1.5, 2.5) best-fit model information

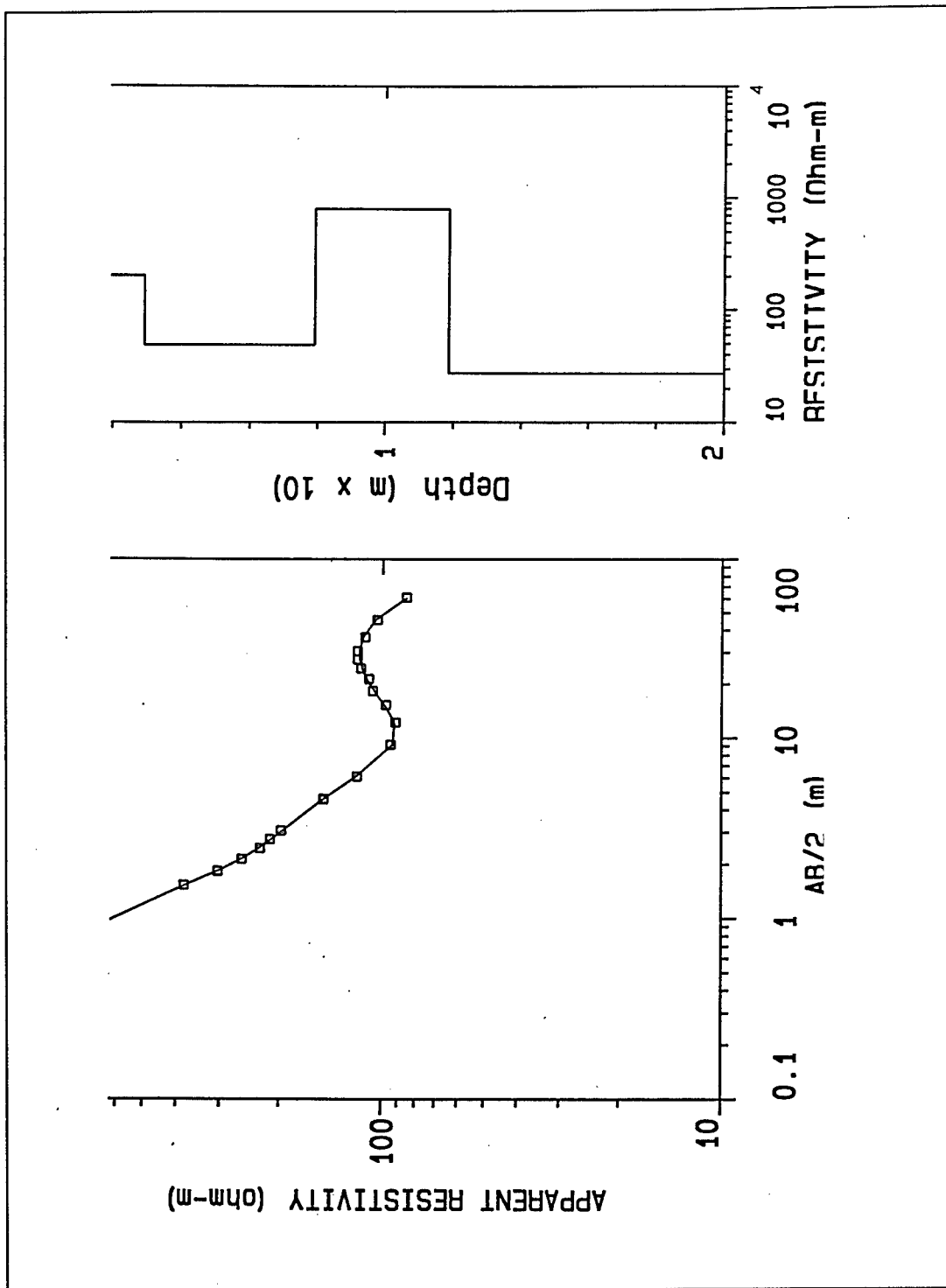


Figure B5. Long line electrical resistivity sounding (2.5, 1.5)

DATA SET: 3

CLIENT: Aberdeen Proving Ground DATE: Nov 1994
 LOCATION: Cluster 13 SOUNDING: 3
 COUNTY: AZIMUTH:
 PROJECT: EQUIPMENT:
 ELEVATION: 6.95
 SOUNDING COORDINATES: X: 2.5000 Y: 1.5000

Schlumberger Configuration

FITTING ERROR: 0.962 PERCENT

L #	RESISTIVITY (ohm-m)	THICKNESS (meters)	ELEVATION (meters)	LONG. COND. (Siemens)	TRANS. RES. (Ohm-m ²)
			6.95		
1	1082.5	0.485	6.46	4.482E-04	525.1
2	201.9	2.43	4.02	0.0120	492.1
3	48.40	4.99	-0.968	0.103	241.8
4	796.1	3.95	-4.92	0.00497	3147.7
5	27.16				

ALL PARAMETERS ARE FREE

No.	SPACING (m)	RHO-A (ohm-m)		DIFFERENCE (percent)
		DATA	SYNTHETIC	
1	0.914	670.5	671.5	-0.149
2	1.52	381.0	378.8	0.575
3	1.82	304.7	305.2	-0.153
4	2.13	259.0	259.9	-0.344
5	2.43	228.6	231.1	-1.09
6	2.74	213.3	211.4	0.886
7	3.04	198.1	196.7	0.672
8	4.57	149.3	149.7	-0.277
9	6.09	118.8	119.6	-0.633
10	9.14	94.48	93.32	1.23
11	12.19	91.44	92.10	-0.728
12	15.24	97.53	98.63	-1.12
13	18.28	106.6	105.7	0.828
14	21.33	109.7	111.4	-1.53
15	24.38	115.8	115.0	0.660
16	27.43	118.8	116.8	1.66
17	30.48	118.8	117.1	1.42
18	36.57	112.7	114.2	-1.34
19	45.72	103.6	104.7	-1.10
20	60.96	85.34	84.89	0.526

Figure B6. Long line electrical resistivity sounding (2.5, 1.5) best-fit model information

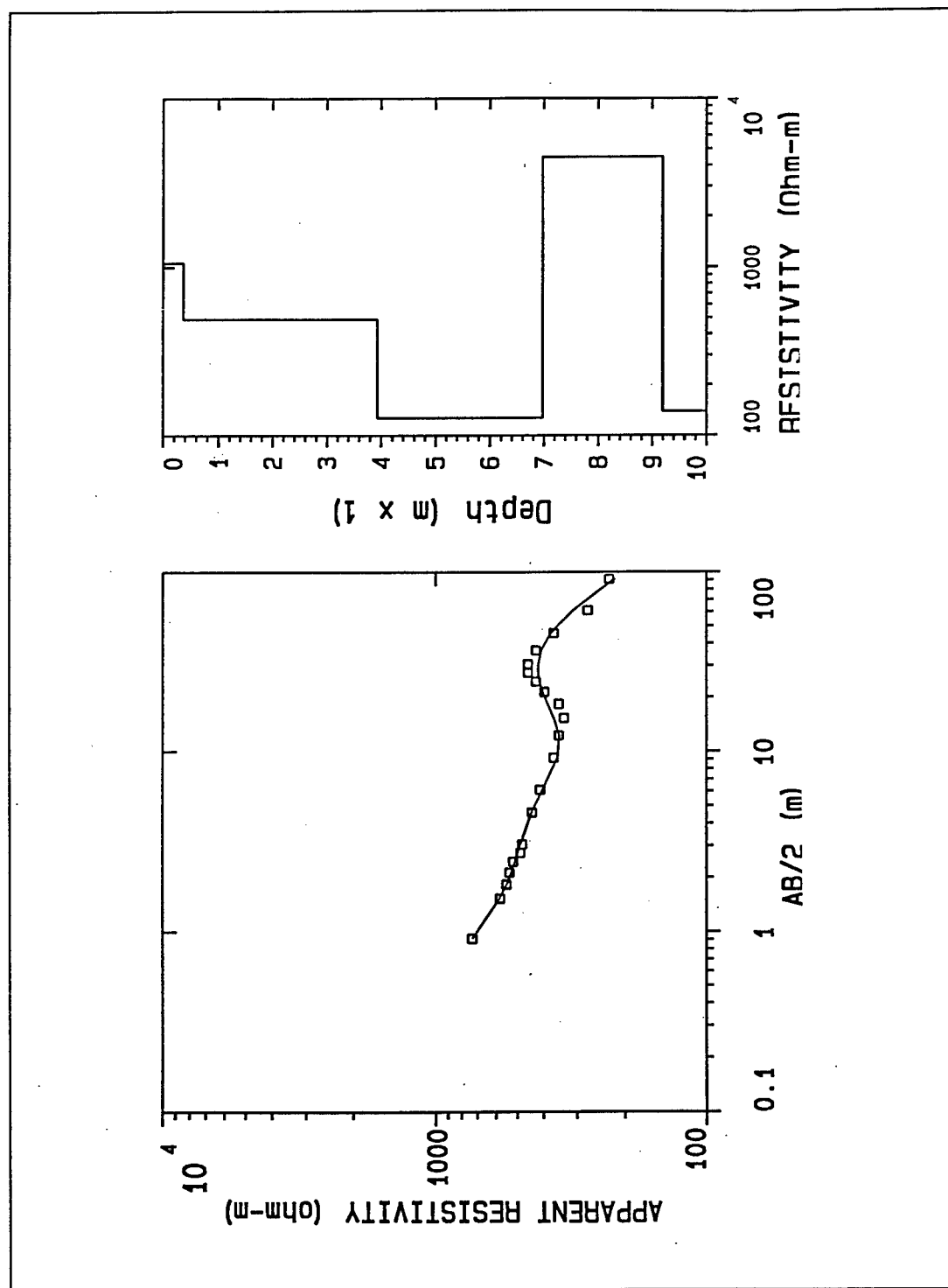


Figure B7. Long line electrical resistivity sounding (3.5, 0.5)

DATA SET: 4

CLIENT: Aberdeen Proving Ground	DATE: Nov 1994
LOCATION: Cluster 13	SOUNDING: 4
COUNTY:	AZIMUTH:
PROJECT:	EQUIPMENT:
ELEVATION: 0.00	
SOUNDING COORDINATES: X: 3.5000 Y: 0.5000	

Schlumberger Configuration

FITTING ERROR: 5.339 PERCENT

L #	RESISTIVITY (ohm-m)	THICKNESS (meters)	ELEVATION (meters)	LONG. COND. (Siemens)	TRANS. RES. (Ohm-m ²)
			0.0		
1	1057.5	0.367	-0.367	3.472E-04	388.3
2	492.4	3.56	-3.93	0.00724	1755.8
3	127.3	3.03	-6.97	0.0238	387.0
4	4492.6	2.22	-9.19	4.943E-04	9976.5
5	138.2				

ALL PARAMETERS ARE FREE

No.	SPACING (m)	RHO-A (ohm-m)		DIFFERENCE (percent)
		DATA	SYNTHETIC	
1	0.914	731.5	730.8	0.0874
2	1.52	579.1	581.6	-0.428
3	1.82	548.6	548.1	0.0830
4	2.13	533.4	526.6	1.26
5	2.43	518.1	511.3	1.31
6	2.74	487.6	499.2	-2.38
7	3.04	480.0	488.8	-1.83
8	4.57	441.9	443.7	-0.399
9	6.09	411.4	403.4	1.95
10	9.14	365.7	354.6	3.04
11	12.19	350.5	349.1	0.393
12	15.24	335.2	365.1	-8.90
13	18.28	350.5	385.3	-9.93
14	21.33	396.2	402.0	-1.46
15	24.38	426.7	412.8	3.24
16	27.43	457.2	417.8	8.60
17	30.48	457.2	417.8	8.60
18	36.57	426.7	406.7	4.67
				-2.34
19	45.72	365.7	374.3	-13.24
20	60.96	274.3	310.6	4.53
21	91.44	228.6	218.2	

Figure B8. Long line electrical resistivity sounding (3.5, 0.5) best-fit model information

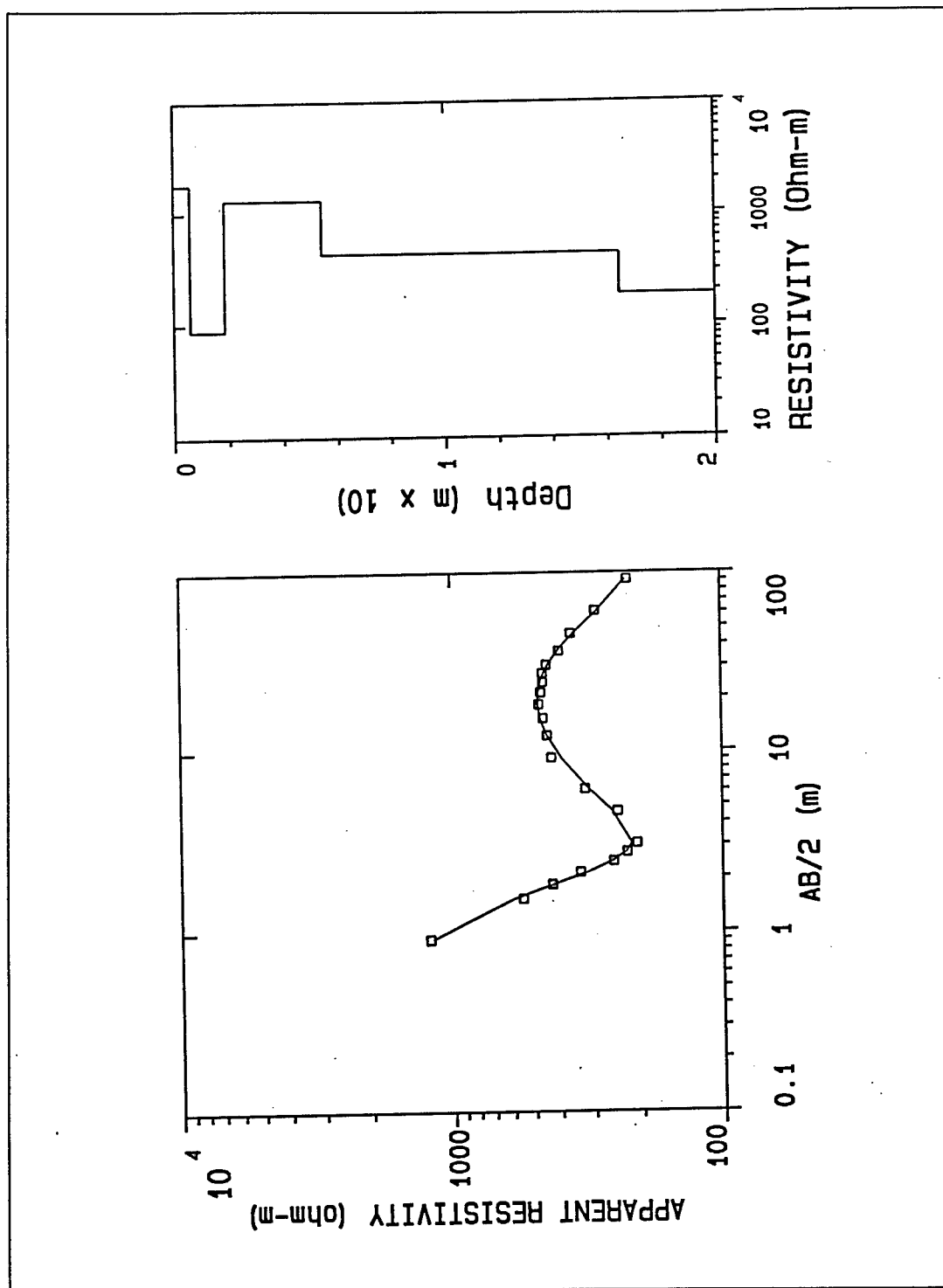


Figure B9. Long line electrical resistivity sounding (4.5, -0.5)

DATA SET: 5

CLIENT: Aberdeen Proving Ground DATE: Nov 1994
 LOCATION: Cluster 13 SOUNDING: 5
 COUNTY: AZIMUTH:
 PROJECT: EQUIPMENT:
 ELEVATION: 0.00
 SOUNDING COORDINATES: X: 4.5000 Y: -0.5000

Schlumberger Configuration

FITTING ERROR: 3.605 PERCENT

L #	RESISTIVITY (ohm-m)	THICKNESS (meters)	ELEVATION (meters)	LONG. COND. (Siemens)	TRANS. RES. (Ohm-m ²)
			0.0		
1	1799.0	0.601	-0.601	3.343E-04	1081.8
2	88.20	1.24	-1.84	0.0141	109.7
3	1299.4	3.57	-5.41	0.00275	4642.7
4	430.5	11.04	-16.46	0.0256	4755.4
5	183.7				

ALL PARAMETERS ARE FREE

No.	SPACING (m)	RHO-A (ohm-m)		DIFFERENCE (percent)
		DATA	SYNTHETIC	
1	0.914	1219.1	1192.0	2.22
2	1.52	548.6	592.7	-8.03
3	1.82	426.7	418.4	1.94
4	2.13	335.2	312.9	6.67
5	2.43	252.9	254.6	-0.656
6	2.74	225.5	226.5	-0.462
7	3.04	207.2	216.3	-4.38
8	4.57	243.8	254.3	-4.33
9	6.09	320.0	309.8	3.18
10	9.14	426.7	392.4	8.03
11	12.19	441.9	442.1	-0.0334
12	15.24	457.2	468.0	-2.38
13	18.28	472.4	477.6	-1.10
14	21.33	464.8	476.0	-2.40
15	24.38	457.2	467.0	-2.14
16	27.43	457.2	453.4	0.828
17	30.48	441.9	437.0	1.10
18	36.57	396.2	401.2	-1.26
19	45.72	358.1	349.9	2.28
20	60.96	289.5	285.6	1.34
21	91.44	220.9	223.9	-1.32

Figure B10. Long line electrical resistivity sounding (4.5, -0.5) best-fit model information

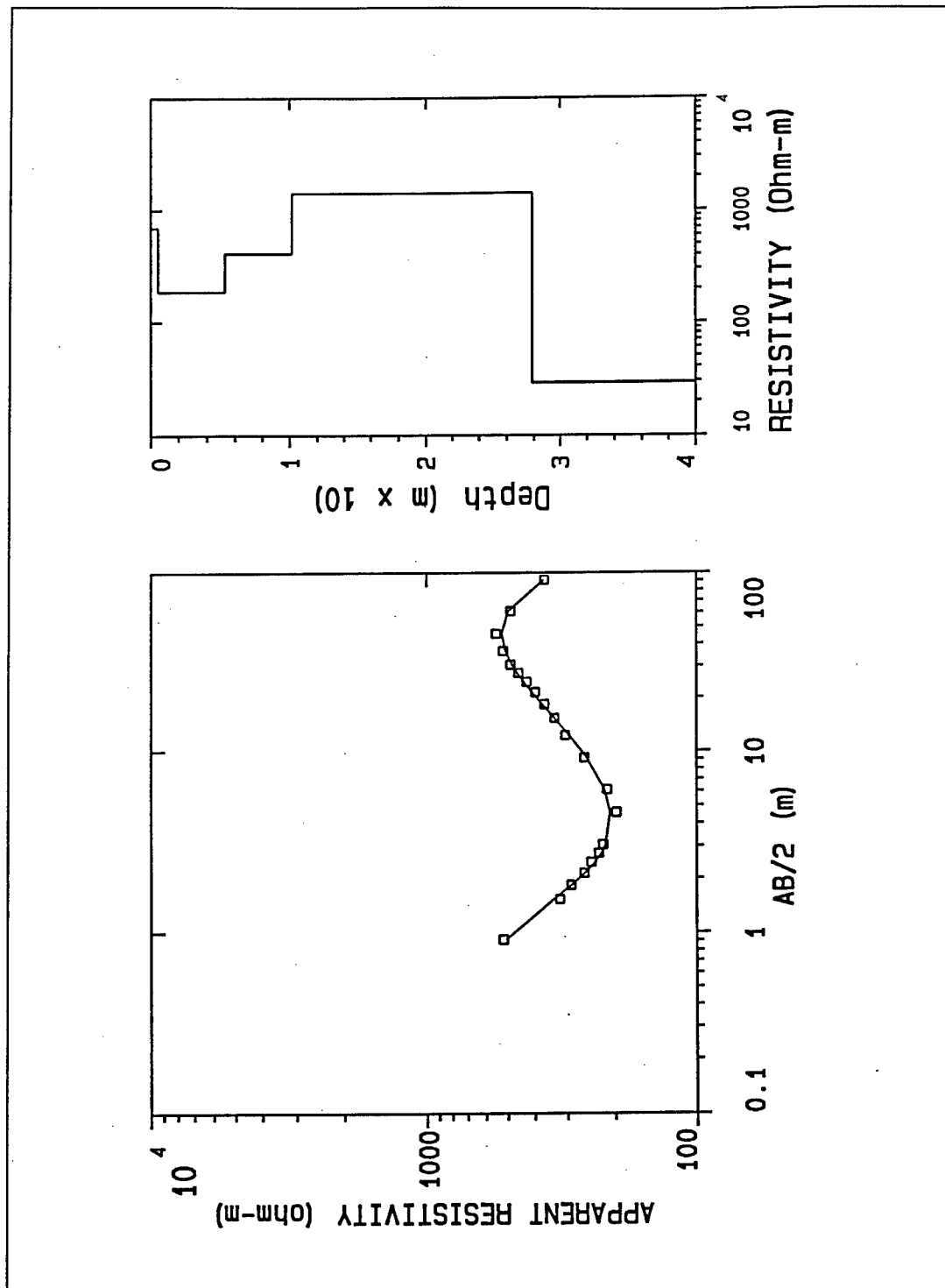


Figure B11. Long line electrical resistivity sounding (5.5, -1.5)

DATA SET: 6

CLIENT: Aberdeen Proving Ground
 LOCATION: Cluster 13
 COUNTY:
 PROJECT:
 ELEVATION: 0.00
 SOUNDING COORDINATES: X: 5.5000 Y: -1.5000

DATE: Nov 1994
 SOUNDING: 6
 AZIMUTH:
 EQUIPMENT:

Schlumberger Configuration

FITTING ERROR: 2.721 PERCENT

L #	RESISTIVITY (ohm-m)	THICKNESS (meters)	ELEVATION (meters)	LONG. COND. (Siemens)	TRANS. RES. (Ohm-m ²)
			0.0		
1	694.5	0.545	-0.545	7.854E-04	378.8
2	186.2	4.72	-5.27	0.0253	880.0
3	409.0	4.88	-10.15	0.0119	1998.5
4	1419.5	17.71	-27.87	0.0124	25154.2
5	28.89				

ALL PARAMETERS ARE FREE

No.	SPACING (m)	RHO-A (ohm-m)		DIFFERENCE (percent)
		DATA	SYNTHETIC	
1	0.914	518.1	506.9	2.16
2	1.52	320.0	338.1	-5.65
3	1.82	289.5	288.8	0.245
4	2.13	259.0	256.9	0.820
5	2.43	243.8	236.8	2.88
6	2.74	228.6	224.2	1.89
7	3.04	220.9	216.5	2.01
8	4.57	198.1	208.6	-5.30
9	6.09	213.3	218.1	-2.25
10	9.14	259.0	252.7	2.43
11	12.19	304.7	294.0	3.54
12	15.24	335.2	335.0	0.0613
13	18.28	365.7	373.2	-2.05
14	21.33	396.2	407.3	-2.80
15	24.38	426.7	436.8	-2.38
16	27.43	457.2	461.6	-0.982
17	30.48	487.6	481.9	1.18
18	36.57	518.1	509.4	1.67
19	45.72	548.6	523.6	4.56
20	60.96	487.6	497.1	-1.93
21	91.44	365.7	367.7	-0.557

Figure B12. Long line electrical resistivity sounding (5.5, -1.5) best-fit model information

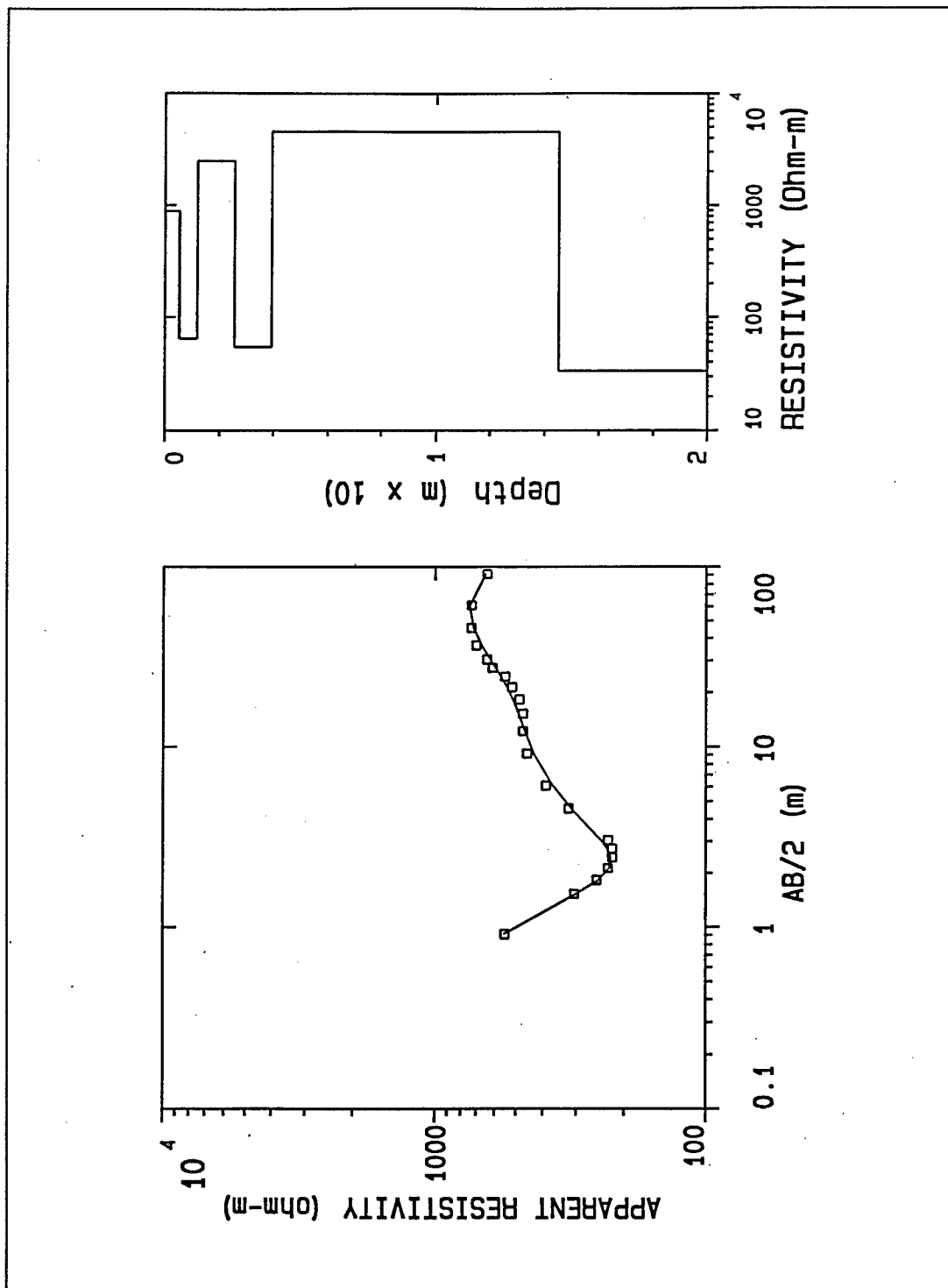


Figure B13. Long line electrical resistivity sounding (6.5, -2.5)

DATA SET: 7

CLIENT: Aberdeen Proving Ground DATE: Nov 1994
 LOCATION: Cluster 13 SOUNDING: 7
 COUNTY: AZIMUTH:
 PROJECT: EQUIPMENT:
 ELEVATION: 0.00
 SOUNDING COORDINATES: X: 6.5000 Y: -2.5000

Schlumberger Configuration

FITTING ERROR: 3.450 PERCENT

L #	RESISTIVITY (ohm-m)	THICKNESS (meters)	ELEVATION (meters)	LONG. COND. (Siemens)	TRANS. RES. (Ohm-m ²)
			0.0		
1	888.6	0.538	-0.538	6.062E-04	478.7
2	64.83	0.659	-1.19	0.0101	42.77
3	2481.4	1.33	-2.53	5.380E-04	3312.7
4	54.35	1.39	-3.93	0.0256	75.90
5	4536.7	10.58	-14.51	0.00233	48033.3
6	33.26				

ALL PARAMETERS ARE FREE

No.	SPACING (m)	RHO-A (ohm-m)		DIFFERENCE (percent)
		DATA	SYNTHETIC	
1	0.914	548.6	554.3	-1.04
2	1.52	304.7	301.3	1.13
3	1.82	251.4	248.0	1.35
4	2.13	228.6	226.2	1.01
5	2.43	220.9	223.2	-1.01
6	2.74	220.9	230.4	-4.26
7	3.04	228.6	242.4	-6.04
8	4.57	320.0	312.8	2.23
9	6.09	388.6	366.9	5.57
10	9.14	457.2	431.1	5.70
11	12.19	472.4	465.2	1.51
12	15.24	472.4	489.9	-3.69
13	18.28	487.6	513.7	-5.35
14	21.33	518.1	539.5	-4.12
15	24.38	548.6	566.9	-3.33
16	27.43	609.5	594.7	2.43
17	30.48	640.0	621.7	2.85
18	36.57	701.0	669.6	4.48
19	45.72	731.5	718.9	1.71
20	60.96	731.5	741.2	-1.33
21	91.44	640.0	645.8	-0.904

Figure B14. Long line electrical resistivity sounding (6.5, -2.5) best-fit model information

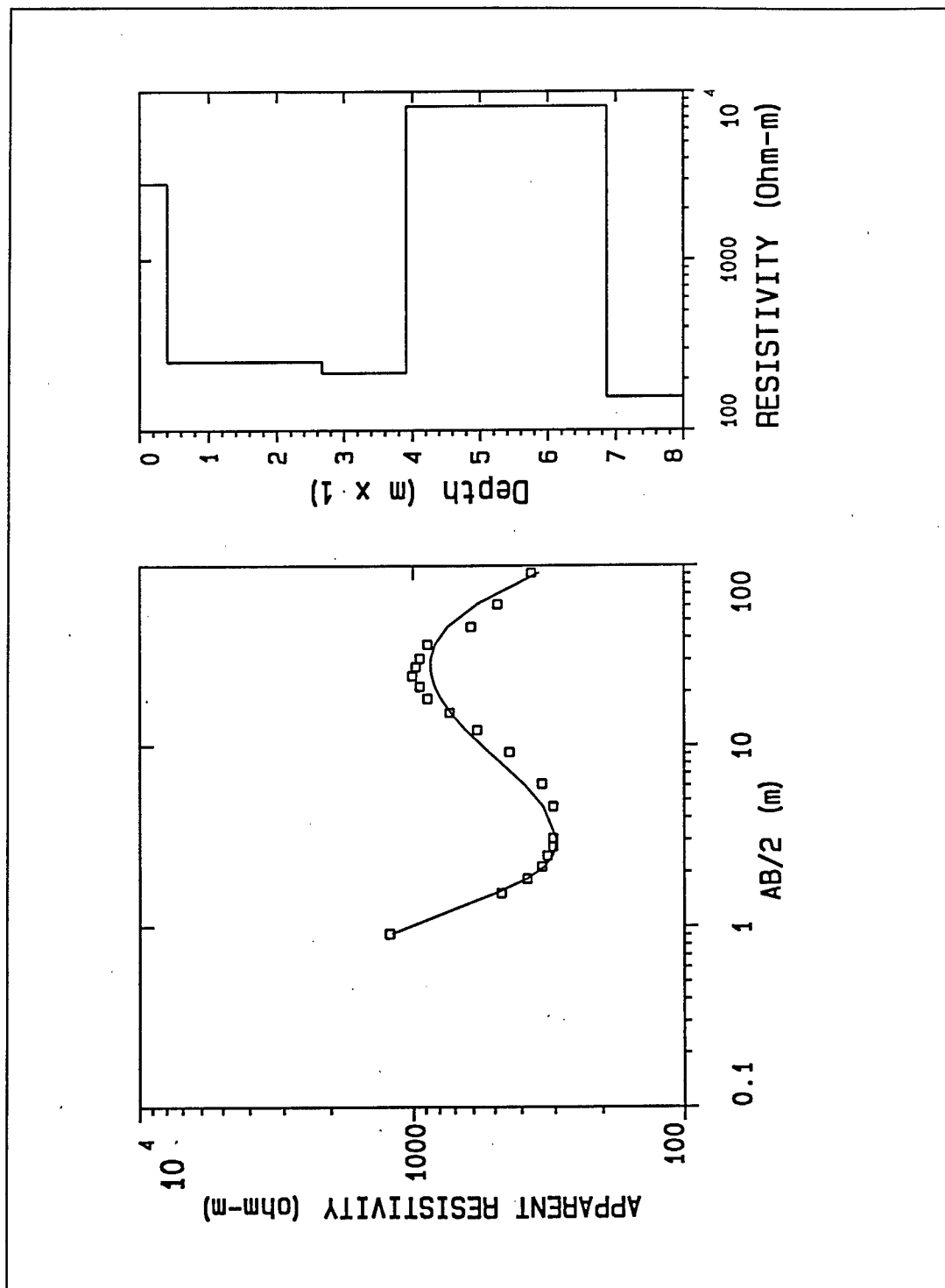


Figure B15. Long line electrical resistivity sounding (7.5, -3.5)

DATA SET: 8					
CLIENT: Aberdeen Proving Ground			DATE: Nov 1994		
LOCATION: Cluster 13			SOUNDING: 8		
COUNTY:			AZIMUTH:		
PROJECT:			EQUIPMENT:		
ELEVATION: 0.00					
SOUNDING COORDINATES: X:			7.5000	Y:	-3.5000
Schlumberger Configuration					
FITTING ERROR:			11.155 PERCENT		
L #	RESISTIVITY (ohm-m)	THICKNESS (meters)	ELEVATION (meters)	LONG. COND. (Siemens)	TRANS. RES. (Ohm-m^2)
			0.0		
1	2833.8	0.398	-0.398	1.406E-04	1128.8
2	252.9	2.27	-2.67	0.00898	574.8
3	217.4	1.23	-3.90	0.00569	269.1
4	8162.1	2.95	-6.86	3.621E-04	24125.9
5	157.2				
ALL PARAMETERS ARE FREE					
No.	SPACING (m)	RHO-A (ohm-m)		DIFFERENCE (percent)	
		DATA	SYNTHETIC		
1	0.914	1219.1	1198.1		1.72
2	1.52	472.4	495.4		-4.86
3	1.82	381.0	380.4		0.134
4	2.13	335.2	328.1		2.11
5	2.43	320.0	305.8		4.43
6	2.74	304.7	297.8		2.28
7	3.04	304.7	296.8		2.59
8	4.57	304.7	331.7		-8.83
9	6.09	335.2	391.0		-16.64
10	9.14	441.9	522.3		-18.18
11	12.19	579.1	636.0		-9.83
12	15.24	731.5	723.7		1.06
13	18.28	883.9	786.7		10.98
14	21.33	944.8	828.5		12.30
15	24.38	1005.8	852.4		15.24
16	27.43	975.3	861.6		11.66
17	30.48	944.8	858.8		9.10
18	36.57	883.9	827.4		6.38
19	45.72	609.5	743.3		-21.94
20	60.96	487.6	580.1		-18.95
21	91.44	365.7	342.3		6.39

Figure B16. Long line electrical resistivity sounding (7.5, -3.5) best-fit model information

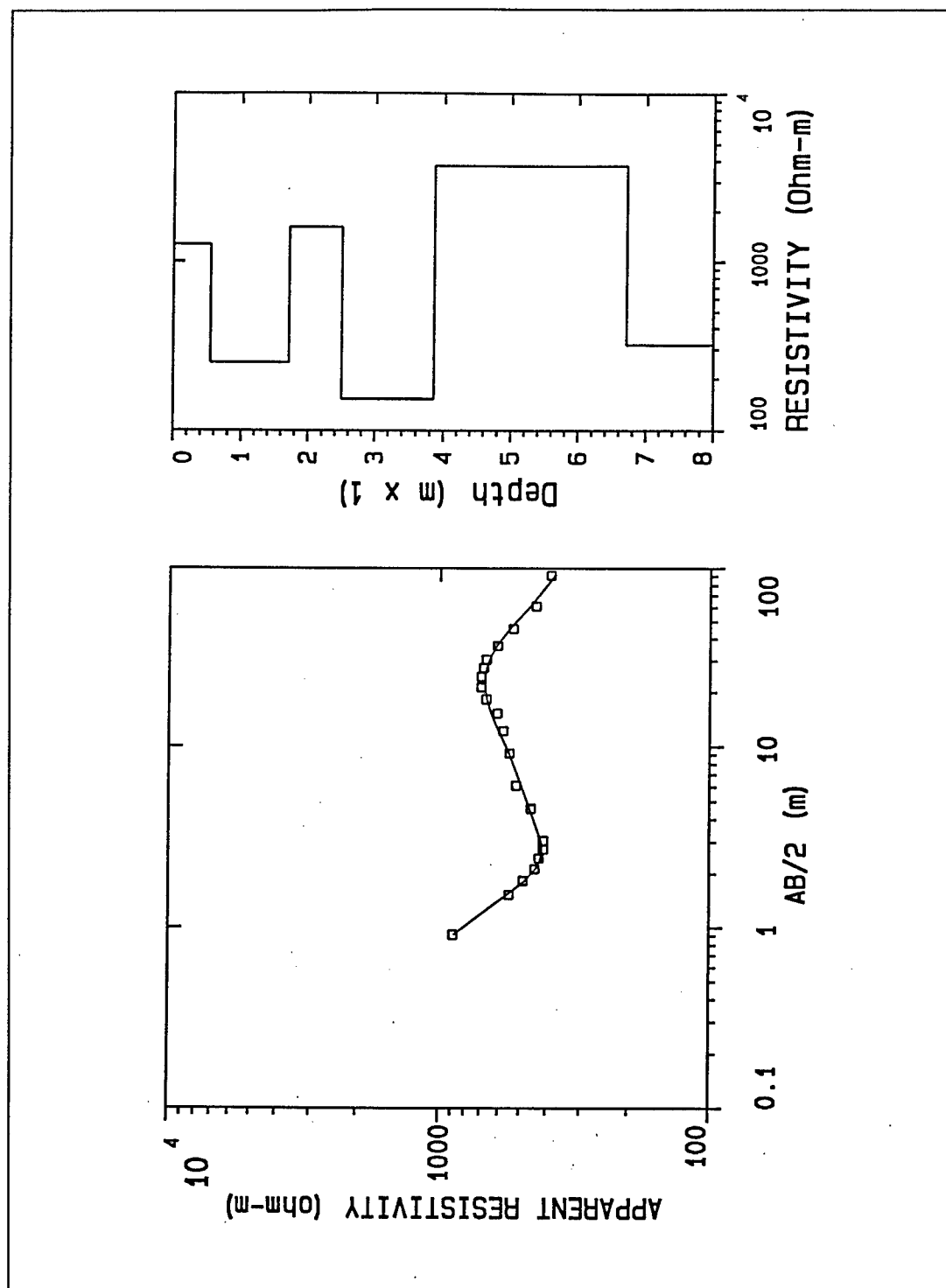


Figure B17. Long line electrical resistivity sounding (8.5, -4.5)

DATA SET: 9

CLIENT: Aberdeen Proving Ground
LOCATION: Cluster 13
COUNTY:
PROJECT:
ELEVATION: 0.00
SOUNDING COORDINATES: X: 8.5000 Y: -4.5000

DATE: Nov 1994
SOUNDING: 9
AZIMUTH:
EQUIPMENT:

Schlumberger Configuration

FITTING ERROR: 2.748 PERCENT

L #	RESISTIVITY (ohm-m)	THICKNESS (meters)	ELEVATION (meters)	LONG. COND. (Siemens)	TRANS. RES. (Ohm-m ²)
			0.0		
1	1266.7	0.541	-0.541	4.276E-04	686.1
2	250.0	1.17	-1.71	0.00470	293.9
3	1613.9	0.785	-2.50	4.868E-04	1268.1
4	152.4	1.36	-3.86	0.00893	207.6
5	3737.4	2.84	-6.71	7.617E-04	10640.4
6	318.0				

ALL PARAMETERS ARE FREE

No.	SPACING (m)	RHO-A (ohm-m)		DIFFERENCE (percent)
		DATA	SYNTHETIC	
1	0.914	883.9	880.0	0.435
2	1.52	548.6	560.2	-2.12
3	1.82	487.6	480.6	1.44
4	2.13	441.9	438.5	0.776
5	2.43	426.7	420.3	1.50
6	2.74	411.4	416.2	-1.15
7	3.04	411.4	419.6	-1.98
8	4.57	457.2	462.2	-1.10
9	6.09	518.1	496.6	4.14
10	9.14	548.6	551.1	-0.451
11	12.19	579.1	601.8	-3.91
12	15.24	609.5	642.1	-5.33
13	18.28	670.5	667.4	0.467
14	21.33	701.0	678.3	3.24
15	24.38	701.0	677.5	3.34
16	27.43	685.7	668.2	2.55
17	30.48	670.5	653.1	2.59
18	36.57	609.5	613.5	-0.653
19	45.72	533.4	549.5	-3.03
20	60.96	441.9	462.9	-4.75
21	91.44	388.6	375.8	3.29

Figure B18. Long line electrical resistivity sounding (8.5, -4.5) best-fit model information

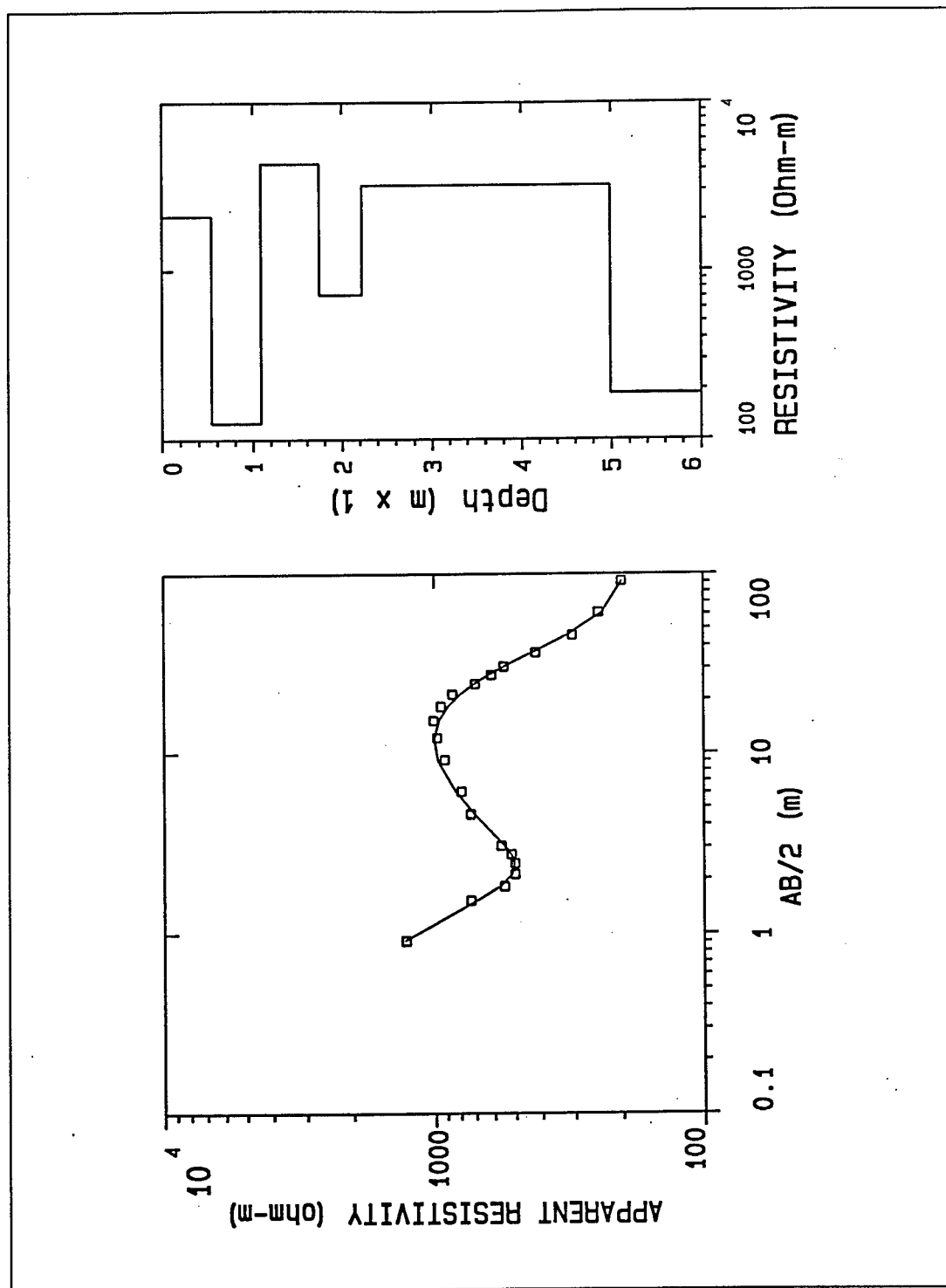


Figure B19. Long line electrical resistivity sounding (9.5, -5.5)

DATA SET: 10

CLIENT: Aberdeen Proving Ground DATE: Nov 1994
 LOCATION: Cluster 13 SOUNDING: 10
 COUNTY: AZIMUTH:
 PROJECT: EQUIPMENT:
 ELEVATION: 0.00
 SOUNDING COORDINATES: X: 9.5000 Y: -5.5000

Schlumberger Configuration

FITTING ERROR: 3.678 PERCENT

L #	RESISTIVITY (ohm-m)	THICKNESS (meters)	ELEVATION (meters)	LONG. COND. (Siemens)	TRANS. RES. (Ohm-m ²)
			0.0		
1	2098.2	0.540	-0.540	2.574E-04	1133.4
2	125.8	0.547	-1.08	0.00435	68.92
3	4310.2	0.652	-1.74	1.513E-04	2810.6
4	715.9	0.486	-2.22	6.796E-04	348.3
5	3202.8	2.76	-4.99	8.631E-04	8853.6
6	187.5				

ALL PARAMETERS ARE FREE

No.	SPACING (m)	RHO-A (ohm-m)		DIFFERENCE (percent)
		DATA	SYNTHETIC	
1	0.914	1280.1	1298.9	-1.47
2	1.52	731.5	694.8	5.01
3	1.82	548.6	567.2	-3.39
4	2.13	502.9	514.1	-2.23
5	2.43	502.9	505.1	-0.434
6	2.74	518.1	519.9	-0.344
7	3.04	563.8	546.1	3.14
8	4.57	731.5	705.0	3.62
9	6.09	792.4	831.0	-4.86
10	9.14	914.4	971.4	-6.23
11	12.19	975.3	1001.3	-2.66
12	15.24	1005.8	963.1	4.24
13	18.28	944.8	888.8	5.93
14	21.33	853.4	799.8	6.27
15	24.38	701.0	709.3	-1.18
16	27.43	609.5	624.7	-2.49
17	30.48	548.6	549.3	-0.136
18	36.57	419.1	429.9	-2.58
19	45.72	304.7	317.9	-4.30
20	60.96	243.8	236.7	2.91
21	91.44	201.1	199.9	0.591

Figure B20. Long line electrical resistivity sounding (9.5, -5.5) best-fit model information

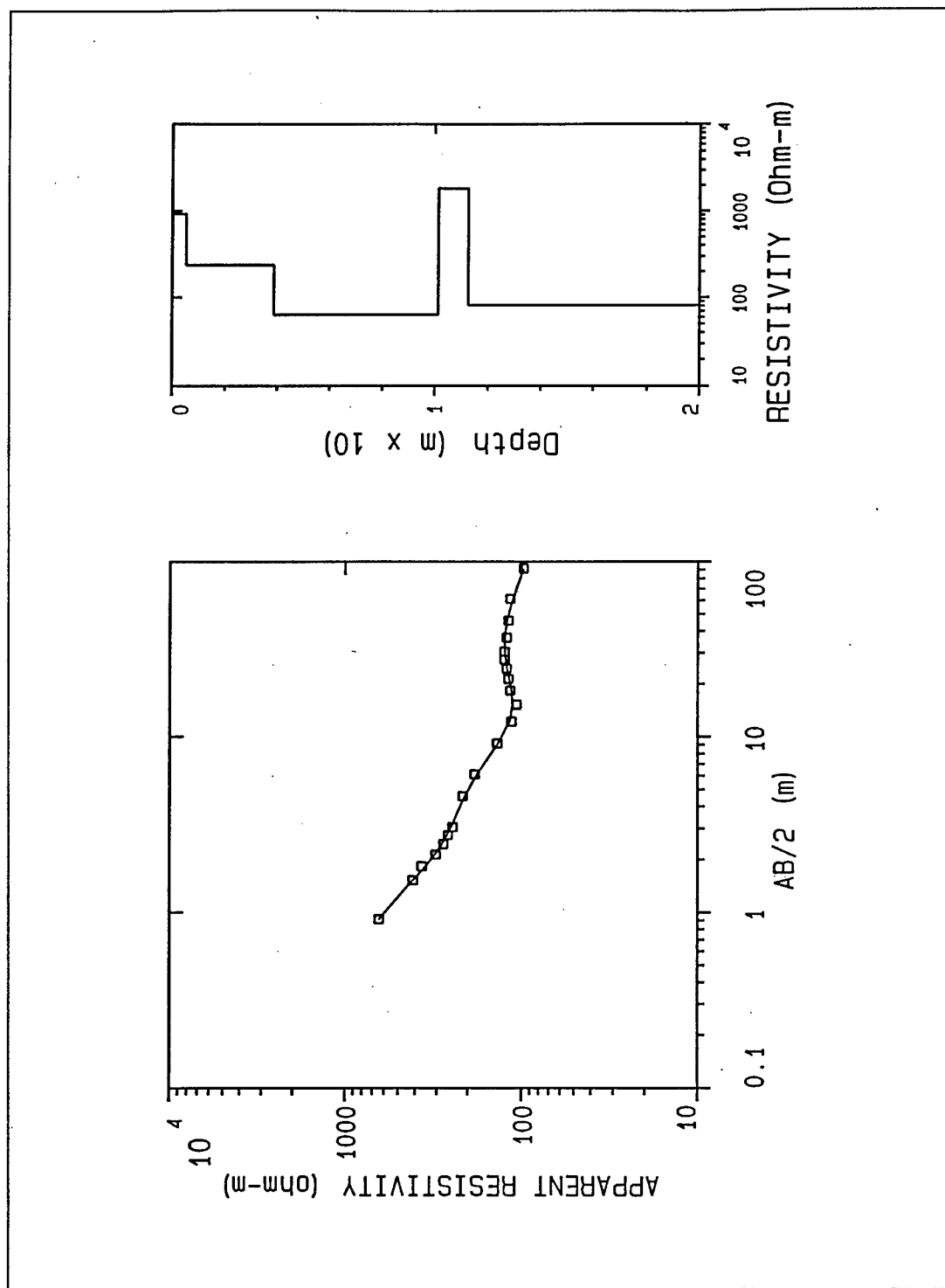


Figure B21. Cross line 1 electrical resistivity sounding (3.5, 2.5)

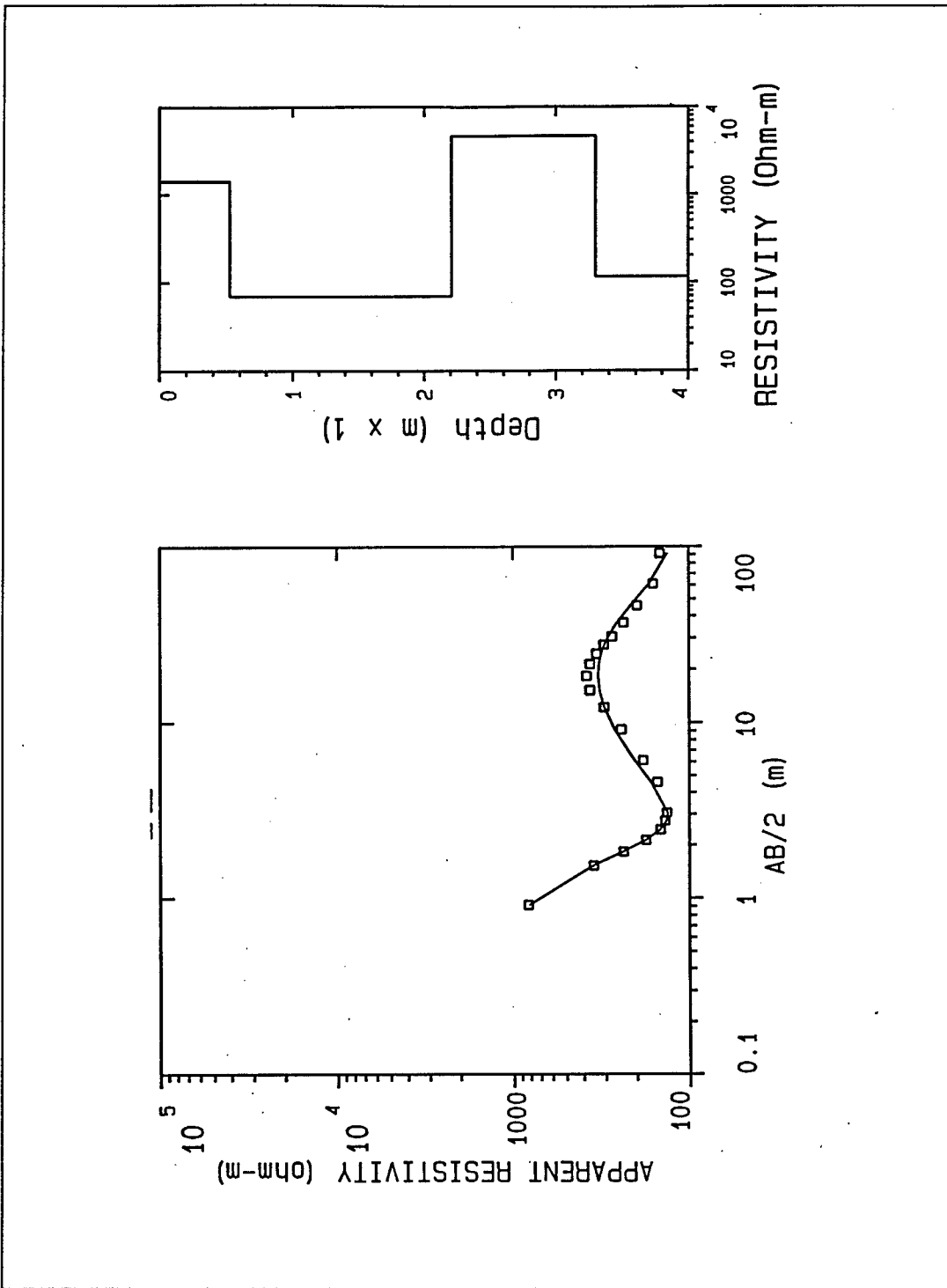


Figure B22. Cross line 2 electrical resistivity sounding (5.5, -3.5)

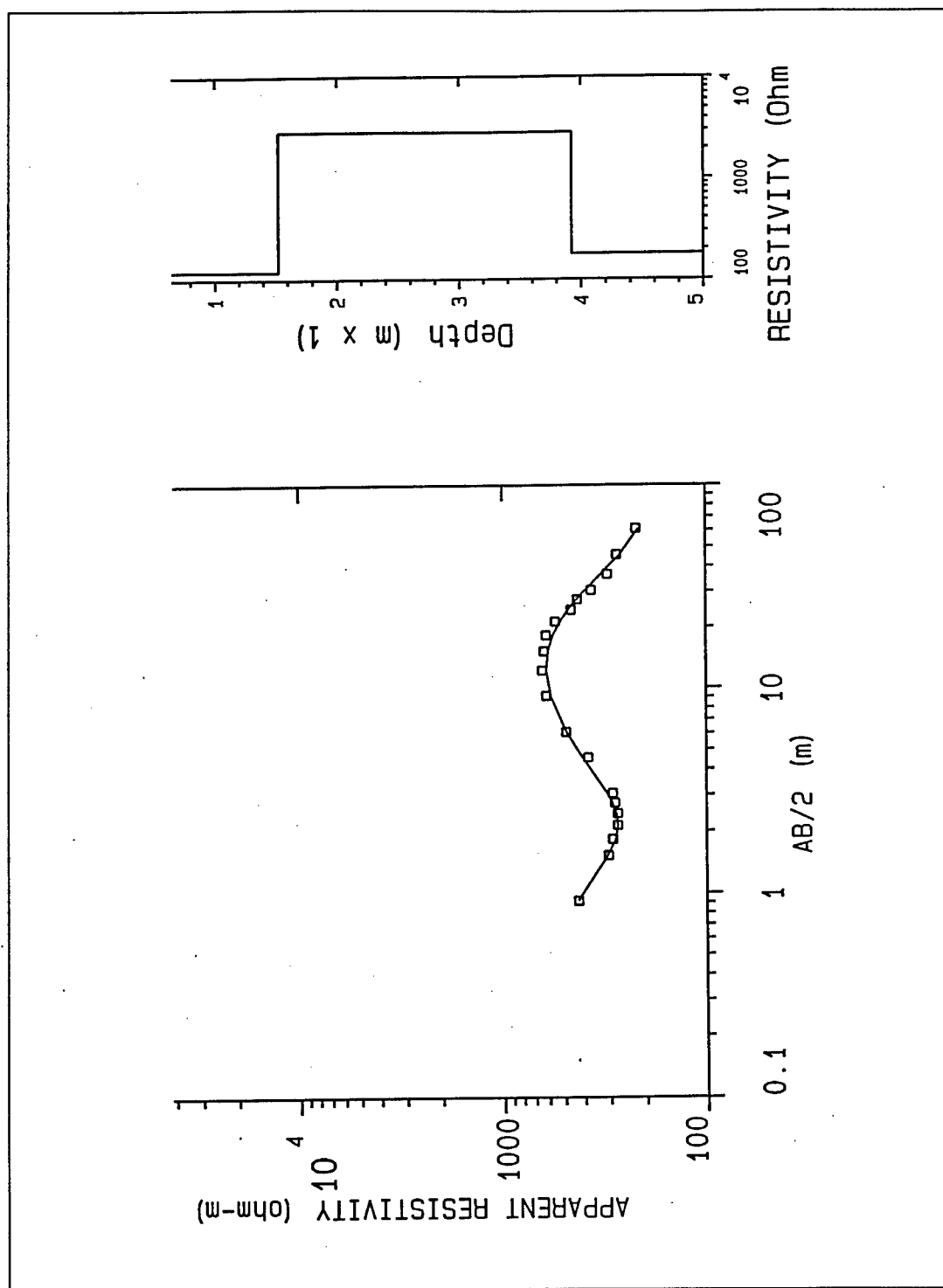


Figure B23. Cross line 2 electrical resistivity sounding (6.5, -2.5)

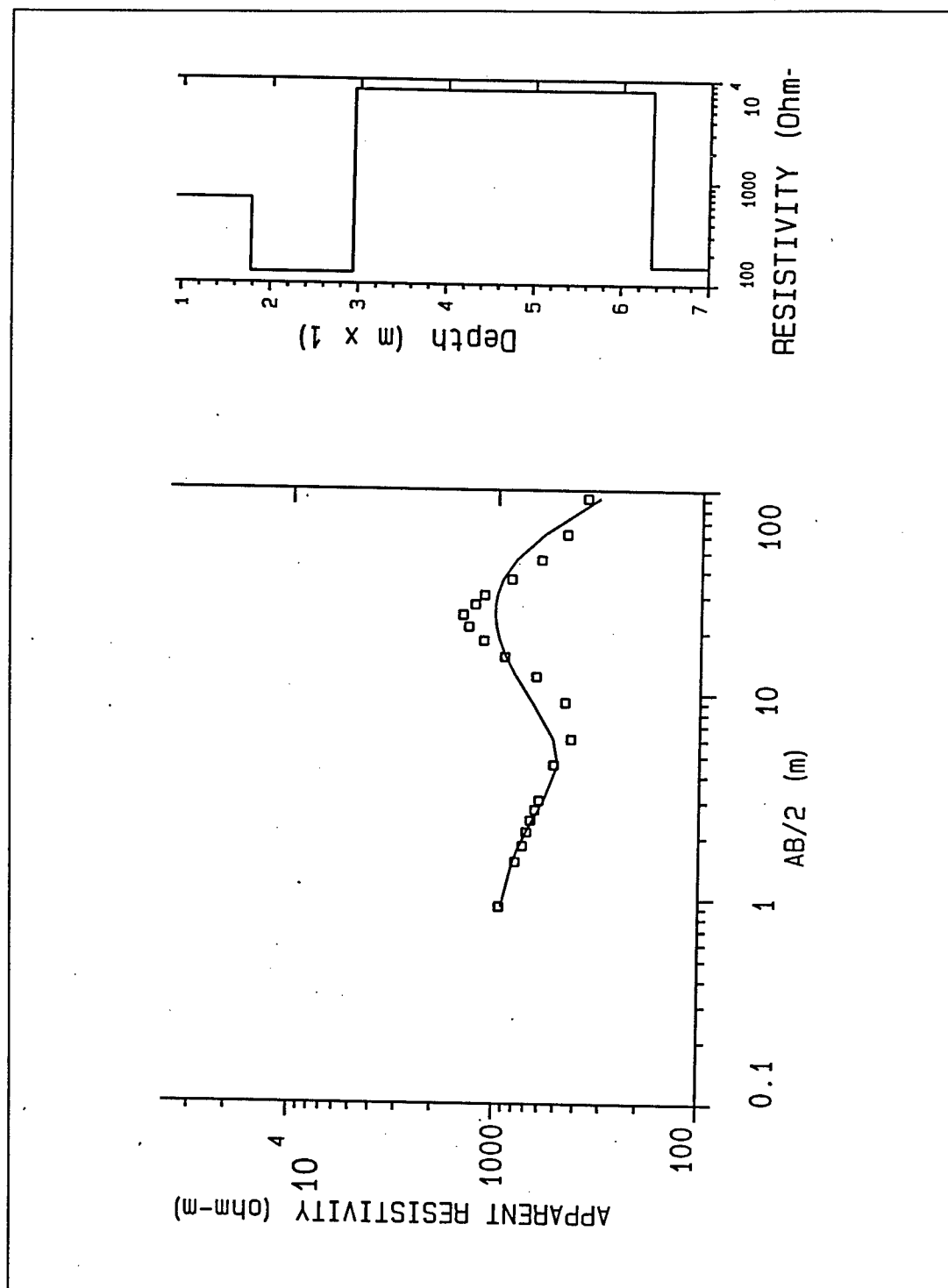


Figure B24. Cross line 2 electrical resistivity sounding (7.5, -1.5)

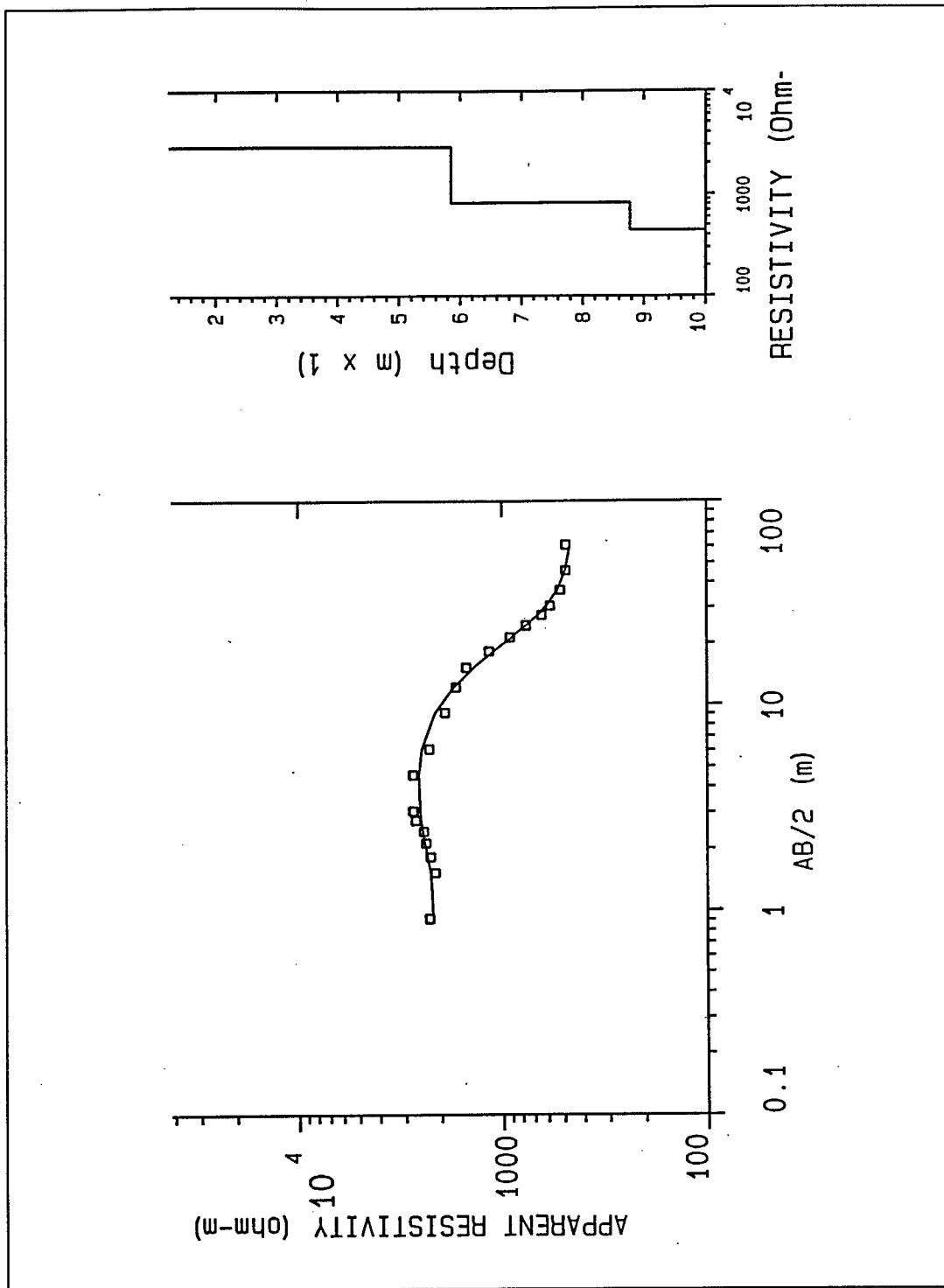


Figure B25. Cross line 3 electrical resistivity sounding (9.5, -7.5)

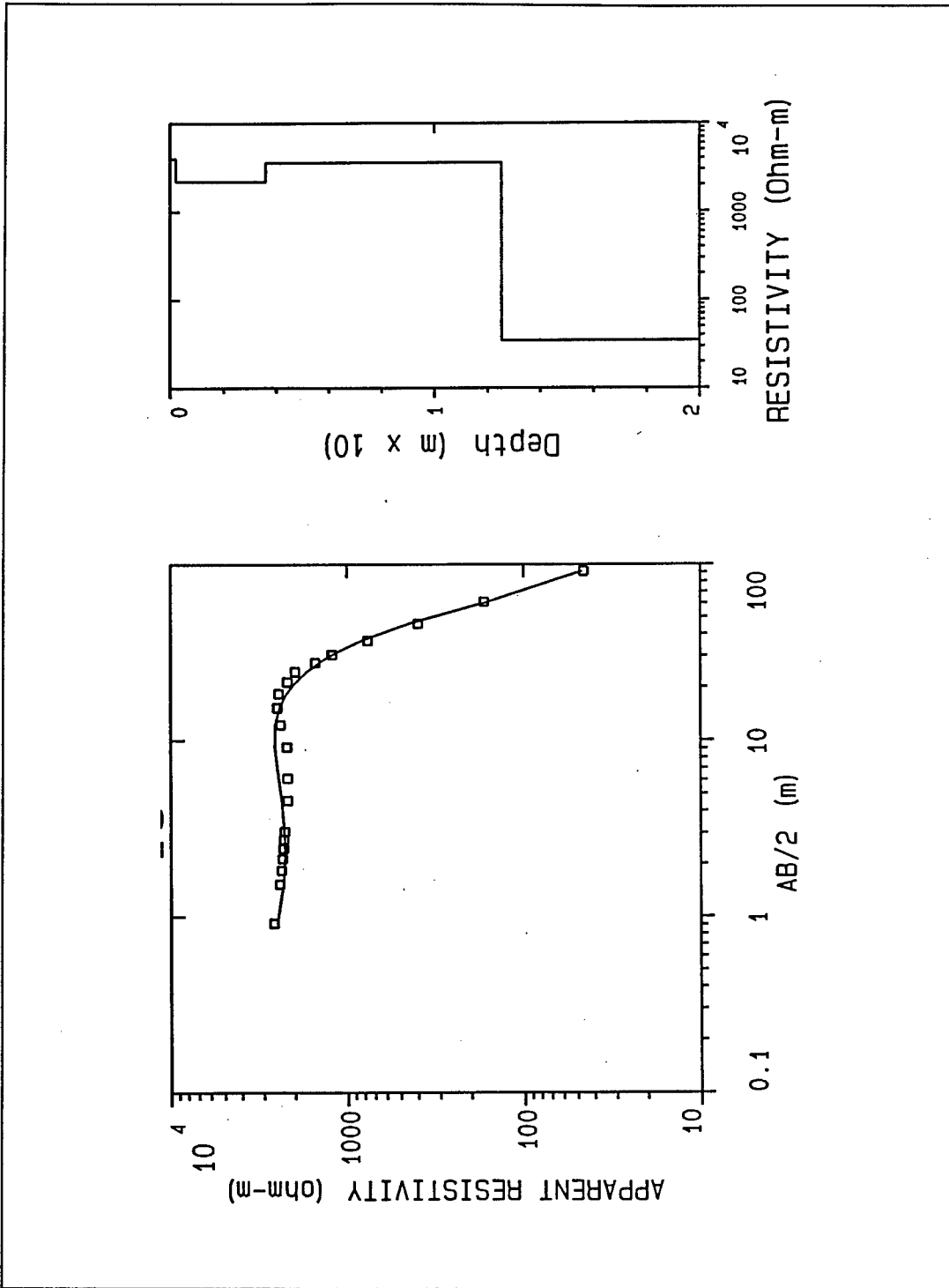


Figure B26. Cross line 3 electrical resistivity sounding (10.5, -6.5)

Appendix C

Transient Electromagnetic Sounding Data

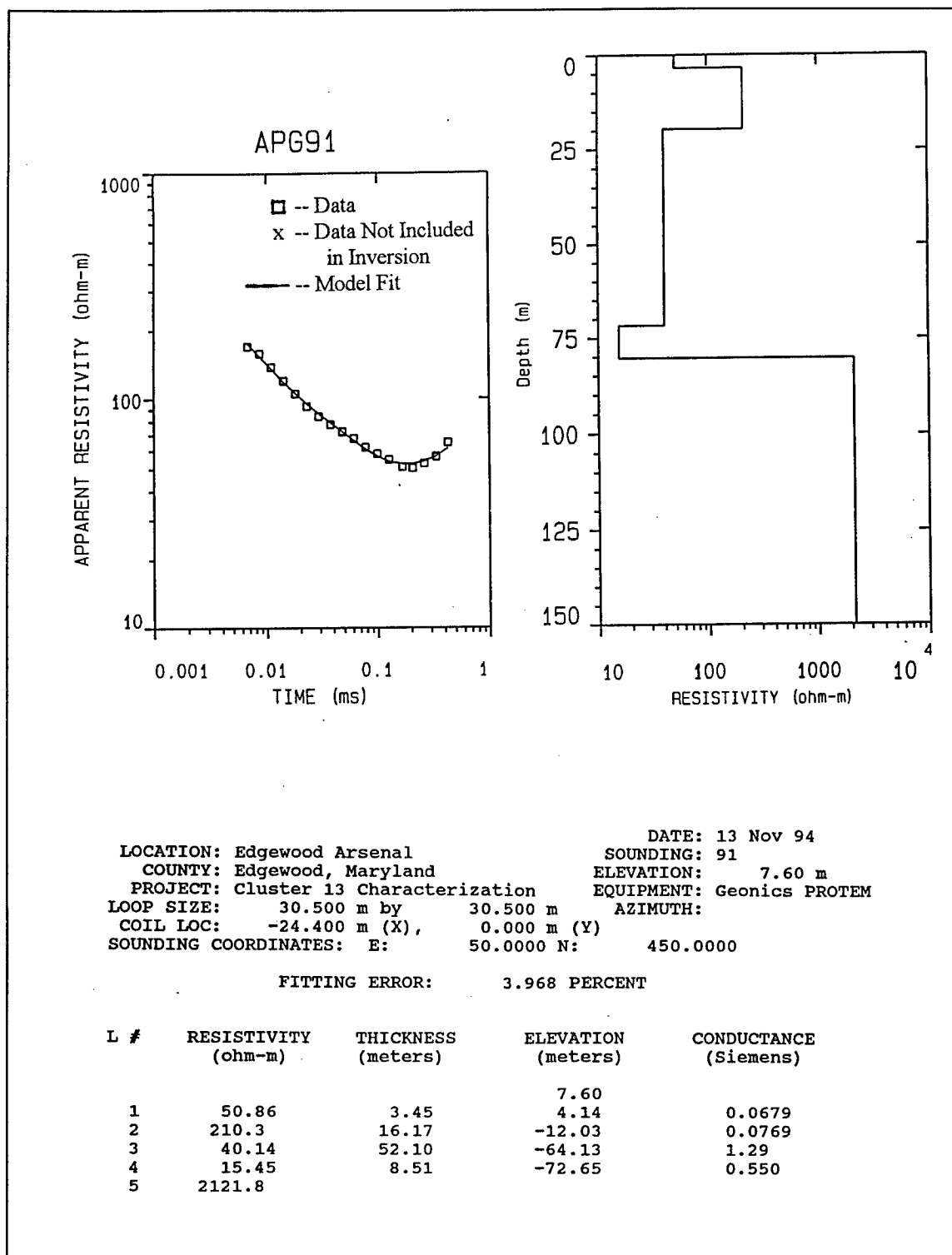


Figure C1. Transient electromagnetic data, best-fit model, and best-fit model parameters list for sounding APG91

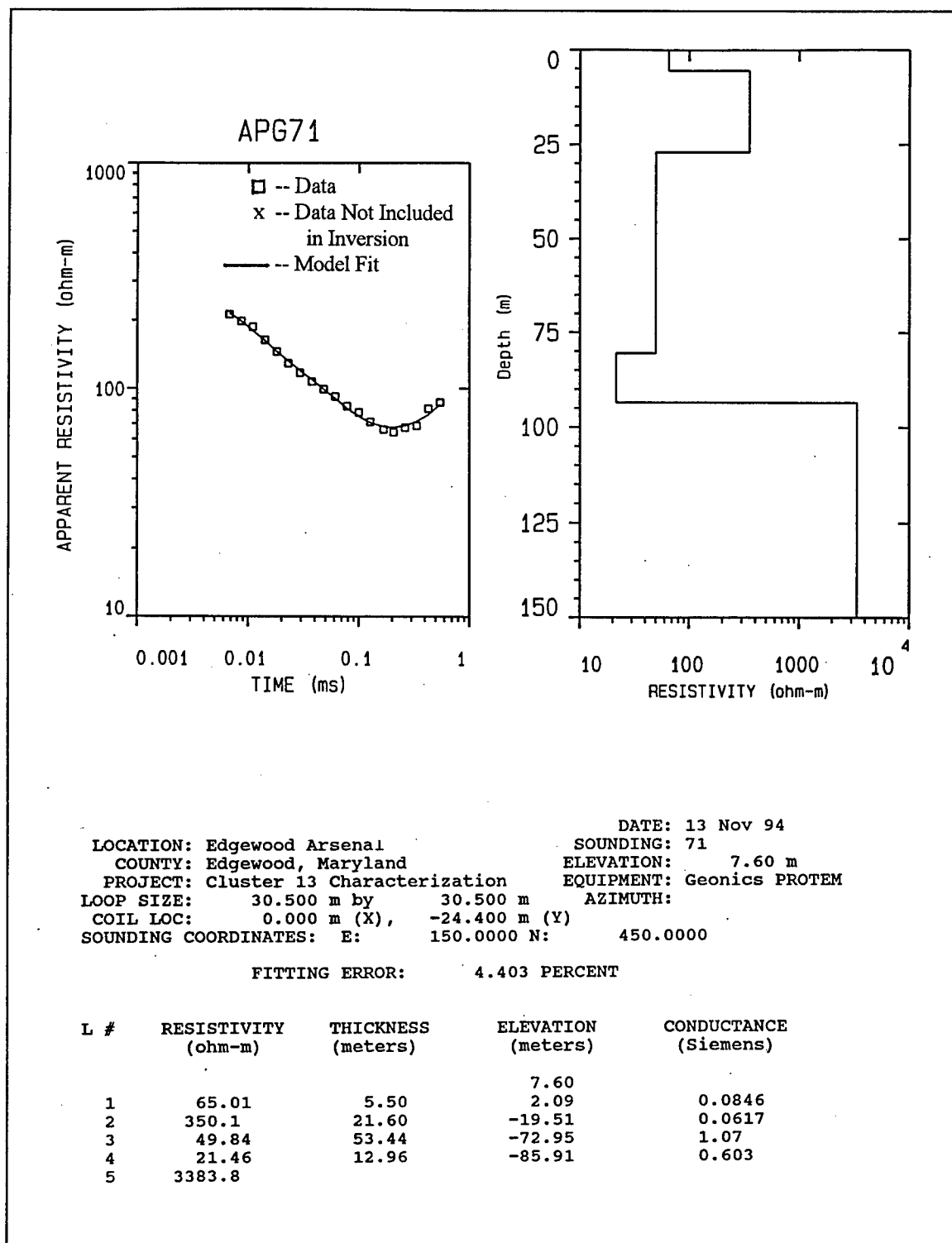


Figure C2. Transient electromagnetic data, best-fit model, and best-fit model parameters list for sounding APG71

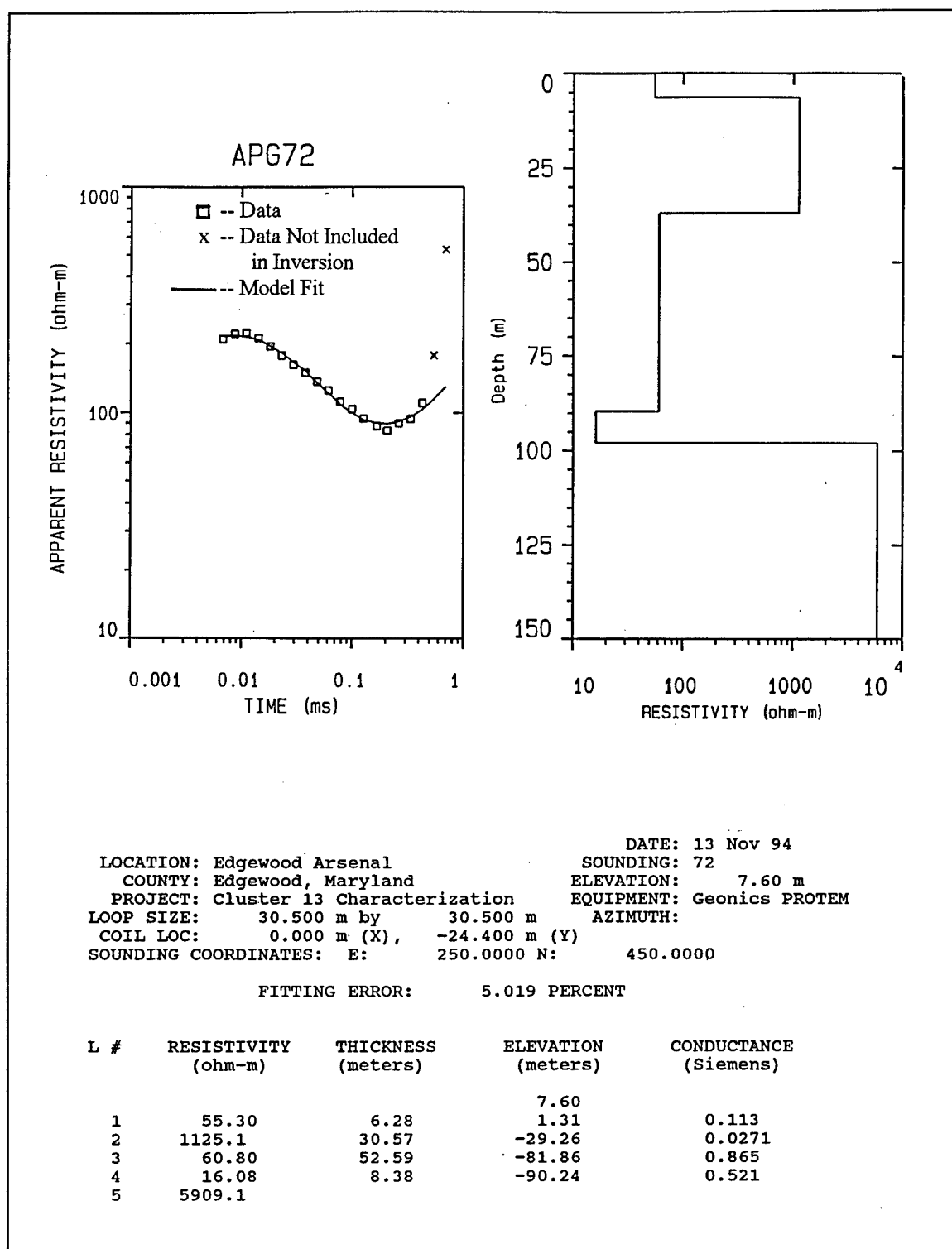


Figure C3. Transient electromagnetic data, best-fit model, and best-fit model parameters list for sounding APG72

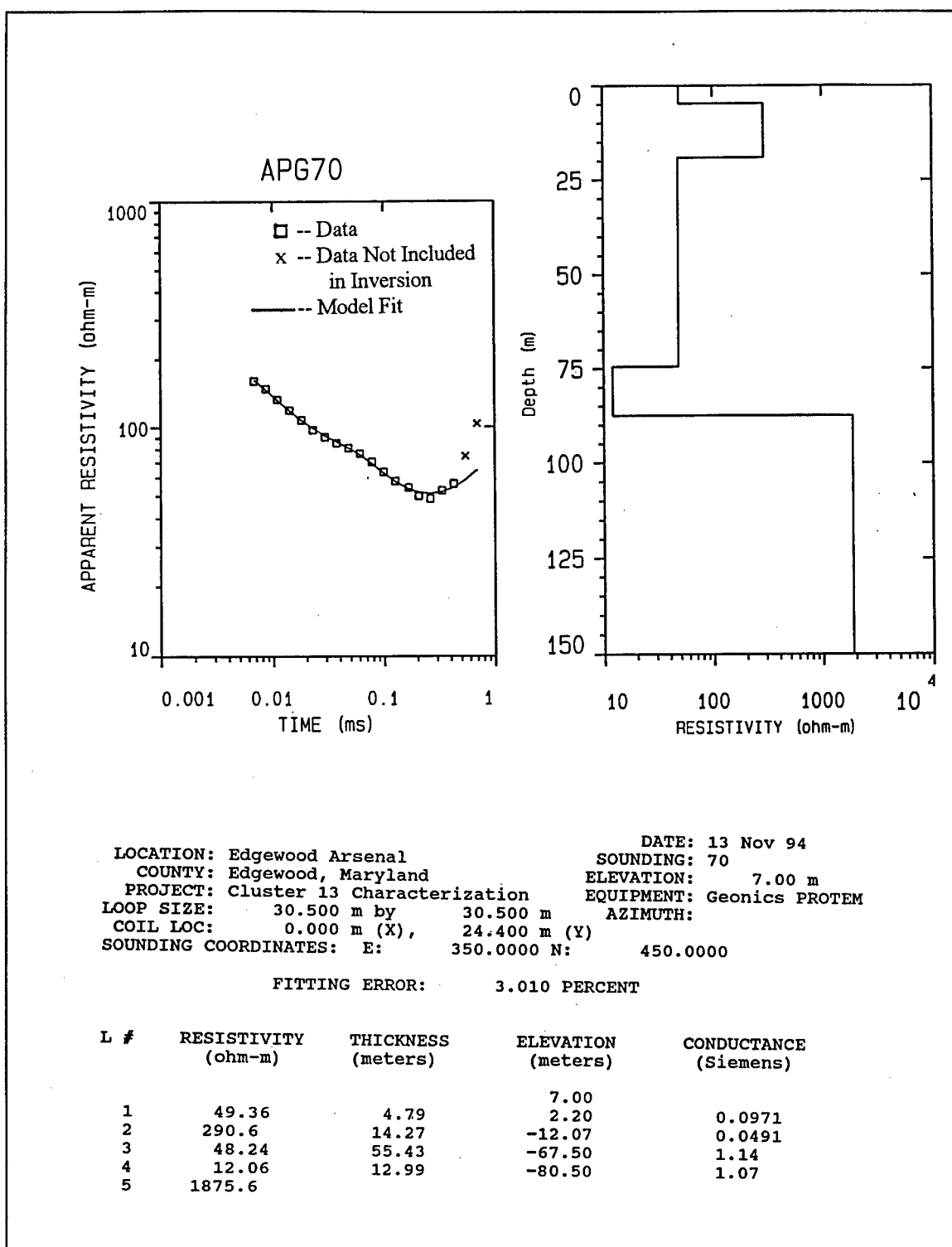


Figure C4. Transient electromagnetic data, best-fit model, and best-fit model parameters list for sounding APG70

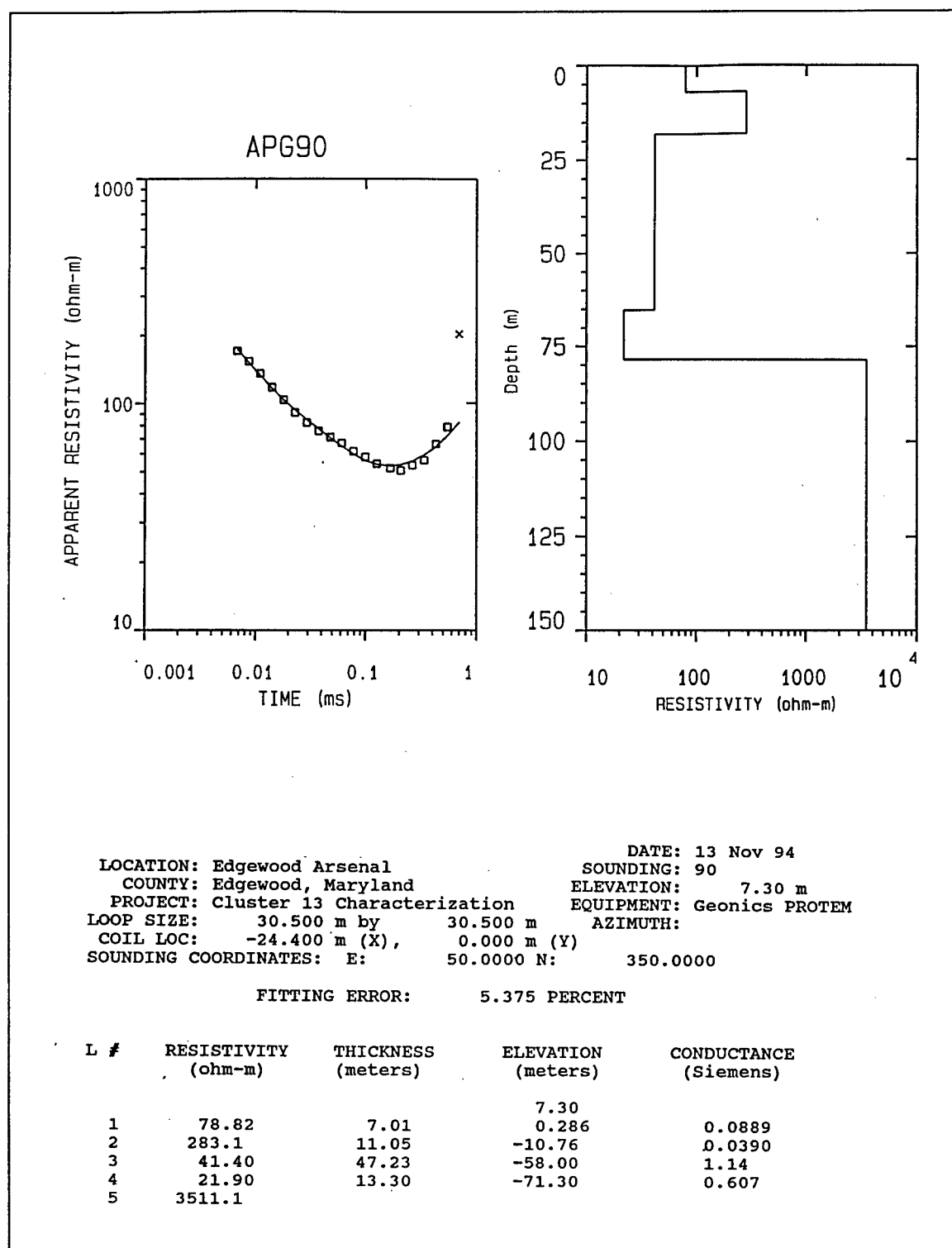


Figure C5. Transient electromagnetic data, best-fit model, and best-fit model parameters list for sounding APG90

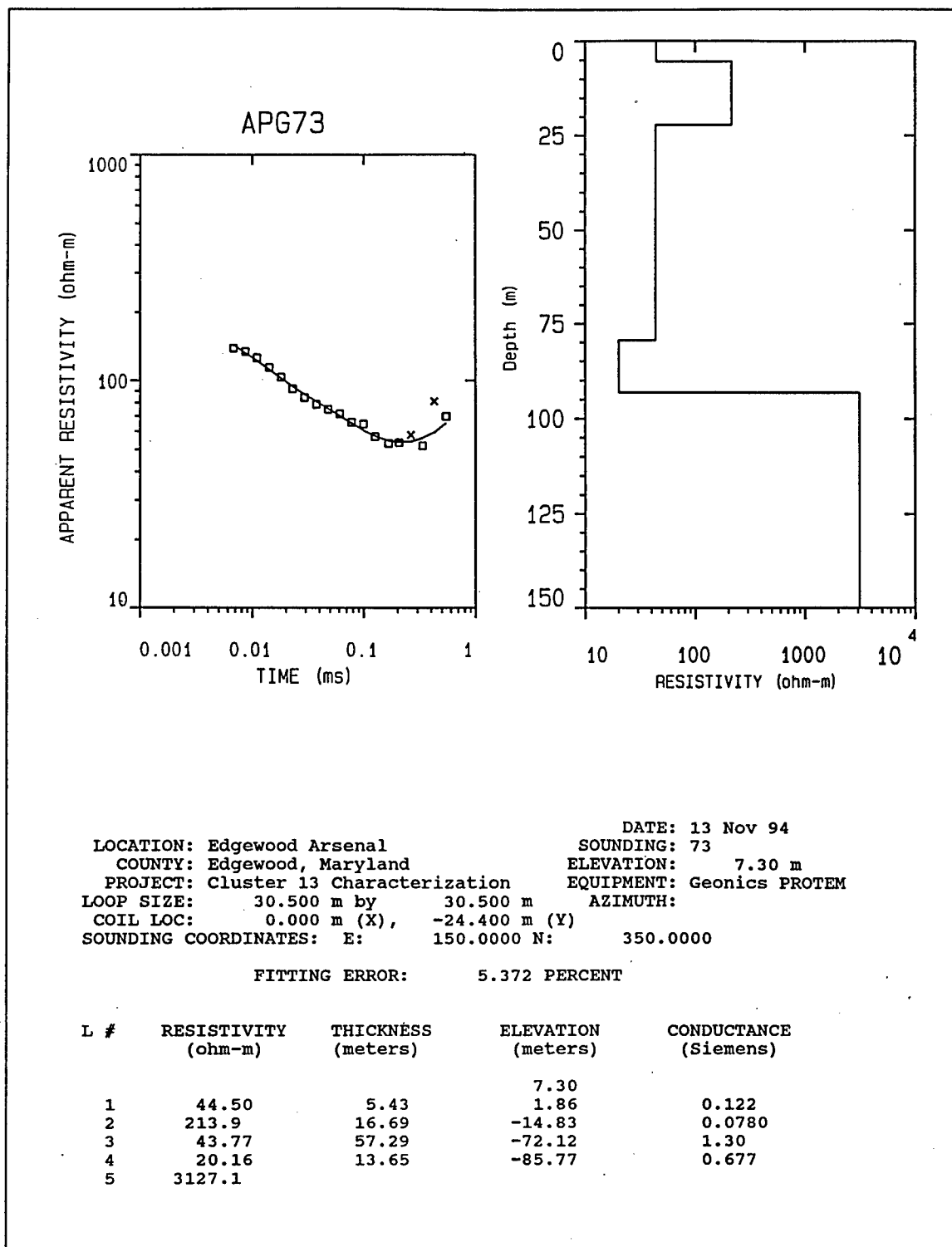


Figure C6. Transient electromagnetic data, best-fit model, and best-fit model parameters list for sounding APG73

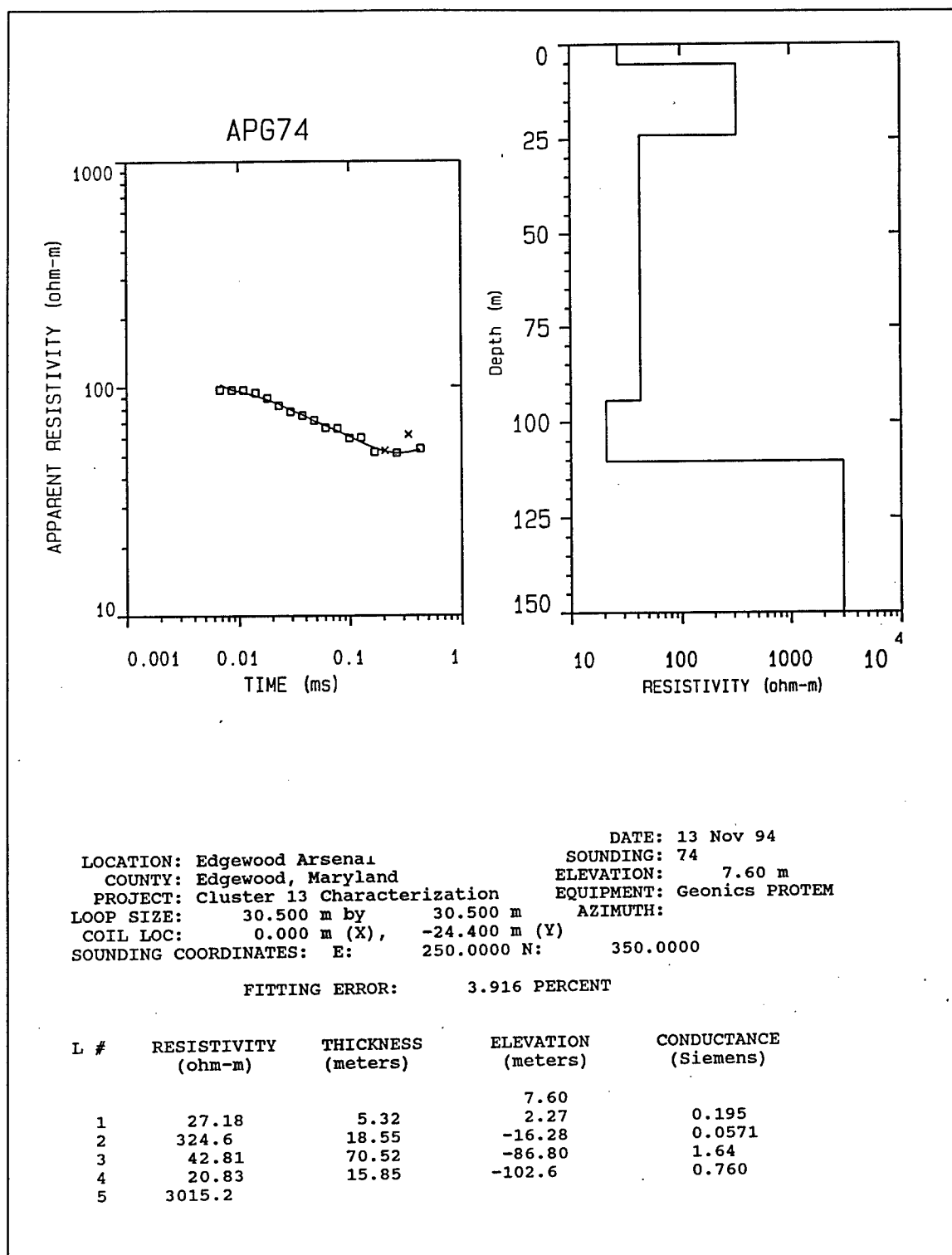


Figure C7. Transient electromagnetic data, best-fit model, and best-fit model parameters list for sounding APG74

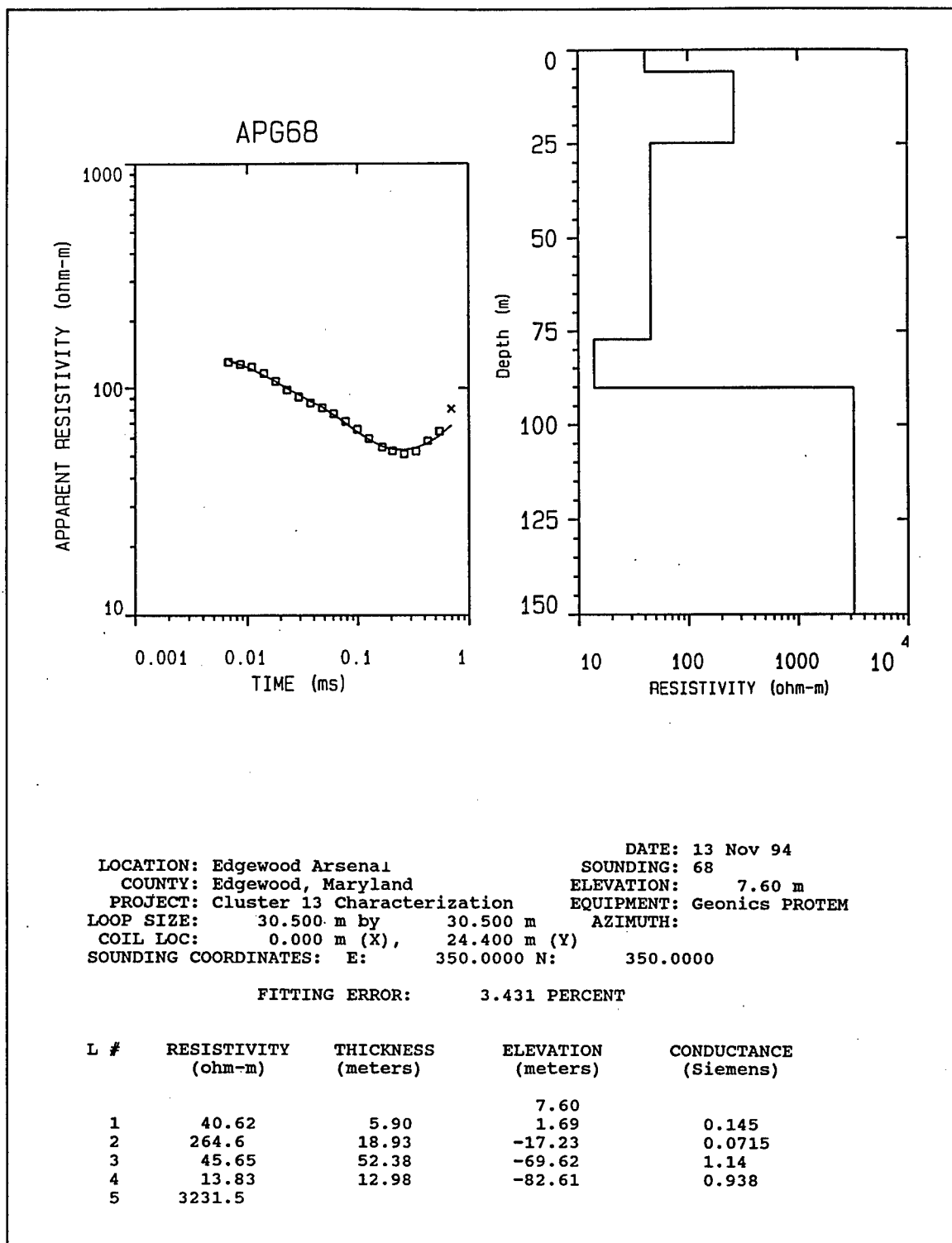


Figure C8. Transient electromagnetic data, best-fit model, and best-fit model parameters list for sounding APG68

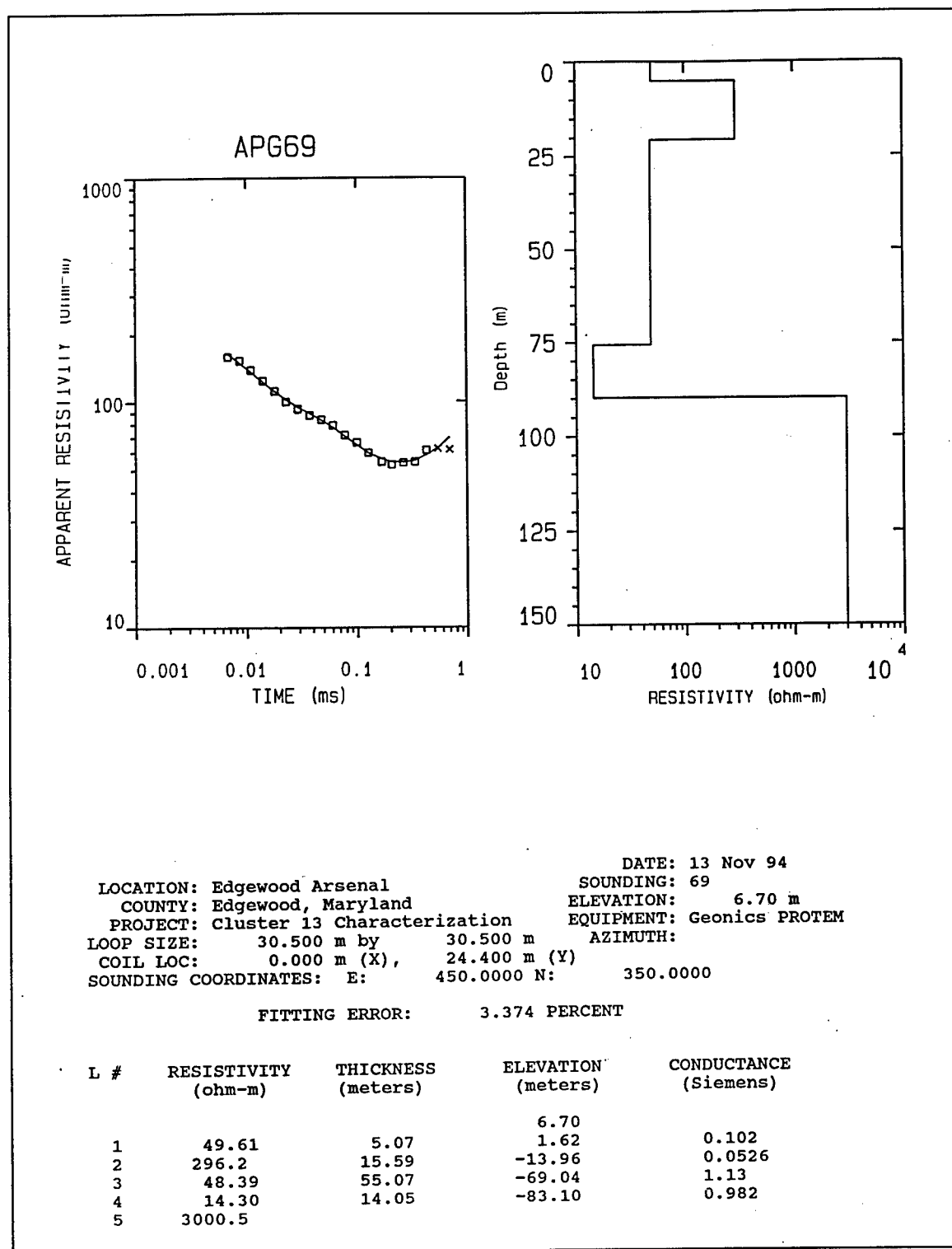


Figure C9. Transient electromagnetic data, best-fit model, and best-fit model parameters list for sounding APG69

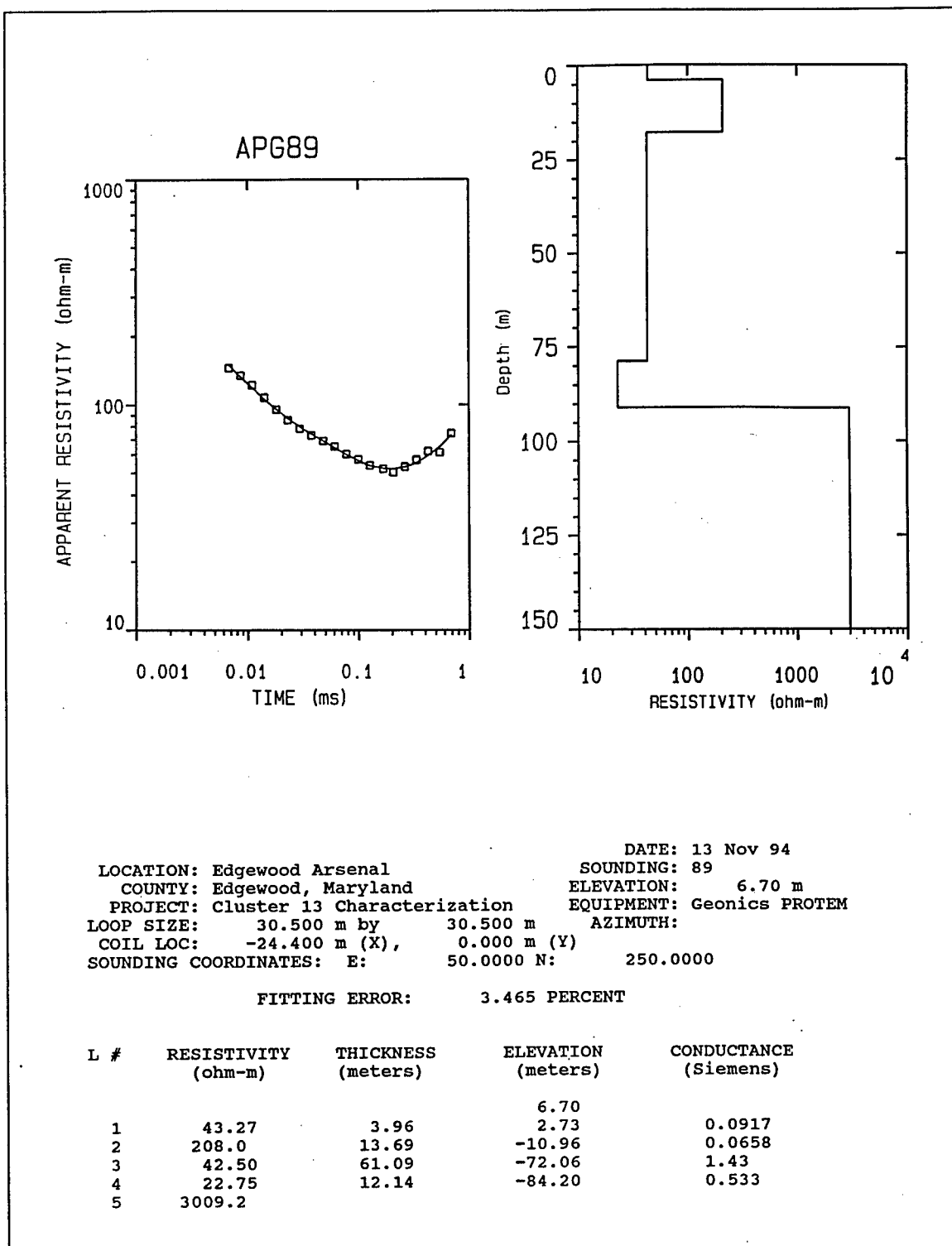


Figure C10. Transient electromagnetic data, best-fit model, and best-fit model parameters list for sounding APG89

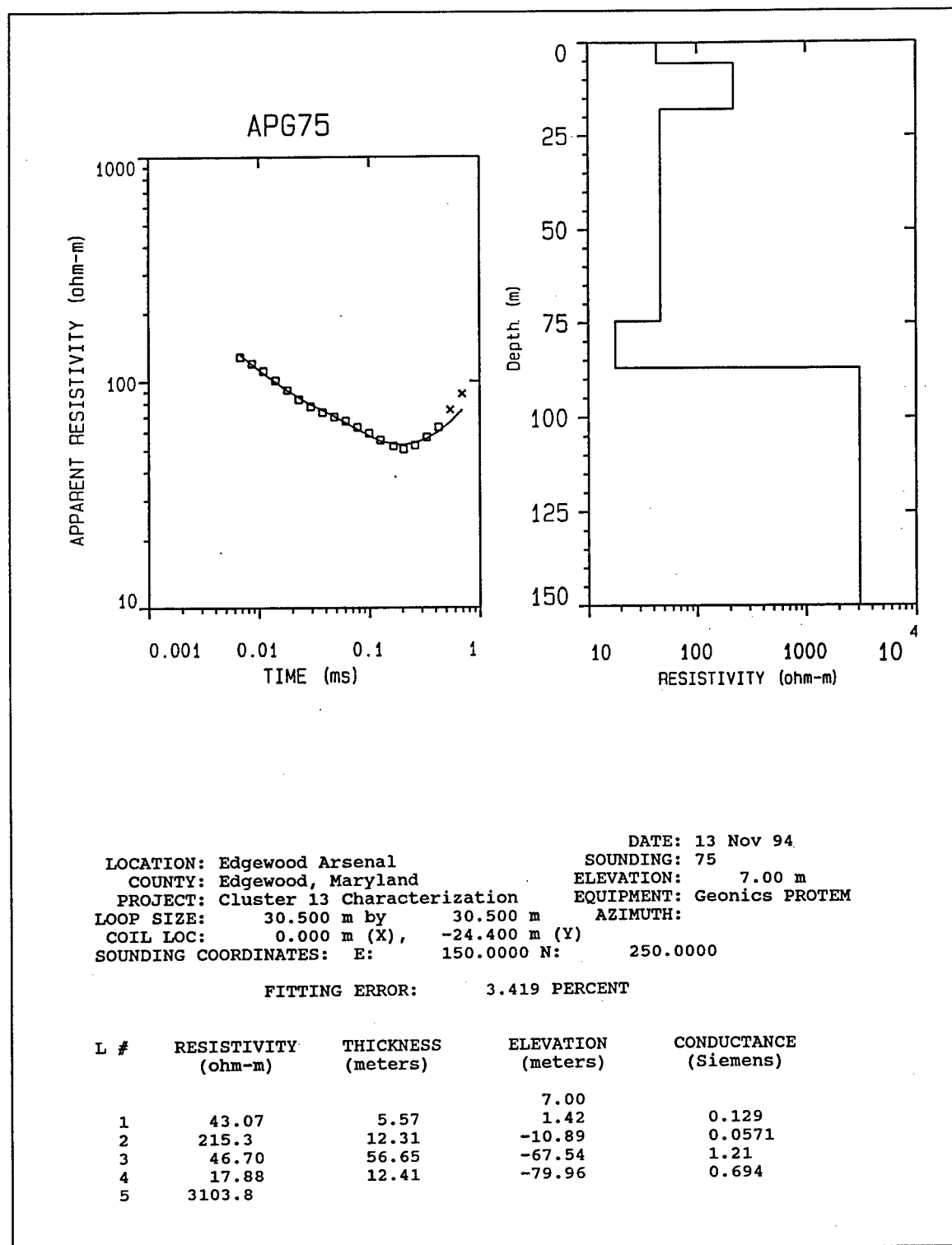


Figure C11. Transient electromagnetic data, best-fit model, and best-fit model parameters list for sounding APG75

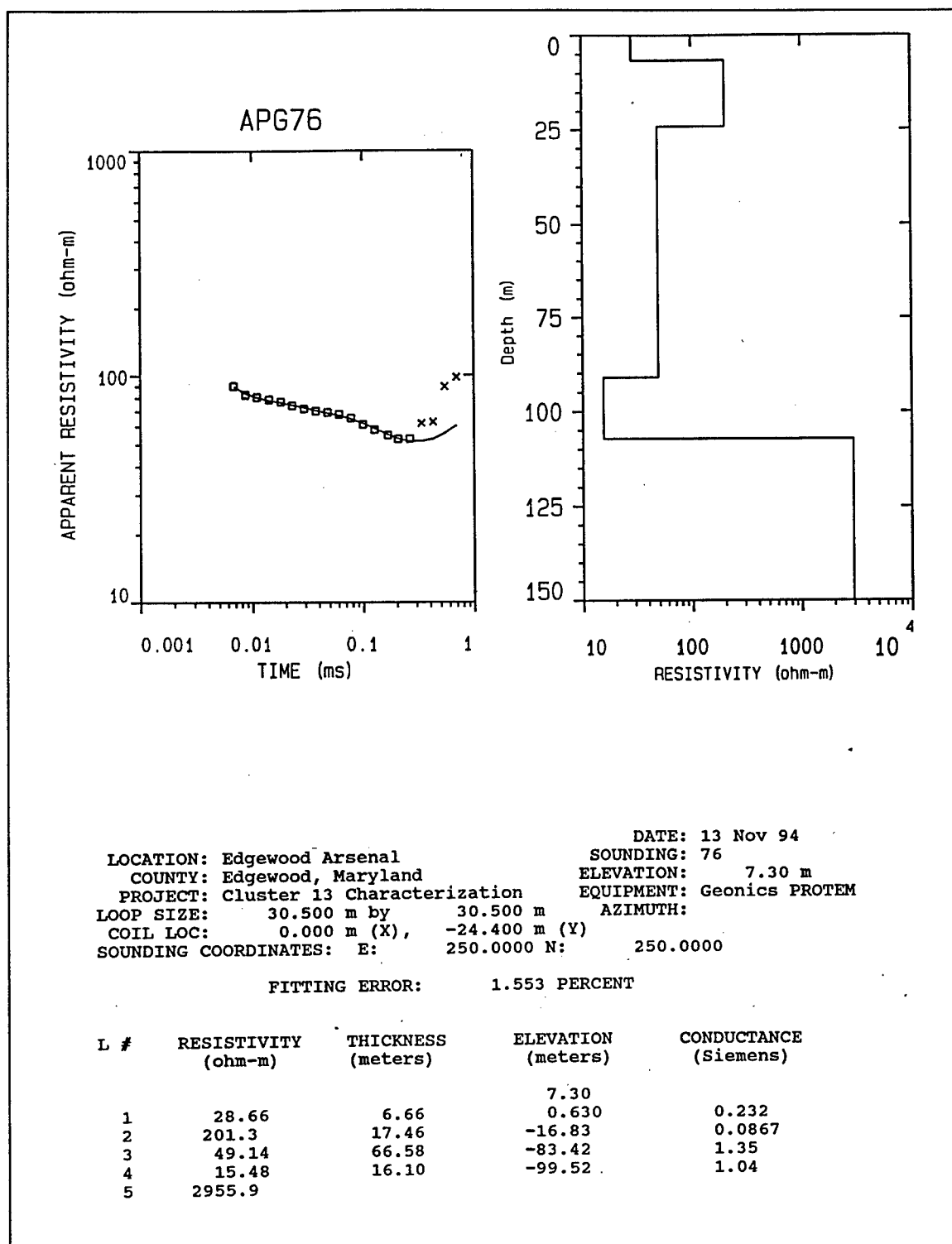


Figure C12. Transient electromagnetic data, best-fit model, and best-fit model parameters list for sounding APG76

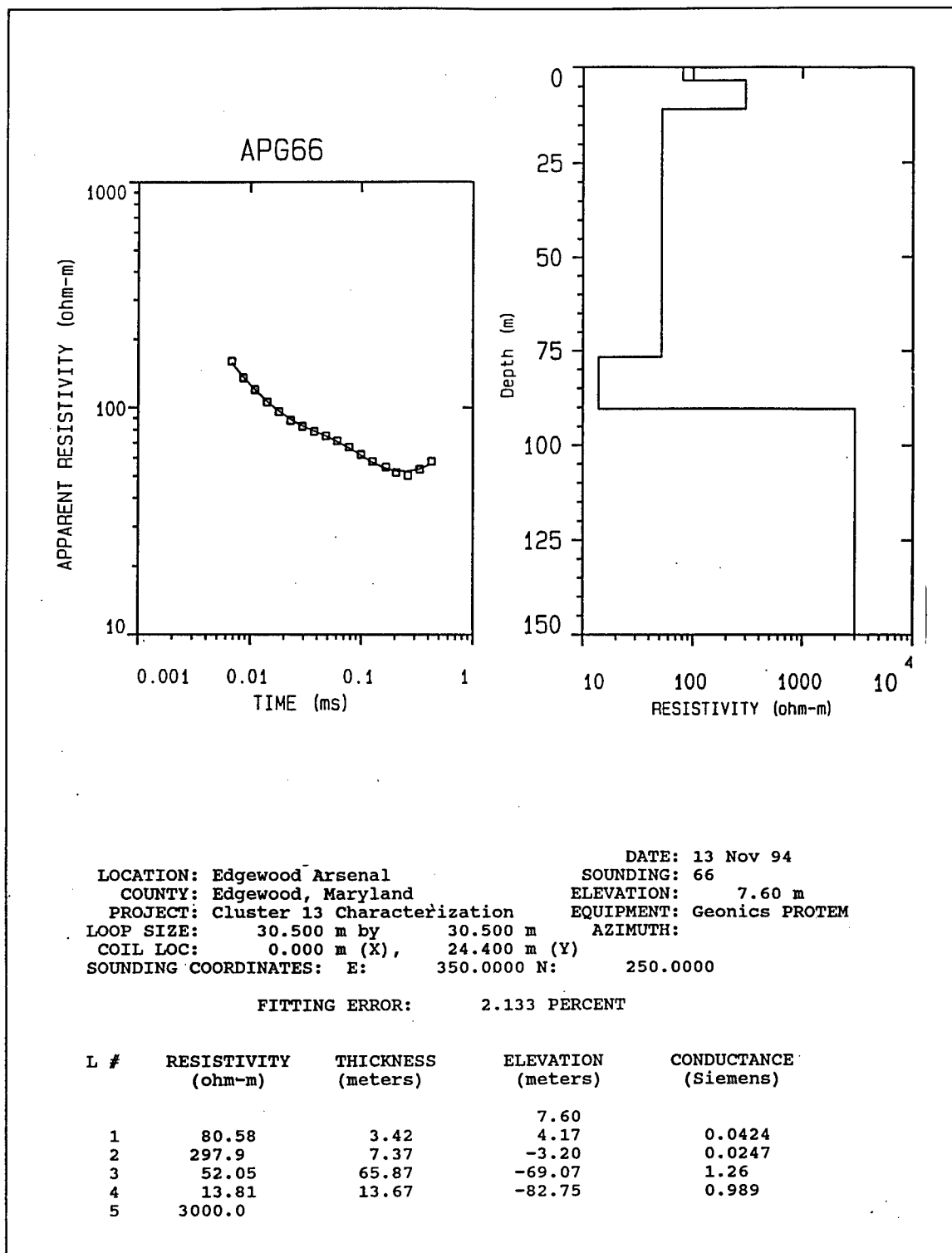


Figure C13. Transient electromagnetic data, best-fit model, and best-fit model parameters list for sounding APG66

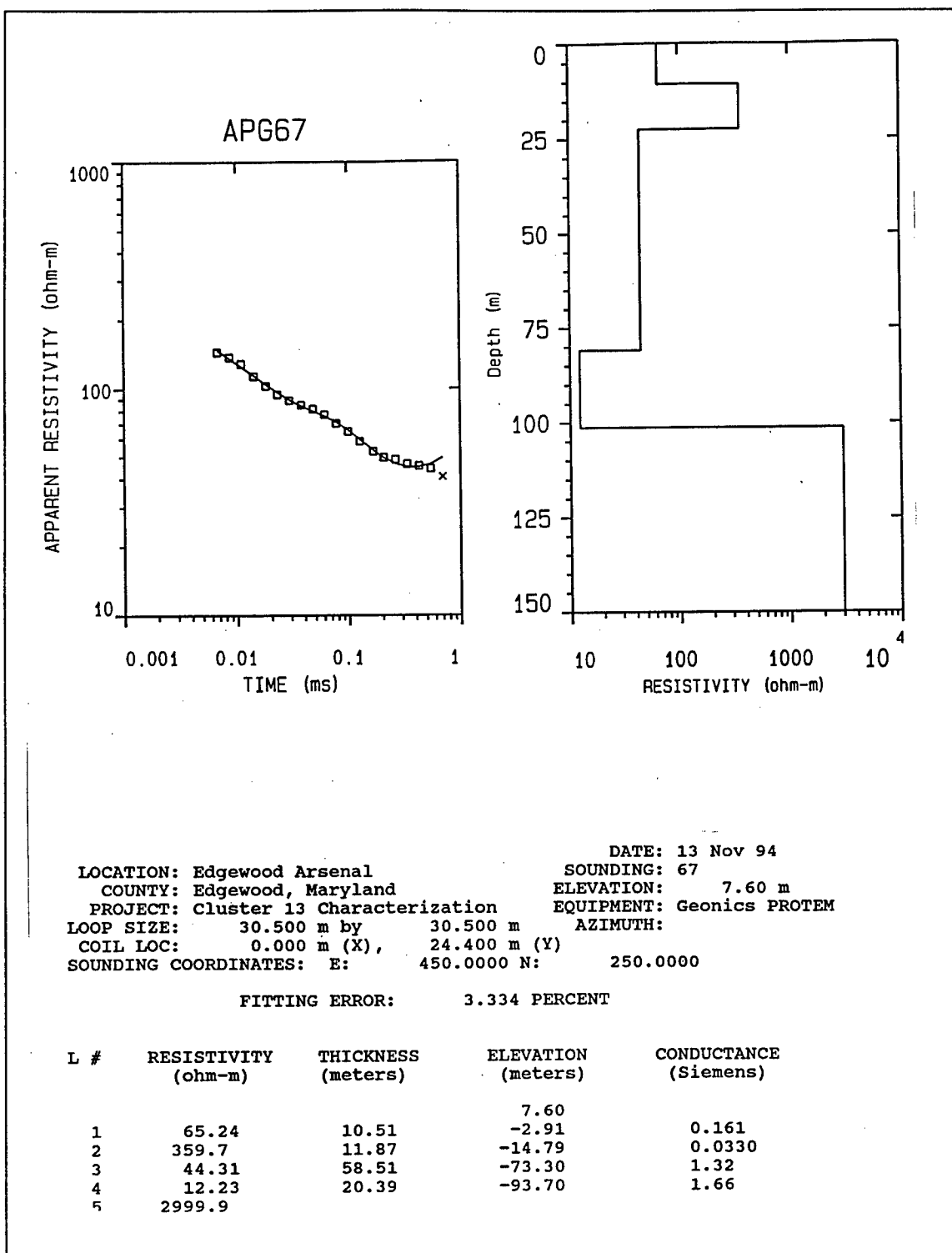


Figure C14. Transient electromagnetic data, best-fit model, and best-fit model parameters list for sounding APG67

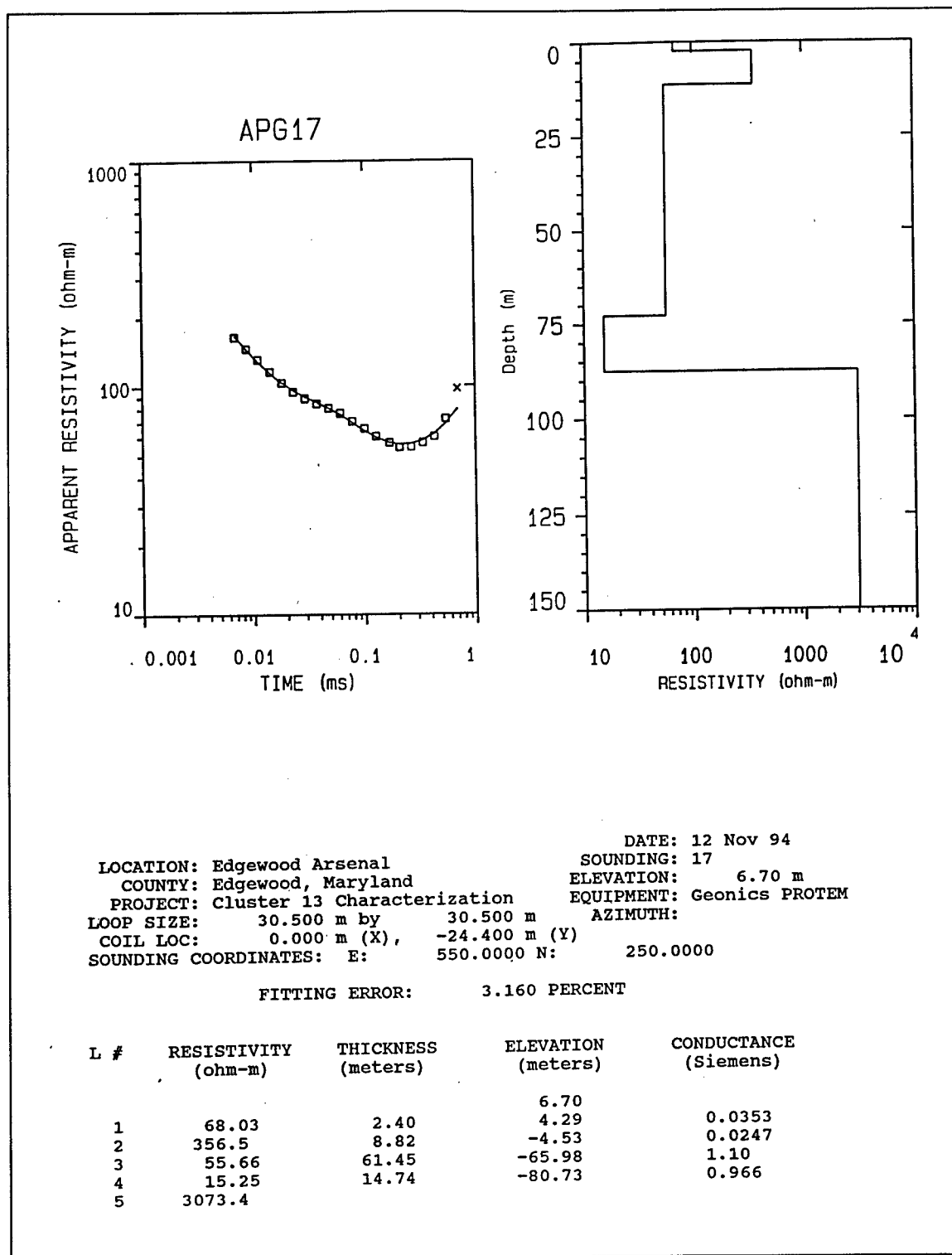


Figure C15. Transient electromagnetic data, best-fit model, and best-fit model parameters list for sounding APG17

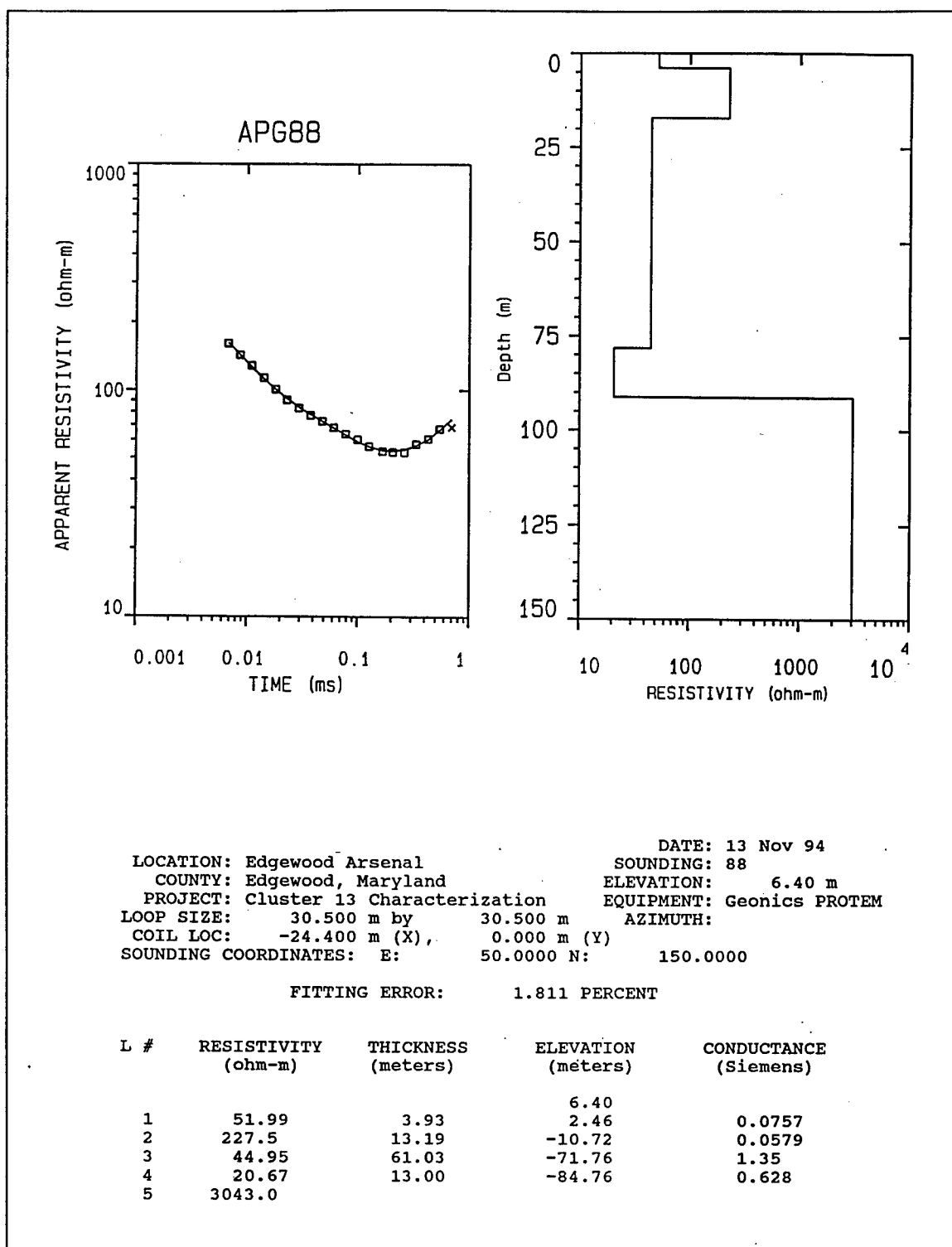


Figure C16. Transient electromagnetic data, best-fit model, and best-fit model parameters list for sounding APG88

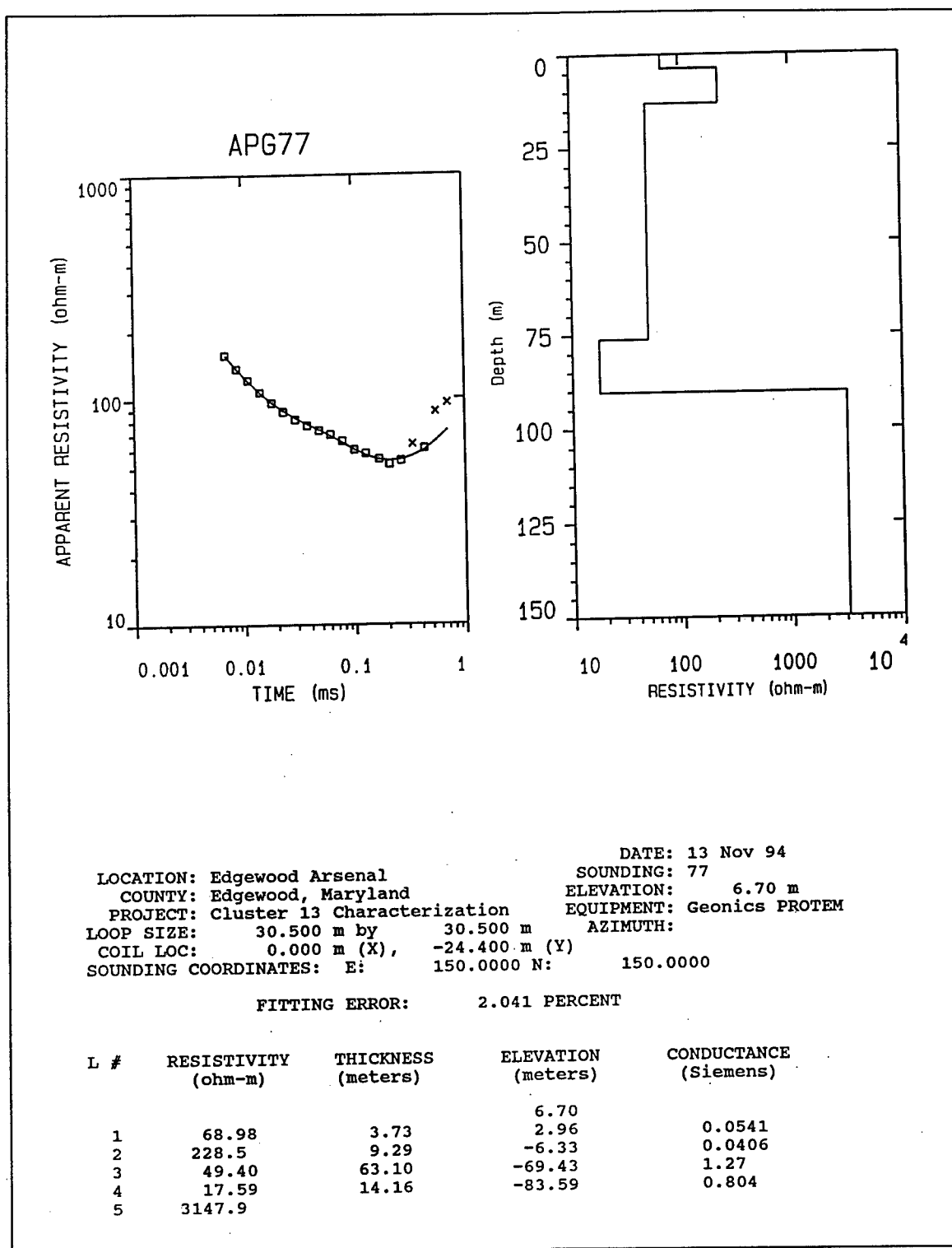


Figure C17. Transient electromagnetic data, best-fit model, and best-fit model parameters list for sounding APG77

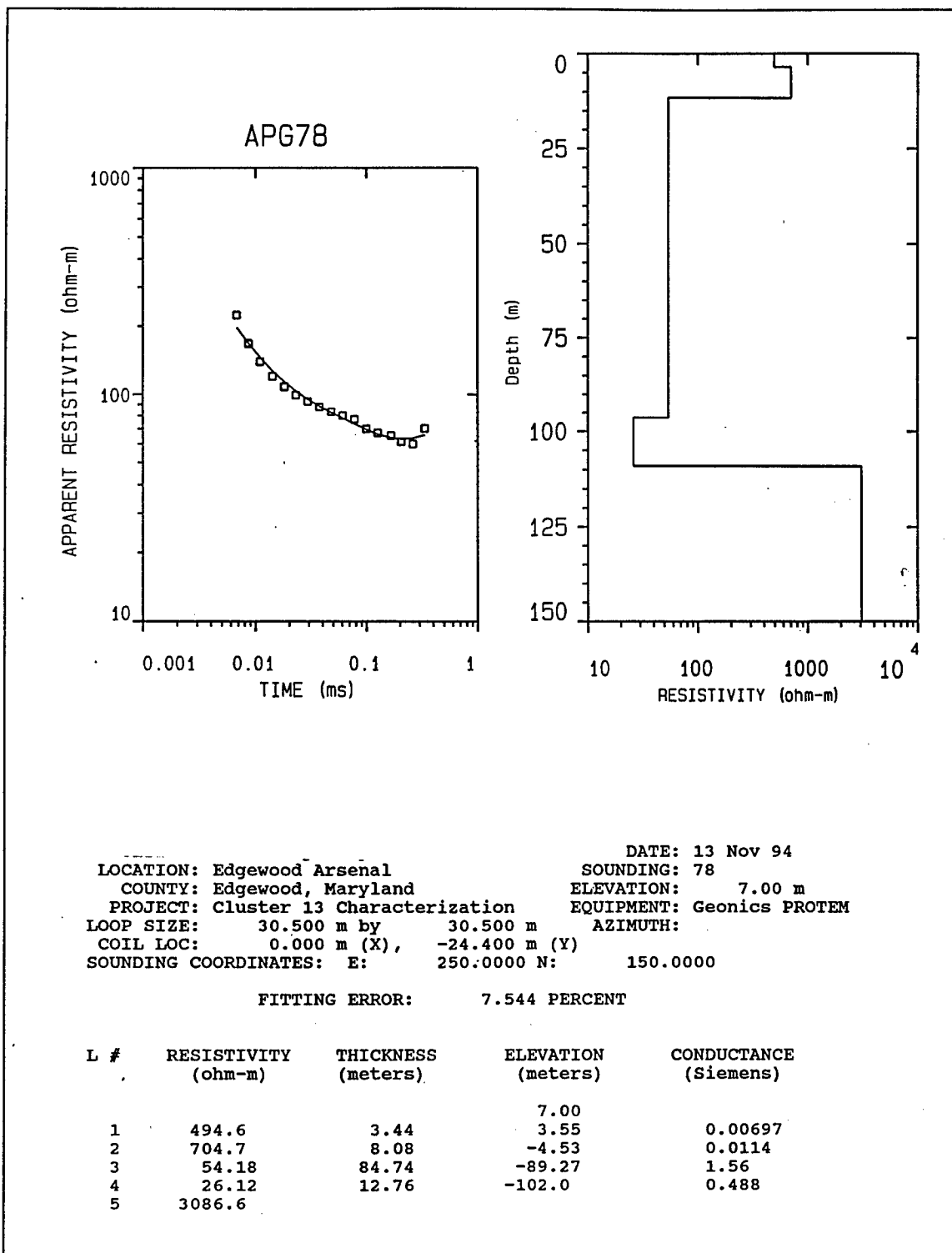


Figure C18. Transient electromagnetic data, best-fit model, and best-fit model parameters list for sounding APG78

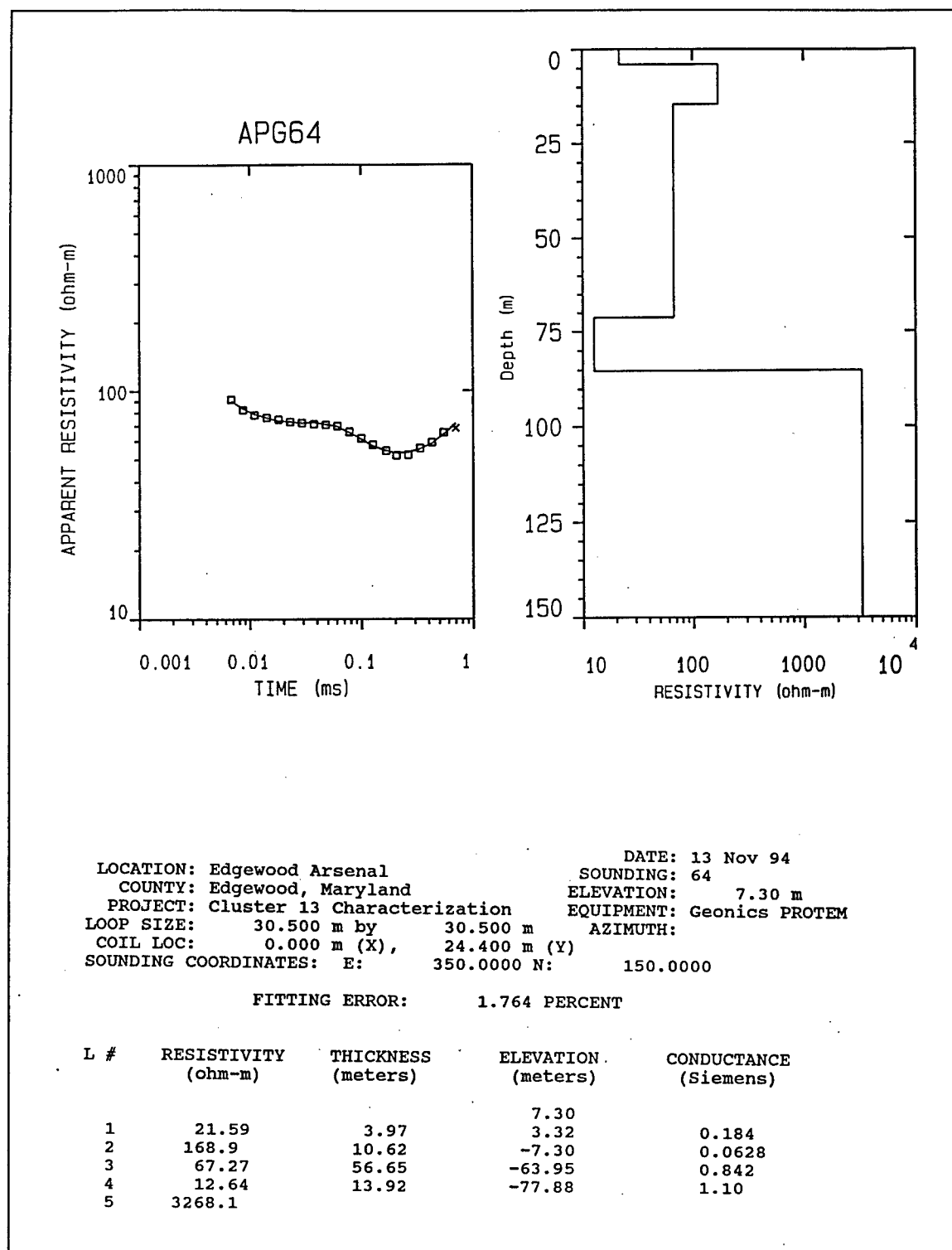


Figure C19. Transient electromagnetic data, best-fit model, and best-fit model parameters list for sounding APG64

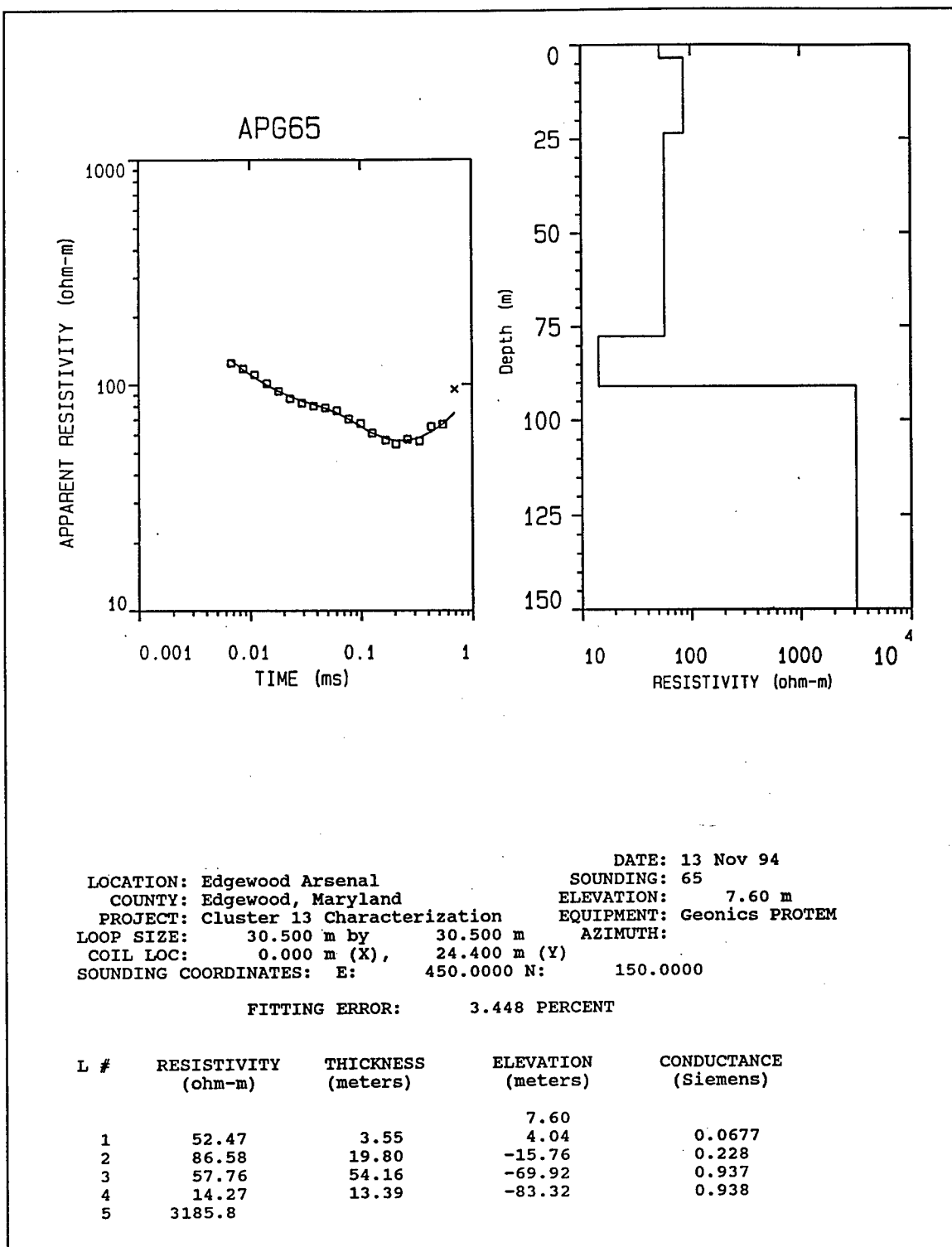


Figure C20. Transient electromagnetic data, best-fit model, and best-fit model parameters list for sounding APG65

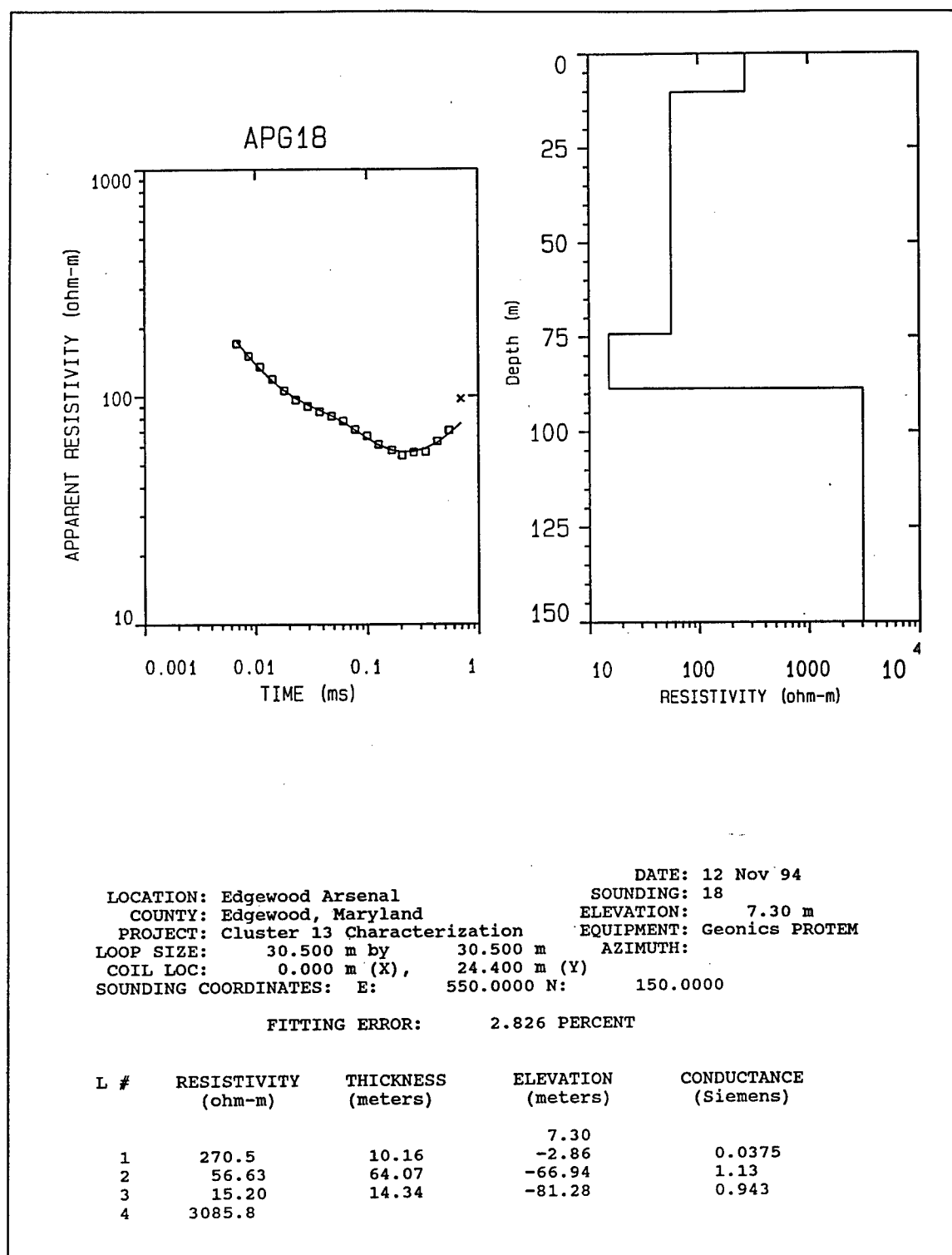


Figure C21. Transient electromagnetic data, best-fit model, and best-fit model parameters list for sounding APG18

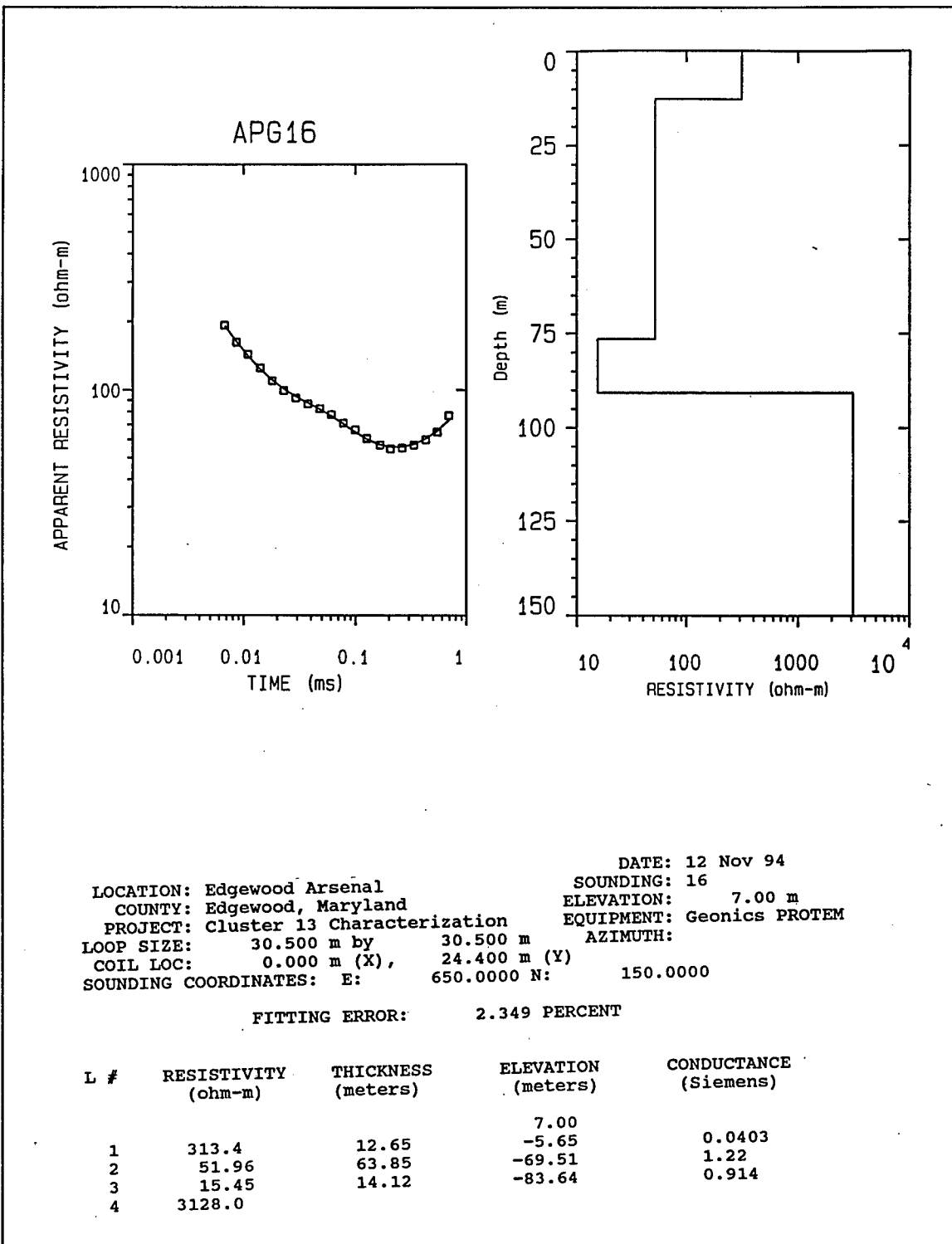


Figure C22. Transient electromagnetic data, best-fit model, and best-fit model parameters list for sounding APG16

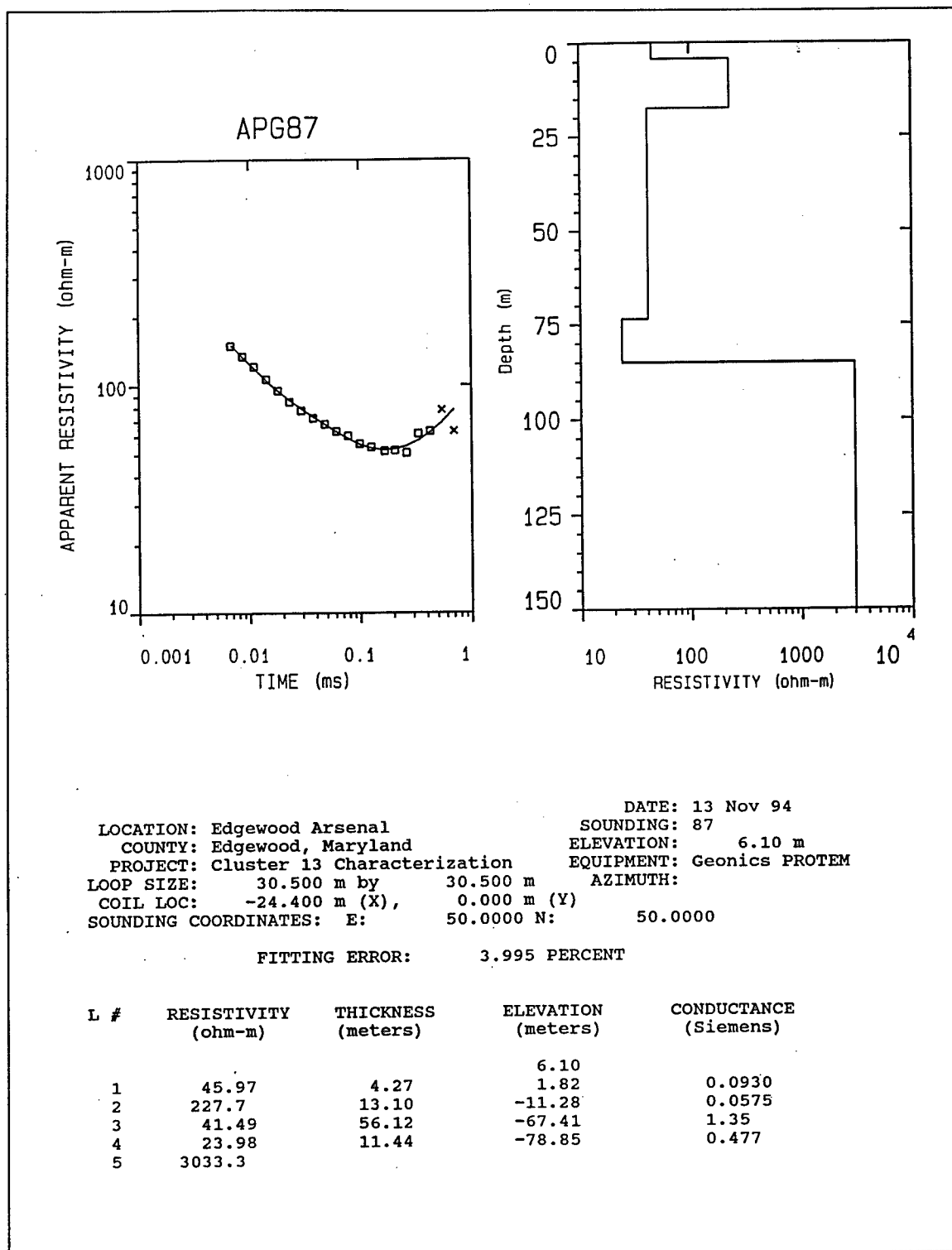


Figure C23. Transient electromagnetic data, best-fit model, and best-fit model parameters list for sounding APG87

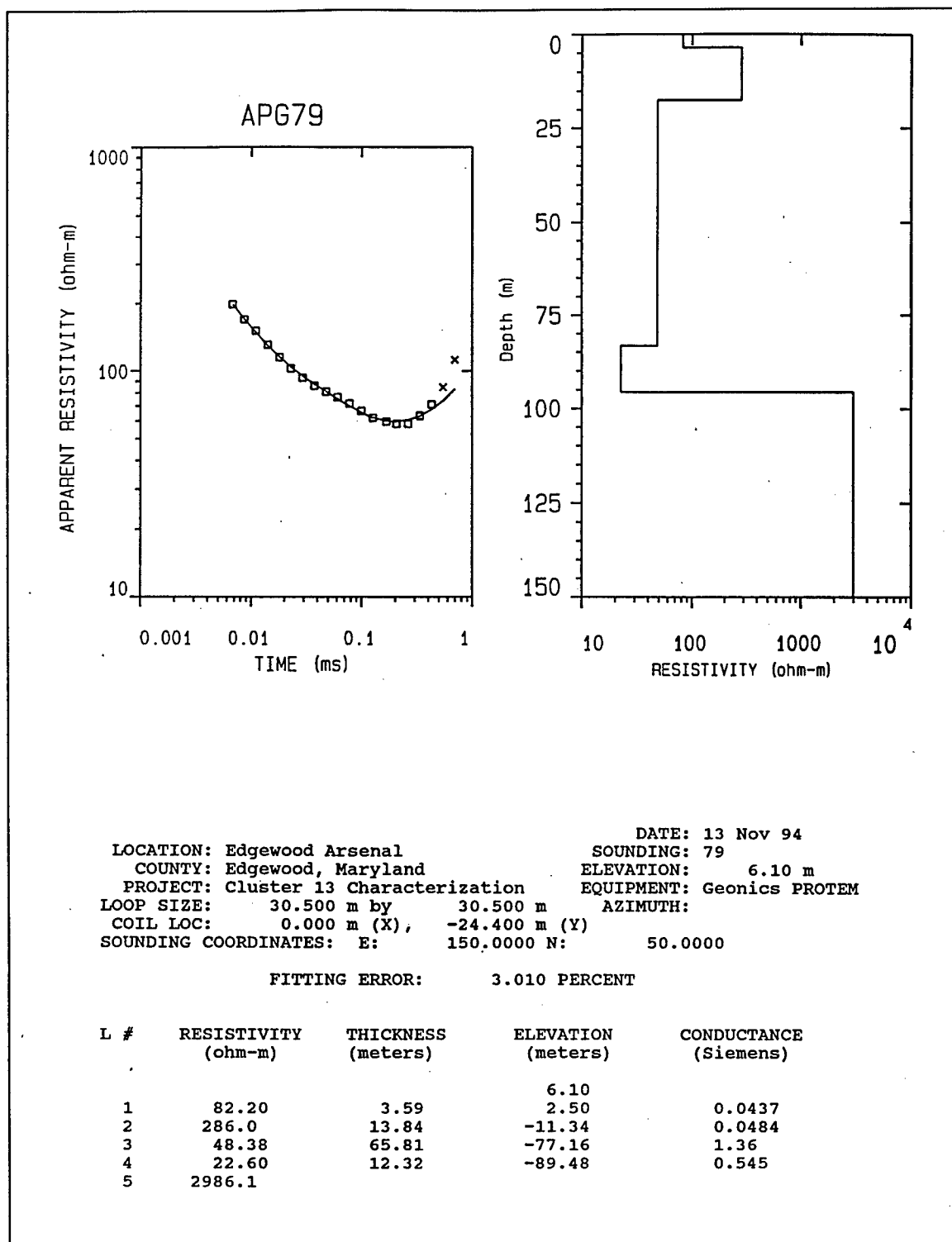


Figure C24. Transient electromagnetic data, best-fit model, and best-fit model parameters list for sounding APG79

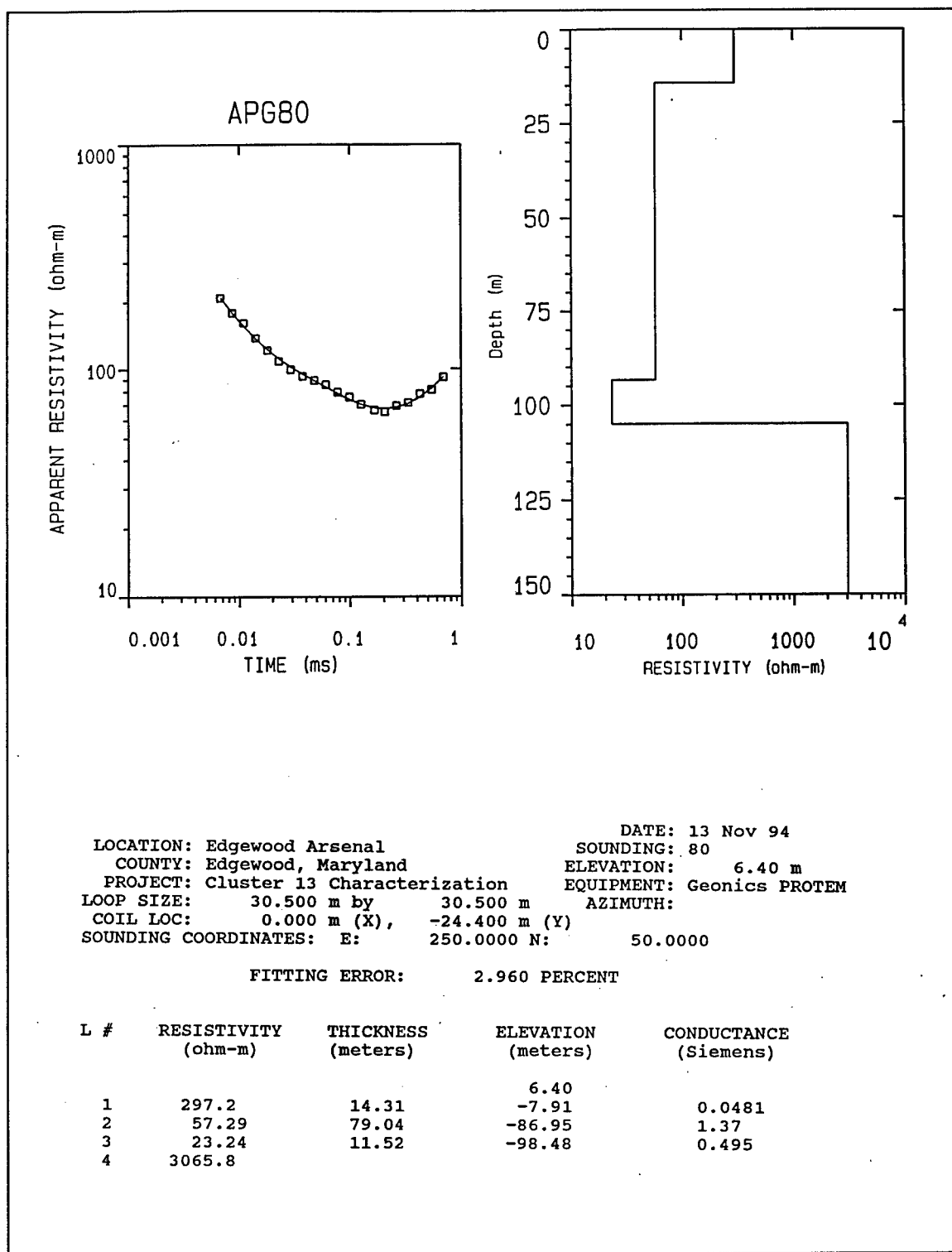


Figure C25. Transient electromagnetic data, best-fit model, and best-fit model parameters list for sounding APG80

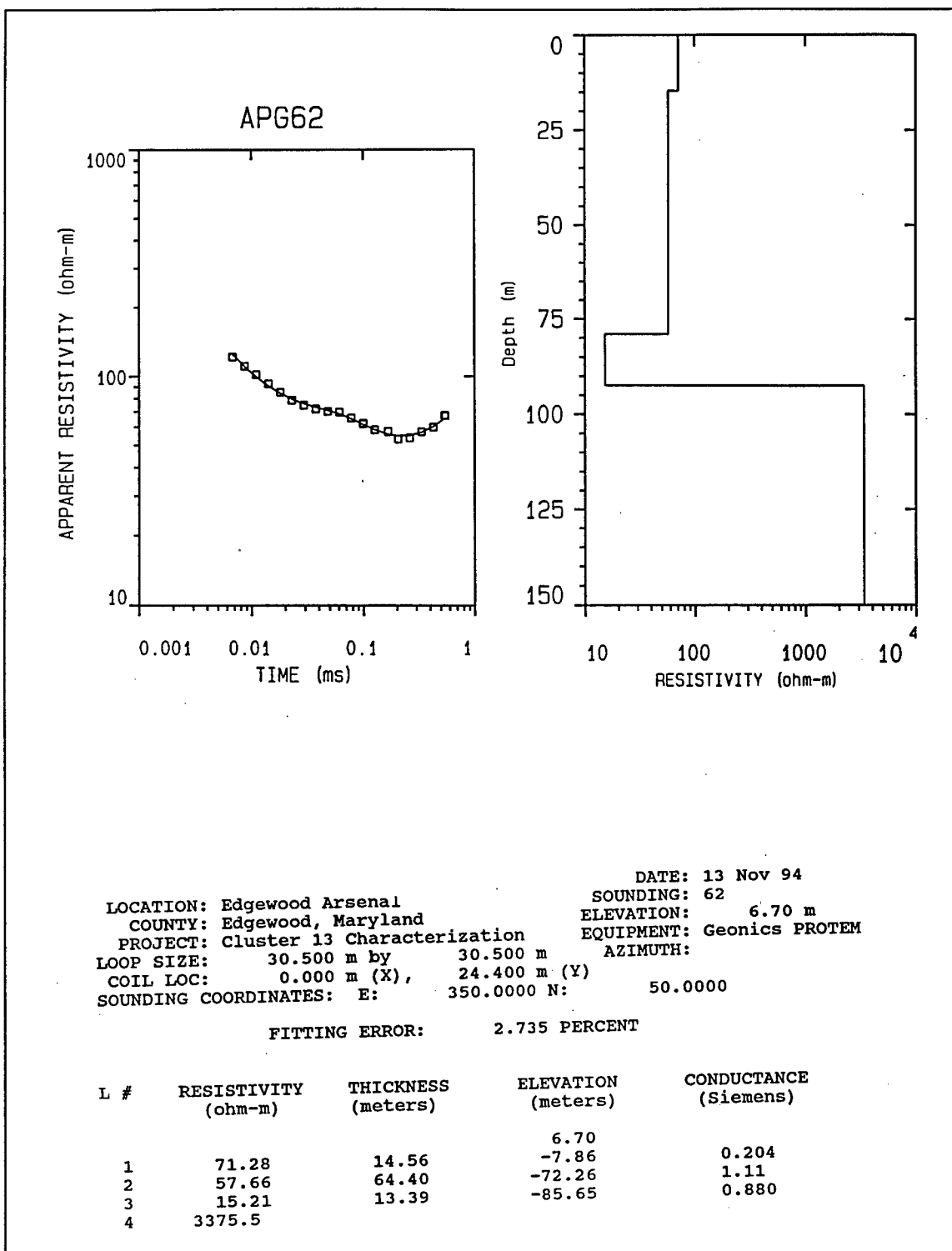


Figure C26. Transient electromagnetic data, best-fit model, and best-fit model parameters list for sounding APG62

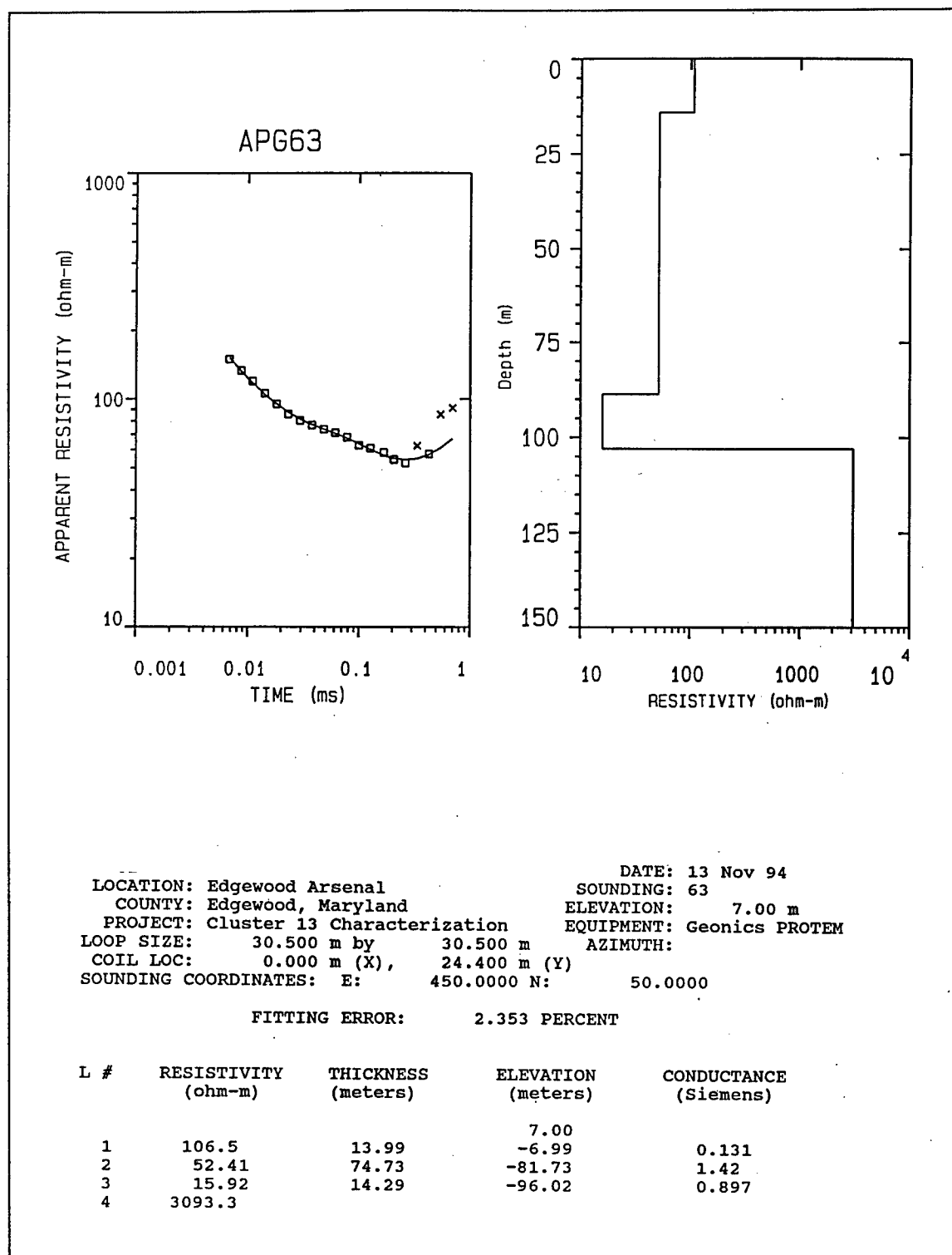


Figure C27. Transient electromagnetic data, best-fit model, and best-fit model parameters list for sounding APG63

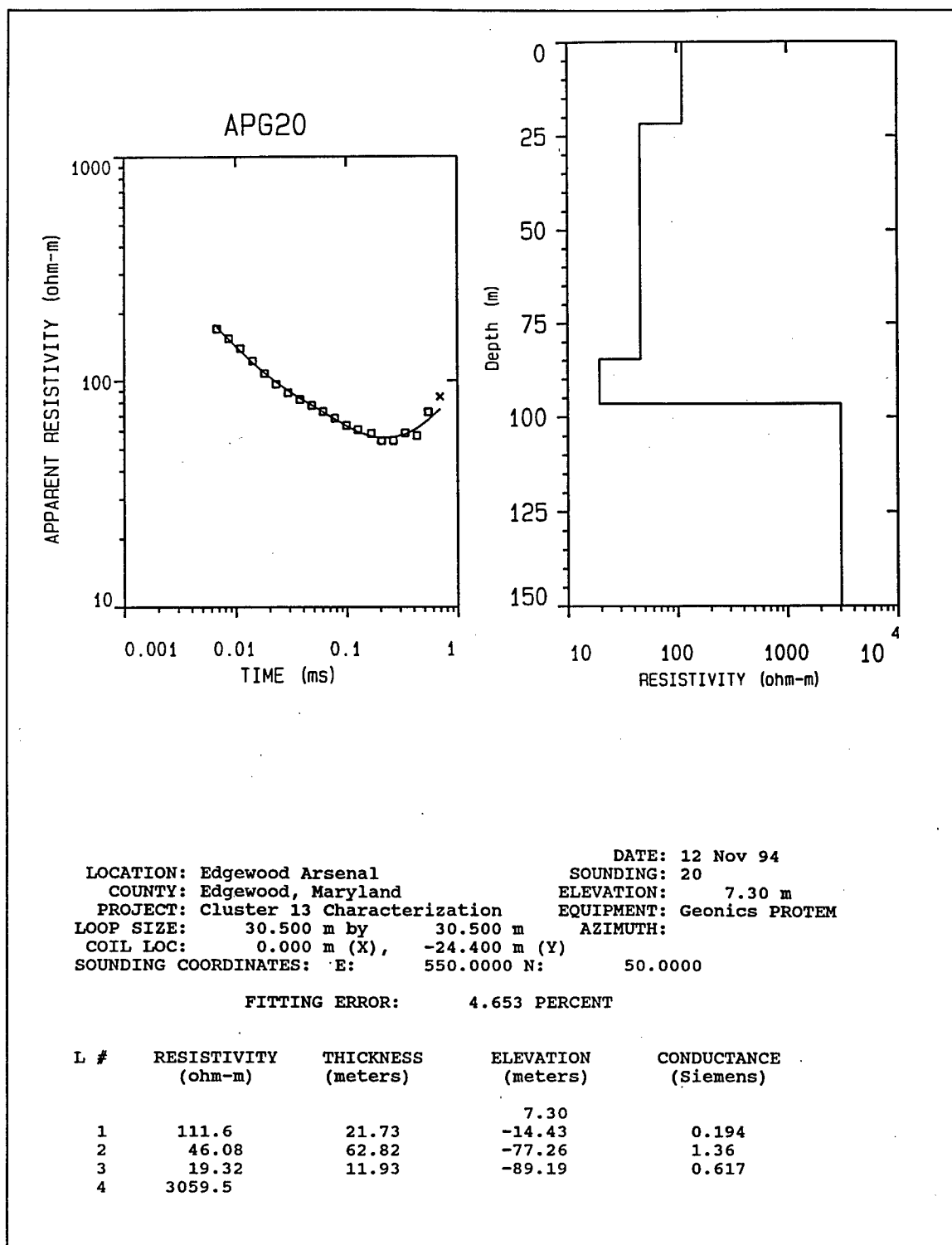


Figure C28. Transient electromagnetic data, best-fit model, and best-fit model parameters list for sounding APG20

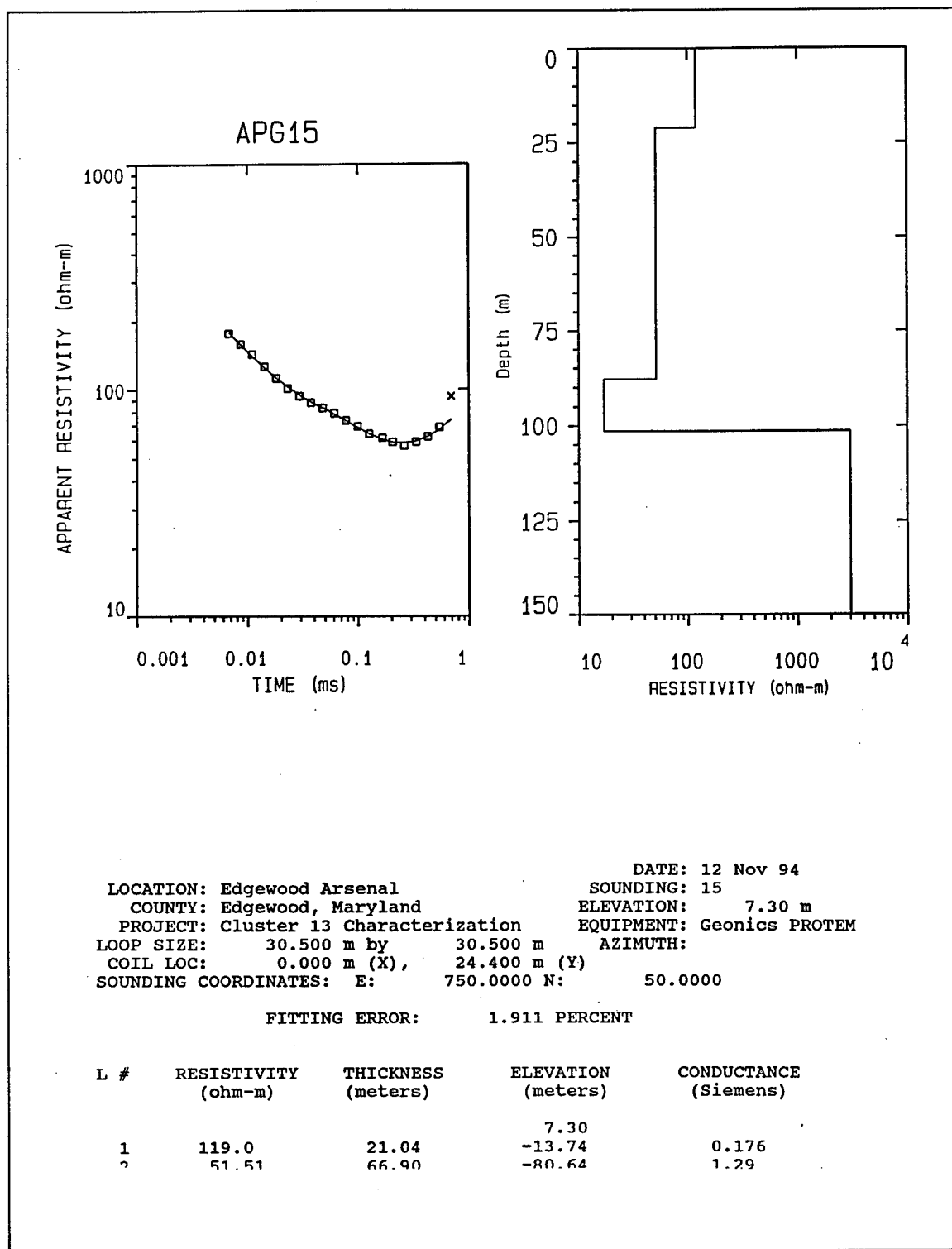


Figure C29. Transient electromagnetic data, best-fit model, and best-fit model parameters list for sounding APG15

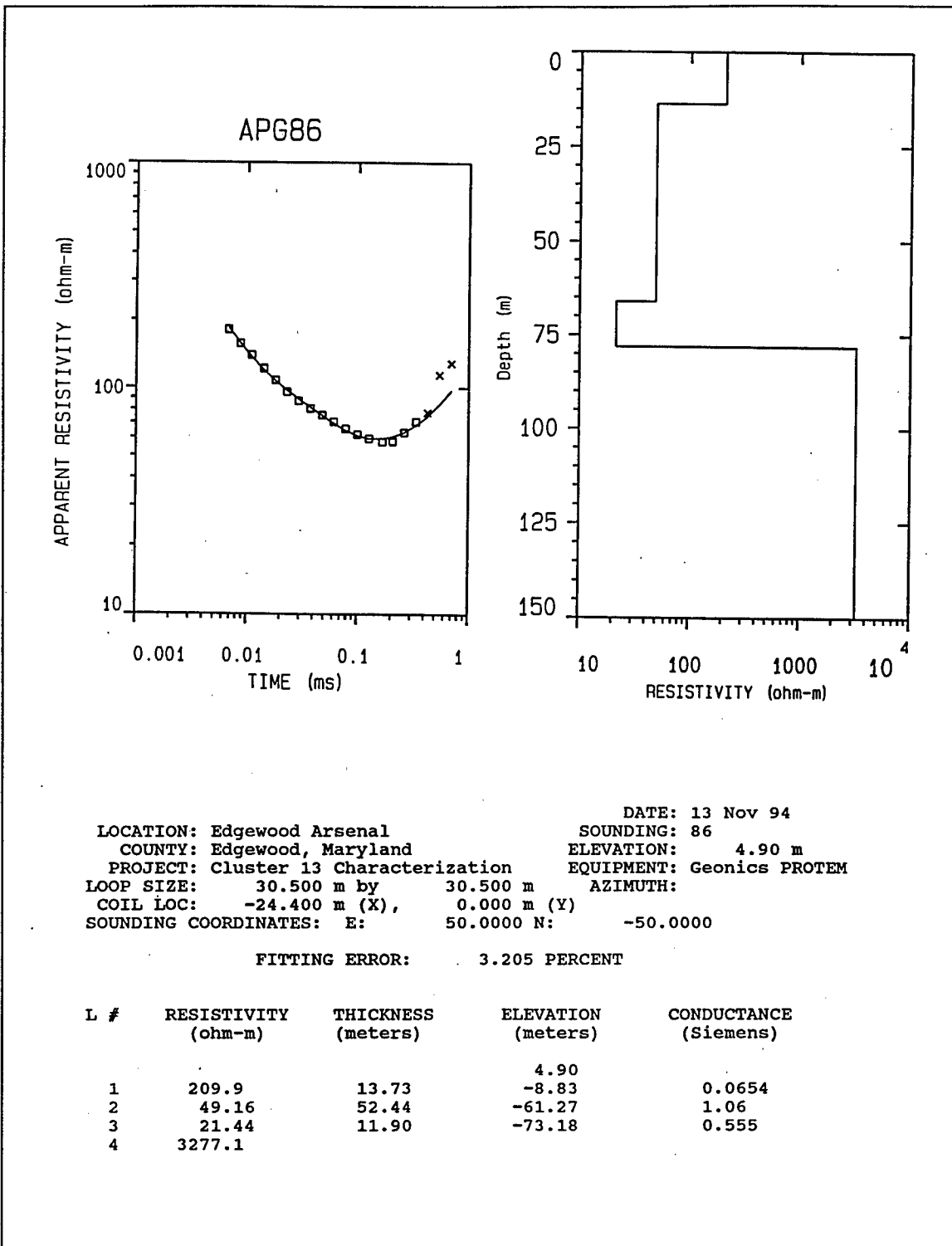


Figure C30. Transient electromagnetic data, best-fit model, and best-fit model parameters list for sounding APG86

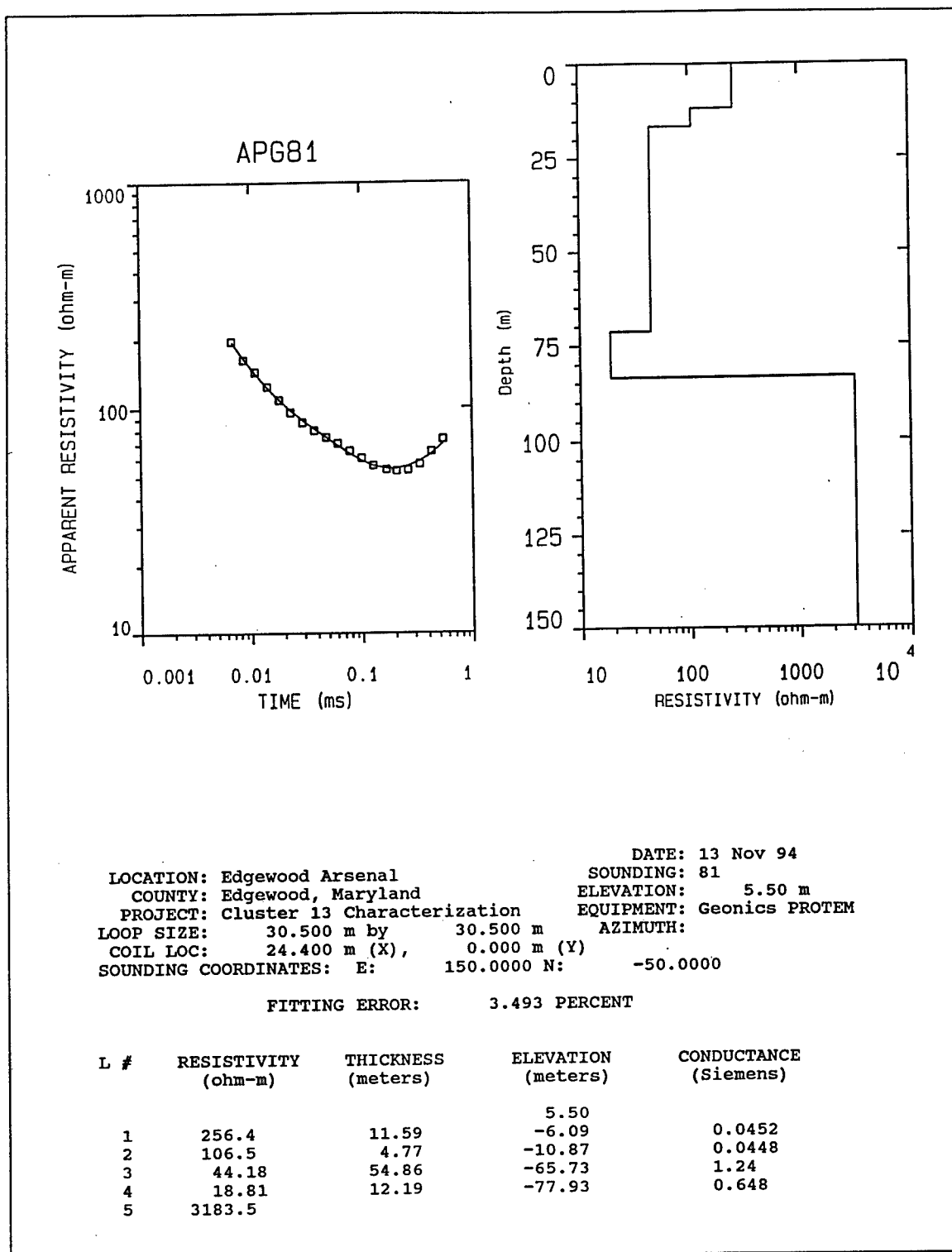


Figure C31. Transient electromagnetic data, best-fit model, and best-fit model parameters list for sounding APG81

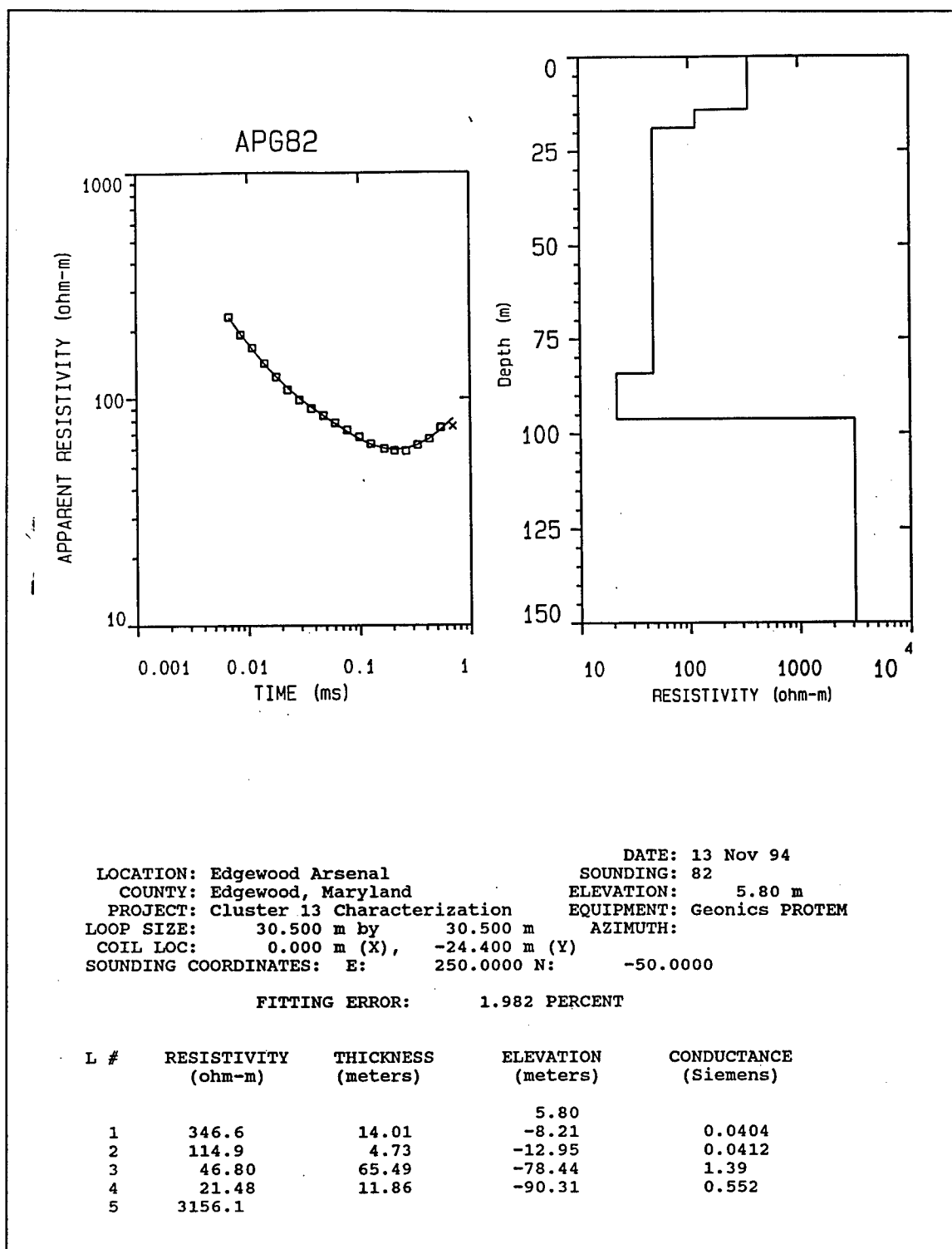


Figure C32. Transient electromagnetic data, best-fit model, and best-fit model parameters list for sounding APG82

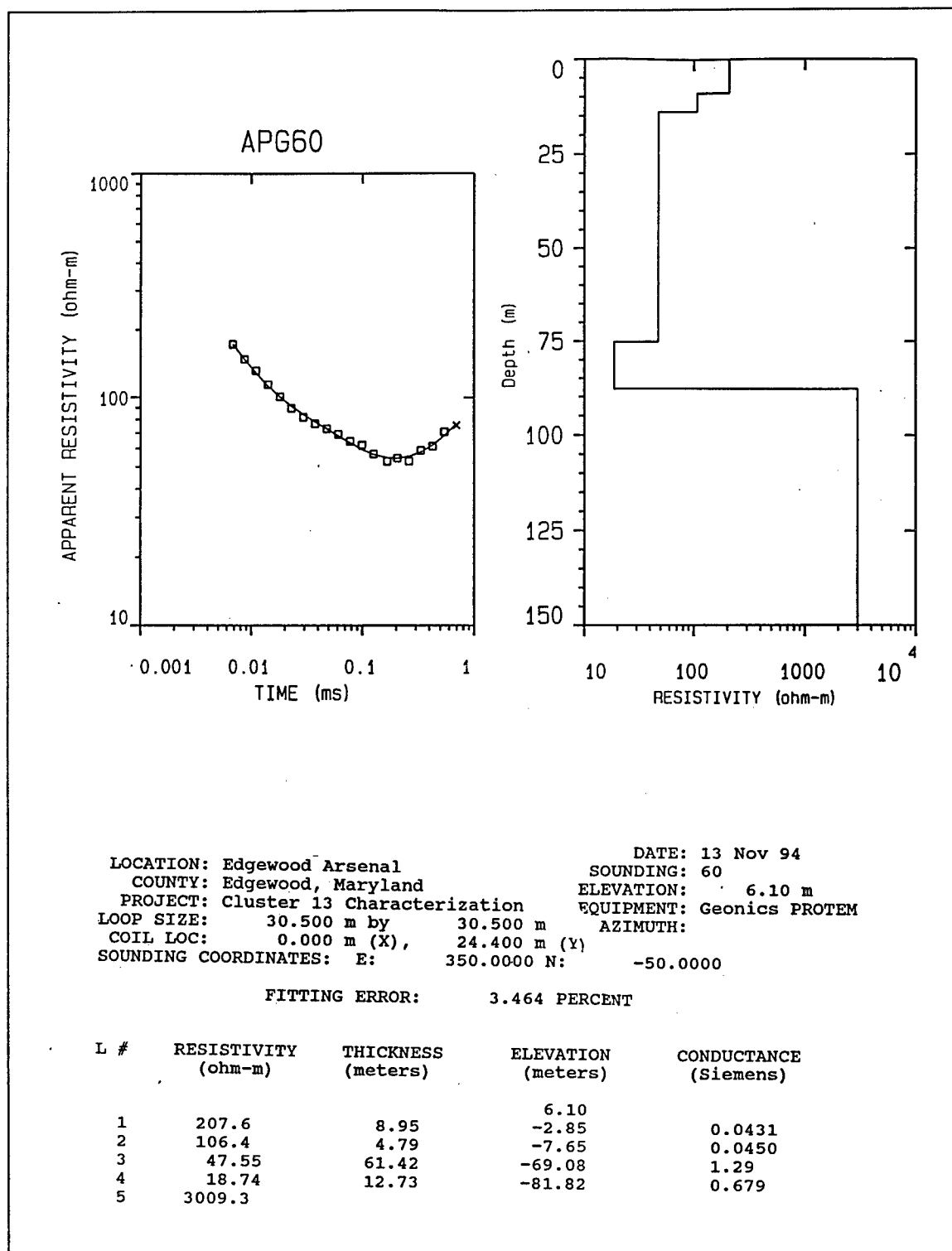


Figure C33. Transient electromagnetic data, best-fit model, and best-fit model parameters list for sounding APG60

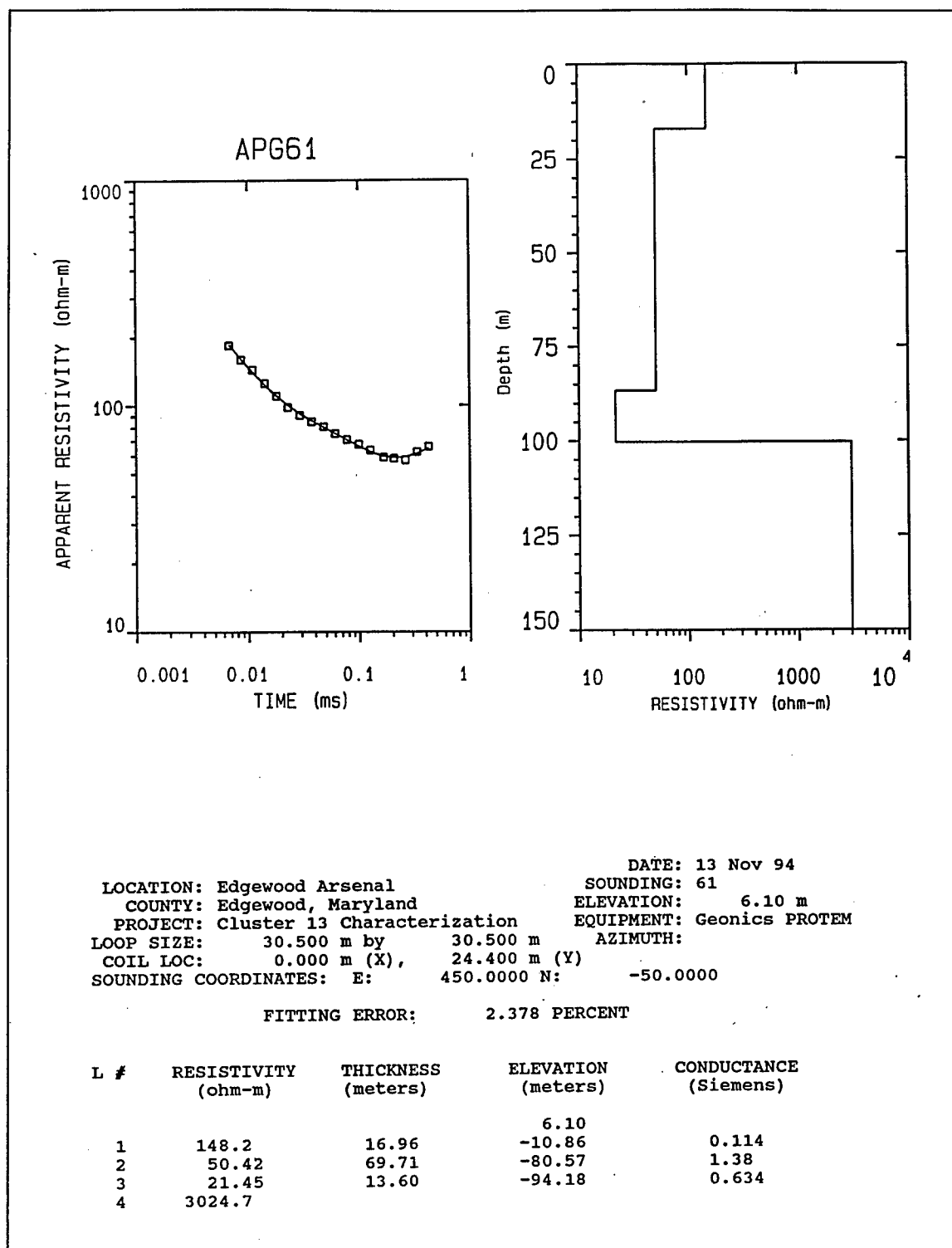


Figure C34. Transient electromagnetic data, best-fit model, and best-fit model parameters list for sounding APG61

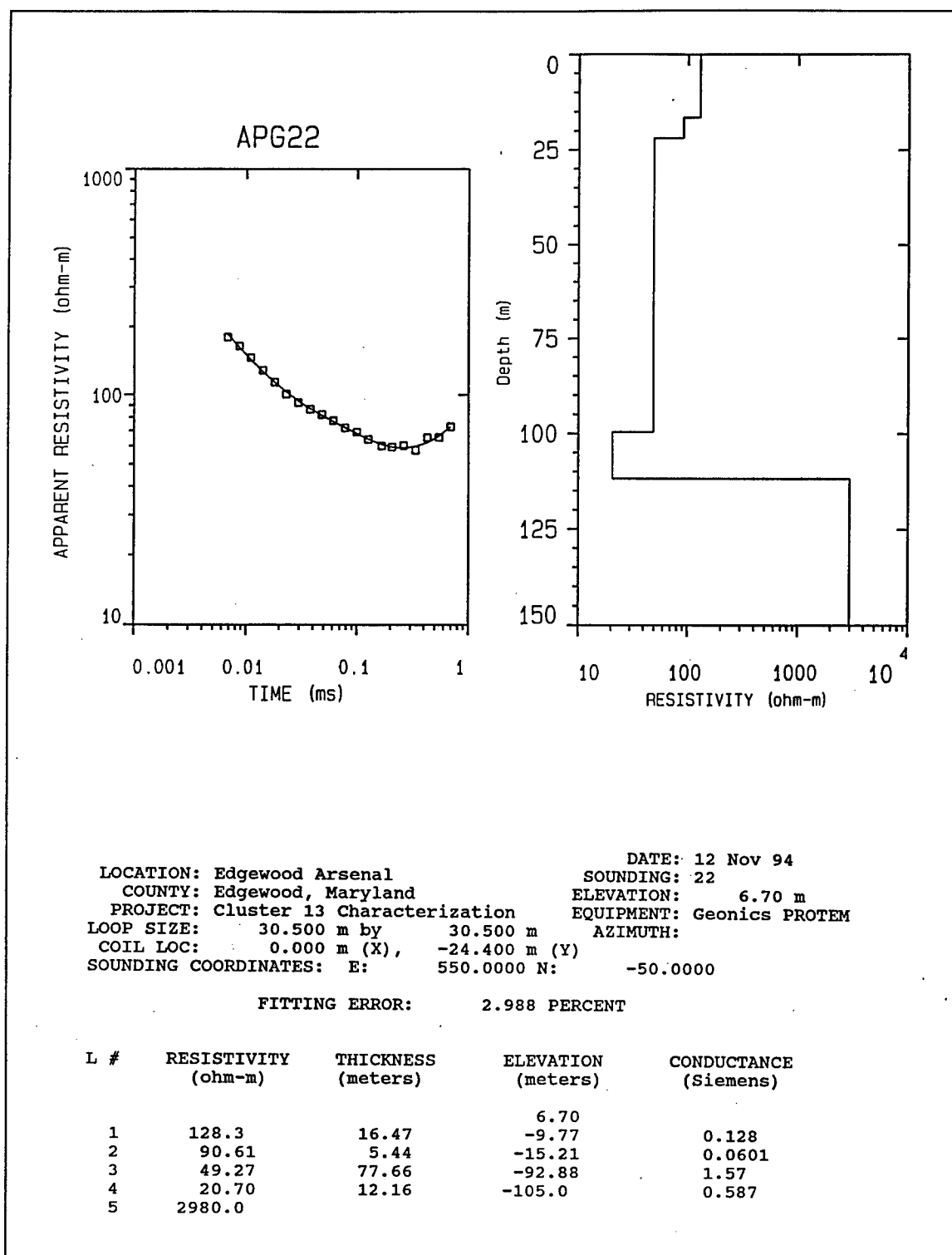


Figure C35. Transient electromagnetic data, best-fit model, and best-fit model parameters list for sounding APG22

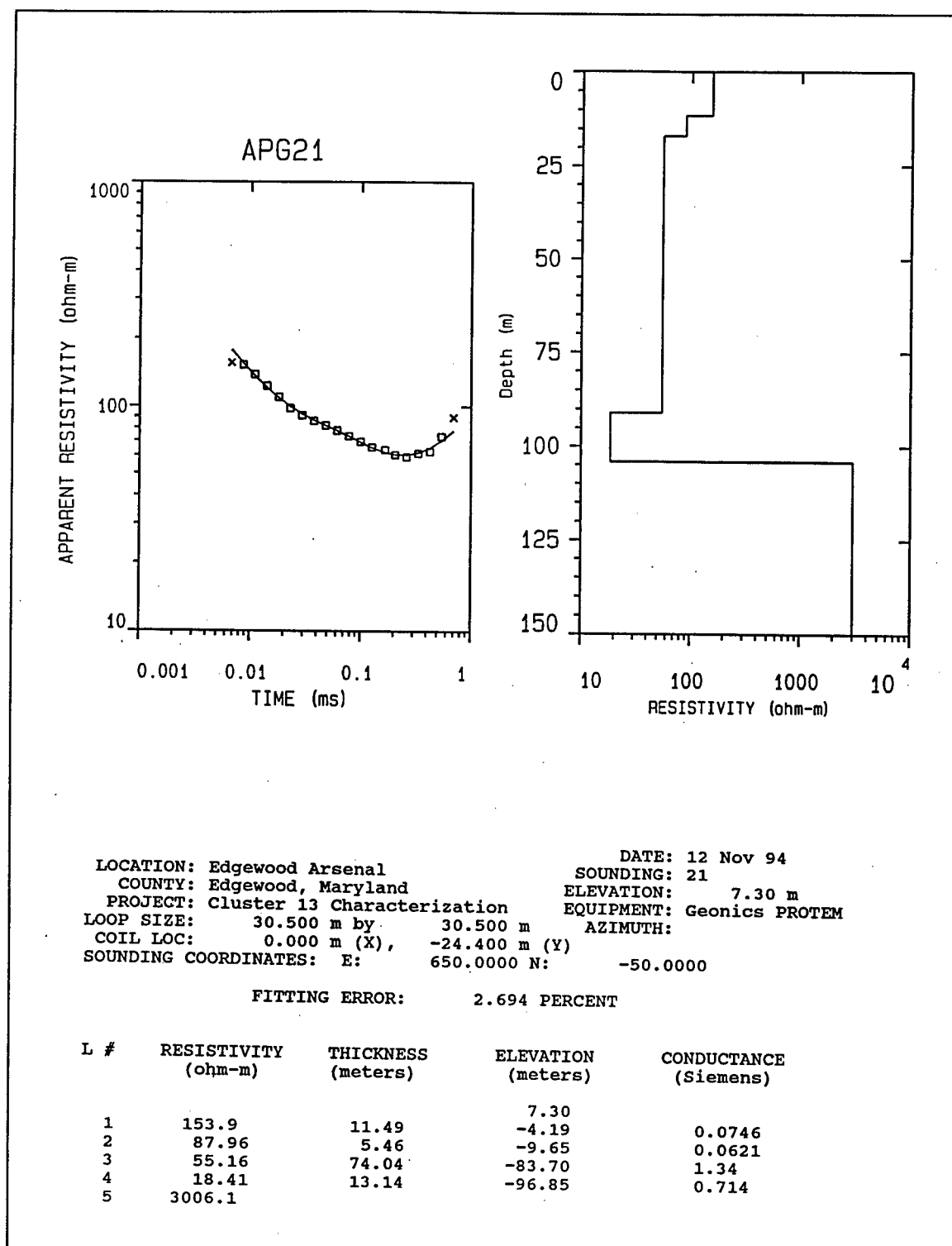


Figure C36. Transient electromagnetic data, best-fit model, and best-fit model parameters list for sounding APG21

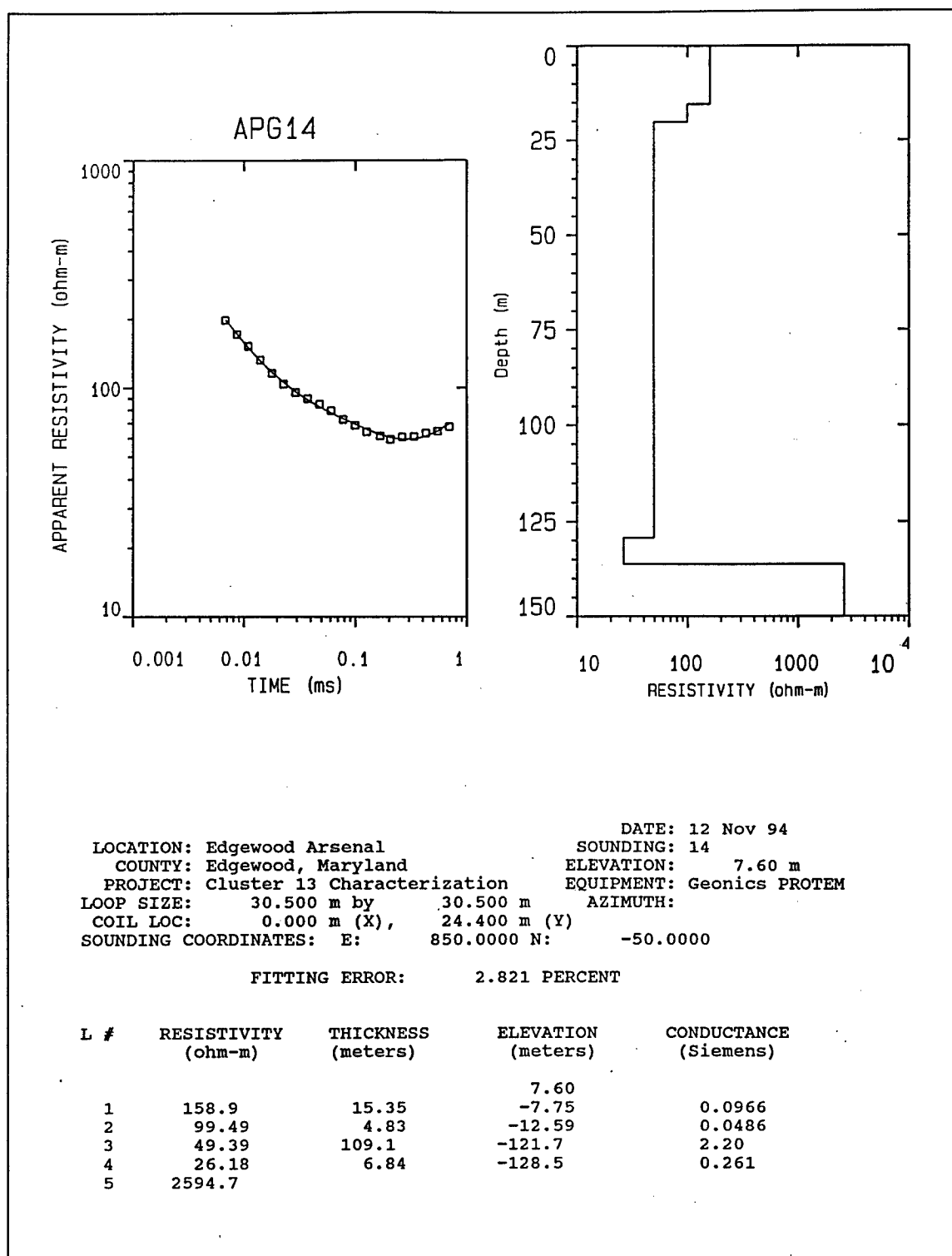


Figure C37. Transient electromagnetic data, best-fit model, and best-fit model parameters list for sounding APG14

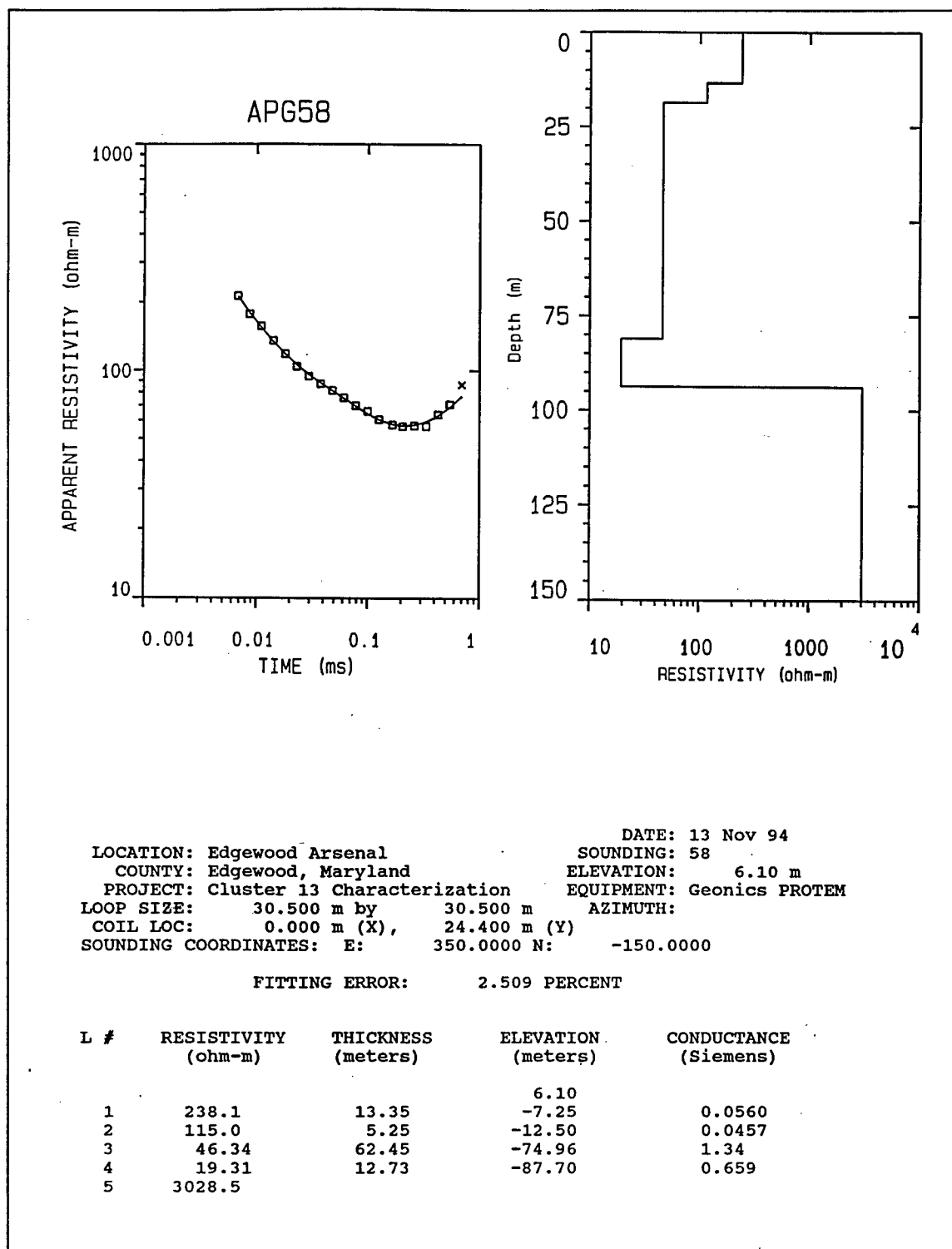


Figure C38. Transient electromagnetic data, best-fit model, and best-fit model parameters list for sounding APG58

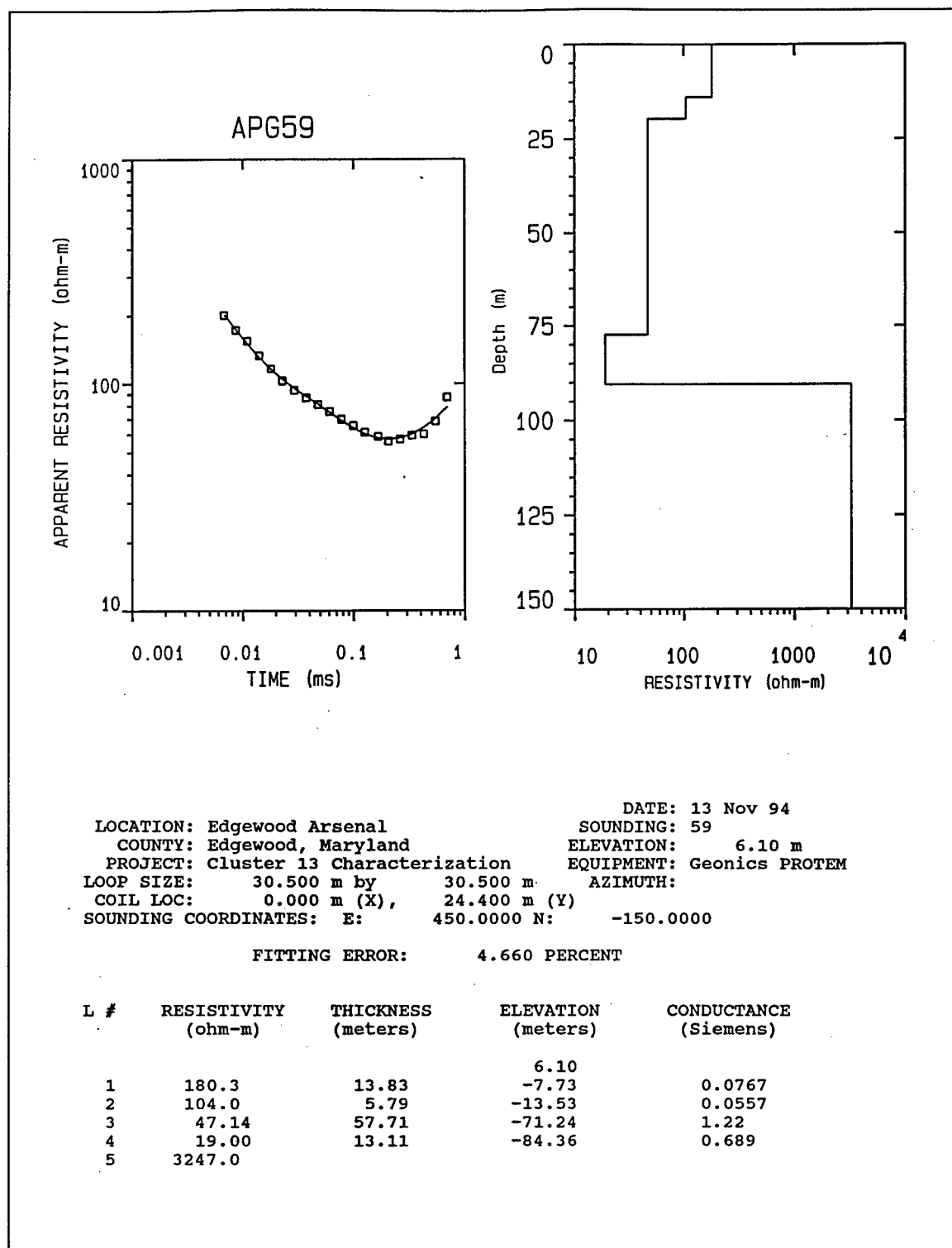


Figure C39. Transient electromagnetic data, best-fit model, and best-fit model parameters list for sounding APG59

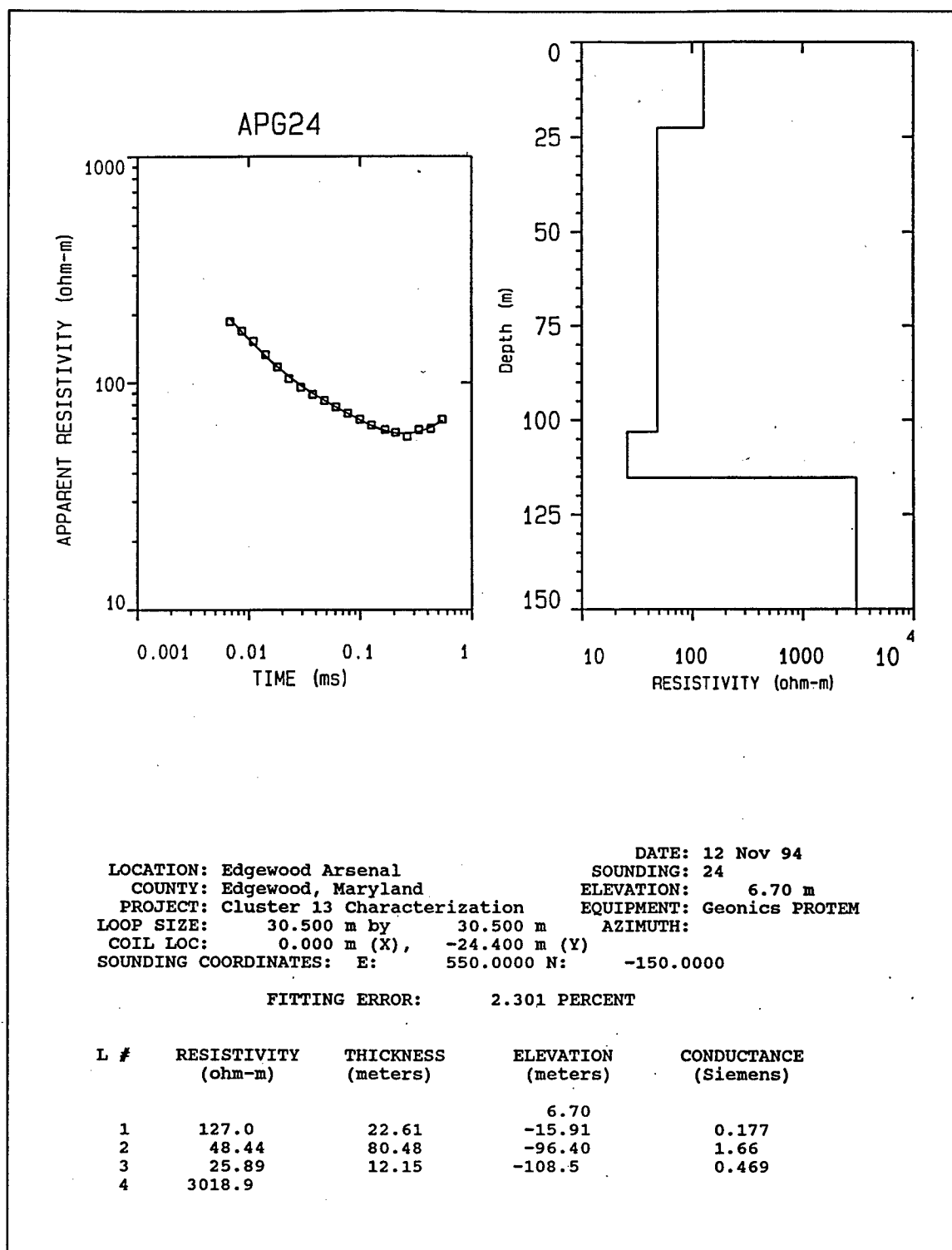


Figure C40. Transient electromagnetic data, best-fit model, and best-fit model parameters list for sounding APG24

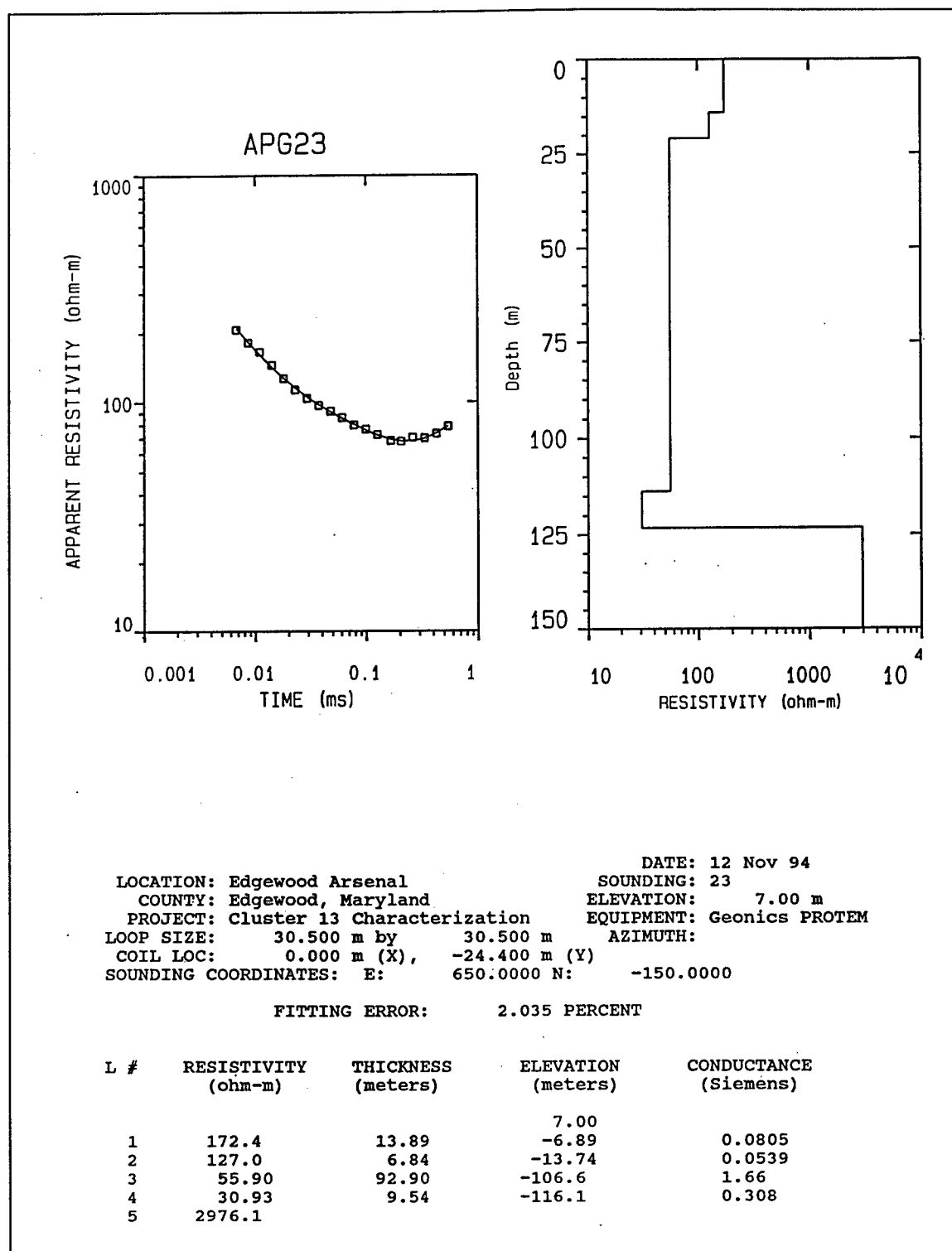


Figure C41. Transient electromagnetic data, best-fit model, and best-fit model parameters list for sounding APG23

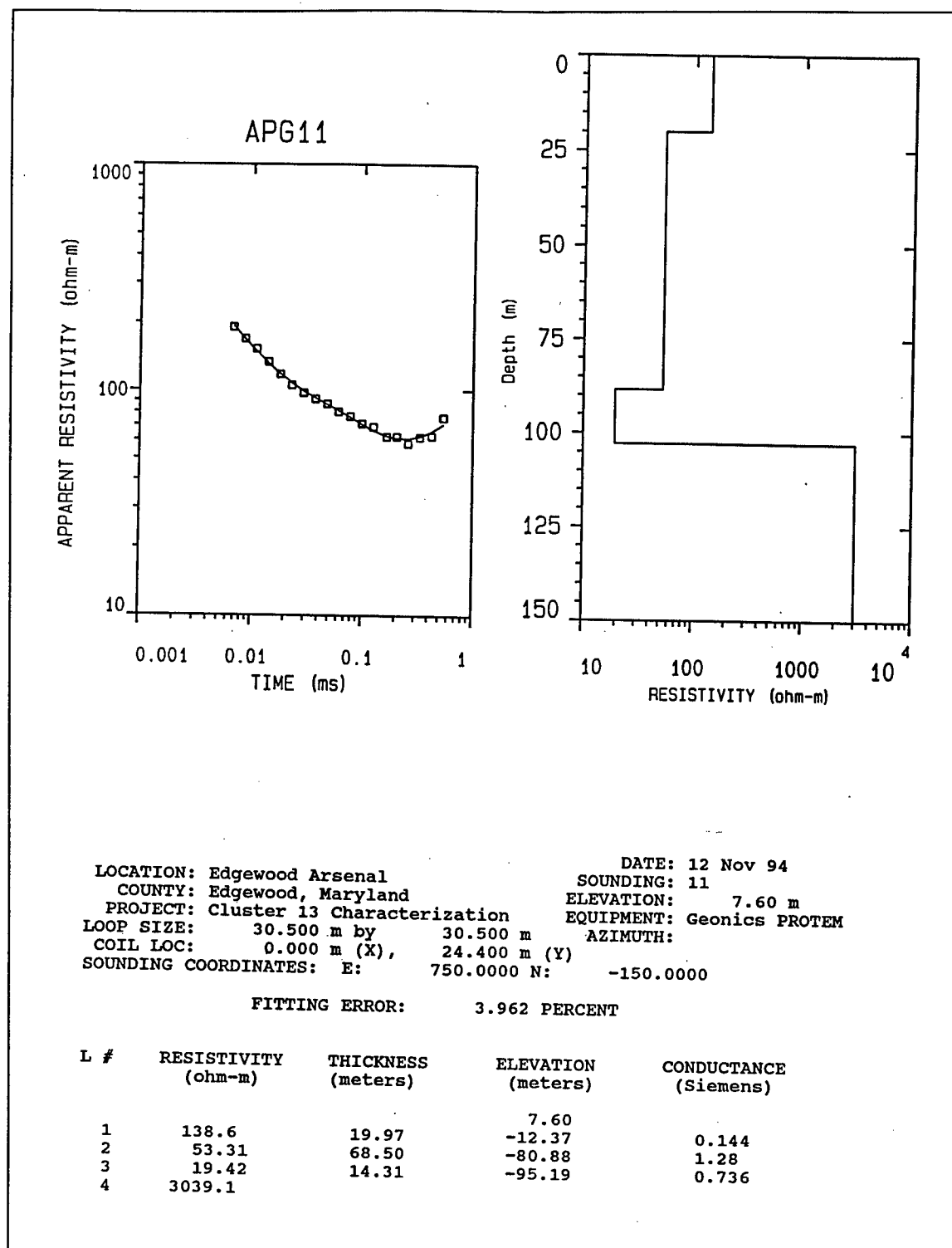


Figure C42. Transient electromagnetic data, best-fit model, and best-fit model parameters list for sounding APG11

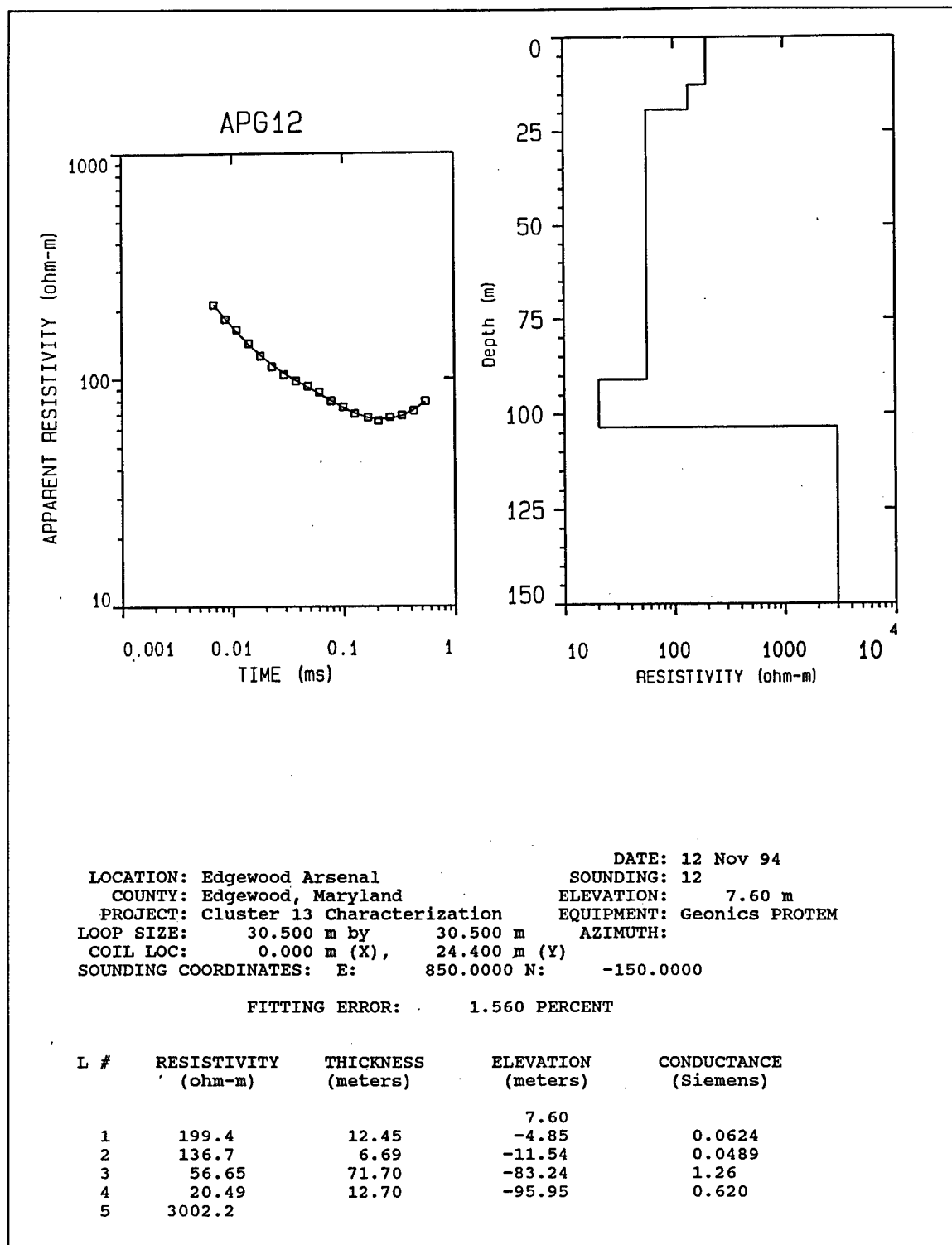


Figure C43. Transient electromagnetic data, best-fit model, and best-fit model parameters list for sounding APG12

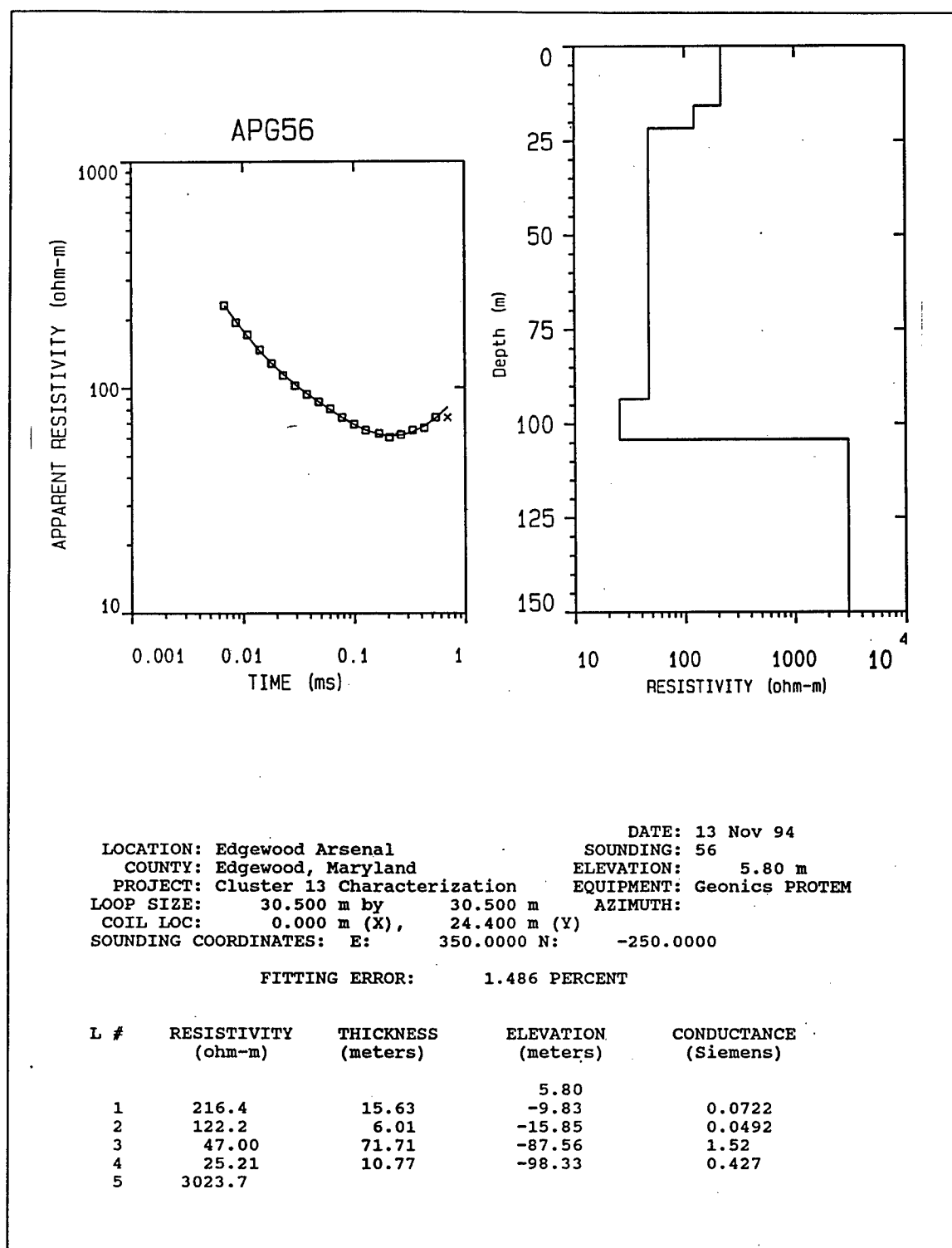


Figure C44. Transient electromagnetic data, best-fit model, and best-fit model parameters list for sounding APG56

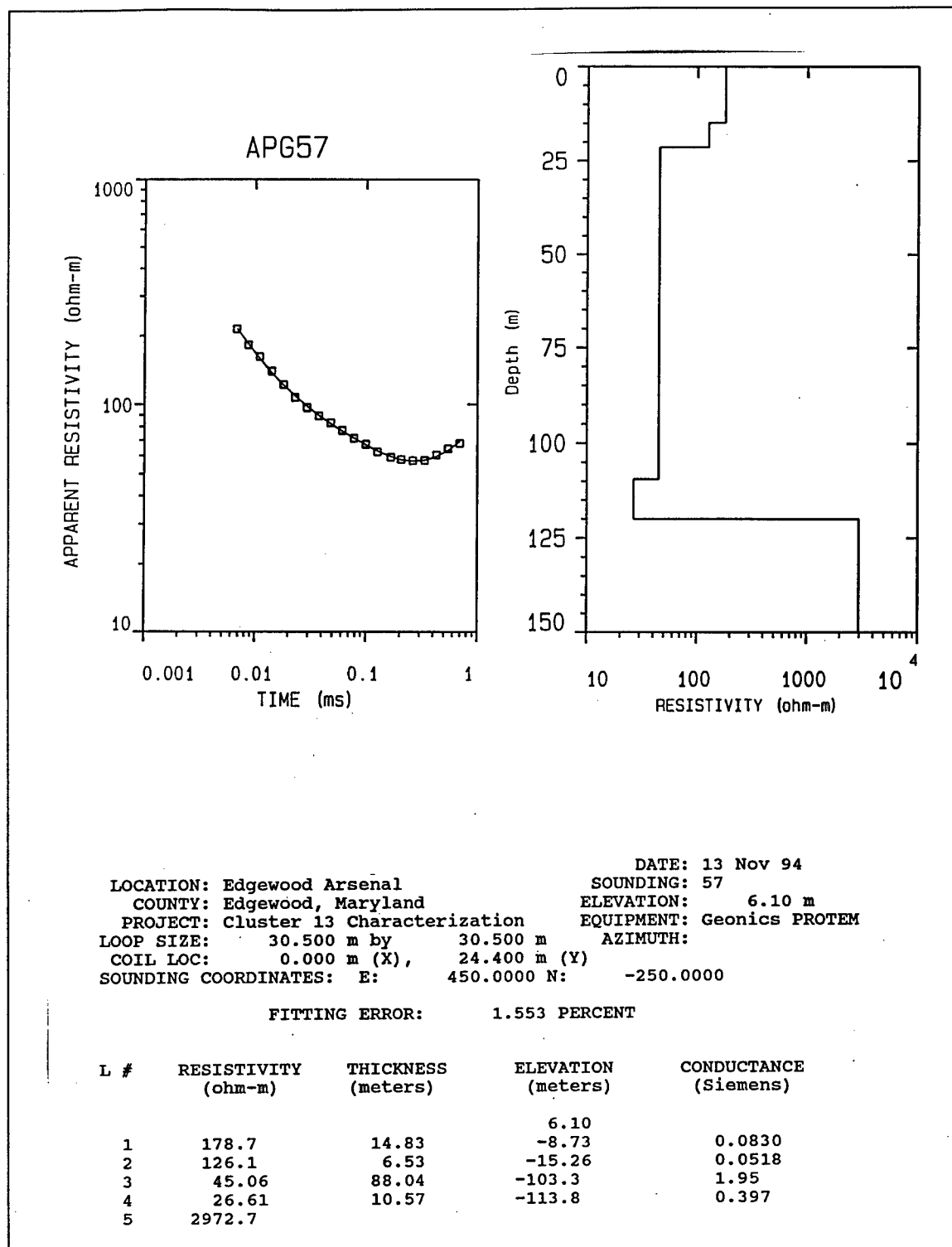


Figure C45. Transient electromagnetic data, best-fit model, and best-fit model parameters list for sounding APG57

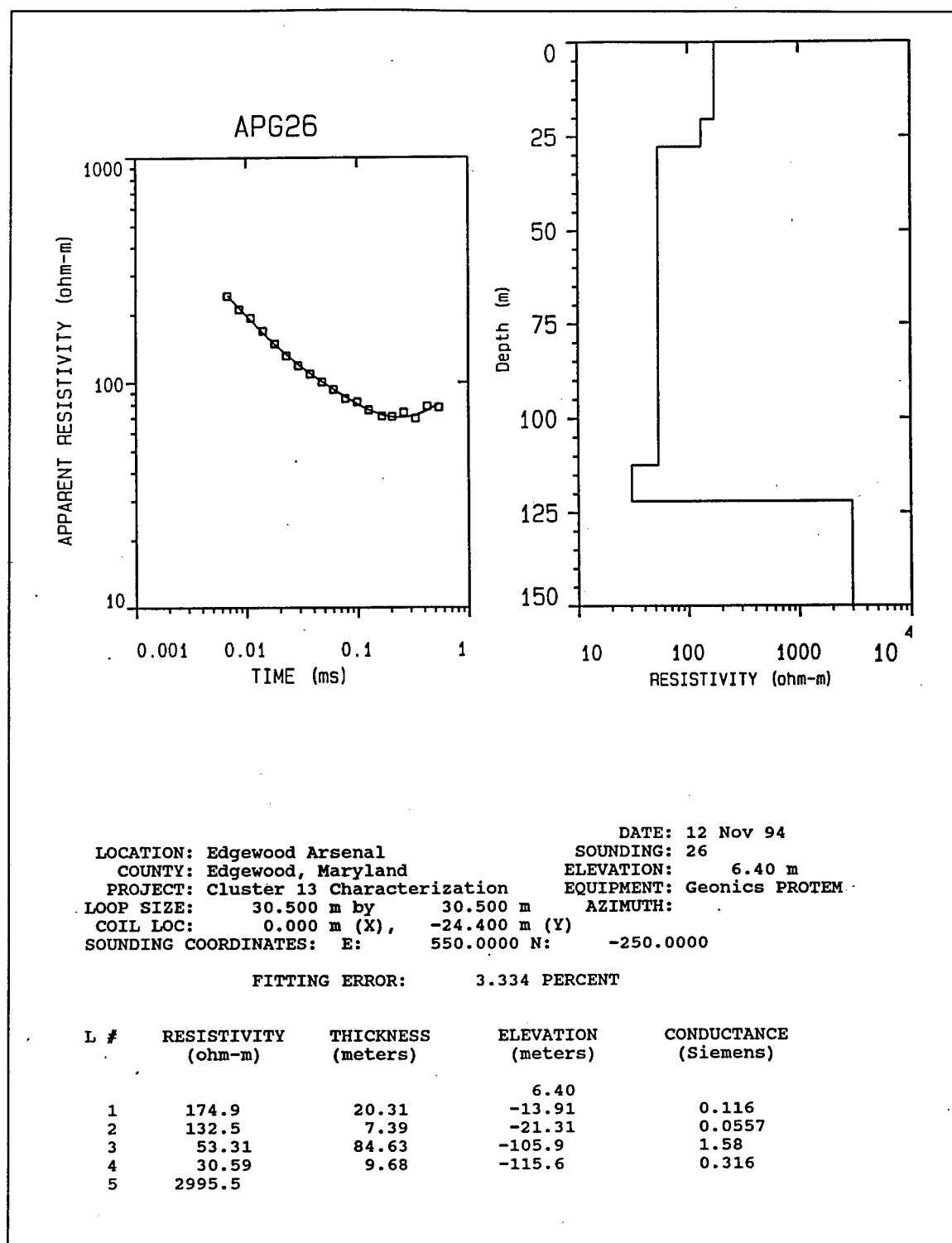


Figure C46. Transient electromagnetic data, best-fit model, and best-fit model parameters list for sounding APG26

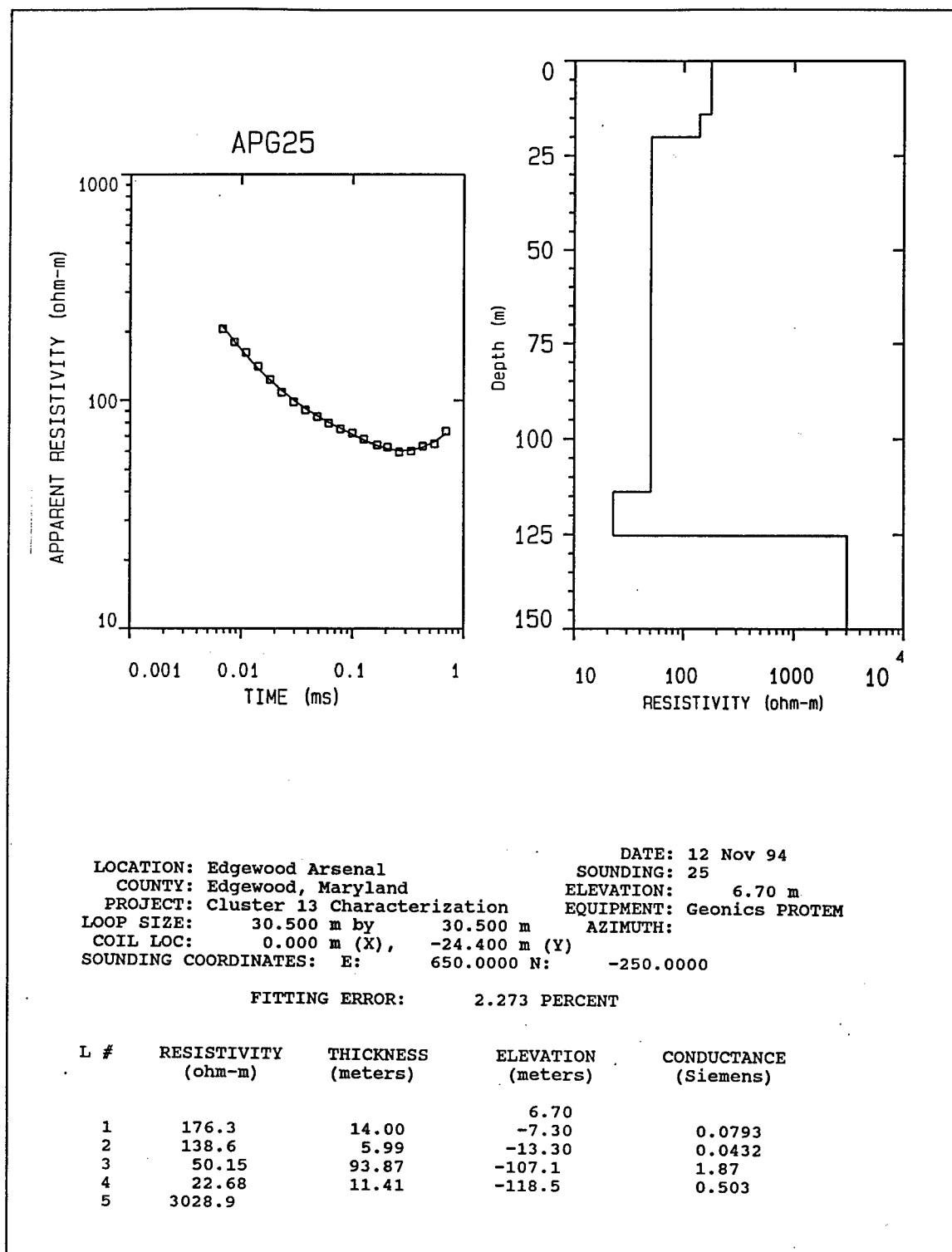


Figure C47. Transient electromagnetic data, best-fit model, and best-fit model parameters list for sounding APG25

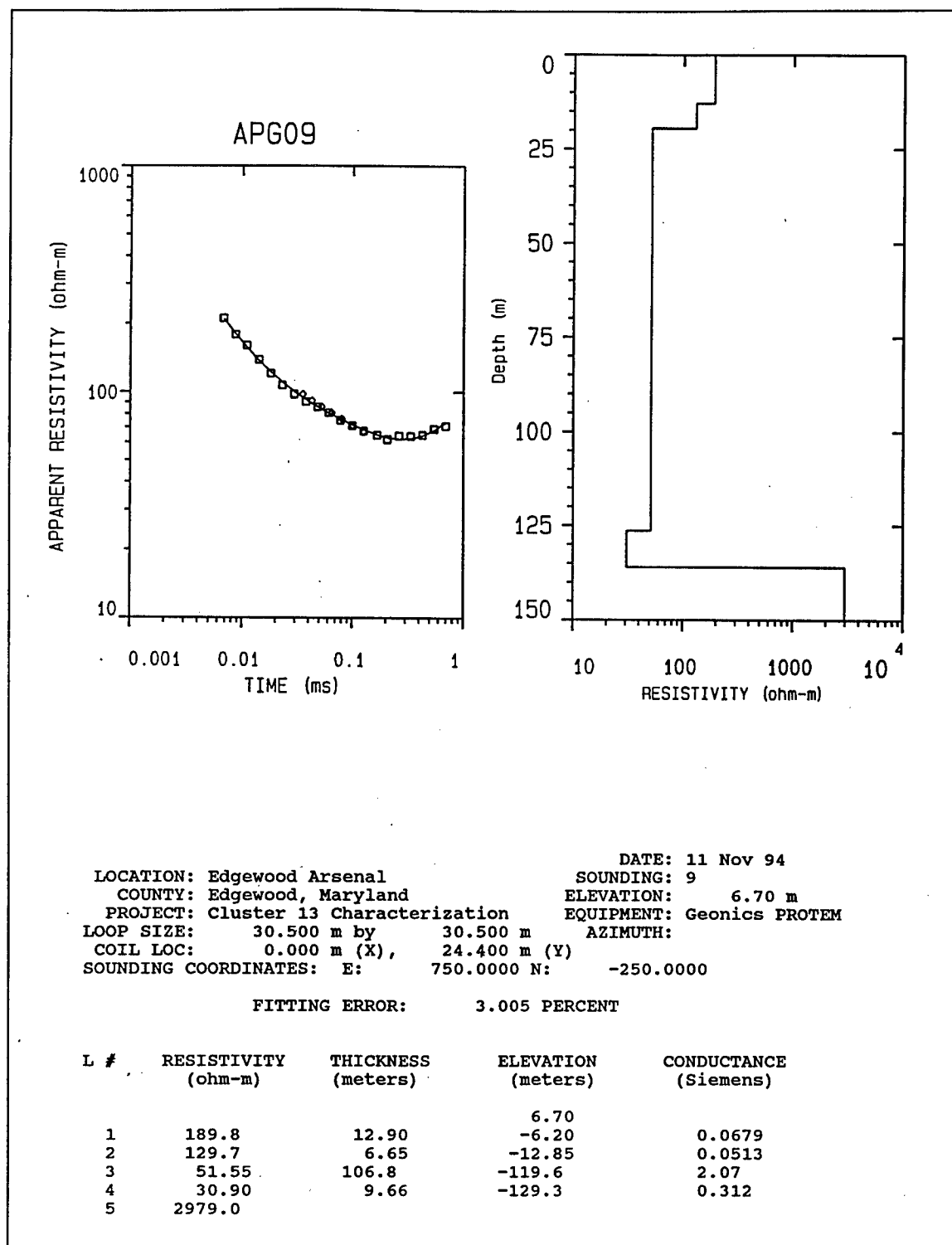


Figure C48. Transient electromagnetic data, best-fit model, and best-fit model parameters list for sounding APG09

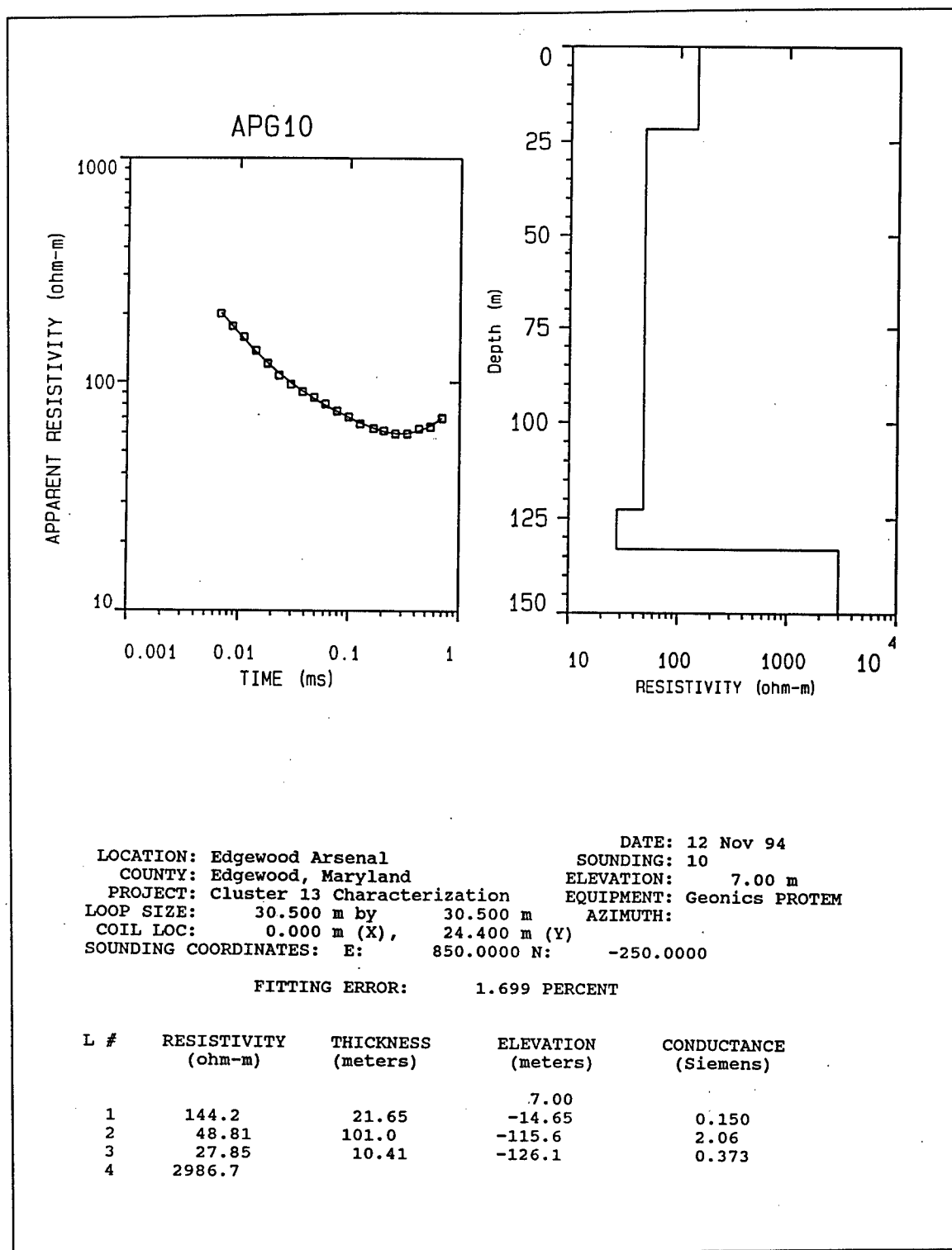


Figure C49. Transient electromagnetic data, best-fit model, and best-fit model parameters list for sounding APG10

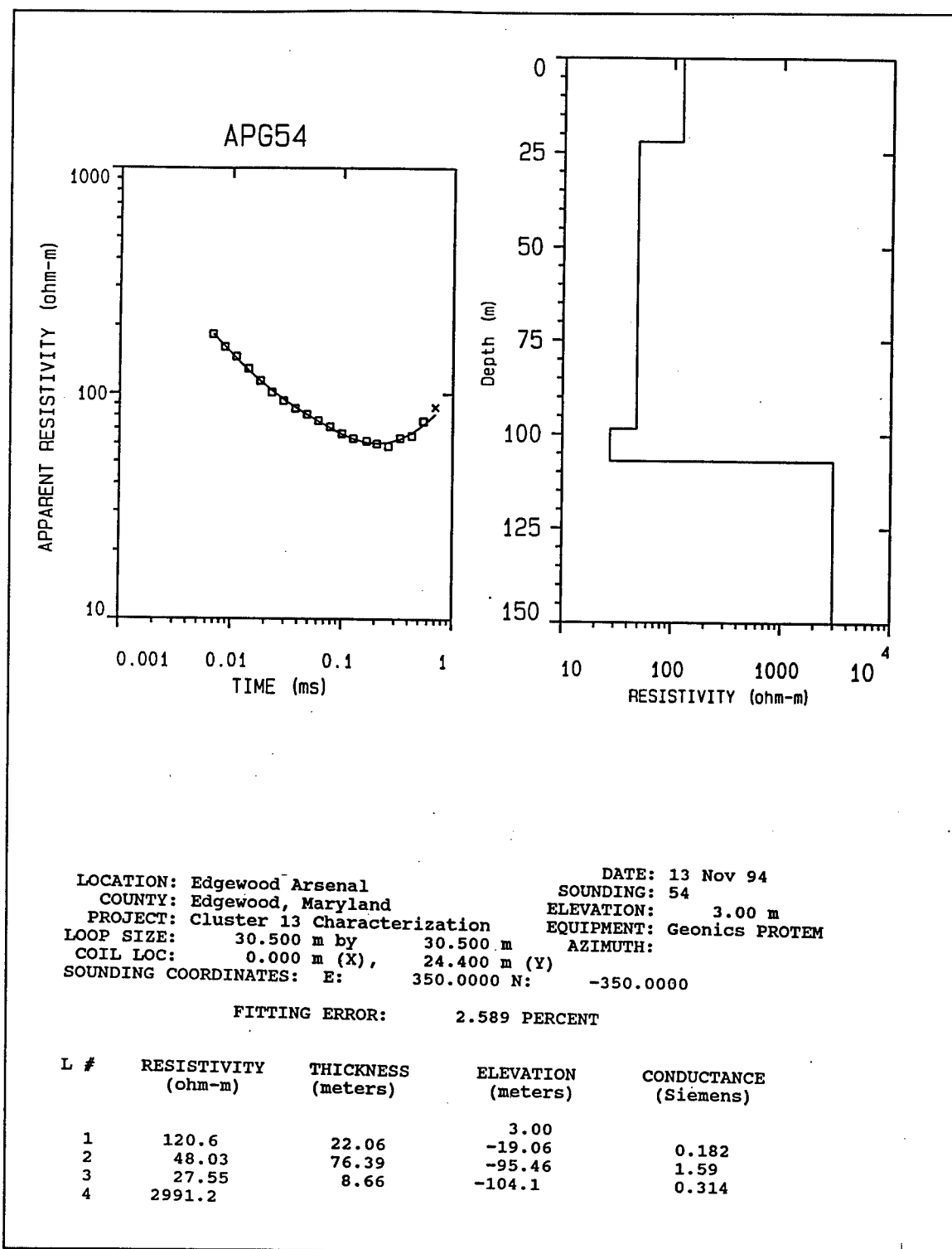


Figure C50. Transient electromagnetic data, best-fit model, and best-fit model parameters list for sounding APG54

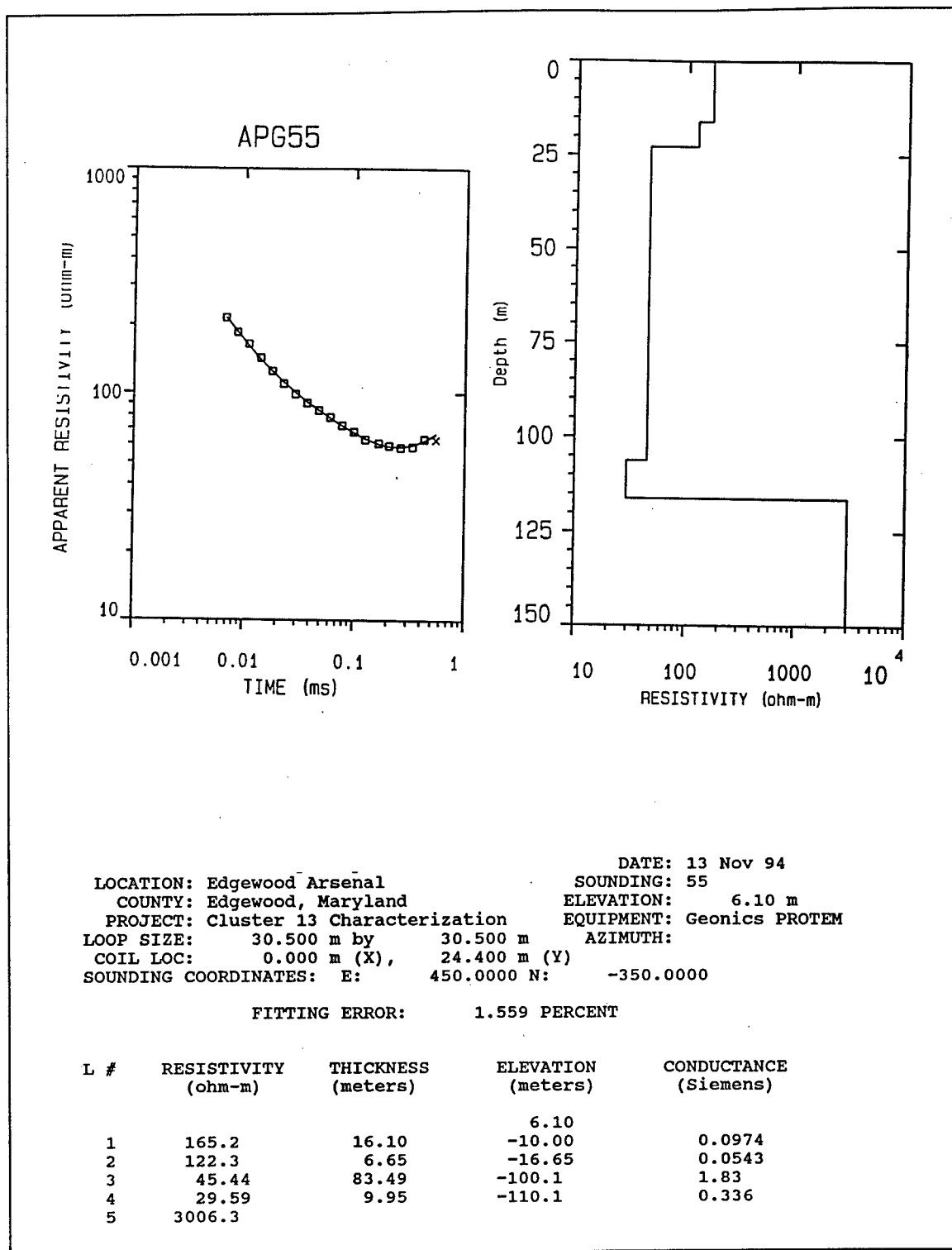


Figure C51. Transient electromagnetic data, best-fit model, and best-fit model parameters list for sounding APG55

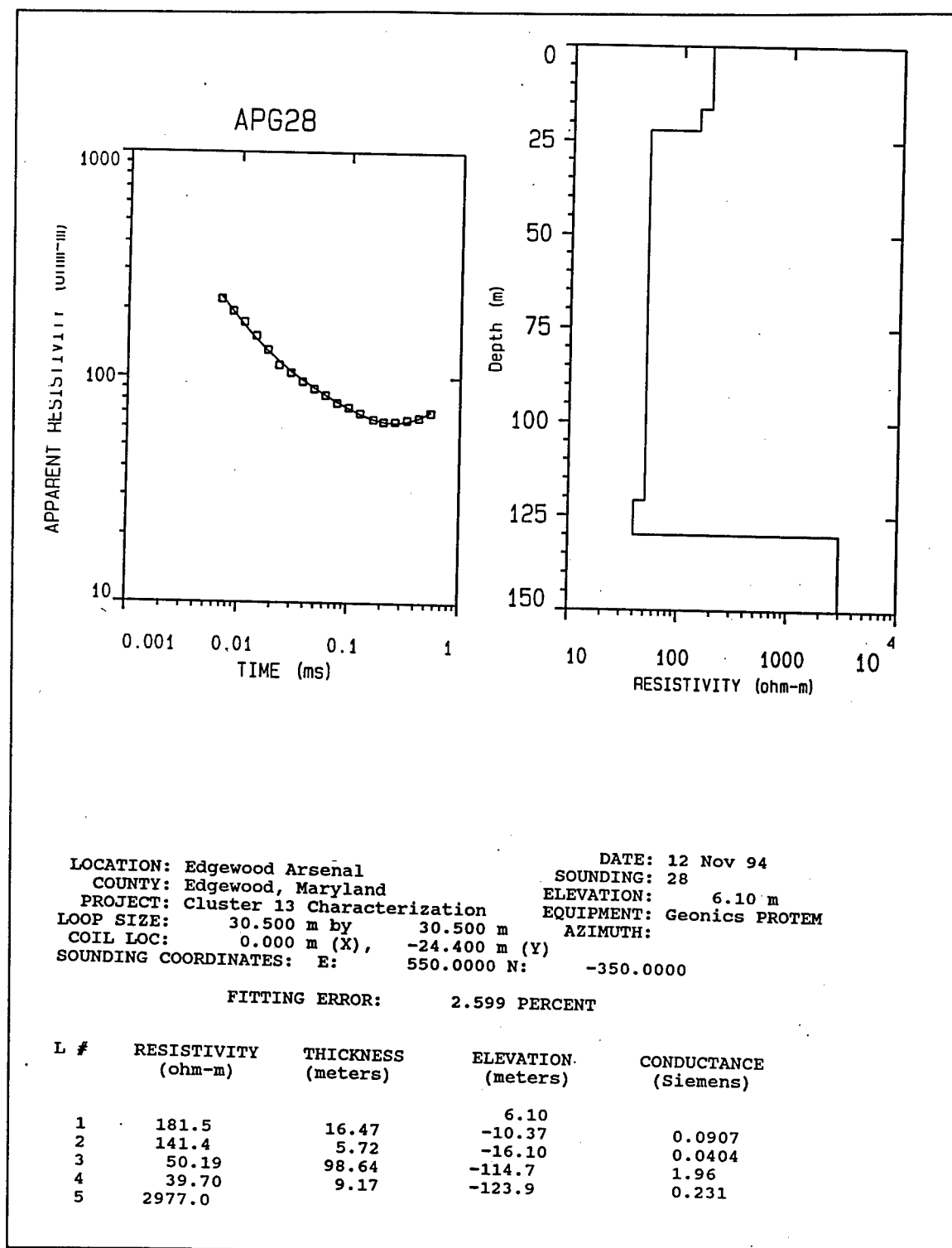


Figure C52. Transient electromagnetic data, best-fit model, and best-fit model parameters list for sounding APG28

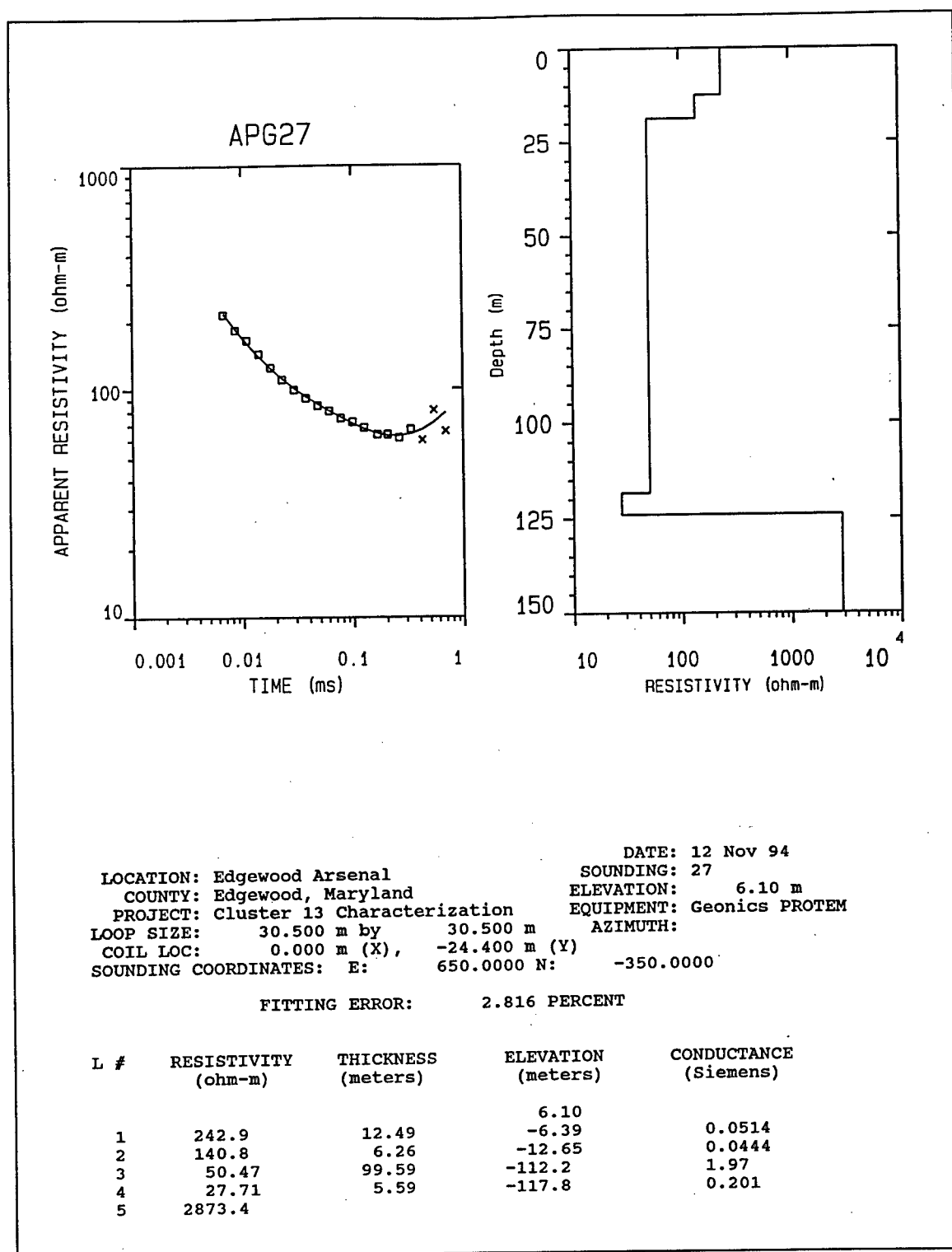


Figure C53. Transient electromagnetic data, best-fit model, and best-fit model parameters list for sounding APG27

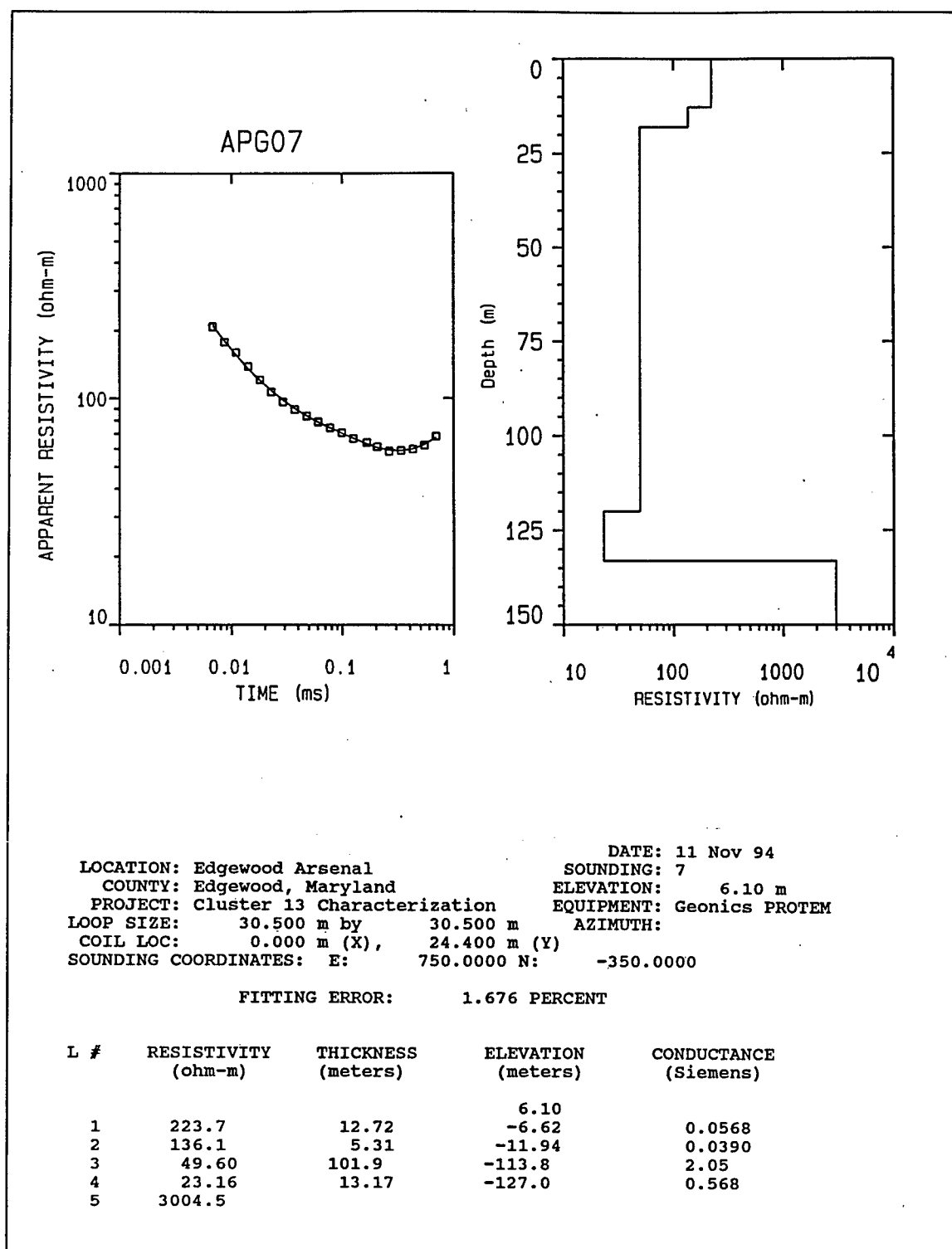


Figure C54. Transient electromagnetic data, best-fit model, and best-fit model parameters list for sounding APG07

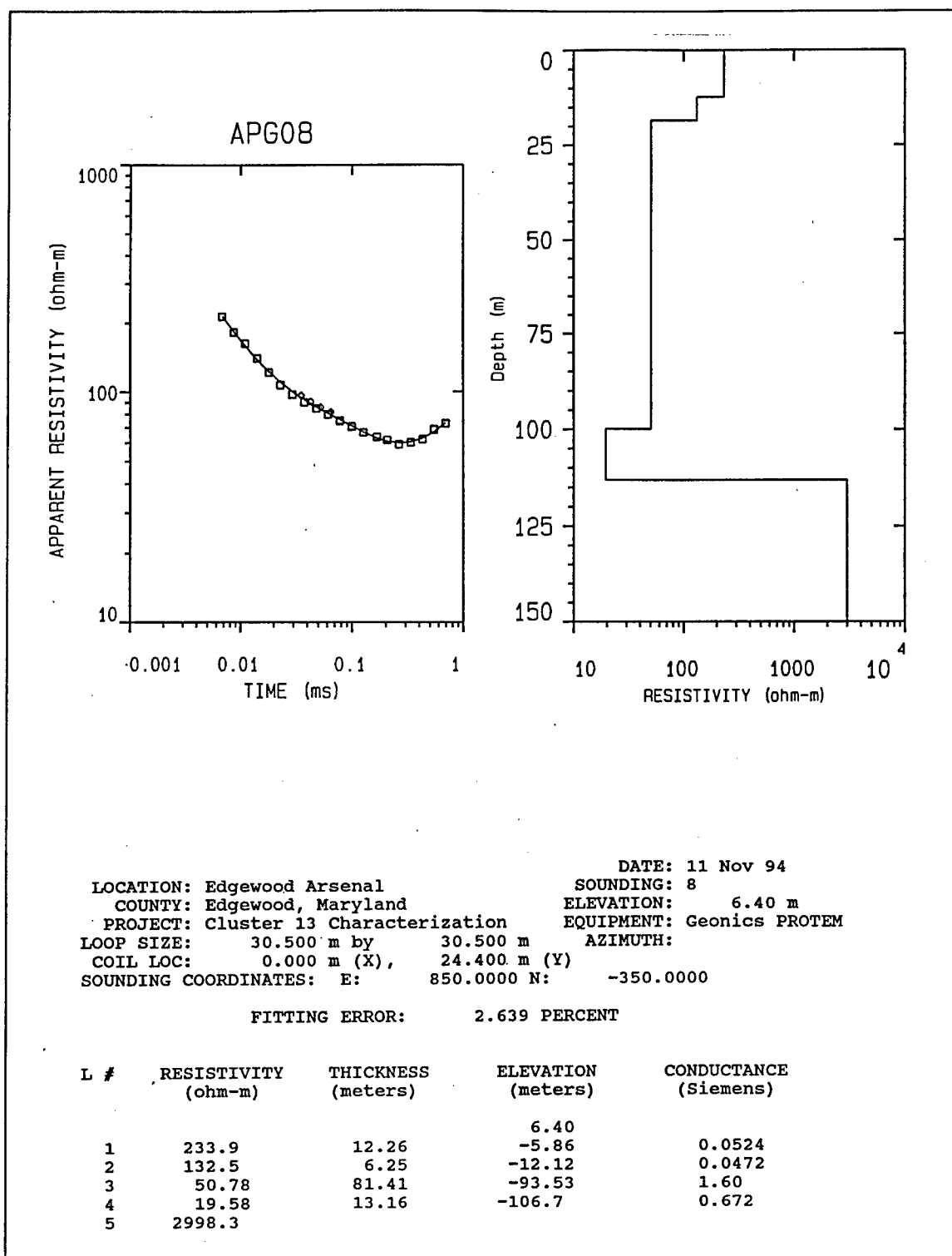


Figure C55. Transient electromagnetic data, best-fit model, and best-fit model parameters list for sounding APG08

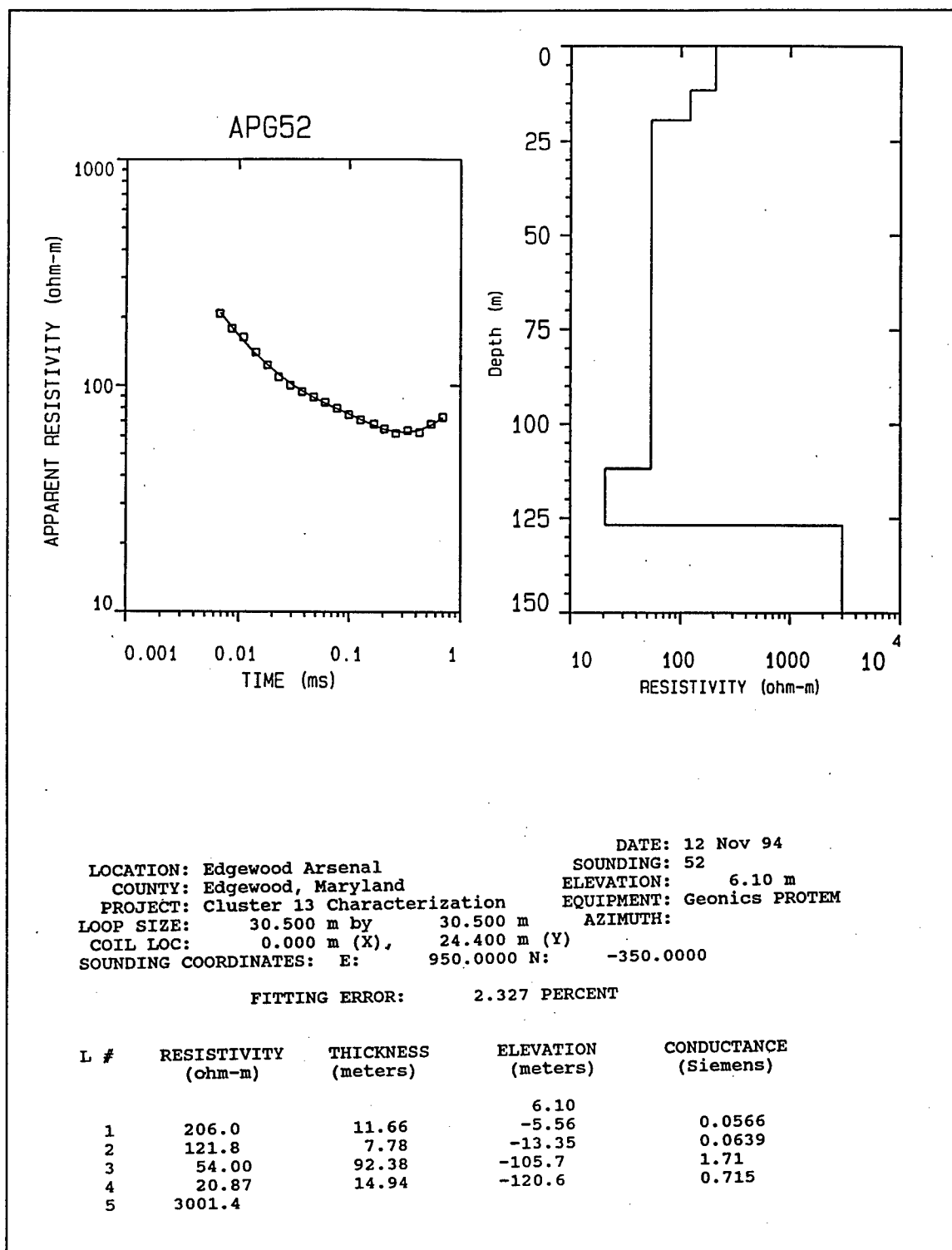


Figure C56. Transient electromagnetic data, best-fit model, and best-fit model parameters list for sounding APG52

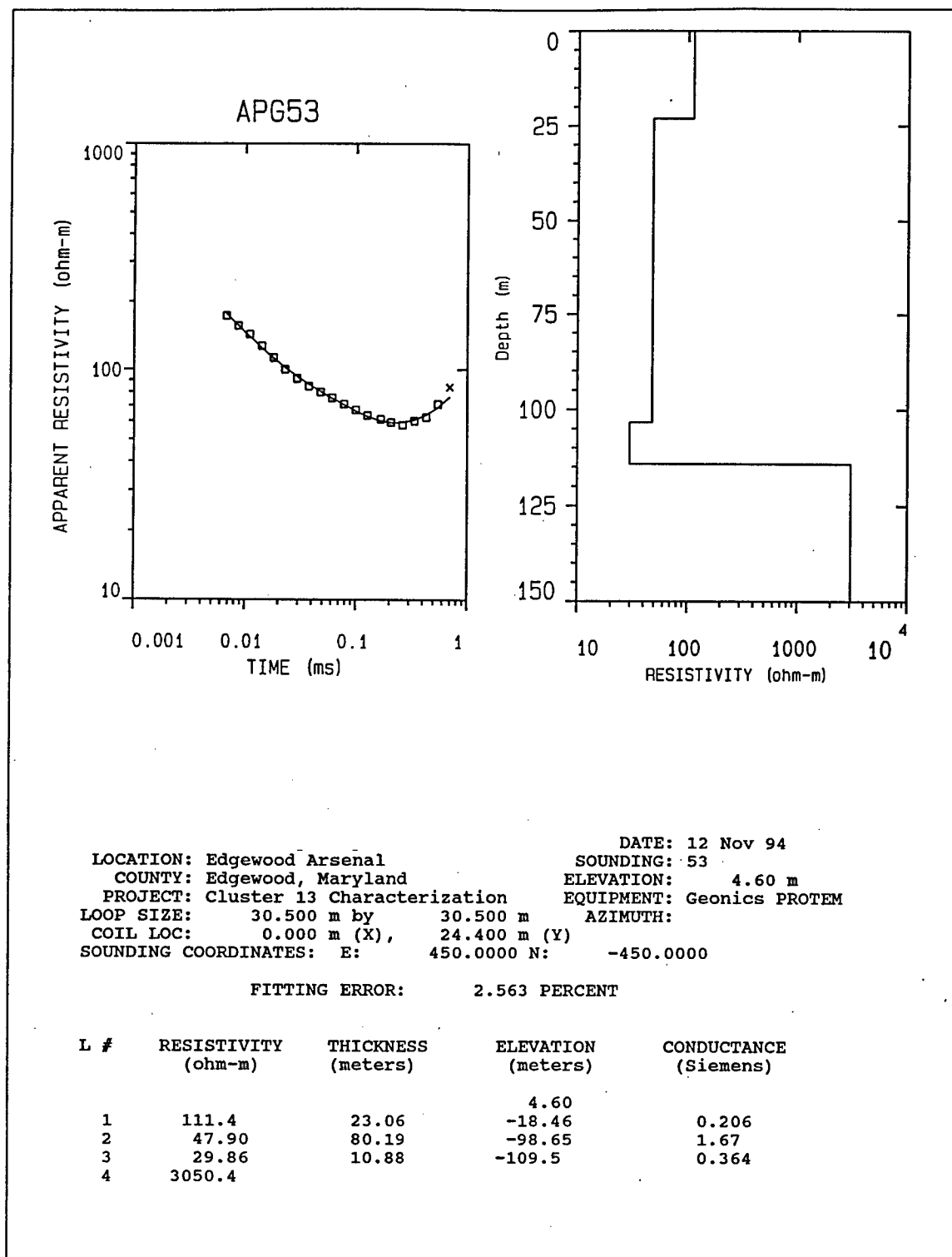


Figure C57. Transient electromagnetic data, best-fit model, and best-fit model parameters list for sounding APG53

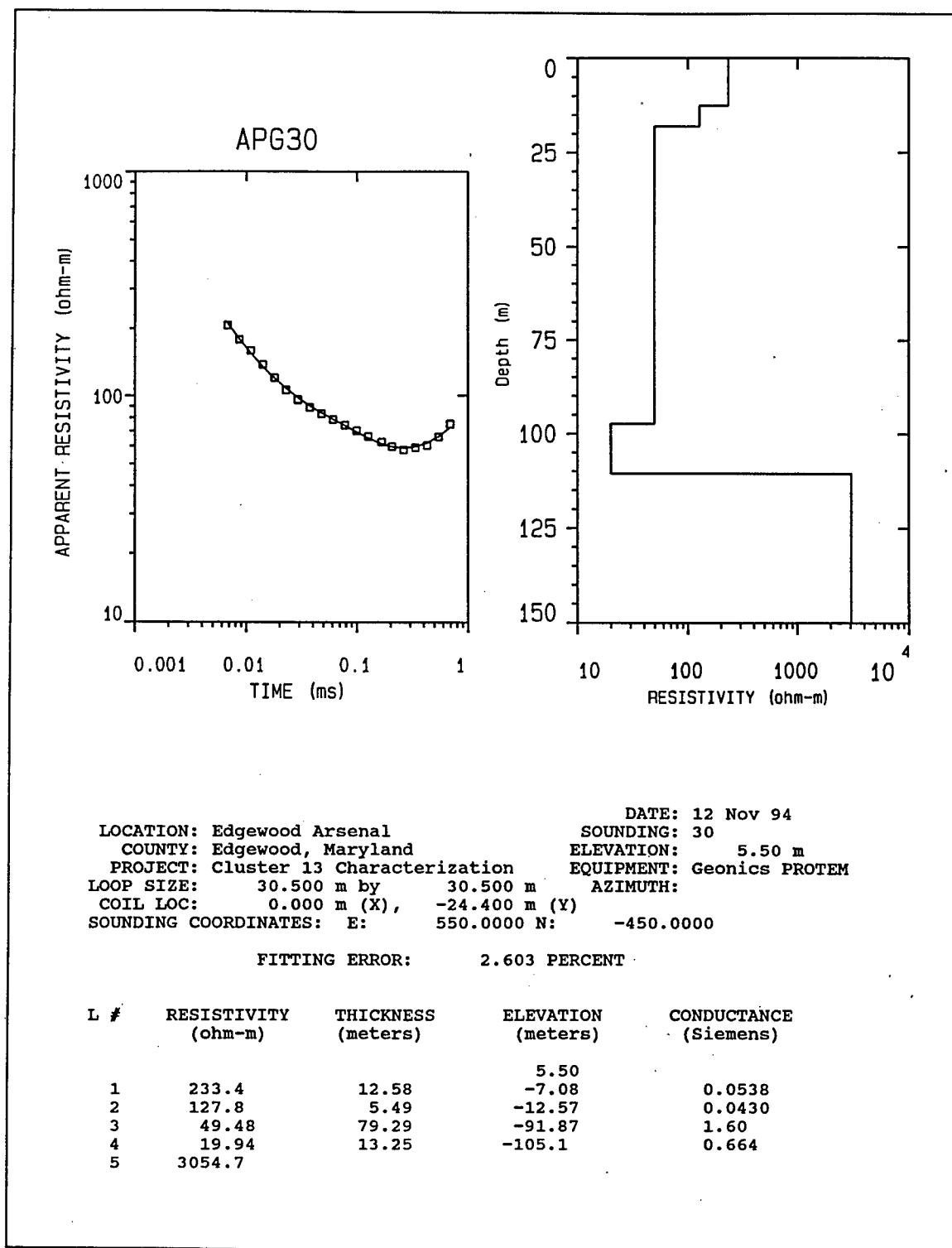


Figure C58. Transient electromagnetic data, best-fit model, and best-fit model parameters list for sounding APG30

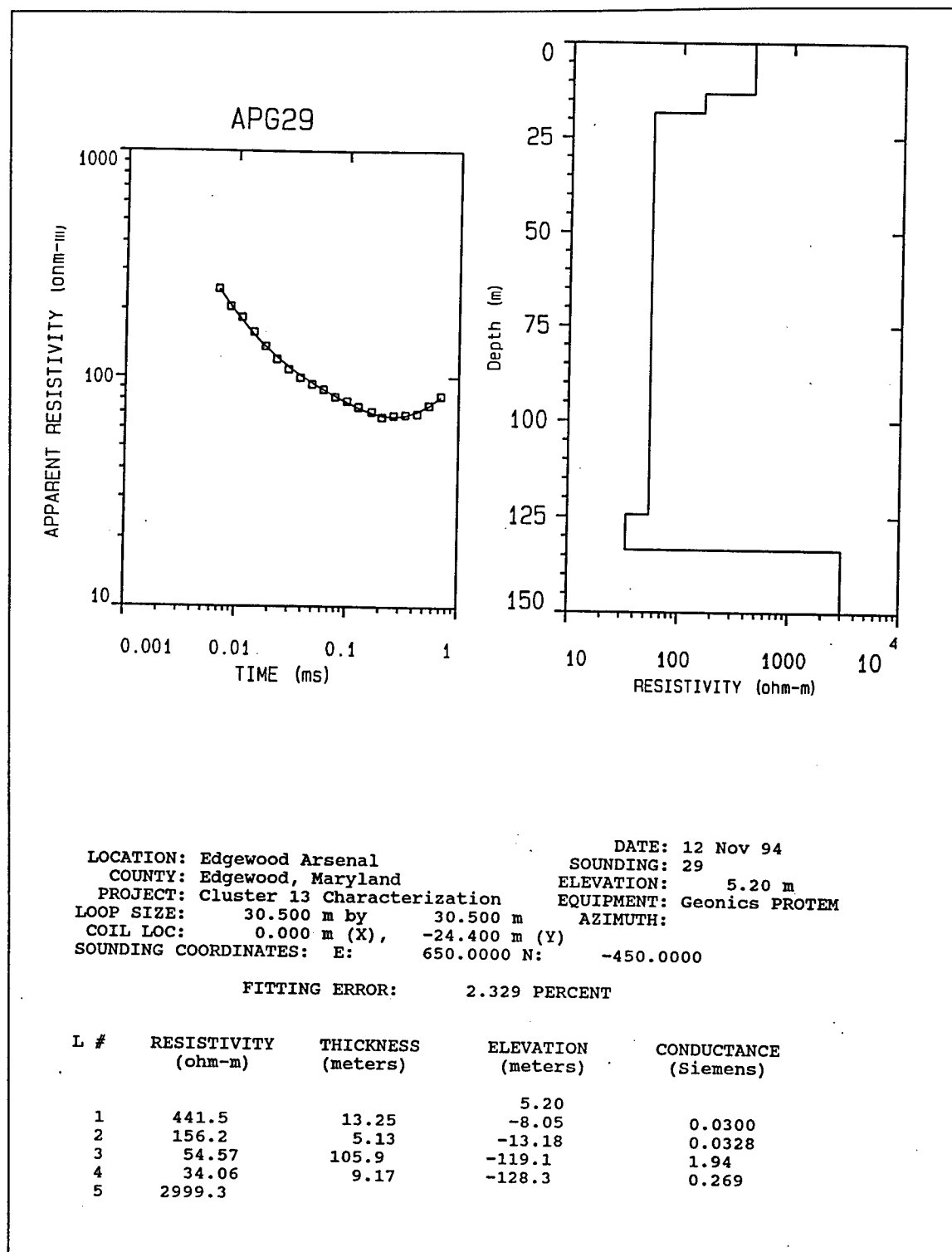


Figure C59. Transient electromagnetic data, best-fit model, and best-fit model parameters list for sounding APG29

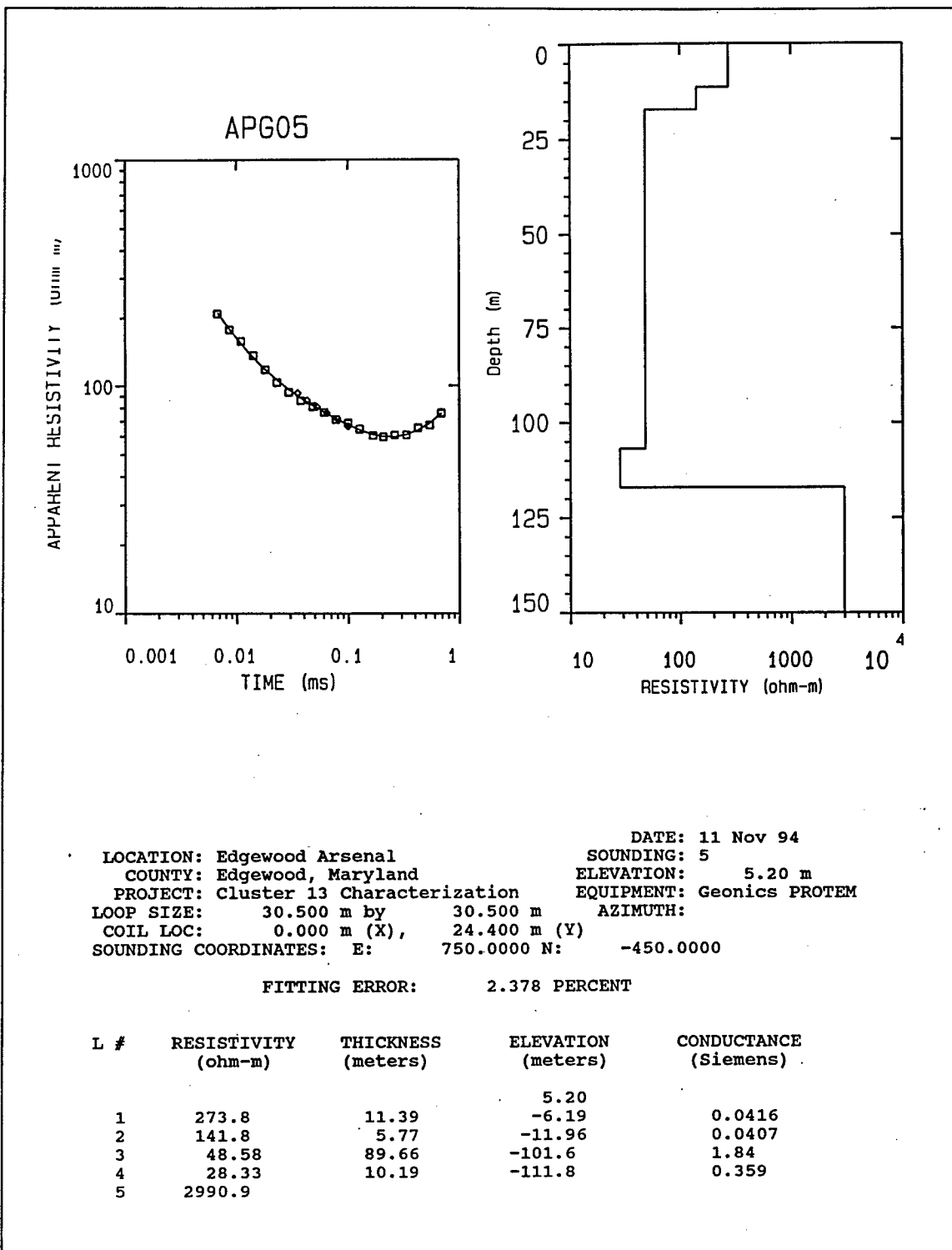


Figure C60. Transient electromagnetic data, best-fit model, and best-fit model parameters list for sounding APG05

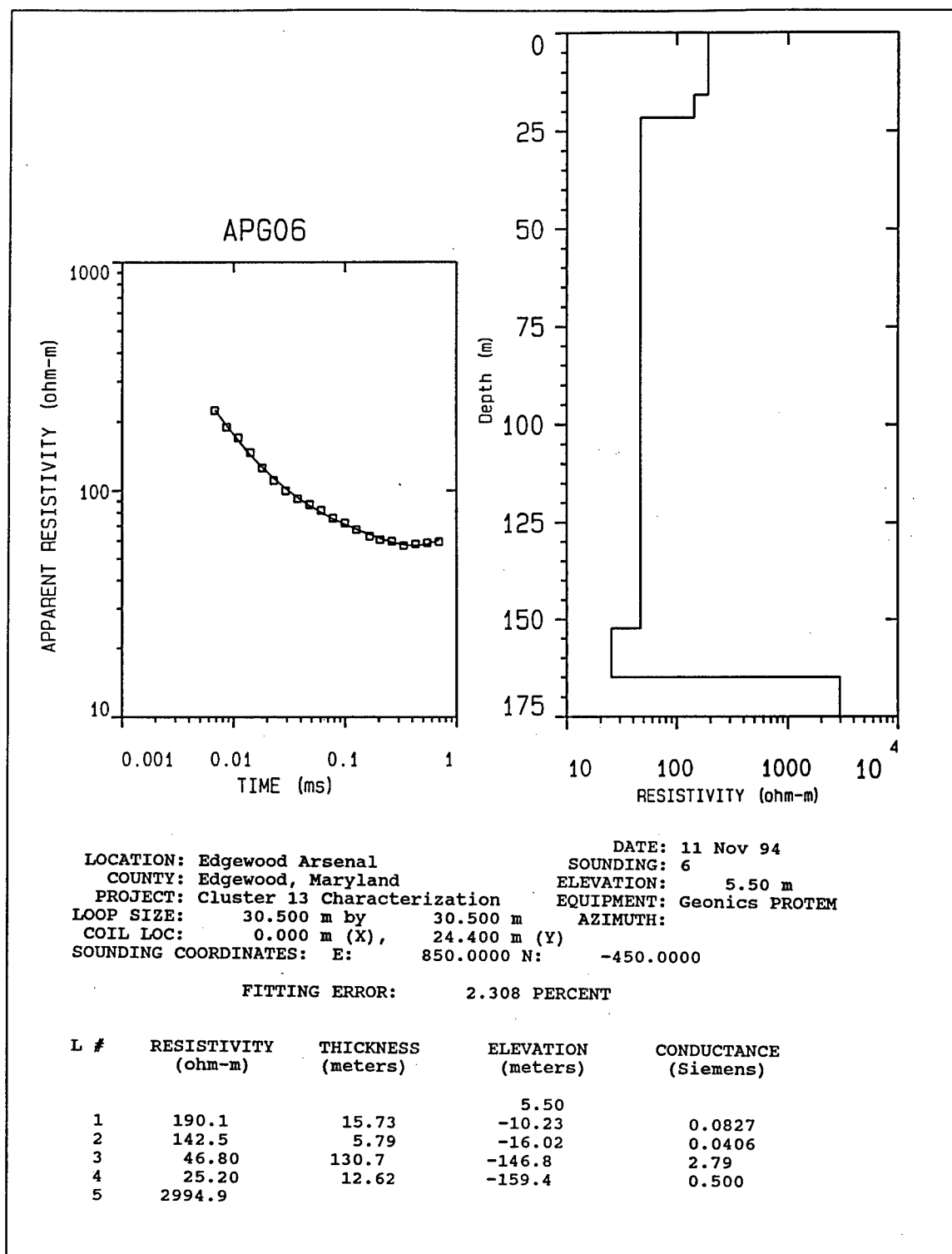


Figure C61. Transient electromagnetic data, best-fit model, and best-fit model parameters list for sounding APG06

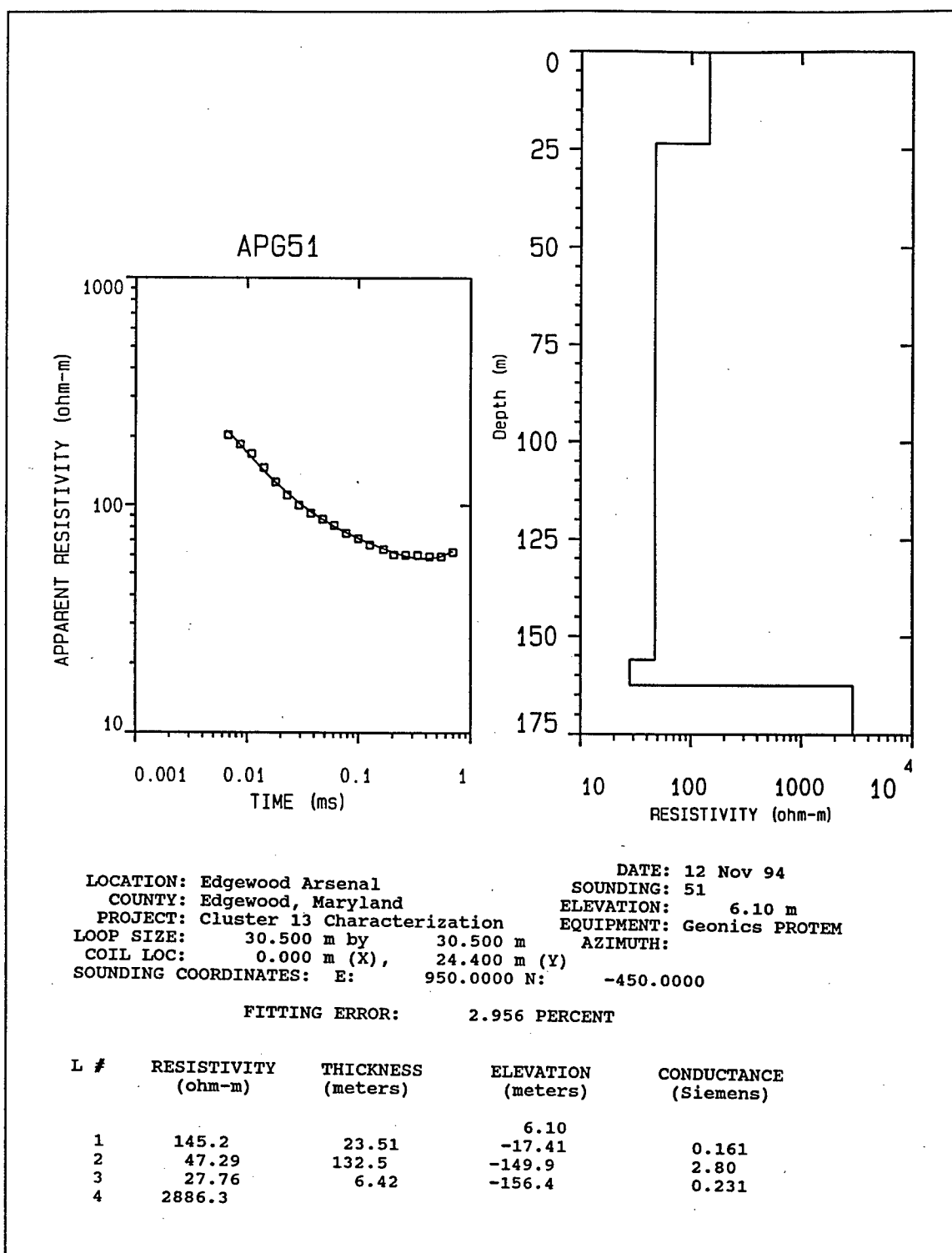


Figure C62. Transient electromagnetic data, best-fit model, and best-fit model parameters list for sounding APG51

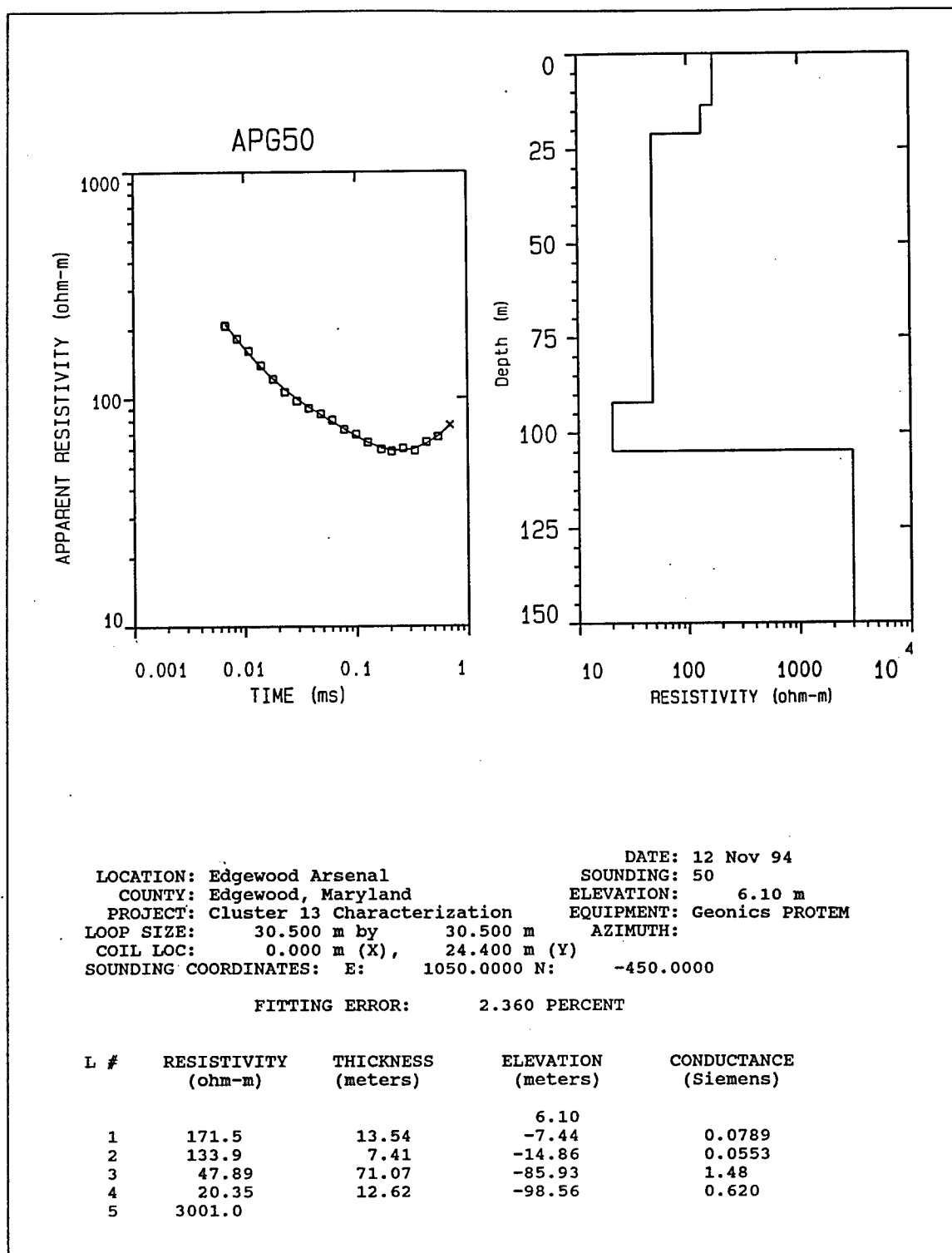


Figure C63. Transient electromagnetic data, best-fit model, and best-fit model parameters list for sounding APG50

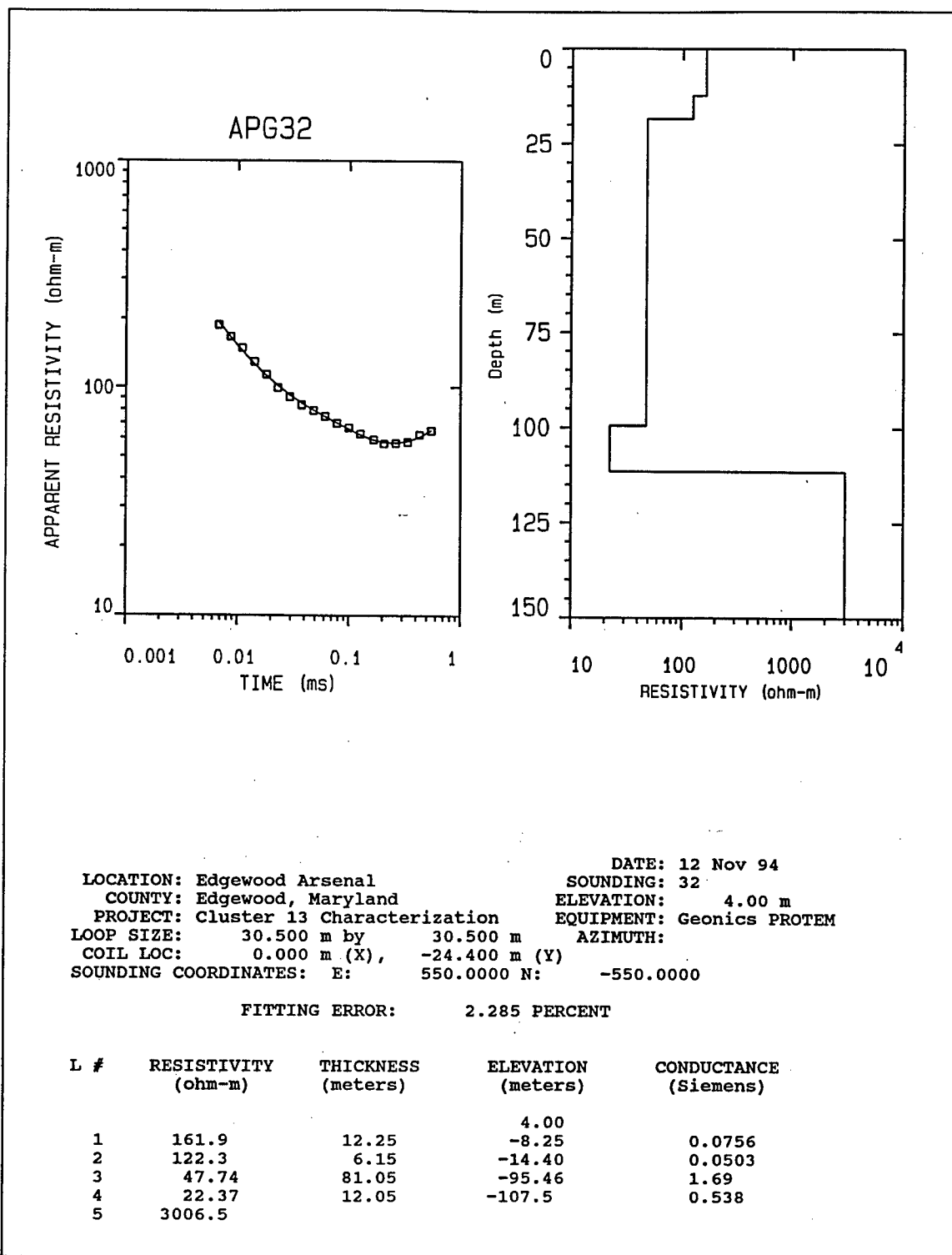


Figure C64. Transient electromagnetic data, best-fit model, and best-fit model parameters list for sounding APG32

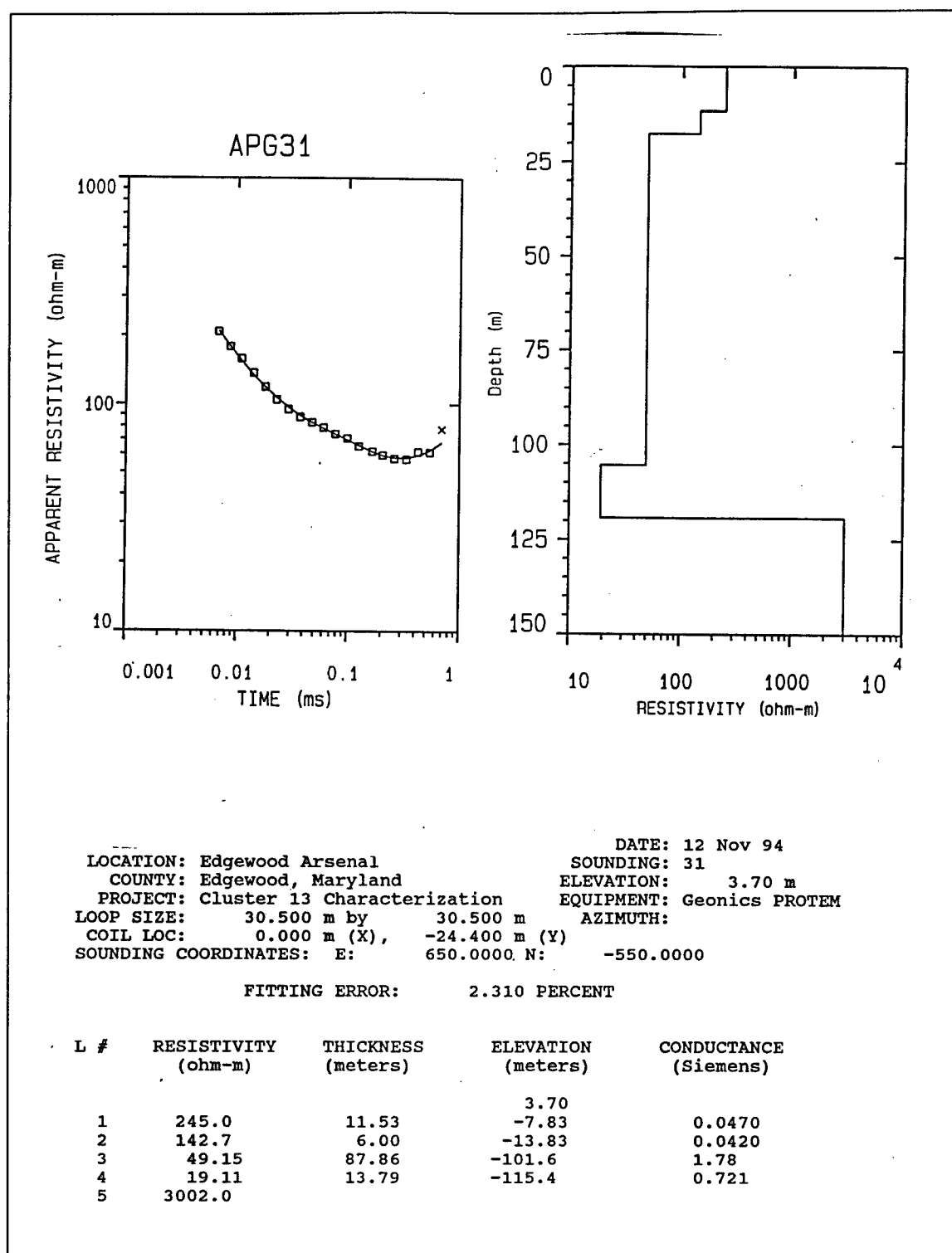


Figure C65. Transient electromagnetic data, best-fit model, and best-fit model parameters list for sounding APG31

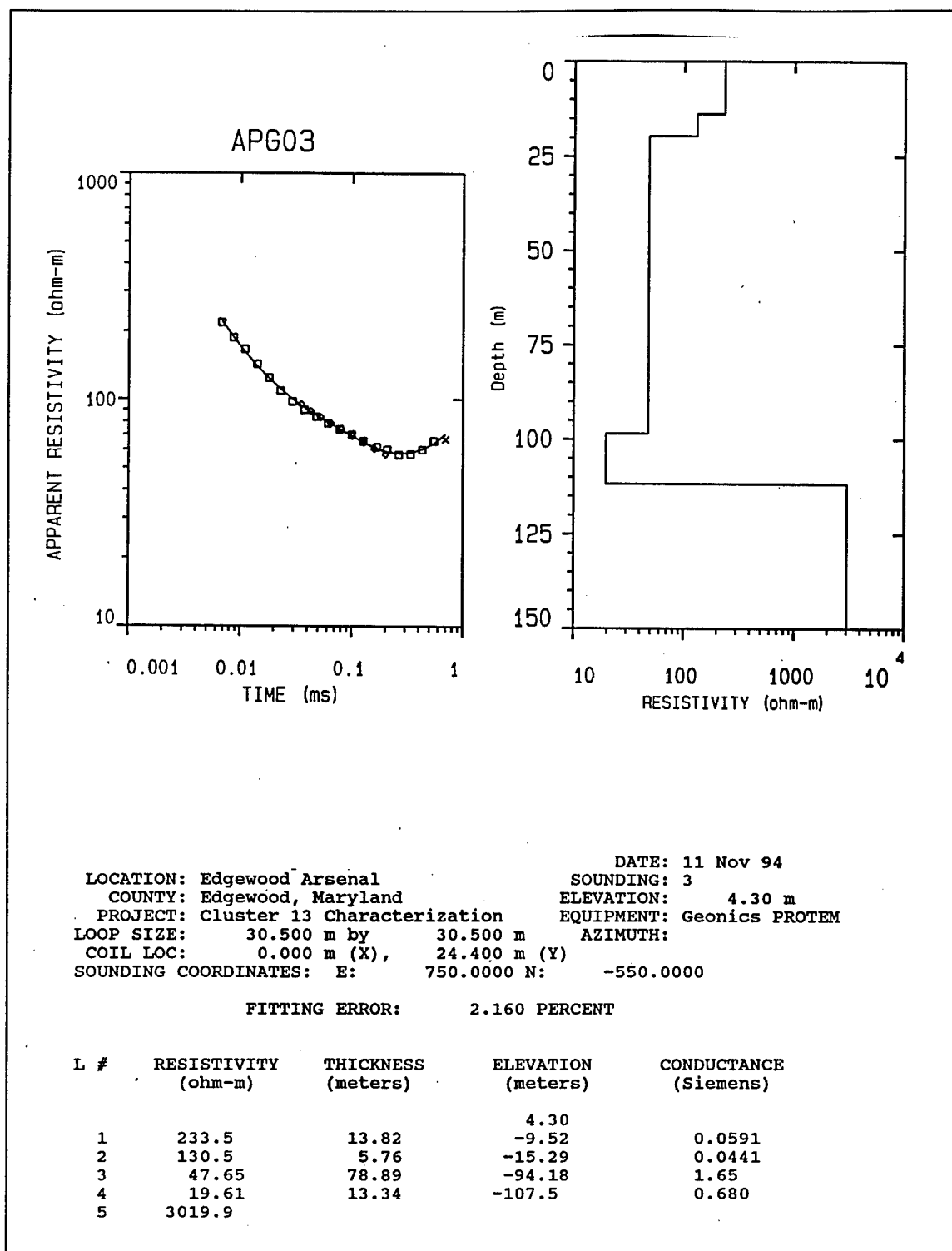


Figure C66. Transient electromagnetic data, best-fit model, and best-fit model parameters list for sounding APG03

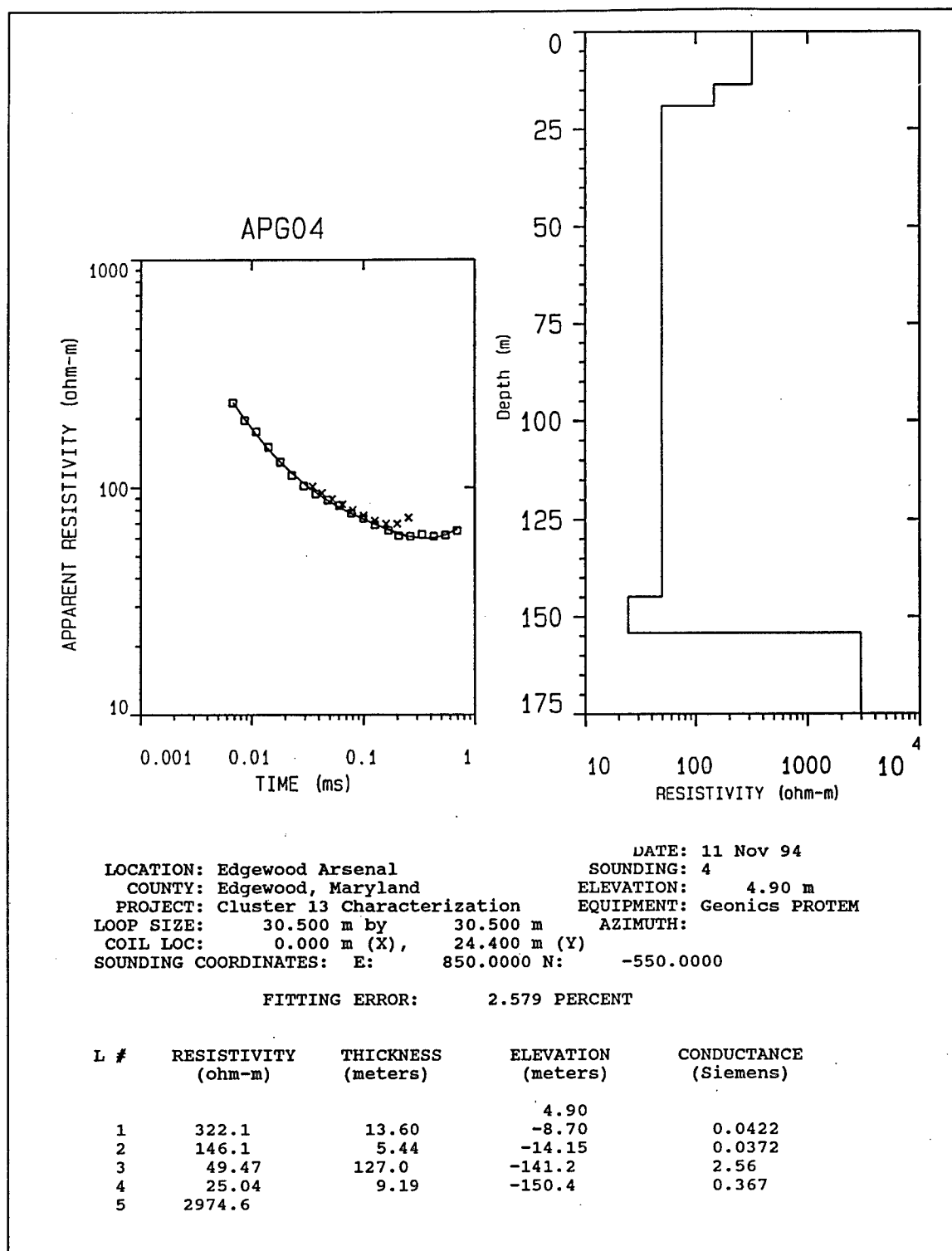


Figure C67. Transient electromagnetic data, best-fit model, and best-fit model parameters list for sounding APG04

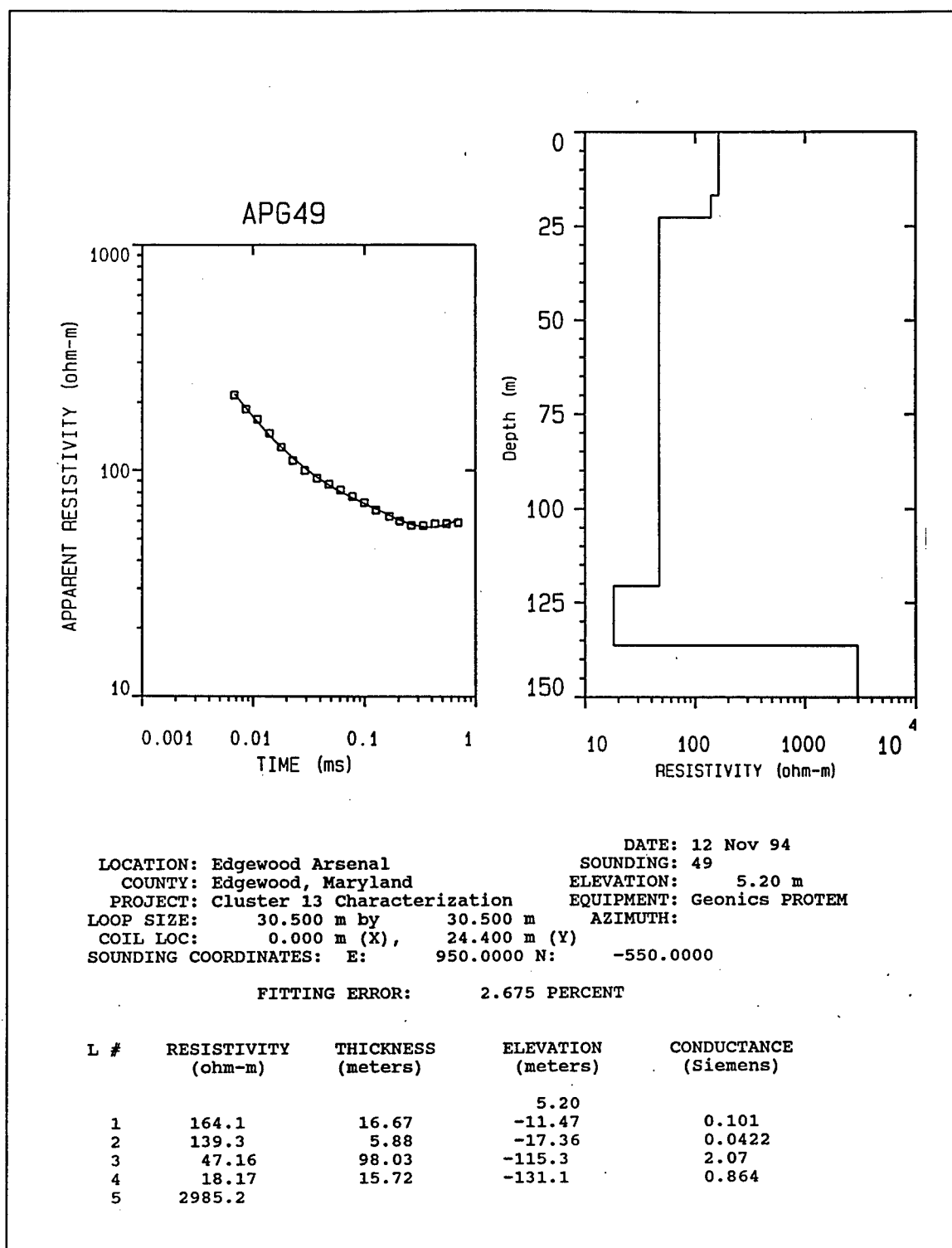


Figure C68. Transient electromagnetic data, best-fit model, and best-fit model parameters list for sounding APG49

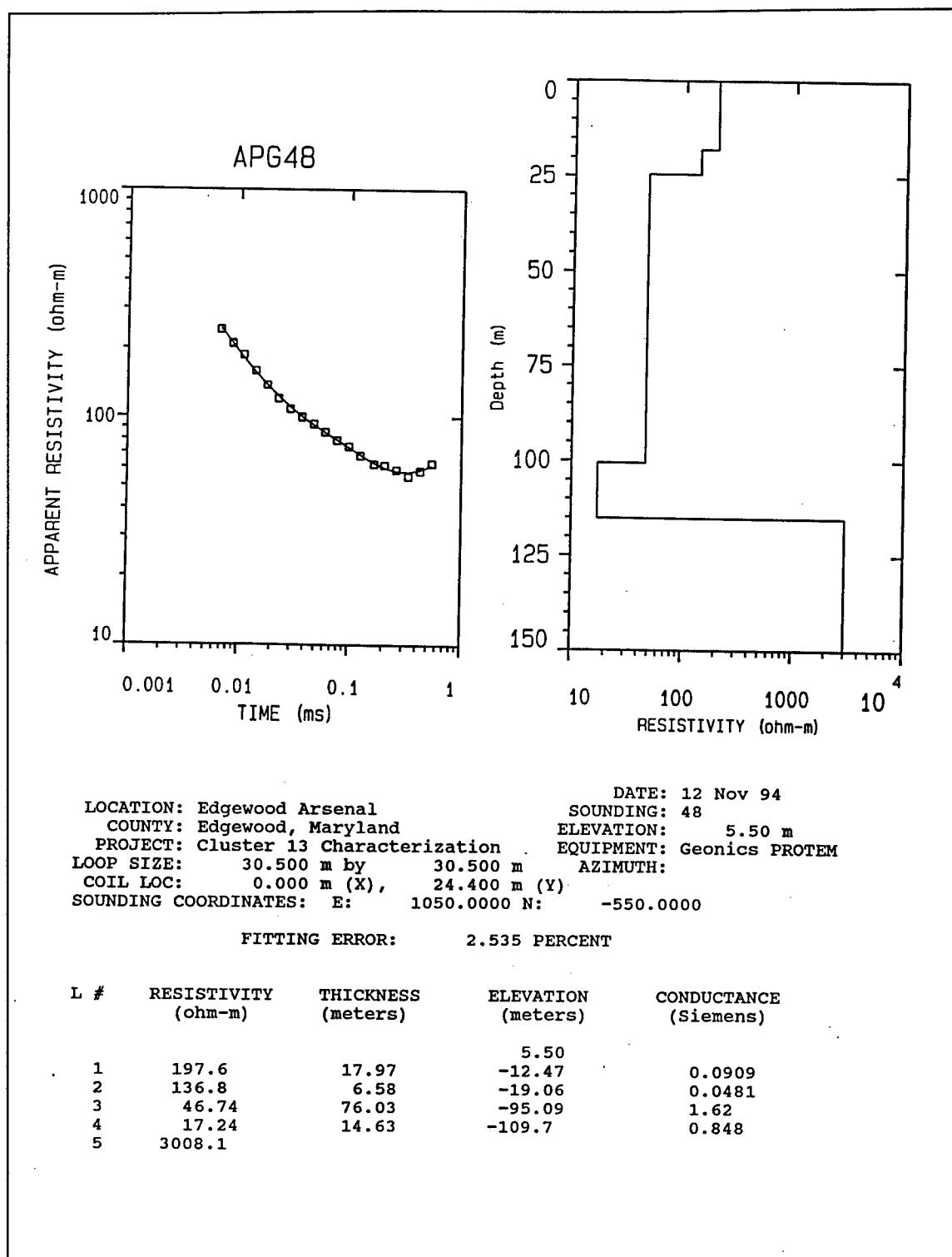


Figure C69. Transient electromagnetic data, best-fit model, and best-fit model parameters list for sounding APG48

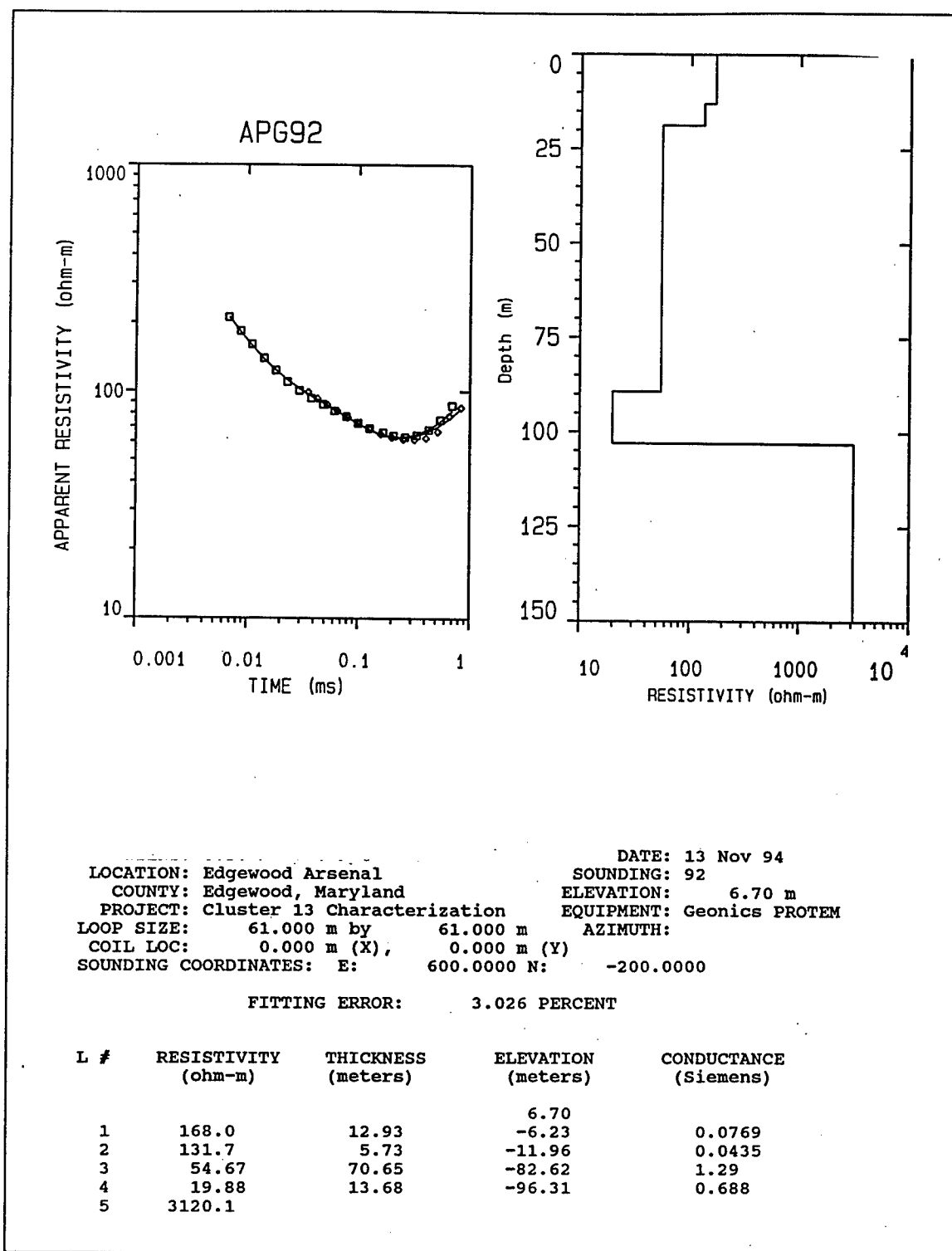


Figure C70. Transient electromagnetic data, best-fit model, and best-fit model parameters list for sounding APG92

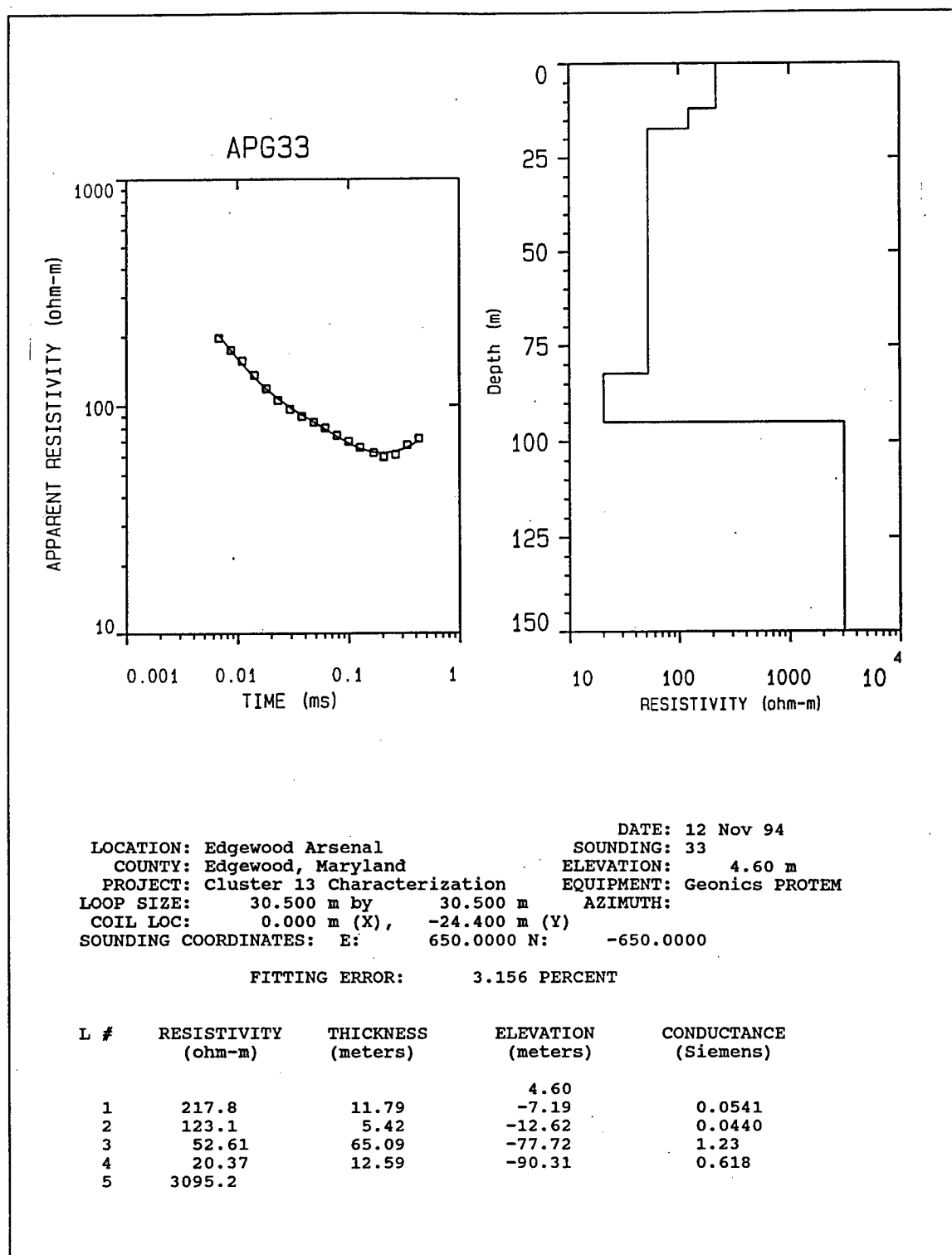


Figure C71. Transient electromagnetic data, best-fit model, and best-fit model parameters list for sounding APG33

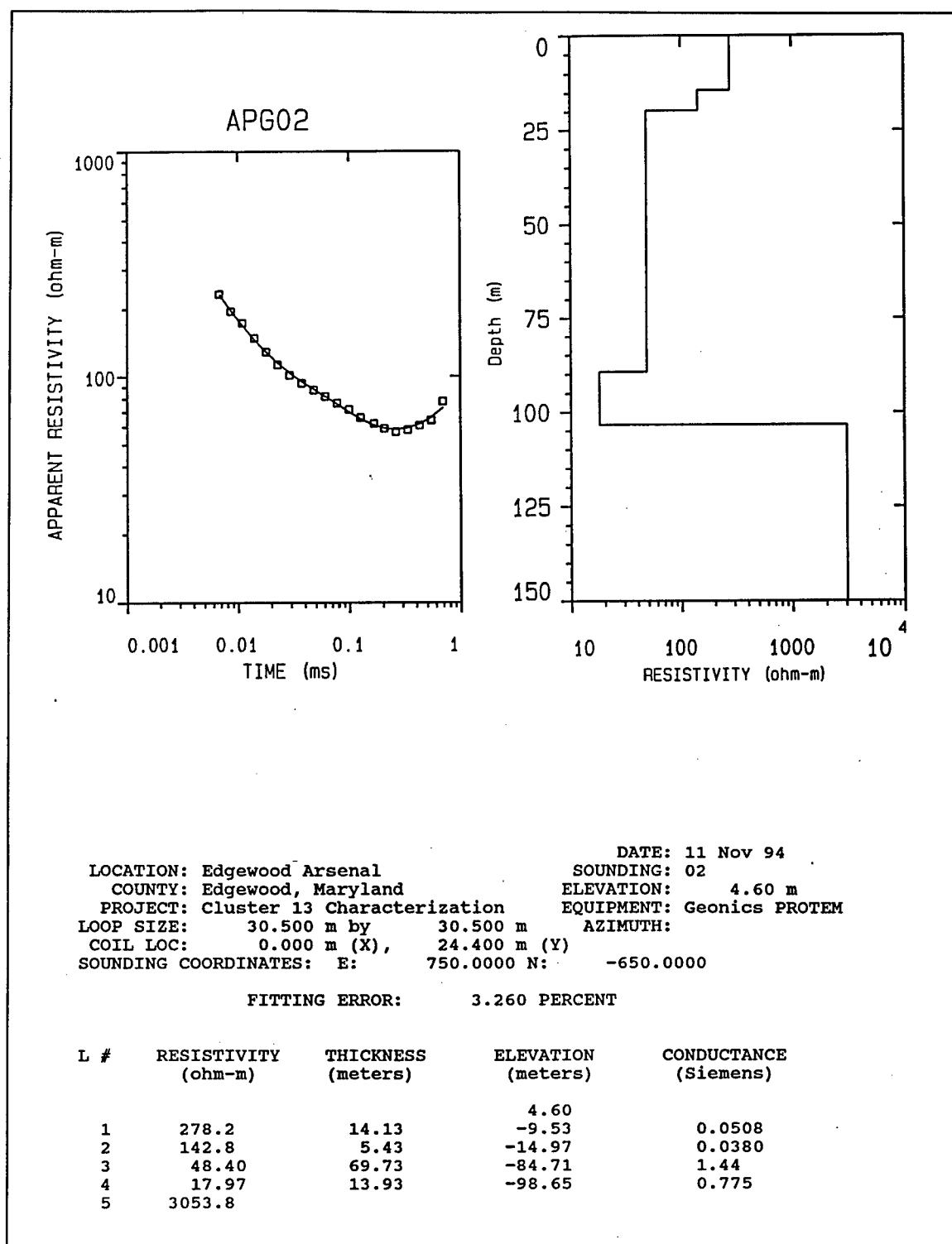


Figure C72. Transient electromagnetic data, best-fit model, and best-fit model parameters list for sounding APG02

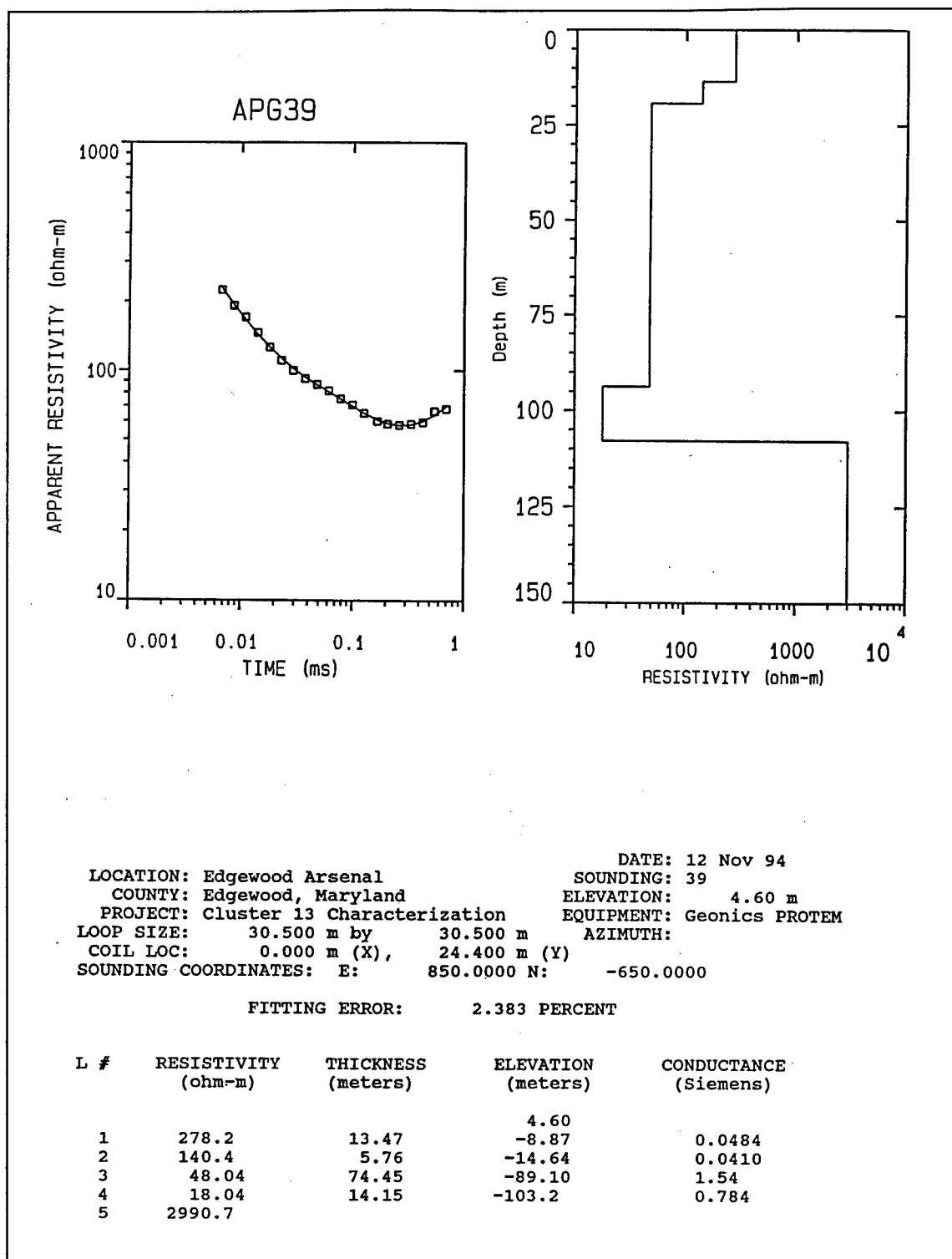


Figure C73. Transient electromagnetic data, best-fit model, and best-fit model parameters list for sounding APG39

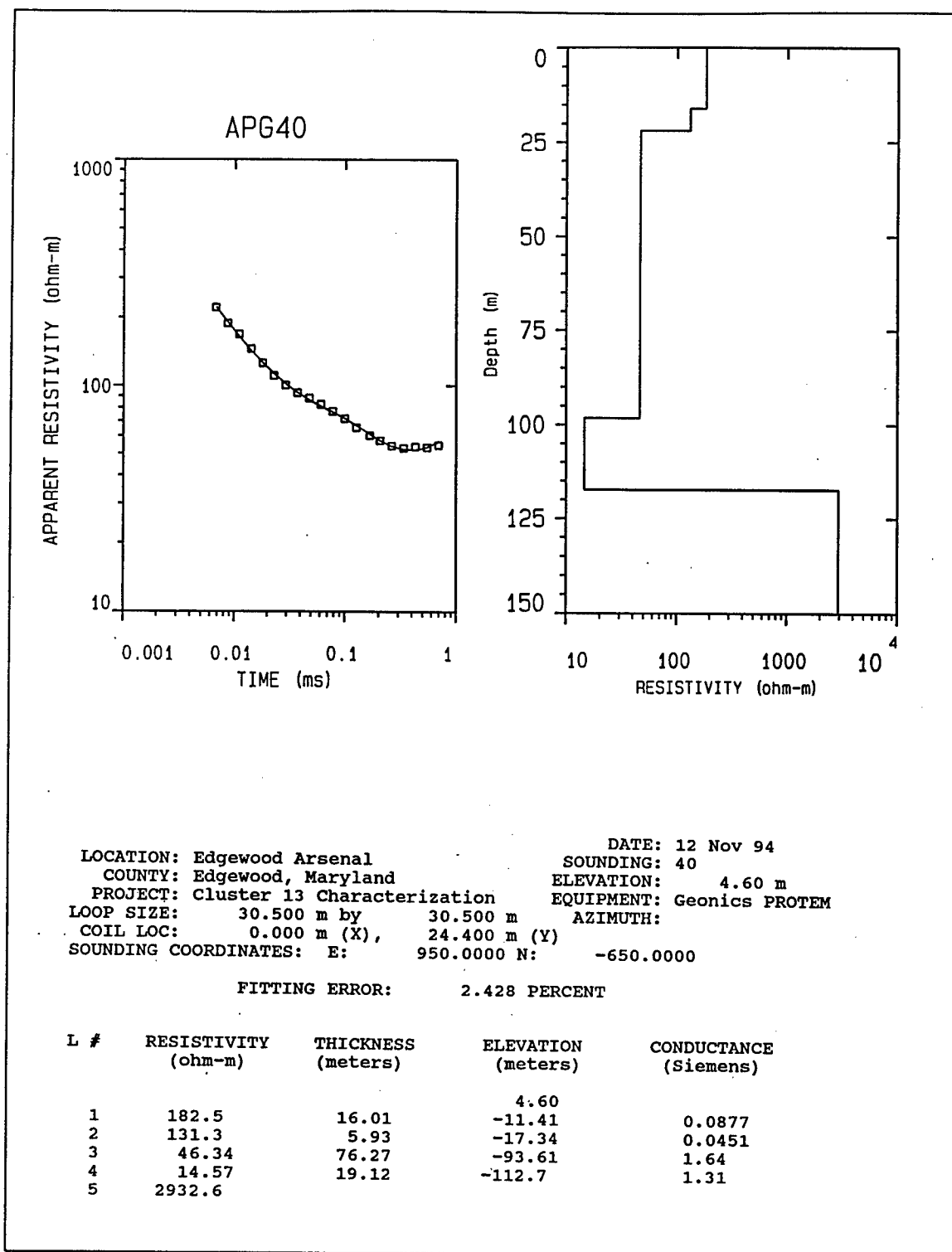


Figure C74. Transient electromagnetic data, best-fit model, and best-fit model parameters list for sounding APG40

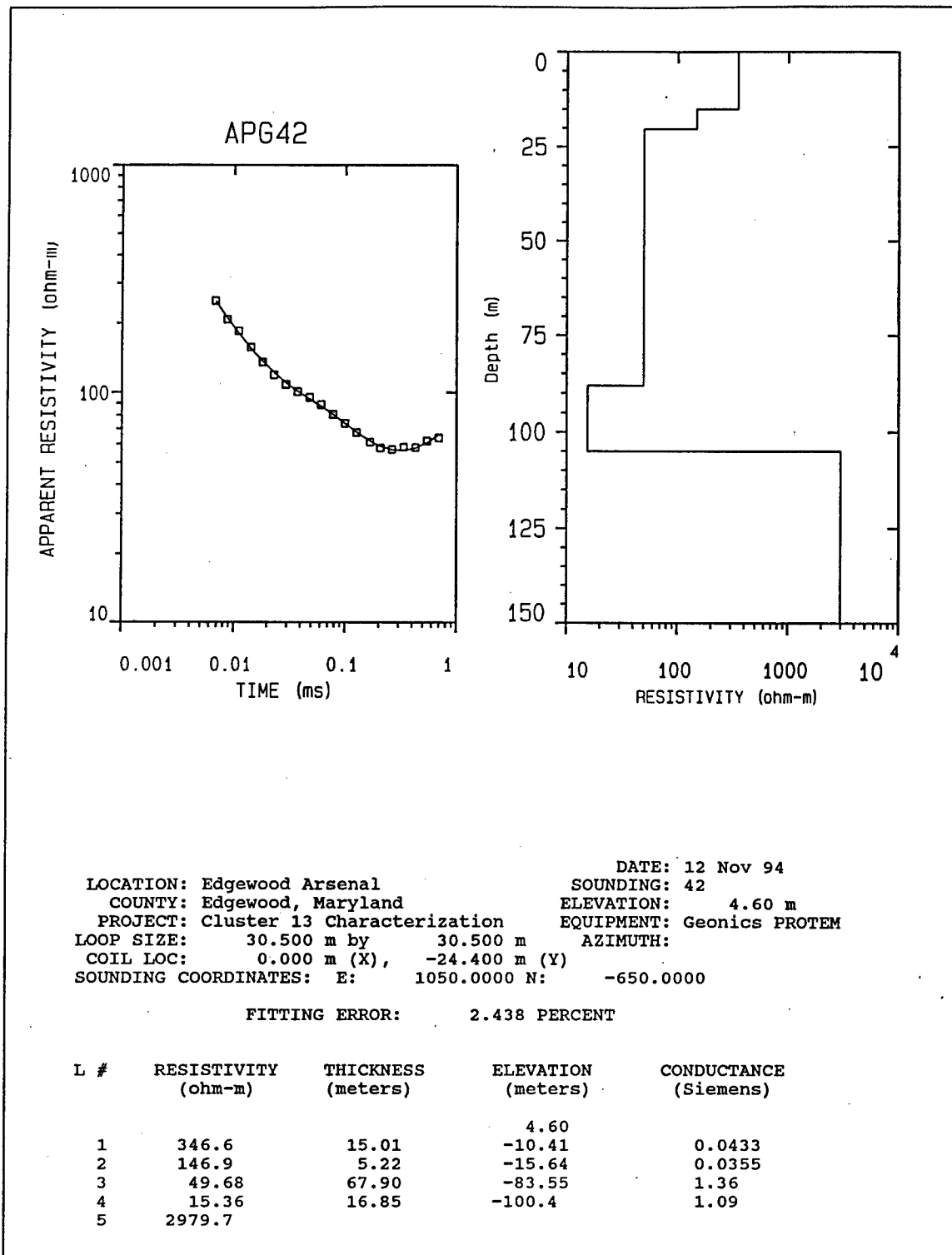


Figure C75. Transient electromagnetic data, best-fit model, and best-fit model parameters list for sounding APG42

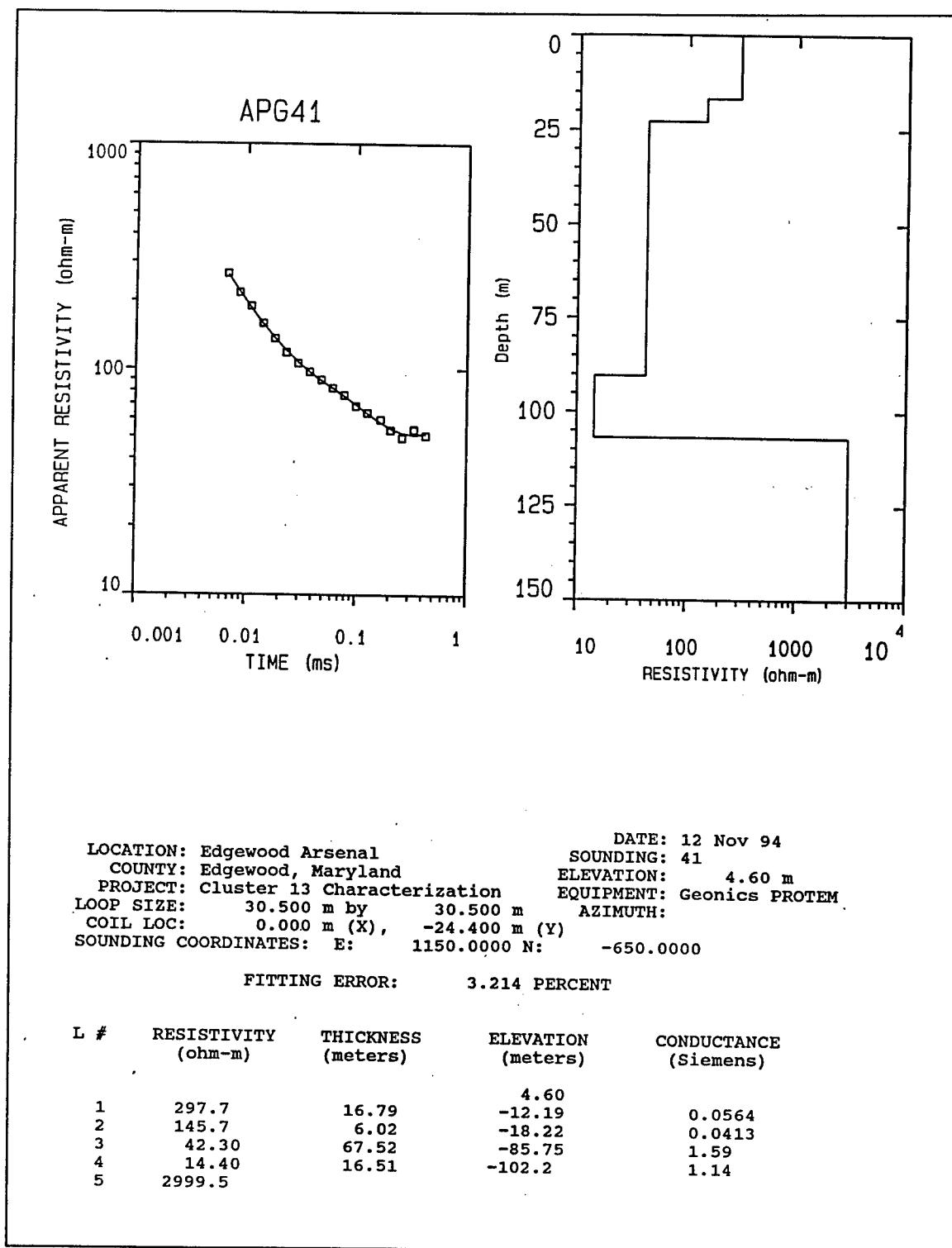


Figure C76. Transient electromagnetic data, best-fit model, and best-fit model parameters list for sounding APG41

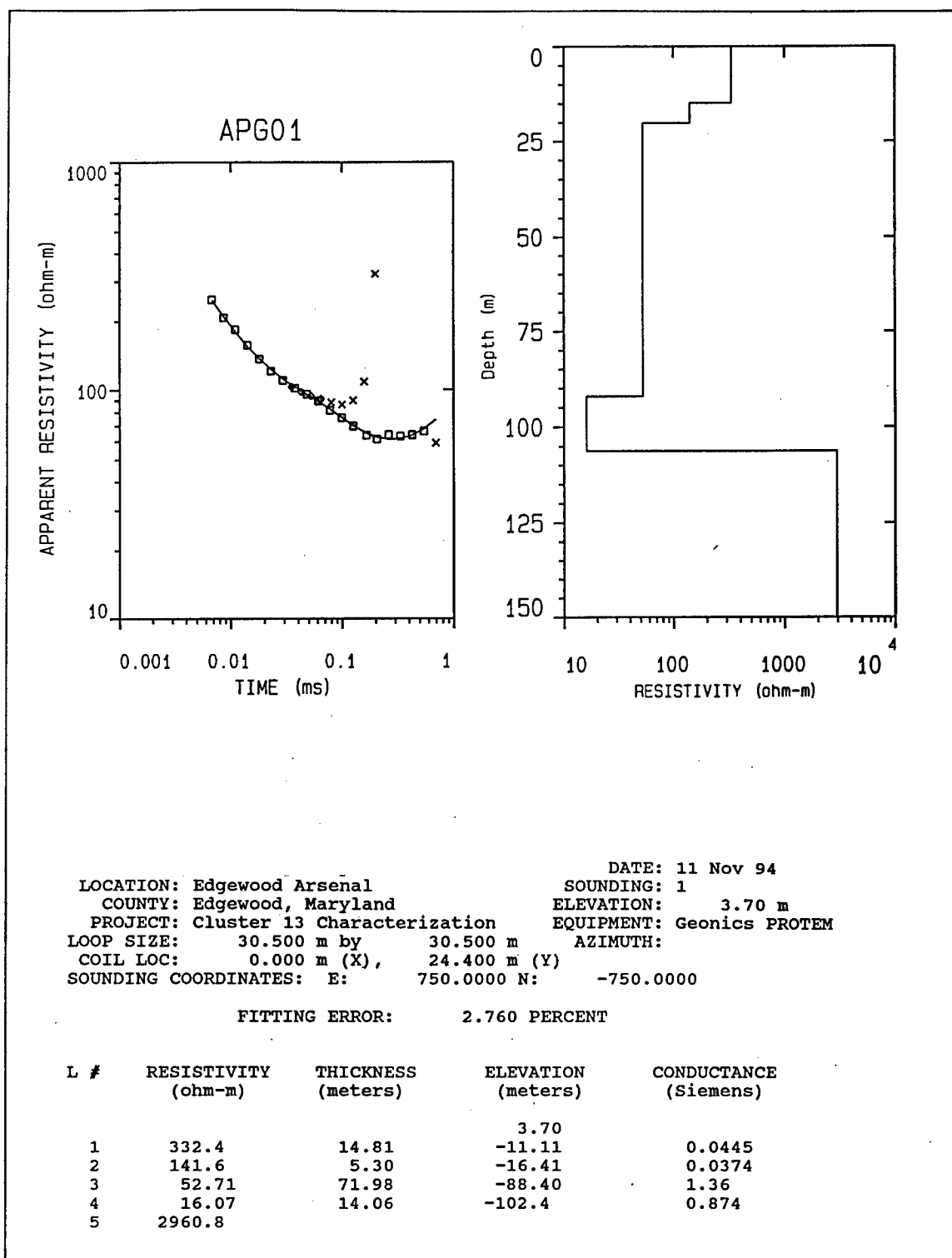


Figure C77. Transient electromagnetic data, best-fit model, and best-fit model parameters list for sounding APG01

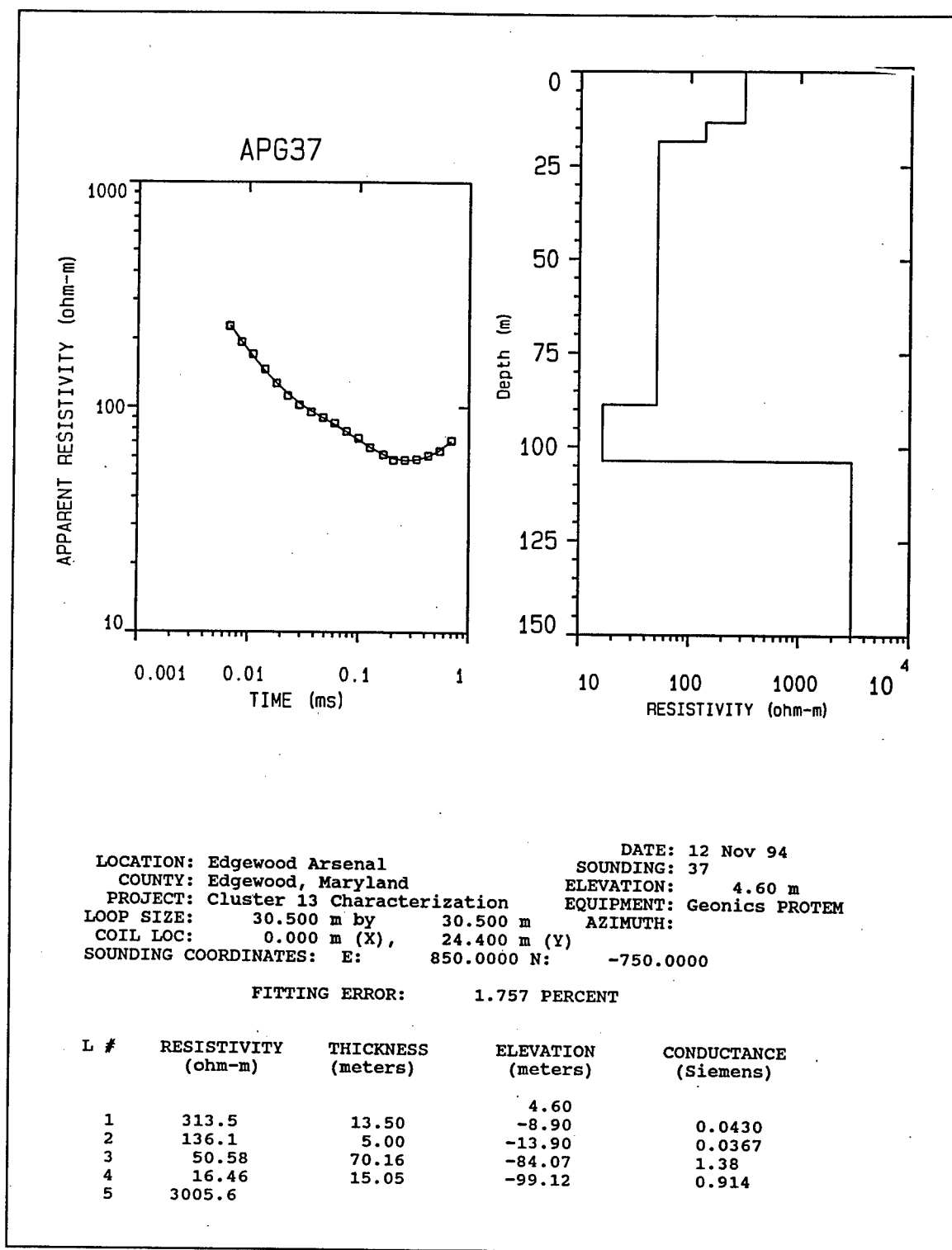


Figure C78. Transient electromagnetic data, best-fit model, and best-fit model parameters list for sounding APG37

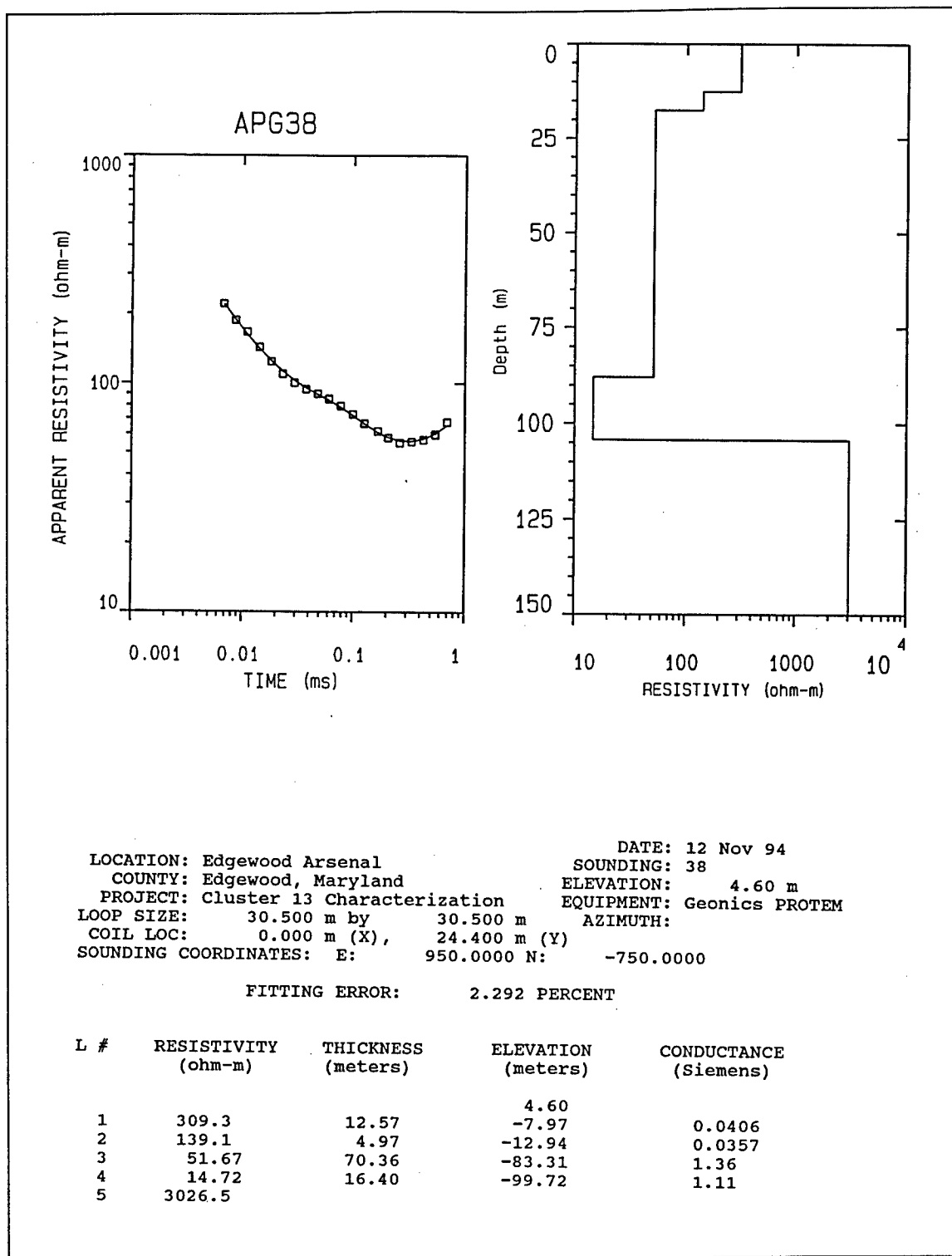


Figure C79. Transient electromagnetic data, best-fit model, and best-fit model parameters list for sounding APG38

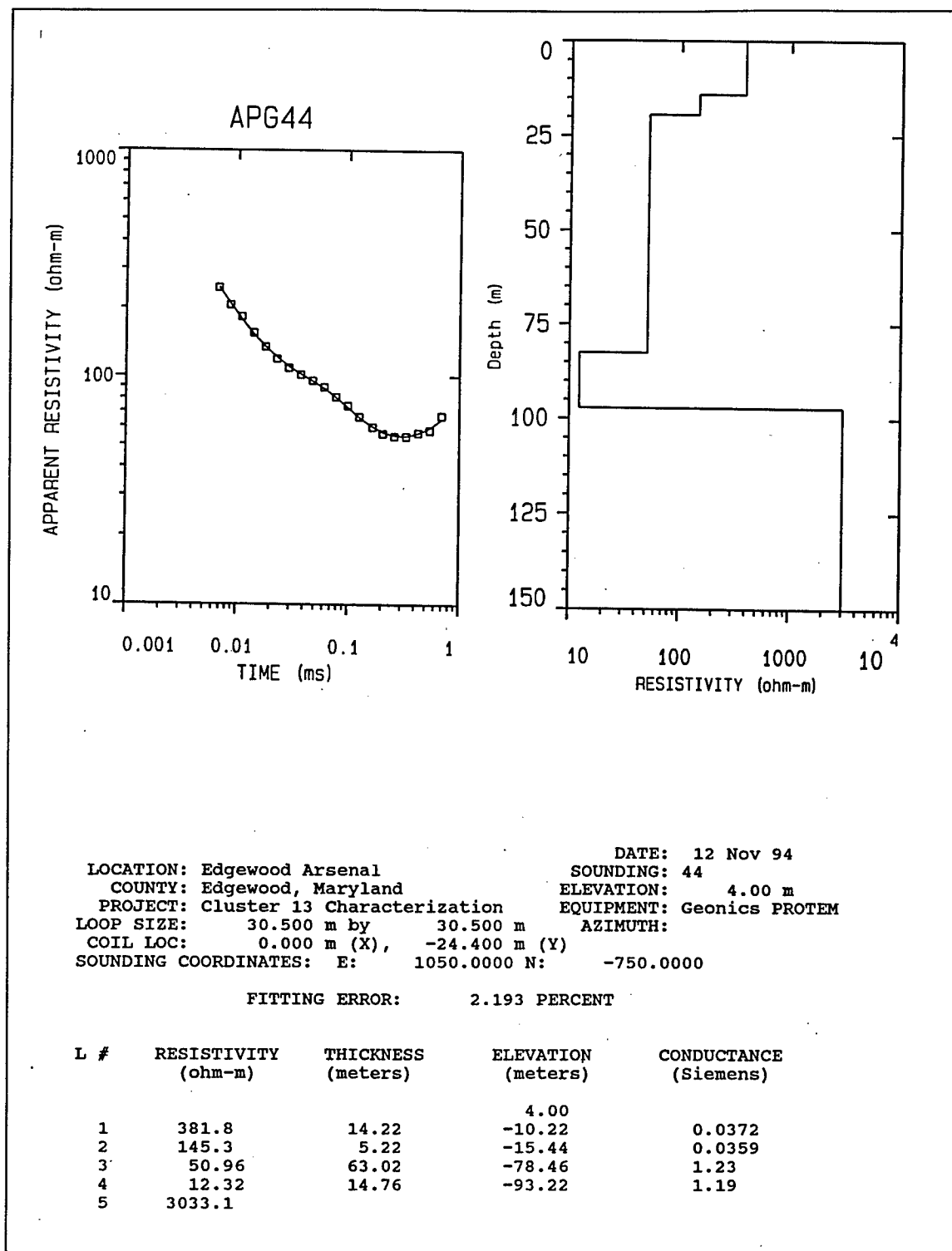


Figure C80. Transient electromagnetic data, best-fit model, and best-fit model parameters list for sounding APG44

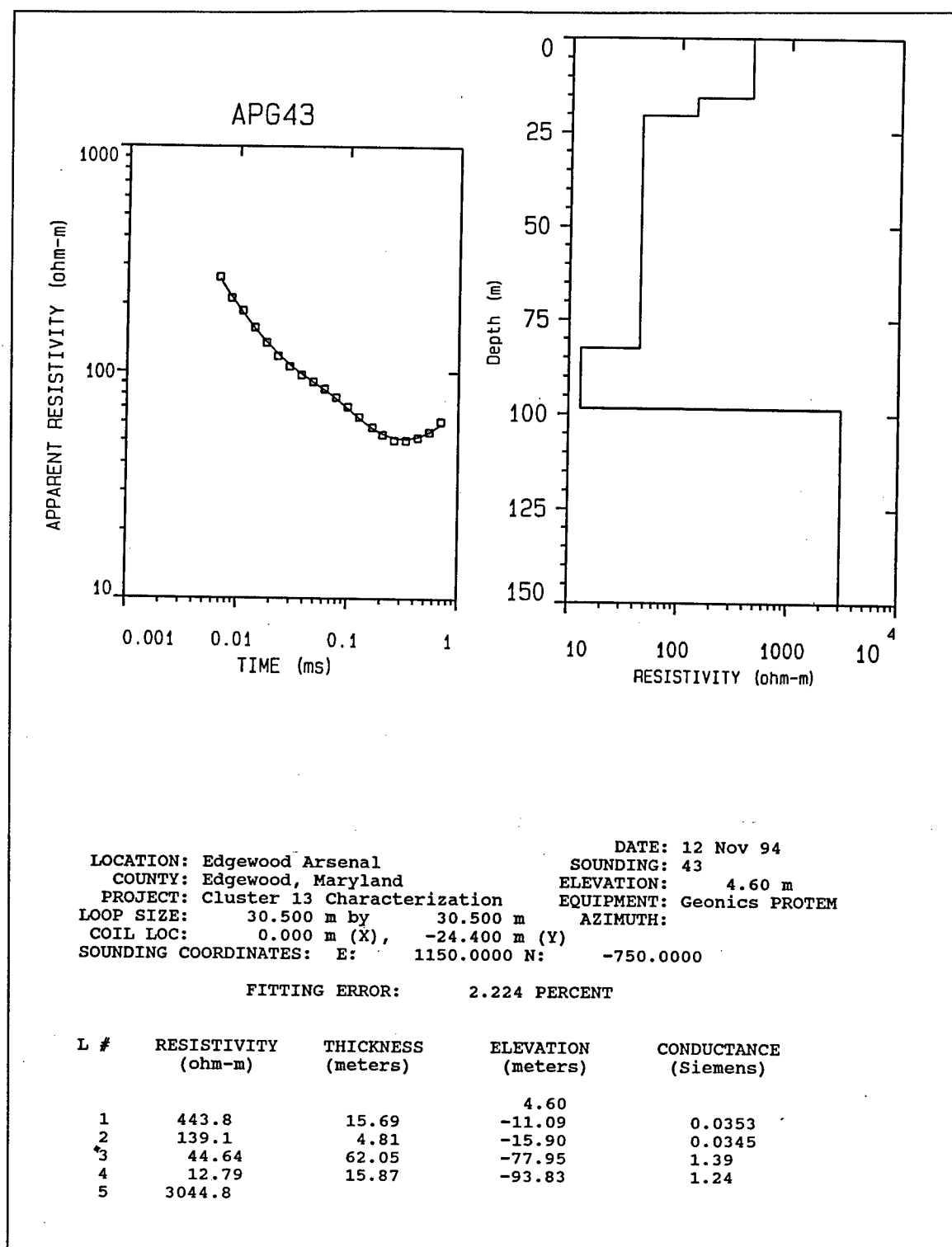


Figure C81. Transient electromagnetic data, best-fit model, and best-fit model parameters list for sounding APG43

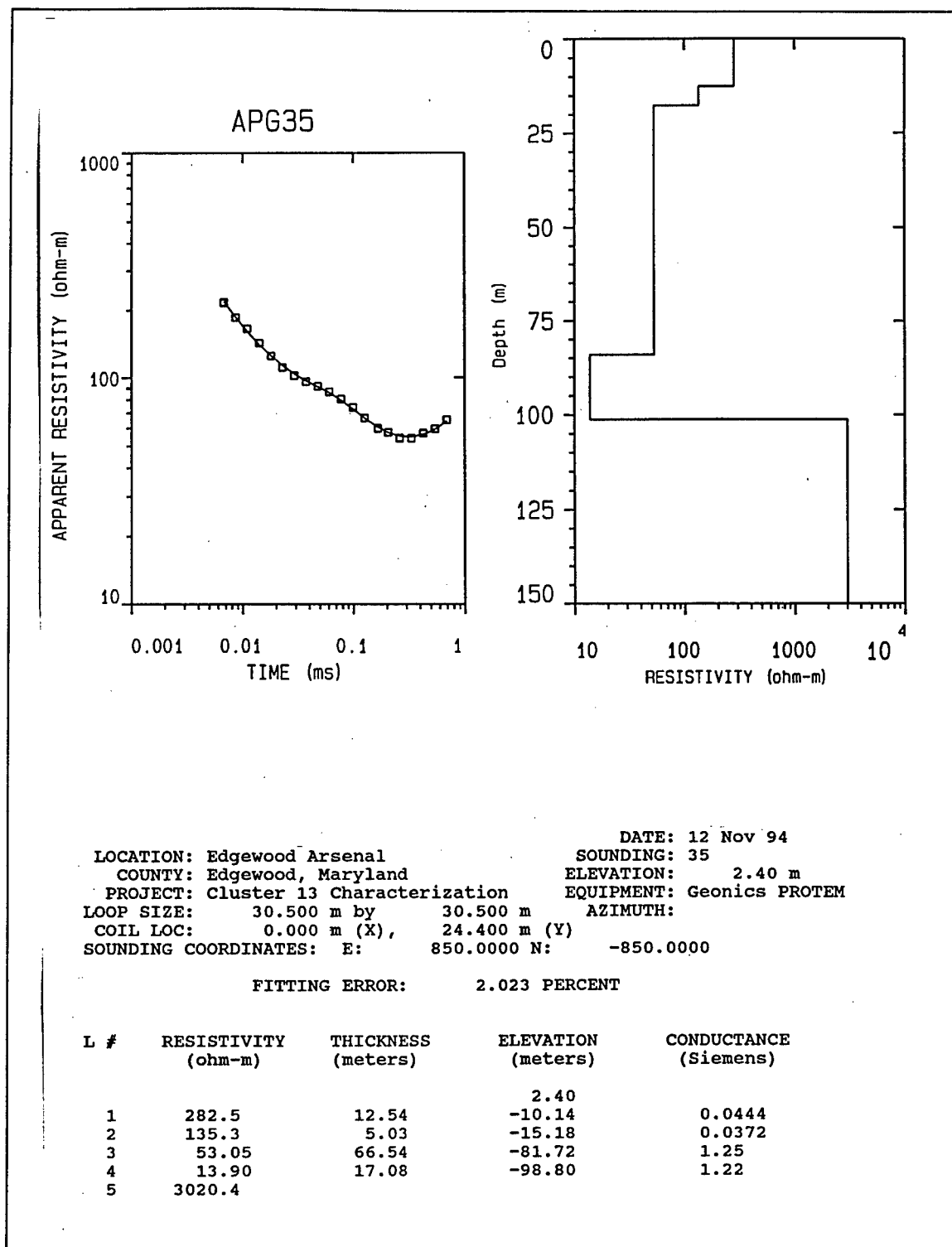


Figure C82. Transient electromagnetic data, best-fit model, and best-fit model parameters list for sounding APG35

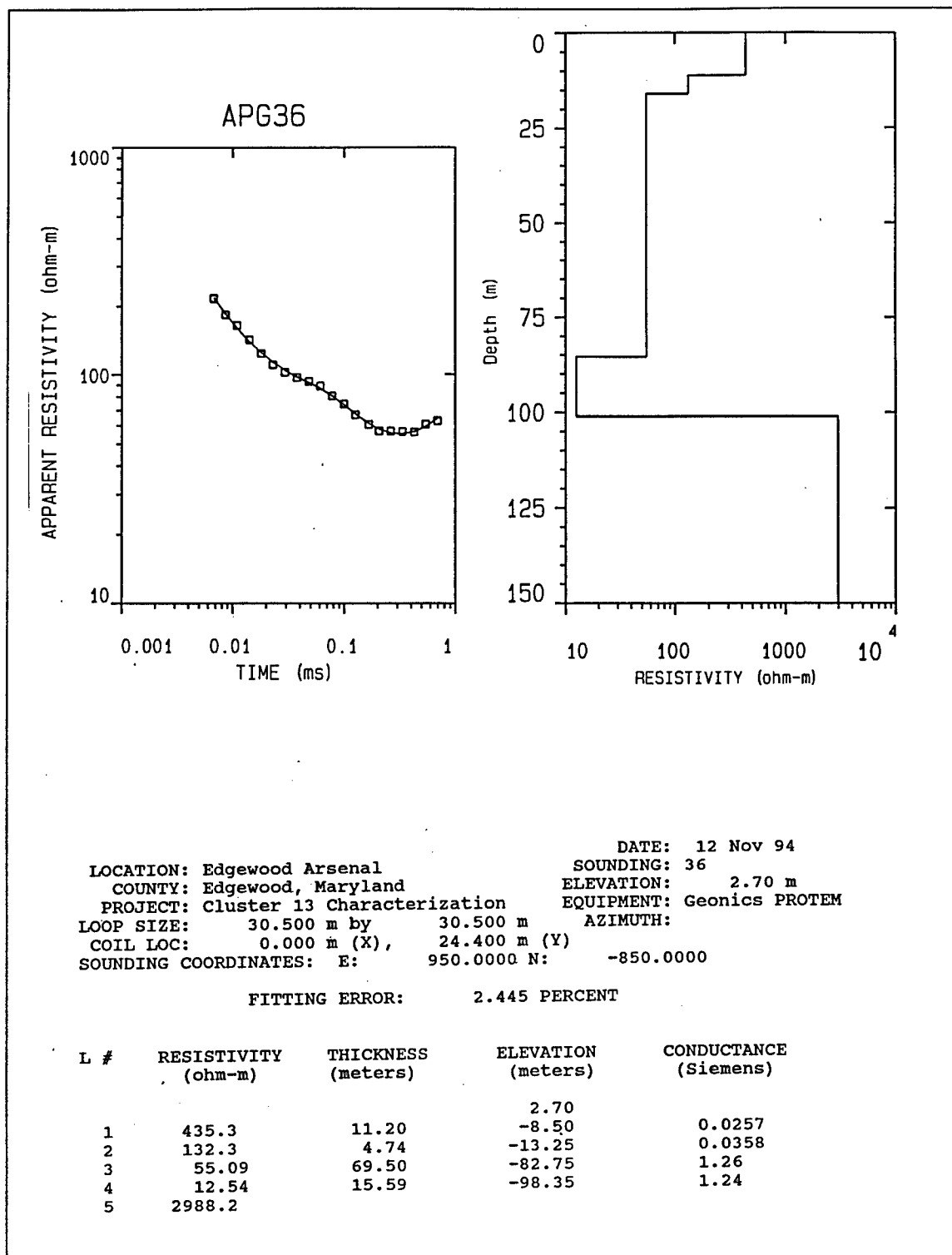


Figure C83. Transient electromagnetic data, best-fit model, and best-fit model parameters list for sounding APG36

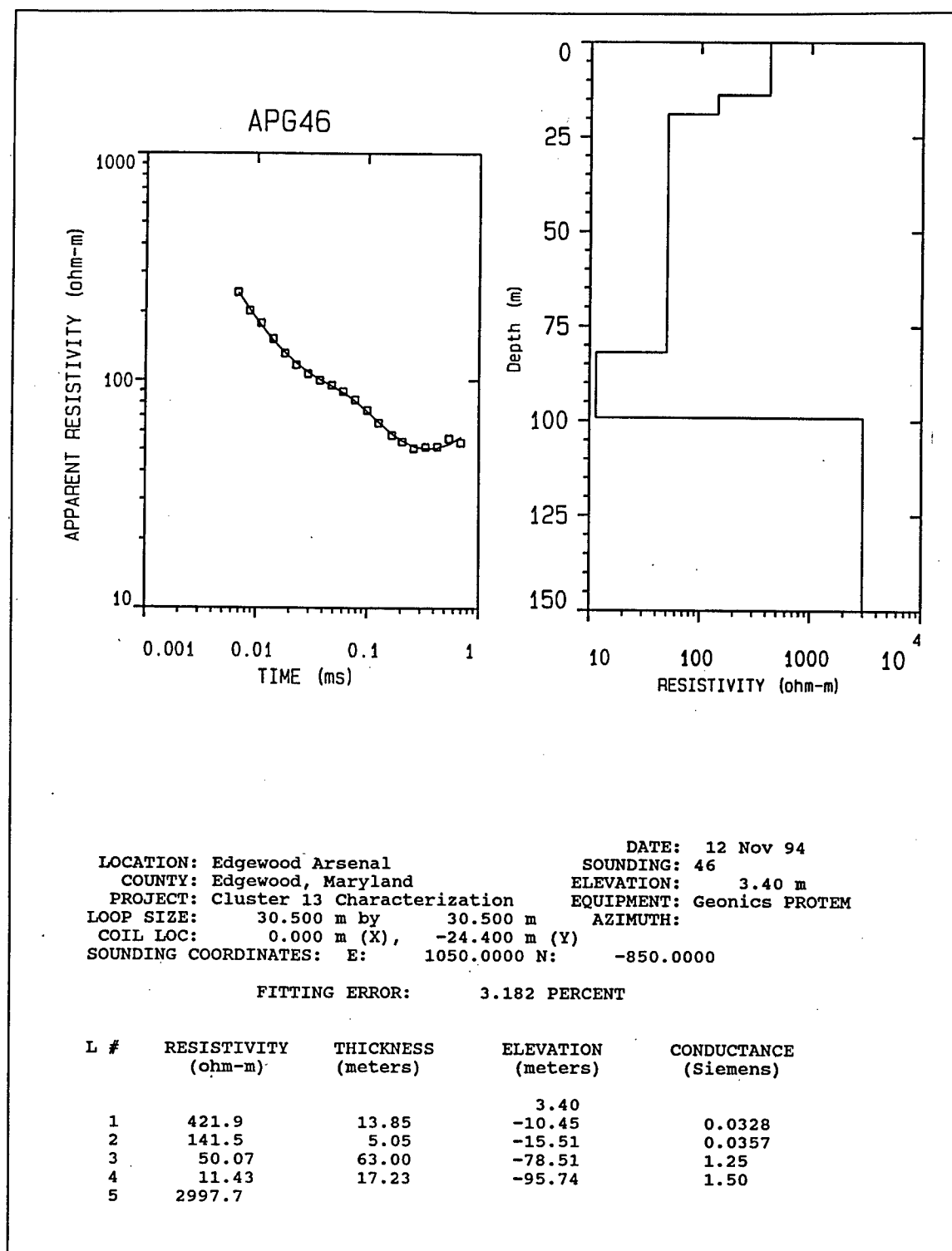


Figure C84. Transient electromagnetic data, best-fit model, and best-fit model parameters list for sounding APG46

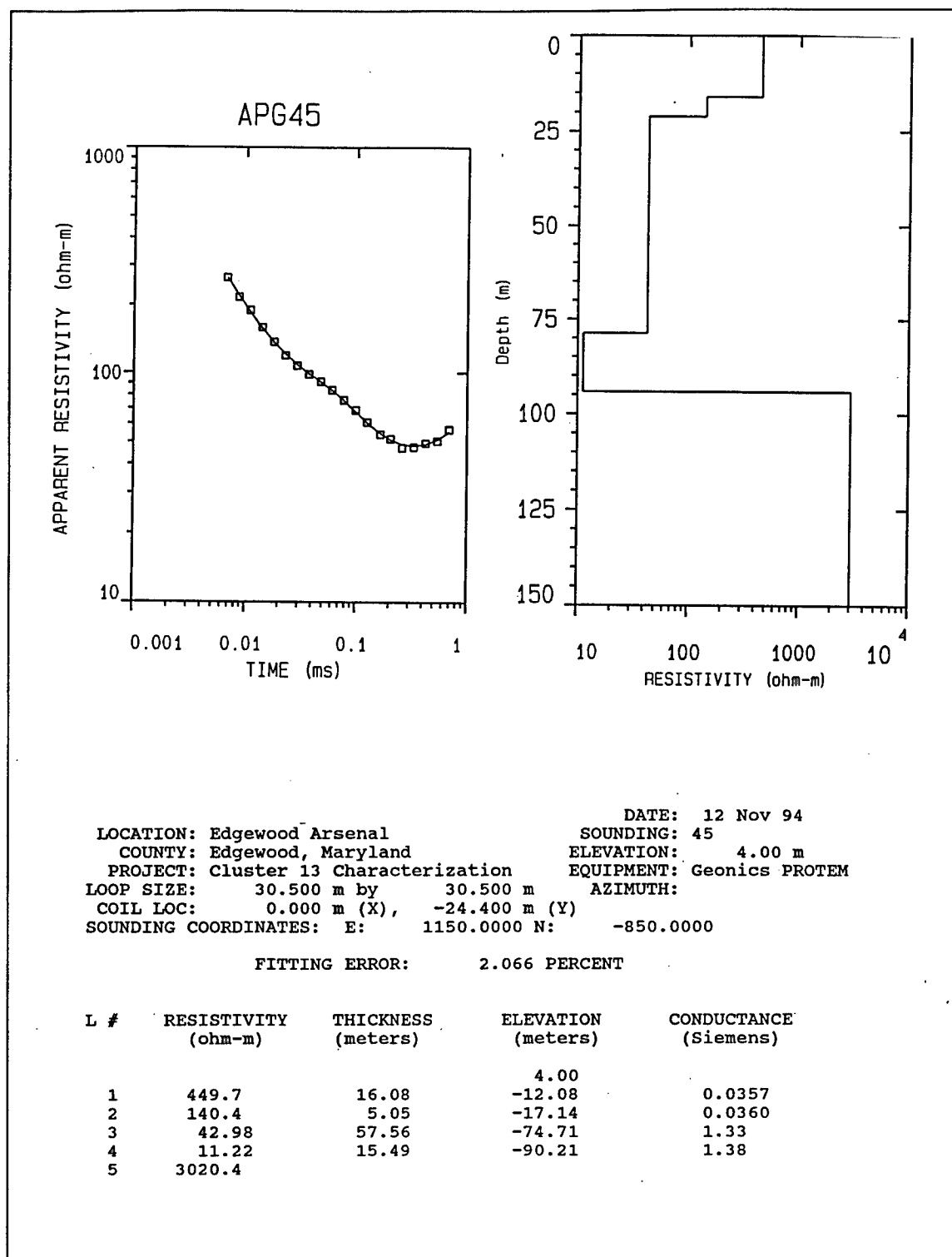


Figure C85. Transient electromagnetic data, best-fit model, and best-fit model parameters list for sounding APG45

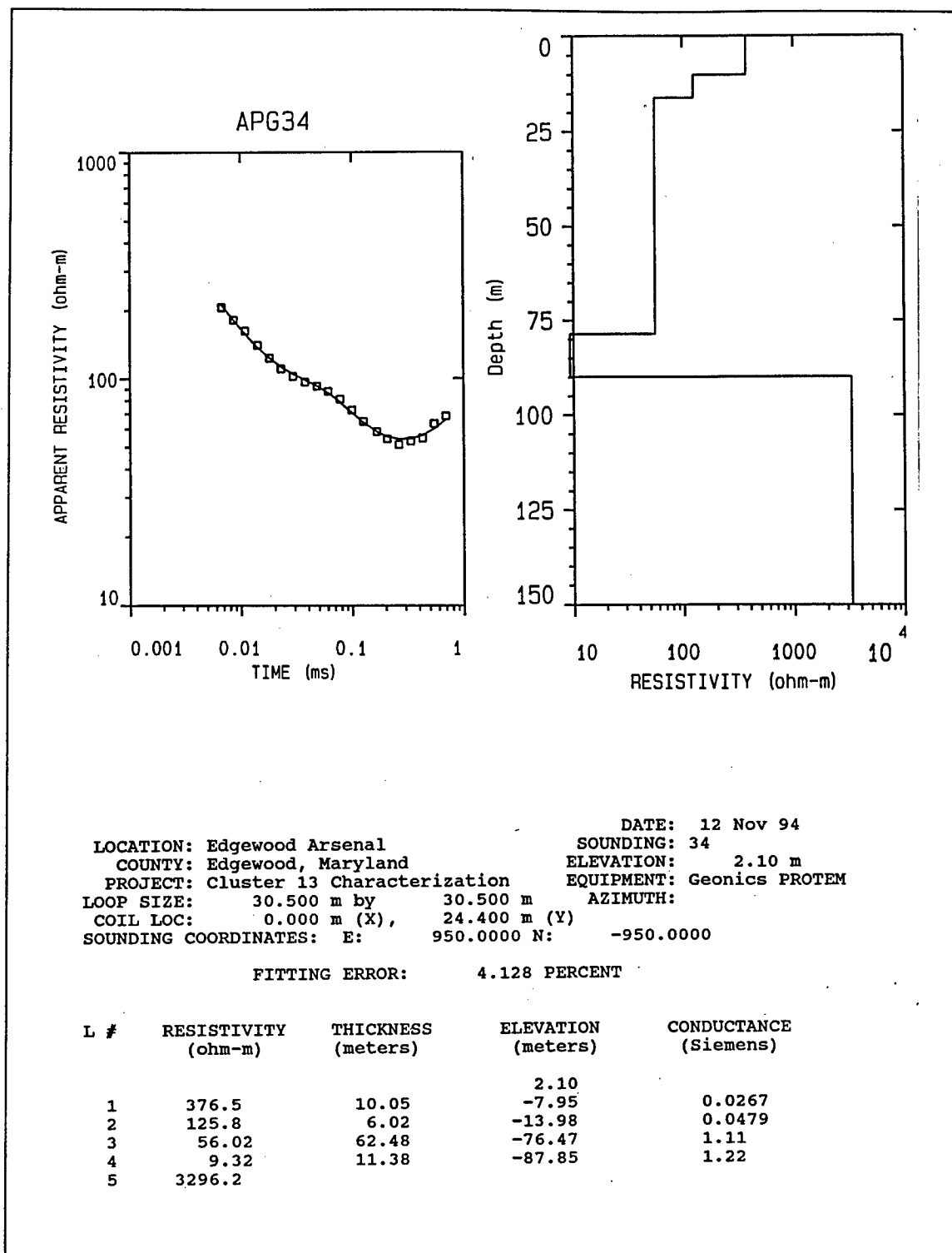


Figure C86. Transient electromagnetic data, best-fit model, and best-fit model parameters list for sounding APG34

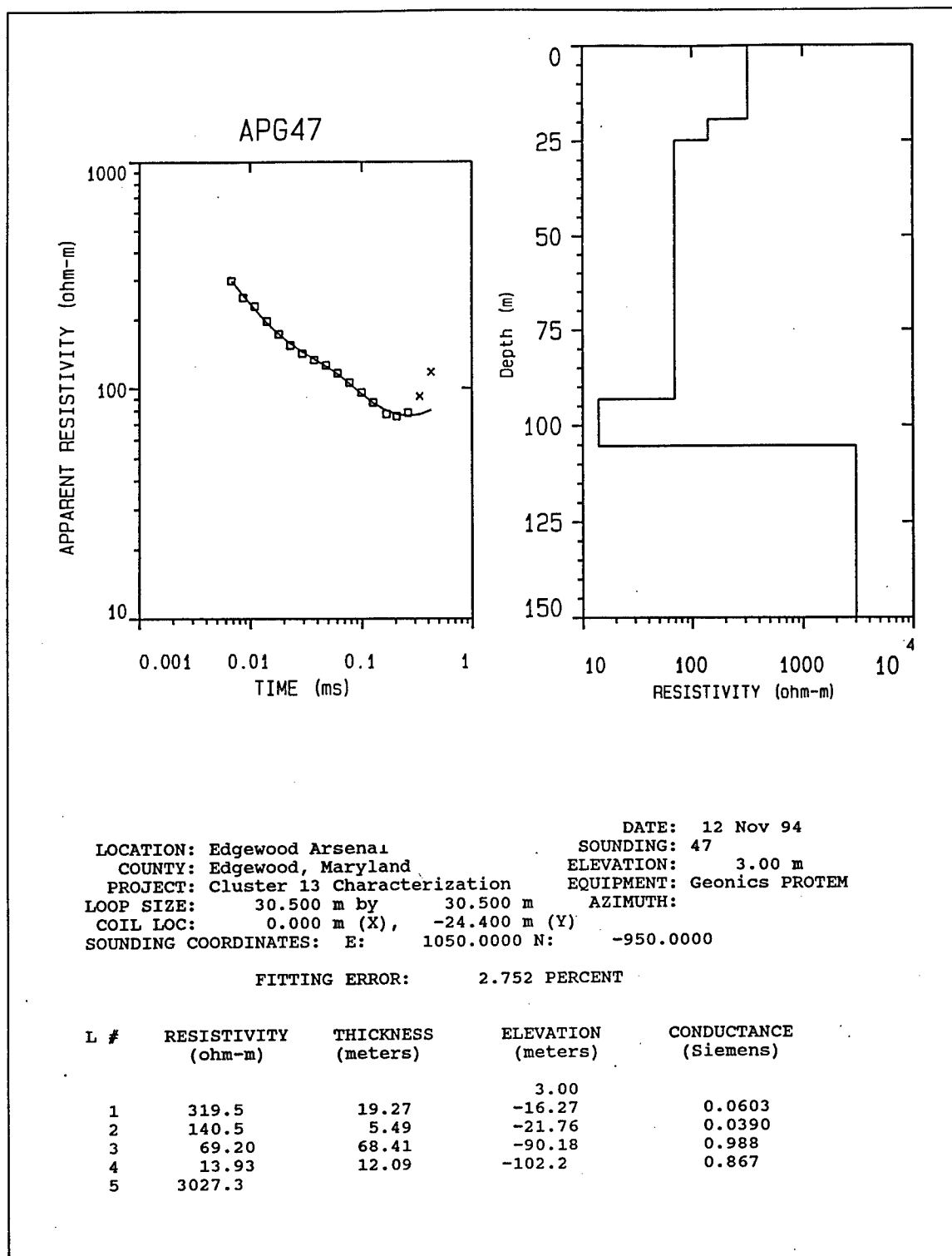


Figure C87. Transient electromagnetic data, best-fit model, and best-fit model parameters list for sounding APG47

Appendix D

Borehole Geophysical Logs

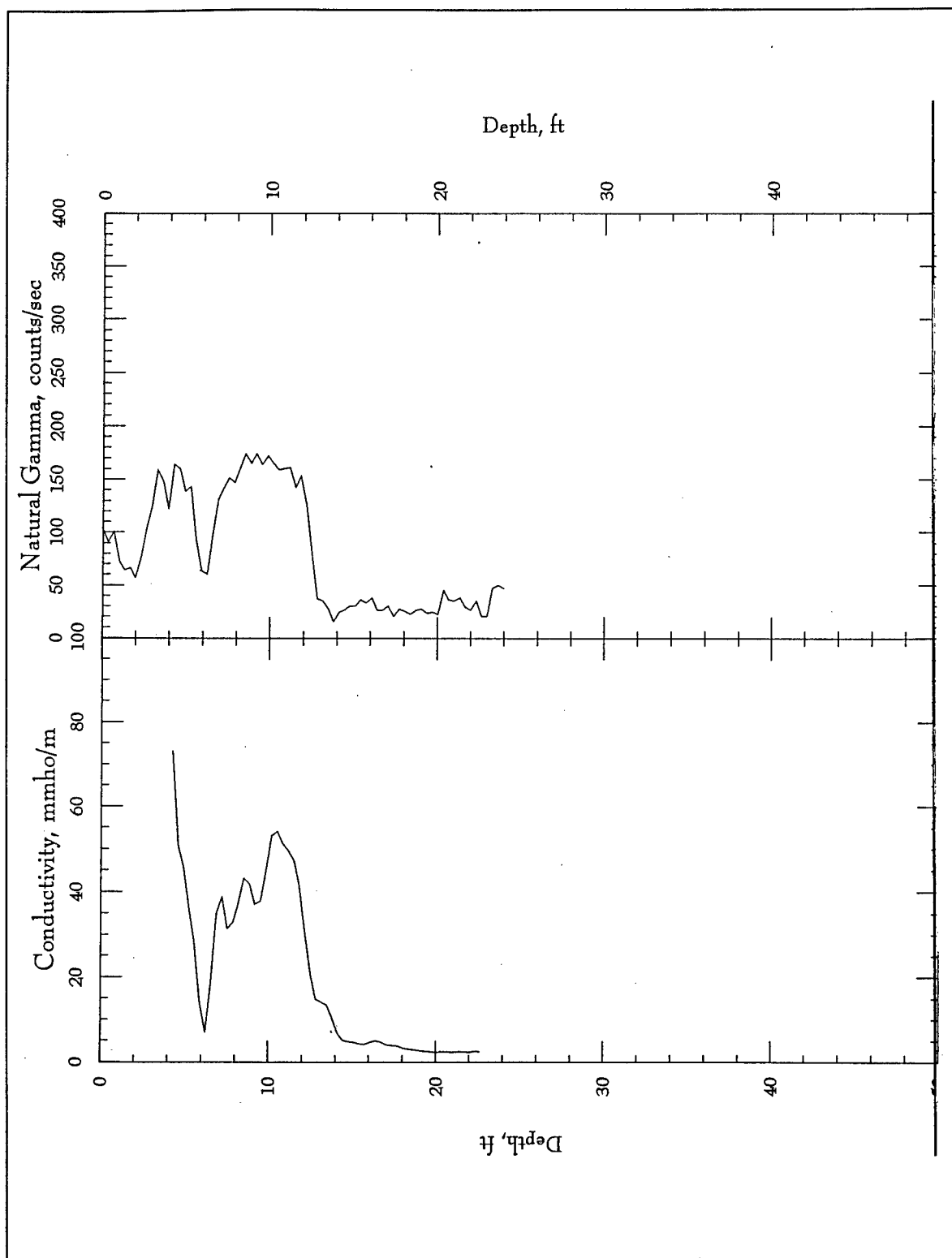


Figure D1. Borehole geophysical logs, WLC-24

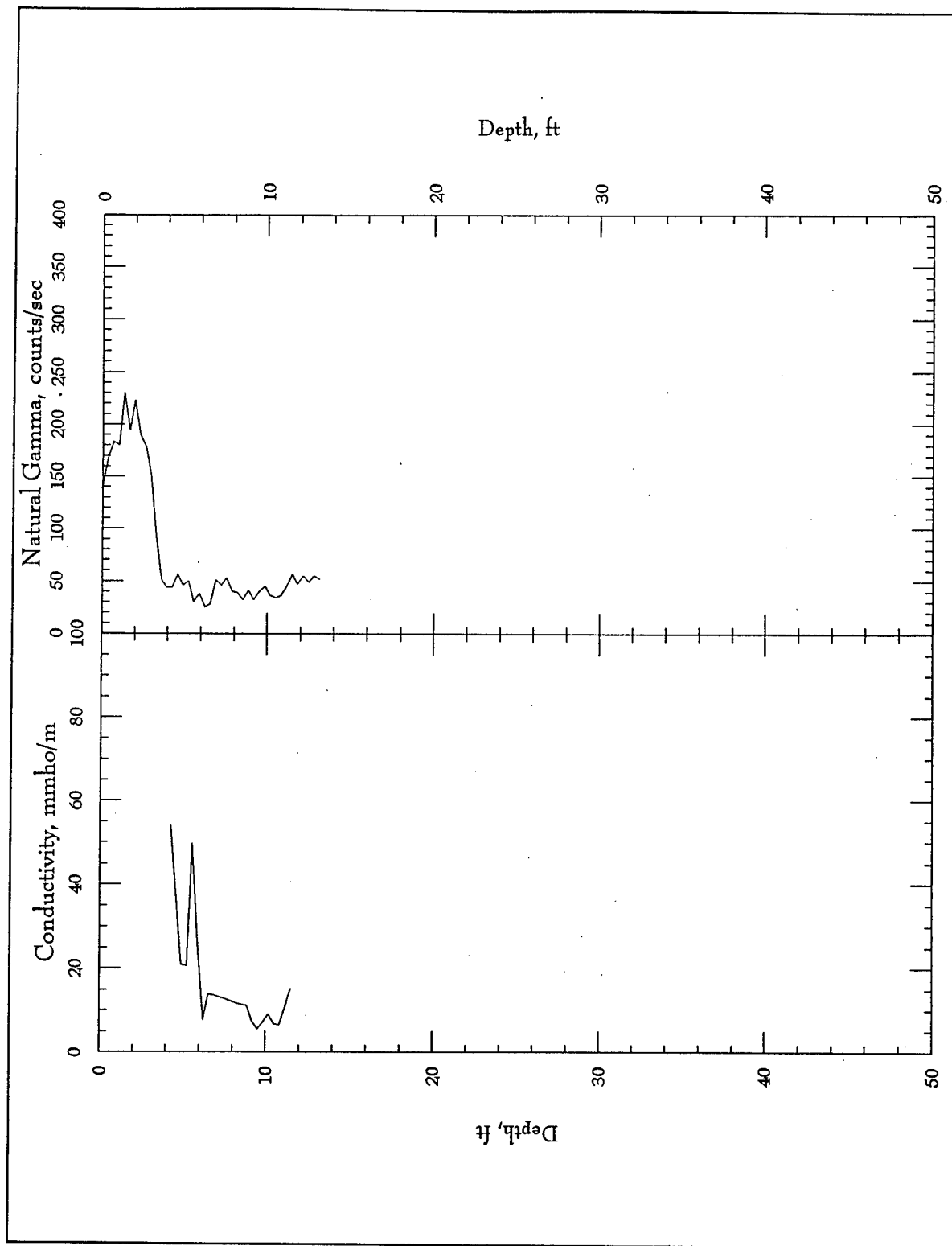


Figure D2. Borehole geophysical logs, WLC-25

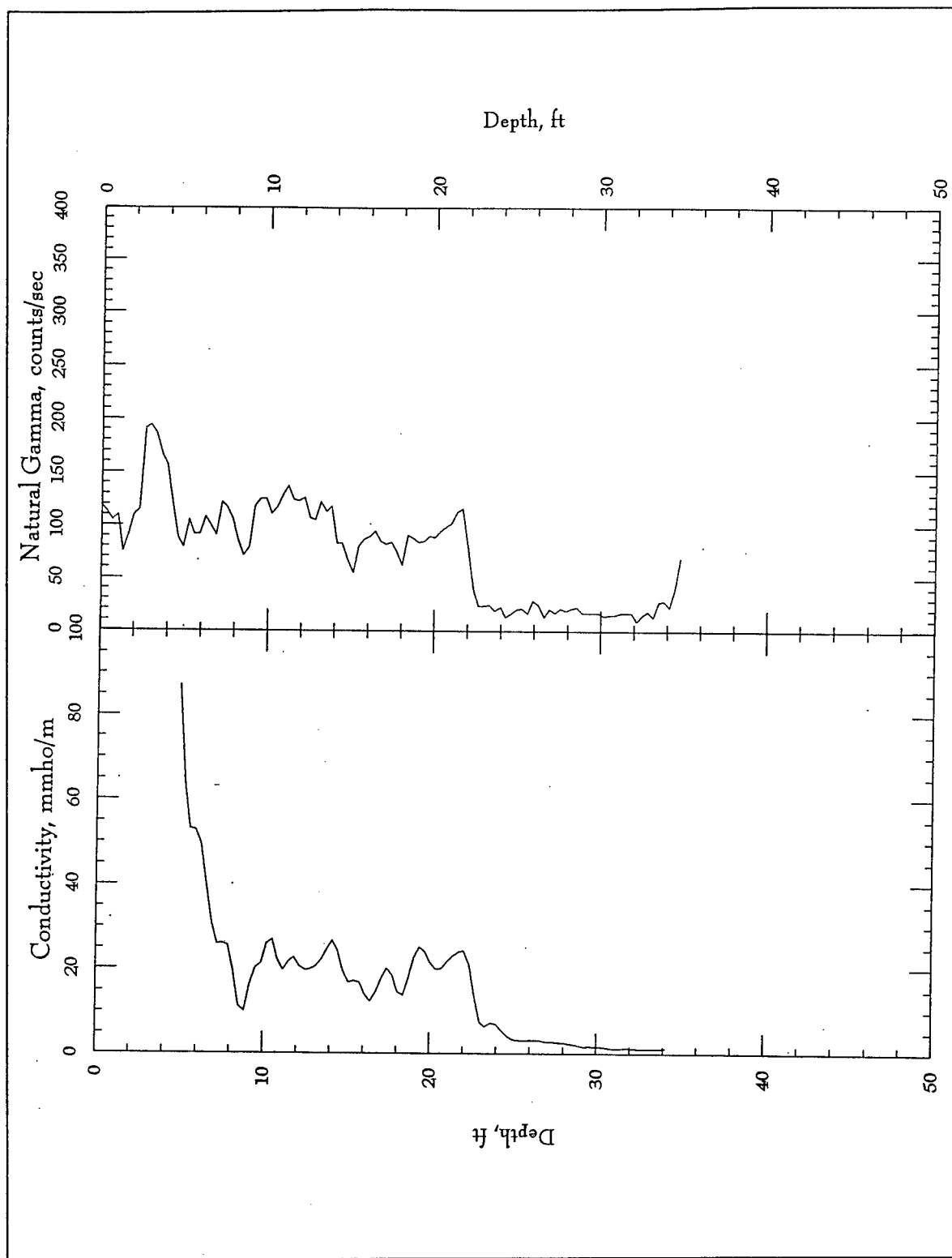


Figure D3. Borehole geophysical logs, WLC-26

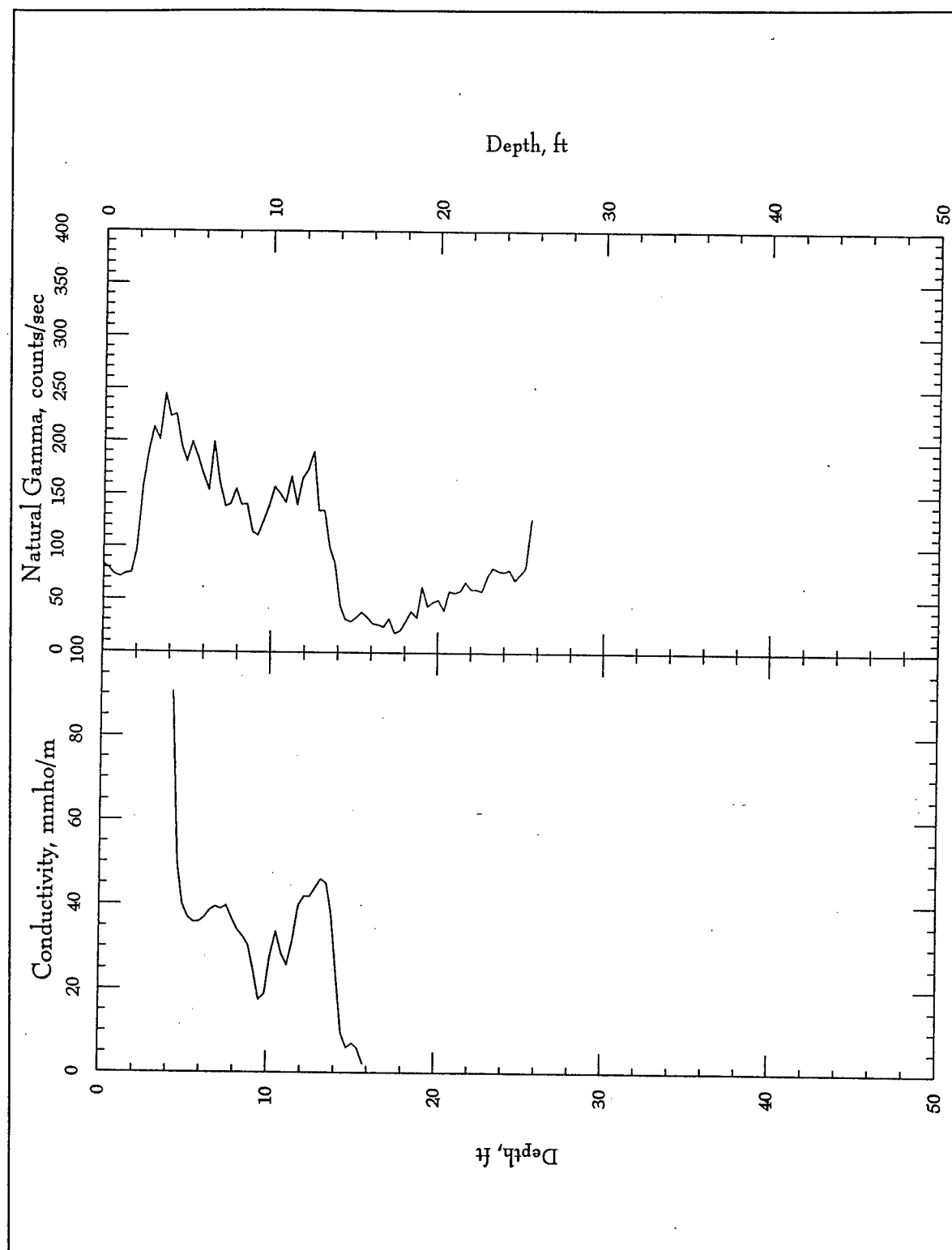


Figure D4. Borehole geophysical logs, WLC-27

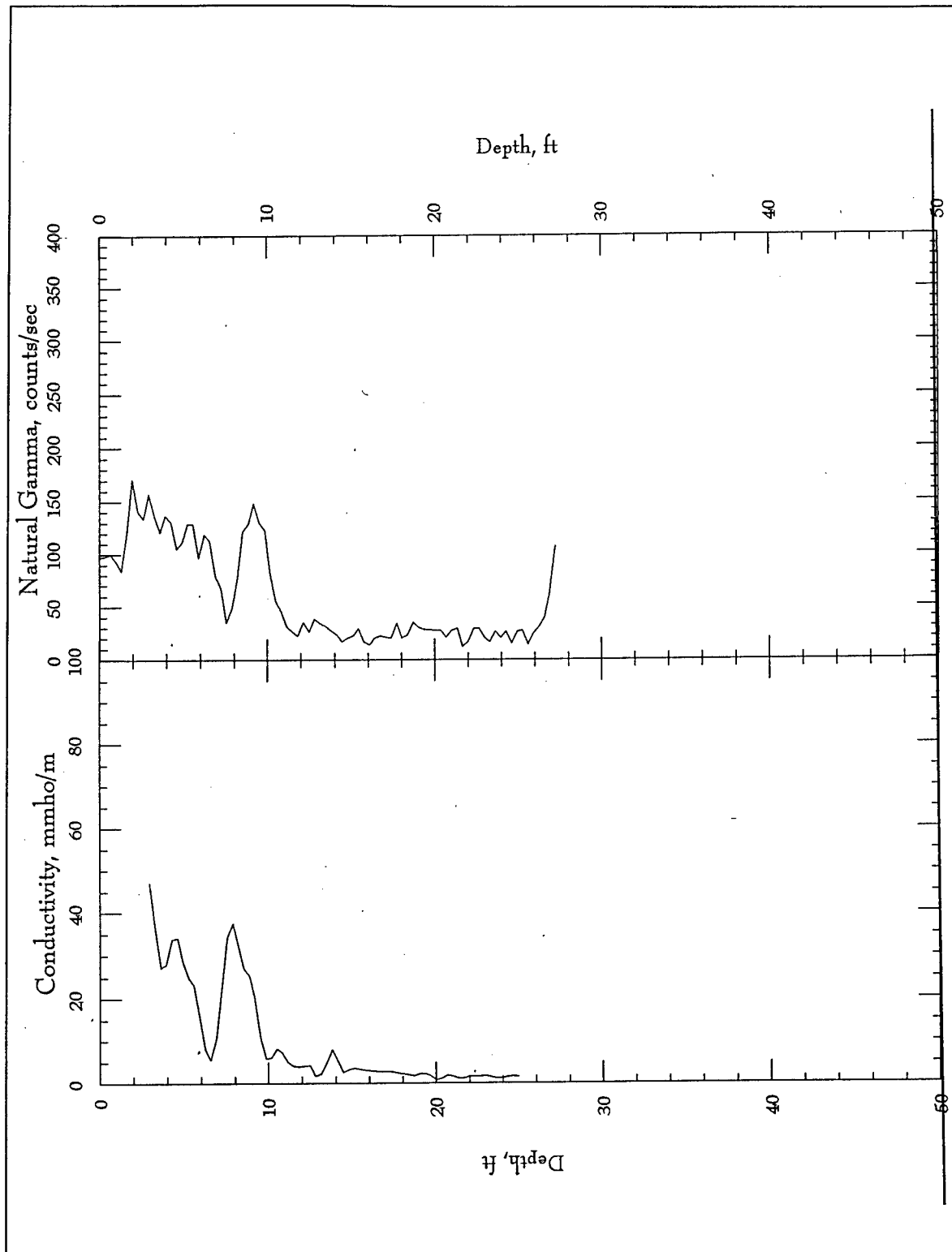


Figure D5. Borehole geophysical logs, WLC-28

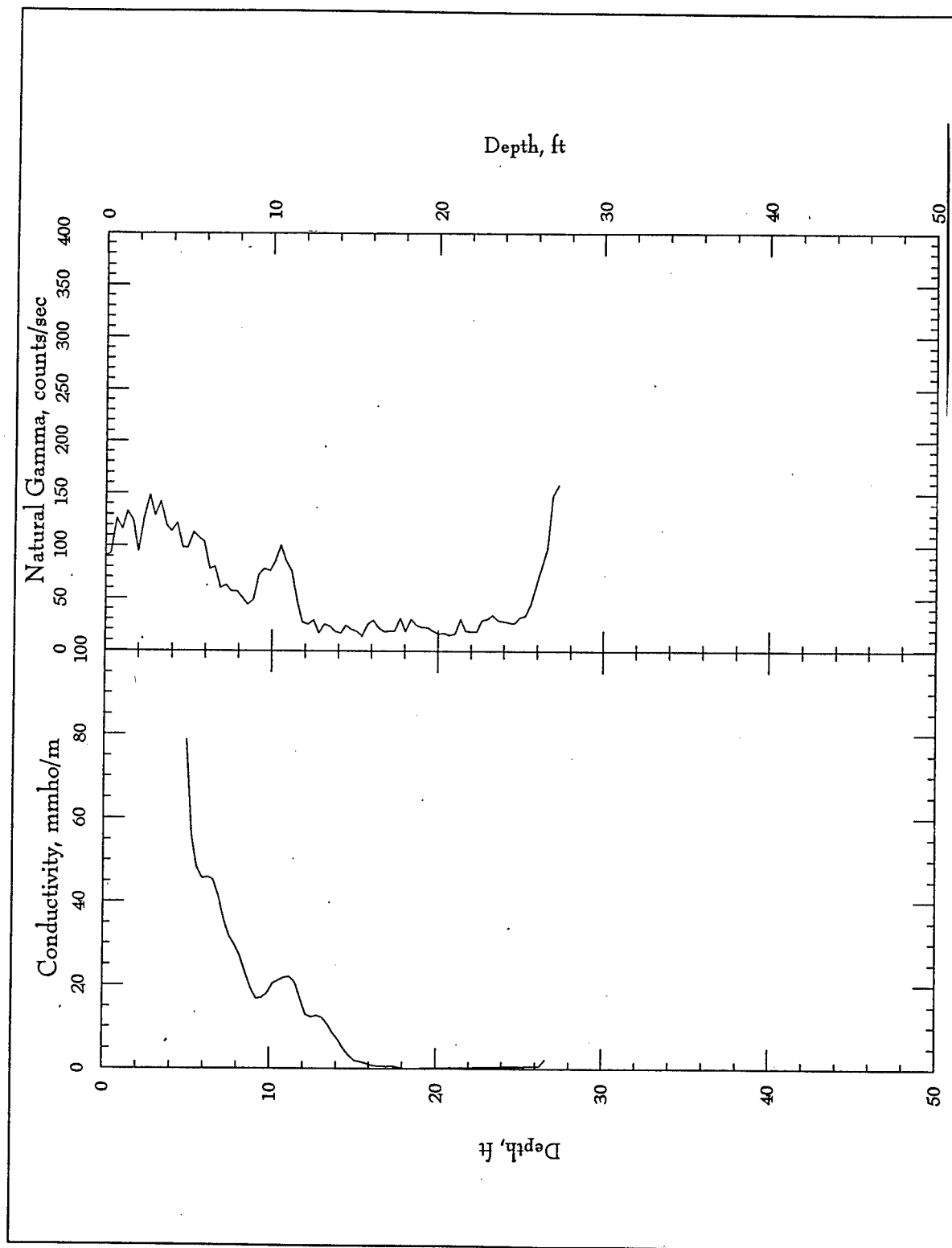


Figure D6. Borehole geophysical logs, WLC-29

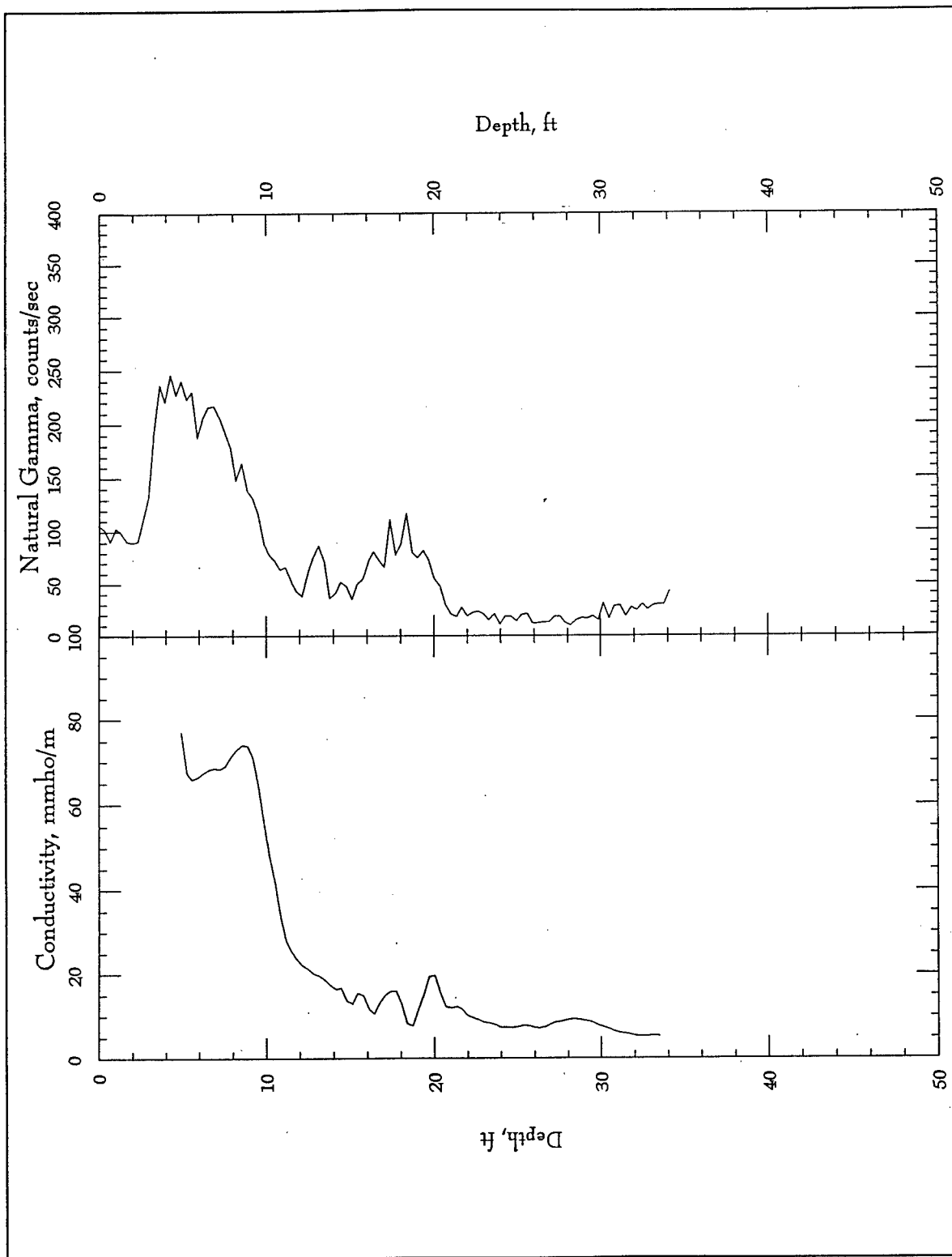


Figure D7. Borehole geophysical logs, WLC-30

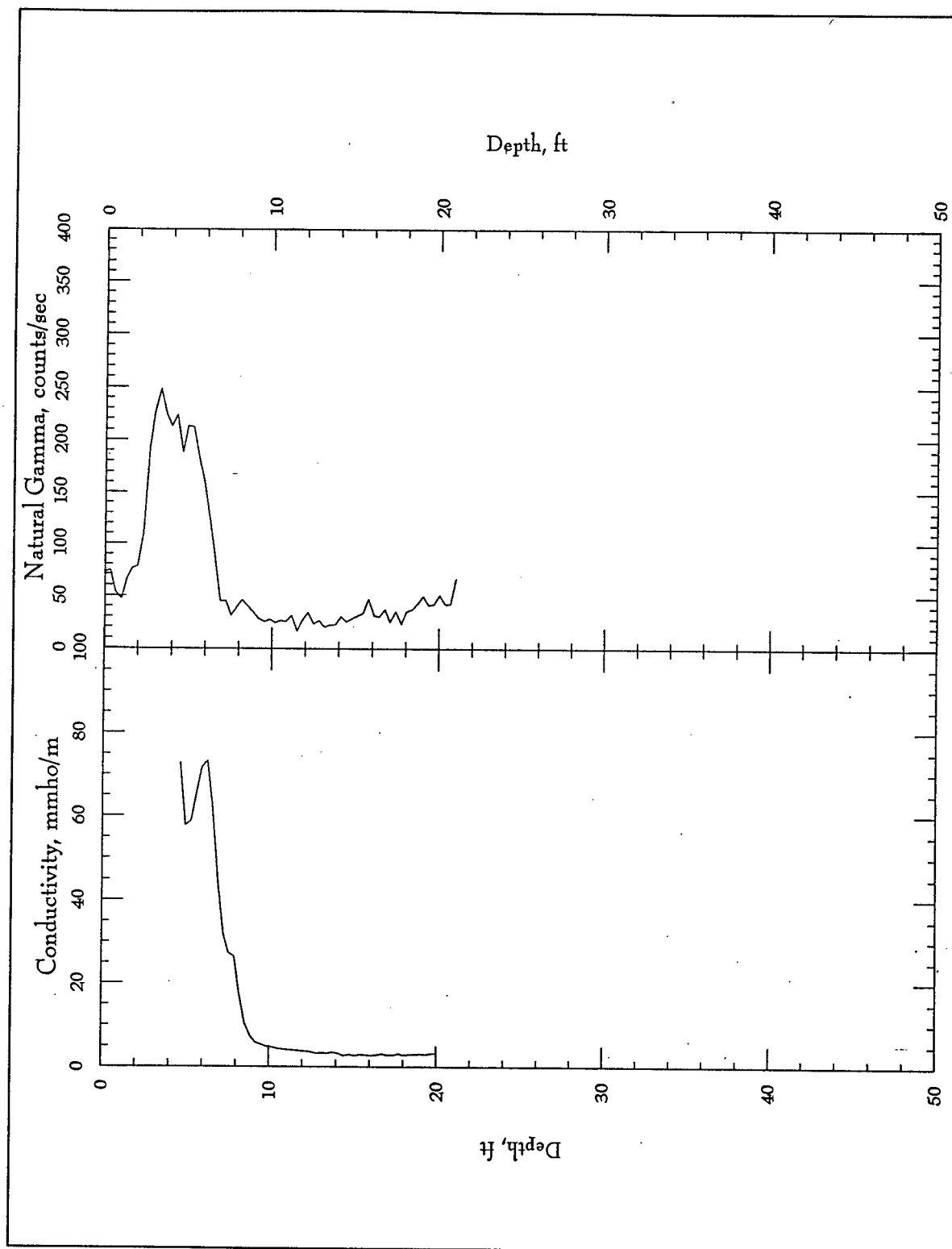


Figure D8. Borehole geophysical logs, WLC-31

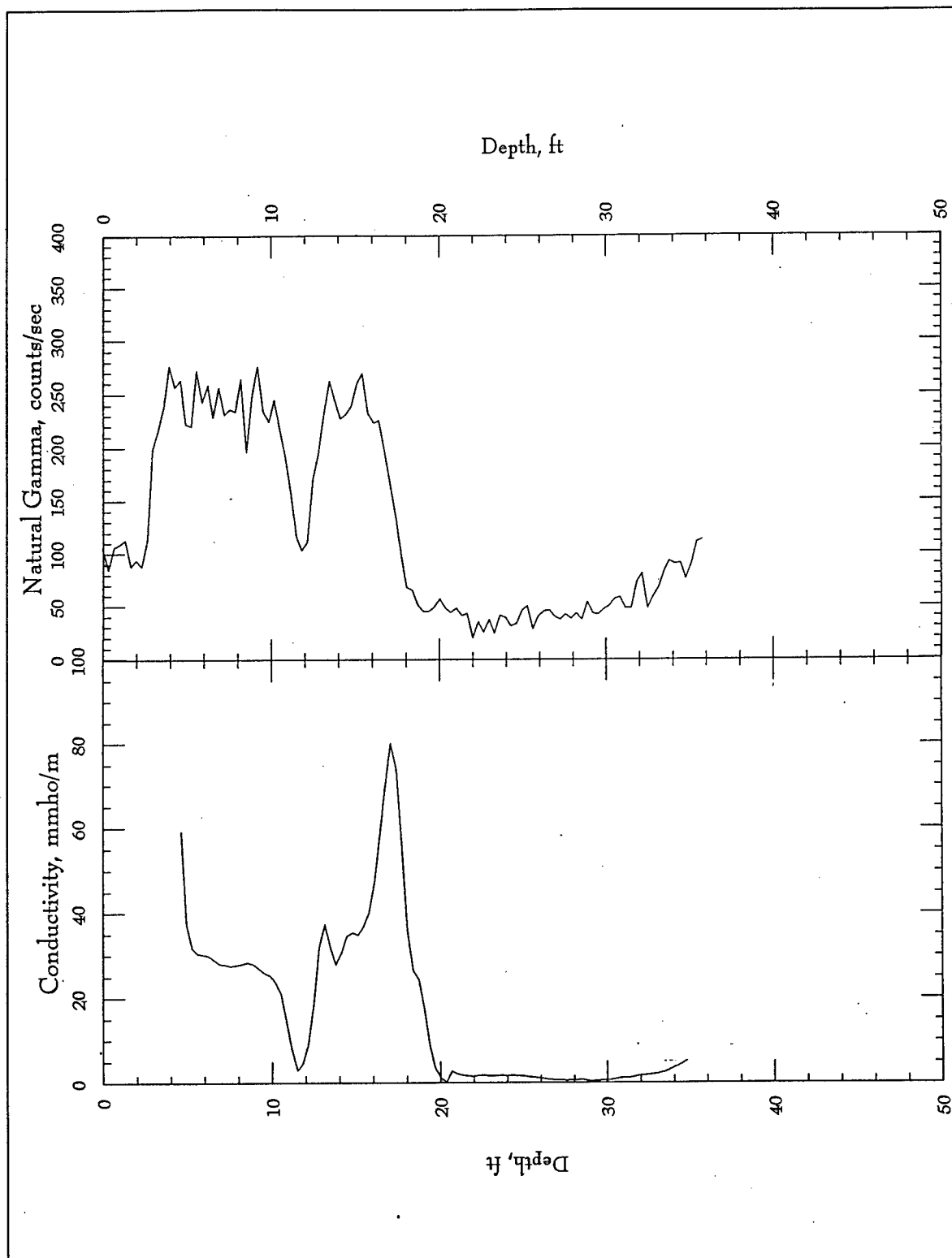


Figure D9. Borehole geophysical logs, WLC-33

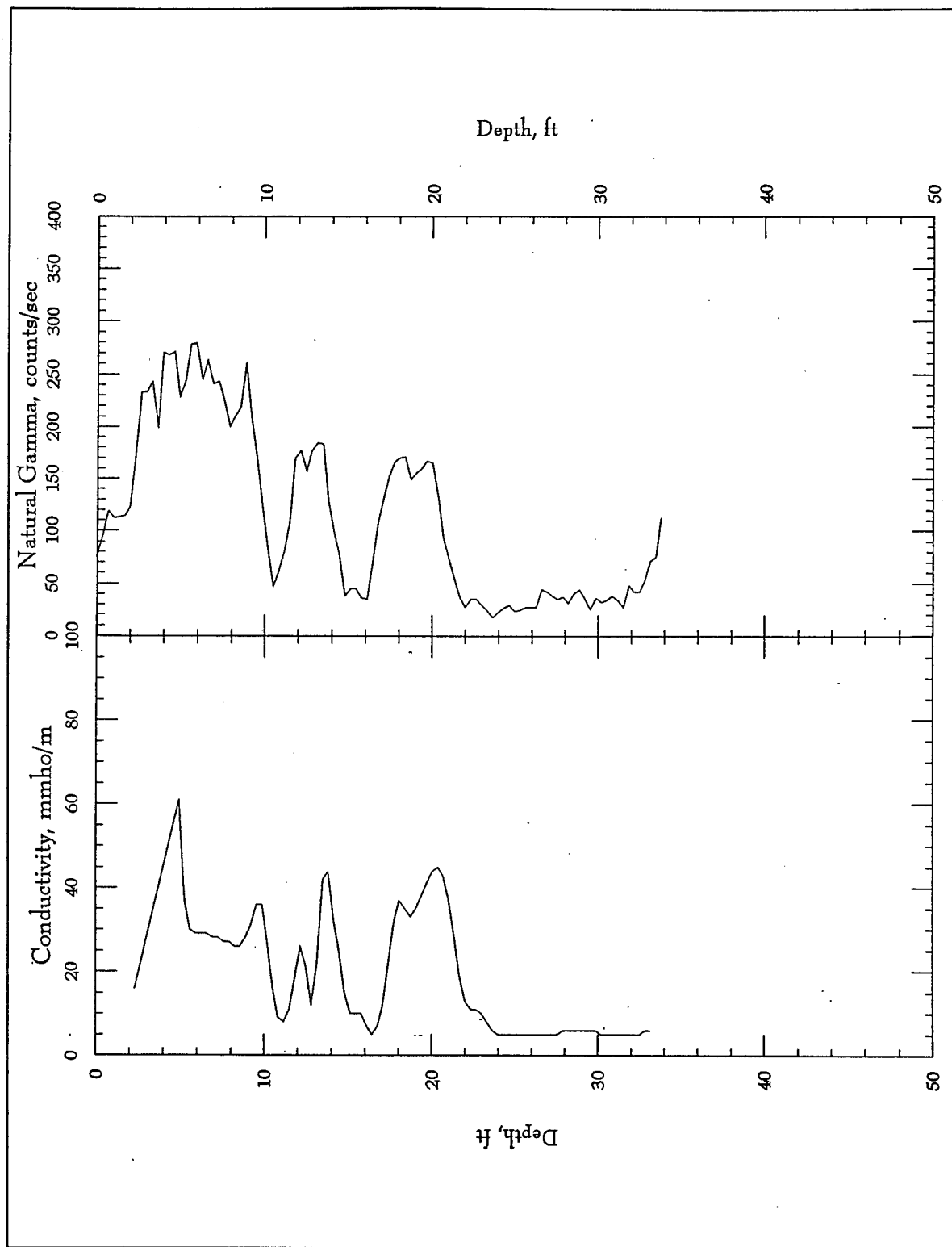


Figure D10. Borehole geophysical logs, WLC-34

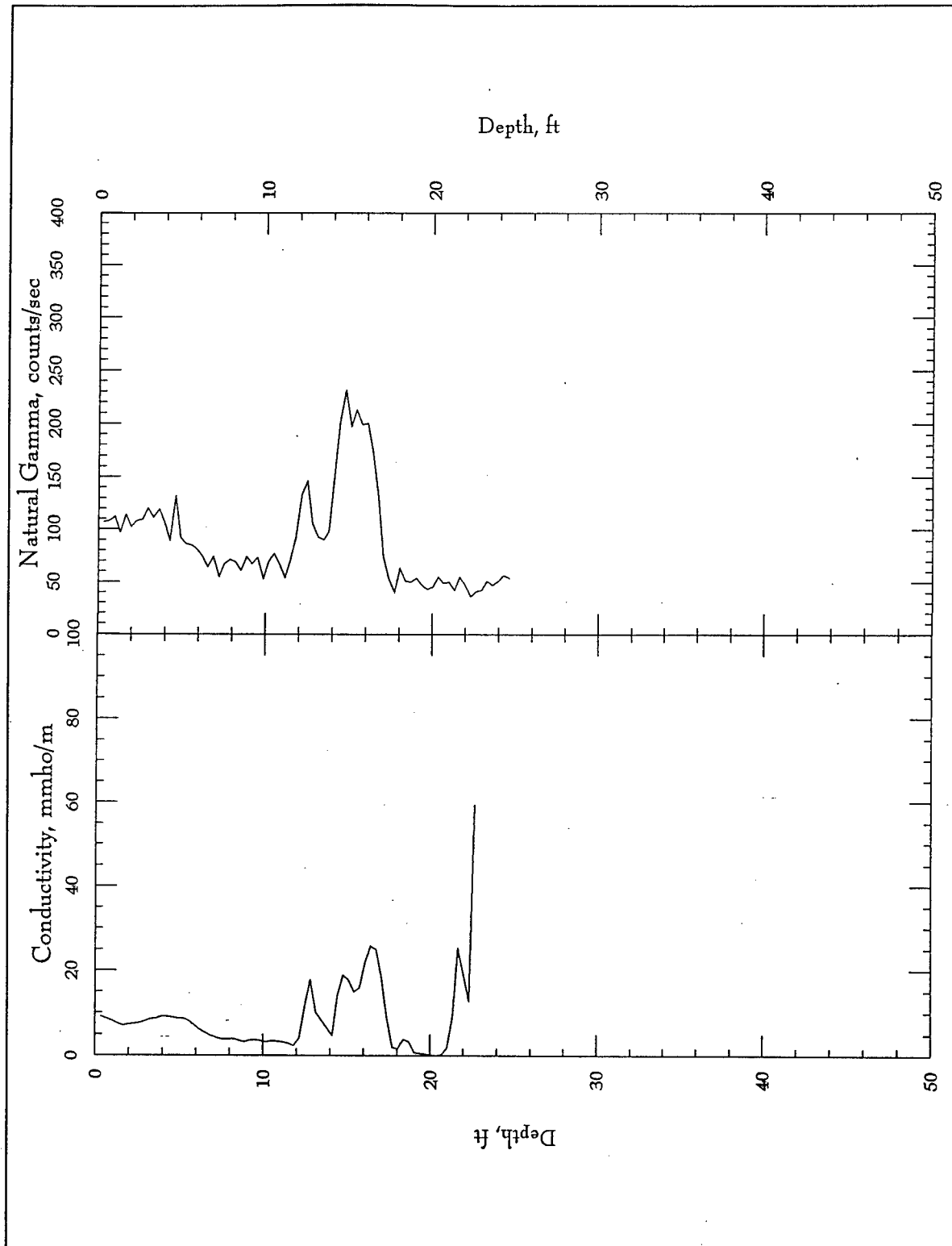


Figure D11. Borehole geophysical logs, WLC-36

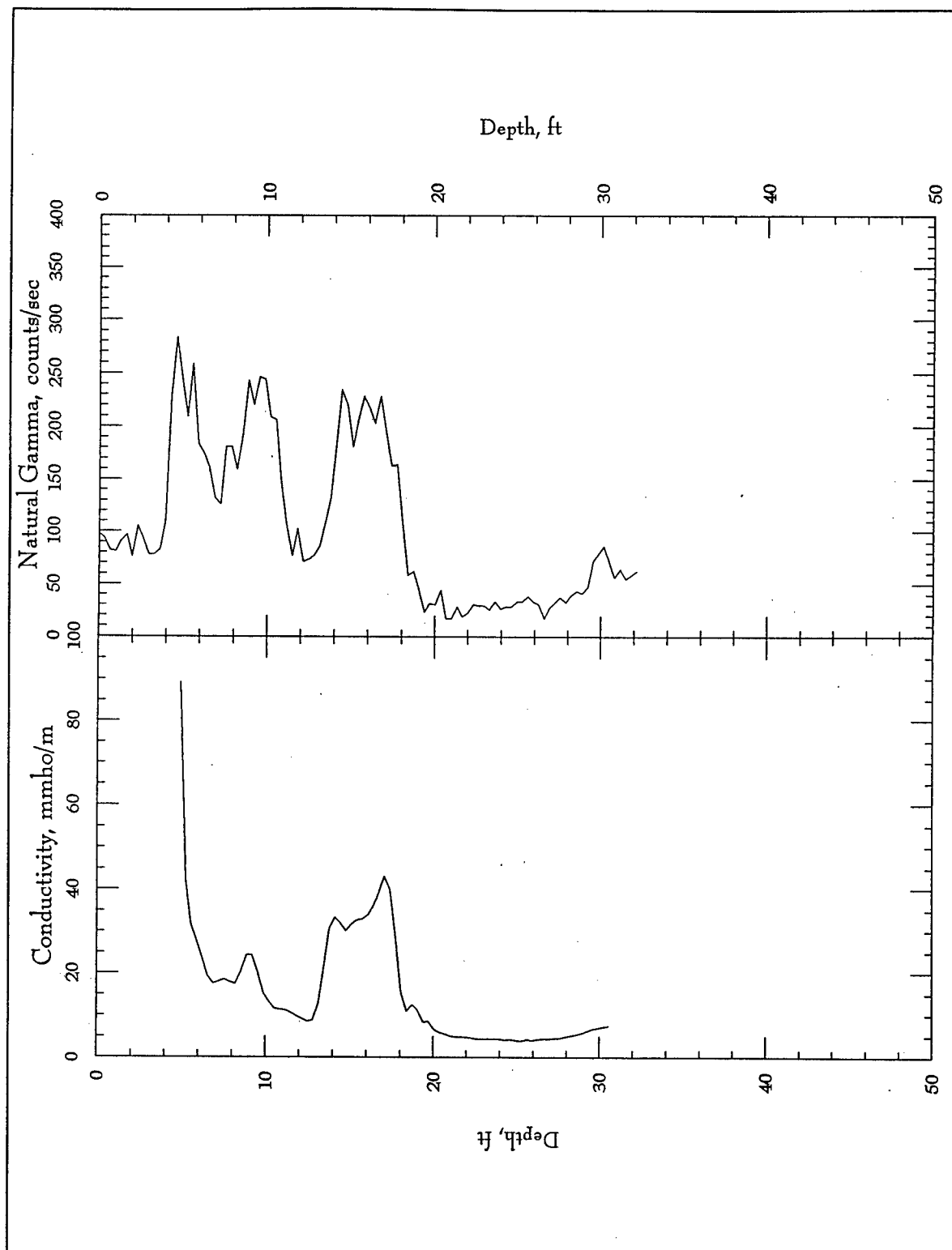


Figure D12. Borehole geophysical logs, WLC-37

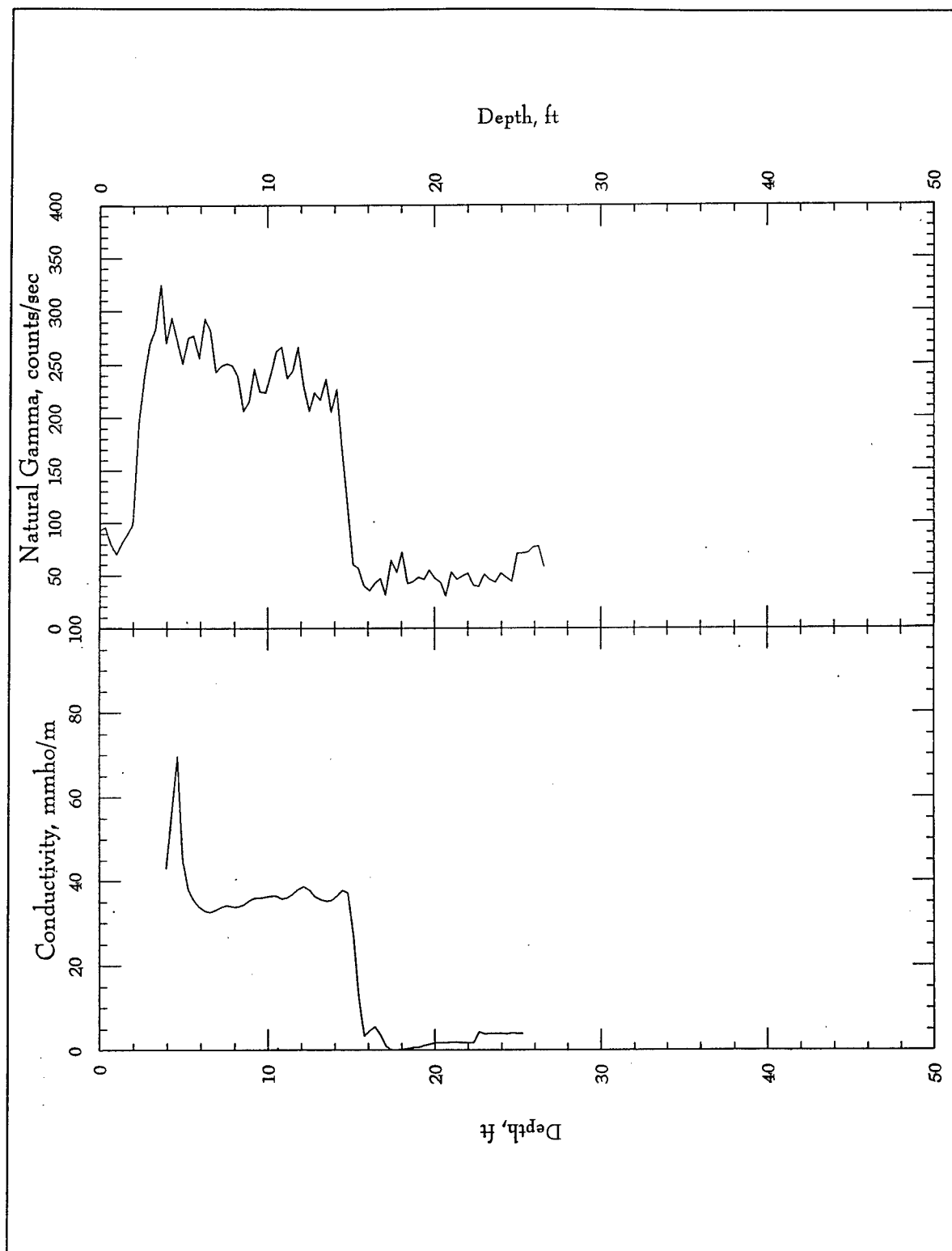


Figure D13. Borehole geophysical logs, WLC-39

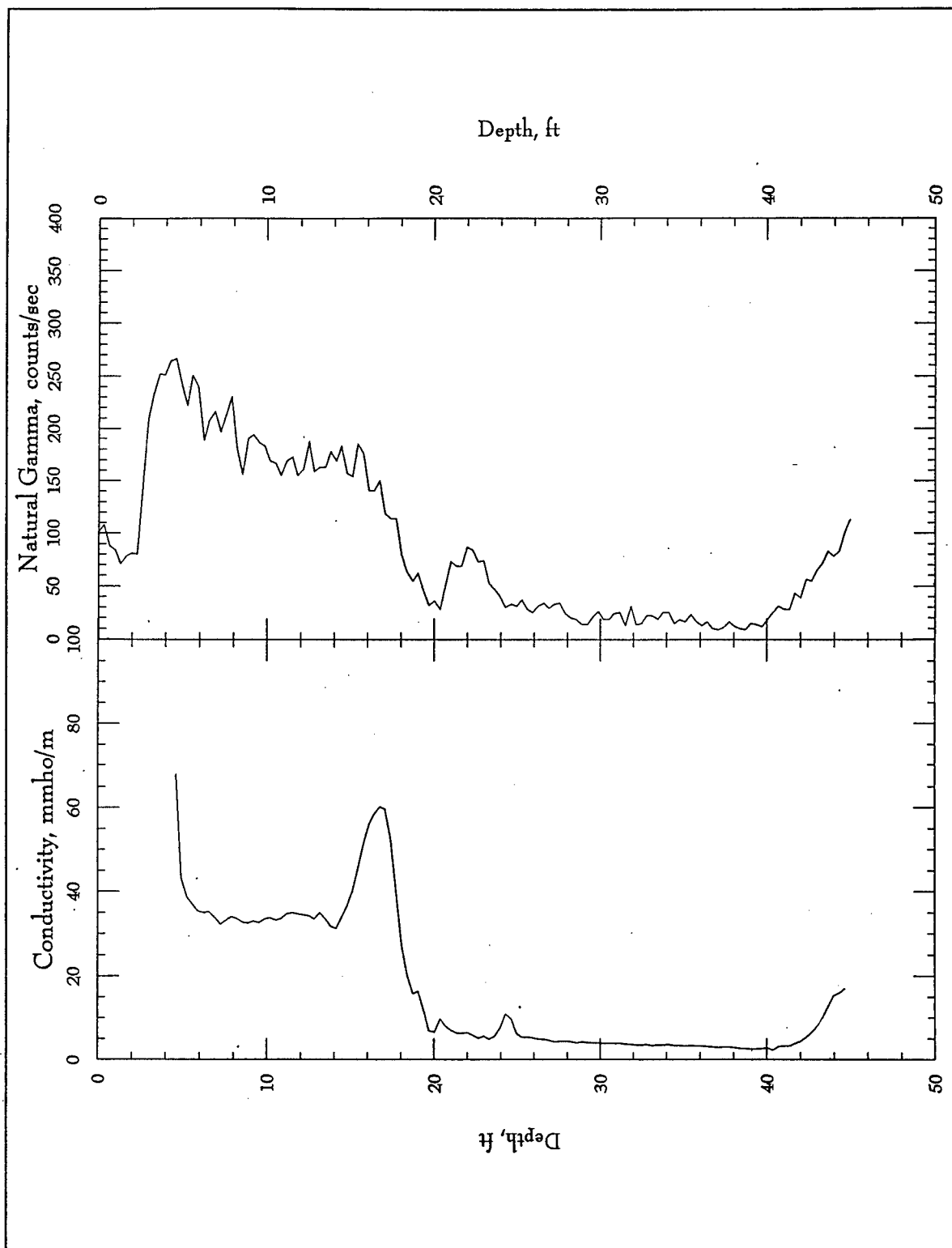


Figure D14. Borehole geophysical logs, WLC-41

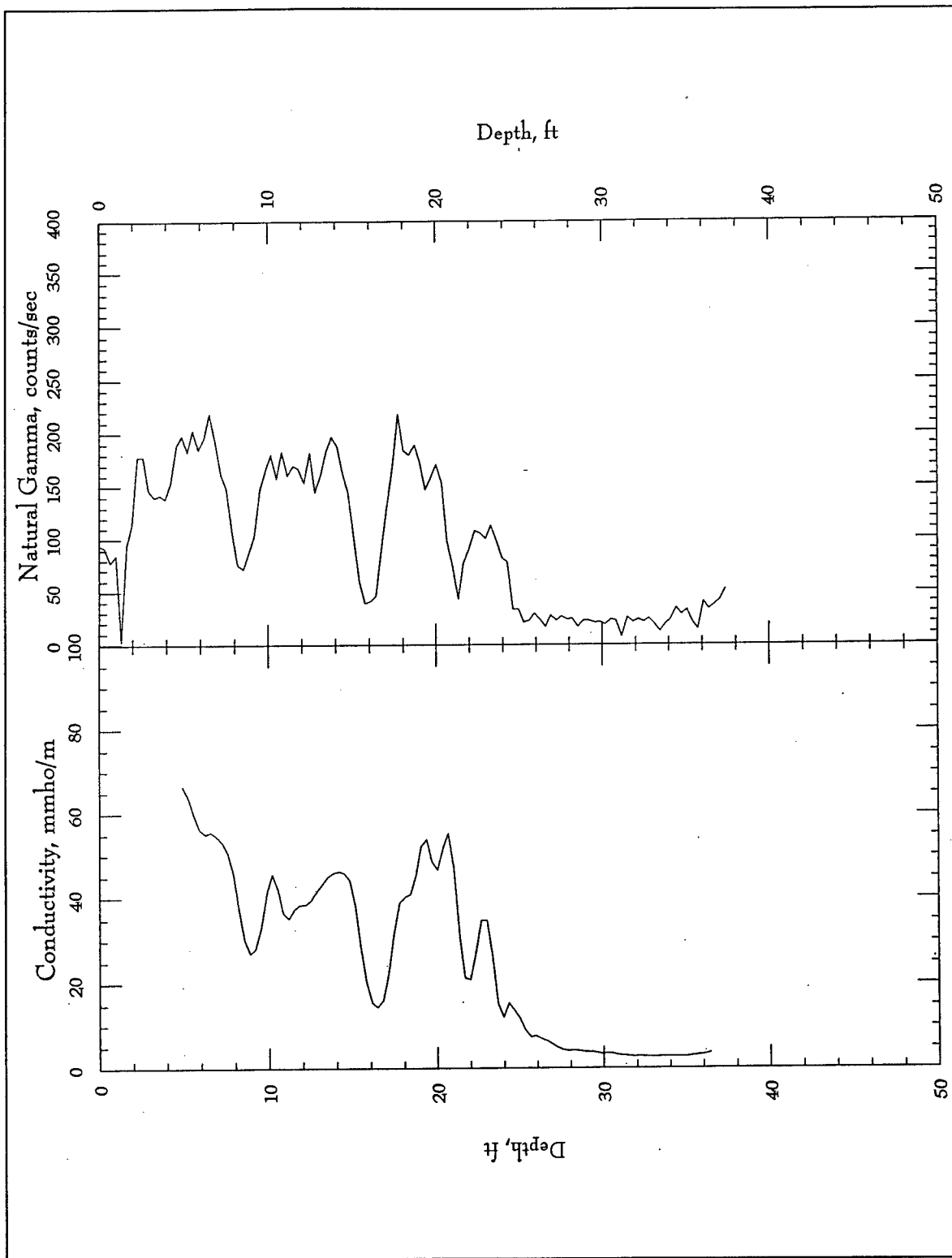


Figure D15. Borehole geophysical logs, WLC-42

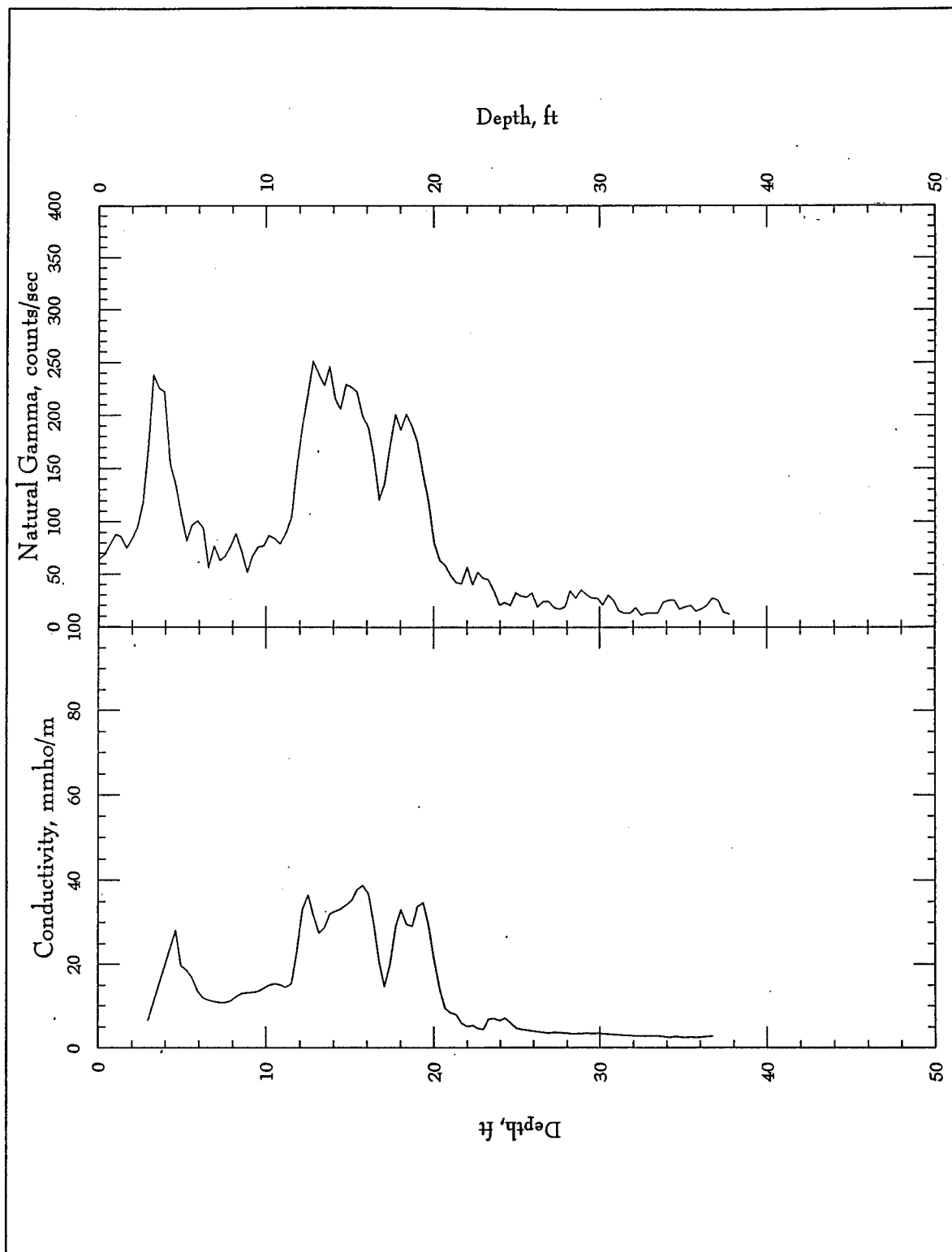


Figure D16. Borehole geophysical logs, WLC-43

REPORT DOCUMENTATION PAGE

Form Approved
OMB No. 0704-0188

Public reporting burden for this collection of information is estimated to average 1 hour per response, including the time for reviewing instructions, searching existing data sources, gathering and maintaining the data needed, and completing and reviewing the collection of information. Send comments regarding this burden estimate or any other aspect of this collection of information, including suggestions for reducing this burden, to Washington Headquarters Services, Directorate for Information Operations and Reports, 1215 Jefferson Davis Highway, Suite 1204, Arlington, VA 22202-4302, and to the Office of Management and Budget, Paperwork Reduction Project (0704-0188), Washington, DC 20503.

1. AGENCY USE ONLY (Leave blank)		2. REPORT DATE October 1996	3. REPORT TYPE AND DATES COVERED Final report	
4. TITLE AND SUBTITLE Assessment of Geophysical Methods for Subsurface Geologic Mapping, Cluster 13, Edgewood Area, Aberdeen Proving Ground, Maryland			5. FUNDING NUMBERS	
6. AUTHOR(S) Dwain K. Butler, Michael K. Sharp, Keith J. Sjostrom, Janet E. Simms, Jose L. Llopis, David V. Fitterman				
7. PERFORMING ORGANIZATION NAME(S) AND ADDRESS(ES) See reverse.			8. PERFORMING ORGANIZATION REPORT NUMBER Technical Report GL-96-17	
9. SPONSORING/MONITORING AGENCY NAME(S) AND ADDRESS(ES) Installation Restoration Program Directorate of Safety, Health, and Environment Aberdeen Proving Ground, Maryland 21005			10. SPONSORING/MONITORING AGENCY REPORT NUMBER	
11. SUPPLEMENTARY NOTES Available from National Technical Information Service, 5285 Port Royal Road, Springfield, VA 22161.				
12a. DISTRIBUTION/AVAILABILITY STATEMENT Approved for public release; distribution is unlimited.			12b. DISTRIBUTION CODE	
13. ABSTRACT (Maximum 200 words) Seismic refraction, electrical resistivity, and transient electromagnetic surveys were conducted at a portion of Cluster 13, Edgewood Area of Aberdeen Proving Ground, Maryland. Seismic refraction cross sections map the "topsoil" layer and the water table (saturated zone). The water table elevations from the seismic surveys correlate closely with water table elevations in nearby monitoring wells. Electrical resistivity cross sections reveal a very complicated distribution of sandy and clayey facies in the upper 10 - 15 m of the subsurface. A continuous surficial (topsoil) layer correlates with the surficial layer of the seismic section and nearby boring logs. Below the surficial layer, the complicated facies distribution has resistivities ranging from 25 ohm-m (likely clay) to several thousand ohm-m (dry sands and/or gravels). The complexity and details of the electrical resistivity cross section correlate well with boring and geophysical logs from nearby wells. The transient electromagnetic surveys map the Pleistocene-Cretaceous boundary, the saprolite, and the top of the Precambrian crystalline rocks. Conducting the transient electromagnetic surveys on a grid pattern allows the construction of a three-dimensional representation of subsurface geology (as represented by variations of electrical resistivity). Depths to the Cluster 13 and other areas of the Edgewood Area. (Continued)				
14. SUBJECT TERMS Borehole geophysical logs Electrical resistivity Geologic mapping			15. NUMBER OF PAGES 288	
Geophysical methods Integrated interpretation Seismic retraction			16. PRICE CODE	
17. SECURITY CLASSIFICATION OF REPORT UNCLASSIFIED	18. SECURITY CLASSIFICATION OF THIS PAGE UNCLASSIFIED	19. SECURITY CLASSIFICATION OF ABSTRACT	20. LIMITATION OF ABSTRACT	

7. (Concluded).

U.S. Army Engineer Waterways Experiment Station
3909 Halls Ferry Road
Vicksburg, MS 39180-6199

U.S. Geological Survey
Box 25046, MS 964
Denver Federal Center
Denver, CO 80225

13. (Concluded).

Thickness and depth of the saprolitic layer and depth to top of the Precambrian rocks are consistent with generalized geologic cross sections for the Edgewood Area and depths projected from reported depths at the Aberdeen Proving Ground NW boundary using regional dips.